Development of a High-Throughput Analytical Platform for the Characterisation of Biopharmaceuticals Generated from Multi-Gene Engineered CHO Cells

By:

Giulia Lambiase

A thesis submitted in partial fulfilment of the requirements for the degree of Doctor of Philosophy.

Faculty of Engineering

Department of Chemical and Biological Engineering

The University of Sheffield

March 2022

This page was intentionally left blank.

Declaration of Originality

In accordance with The University of Sheffield regulations, I, Giulia Lambiase, hereby declare that I am the sole author of this thesis. The results presented within are the fruits of my own labour, efforts and achievements. Where this was not the case, it has clearly been stated. I confirm that the present work has not been submitted in part or whole for any other degree or qualification.

This page was intentionally left blank.

Acknowledgements

This research would not have been possible without the sponsorship of AstraZeneca, the Biotechnology and Biological Sciences Research Council, and The University of Sheffield.

I would like to express my special thanks of gratitude to my supervisors Prof David C. James, Prof Mark J. Dickman, and Dr Vivian Lindo for giving me the opportunity to pursue a PhD and realise my dream to become a scientist. I also thank them for their endless guidance and support throughout my PhD journey, for encourage research ideas, providing scientific vision, wisdom and respond with a joke every time things went wrong. I am grateful to them and AstraZeneca for allowing the pursue of this research at the company site, providing extended funding during the COVID-19 pandemic as well as giving me the possibility to carry on research work after my thesis submission.

I owe a huge thanks to Dr Sophie Inman for teaching me mass spectrometry and assisting me in troubleshooting the various instruments in the Characterisation Lab, especially our good old triple quad! I am sincerely grateful for her outstanding enthusiasm and dedication to science as well as care for others which have been and will always be an excellent role model to me.

A debt of gratitude is owed to Dr Maurizio Muroni for training me in various industrial methodologies for protein analysis, for his guidance and, most of all, for teaching me to approach science with a smile, especially when experiments do not work.

I would like to thank Samuel Shepherd for providing the scripts to automate the analytical methods, training and helping me troubleshooting the robot. A special thanks for the long working hours powered through with double-shot Starbucks coffee.

It has been a great pleasure to work in the Analytical Science team at AstraZeneca. I thank the Cell Culture and Fermentation Science team in AstraZeneca and Prof David C. James research group at the University of Sheffield for the strong collaboration, particularly for providing the case study samples for my project. A special thanks to Dr Jennifer Spooner for her assistance in protein purification, Dr James Savery and the AZ Data Science Academy.

Finally, I would like to thank my parents Luigi and Paola, family and friends who have always been close to me even when far away; and to Freddie and Family Greatrex for their love and support – *without you, none of this would have indeed been possible.*

This page was intentionally left blank.

Abstract

The biopharmaceuticals market was valued $325 billion in 2020 with revenues forecasted to rise in the upcoming decade. High-throughput process development (HTPD) tools characterised by miniaturisation, parallelisation and automation of industrial bioprocessing workflows have emerged as the key enabler for leveraging costs and rapidly launching new products to market. However, the small sample generated from HTPD experiments and the fast timelines introduce analytical bottlenecks. Hence, more efficient high-throughput (HT) analytical tools are required to ensure the quality necessary to meet regulatory approval. This study aims to address some of the gaps in the current methodologies for the characterisation of protein-based biopharmaceuticals and implement new HT analytical solutions for driving product development in the industry. The first part of this work presents the generation of a flexible HT platform for the analysis of proteins expressed in microscale cell culture systems. Chemometric tools such as design-of-experiment (DoE), multivariate analysis (MVA) and predictive modelling were used to leverage method development and support product quality (PQ) analysis with statistical data, in line with the quality-by-design (QbD) approach. Fully automated pipette-tip based methods were optimised for the purification and preparation of low volume samples. Rapid HT size-exclusion (SEC) and cation-exchange chromatography (CEX) methods enabled the profiling of size and charge variants with sub-2 μg sensitivity. Online coupling of SEC with CEX in a two-dimensional liquid chromatography (2D-LC) set up with mass spectrometry (MS) detection (2D SEC-CEX-MS) combined aggregation analysis and charge variants peak identification in a single method maximising the data acquired from minimal sample requirements. Targeted MS analysis of cysteine modifications by multiple-reaction monitoring (MRM) was used to quantitate aggregates and fused into multi-attribute method (MAM) for supporting the analysis of cysteine modifications, glycosylation, deamidation and C-terminal Lys processing throughout the development of a bispecific antibody product. Finally, the methods were integrated into a HT analytical platform supporting HTPD experiments for cell line development (CLD). The HT analytical platform processed several hundreds of small volume samples providing PQ data necessary for clone selection. This demonstrated the benefits of hyphenating HT analytics as early as possible to drive CLD activities and gather a deeper understanding of the scientific and engineering principles that govern protein expression in cells. The HT analytics developed in this research will be implemented in the industrial analytical workstream to support AstraZeneca pipeline.

This page was intentionally left blank.

List of Tables

Table 1.1 Summary of the Most Common mAbs Quality Attributes and their Effect on the Bioactivity, Safety and Efficacy of the Final Product. 18

Table 1.2 List of the PTMs and Product Degradation Events Commonly Known to Cause Charge Heterogeneity in mAbs and BsAbs. 20

Table 1.3. Comparison between Conventional LT and State-of-the-Art HT Analytics for Biopharmaceutical Process Development. 38

Table 1.4. IEX Column Stationary Phases and Characteristics 46

Table 2.1 List of the LC and LC-MS methods and the columns used for method development with their respective providers and final applications 63

Table 2.2 Summary of the samples used for research with the respective providers and application description. 64

Table 3.1 Summary of estimates of the PhyTip purification MESD model parameters with t-test results 82

Table 3.2 Summary of the estimates of the PhyTip purification CCD model parameters with t-test results 85

Table 3.3 Optimised PhyTip purification method 88

Table 3.4 PhyTip purification method assessment results. 92

Table 3.5 Effect summary report of the HT SEC MESD model estimates. 96

Table 3.6 BsAbs HT SEC method development DoE effect summary 100

Table 3.7 HT SEC method 105

Table 3.8 HT SEC method assessment results. 106

Table 3.9 Summary of the DoE2 model parameters effects. 117

Table 3.10 Summary of the optimised HT CEX method. 118

Table 3.11 HT CEX method assessment results. 120

Table 4.1 DoE factors effects summary. 130

Table 4.2 2D SEC-CEX-UV final method conditions. 138

Table 4.3 2D SEC-CEX-UV method assessment results. 140

Table 4.4 2D SEC-CEX-UV PQ analysis of mAb-1 at the start and endpoint of the accelerated forced degradation and stability study..... 142

Table 4.5 2D-LC SEC-CEX-UV-MS final method conditions. 156

Table 4.6 2D SEC-CEX-UV-MS PQ analysis of mAb-1 at the start and endpoint of the accelerated forced degradation and stability study..... 157

Table 5.1 Sample groups used for BsAb-1 disulphide bonds mapping..... 172

Table 5.2 Random effect model report. 193

Table 5.3 MAM method assessment results 196

Table 9.1 PhyTip purification method development MESD factors, responses and constant parameters. 287

Table 9.2 PhyTip purification CCD factors, responses and constant parameters. 288

Table 9.3 Full dataset of the linearity study and determination of the column loading range %R. 289

Table 9.4 T-test of the %HMWS analysed before and after PhyTip purification by SEC for the assessment of the method suitability-for-Use..... 290

Table 9.5 SEC Methods employed for analysing the %HMWS during the assessment of PhyTip purification suitability-for-Use. 291

Table 9.6. List of factors and responses of the MESD for HT SEC method development. 292

Table 9.7 List of the 2x2x3 FFD DoE factors, responses and analysis conditions. 293

Table 9.8 HT SEC throughput gain by injection overlapping. 294

Table 9.9 HT SEC accuracy study. 297

Table 9.10 Analysis conditions of HT CEX method development DoE1. 302

Table 9.11 Analysis conditions of the HT CEX DoE2..... 303

Table 9.12 HT CEX DoE2 parameter estimates analysed for each response. 304

Table 10.1 2D SEC-CEX-UV column screening and mobile phase composition selection DoE table. 308

Table 10.2 T-test evaluating the difference between the mean %peak area of mAb-1 size and charge variants for the RS and control samples. 313

Table 10.3 ANOVA test for the %LMWS observed during the accelerated stability study. 315

Table 10.4 ANOVA test for the %LMWS observed during the low pH stress. 317

Table 10.5 ANOVA test for the %LMWS observed during the high pH stress. 318

Table 10.6 ANOVA test for the %acidic species observed during the low pH stress.....319

Table 10.7 ANOVA test for the %acidic species observed during the high pH stress.....320

Table 10.8 ANOVA test for the %acidic species observed during the stress conditions applied during the accelerated stability study. 321

Table 10.9 ANOVA test for the %basic species observed during low pH stress.....322

Table 10.10 ANOVA test for the %basic species observed during high pH stress.....323

Table 10.11 ANOVA test for the %basic species observed under the accelerated stability study stress conditions. 324

Table 10.12 Method assessment accuracy data for the analysis of heat-stressed mAb-1..327

Table 10.13 MS peak assignment.....330

Table 11.1 ANOVA test for the sample plate position. 341

Table 11.2 T-test of the manual *vs.* the automated sample preparation procedures.....343

Table 11.3 Summary of the variability gauge analysis for BsAb-1 PTMs quantitation by manual and automated sample preparation. 346

Table 11.4 Summary HMWS quantitation regression model. 347

Table 11.5 Summary of the factors effects in the HMWS quantitation model. 348

Table 11.6 Summary of the Variability gauge analysis to assess the overtime stability of the tryptic digested peptides under process conditions before LC-MS injection within 48 samples. 348

Table 12.1 Example of PhyTip purification/HTSEC Python script 1. 369

This page was intentionally left blank.

List of Figures

Figure 1.1 IgG1 Molecular Structure with Commonly Occurring Quality Attributes. 17

Figure 1.2 Biopharmaceutical Development Lifecycle. 27

Figure 3.1 Schematic representation of DFC mechanism on resin-filled pipette-tips.....79

Figure 3.2 Non-reducing SDS-PAGE gel electrophoretogram of the purification of a mAb from the cell culture supernatant. 80

Figure 3.3 PhyTip purification MESD prediction profiler.....83

Figure 3.4 Box-Wilson CCD points representation on a cube. 84

Figure 3.5 PhyTip purification CCD prediction profiler. 86

Figure 3.6 Assessment of the effect of different elution buffers on PQ. 88

Figure 3.7 PhyTip linearity and column loading range. 90

Figure 3.8 Assessment of the PhyTip purification method suitability for use. 91

Figure 3.9 HT SEC MESD prediction profiler.....97

Figure 3.10 BsAb-1 size variants profile of BsAb-1 with peak assignment details. 99

Figure 3.11 FFD model prediction profiler for BsAbs method development. 101

Figure 3.12 Evaluation of the HT SEC method optimal injection volume range. 103

Figure 3.13 Overlay of 10 µL injection of samples with different concentrations. 104

Figure 3.14 HT SEC of samples with various degrees of HMWS impurities. 108

Figure 3.15 Visualisation of the DoE1 data points on a cube. 113

Figure 3.16 DoE1 heatmap of the ePC response in relation to the column chemistry and mobile phase pH. 115

Figure 3.17 CEX charge variants profile of mAb-1 by using different column chemistries and mobile phase chromatograms. 115

Figure 3.18 Visualisation of the data points of the DoE2 on a cube. 116

Figure 3.19 HT CEX DoE2 prediction profiler. 118

Figure 3.20 HT CEX method stability-indicating capability. 119

Figure 4.1 Contour plot showing the effect of the mobile phase composition and column chemistry on SEC separation. 131

Figure 4.2 Overlay of heat-stressed mAb-1 chromatograms obtained by using the same ionic strength mobile phase across three columns. 132

Figure 4.3 DoE prediction profiler for the 2D SEC-CEX-UV method ^{1}D column selection. 134

Figure 4.4 Schematic of the 2D-LC system with 2D valve plumbing flow path. 135

Figure 4.5 DoE verification and evaluation of the ^{1}D SEC mobile phase compatibility with the ^{2}D CEX separation. 136

Figure 4.6 2D heart-cutting SEC-CEX-UV analysis of a mAb. 138

Figure 4.7 Analysis of AAPH stress-induced degradation pathway of mab-1 over time by 2D SEC-CEX-UV. 144

Figure 4.8 Analysis of H_2O_2 stress-induced degradation pathway of mab-1 over time by 2D SEC-CEX-UV. 145

Figure 4.9 Effect of buffer ionic strength and pH on the ^{1}D SEC separation. 149

Figure 4.10 ^{2}D CEX gradient slope optimisation. 151

Figure 4.11 Intact mAb-1 Analysis under denaturing and native conditions with increasing in-source CID setting. 154

Figure 4.12 mAb-1 RS charge variants peak identification by 2D SEC-CEX-UV-MS.... 159

Figure 4.13 H_2O_2-stressed mAb-1 charge variants peak identification by 2D SEC-CEX-UV-MS. 159

Figure 4.14 AAPH-stressed mAb-1 charge variants peak identification by 2D SEC-CEX-UV-MS. 160

Figure 5.1 Schematic representation of BsAb-1 molecular structure and disulphide bond linkage. 168

Figure 5.2 EThcD-assisted MS and MS/MS spectra of the scFv tripeptide in BsAb-1 SEC fractions. 172

Figure 5.3 Schematic representation of the scFv tripeptide disulphide bonds and site-specific modifications. 174

Figure 5.4 XIC of peptide-3 $[M+2H]^{2+}$ (1501 m/z) and peptide-1 $[M+1H]^{1+}$ (1075 m/z).174

Figure 5.5 EThcD MS/MS spectra of glutathionylation on Cys640 observed in fraction 1. 175

Figure 5.6 EThcD MS/MS spectra of cysteinylation on Cys640 observed in fraction 1...175

Figure 5.7 EThcD MS/MS spectra of glutathionylation on Cys442 observed in fraction 1. 176

Figure 5.8 EThcD MS/MS spectra of cysteinylation on Cys442 observed in fraction 1...176

Figure 5.9 MAM analysis of BsAb-1: proof-of-concept of targeted PTMs monitoring. ..179

Figure 5.10 Quantitative analysis of BsAb-1 Cys modifications by MAM.....180

Figure 5.11 MVA report. 182

Figure 5.12 Inferring the quantitation of HMWS from Cys modifications by Ridge regression analysis. 184

Figure 5.13 Variability gauge chart for site-specific PTMs relative peak area between manual and automated procedures. 188

Figure 5.14 Assessment of the overtime sample stability across 48 injections. 190

Figure 5.15 Day-to-day reproducibility parallelism plot. 191

Figure 5.16 Variability gauge charts of day-to-day reproducibility. 192

Figure 5.17 Qualifier/quantifier ion ratio CVs for the assessment of method suitability for the analysis of in-process samples and stability-indicating capability. 194

Figure 5.18 PTMs quantitation for the assessment of method suitability for the analysis of in-process samples and stability-indicating capability. 195

Figure 6.1 Schematics of the PhyTip-purification/HT SEC workflow 202

Figure 6.2 Visual representation of the %HMWS in each 96-DWP analysed during the SPOG screen.....204

Figure 6.3 Effect of the cell culture conditions under investigation on the %HMWS impurities analysed in samples harvested on day 9 and day 14 of the overgrowth.....207

Figure 6.4 Effect of the cell culture experimental conditions on BsAb-1 C-terminal retention on days 9 and 14 of the overgrow analysed by MAM. 208

Figure 6.5 Effect of the cell culture experimental conditions on BsAb-1 deamidation on days 9 and 14 of the overgrow analysed by MAM. 209

Figure 6.6 Effect of the cell culture experimental conditions on BsAb-1 glycosylation on days 9 and 14 of the overgrow analysed by MAM. 210

Figure 6.7 Effect of the cell culture experimental conditions on BsAb-1 Cys modifications on days 9 and 14 of the overgrow analysed by MAM..... 211

Figure 6.8 HMWS quantitation by MRM..... 212

Figure 6.9 Comparison of the HMWS quantitation data analysed by MAM and HT SEC. 213

Figure 6.10 Size and charge variants profile of mAb-1 samples in the 24-DWP screen .. 216

Figure 6.11 Size and charge variants of mAb-1 in the 10 mL culti-flasks experiment..... 217

Figure 7.1 Schematics of the HT Analytical Platform. 223

Figure 7.2 A view of the direction of the biopharmaceutical analytics from the current HT and conventional tools towards future technologies..... 232

Figure 9.1 PhyTip purification method development MESD actual-by-predicted plot. ... 287

Figure 9.2 PhyTip purification CCD actual-by-predicted plot. 288

Figure 9.3 Analysis of mAb-1, mAb-2 and BsAb-1 HMWS impurities by AZ SEC SOP. 291

Figure 9.4 HT SEC MESD actual-by-predicted plot for the responses analysed separately. 292

Figure 9.5 HT SEC 2x2x3 FFD DoE actual-by-predicted plot..... 293

Figure 9.6 HT SEC specificity assessment. 294

Figure 9.7 HT SEC repeatability study..... 295

Figure 9.8 HT SEC stability-indicating capability. 295

Figure 9.9 Linearity test of the UV absorbance response *vs.* %HMWS..... 296

Figure 9.10 Determination of the HT SEC method LOQ and LOD from a calibration curve. 300

Figure 9.11 Proof-of-concept application of the HT SEC method..... 301

Figure 9.12 HT CEX Method development DoE1 actual-by-predicted plot. 302

Figure 9.13 HT CEX method development DoE2 actual-by-predicted plot. 303

Figure 9.14 HT CEX specificity test.....305

Figure 9.15 HT CEX repeatability study. 305

Figure 9.16 HT CEX linearity. 306

Figure 10.1 SEC profile of heat-stressed mAb-1 analysed by the AZ SOP SEC method. 307

Figure 10.2 Actual-by-predicted plot for resolution (A) and %HMWS (B) with the respective lack of fit tables reporting the DoE Model summary for each response.....309

Figure 10.3 ^{1}D SEC DoE verification. 310

Figure 10.4 SEC-CEX-UV specificity test. 311

Figure 10.5 2D SEC-CEX-UV stability-indicating study. 312

Figure 10.6 SEC-CEX-UV RS-control samples overlay over time. 312

Figure 10.7 ^{2}D accelerated stability study SEC-CEX-UV chromatograms. 314

Figure 10.8 2D low and high pH treatment SEC-CEX-UV chromatograms overlays. 316

Figure 10.9 Linearity study. 325

Figure 10.10 Peak area *vs.* proportional protein load for LOQ determination.....326

Figure 10.11 Comparison of %HMWS quantitation obtained by SEC-CEX-UV method *vs.* the AZ SOP SEC. 329

Figure 10.12 Overlay of the mAb-1 RS ^{1}D SEC profiles obtained by using volatile and non-volatile buffers. 329

Figure 11.1 BsAb-1 SEC profile displaying the time window of the HMWS impurities and main product peak fractions. 333

Figure 11.2 EThcD-assisted MS/MS spectra of the Cys23-Cys88 disulphide bond linked peptide. 334

Figure 11.3 EThcD-assisted MS/MS spectra of the Cys134-Cys194 disulphide bond linked peptide. 335

Figure 11.4 EThcD-assisted MS/MS spectra of the Cys148-Cys204 disulphide bond linked peptide. 336

Figure 11.5 EThcD-assisted MS/MS spectra of the Cys265-Cys325 disulphide bond linked peptide. 337

Figure 11.6 EThcD-assisted MS/MS spectra of the Cys371-Cys698 disulphide bond linked peptide. 338

Figure 11.7 EThcD-assisted MS/MS spectra of the Cys420-Cys494 disulphide bond linked peptide. 339

Figure 11.8 Comparison of the qualifier/quantifier ion ratio CVs obtained when using the manual and automated sample preparation procedures. 340

Figure 11.9 Comparison of the MAM relative quantitation data of BsAb-1 PTMs obtained when using the manual *vs.* the automated sample preparation procedures. 340

Figure 11.10 Comparison of the standard deviation observed in relation to the ms signal intensity. 349

Figure 11.11 Comparison between the HT SEC and MAM method precision in quantifying BsAb-1 HMWS impurities. 350

Figure 12.1 T-test of the variation in HMWS levels analysed by HT SEC on day 9 and day 14. 351

Figure 12.2 ANOVA of the %HMWS analysed on day 9 across the experimental conditions. 352

Figure 12.3 ANOVA of the %HMWS analysed on day 14 across the experimental conditions. 353

Figure 12.4 ANOVA of C-terminal Lys retention across the experimental conditions on day 9. 354

Figure 12.5 ANOVA of C-terminal Lys retention across the experimental conditions on day 14. 355

Figure 12.6 T-test of C-terminal Lys retention between day 9 and day 14. 356

Figure 12.7 ANOVA of MAM predicted HMWS across the experimental conditions on day 9. 357

Figure 12.812.9 ANOVA of MAM predicted HMWS across the experimental conditions on day 14. 358

Figure 12.10 T-test of MAM predicted %HMWS between day 9 and day 14.....359

Figure 12.11 ANOVA of deamidation of Asn54 across the experimental conditions on day 9. 360

Figure 12.12 ANOVA of deamidation of Asn54 across the experimental conditions on day 14. 361

Figure 12.13 T-test of deamidation of Asn54 between day 9 and day 14. 362

Figure 12.14 ANOVA of deamidation of Asn365 across the experimental conditions on day 9. 363

Figure 12.15 ANOVA of deamidation of Asn365 across the experimental conditions on day 14. 364

Figure 12.16 T-test of deamidation of Asn365 between day 9 and day 14. 365

Figure 12.17 ANOVA of deamidation of Asn662 across the experimental conditions on day 9. 366

Figure 12.18 ANOVA of deamidation of Asn662 across the experimental conditions on day 14. 367

Figure 12.19 T-test of deamidation of Asn662 between day 9 and day 14. 368

List of Acronyms and Abbreviations

ω_h: peak width at half height

µL: microliter

µm: micrometre

1D-LC: one-dimensional liquid chromatography

2D-LC: two-dimensional liquid chromatography

AAPH: azodiisobutyramidine dihydrochloride

AcOOH-3.6: acetate buffer, pH 3.6

ADC: antibody-drug conjugate

ADDC: antibody-dependent cellular cytotoxicity

AEX: anion exchange

ANOVA: analysis of variance

API: active principal ingredient

AQbD: analytical quality by design

Arg (or R): arginine

Asn (or N): asparagine

ASO: antisense oligonucleotide

ATMP: advanced therapy medicinal products

AZ SEC SOP: AstraZeneca size exclusion chromatography standard operating procedure

AZ: AstraZeneca

BBD: Box-Behnken design

BEH: ethylene bridge hybrid technology

BHK: baby hamster kidney cells

BiTE: bispecific T-cell engager

BLI: bio-layer interferometry

BsAb: bispecific antibody

CAP-T: Human amniocentesis cells

CCD: central composite design

CDR: complementarity-determining region

CE: capillary electrophoresis

CE-MS: capillary electrophoresis-mass spectrometry

CEX: cation exchange

CGE: capillary gel electrophoresis

cGMP: current good manufacturing practice

CH: heavy chain constant domain

CHO: Chinese hamster ovary cells

CID: collision-induced dissociation

cIEF: capillary isoelectric focusing

CL: light chain constant domain

CLD&E: cell line development and engineering

CLD: cell line development

-COOH: carboxylic group

CPP: critical process parameter

CQA: critical quality attribute

Cys (or C): cysteine

CZE: capillary zone-electrophoresis

DAD: diode array detector

DFC: dual flow chromatography

DHFR: dihydrofolate reductase

DLS: dynamic light scattering

DNA: deoxyribonucleic acid

DoE: design of experiment

dp: particle diameter

DSP: downstream processing

DTE: difficult to express

DTT: dithiothreitol

DWP: deep-well plate

E. coli: Escherichia coli

EDTA: ethylenediaminetetraacetic acid

ELISA: enzyme-linked immunosorbent assay

EMA: European Medicines Agency

EP: European Pharmacopoeia

ePC: experimental peak capacity

ER: endoplasmic reticulum

ERAD: endoplasmic reticulum-associated degradation

ESI: electrospray ionisation

ESI-MS: electrospray ionisation-mass spectrometry

EThcD: electron-transfer/higher-energy collision dissociation

eV: electronvolt

F: flow rate

Fab: antigen-binding fragment

Fc: fragment crystallisable

FDA: Food and Drug Administration

FDR: false discovery rate

FFD: factorial design

FIH: first-in-human

FTICR: Fourier transform ion cyclotron resonance

GalNAc: N-acetylgalactosamine

Gly (or G): glycine

Gly·HCl-2.6: glycine hydrochloride, pH 2.6

GS: glutamine synthetase

GSH: glutathione

H2O2: hydrogen peroxide

HC: heavy chain

HCCF: host cell culture fluid

HCP: host cell protein

HEK-293: Human Embryonic Kidney cells

HILIC: hydrophilic interaction chromatography

His (or H): histidine

HMWS: high-molecular-weight species

HOS: higher-order structure

HPLC: high-performance liquid chromatography

HPSEC: high-performance size-exclusion chromatography

HRMS: high-resolution mass spectrometry

HT SEC: high-throughput size-exclusion chromatography

HT SPR: high-throughput surface plasmon resonance

HT: high-throughput

HTPD: high-throughput process development

HTS: high-throughput screening

ICH: International Council for Harmonisation of Technical Requirements for Pharmaceuticals for Human Use

ID x L: internal diameter x length

ID: internal diameter

IEX: ion-exchange chromatography

Ig: immunoglobulin

IND: Investigational new drug

KCl: potassium chloride

kV: kilovolt

LC: light chain

LC-FLR-MS: liquid chromatography-fluorescence-mass spectrometry

LC-MS/MS: liquid chromatography-tandem mass spectrometry

LC-MS: liquid chromatography-mass spectrometry

LDPE: low-density polyethylene

LDR: linear dynamic range

LMWS: low-molecular-weight species

LOD: limit of detection

LOQ: limit of quantification

LT: low-throughput

m/z: mass to charge ratio

M: molar

mAb: monoclonal antibody

MALDI: matrix-assisted laser desorption ionisation

MAM: multi-attribute method

MBR: microbioreactor

mD LC: multi-dimensional liquid chromatography

MES: 2-(N-morpholino)ethanesulfonic acid

MESD: main effects screening design

Met (or M): methionine

min: minute(s)

mL: millilitre

mm: millimetre

mM: millimolar

MRM: multiple reaction monitoring

mRNA: messenger ribonucleic acid

MS/MS: tandem mass spectrometry

MS: mass spectrometry

msAb: multi-specific antibody

MSX: methionine sulfoximine

MTX: methotrexate

MVA: multi-variate analysis

MWD: multi-wavelength detector

-N(C2H5)2: secondary amine group

-N(CH3)3: quaternary amine group

Na_3PO_4: sodium phosphate

NaCl: sodium chloride

NBE: new biological entity

NEM: N-ethylmaleimide

NGA: next-generation antibody

NGNA: N-glycolylneuraminic acid

nm: nanometer

np: non-porous

NPLC: normal phase chromatography

NRPM: non-reduced peptide mapping

NS0/1: Mouse Myeloma cells

NTA: nanoparticle tracking analysis

OD: outside diameter

-OH: hydroxyl group

PAT: Process Analytical Technology

PEEK: polyetheretherketone

PerC6: Human Embryonic Retina-derived cells

PES: polyethersulfone

pI: isoelectric point

PK: pharmacokinetics

PL: protein load

pM: picomolar

PNGaseF: Peptide -N-glycosidase F

PO_4^{3-}: phosphate

PPL: proportional protein load

PQ: product quality

PQA: product quality attribute

Pro (or P): proline

PS/DVB: poly(styrene-divinylbenzene)

PTM: post-translational modification

QbD: quality by design

QC: quality control

QqQ: triple quadrupole mass spectrometer

QTPP: quality target product profile

R&D: Research and development

R^2: coefficient of determination

rDNA: recombinant DNA

RM: reference material

RMSE: root mean square error

RNA: ribonucleic acid

RPLC: reverse-phase liquid chromatography

RPM: reduced peptide mapping

rpm: revolution per minute

RS: reference standard

Rs: resolution

RSM: response surface methodology

S/N ratio: signal-to-noise ratio

s: second(s)

SARS-Cov-2: Coronavirus 2

SAX: strong anion exchange

scFv: single-chain variable fragment

SCX: strong cation exchange

SDS-CGE: sodium dodecyl sulphate capillary gel electrophoresis

SEC: size-exclusion chromatography

Ser (or S): serine

SiA: sialic acid

siRNA: small interfering RNA

-SO3H: sulfonic group

SO_4^{2-}: sulphate

SOP: standard operating procedure

SPE: solid-phase extraction

SPR: surface plasma resonance

SRP: signal recognition particle

SST: system suitability

Std Error: standard error

Thr (or T): threonine

TOF: time-of-flight

TR-FRET: time-resolved-fluorescence resonance energy transfer technology

Ts: tailing factor (or symmetry)

U/LLOD: upper/lower limit of detection

U/LLOQ: upper/lower limit of quantification

UHPLC: ultra-high pressure liquid chromatography

UHP-SEC: ultra-high-performance size exclusion chromatography

UPR: unfolded protein response

US: United States of America

USP: upstream processing

USPD: upstream process development

UV: ultra-violet

VCD: viable cell density

VH: heavy chain variable domain

VL: light chain variable domain

WAX: weak anion exchange

WCX: weak cation exchange

WP: well pate

XIC: extracted ion chromatogram

ZFN: Zinc Finger Nuclease

α-gal: galactose-α1,3-galactose

Table of Contents

Introduction 1

1.1 Pharmaceutical Biotechnology and Biopharmaceuticals 2

1.1.1 Introduction to Biopharmaceutical Industry 2

1.1.2 Biopharmaceuticals 4

1.1.3 The Biopharmaceutical Market 6

1.2 Cell Culture Technology 8

1.2.1 Expression Systems 8

1.2.2 Mammalian Cell Culture 8

1.2.3 Chinese Hamster Ovary Cells Factories 10

1.3 Insights into CHO-expressed Recombinant Proteins 12

1.3.1 Protein Expression, Folding and Assembly 12

1.3.2 The Structure of Monoclonal Antibodies 13

1.3.3 The Structure of Bispecific Antibodies 14

1.3.4 Quality Attributes of mAbs and BsAbs 16

1.4 The Biopharmaceuticals Research and Development: An Analytics-Driven Process 25

1.4.1 Overview 25

1.4.2 CHO Cell Line Development and Engineering 27

1.4.3 Upstream and Downstream Process Development and Optimisation 29

1.4.4 Quality Analysis in Biopharmaceuticals Process Development 30

1.5 High-Throughput Process Development Technology 31

1.5.1 Background 31

1.5.2 What Makes a Technology High-Throughput? 32

1.5.3 High-Throughput Technologies for Upstream Development 34

1.5.4 High-Throughput Technologies for Downstream Process Development 35

1.6 Advanced Analytical Methodologies for Biopharmaceuticals Analysis and their Application to High-Throughput Process Development 37

1.6.1 Bioassays and High-Throughput Quantitation of Expression Titre and Residuals 38

1.6.2 High-Throughput Analysis of Glycosylation 39

1.6.3 High-Throughput Analysis of Charge-Variants 42

1.6.4 High-Throughput Analysis of Size Variants 46

1.6.5 High-Throughput Mass Spectrometry-based Methods 47

1.6.6 Challenges in High-Throughput Analysis of Biopharmaceuticals 49

1.7 Theoretical framework: Aim of Thesis and Overview 52

Materials and Methods 56

2.1 Liquid Chromatography-Mass Spectrometry Materials and Equipment..... 57

2.1.1 Chemicals and Materials 57

2.1.2 LC Equipment 57

2.1.3 Software for Method Development and Data Analysis 58

2.1.4 Methods 59

2.1.5 Samples used for Method Development, as Controls and System Suitability Checks 64

2.2 Purification of CHO Cell Culture..... 65

2.2.1 Chemicals 65

2.2.2 Low-Throughput Purification..... 65

2.2.3 High-Throughput Purification 65

2.3 CHO Cell Culture 66

2.3.1 Cell Lines and Model Molecules 66

2.3.2 Cell Culture Maintenance..... 66

2.3.3 Cryopreservation, Cell Bank Generation and Revival..... 67

2.3.4 Shake-Flasks Fed-Batch Overgrows of CHO Cells..... 67

2.3.5 Harvesting 68
2.4 Recombinant Protein Quantification 68
2.4.1 Titre Analysis by Analytical Protein-A Affinity Chromatography 68
2.4.2 UV/Vis Absorption Spectroscopy 68
2.5 Equations 69
2.5.1 Chromatography Peak Analysis 69
2.5.2 Method Assessment 69
2.6 Statistics 71
2.6.1 Actual-by-Predicted Plot 71
2.6.2 Effect Summary Report 71
2.6.3 Parameter Estimates Table 72
2.6.4 Prediction Profiler 72
2.6.5 Desirability Function 72
Part A: High-throughput platform workflow for the purification and aggregation analysis of mAbs and BsAbs 75
3.1 Abstract 75
3.2 Introduction 76
3.3 Results and Discussions 78
3.3.1 A Fully Automated Platform Method for Small Scale Purification mAbs and BsAbs by PhyTip Columns 78
3.3.2 Fast and Sensitive Aggregation Analysis by Size-Exclusion Chromatography 93
3.3.3 Proof-of-Concept Application of the HTSEC Method 107
Part B: DoE-Assisted Method Development for the Analysis of mAb Charge Variants by Cation Exchange Chromatography 110
3.4 Abstract 110

3.5 Introduction 111

3.5.1 DoE1: 4X2 Factorial Design 112

3.5.2 DoE2: Box-Behnken Design 116

3.5.3 Model Verification and Method Assessment 119

3.6 Conclusions 121

Integrating aggregation and charge variants analysis in one single method by heart-cutting 2D SEC-CEX-MS. 124

4.1 Abstract 124

4.2 Introduction 125

4.3 Results and Discussion 129

4.3.1 Heart-cutting 2D SEC-CEX-UV method development, Part A: selection of the ^{1}D SEC conditions for coupling CEX in the ^{2}D 129

4.3.2 Application of the 2D SEC-CEX-UV Method to Support the Analysis of Size and Charge Variants during mAb-1 Accelerated Forced-Degradation and Stability Study 141

4.3.3 Part B: Online hyphenation of heart-cutting SEC-CEX-UV to MS detection 147

4.3.4 SEC-CEX-UV-MS Characterisation of mAb-1 Structural Modifications Resulting from Accelerated Forced Degradation and Stability Study 157

4.4 Conclusions 162

Targeted mass spectrometry for aggregates assessment in a MAM workflow 166

5.1 Abstract 166

5.2 Introduction 167

5.3 Results and Discussions 171

5.3.1 Analytical Discovery of BsAb-1 Quality Attributes 171

5.3.2 Development of the Multi-Attribute Method 178

5.3.3 Development of Automated Sample Preparation 186

5.3.4 MAM Method Assessment 189

5.4 Conclusions 197

Hyphenation of the high-throughput analytical platform to cell engineering 199

6.1 Abstract 199

6.2 Introduction 200

6.3 Results and Discussions 201

6.3.1 Application of the PhyTip-purification/HT SEC workflow to 96-DWPs CHO cell cultures 201

6.3.2 Application of the PhyTip purification/HT SEC/MAM workflow to understand the effect of small molecule-enriched media on the product quality of CHO-expressed bispecific antibodies 206

6.3.3 Understanding the effect of targeted gene expression strategies on CHO-expressed mAbs product quality by the PhyTip-purification/2D SEC-CEX-UV analytical workflow 214

6.4 Conclusions 219

Concluding Remarks and Future Work 223

7.1 One-dimensional chromatography methods for flexible high-throughput purification and characterisation of mAbs and BsAbs 224

7.2 Multiple Attribute Analysis of Therapeutic Proteins using LC-MS methods. 227

7.3 Future Work 229

7.4 Considerations on the implementation of the High-Throughput Analytical Platform in Industry 231

Bibliography 234

Appendix A 287

Appendix B 307

Appendix C.....333

Appendix D.....351

This page is intentionally left blank

Chapter 1

Introduction

This study focuses on the development of high-throughput (HT) analytical solutions for characterising the quality attributes of recombinant therapeutic proteins expressed in small-scale CHO cells cultures. This research seeks the establishment of a feedback loop system between analysis and cell engineering to support cell line development for biopharmaceuticals production, aiming to identify and understand the variables that impact the quality profile of CHO cell-expressed recombinant proteins. The following introductory chapter provides an overview of the biopharmaceuticals development process in industry highlighting the challenges to overcome for fulfilling the regulatory requirements to launch new products to market. Subsequently, the state-of-the-art HT technologies used for process development will be discussed with particular emphasis on the HT analytical methodologies currently applied in early biopharmaceutical development. The need for analytical tools that can combine ease of operation, rapid analysis, and accuracy in an analytical Quality-by-Design (QbD) framework is presented. Finally, the chapter comes full circle to outline how more efficient analytical methods could lead to effective innovations for advanced bioprocess control.

1.1 Pharmaceutical Biotechnology and Biopharmaceuticals

1.1.1 Introduction to Biopharmaceutical Industry

Biotechnological manufacturing of pharmaceutical products implies the use of living systems, such as bacteria, yeasts, plants, and animals or parts of thereof for the development of products that can be used for medicinal, prophylactic or diagnostic purposes. Biological sources have long been exploited in medicine and there are many examples supporting the relevance of this practice. Amongst the best known of them are, the introduction of vaccination by Edward Jenner against smallpox from cowpox (*variolae vaccinae*, 1796); later adopted by Louis Pasteur for the first attenuated bacteria-based vaccines against anthrax and chicken cholera (the 1800s); the extraction of insulin from animal pancreas by Frederick Banting and J.J.R. Macleod (Nobel Prize, 1923); the serendipitous discovery of penicillin from colonies of Staphylococcus by Alexander Fleming (Nobel Prize, 1945 with Howard Florey and Ernst Boris Chain) along with its mass production achieved thanks to the chemical engineer Margaret Hutchinson Rosseau, who developed the first deep-tank fermentation plant, granting large-scale supply of pharmaceutical-grade penicillin during the Second World War.

Besides all the great advancements being made in the pharmaceutical industry and technology, all these drugs were still directly extracted from native biological sources. It was only during the post-World War II era that the pioneers of molecular biology brought forward novel notions on deoxyribonucleic acid (DNA) gene expression and cellular process control. Paul Berg's first paper on recombinant DNA technology (rDNA) in living organisms (Paul Berg, Nobel Prize,1980) paved the way for Stanley Cohen and Herbert Boyer to perform cellular and genetic engineering laying the foundations of modern biotechnology and its application to the discovery and production of medicinal products.

The first recombinant therapeutic protein, *insulin*, was introduced as biopharmaceutical in 1982 under the trade name *Humulin* by Genentech and Eli Lilly (Quianzon and Cheikh, 2012; Walsh, 2013). This was followed by *Proleukin* (aldesleukin – IL-2-like protein), and *Zenapax* (daclizumab – a humanised monoclonal antibody) in the 1990s. The first therapeutic mAb, muromonab-CD3 (Orthoclone OKT3), was approved by the US FDA in 1986 and comprised a murine mAb targeting T cell-expressed CD3 for the treatment of acute transplant rejection (Lu et al. 2020; Ecker et al. 2015). In 2003, the first fully human antibody

Humira (adalimumab) was approved by the US Food and Drug Administration (FDA) for the treatment of Crohn's disease, ulcerative colitis, psoriasis and other autoimmune disorders (Brekke and Sandlie 2003). Novel biotechnological techniques achieved the production of proteins, peptides and genetic materials at higher quality and quantity than direct extraction from native biological sources (Ho and Gibaldi, 2013). Moreover, bioprocess engineering technologies improved product functionality, productivity and structural characteristics extending the application of these medications for the treatment of unmet needs (Shukla and Thömmes, 2010). Along this line, bispecific antibodies (BsAbs) and fusion proteins are biopharmaceuticals specifically engineered to optimise the bioactivity, immunogenicity and pharmacokinetics (PK) of medicinal products (Walsh, 2014; Czajkowsky et al., 2012). Moreover, research and development (R&D) of nucleic acid-based products, such as antisense oligonucleotides (ASO), gene therapies and gene-engineered cells have also increased over the last years. As a result of scientific advancements, the last few decades have seen the field of drug development move its focus from conventional chemically synthesised small-molecules to cell-expressed large-molecule biopharmaceuticals. Hundreds of start-up biopharmaceutical companies were founded in the late 20th century, notably in the USA and Europe. Many other firms then diversified into this area or formed strategic alliances. Amgen, Biogen and Genentech represent the three pioneering biopharmaceutical companies that are still competitive in the business (Walsh, 2014; Zhang and Liu, 2020; Crunkhorn, 2014; Yip, 2019; Estes, Melville, and Chinese, 2014). The biopharmaceutical industry has continued to flourish into the 21st century, expanding to Asia and South America (K. Zhang and Liu, 2020; Alzahrani, 2020; Rezaie et al., 2012; Pimenta and Monteiro, 2019). However, several challenges remain in the production of biopharmaceuticals which are more costly and more difficult to manufacture than conventional drugs (Rader 2008; Walsh, 2013; Kesik-brodacka, 2018; Kaplon et al., 2020). An in-depth review of the current issues in biopharmaceuticals development will be discussed in this chapter.

1.1.2 Biopharmaceuticals

Biopharmaceuticals include therapeutics, vaccines and biological diagnostic agents which have revolutionised the last century's diagnosis, prevention, and treatment of human diseases, particularly cancer, respiratory, inflammatory and autoimmune diseases (Crunkhorn, 2014; Walsh, 2018; Craik, Fairlie, Liras, and Price, 2013; Lonardo and Baldelli, 2020). In comparison to conventional small molecule pharmaceutical drugs, biopharmaceuticals demonstrated an extraordinary specificity and activity, resulting in more targeted mechanisms of action with fewer off-target effects extending the horizons towards the treatment of severe life-threatening diseases (Kesik-brodacka, 2018; Crunkhorn, 2014).

The term 'biopharmaceuticals' first appeared in the 1980s and refers to pharmaceuticals manufactured using biotechnological techniques (Walsh, 2013; Rader, 2008; Kesik-brodacka, 2018). They are part of the broad category of biologics comprising products that are inherently biological thus, composed of sugars, proteins, nucleic acids, complex combinations of these substances or living entities such as cells or tissues (Rader, 2008; Walsh, 2013). Along with biopharmaceuticals, biologics include tissue-, gene- and cell-therapy agents also referred to as advanced therapy medicinal products (ATMPs) (Ham et al., 2018). Whilst biologics may be isolated from natural sources (humans, animals, plants and microorganisms), biopharmaceuticals are exclusively produced by genetic engineering of living systems such as cells, often employing cloning, tissue culture as well as other cutting-edge biotechnology tools used to cut, insert, link, and recombine DNA fragments to gain useful therapeutic products. The majority of them are created via recombinant DNA technology (Khan et al., 2016) involving the insertion of DNA molecules from different species into a host organism aiming to produce new genetic combinations. The development of genetic engineering and cloning technology has opened many possibilities for expressing and isolating recombinant proteins for medicinal use. Cell engineering has so far been the most proficient technology for producing recombinant proteins. Another technology worth acknowledgement relies on the use of transgenic animals. The anticoagulant agent ATryn® (rEVO Biologics, Ltd.) expressed in transgenic goat's milk, is an example of a transgenic animal-derived medicine that was granted regulatory approval by both EMA (2006) and FDA (2009) and is currently available on the market. Nevertheless, the biopharma industry has been slow to embrace this platform favouring cell engineering tools that prove more promising in gaining productivity and compliance to process technologies (Scott and Melville, 2014).

To date, protein-based biopharmaceuticals lead the market with monoclonal antibodies (mAbs) representing the largest class (Walsh, 2018; Kaplon et al., 2020). Other types include hormones, growth factors, cytokines, blood factors, enzymes, vaccines and anti-coagulant agents (Aggarwal, 2014). Further advancements in protein engineering led to the development of next-generation biopharmaceuticals. To name a few, fusion proteins, antibody fragments such as antigen-binding fragments (Fab) or single-chain variable fragments (scFvs), antibody-drug conjugates (ADC) and multi-specific antibodies (msAbs) are examples of the recent innovations in antibody formats (Evans and Syed, 2014). Moreover, the last decade's R&D breakthroughs have led to a rise in the number of nucleic acid-based biopharmaceuticals on the market. These include antisense RNA and DNA, small interfering RNA (siRNA), ribozymes and aptamers used to selectively target disease-causing genes (Mergener, 2021). Notably, the COVID-19 outbreak caused by severe acute respiratory syndrome Coronavirus 2 (SARS-CoV-2) has demonstrated the effectiveness of cutting edge biotechnological tools in delivering rapid and adaptable vaccination strategies on a global scale in only 9 months from the start of the pandemic (Pichon and Perche, 2021). This laid the foundation for new research and business strategies with mRNA vaccines being at the centre of scientific interest (Philippidis, 2021).

Despite the success of biopharmaceuticals advancements, the COVID-19 pandemic has also highlighted the scientific gaps and demands of the industry concerning the technology, production, and distribution of its products (Stoll et al., 2021; Balcerek, Bednarek, and Sobie, 2021; Sarkis et al., 2021; Ibrahim et al., 2021). Indeed, biopharmaceuticals are inherently complex; their large size, structural heterogeneity, and post-translational and chemical modifications pose a safety risk that must be monitored at all stages of development (Garripelli, Wu, and Gupta, 2020). High-expressing industrial cell lines that are stable throughout multiple cell generations along with production processes that guarantee the delivery of the final product with consistency are essential for regulatory approval (Balcerek, Bednarek, and Sobie, 2021). Moreover, due to the complexity of their structure, biopharmaceuticals are prone to degradation events and require specialised services for their supply chain such as low-temperature storage (Ibrahim et al., 2021). This adds to the costs of process development which is particularly high compared to conventional pharmaceutical drugs (Silva, Eppink, and Ottens, 2021).

The introduction of next-generation biomolecules posed further industrial challenges (Rader, 2008; Walsh, 2013; Kesik-brodacka, 2018; Kaplon et al., 2020). This is due to a number of

reasons. Firstly, the engineered molecules can be more "difficult-to-express" (DTE) than natural ones due to the lack of cellular competency resulting in low expression titres (Johari et al., 2015). Secondly, the need for a more complex structure and post-translational processing may lead to further quality burdens that can be missed during the discovery process (Jarasch et al., 2015). Finally, insufficient process knowledge for producing (expressing, purifying and analysing) these new molecular entities results in a deceleration of the timelines and an increase in the costs for process development (Silva, Eppink, and Ottens, 2021).

This landscape explains why the biopharmaceutical industry has strategically continued investing in quick and cost-effective HT technologies as a means of leveraging process development along with creating a diversified product portfolio to rapidly launch new products to market.

1.1.3 The Biopharmaceutical Market

The biopharmaceutical industry is a growing multi-billion-dollar business totalling $230 billion in 2020 and is projected to reach $345 billion by 2026 (Biopharmaceutical Market). Global market sales have continued rising since the approval of Humulin, totalling $140 billion in 2013, $228 billion in 2016 (Moorkens et al., 2017), and $186 billion in 2017 (Rathore and Bhargava, 2020). Market statistics show that mAbs are both the most profitable and most rapidly growing class of biopharmaceuticals (Newswire, 2016; Walsh, 2010; Kesik-brodacka, 2018; Rathore and Bhargava, 2020; Kaplon et al., 2020; Yip, 2019) with sales expected to continue rising over the next several years (Ecker, Jones and Levine, 2015; Jiang et al., 2019; Zeitlin, 2021). During 2010-2019, more than 50 mAbs were approved in the EU and US market encompassing over half (53%) of all first-time approvals (Walsh, 2018; Kaplon et al., 2020). During the COVID-19 pandemic, the biopharmaceutical industry has thrived on vaccines as well as next-generation biopharmaceuticals, and gene therapies (Sedykh et al., 2018; Philippidis, 2021). New drug candidates were proposed for the treatment of the COVID-19 symptoms and are expected to join the market in the upcoming months (Philippidis, 2021).

Nevertheless, the high costs associated with biopharmaceuticals R&D represent the major challenge for biopharmaceutical companies (Thakor et al., 2017; Kesik-brodacka, 2018; Silva, Eppink, and Ottens, 2021). Indeed, cost-effectiveness and time-to-market along with

therapeutic efficiency, patient safety, and product quality (PQ) are the key aspects that govern production and sales. Therefore, it is of paramount importance for the biopharmaceutical industry to attain a product development workstream that fulfils these criteria. Not surprisingly, one of today's main focus areas of the business is the integration of high-throughput process development (HTPD) technologies to accelerate biopharmaceutical drug development (Silva, Eppink, and Ottens, 2021). Further insights into the state-of-the-art biopharmaceutical HTPD tools are discussed in Section 1.5 of this Chapter.

1.2 Cell Culture Technology

1.2.1 Expression Systems

The expression machinery of living cells can be manipulated and harnessed to produce biopharmaceuticals. This implies the use of cell culture procedures to isolate the cells from their native substrate and subsequently grow them in an artificial environment under controlled conditions. A specific cell type can be genetically engineered to express the product of interest as part of its gene expression machinery hence, called the "host cell system". Recombinant systems are constructed by introducing a gene coding for the protein of interest into a well-characterised strain of the producer cell line (Cox Gad, 2007; Hu et al., 2012; Hu, 2020).

The selection of the appropriate host cell type is a fundamental step in biopharmaceutical production. Many factors influence the choice of the host and are mostly related to the physicochemical properties of the molecule to be expressed, costs of goods, time required to express a certain amount of protein and maximum yield achievable. A plethora of expression systems has been exploited and implemented for the production of biopharmaceuticals, including bacteria, yeast, insects, plant and mammals (Walsh, 2004; Hu et al., 2012; Kesik-brodacka, 2018). Amongst them, mammalian cells are the preferred and most utilised host for producing complex protein-based biopharmaceuticals, such as mAbs (Walsh, 2004; Hu et al., 2012; Kiss and Gottschalk, 2018).

As highlighted in the "Biopharmaceutical benchmarks" series by Walsh, mammalian cell culture, and particularly CHO expression systems, currently support the production of both the vast majority and best-selling drugs (Walsh, 2010, Walsh, 2014, Walsh, 2018). More details on the characteristics of this successful host cell type are discussed in Section 1.2.2.

1.2.2 Mammalian Cell Culture

Mammalian cells are the most used cell type for biopharmaceutical production owing to the capability of their cellular machinery of folding and assembling complex polypeptide chains as well as performing post-translational modifications (PTMs) similarly to endogenous human proteins (Walsh, 2004; Hu et al., 2012; Kiss and Gottschalk, 2018). These features are fundamental for the safety and efficacy of the final therapeutic product and explain why

they are often the cell type of choice despite being more complex, time-consuming and costly than other prokaryotic and eukaryotic cell culture processes. Moreover, mammalian cells are high yielding and easily scalable. In this context, technology advancements have contributed to boosting titres from 0.1 g/L to 10 g/L to meet the demand of the clinical supply (Kiss and Gottschalk, 2018; Kesik-brodacka, 2018; Hu, 2020).

Currently, a great array of mammalian cell lines is available for recombinant protein production. Historically, rodent-derived cell lines such as Chinese Hamster Ovary (CHO) cells, Mouse Myeloma cells (NS0/1), Mouse Fibroblast cells, and Baby Hamster Kidney cells (BHK) are the most common mammalian cells. These hosts express proteins with human-like PTMs but can also produce non-human structural modifications which can impact drug safety. As an example, galactose-α1,3-galactose (α-gal) and N-glycolylneuraminic acid (NGNA) are N-glycans expressed in mice but not in humans and are associated with immunogenicity and bioactivity, protein stability and *in vivo* clearance (Dumont et al., 2015; Kiss and Gottschalk, 2018). This can yield dangerous off-target effects, for instance, patients treated with Erbitux® (cetuximab, Merck Group & Eli Lilly), the antineoplastic agent expressed in SP2/0 cells, underwent anaphylaxis shock due to pre-existing IgE antibodies directed against α-1,3-gal residues (Chung et al., 2008; Estes, Melville, and Chinese, 2014).

On the other hand, human-derived hosts can perform fully human optimised PTM profiles (Dumont et al., 2015; Kiss and Gottschalk, 2018; Havenga, Holterman, and Melis, 2008; Swiech, Picanço-Castro, and Tadeu, 2012; Blanchard et al., 2011). Amongst these, Human Embryonic Kidney cells (HEK-293), Human Fibrosarcoma cells (HT-1080), Human Amniocentesis (CAP-T) cells, and Human Embryonic Retina-derived (PerC6) cells have been adopted for the production of biopharmaceuticals (Dumont et al., 2015; Kiss and Gottschalk, 2018; Swiech, Picanço-castro, and Tadeu, 2012; Walsh, 2014). Nevertheless, the analytical characterisation of proteins expressed in human cells showed different quality profiles than the endogenous human proteins (Scott and Melville, 2014). To date, there is no clear evidence demonstrating that recombinant proteins expressed in human cells are safer than those produced in mouse-derived cells.

Most of the presently licensed biopharmaceuticals are produced in non-human mammalian expression systems. CHO cells are the preferred industry-standard expression platform, accounting for more than 70% of the approved therapeutic proteins (Birch and Racher, 2006;

Jayapal et al., 2007; Omasa et al., 2010; Walsh, 2010; Zhu, 2012; Walsh 2014). More details on the characteristics and the success of this host are given in Section 1.2.3.

1.2.3 Chinese Hamster Ovary Cells Factories

Originally isolated from an adult Chinese Hamster's ovary biopsy *(Lat. Cricetulus griseus*) by Puck in 1985 (Tjio and Puck, 1958), CHO cells have become the favoured host for biopharmaceutical production (Kuo et al., 2018 Walsh, 2014; Dumont et al., 2015; Kiss and Gottschalk, 2018). The success of this host has been extensively reviewed in the literature and relies on a number of reasons. Owing to its mammalian origin, CHO expression machinery can efficiently fold and assemble complex, multi-chain and multi-domain proteins with human-like PTMs (Walsh, 2004; Hu et al., 2012; Kiss and Gottschalk, 2018). Regulatory approval is eased by the comprehensive industry process expertise and well-documented safety profile built over the years (Walsh 2014; Kesik-brodacka, 2018; Zhang, 2010; Kiss and Gottschalk, 2018). Furthermore, CHO genetic instability has cleverly been exploited for the isolation of clonal cell lines with functional characteristics that fulfil the industrial requirements (Davies et al., 2013). Amongst them, adaptation to growing at high densities in both suspension and serum-free media, ease of transfection, powerful gene amplification system, and low susceptibility to human viral infection ensured high productivity in both transient (>2 g/L) (Daramola et al., 2013) and stable industrial cell lines (>10 g/L) (Huang et al., 2010; Costa et al., 2010; Wurm, 2004). These beneficial attributes increase the confidence that two key industry requirements will be met, namely, the production of high titre biopharmaceuticals and desired structural attributes (Budge et al., 2020; Fischer, Handrick, and Otte 2015; Hernandez, 2015; Kiss and Gottschalk, 2018). To date, a variety of CHO cell lineages have been developed, including CHO-DG44, DUKX-B11 isolated at Columbia University (Urlaub and Chasin, 1980), CHO-S, CHO-K1, and its derivative CHOK1SV (developed by Lonza) (Fischer, Handrick, and Otte, 2015; Scott and Melville, 2014; J. Zhang, 2010; Kiss and Gottschalk, 2018). These cell lines have been adapted and optimised for satisfying the requirements of biopharmaceuticals production so that today's biopharmaceutical companies own proprietary CHO cell lines. In this context, cell line stability, productivity and quality have been the major focus of CHO CLD and engineering (CLD&E) (reviewed by Hong et al., 2018).

Despite the advantages, CHO cells are neither naturally perfect nor their cellular mechanism has completely been explored and well-understood yet. Furthermore, the same genetic and epigenetic instability that facilitates engineering manipulation may also lead to a discrepancy in growth, metabolism, biosynthesis and post-translational processing. This is due to the unpredictable phenotypic variations arising from the genome restructuring during continuous subculture. Moreover, enhanced cellular stress can cause low cell growth, low productivity and induction of protein aggregation (Yuk et al., 2015; Graham, Bhatia, and Yoon, 2019; Chung et al., 2019; Das et al., 2020; Hong et al., 2020).

Despite cell engineering advancements have substantially improved product yield, uncharacterised cellular processes and gene regulatory mechanisms still hamper PQ (Kuo et al., 2018). Therefore, both clone selection and cell line development (CLD) can be time-consuming and labour intensive (Davies et al., 2013). Fundamentally, a better understanding of the scientific and engineering principles involved in CHO cells manufacturing, and the identification of the variables that affect PQ are needed to gain control of their cellular expression machinery. This could result in a substantial reduction in costs and timeline for the launching of novel life-saving medicines to market and their bioprocessing.

Another aspect to take into consideration is that culturing of CHO cells remains more expensive and slower than prokaryotic and eukaryotic expression systems, such as bacteria and yeast (Jiang et al., 2019). This is mainly because animal-derived cells have a low proliferation rate, require complex media, refined feed and stringent sterility protocols due to their vulnerability to contamination (Jiang et al., 2019; Fischer, Handrick, and Otte, 2015).

All these factors contribute to the overall flare of process costs and timelines, which remain the major burden of the market and hamper the access of medicines worldwide (Jiang et al., 2019). In recent years, the implementation of HTPD methodologies has leveraged CHO CLD with a substantial reduction in time and costs associated with conducting the large screening experimentation required in upstream process development (USPD). Detailed information on the state-of-the-art HTPD tools used in USPD is given in Section 1.5.3.

1.3 Insights into CHO-expressed Recombinant Proteins

1.3.1 Protein Expression, Folding and Assembly

The mammalian cells expression of correctly folded proteins at high titres requires adequate degrees of transcription and post-transcriptional steps such as messenger ribonucleic acid (mRNA) translation, polypeptide translocation, folding, assembly and addition of PTMs. After a protein is translated, the N-terminal signal peptide of the unfolded polypeptide chain forms a complex with the signal recognition particle (SRP) and enters the endoplasmic reticulum (ER). Here, the signal peptidase cleaves the signal peptide and the polypeptide chain undergoes folding and assembly. The rough ER is primarily responsible for protein folding, the addition of high mannose core oligosaccharides to the N-glycosylation site, trimming of terminal glucose and mannose residues from initial glycan, and formation of disulphide bonds (Hu et al., 2012). Next, the nascent protein progresses through the Golgi apparatus where it receives the addition of PTMs such as glycoform modifications, peptide proteolytic cleavage, γ-carboxylation of glutamic acid and β-hydroxylation of aspartic acid (Hu et al., 2012). Finally, at the completion of its three-dimensional structure, the newly synthesised protein is secreted into the cell culture media. These steps are dependent on the recombinant protein characteristics and constraints in their mechanisms may be the cause of aggregation and low productivity (Pybus et al., 2014; Johari et al., 2015; Kiss and Gottschalk, 2018).

The ER and Golgi apparatus constitute the control system for protein folding and assembly. A variety of stress events may perturb the ER homeostasis exceeding its capacity for protein folding. The resulting misfolded and unfolded proteins accumulated in the ER are either sent back through the folding cycle or tagged for degradation via the ER-associated degradation (ERAD) pathway. An excessive cargo of unfolded proteins can lead to the activation of the unfolded protein response (UPR) and upregulation of degradative enzymes (Chakrabarti, Chen, and Varner, 2011). In this context, it is important to notice that ER stress contributes to low productivity, cell death, misfolding, and aggregation. Hence, research efforts have been focused on studying and understanding the UPR mechanism (Du et al., 2013; Kober, Zehe, and Bode, 2012) and unravel the enigma behind DTE proteins (Le Fourn et al., 2014; Pybus et al., 2014; Johari et al., 2015).

1.3.2 The Structure of Monoclonal Antibodies

Gerald Edelman and Rodney Porter were the first to discover the distinctive Y-shaped molecular structure of antibodies (Edelman and Porter, Nobel Prize, 1972). Unlike endogenous antibodies, mAbs originate from a single B-cell clone and show binding specificity to one single epitope (Bakhtiar, 2012; Frye et al., 2016; Ko et al., 2018; Sedykh et al., 2018). Although this class of therapeutics includes IgA, IgD, IgE, IgG, and IgM, most of marketed mAbs are IgG – precisely human/humanised IgG1, to some extent IgG2, and IgG4 (Bakhtiar, 2012; Beck, Sanglier-Cianférani, and Van Dorsselaer, 2012; Higel et al., 2016; Walsh, 2018). The schematic representation of a mAb structure is depicted in Figure 1.1.

MAbs bear a large and complex chemical structure resulting in 146-160 kDa mass range organised into four polypeptide chains – two heavy chains (HC, ~50 kDa each) and two light chains (LC, ~25 kDa each). These are held together by 2-4 interchain disulphide bonds in the so-called "hinge region", giving the mAb its characteristic Y-shape (Lakbub, Shipman, and Desaire, 2018). One additional interchain disulphide bond connects the fifth cysteine (Cys) residue of each HC with the last Cys of each LC. Furthermore, the IgG polypeptide chains are organised in 6 globular domains joined together by 12 intrachain disulphide bonds (Liu and May, 2012; Lakbub, Shipman, and Desaire, 2018; Beck, Sanglier-Cianférani, and Van Dorsselaer, 2012). The variable regions of the HC and LC are located at the N-termini and bear the complementarity-determining regions (CDRs) that provide the specificity for antigen-binding site (Bhat and Rao, 2020; Beck, Sanglier-Cianférani, and Van Dorsselaer, 2012; Lakbub, Shipman, and Desaire, 2018; Sjögren, Olsson, and Beck, 2016).

According to the functional characteristics of the IgG domains, three main regions can be distinguished in two Fabs, and one fragment crystallisable (Fc). The Fab is composed of the CDRs, variable regions, and the first domain of the HC (CH1) and is responsible for antigen-binding specificity. The Fc region is composed of CH2 and CH3 of both heavy chains and binds the cell surface receptors activating the complement system (Bhat and Rao, 2020; Beck, Sanglier-Cianférani, and Van Dorsselaer, 2012; Lakbub, Shipman, and Desaire, 2018; Sjörgen, Olsson, 2016). The large size of mAbs and their complex cellular mechanism of expression lead to a vast physicochemical and structural heterogeneity (Higel et al., 2016; Bakhtiar, 2012; Zhang, Cui, and Gross, 2014; B. Zhang et al., 2016; Brunner et al., 2017; Reusch and Tejada, 2015).

Detailed information on the most common mAb quality attributes including PTMs as well as chemical modifications resulting from degradation events will be examined in Section 1.3.4.

1.3.3 The Structure of Bispecific Antibodies

Multi-specific antibodies can bind more than one antigen and belong to a class of therapeutics appointed as "next-generation antibodies" (NGAs) by *Nature Reviews Drug Discovery* journal in 2014 (J. B. Evans and Syed, 2014). Bispecific antibodies (BsAbs) bear two different antigen-binding sites and were proven auspicious for the treatment of cancer, autoimmune diseases and several other conditions due to their multi-target mechanism of action (Sedykh et al., 2018; Reichert, 2019; Krishnamurthy and Jimeno, 2018; Nuñez-Prado et al., 2015). This class of therapeutics encompasses several different species and a variety of formats whose characteristics along with their therapeutic and engineering principles have extensively been reviewed (U. Brinkmann and Kontermann, 2017; Reichert, 2019). BsAbs that are currently available on the market are the antineoplastic agent Blincyto® (bispecific T-cell engager (BiTE) blinatumomab, Amgen/Micromet) and Hemlibra® (full-length IgG-like BsAb emicizumab-kxwh, Chugai/Genentech, a subsidiary of Roche) used against cancer and haemophilia A, respectively.

Despite holding therapeutic promise, the challenges associated with BsAbs developability have hindered their market thrive (Brinkmann and Kontermann, 2017; Reichert, 2019). B. Trout and co-workers have significantly contributed to the determination of protein-based therapeutics developability on the basis of their physicochemical characteristics (Chennamsetty et al. 2009; Lai et al. 2021; Chennamsetty et al. 2010; Courtois et al. 2016; Lauer et al. 2011). Due to the increased molecular complexity, these products are often DTE and show poor stability resulting in high levels of both aggregates and clipped species (Gomez et al., 2020; Manikwar et al., 2020; Phung et al., 2020; C. Wang et al., 2018; Schachner et al., 2016; Cao et al., 2018). As an example, Cao et al. (2018) have reported the formation of head-to-tail dimers of an IgG-scFv fusion BsAb (BsAb-1) molecules as a consequence of cysteinylation and glutathionylation of the Cys residues constituting the engineered disulphide bond in the scFv region.

BsAb-1 is a full length symmetric IgG1-like BsAb with scFv fused in the CH3 domain stabilised by an engineered disulphide bond. Supported by Cao's work, the mechanism and

causes of aggregation of this model molecule will be the subject of study in this research project.

1.3.4 Quality Attributes of mAbs and BsAbs

Biopharmaceuticals are defined by their quality attributes. These attributes depend on the physical, molecular, cellular, immunochemical, microbiological and biological characteristics of the molecule of interest and must be fully characterised during product development. Some of them are considered "critical" to ensure the delivery of a product with the desired quality. Thus, the critical quality attributes (CQAs) must be defined as early as possible and monitored throughout the product development process (ICH, 2009).

Examples of mAbs and BsAbs quality attributes include product appearance, identity, purity, impurities, potency, quantity, etc. Amongst the most common CQAs are PTMs occurring after translation and other non-enzymatic chemical modifications resulting from product degradation events. PTMs are covalent and generally enzymatic modifications occurring as part of protein biosynthesis. Conversely, other covalent and non-covalent chemical modifications may result as a consequence of product degradation events during upstream (USP) and downstream processes (DSP), formulation and storage. Such modifications define the physicochemical properties of the mature proteins hence, its bioactivity, interactions, and in turn, the safety and efficacy of the final product (Deribe, Pawson and Dikic, 2010; Zhao *et al.*, 2010; Martin, 2003; Greer and Shi, 2012; Chirmule and Nair, 2016).

Glycosylation, disulphide bonds scrambling, aggregation, fragmentation, deamidation, oxidation, phosphorylation, methylation, acetylation, and amidation are amongst the most common enzymatic PTMs found in mAbs and known to be influenced by cell engineering strategies (Santos and Lindner, 2017; Duan and Walther, 2015; Reason *et al.*, 2018). However, some of them such as aggregation, fragmentation, oxidation, and deamidation can occur after protein expression, as part of product degradation events (Arosio et al. 2011; Oyetayo et al., 2017; Wecksler et al., 2018; Alam et al., 2020).

Figure 1.1 illustrate the quality attributes occurring in mAbs and their specific sites, whilst Table 1.1 summarises their effect on the bioactivity, safety and efficacy of the final product. The following sections give an overview of the most common PTMs and chemical modifications found in mAbs and BsAbs that may be dependent on upstream process conditions and investigated in this research project.

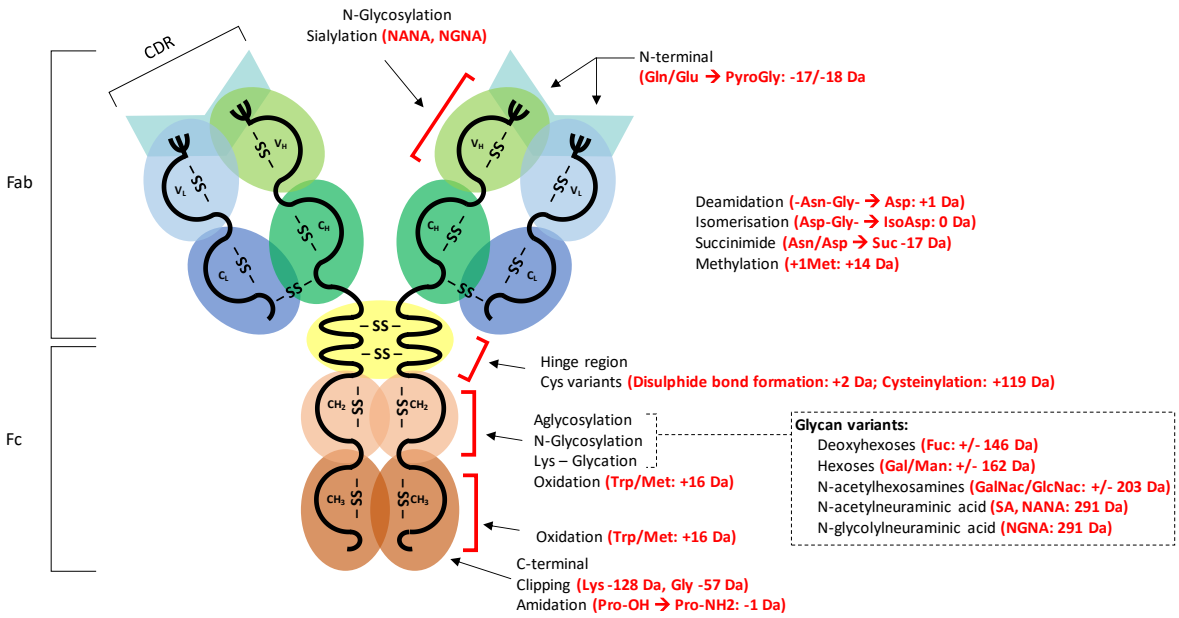

Figure 1.1 IgG1 Molecular Structure with Commonly Occurring Quality Attributes. Schematic of an ordinary IgG1 molecular structure showing the location of the PTMs and chemical modifications that typically occur in CHO-expressed mAbs. The shift in molecular weight caused by each modification is indicated in terms of nominal mass difference as reported at https://www.sigmaaldrich.com/life-science/proteomics/post-translational-analysis/phosphorylation/mass-changes.html.

Table 1.1 Summary of the Most Common mAbs Quality Attributes and their Effect on the Bioactivity, Safety and Efficacy of the Final Product.

Modification	Formation	Quality Effect	Reference
C-terminal clipping of Lys and Gly	Enzymatically-induced incomplete cleavage of the Lys residues. Gly clipping is followed by amidation of the neighbouring Pro.	May affect PK and is indicative of increased cellular stress altering protein expression	(Hu et al., 2017; Liu et al., 2014).
N-terminal pyroGlu	Non-enzymatically-induced cyclisation of the N-terminal Gln or Glu with loss of -NH3.	No substantial effect on efficacy and safety reported	(Leblanc et al., 2017; Liu et al., 2014)
Incomplete glycosylation (such as afucosylated protein species)	Incomplete enzymatic processing of glycoforms	Alteration of PK, protein activity, stability, and efficacy.	(Pereira et al., 2018; Liu et al., 2014; Gaza-bulseco et al., 2008).
Glycosylation	Enzymatic addition of glycan residues, mainly sialic acid, fucose, galactose and mannose.	Affects PK, protein function, activity and stability as well as immunogenicity	(Kuriakose et al., 2016; Liu, 2015; Liu et al., 2014; Grainger and James, 2013; Jefferis, 2012; Zheng et al., 2011; Arnold et al., 2007).
Glycation	Non-enzymatic addition of glycan residues mainly deriving from formulation excipients and usually involving reducing sugars binding Lys amine residues covalently.	Affects PK, protein function, activity and stability as well as immunogenicity	(Leblanc et al., 2016; Liu et al., 2014; Quan et al., 2008)
Deamidation and succinimide formation	Loss of ammonia (-NH3), typically occurring on Asn and Gln residues with subsequent conversion to Asp and Glu, respectively. Deamidation can be induced by both enzymatic and non-enzymatic mechanisms.	Reduced affinity and stability	(Alam et al., 2020; Qiu et al., 2019; Luo et al., 2011; Vlasak et al., 2009).

Aggregation	Various mechanisms, both enzymatic and non-enzymatic, such as cellular stress over secretory pathways resulting in protein unfolding and misfolding, media composition, and process parameters, downstream processing and incorrect storage.	Immunogenic reactions and impairment of patient safety.	(Le Fourn et al., 2014; Chung et al., 2018; Hansen et al., 2017; Ho et al., 2013; Chakrabarti, Chen, and Varner, 2011; Gomez et al., 2012; Jing et al., 2012; Vázquez-Rey and Lang, 2011; Ambrogelly et al., 2018; Albert Jesuran Paul, Handrick et al., 2017).
Disulphide bonds scrambling	Incorrect formation of a covalent bond between free thiols leading to non-native disulphide bonds. Disulphide bond scrambling can be induced enzymatically as well as non-enzymatically promoted by alkaline environments.	Often leading to fragmentation and aggregation resulting in immunogenic reaction, and reduction of the bioactivity.	(Lakbub et al., 2018; Liu and May, 2012; Strand et al., 2013; X. Wang et al., 2011
Oxidation	Loss of electrons mostly occurring on tryptophan and methionine residues but also lysine, cysteine, and histidine residues. Oxidation can be induced by both enzymatic and non-enzymatic mechanisms.	Oxidation of a mAb CDR can reduce the potency of the drug; when occurring on the Fc oxidation can affect the molecule stability and higher-order structure (HOS) with loss of the FcRn binding capacity.	(Xiaojuan Li, Wei Xu, Yi Wang, Jia Zhao, Yan-Hui Liu, Daisy Richardson, Huijuan Li, Mohammed Shameem 2016; Sokolowska et al. 2017; Dion et al. 2018; Zheng et al. 2021)
Isomerisation	Non-enzymatic PTM typically occurring as a consequence of Asn deamidation with consequent formation of isoAsp. When preceded by aromatic residues, Pro is prone to cis/trans isomerisation.	Isomerisation can affect HOS leading to product stability, safety and potency issues.	(Guttman et al. 2020; Vlasak et al. 2009; Z. Zhang, Shah, and Guan 2019).

1.3.4.1 Charge Variants

The cumulative effect of the enzymatic and non-enzymatic processes occurring after protein translation may give rise to protein isoforms with varying surface net charge (Xie et al., 2016; Hu et al., 2017; Leblanc et al., 2017). Acidic species have lower pI values than the main species peak leading to an increase of negative charge. Conversely, basic variants have higher pIs than the main species peak and contribute to extend the positive charge distribution (Fekete, Beck, and Guillarme, 2015; Reusch et al., 2015; Parr, Montacir, and Montacir, 2016; Sissolak et al., 2019). Charge heterogeneity may be indicative of certain modifications that could significantly impact the quality, safety and efficacy of the final product (Rathore, Singh, and Narula, 2016). Hence, monitoring and understanding the principles behind therapeutic protein charge variants are essential throughout all development phases, release testing, and control of manufacturing processes (Sissolak et al., 2019). Table 1.2 lists the most common mAbs and BsAbs PTMs and non-enzymatic chemical modifications associated with alteration of the surface charge distribution.

Table 1.2 List of the PTMs and Product Degradation Events Commonly Known to Cause Charge Heterogeneity in mAbs and BsAbs.

Modification	Charge	Reference
C-terminal clipping of Lys and Gly	Basic	(Hu et al., 2017; Liu et al., 2014).
N-terminal pyroGlu	Basic	(Leblanc et al., 2017; Liu et al., 2014).
Glycosylation	Acidic	(Kuriakose et al., 2016; Liu, 2015; Liu et al., 2014; Grainger and James, 2013; Jefferis, 2012; Zheng et al., 2011; Arnold et al., 2007).
Glycation	Acidic	(Leblanc et al., 2016; Liu et al., 2014; Quan et al., 2008).
Deamidation and succinimide formation	Acidic	(Alam et al., 2020; Qiu et al., 2019; Luo et al., 2011; Vlasak et al., 2009).

1.3.4.2 Glycosylation

Glycosylation refers to the covalent addition of carbohydrate molecules (glycans) to specific sites of the protein surface. Glycans post-translational processing starts in the ER, where a glycan chain is trimmed by the action of various glycosidases. Next, the resultant glycoprotein is transported to the Golgi apparatus for further modifications and release of the diverse glycan structures. Protein glycoprofiles are complex, heterogeneous and their intrinsic chemical characteristics can significantly influence protein solubility, folding,

stability and interactions. Indeed, glycosylation is considered a CQA of mAbs and related products and several studies have demonstrated how glycosylation critically affects serum half-life, immunogenicity and potency (Arnold et al., 2007; Kuriakose, Chirmule, and Nair, 2016; Liu, 2015; Grainger and James, 2013; Jefferis, 2012; Zheng, Bantog, and Bayer, 2011).

Glycan heterogeneity depends on glycans type, structure, site, and occupancy. Most of the glycoproteins expressed in CHO and other mammalian cells bear N- and O-liked glycans. N-glycosylation occurs at the consensus sequence of Asn-X-Ser/Thr (where X is any amino acid except Pro). This site is generally located in the Fc region of mAb molecules, in position Asn297 of the CH2 domain (Figure 1.1). Moreover, it was reported that 20% of mAbs bears a second N-glycosylation site on the VH domain (Qian et al., 2007; Higel et al., 2016). O-linked glycosylation, however, happens via an α-O-glycosidic bond formed between N-acetylgalactosamine (GalNAc) and the hydroxyl group (-OH) of Ser/Thr (Z. Wang, Zhu, and Lu, 2020; Plomp et al., 2015). O-linked glycans are inherently different from N-linked glycans and rare in CHO cells-expressed mAbs (Batra & Rathore, 2016; L. Zhang et al., 2016; Liu, 2015).

The most common glycoforms found in CHO-expressed mAbs are of limited size and involve high mannose, complex and hybrid types – generally, bi-antennary with core-fucosylation and low content of sialic acid (SiA) glycoforms (Higel et al., 2016; Sha et al., 2016; Reusch and Tejada, 2015). Despite CHO cells capability of performing human-like glycosylation, they cannot process certain human types of glycans such as α-2,6-sialylation and α-1,3/4-fucosylation (Lalonde and Durocher, 2017). Furthermore, CHO cells produce glycans that are not present in humans such as NGNA and terminal α-Gal modifications. In this context, non-endogenous glycans are of particular concern for PQ analysis since they can trigger immunogenic responses when injected into humans (Lalonde and Durocher, 2017; Zhang, Luo and Zhang, 2016; Kuriakose, Chirmule, and Nair, 2016).

As a result of the strong evidence in the literature regarding the influence of N-glycosylation on mAbs therapeutic activity and product developability, several engineering strategies focused on improving the efficacy and safety of this class of therapeutics by manipulating their glycosylation profile have been reported (Mimura et al., 2018; Batra and Rathore, 2016; Grainger and James, 2013; Jefferis, 2012). Examples of which include, in-process controls of cell culture parameters such as temperature, pH, and media composition (Graham, Bhatia,

and Yoon, 2019; Gramer et al., 2011) genetic engineering strategies concerning the use of small interfering RNAs (siRNAs) (Chang et al., 2019), gene knockdown/knockout (Chang et al., 2019), small molecule enhancers (Chang et al., 2019), and Zinc Finger Nuclease (ZFN) technology (Malphettes et al., 2010). Glycoengineering approaches have been adopted to produce afucosylated mAbs that can enhance the antibody-dependent cellular cytotoxicity (ADDC) activity and their efficacy and specificity against tumour cells (Pereira et al., 2018). In this context, HT technologies and mathematical modelling have aided the advancement of novel CHO cell engineering strategies and understanding of the principles behind protein glycosylation (Galleguillos et al., 2017; Tejwani et al., 2018; Sha et al., 2016; Grainger and James, 2013).

1.3.4.3 Aggregation

Aggregation is a highly immunogenic protein modification occurring in mAbs and derivatives, thus, classified as a CQA (Ambrogelly et al., 2018; Paul et al., 2017; Williams et al., 2017; Moussa et al., 2016). Multiple mechanisms lie behind the formation of protein aggregates which are often unique to the protein of interest and remain overall not well-understood. For example, cellular stressors over secretory pathways can lead to improper folding or misfolding and ultimately result in the formation of aggregates (Le Fourn et al., 2014; Chung et al., 2018; Hansen et al., 2017; Ho et al., 2013; Chakrabarti, Chen, and Varner, 2011). Aggregation can also be induced by media composition (Luo et al., 2011) and process parameters such as pH, temperature, osmolality, agitation, dissolved oxygen, downstream processing (DSP) and formulation (Gomez et al., 2012; Jing et al., 2012; Vázquez-Rey and Lang, 2011; Ambrogelly et al., 2018; Albert Jesuran Paul, Handrick, et al., 2017).

In addition to the various mechanism of formation, the physicochemical properties of aggregates are diverse and complex. Aggregates can be classified as soluble/insoluble, covalent/non-covalent, reversible/non-reversible, and native/denatured (Cromwell, Hilario, and Jacobson, 2006). Philo (2006) classified aggregates based on their molecular chemistry and size into 1) rapidly reversible non-covalent small oligomers (dimers, trimer, tetramer, etc.); 2) irreversible non-covalent oligomers; 3) covalent oligomers; 4) large aggregates (>10-mer); 5) very large aggregates (diameter ~50 nm to 3000 nm); 6) “snow” referring to generally irreversible visible particles (Philo, 2006).

The complex nature of protein aggregation poses a difficult challenge in biopharmaceutical development. Developability issues concern not only the safety and efficacy of the final product but also the increased time and costs of manufacturing goods. Indeed, aggregates are removed during downstream processing thus, a high percentage of aggregation may result in considerable product waste (Vázquez-Rey and Lang, 2011). Moreover, the molecule is required to be stable in formulation buffer and storage conditions (Basle et al., 2020). To overcome these challenges, bioprocess engineering strategies have been focusing on increase expression titres and purification yield as well as minimising protein aggregation and reducing the costs of goods (Gomez et al., 2019; Jing et al., 2012; Paul et al., 2017; Saunders et al., 2016).

It is for the reasons described above that considerable emphasis is given towards protein characterisation by analytical methods from early-stage process development to help understand and control aggregation. High-throughput technologies are fundamental to efficiently identify aggregation-prone candidates during both discovery and development (Paul et al., 2015; Madadkar et al., 2017; Williams et al., 2017). Recent years have seen a surge of computational approaches and machine learning for studying and predicting protein aggregation propensity in drug discovery and development (Ebo et al., 2020; Chennamsetty et al. 2009; Lai et al. 2021; Chennamsetty et al. 2010; Courtois et al. 2016; Lauer et al. 2011). Key publications in this area are from the group of Bernhardt L. Trout on the development of methods for measuring the developability index of protein-based drug candidates and machine learning algorithms to support developability assessment at the early stages of product development (Chennamsetty et al. 2009; Lai et al. 2021; Chennamsetty et al. 2010; Courtois et al. 2016; Lauer et al. 2011). An overview of the state-of-the-art analytical methodologies employed for the analysis of aggregates is illustrated in Section 1.6.4 of the present chapter.

1.3.4.4 Disulphide Bond Scrambling

Disulphide bonds are PTMs occurring inside the cell as part of protein biosynthesis and involve the formation of covalent bonds between the free thiol (-SH) groups of side-chain Cys residues catalysed by enzymes. Disulphide bonds play a key role in the folding and stability of the protein. Incorrect disulphide bonds formation, reshuffling and Cys modifications can lead to the formation of structural isomers, size variants and aggregates with serious consequences on the biological activity and safety of the final product (Lakbub

et al., 2018; Liu nd May, 2012; Strand et al., 2013; Wang et al., 2011). Disulphide bond mapping in proteins is generally accomplished by bottom-up LC-MS/MS analysis (Lakbub, Shipman, and Desaire, 2018). Further insights on disulphide bond characterisation and Cys modifications is discussed in Chapter 5.

1.4 The Biopharmaceuticals Research and Development: An Analytics-Driven Process

1.4.1 Overview

Biopharmaceutical discovery programs screen for a new biological entity (NBE) with sufficient evidence of biological activity and safety profiles to be selected as novel therapeutic candidates. Following discovery, biopharmaceutical process development involves all the steps necessary to take a therapeutic candidate to market. Once the lead compounds have been identified, *in-vivo* and *in-vitro* testing is conducted for early safety and efficiency assessment. During this stage, the physicochemical and immunochemical properties of the compounds of interest are thoroughly characterised. Analytical testing must be compliant with the ICH quality guidelines detailing the characterisation of the product physicochemical and immunochemical properties, biological activity, purity, identified impurities and contaminants and quantity. The guidelines also require the analysis of both the drug substance and drug product appearance, identity, purity and impurities, potency and quantity. All the analytical methods used for product release must be validated according to the ICH specifications (ICH Q2(R1-2)) and the laboratory procedures must adhere to the current Good Manufacturing Practice (cGMP). Moreover, initial development and optimisation of the upstream and downstream process and investigation of a suitable route of administration are also carried out. This phase is called preclinical development and aims at gathering as much information as possible on the product and the process to support development at later stages and provide preliminary information on dosing and toxicity levels for first-in-human (FIH) studies.

Clinical development begins after the completion and approval of the preclinical data by the regulatory agencies. The process follows the ICH guidelines on Good Clinical Practice and involves three phases where the product is tested on an increasing number of trial subjects and ends with the submission of a dossier to be approved by the regulatory authorities. If the process is successful, the product can be licensed for wider patient use. Finally, pharmacovigilance and post-marketing surveillance activities are carried out for more than a decade from market approval. The average cost of biopharmaceutical process development is estimated to be $2.6 billion (DiMasi, Grabowski, and Hansen, 2016; Mohs and Greig, 2017).

More information on both preclinical and clinical development guidelines can be found at https://www.ich.org/page/search-index-ich-guidelines). Figure 1.2 illustrates a schematic of an NBE development process, while more information can be found at the FDA's website https://www.fda.gov/drugs/cder-small-business-industry-assistance-sbia/new-drug-development-and-review-process.

Several authors have pointed out how the biopharmaceuticals properties significantly depend on the manufacturing method, hence process development is considered an integral part of product development and critical for delivering a new product to market (Lim et al., 2006; Carter, 2011; Dimitrov, 2012; Kesik-brodacka, 2018). In this scenario, analytical technologies are the key enabler for building robust, time- and cost-effective manufacturing processes to ultimately supply affordable medicines that consistently meet regulatory specifications. Process development involves the coordination of many teams across the business that work together on the establishment of a *design space* for product manufacture. Although sometimes challenging, the coordination between these groups is essential for the success of the product (Papathanasiou, Maria M Kontoravdi, 2019; Kiss and Gottschalk, 2018). In this framework, it is not uncommon for analytical scientists to work in synergy with other departments that strongly depend on analytical testing to answer questions such as "*What? Where? How much? What arrangement, structure or form?*" (Christian, 2005). By answering these questions, the analyst provides the tools for understanding the scientific principles that govern biopharmaceuticals production.

As evidence of the importance of analytical testing in driving biopharmaceutical development, the FDA implemented the quality-by-design (QbD) principles in biomanufacturing aiming to deliver quality throughout the whole process. The QbD practice is a data-driven approach that follows rigorous scientific methods and principles, including risk assessment to build quality into the process. According to the QbD dogma, undertaking process development in a *design space* ensures the attainment of specific objectives with a comprehensive understanding of both product and process, leading to the identification of the risks impacting the quality of the outcome (ICH Q8-R2, 2009; Sangshetti et al., 2017; Kumar, 2019; Papathanasiou, Kontoravdi, 2019; Kiss and Gottschalk, 2018). The process is dependent on and driven by analytical data, which build process knowledge, drive the scientific and process engineering choices and shape market strategies. This study focuses on addressing challenges relative to early-stage biopharmaceutical development, therefore, the literature and discussions related to late-stage product development, clinical studies and

manufacture were not reviewed in-depth. Nevertheless, a brief overview of the research setting was outlined to put the importance of this work into context.

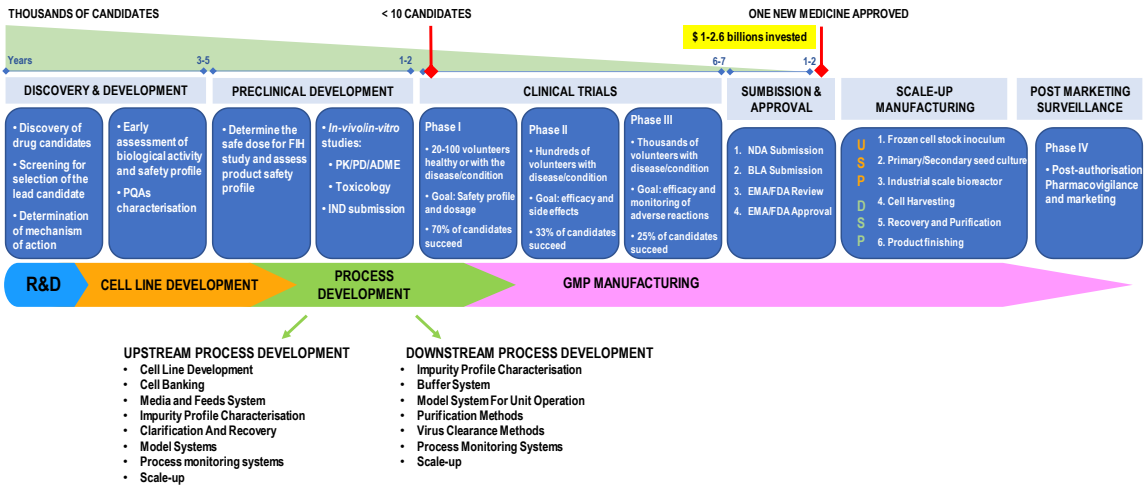

Figure 1.2 Biopharmaceutical Development Lifecycle.
Flowchart showing all the phases of a biopharmaceutical lifecycle from discovery to preclinical development, clinical trials, and regulatory approval with the respective timeline and average money invested. After the approval of a new drug, the manufacturing and post-marketing surveillance phases are described. The steps necessary for the USP and DSP development are also listed.

1.4.2 CHO Cell Line Development and Engineering

Following the selection of the lead candidate molecules, initial consideration of the manufacturing process is brought to the fore with the development of a suitable cell line. A typical industrial CHO CLD workflow starts with the selection of a host appropriate for producing the molecule of interest and the design of an expression vector for delivering the transgene into the host. These two steps are dependent on one another as the expression vector selection system needs to be compatible with the host expression machinery. Subsequently, the expression vector is amplified (usually in bacteria cells such as E. coli), isolated and transfected into the CHO cell host to obtain producing clones.

The most common transfection method used in CHO cells is electroporation, however, lipofection and polymer-mediated gene transfer are also used. Transient transfection is useful in the initial phase of CLD as a quick (~10 days) and more economical way to provide sufficient material for early assessment of the product characteristics, efficacy and engineering strategies to be taken further. However, in transient transfection, the gene expression ability is rapidly lost since the DNA product is replicated as an extrachromosomal unit (Ozturk and Kompala, 2006; Rita Costa et al., 2010). Although more lengthy (12-14

weeks) and expensive, stable transfection accomplishes the permanent expression of a recombinant protein (Wurm, 2004; Hu, 2012; Rita Costa et al., 2010). Moreover, as a means of ensuring therapy consistency, the ICH guidelines require that biopharmaceuticals must derive from a clonal cell line. Hence, stable transfection is most suitable for large-scale production. Here, the vector DNA is usually transfected with a marker gene to guarantee integration into the host genome and subsequent selection of the cells that stably express the protein of interest.

The most common marker genes used in CHO cells are dihydrofolate reductase (DHFR) and glutamine synthetase (GS). DHFR is an enzyme involved in purine and pyrimidine synthesis, catalysing the conversion of dihydrofolate into tetrahydrofolate. The addition of methotrexate (MTX – folic acid antagonist), inhibits the function of DHFR. Only the transfected cells containing the DHFR gene can survive in the presence of MTX. Moreover, an antibiotic resistance gene is added to act as a selectable marker to facilitate vector amplification. In this system, the selection is performed by culturing the cells in a medium lacking hypoxanthine and thymidine and containing G-418 (aminoglycoside antibiotic – polypeptide synthesis inhibitor). Differently from the DHRF, the GS expression system principle is based on the synthesis of glutamine from glutamate and ammonium catalysed by the GS enzyme. Since glutamine is an essential amino acid, only the transfected cells can grow in glutamine-free media. Even for cells that do express functional levels of GS endogenously (i.e. CHO cell lines), including GS inhibitor methionine sulfoximine (MSX), enables the use of the GS expression vectors. In this case, only the transfectants with additional GS activity (i.e. the GS gene from the expression vector) can survive. Once selected, the highly expressing clonal populations are finally expanded and used for screening and further analysis.

Following the establishment of expressing pools, cells are screened for selection of the highest producing clones. The cell clones are subcultured in small scale bioreactors, usually in fed-batch mode, providing accurate scale-down model data useful for large scale reactions. At this stage, small-scale downstream models and thorough analytical characterisation are integrated and clone selection is driven by both cell line productivity and product quality. The CLD process culminates with the selection of a final production clone with suitable characteristics to proceed to scale-up manufacturing. Eventually, research banks of the top clones can be made and process development pursued with a focus on media optimisation and process conditions. Analytical data gathered during this stage are

fundamental for identifying the challenges in the development and production of the molecule of interest and consequently drive process development and optimisation before scale-up and clinical manufacturing (Lewis et al., 2013).

1.4.3 Upstream and Downstream Process Development and Optimisation

Biopharmaceutical USP is the iterative approach used in the industrial and academic environment to express recombinant proteins in cells. This involves inoculum and media development and culminates with the harvesting of the final product from cell culture. The performance of the cell line is strongly affected by the process conditions, including media and feed composition thus these factors need thorough optimisation. On the other hand, DSP encompasses all the steps required for the purification of the protein of interest from cell culture (Figure 1.2).

The development and optimisation of both USP and DSP have largely benefitted from the adoption of platform technology (Shukla et al., 2017). Namely, standardised methodologies are applied across multiple products belonging to the same class or having similar characteristics. Industries develop their proprietary platform methods and combine them in a logical sequence to create platform processes that serve as a guidance scheme to develop and manufacture multiple products. This is performed to limit experimentation and costs required to reach a bioprocessing solution for a given candidate (Shukla et al., 2007; Gronemeyer, Ditz, and Strube, 2014). One of the advantages of platform technology is the predictability for process optimisation and consistency of manufacturing. Undeniably, the implementation of platform process technology played a key part in the growth of mAb molecules (Shukla et al., 2007; Gronemeyer, Ditz, and Strube, 2014). Furthermore, the integration of platform approaches with HT technologies delivered biopharmaceutical development an extraordinary QbD toolbox that reduces costs and time on the process along with ensuring quality. More details on HTPD follows in Section 1.5.

1.4.4 Quality Analysis in Biopharmaceuticals Process Development

Analytical methodologies play an important role in assessing the quality of biopharmaceuticals throughout the entire lifecycle from discovery to development, manufacturing, marketing and post-marketing (Siddiqui, AlOthman, and Rahman, 2017). The subjects of analytical investigation are the drug substance (active ingredient), intermediates, drug product, impurities and degradation products, process parameters, cells and biological samples containing the active ingredient and its metabolites. Analytical methods used for biopharmaceutical analysis include techniques such as spectroscopy, chromatography, electrophoresis, and mass spectrometry.

Advancements in biopharmaceutical analysis are moving towards technologies that can support the QbD approach and speed up the launch of novel medicines to market. Hence, HTPD tools involve the use of rapid and sensitive methods that can be integrated with automated platform technologies. Along these lines, Process Analytical Technology (PAT) involves the use of analytical methods that enable real-time measurements and online monitoring of process conditions and PQ directly from bioreactors (Strasser, Farrell, et al. 2021; Floris et al. 2020). Both HTPD and PAT focus on the realisation of the QbD framework and combine technologies ranging from analytical chemistry, control theory and statistical modelling (FDA, 2004; Rolinger and Matthias, 2020; Read, Park, et al., 2010; Read, Shah, et al. 2010). The goal of both HT analytics and PAT tools during the product development phases is to ease the assessment of drug developability and process optimisation, define the Quality Target Product Profile (QTPP), and identify the Critical Process Parameters (CPPs) related to bioprocess engineering strategies to meet the CQAs. The overall aim is to enhance process understanding and control to finally deliver quality products with consistency (Schaefer et al. ,2014; Glassey et al., 2011; Bhambure, Kumar, and Rathore, 2011; Łącki, 2014).

1.5 High-Throughput Process Development Technology

1.5.1 Background

The last decades have seen the surge of HTPD technology in an industrial setting driven by the ever-increasing pressure of biopharmaceutical companies towards lowering the time and costs necessary for the development of novel therapeutic products before clinical entry. Furthermore, following the introduction of regulatory initiatives such as the QbD approach, pharmaceutical development and manufacturing require a thorough process understanding and control of all the variables that impact PQ. Hence, the expansion and improvement of HTPD technologies have become the point of convergence for shortening the process upfront and ensuring the delivery of a final product with the targeted quality profile.

With rapid and cost-efficient workflows, HTPD tools aim to ease the assessment of drug developability and identify the product CQAs related to bioprocess engineering strategies (Bhambure, Kumar, and Rathore, 2011). Similarly, HTPD can also aid late-stage activities such as commercial process development, characterisation and scale-down validation to efficiently and fully explore the design space for quality assurance, in line with the QbD framework (Kiss and Gottschalk, 2018; Manahan et al., 2019). The central goal of HTPD is the generation of large experimental datasets directly relevant to large-scale biopharmaceutical manufacturing. The impact of these methodologies was confirmed by several publications describing their application from clone selection and upstream optimisation to downstream purification, formulation and quality analysis (Evans et al., 2017; Łącki, 2014; Sandner et al., 2019; Reema et al., 2012; Goldberg et al., 2017).

The HTPD tools efficiently drive process development in a time- and resource-constraint environment. However, HT workflows are not without flaws that still hamper the implementation of these technologies. Indeed, to fully exploit the potential of HTPD, further technology improvements in the field of automation, analytics and data evaluation need to be attained (Łącki, 2014).

What follows is a summary of the features and the state-of-the-art of HTPD methodologies along with a critical discussion on the challenges and future perspectives of this technology as it applies to cell culture, downstream purification and analysis.

1.5.2 What Makes a Technology High-Throughput?

The common denominators of HTPD technologies are miniaturisation, parallelisation and automation. These are the fundamental features of HTPD tools that, supported by DoE, multivariant analysis, statistical modelling and platform approaches, enforce process efficiency while fully exploring the multidimensional design space, requested by the QbD framework.

1.5.2.1 Miniaturisation

The main benefit of miniaturisation is the reduction of reagent volumes and resources required per experiment, which results in a substantial decrease in cost and time. Over the years, small scale bioprocess technologies have evolved from test-tube-based to micro-well-plate-based assays enabling the handling of microliter samples. The miniaturisation of chromatography columns assisted both the downstream purification of small volume samples and the development of sensitive analytical characterisation methods (Evans et al., 2017; Petroff et al., 2016; Stoll et al., 2019). Recently, the introduction of chip technology allowed a further reduction of sample volume, from micro- to nanolitres (Ou et al., 2020; Wheeler et al., 2014).

1.5.2.2 Parallelisation

Parallel experimentation consists of the concurrent execution of multiple experimental runs in a flexible and dynamic scheme. Parallelisation aims to accelerate the investigation of a wide experimental space which is key to process understanding and optimisation. The concept of parallelisation was first proposed by the FDA with the “Pharmaceutical Current Good Manufacturing Practices (CGMPs) for the 21st Century – A Risk-Based Approach” in 2002 and became an integral part of PAT and QbD workflows (FDA, 2004).

1.5.2.3 Automation

Automation facilitates both miniaturisation and parallelisation allowing for the processing of hundreds of small volume samples simultaneously. Consequently, both the reduction in experimental cycle time and the boost of productivity are the key drivers for the advancement of such technology in the biopharmaceutical industry. Moreover, the positive impact of

process automation is seen in the betterment of process control, robustness and decrease of labour time. Indeed, automation leverages the workload by freeing scientists from many hours of assiduous and error-prone lab tasks, enabling them to focus their time in more valuable areas. Additionally, robot enclosure systems also allow the execution of hazardous experiments in a safe environment. A large and growing body of literature recognises the progressive wave and great potential of HT automation technology when applied to different research and industry settings to increase data and knowledge generation by interrogating multidimensional experimental spaces. However, some authors such as Scott and Melville (2014) also admitted how complications due to instrument expenses and "fit-for-purpose" integration of such technologies in laboratory workflows retarded, and still hinder, the uptake of automation in the biopharmaceutical industry (Scott and Melville, 2014). The most successful automation tools implemented in biopharmaceutical industry laboratories are liquid handling robots. Companies such as Hamilton, Tecan and Opentrons have been focused on developing liquid handling robots fit for laboratory purposes with user-friendly graphical interphases and operating systems to ease usability by chemists and biologists (Byrne and Swindley, 2020; Bhambure, Kumar, and Rathore, 2011). Indeed, these systems are usually affordable by both industrial and small research laboratories. Secondly, they offer several functionalities such as handling a wide range of sample volumes, shaking, incubation heat-block stations, and vacuum pump attachments. Therefore, liquid handling robots can be adapted to support different workflows from cell culture feeding and clone selection, to downstream purification, analytical assays and sample preparation before LC-MS characterisation. Finally, they offer a great improvement in the overall efficiency and safety of the workplace. Additionally, a central component of the HTPD framework consists of the rapid manipulation of broad datasets in an automated fashion (Gangadharan et al., 2019). Automated software packages for data analysis has successfully been incorporated into HTPD platforms (Jansen et al., 2018; Rathore et al., 2017; Lumley et al., 2020; Pfeuffer et al., 2017). However, data analysis is still considered a lengthy and burdensome task due to the complexity of certain types of datasets, such as those coming from analytical characterisation by LC-MS. Moreover, the necessity of demanding data interpretation challenges the development of automated data processing platforms.

Statistical modelling has become an integral part of HTPD decision-support tools as it leverages the vast quantity of data collected throughout the biopharmaceutical lifecycle (Papathanasiou et al., 2017; Kroll et al., 2017; Łącki, 2014; Bhambure, Kumar, and Rathore,

2011; Rolinger and Matthias, 2020). Several studies have demonstrated how mathematical modelling guided the information obtained through screening experimentation and helped to define optimal conditions for tailoring the subsequent experiments (Goudar, McFarland, and Betenbaugh, 2018).

Although there are still challenges to overcome before fully automated "from-sample-to-report" workflows will become routine, the trend in HTPD and automation technology development is moving towards making life science cheaper, faster, safer and more accessible with robots and AI forecasted to become the workhorse of the lab (Feidl et al., 2020).

1.5.3 High-Throughput Technologies for Upstream Development

The technology used in HTPD must be fit for the screening-led assays adopted in CLD activities for clone selection, media and process development. This area of application has been focusing on integrating cell line engineering approaches involving in-silico modelling, omics-technology, systems biology and genome editing (Kuo et al., 2018) with microbioreactor systems (MBRs) mimicking large-scale production stirred tank bioreactors (Cartwright et al., 2018).

As reviewed by Hemmerich, MBRs are organised in two classes: shaken and stirred impeller cultures (Hemmerich et al., 2018). Recently, these systems have replaced shake T-flasks and lab-scale bioreactors in early- and mid-stage process development (Hemmerich et al., 2018). The most commonly used shake culture-based MBRs use microtiter multi-well plates, spin tubes, and microfluidics for cell culture (Kiss and Gottschalk, 2018; Hemmerich et al., 2018). Commercial products involve Deep-Well Plates (DWPs), TubeSpin®Bioreactor (tpp.ch), microMatrix (applikonbio.com), SimCell™ platform (BioProcess Corp.), M24 micro-bioreactor (MicroReactor Technologies, Inc.), Growth Profiler (enzyscreen.com), Micro-24 (pall.com), BioLector (m2p-labs) and many others. These systems represent a cost-effective solution with minimal setup. Moreover, they allow for high-level parallelisation and are particularly suitable for large-number high-throughput screening (HTS) experiments. For instance, DoE experiments can be easily set up on these systems in batch or fed-batch mode following automated and unsupervised workflows. The main drawback of shaken culture MBRs is their fundamental differences to large-scale bioreactors along with the inefficient control of key process parameters such as agitation rate, dissolved

gasses (e.g. O_2, CO_2, N_2), and pH (Hemmerich et al., 2018; Kiss and Gottschalk, 2018; Rameez et al., 2014). This may lead to further issues when it comes to scale-up as the results may not be comparable and model prediction may not be accurate.

On the other hand, stirred variants offer a flexible small-scale system that better mimics the large-scale bioreactor operations and hence facilitates the following scale-up steps. These systems can monitor and control process parameters such as temperature, dissolved gasses and pH. The stirred MBRs hydrodynamics is similar to large-scale units thus, with the help of computational simulation, further understanding of process development conditions is gained before scale-up. Currently, the most employed stirred MBRs are ambr® systems (tapbiosystems.com) and bioREACTOR (2mag.de). These systems allow the accessibility of culture volumes in the range of 10-250 mL facilitating the integration of analytical testing for PQ monitoring (Strasser et al. 2021; Manahan et al., 2019; Sandner et al., 2019). Nevertheless, the technical setup for these systems is more complex with higher costs than the shaken culture variants. Thus, stirred MBRs are generally for smaller-number screening and optimisation experiments prior to scale up, whereas, shaken-culture MBRs are a better fit for large-number screening experiments where less process information is needed. Several published articles testify to the extensive use of both shaken and stirred MBRs for CLD application such as strain screening, growth parameter optimization, media and feed development (Cartwright et al., 2020; Amanullah et al., 2010; Legmann et al., 2009; Lamping et al., 2003; Isett et al., 2007; De Jesus et al., 2004).

1.5.4 High-Throughput Technologies for Downstream Process Development

Cell culture purification may be necessary at numerous stages of biopharmaceuticals development and not just at the final stage of their production (Schmidt et al., 2016). In contrast to manufacturing, R&D applications place a greater emphasis on the selection of the lead candidate molecule with desirable functional characteristics for therapeutic development. In this context, PQ analysis, biological activity and stability are of major focus, thus, fast purification processes without polishing are usually performed to rapidly achieve an adequate level of purity for testing. Nevertheless, HTPD downstream processing aims to find the parameters influencing yield and PQ profile of the recovered protein, front-loading method development and optimisation of the operating conditions before scale-up (Chhatre, Bracewell, and Titchener-Hooker, 2009; Baumann and Hubbuch, 2017; Liu et al., 2017;

Stamatis et al., 2019). Hence, the choice of a scale-down purification model that is representative of the downstream unit operation at the process scale is critical and also one of the most challenging issues of downstream HTPD (Łącki, 2014).

Not surprisingly, most of the HTPD purification tools developed in recent years are based on affinity chromatography principles (Evans et al., 2017; Liu et al., 2017; Stamatis et al., 2019). In comparison to other modes of chromatography, affinity separation provides a fast one-step purification method to generate material suitable for screening and primary characterisation in early process development (Chhatre, Bracewell, and Titchener-Hooker, 2009; Evans et al., 2017). Affinity chromatography separations require the fine-tuning of a series of steps (capture, wash and elution) to recover the product of interest from the cell culture supernatants (Arora, Saxena, and Ayyar, 2017). The success of the purification step is the result of a complex cascade of events depending not only on the method specifications such as buffer composition, pH, temperature, column etc. but is also highly influenced by the upstream process conditions. Furthermore, handling of small volume samples easily and rapidly may constitute further complications (Treier et al., 2012). Indeed, the development of small-scale affinity chromatography methods that maximise yield without affecting PQ remains one of the most challenging steps of HT downstream purification (Evans et al., 2017; Treier et al., 2012).

HT downstream tools come in various scales and formats: microliter plates, pipette tips and microcolumns pre-packed with chromatography resins (reviewed by Evans et al., 2017). Previously published papers demonstrate how these methodologies can purify small cell culture volumes with levels of recovery comparable to large-scale purification. Moreover, workflows are designed to be fully automated on liquid handling platforms including neutralisation or buffer-exchange post-purification resulting in an overall gain in time and process costs (Treier et al., 2012).

1.6 Advanced Analytical Methodologies for Biopharmaceuticals Analysis and their Application to High-Throughput Process Development

The full potential of HTPD is achieved when HT analytics is integrated into a feedback loop engine that generates information necessary for assessing drug developability and process control parameters. Analytical method development for HT operations aims to provide tools that rapidly and accurately support the analysis of large numbers of low volume samples coming from both HT upstream and downstream process development to efficiently generate a large amount of data for deepening product and process understanding (Bhambure, Kumar, and Rathore, 2011; Ma et al., 2020; Trappe et al., 2018; Jonnalagadda et al., 2016; Redman et al., 2015; Lanter et al., 2020). The application of HT analytics is particularly valuable for routine analysis when conventional methods are lengthy and lack sensitivity. In this context, HT tools are designed to give comparable information to those obtained with traditional analytical methods, but with greater throughput capabilities. Table 1.3 compares the conventional low-throughput (LT) analytical methodologies with the state-of-the-art HT tools supporting the various steps of process development.

As reviewed by Konstantinidis (2013), HT analytical methods are defined by the time and sample amount required for the analysis. Both time and sample amount are directly influenced by the method linear dynamic range (LDR) and limits of quantification (U/LLOD and U/LLOQ), the complexity of sample preparation and measurement, as well as the possibility of implementing parallelisation and automation to the workflows (Konstantinidis, Kong, and Titchener-Hooker, 2013). Therefore, when developing or choosing the method, the analyst needs to make sure that the method is suitable for working in a HTPD environment. The quality attributes to be monitored during development mainly depend on the physicochemical properties of the molecule of interest, scale and process characteristics. However, in early-stage development, when little process knowledge is gathered, product analysis usually gravitates towards titre, potency, glycosylation, size and charge variant profiles (Kahle and Hermann, 2018). The HT analysis of these quality attributes is discussed hereafter whilst the challenges of the current HT analytical tools are examined in Section 1.6.6.

Table 1.3. Comparison between Conventional LT and State-of-the-Art HT Analytics for Biopharmaceutical Process Development.

Quality Attribute	LT Methodology	HT Methodology
Titre, Residuals, Purity, Identity	ELISA, CE-MS, LC-FLR-MS (HILIC, NPLC, RPLC, WAX)	BLI, FRET-TR, Fluorescence Spectroscopy, Smart assays kits, Microfluidics, Automated immunoassays
Potency	ELISA, SPR	BLI, HT SPR
Size Variants	SDS-PAGE, CGE, SEC-HPLC	Microfluidics, capillary-based western blots, automated assay kits, cartridge-based assays, UHPLC
Charge Variants, pI	cIEF-gel, CE, IEX (HPLC)	iCE, IEX (UHPLC)
Glycosylation	PNGaseF digested or intact protein HILIC-MS	Smart assays kits, UHPLC, microfluidics
Other PTMs	Peptide-mapping RPLC/MS	Smart assay kits, UHPLC-MS, MAM, direct infusion MS

* ELISA: enzyme-linked immunosorbent assay; CE-MS: Capillary electrophoresis–mass spectrometry; LC-FLR-MS: liquid chromatography–fluorescence–mass spectrometry; HILIC: Hydrophilic interaction chromatography; NPLC: normal phase liquid chromatography; RPLC: reverse-phase liquid chromatography; WAX: weak anion exchange chromatography; BLI: bio-layer interferometry; TR-FRET: time-resolved-fluorescence resonance energy transfer technolog; SPR: surface plasma resonance; HT SPR: high-throughput surface plasma resonance; SDS-PAGE: sodium dodecyl sulphate capillary gel electrophoresis; CGE: capillary gel electrophoresis; HPSEC: high-performance size-exclusion chromatography; cIEF: capillary isoelectric focusing; CE: capillary electrophoresis; IEX: ion exchange chromatography; UHPLC: ultra-high performance liquid chromatography; MAM: multi-attribute method (see *List of Acronyms and Abbreviations*).

1.6.1 Bioassays and High-Throughput Quantitation of Expression Titre and Residuals

A diverse array of HT assays provides analytical methods for measuring protein expression titre, concentration of residuals, kinetic and binding affinity through the various steps of biopharmaceutical discovery and development. Most of these methodologies consist of immunoassays combined with optical analytical detection based on bio-layer interferometry (BLI) (Octet® platform, ForteBio), time-resolved-fluorescence resonance energy transfer technology (TR-FRET) (HTRF® Technology, Cisbio), fluorescence polarization (Valitacell's ValitaTITER IgG assay), UV and fluorescence spectroscopy (Gyrolab™ platform, Gyros Protein Technologies). The technology comprises multi-well plates, biosensors and microfluidic devices; the procedures can be performed in a semi- or fully automated fashion. These tools offer lower LOD, LOQ and faster analysis in comparison to the standard analytical HPLC methods and ELISA assays which are now considered of lower throughput.

The BLI technology offers a few advantages in comparison to fluorescence polarisation, TR-FRET, UV and fluorescence spectroscopy-based techniques. Firstly, it is less susceptible to matrix composition hence, it can be applied on crude, purified and formulated samples of various buffers and pH values. Secondly, it can cover the analysis of a wide range of molecules from small to large molecular weights. Finally, titre, residuals, impurity and potency analysis can be integrated into a single platform.

One of the most successful examples of HT tools applied for the analysis of mAbs and other proteins are the Octet® instruments (ForteBio). Each Octet® system involves biosensors and microplates assay kits. The technology is based on BLI consisting in the measurement of the shift in the interference pattern of white light caused by an increase in optical thickness resulting from the binding between the target molecule and the ligand immobilised on the biosensor tip. The real-time, label-free measurement of this interaction allows monitoring of the protein concentration as well as kinetics and binding specificity, association and dissociation rate in a unique system. The Octet® instruments are routinely used in industry labs as a HT platform for the analysis of expression titre, potency, host cell proteins (HCPs) and other process-related impurities in both crude and purified samples. The Octet HTX is the highest throughput system of the Octet platform and allows the use of as low as 40 µL sample volume with LDR falling between 10 pM and 1 mM sample concentration. The analysis procedure is designed to be fully automated and the measurement time for running up to 384 samples is only 15 min (https://www.fortebio.com/). The remarkable increase in throughput balances the heavy costs associated with this technology (Kiss and Gottschalk, 2018).

Besides the Octet®, the most successful HT tools for potency analysis are based on SPR and combine automation and microfluidics. Examples of commercially available tools are the OneStep SPR System (ForteBio), Carterra LSA platform (SensiQ Technologies), Biacore™ System (Cytiva Life Sciences) and ProteOn™ XPR36 System (Bio-Rad Laboratories, Inc.) offering a substantial improvement in analysis time and sensitivity compared to automated potency binding ELISAs (Joelsson et al., 2008; Kiss and Gottschalk, 2018).

1.6.2 High-Throughput Analysis of Glycosylation

Glycan heterogeneity poses a daunting analytical challenge, usually requiring the use of hyphenated methods for assessing specific glycosylation attributes, including site, structure

and abundance (Dotz et al., 2015; Hajba, Csanky, and Guttman, 2016). Typically, glycosylation analysis is classified as macro- and micro-heterogeneity analysis. Macro-heterogeneity refers to the glycans site-occupancy assessment, whilst micro-heterogeneity analysis involves the determination of the glycan structure present at specific sites in the mAb molecule. Glycosylation profiling involves the enzymatic deglycosylation of the mAb molecule followed by released glycan analysis.

Zhang (2016) reviewed the approaches used for biopharmaceuticals N-glycan analysis (Zhang, Luo, and Zhang, 2016). The diverse state-of-the-art analytical methods for mAb glycosylation analysis were reported by Leoz et al. (2020) in an extensive interlaboratory study having the NISTmAb as a model molecule (Leoz et al., 2020). High-throughput analytical strategies for glycan analysis have been focusing on speed, automation and miniaturisation of sample preparation and separation methods (Hajba, Csanky, and Guttman, 2016).

Sample preparation protocols involved the automation of digestion, purification and labelling by liquid handling (reviewed by Aich, Lakbub, and Liu, 2016). Released-glycan sample preparation assays based on magnetic beads (Váradi, Lew, and Guttman, 2014), microcolumns (Szigeti et al., 2016), tips (Yang et al., 2017) and microarrays (Fanayan, Hincapie, and Hancock, 2012) were proven successful when hyphened with HT liquid-phase separation methods such as UHPLC, CE, and microfluidics. Published works account for the advantageous use of commercially available HT kits such as ProZyme and Waters proprietary glycan kits showing 90% improvement in throughput compared with conventional LC-FLR-based methods (Zhang et al., 2020). Furthermore, recent glycan-labelling techniques improved the sensitivity of MS acquisition which is key when working at a small scale (Kimzey et al., 2015; Keser et al., 2018).

Beads- and sensors-immobilised lectins binding assays coupled to biolayer interferometry (Octet QK384 platform) or fluorescence detection (e.g. PAIA assay technology) were adopted for the rapid quantification of mAbs glycoforms in early CLD (Jonnalagadda et al., 2016; Spier and Griffiths, 2012). Despite the great gain of analysis time and easiness of operations, these technologies lack the specificity, resolving power and robustness ensured by LC/MS-based methods (Lazar, 2011; Chi et al., 2020). Hence, current analytical efforts focus on improving the throughput capability of MS-based detection (Chi et al., 2020; Lanter

et al., 2020) and their potential integration with fully automated sample preparation protocols and microfluidic-based separations (Lazar, 2011; Redman et al., 2015).

1.6.3 High-Throughput Analysis of Charge-Variants

As previously discussed, therapeutic proteins charge variants profile can be indicative of important CQAs thus, must be monitored throughout lead candidate, CLD and other development activities (Chung et al., 2018; Wagner-rousset et al., 2017; Leblanc et al., 2017). Charge variants analysis is mostly based on ion-exchange chromatography (IEX) and electrophoretic techniques such as capillary gel electrophoresis (CGE), capillary electrophoresis (CE), capillary isoelectric focusing (cIEF) with or without MS detection (Carillo, Jakes, and Bones 2020; Füssl et al. 2020; Kahle and Hermann, 2018; Ma et al., 2020; Liu, Ren, Zong and Zhang, 2019; Leblanc et al., 2017). Analysis workflows involve the determination of charge heterogeneity at the intact, subunit and peptide levels with the Fab region being of particular interest since CDR modification are those that most influence mAb activity (Liu, Ren, Zong and Zhang, 2019). The on/offline coupling of liquid-phase separations with mass spectrometry is necessary for the identification of the charge variants (Liu, Ren, Zong, and Zhang, 2019; Leblanc et al., 2017; Gstöttner et al., 2018; Ma et al., 2020; Dai et al., 2018; Füssl et al., 2019). High-throughput method development has gravitated towards the implementation of fast small-scale liquid-phase separations (Trappe et al. 2018), microfluidic chip devices with laser-induced fluorescence (LabChip GXII, Caliper, PerkinElmer) and MS detection (ZipChip CE-ESI-MS) (Carillo, Jakes, and Bones 2020). Moreover, the use of robotic liquid handers is becoming increasingly frequent for the generation of automated analytical workflows (Millán-Martín et al. 2020; Redman et al., 2016; Herring, Ji, and Richter, 2019).

Wheeler et al. (2014) described the application of the LabChip GXII microchip zone electrophoresis method for mAb charge variants achieving 10-fold faster analysis than conventional methods with minimal method development, data processing and sample volume needed. Other methods that require low sample volume are the cIEF-based methods hence, often adopted for large screening assays (Goyon, Exco, et al., 2017). However, several authors claimed that chromatography methods generally allow for better resolution and are considered more robust than electrophoretic-based separations thus, most suitable for accurate quantification (Du et al., 2012; Alekseychyk et al., 2017; Chung et al., 2018; Herring and Richter, 2019). A brief discussion on the application of IEC for mAb analysis is outlined below with a major focus on HT method development.

1.6.3.1 Ion Exchange Chromatography (IEX)

Together with imaging cIEF, IEX has become the gold standard methodology for the analysis of superficially charged proteins under non-denaturing conditions (Parr, Montacir, and Montacir, 2016; Garripelli, Wu, and Gupta, 2020). IEX retention mechanism is based on the competition between sample ions and mobile phase counter-ions for interaction with the stationary phase functional groups. Hence, IEX columns are characterised by ionised or ionisable groups bonded to the stationary phase surface, whose chemical nature divides cation-exchange (CEX) and anion-exchange (AEX) modes of separations

Table 1.4). Based on the interaction between the stationary phase functional groups and the analyte surface accessible charge, basic and acid variants can be resolved from the main peak isoform. In CEX separations, variants with lower pI values (more acidic) elute before the main peak isoform whilst variants with higher pI values (more basic) elute after. Vice versa, AEX separations are characterised by basic variants eluting earlier and acidic variants eluting after the main peak isoform. Owing to the basic nature of the amino acids, proteins such as mAbs, are positively charged at operating pH values ($5 \leq pH \leq 7$) and usually separated by CEX. On the other hand, AEX is mostly used for purification polishing steps (Elich et al., 2019; Masuda et al., 2020) besides a few studies reveal successful application for the analysis of mAbs and protein glycosylation (Ponniah et al., 2017; Chen et al., 2020; Büttner et al., 2021). Therefore, the CEX mode of separation and its application in a HT environment will be the focus of this section.

CEX separations are complex and strictly dependent on the molecule pI. The optimal resolution is obtained with the fine-tuning of various parameters such as column, mobile phase composition, pH, temperature, flow rate etc. (Fekete, Beck, Veuthey, et al., 2015). Notably, the large size and complex surface charge distribution of mAbs can pose challenges in CEX method development. Statistical modelling software (e.g. Drylab, Molnár Institute) aid understanding of the separation mechanism (Rea et al., 2011; Fekete, Beck, Veuthey, et al., 2015) and ease method optimisation, reducing time and complexity of development – a considerable advantage for HT applications (Fekete, Beck, Fekete, et al., 2015; Guillarme, Fekete, and Beck, 2015; Joshi, Kumar, and Rathore, 2017; Kumar et al., 2015; Schmidt, Hafner, and Frech, 2014). A few authors revealed how both pH and salt-gradients can serve as a multi-product approach by testing 10 mAbs with pI values ranging between 6.7-9.0. Salt-based separations are an established PAT tool since guarantee robustness and better resolution (Guillarme, Fekete, and Beck, 2015; Fekete, Beck, Fekete, et al., 2015; Farsang et al., 2019). On the other hand, pH-based gradients are MS-compatible, which guarantees online characterisation of the acid and basic variants (Leblanc et al., 2017).

As extensively reviewed in the literature, the physicochemical properties of CEX stationary phase particles play a critical role in resolving protein charge variants (Fekete, Beck, and Guillarme, 2015; Murisier et al., 2019). Indeed, non-porous particles minimise the transparticle mass transfer resistance band-broadening effect related to the electrostatic interactions provided by the large molecular size and complex surface charge of proteins. The majority of modern CEX columns commercially available are packed with non-porous

particles presenting a hydrophobic core coated with a thin layer of hydrophilic material, such as highly cross-linked poly(styrene-divinylbenzene) (PS/DVB). The hydrophilic nature of the PS/DVB coating material allows for non-specific interactions, extended pH range stability ($2 \leq pH \leq 12$) and high-temperature operation (up to 60 °C) (Fekete, Beck, and Guillarme, 2015). Moreover, it was demonstrated how IEX retention can directly depend on column particle size (Murisier, Farsang, et al., 2019; Fekete, Beck, and Guillarme, 2015). Today, UHPLC CEX columns with dp in the range 1.7-6.0 µm are commercially available and adopted in the HTPD environment. Nonetheless, Murisier et al., explained how reducing particle size below 2-2.5 µm does not improve IEX separations, opposite to other modes of chromatography (Pauw et al., 2014; Sanchez et al., 2013).

High-throughput applications of CEX offer rapid and sensitive charge variants separations of mAbs by using short narrow-bore columns both with pH and salt-based gradients (Trappe et al., 2018; Alekseychyk et al., 2017; Ma et al., 2020; Joshi, Kumar, and Rathore, 2015). Trappe (2018) achieved a sub-4 min method based on a 2.1 x 50 mm (ID x L) column with a pH gradient for the analysis of trastuzumab charge variants expressed from different CHO and HEK293 cell lines (Trappe et al., 2018).

Table 1.4. IEX Column Stationary Phases and Characteristics

IEX Phases	Functional group	Characteristics
Strong Cation Exchange (SCX)	Sulfonic acid group ($-SO_3H$)	Wide operating pH as the functional group is negatively charged when using strong acids-based mobile phases.
Weak Cation Exchange (WCX)	Carboxylic acid group (-COOH)	Narrow operating pH as the functional group is ionised at basic pH and mostly affected by the mobile phase conditions, temperature and pH shifts. WCX may provide higher selectivity than SCX for large biomolecules.
Strong Anion Exchange (SAX)	Quaternary amine group ($-N(CH_3)_3$)	Wide operating pH as the functional group is positively charged when using mobile phases composed of strong bases.
Weak Anion Exchange (WAX)	Primary/Secondary amine group ($-N(C_2H_5)_2$)	Narrow operating pH as the functional group is ionised at acid pH and mostly affected by the mobile phase conditions, temperature and pH shifts. WAX may provide selectivity that is not met with SAX, especially for large molecules.

1.6.4 High-Throughput Analysis of Size Variants

As previously mentioned, the formation of protein aggregates, also referred to as high-molecular-weight species (HMWS), may derive from various mechanisms and is strictly influenced by the sequence and structural modifications of each protein. Likewise, mechanisms affecting the protein molecular stability may also lead to fragmentation, thus, the formation of low-molecular-weight species (LMWS). The tendency of a lead candidate protein to both aggregate and fragment is critical for product developability (Ebo et al., 2020; Basle et al., 2020). Therefore, HMWS and LMWS levels and mechanisms of formation are monitored and characterised since early-stage development (Jarasch et al., 2015).

According to the US Pharmacopoeia, the gold standard methods for mAb LMWS and HMWS analysis include capillary gel electrophoresis (CGE) and size-exclusion chromatography (SEC), respectively. Conventional SEC workflows require minimal sample preparation and several research groups have developed sensitive HT SEC methods for the analysis of HMWS with sub-10 min isocratic runs (Goyon, Beck, et al., 2017; Goyon, Fekete, et al., 2018; Hong, Koza, and Bouvier, 2012; Diederich et al., 2011; Rea et al., 2012; Goyon, Sciascera, et al. 2018). Another important achievement was the use of non-volatile solvents for online MS coupling enabling the identification and conformational

characterisation of the SEC separated peaks (Goyon, D'Atri, et al., 2017; Ehkirch et al., 2018).

Protein fragments and small impurities are better resolved by CGE; therefore, HT technology development has implemented the use of microfluidic chip electrophoretic separation methods. Amongst the commercially available platforms for size variants analysis are the Caliper®, Maurice®, and Peggy-Sue® from ProteinSimple Inc. which make use of microfluidics technology. Besides the net increase in throughput, the main advantages of these tools are the easiness of use and compatibility with automation (Ou et al., 2020). However, their resolving power remains lower than standard HPLC and CGE methods and are unable to provide detailed information at the molecular level such as those obtained by MS (Ou et al., 2020; Chi et al., 2020).

Together with SEC and CGE, dynamic light scattering (DLS), nanoparticle tracking analysis (NTA), micro-flow imaging, sodium dodecyl sulphate-polyacrylamide gel electrophoresis (SDS-CGE), analytical ultracentrifugation, and asymmetrical flow field-flow fractionation are also used for understanding the size variants (Basle et al., 2020). The analytical methods used to support protein size variants during all phases of development were reviewed by Basle et al. (2020).

1.6.5 High-Throughput Mass Spectrometry-based Methods

Since the 2002 Nobel laureate John Fenn first presented the analysis of proteins by electro-spray ionisation-mass spectrometry (ESI-MS), this technique has become indispensable in the analytical characterisation labs of biopharmaceutical industries and academic research centres (Fenn et al., 1989). Generally hyphened with RPLC separations, ESI-MS detection is widely used for product characterisation during CLD. Thanks to the introduction of high-resolution mass spectrometers (HRMS), such as time-of-flight (TOF), orbitrap and Fourier transform ion cyclotron resonance (FTICR) excellent protein structural characterisation was achieved with a level of accuracy, sensitivity and resolution significantly superior to other analytical techniques (Srebalus-Barnes and Lim, 2007; Rosati et al., 2013; Koen, Vandenheede, and Pat, 2014). Although MS-based methods are usually considered of mid- or low-throughput, several steps forward were taken to speed measurement time, ease of data processing and application to crude samples (Chi et al., 2020).

In this context, recently published scientific papers described the development of HT methods combining fast sample preparation protocols with targeted monitoring of protein product quality attributes (PQAs) at the molecular level by LC-MS (Chi et al., 2020; Wang et al., 2016; Qian et al., 2020; Lanter et al., 2020; Li, 2016). Particularly, Multi-Attribute method (MAM) is gaining momentum amongst the MS-based HT techniques providing a solution for the simultaneous detection, identification and quantitation of multiple PQAs in a single automated method with sensitivity and resolution far superior to other HT tools (Carillo et al. 2021; Wang et al., 2016; Kiss and Gottschalk, 2018). MAM methodology is based on peptide mapping analysis using HRMS instrumentation capable of accurate identification of residue-specific product quality attributes and quantitation (Rogers et al. 2018). When first presented by Rogers et al in 2015, MAM involved a quantitative tryptic-digested peptide mapping method by RPLC-Orbitrap MS (Thermo Scientific Exactive Plus mass spectrometer) combined with automated data processing by Pinpoint software (Thermo Scientific) (Rogers et al., 2015). The MAM method was built based on the MS2 data previously acquired to characterise the molecule of interest – an anti-streptavidin IgG2 – and a Pinpoint workbook reporting each modification. Following, the MS1 only precursor ions were targeted by retention time, accurate mass and isotopic distribution (Rogers et al., 2015). Rogers' method was able to simultaneously monitor the mAb primary sequence coverage and the PTMs on targeted amino acids, namely glycosylation, deamidation, oxidation, isomerisation, and glycation in a single analysis and compared to traditional assays such as HILIC-MS for glycans (Rogers et al., 2015). A few years later, supported by several published works, Rogers restated the advantages of MAM implementation in QbD over conventional profile-based techniques such as chromatographic and electrophoretic separations with UV/Vis or fluorescence detection (Rogers et al., 2018; Xu et al., 2017; Berger and Fredette, 2017; Dong et al., 2016; Zhang and Guo, 2017). Indeed, MAM provides the capability and sensitivity to indicate the site of PTMs and chemical modifications with high specificity, typical of MS-based methods. This is particularly advantageous when such a level of information is required for CQA monitoring and provide the flexibility of application for the analysis of biomolecules other than mAbs (Buettner et al., 2020).

Additionally, the function of New Peak Detection (NPD) can be used to detect new peaks in samples tested against their reference standards empowering a broader detection spectrum. Moreover, several research groups have employed MAM on the intact and subunits (Lanter et al., 2020) as well as incorporating quick, fully automated sample preparation workflows.

These works demonstrated that MAM-based tools can offer a robust HT platform to monitor a product CQAs during process development activities such as clone selection, product comparability, and stability assessment under cGMP environment (Carillo et al. 2021; Zhang, Shah, and Guan, 2019; Rogstad et al., 2019; Jameel, Skoug, and Nesbitt, 2020).

Despite the several advantages, MAM methods remain difficult to develop and require comprehensive knowledge of the structure and sequence liability of the molecule of interest as well as expert scientists. Moreover, scientific literature on MAM application for the assessment of disulphide bond variants and cysteine adducts is scarce since sample preparation protocols generally require reduction (Liu, Ludwig, and Leone, 2019; Rogers et al., 2018; Lanter et al., 2020). Additionally, MAM has so far been inadequate to measure aggregation and higher-order structure (HOS) nor has been used for the site-specific analysis of intact large molecule structure with high sensitivity. Likewise, the analysis of non-proteinaceous molecules such as DNA and RNA has been hindered by the large size of these molecules and the fact that they are not amenable to proteolytic peptide mapping conditions (Rogers et al., 2018). Future applications may, therefore, envisage MAM as an in-process, easy-to-implement, and regulatory-compliant tool for monitoring aggregation and HOS during biopharmaceuticals development.

1.6.6 Challenges in High-Throughput Analysis of Biopharmaceuticals

As reviewed in Section 1.5, HT technologies are increasingly rising as integral elements of biopharmaceutical development activities enabling more rapid and efficient experimental workflows during cell culture, downstream purification and quality assessment (Kiss and Gottschalk, 2018). The use of HT screening platforms based on miniaturised cell culture systems and automation technology has significantly improved the throughput capability of cell culture clone selection and USP development. However, the implementation of small-scale screening studies suffers from analytical bottlenecks (Berkowitz et al., 2012; Guerra, von Stosch, and Glassey, 2019).

Despite the great advancements in HT analytical methodologies based on chromatography, electrophoresis, microfluidics, spectroscopy and mass spectrometry (previously reviewed in Section 1.6), several challenges hamper their application in industrial HTPD workstreams. This is due to the poor comparability with benchmark low-throughput methods and compliance with regulatory requirements. Although several HT analytical technologies may

prove successful, their application in industry settings must conform to the regulatory guidelines for “Analytical Procedures and Methods Validation for Drugs and Biologics” from FDA (US FDA Center for Drug Evaluation and Research, 2015).

Moreover, such methods are difficult to develop due to a series of analytical challenges involving the sample characteristics such as 1) the large number; 2) the complex matrix, due to the rich media composition, cell debris and metabolites; 3) the low amount of material available for analysis, due to both the small volume and the poor productivity of cells during early-stage CLD.

A further challenge of the current HT analytical methods involves the inherent structural complexity of biomolecules. Because of the multiple PTMs, chemical modifications, and HOS impacting on the potency, safety and efficacy, most biopharmaceuticals CQAs are related to the therapeutic protein structure. Hence, thorough structural characterisation is necessary since early-stage development and must be monitored throughout all phases of a biopharmaceutical lifecycle (Kesik-brodacka, 2018). Microfluidic chip capillary electrophoresis devices such as LabChip GXII (Caliper, PerkinElmer Company, Alameda, CA) have been implemented in industry labs and provide platform methods for the analysis of titre, size variants, covalent aggregation, purity, stability, charge and N-glycan profiles and are easy to operate by non-expert scientists (Reema et al., 2012; Wheeler et al., 2014). Despite the low sample volume and time required for the analysis and easiness of operation, these tools lack the resolving power typical of MS-based methods (Lazar, 2011; Chi et al., 2020).

On the other hand, the large molecular size of recombinant proteins constitutes a burden to the HT capability (especially for method sensitivity and detection limits) of the most high-resolving mass spectrometers, such as TOF, Orbitrap and FTICR. Indeed, high-resolution analysis is often time-consuming and requires complex analytical devices resulting in analytical methods with poor levels of parallelisation (Berkowitz et al., 2012). Moreover, protein characterisation analysis often involves lengthy sample preparation steps including purification from cell culture supernatant, buffer-exchange, reduction and digestion procedures. Although automation and HT workflows for purification and sample preparation have successfully been implemented, these strategies are known to cause artefacts.

All these reasons explain how difficult the implementation of HT analytical method development can be and why the current analytical methodologies cannot always cope with

the challenges added by bioprocess requirements. Hence, the need for more efficient analytical tools that can support the development of novel therapeutic candidates in line with the industry regulatory specifications (Guerra, von Stosch, and Glassey, 2019).

1.7 Theoretical framework: Aim of Thesis and Overview

Analytical testing drives biopharmaceutical product development providing the data for key-decision making and regulatory approval (see Section 1.4). Therefore, it is essential for analytical scientists to provide analytical tools that are adequate for their final application and meet the requirements of each development stage. Consequently, analytical development is itself influenced and driven by the technological advancements occurring in other sectors of biopharmaceutical bioprocessing and the respective regulatory requirements. As an example, several research works testify how the analytical technology development of the last few decades has been focusing on improving the throughput and real-time measurement capability of the current methodologies to fit into both the HTPD and PAT framework to meet the requirements of the QbD approach at market pace (see Sections 0, 1.5, and 1.6). However, the implementation of HT analytics for protein characterisation is still hampered by the inherent structural complexity of biologics and process limitations. As previously discussed, HTPD CHO cell engineering tools require effective HT analytical tools supporting quality assessment during early-stage CLD (see Section 1.5.3). However, the low sample amount availability and the need for fast analysis time constitute the bottleneck of the current analytical methodologies and hamper the implementation of thorough PQ characterisation early in the process (Section 1.6.6). Currently, orthogonal assays are used for PQ analysis, each tackling different PQAs. No comprehensive analytical method exists that can simultaneously monitor all the potential PQAs of a recombinant protein with minimal sample consumption and analysis time adequate for enabling fast decision making at the CLD level.

From such a perspective, this research project brings HT analytics to the fore of biopharmaceuticals R&D as an indispensable means for maximising the understanding of the engineering principles behind protein expression and efficiently drive the choice of cell engineering strategies during early-stage product development. The enhancement of the technology throughput is seen as the key enabler for identifying as early as possible both the molecules and process conditions that fail to ultimately enable the provision of life-changing medicines to patients at a time and costs affordable worldwide. This justifies the scientific commitment and endeavours devoted to answering questions such as "*How to extrapolate the maximum amount of meaningful PQ information from the minimum amount of sample in a time window that allows cell engineers to quickly modify their strategies within the CLD*

timescale? How to improve the method sensitivity whilst maintaining the resolution and analysis speed? How to sustainably develop flexible analytical methods for an NBE when the current methods are not fit-for-purpose and how to easily integrate them in the current analytical workflows? How should the future analytical tools be to overcome the limitation of the current technologies and better drive the development of life-changing medicines for unmet medical needs?"

This project focuses on the development of a HT analytical platform for the characterisation of therapeutic proteins expressed in CHO cells. The goal of the research is to maximise the PQ information obtained from minimal sample and time required for the analysis to ultimately support clone selection during CLD. Each analytical method was designed for the screening of samples deriving from small scale cell culture systems such as 96-DWPs and stir-tank MBRs suitable to operate in automated workflows. Most importantly, the analytical tools were developed in line with the industrial requirements for implementation in the analytical workstream in AZ. The final aim of this work is the hyphenation of HT analytics to HT cell line engineering to create a feedback loop system enabling a deeper understanding of the engineering and scientific principles underlying protein expression in CHO cells. The feedback loop system will ultimately be used to control the variables that affect PQ during the CLD process and help to build a smarter biomanufacturing process.

Part A of Chapter 3 presents the development of a HT analytical workflow for the aggregation analysis of proteins expressed in 96-DWP cell cultures. The workflow involves the implementation of a fully automated HT purification method based on resin-filled pipette tips columns followed by analysis of aggregates by SEC. The SEC method was developed using 2.1 mm ID columns allowing for sensitive and rapid analysis of aggregates in mAbs and BsAbs products. Part B presents the implementation of a split-DoE approach for leveraging the development of CEX methods. The focus is the implementation of the split-DoE approach for developing a HT CEX method for charge variants analysis of a mAb candidate.

Chapter 4 presents the combination of both aggregates and charge variants analysis in a unique 2D-LC set up. Method development focuses on coupling SEC in the first dimension (^{1}D) with CEX in the second dimension (^{2}D) by heart-cutting 2D-LC mode. 2D SEC-CEX separations were developed using both non-volatile and volatile solvents. The advantages and disadvantages of UV detection over direct coupling to MS was thoroughly discussed.

The adoption a 2D-LC approach over conventional 1D-LC methods and its implementation to the industrial analytical workhorse was addressed.

Chapter 5 introduces the development of a MS-based method for quantifying aggregates of a BsAb drug candidate. The method is based on a targeted MS method monitoring Cys modifications associated with aggregates formation in the BsAb candidate. Peptides bearing other PQAs such as glycosylation, deamidation, and C-terminal Lys clipping were also monitored by MRM offering a novel MAM workflow for addressing multiple quality attributes in a single method.

Chapter 6 demonstrates the application of the HT methods previously developed to case study samples. The complete analytical platform is integrated to CLD strategies in support of clone selection to drive better decision making.

This page is intentionally left blank

Chapter 2

Materials and Methods

The coming chapter provides the reader with a detailed description of the materials and methods used to complete the experiments described in the following results chapters. The experimental work was carried out in the laboratories of either the Department of Chemical and Biological Engineering at The University of Sheffield or the Department of Biopharmaceutical Development of AstraZeneca in Cambridge.

2.1 Liquid Chromatography-Mass Spectrometry Materials and Equipment

2.1.1 Chemicals and Materials

The preparation of LC mobile phases for SEC and CEX applications involved the use of sodium phosphate dibasic, sodium phosphate buffer monobasic, sodium chloride, hydrochloric acid, sodium hydroxide, hydrochloric acid, ammonium acetate, acetic acid (Sigma-Aldrich), and 2-(N-morpholino)ethanesulfonic acid (MES) (Fisher Scientific). The pH of all the buffers was confirmed by Benchtop pH Meter (Mettler Toledo) and each was filtered with Nalgene™ Rapid-Flow™ Sterile Disposable Filter Units with a 0.2 µm pore size PES Membrane (Thermo Scientific). IonHance CX-MS pH concentrates A & B kit in MS certified LDPE containers (10X concentrates) were purchased from Waters and dedicated to IEX-MS work. All the buffers for non-MS application were prepared by using deionised water dispensed by Barnstead Nanopure Diamond Lab Water System (Thermo Fisher), whereas those dedicated to MS application were prepared by using LC-MS grade water (Merk Group Ltd.). Buffers for RPLC were prepared by using LC-MS grade water, acetonitrile, methanol, isopropanol, trifluoroacetic acid, and formic acid.

Sample preparation involved the use of tris (hydroxymethyl)aminomethane, dithiothreitol (DTT), N-ethylmaleimide (NEM), guanidine, ethylenediaminetetraacetic acid (EDTA), iodoacetamide, urea, 2-(N-morpholino)ethanesulfonic acid (MES) sodium citrate, tris(hydroxymethyl)aminomethane (Tris-base/Tris-HCl), hydrogen peroxide (H_2O_2) solution, α,α′-azodiisobutyramidine dihydrochloride (AAPH) solution (Sigma-Aldrich), microdialysis devices (Thermo Scientific), trypsin and PNGase F (Promega). Buffer exchange prior to analysis was achieved using Zeba TM Spin Desalting Plates 96-well, 7K (Thermo Scientific), and AZ proprietary platform formulation buffer.

2.1.2 LC Equipment

2.1.2.1 1D-LC System

1D-LC analysis was performed using an Agilent 1260 Infinity II UHPLC System equipped with a degasser, quaternary pump, thermostatted multi-sampler, and diode array detector

(DAD) in conjunction with a multi-column compartment with a column selection valve. All LC parts were joined by 1.6 mm OD, 0.12 µm ID stainless steel capillary tubing with stainless steel fittings. System control and data analysis were accomplished with Agilent OpenLAB CDS ChemStation Edition, version C.01.07. Mobile phase recipes and separation gradients were created using the Agilent Buffer Advisor Software with ZedGraph Library, version 5.0.8.20000, and DotNetZip Library, version 1.9.1.5. LC equipment and software packages were all purchased from Agilent Technologies Inc. The JMP® Pro 15.0 statistical software (SAS Institute Inc.) was used for assisting method development by DoE models and data analysis.

2.1.2.2 2D-LC System

2D-LC analysis was conducted on an Agilent 1290 Infinity II system. The first dimension was composed of a quaternary pump with a degasser, an autosampler with a cooler, a thermostatic column compartment, and a multi-wavelength detector (MWD). The second dimension was equipped with a binary pump, a degasser, and a diode-array detector (DAD). The two dimensions were interconnected by the Agilent 1290 Infinity series 2-position/4-port 2D-LC valve head with 80 uL loops and 2x multiple heart-cutting valves equipped with 40 µL loops. All parts of the 2D-LC system were connected with 1.6 mm OD, 0.13 mm ID PEEK tubing with PEEK fittings. Instrument control and data analysis were achieved with Agilent OpenLAB CDS ChemStation Edition, version C.01.07. All LC instrumentation was purchased from Agilent Technologies Inc. This equipment set-up was used for 2D-LC method development and applications. Mass spectrometry hyphenation to 2D-LC separations was achieved by connecting the 2D-LC system DAD to the Q Exactive HF-X hybrid quadrupole-Orbitrap mass spectrometer with ESI (Thermo Scientific) and BioPharma Option. Source parameters were optimised to a spray voltage of 3.5 kV, a capillary temperature of 250 °C, and in-source CID fragmentation of 80 eV. Further information on method development is reported in Chapter 4.

2.1.3 Software for Method Development and Data Analysis

Statistical method development and data analysis were aided by the use of JMP® Pro 15.0 (SAS Institute Inc.) and Python Software Foundation (Python Language Reference, version 3.7, available at http://www.python.org).

2.1.4 Methods

This section summarises additional chromatography equipment used for the development of LC and LC-MS methods. Further information is reported in the results and discussion chapters dedicated to the development and applications of specific methods. Table 2.1 lists all the LC and LC-MS methods developed throughout this research project, the chromatography columns used for method development, and the respective providers.

2.1.4.1 RP-LC-ESI-MS Intact Mass Analysis

Intact mass analysis was conducted on a Waters Acquity UPLC with a vacuum degasser, binary pump, autosampler with a temperature-controlled sample compartment, a dual-wavelength detector, a switching valve to the MS, and Mass Lynx software coupled with the Waters SYNAPT MS with ESI source (Waters Corp.). Reverse phase separation was achieved following a linear gradient using Acquity UPLC® BEH300 C4 1.7 µm 2.1 x 50 mm column (Waters Corp.) column, flow rate of 0.15 mL/min, and temperature maintained at 60 °C. Mobile phase A was 0.01% TFA and 0.1% formic acid in water, and mobile phase B was 0.01% TFA and 0.1% formic acid in acetonitrile. The ESI source was operated in positive ion mode, capillary voltage was set to 3.4 kV, source temperature 120 °C, sampling cone, 40 kV, extraction cone 3 kV, desolvation temperature 400 °C. Mass spectra were collected at an m/z range of 800–4,500. Further information regarding the method, procedure and specifications have been omitted as they are proprietary to AstraZeneca. Data processing was done by BioPharma Finder 3.2 (Thermo Fischer Scientific) and GPMAW 9.51 (Lighthouse data). BioPharma Finder 3.2 was set for ReSpect deconvolution algorithm.

2.1.4.2 RP-LC-ESI-MS Reduced Peptide Mapping

Protein sample concentrations were diluted to 5.0 mg/mL with HPLC-grade water. Sample denaturation consisted in the addition of the denaturing buffer (7.2 M guanidine HCl, 90 mM Tris, 0.1 mM EDTA, 30 mM dithiothreitol, pH 7.4) and incubation at 37 °C for 30 min. After incubation, alkylation was performed by adding 500 mM IAM to each sample to a final concentration of 70 mM and incubating at room temperature for 30 min in the dark. After alkylation, samples were transferred to a Pierce 96-well 10 K MWCO dialysis plate (catalogue no. 88260; Thermo Fisher Scientific) containing dialysis buffer (6 M urea, 150 mM Tris, pH 7.6), which was shaken for 2 h to desalt the samples. Subsequently, the samples

were recovered and digested with Trypsin Gold (Promega) at a mass ratio of 1:12 (enzyme:sample) and incubated at 37 °C for 4 h. Upon completion, the digestion was quenched by 10% TFA. The reduced peptide mapping (RPM) analysis of tryptic digest samples was performed on a Waters Acquity UPLC with a vacuum degasser, binary pump, autosampler with temperature-controlled sample compartment, dual-wavelength detector, switching valve to the MS and Xcalibur software coupled with the Q Exactive HF-X hybrid quadrupole-Orbitrap mass spectrometer with ESI (Thermo Scientific) and BioPharma Option. Acquity UPLC BEH C18 1.7 µm 2.1 x 150 mm column (Waters Corp.) column with temperature set to 55 °C. Mobile phase A was 0.02% TFA in water, and mobile phase B was 0.02% TFA and in acetonitrile. Samples were eluted with a linear gradient at a flow rate of 0.2 mL/min. The ESI source was operated in positive ion mode, capillary voltage was set to 3.5 kV, capillary temperature 320 °C, and mass range of 250–2,000 m/z. Top 5 data-dependent acquisition was used for peptide identification and PTM localisation and the fragmentation mass spectra were obtained by collision-induced dissociation (CID). Tryptic peptides were identified by their mass corresponding to the amino acid composition, and the fragmentation masses were determined by MS2. BioPharma Finder 3.2 was used for data processing. Full methods procedures and specifications have been omitted as they are proprietary to AstraZeneca.

2.1.4.3 RP-LC-ESI-MS EThcD-Assisted Non-Reduced Peptide Mapping

Non-reduced tryptic peptides were obtained by following a protocol developed in AstraZeneca. Samples were diluted to 1 mg/mL. Alkylation was achieved by adding 200 mM N-ethylmaleimide (NEM) solution and incubating at room temperature in the dark for 30 min. Subsequently, the samples were denatured with 8M urea in 100 mM MES buffer, pH 6.0 and digested with trypsin sequencing grade, (Promega, catalogue number V5111) at a mass ratio of 1:12 (enzyme:sample) and incubated at 37 °C for 4 h. Finally, digestion was quenched by 10% TFA. Non-reduced peptide mapping (NRPM) was executed on a Waters Acquity UPLC with a vacuum degasser, binary pump, autosampler with temperature-controlled sample compartment, dual-wavelength detector, switching valve to the MS, and Xcalibur software coupled to the Orbitrap Fusion™ Tribrid™ mass spectrometer with ESI (Thermo Scientific). Reverse phase separation was achieved using ACQUITY UPLC CSH C18 2.1X150mm column maintained at 60°C. Mobile phase A was 0.02% TFA in water, and mobile phase B was 0.02% TFA and in acetonitrile. Samples were eluted by using a 30 min linear gradient with a flow rate of 0.15 mL/min. The ESI source was operated in positive polarity, and mass range of 250–2,500 m/z with 120K resolution, precursor automatic gain control (AGC) target was set to 2×10^5, and the maximum injection time was set to 50 ms. The MS/MS method was programmed in the data dependent acquisition mode with the 5 most intense peaks subjected EThcD fragmentation with 30K resolution, an automatic gain control (AGC) target of 5×10^4, and maximum injection time of 54 ms. As the method was developed in AstraZeneca, the source and fragmentation parameters were optimised for in-house application but the details are reserved and proprietary of the company. Thermo Xcalibur ™ Software was used for data processing.

2.1.4.4 RP-LC-ESI-MS Non-Reduced Peptide Multiple-Reaction Monitoring

The preparation of non-reduced tryptic peptides was conducted on a Tecan Freedom EVO® 200 robotic liquid handling platform (TECAN Group Ltd.) equipped with a positive pressure HEPA enclosure, a Tecan Liquid Handling (LiHa) arm, and a MultiChannel Arm™ (MCA) 96. Consumables included 25 mL troughs (TECAN Group Ltd.), reagent rack, 1.5 mL Eppendorf tubes, 96-well PCR plates (Thermo Scientific) Greiner 96-well plates with u-bottom with half skirt Eppendorf on top (Greiner Bio-One Ltd.) and 96-well 1 mL V-bottom plate (Waters Corp.). The automation script was written by Samuel Shepherd (AstraZeneca) on Freedom EVOware®, Version 2.7 (TECAN Group Ltd.). NRPM analysis was executed

on a Waters Acquity UPLC with a vacuum degasser, binary pump, autosampler with temperature-controlled sample compartment, CSH C18 130A, 1.7, 1 mm x 150 mm RP-LC column, dual-wavelength detector, switching valve to the MS and Mass Lynx software coupled with the Xevo TQ-S triple quadrupole mass spectrometer with ESI (Waters Corp.). The MS system was operated in multiple-reaction monitoring (MRM) mode which involved filtering of the peptide precursor ions a specific mass-to-charge (m/z) in the first quadrupole (Q1). Subsequently, the precursor ions entering the collision cells (q) were subjected to fragmentation. Finally, the precursor ion fragments with a predefined m/z were filtered in the third quadrupole (Q3) and detected. LC-MS buffers were prepared in-house and the recipes are property of AstraZeneca.

Skyline software was used for the optimisation of the peptides transition list and fragmentation parameters as well as for data analysis. Three transitions were monitored for each peptide precursor ion, of which the most intense fragment ion was used for quantification, whilst the other two served as qualifier ions. The cone voltage and collision energy were optimised for each peptide and the duty cycle was reduced to 0.02 s targeting each peptide for a 1-3 min time window. More information on method development is reported in Chapter 5. JMP® Pro 15.0 (SAS Institute Inc.), and Python Software Foundation (Python Language Reference, version 3.7 available at http://www.python.org) were used for automated data processing and visualisation. The data processing workflow involved various steps encompassing 1) the calculation of the ratio between the qualifier ion *vs.* the quantifier ion peak area of each peptide monitored; 2) the calculation of the coefficient of variation (CV) of each qualifier/quantifier peptide ratio; 3) the relative quantification of each quality attribute displayed as %area of the modified species peak *vs.* the %area of the unmodified species peak. For accurate quantification analysis, the qualifier/quantifier peptide ratio CV was required to be < 20%.

Table 2.1 List of the LC and LC-MS methods and the columns used for method development with their respective providers and final applications

Method	Column	Provider	Application	Reference
HT SEC	ACQUITY UPLC Protein BEH SEC 200 Å, 2.1 x 150 mm, 1.7 µm	Waters	Aggregates	Chapter 3, Part A, Section 3.3.2
	Unix™-C SEC-300, 300 Å, 2.1 x 150 mm, 1.9 µm	Sepax	Aggregates	
HT CEX	AgilentBio WCX column 2.1 x 50 mm, 5 um, np	Agilent	Charge variants	Chapter 3, Part B
	BioResolve SCX mAb 2.1 x 40 mm, 3 µm, np	Waters	Charge variants	
	bioZen WCX 2.1 x 50 mm, 6 um, np	Phenomenex	Charge variants	
	Proteomix SCX 2.1 x 50 mm, 1.7 um, np	Sepax	Charge variants	
2D SEX-CEX-UV	ACQUITY UPLC Protein BEH SEC 200 Å, 4.6 x 150 mm, 1.7 µm column	Waters	Aggregates	Chapter 4
	Agilent AdvanceBio SEC 200A, 4.6 x 150 mm, 1.9 µm	Agilent	Aggregates	
	bioZen™ 4.6 x 150 mm, 1.8 µm	Phenomenex	Aggregates	
	Agilent: AgilentBio WCX column 2.1 x 50 mm, 5 um, np	Agilent	Charge variants	
2D SEX-CEX-UV-MS	Agilent AdvanceBio SEC 200A, 4.6 x 150 mm, 1.9 µm	Agilent	Aggregates	Chapter 4
	BioResolve SCX mAb column, 3 µm, 2.1 mm x 50 mm	Agilent	Charge variants	
MAM	CSH C18 130A, 1.7, 1 mm x 150 mm RPLC	Waters	BsAb-1 PTMs	Chapter 5

2.1.5 Samples used for Method Development, as Controls and System Suitability Checks

The samples used for method development were all CHO-derived and provided by AstraZeneca, namely mAb-1 and mAb-2 reference standards (RS) and BsAb-1 and BsAb-2 reference materials (RM). Proof-of-concept application of the analytical methods was achieved using samples generated by the Cell Line Development (CLD) team in AstraZeneca and Prof David C. James's research team at the University of Sheffield. Detailed information on all the samples used during method development, system suitability (SST) checks, control and application of all the methods developed in this research project are summarised in Table 2.2.

Table 2.2 Summary of the samples used for research with the respective providers and application description.

Sample	Provider	Application
mAb-1, BsAb-1	AstraZeneca	PhyTip purification development
mAb-1, BsAb-1, BsAb-2	AstraZeneca	PhyTip purification application
mAb-1, BsAb-1	AstraZeneca	PhyTip purification control
Gel Filtration Standard	Bio-Rad Laboratories	HT SEC SST
Heat-stressed mAb-1, heat-stressed mAb-2, BsAb-1 RM, BsAb-2 RM.	AstraZeneca	HT SEC development
mAb-1 RS and BsAb-1 RM	AstraZeneca	HT SEC control
BsAb-1, BsAb-2	AstraZeneca/The University of Sheffield	HT SEC proof-of-concept application
mAb-1 RS	AstraZeneca	HT CEX and 2D SEC-CEX-UV(MS) development and control
Stressed mAb-1	AstraZeneca	HT CEX and 2D SEC-CEX-UV(MS) proof-of-concept application
mAb-1	The University of Sheffield	2D SEC-CEX-UV application
Peptide Retention Time Calibration Mixture	Thermo Scientific	MAM SST 1
NR tryptic digested BsAb-1 RM	AstraZeneca	MAM SST 2
BsAb-1	AstraZeneca	MAM development
BsAb-1	AstraZeneca/The University of Sheffield	MAM proof-of-concept application
Peptide Retention Time Calibration Mixture	Thermo Scientific	RPM SST
mAb-2	AstraZeneca	RPM control
mAb-2	AstraZeneca	Intact mass analysis SST/control

2.2 Purification of CHO Cell Culture

2.2.1 Chemicals

Gibco 1x Dulbecco phosphate buffer (DPBS) (Thermo Fisher Scientific), acetic acid glacial, hydrochloric acid, methanol, ethanol and isopropanol (Merk Group Ltd.), glycine hydrochloride, L-histidine hydrochloride monohydrate, sodium acetate anhydrous, sodium chloride, sodium hydroxide, and sucrose (Sigma-Aldrich) were used for protein purification and column storage buffers.

2.2.2 Low-Throughput Purification

The purification protocol was developed by Jennifer Spooner (AstraZeneca) and adapted for this work. Purification was performed using HiTrap MabSelect SuRe 1 mL columns on the ÄKTAxpress™ system, and data were analysed by Unicorn 5.31 software (GE Healthcare Life Sciences). After purification, the samples were buffer exchanged into formulation buffer using disposable PD 10 desalting columns (Merck Group Ltd.). Details of the purification procedure and buffer composition are proprietary to AstraZeneca.

2.2.3 High-Throughput Purification

PhyTip 200 µL volume columns, containing 20 µL of ProPlus (MabSelect SuRe™) affinity resin (PhyNexus Inc.) were operated on a Tecan Freedom EVO® 200 robotic liquid handling platform (TECAN Group Ltd.) equipped with a positive pressure HEPA enclosure, Tecan Liquid Handling (LiHa) arm, and MultiChannel Arm™ (MCA) 96. Consumables used included 25 mL, 100 mL, and 300 mL troughs (TECAN Group Ltd.), 96-well DWP, 2.2 mL, deep-well plates (Thermo Fisher Scientific), Greiner 96-well plates with u-bottom (Greiner Bio-One Ltd.), and V-squared bottom 96-well plates (Agilent Technologies Inc.). All the automation scripts were written by Samuel Shepherd (AstraZeneca,) on Freedom EVOware®, Version 2.7 (TECAN Group Ltd.). The high-throughput (HT) purification procedure and its development are described in Chapter 3 with more information on buffers composition reported in Section 3.3.1.

2.3 CHO Cell Culture

Research involving mammalian cell culture, product purification and analysis were carried out in separate laboratories to prevent cell contamination and ensure culture sterility. Materials and consumables were purchased with high quality and cell culture grade. Single-use sterile material was used for cell culture, particularly when coming into direct contact with living cells. Sterilisation of reusable consumables was achieved by autoclavation at 121 °C as well as membrane filtration with 0.22 µm pore size sterile membranes. Class 2 HEPA filtered laminar airflow cabinets served for handling mammalian cell culture material during experiments and guaranteed cleanliness of the work zone along with protection of both user and samples. All surfaces and consumables were decontaminated with 70% ethanol before entering the airflow cabinet.

2.3.1 Cell Lines and Model Molecules

The cell lines and molecules used for this research are proprietary to AstraZeneca. The company kindly provided pool and clone-derived CAT-S CHO cell lines which were transfected for the expression of an IgG1, kappa monoclonal antibody (mAb-1), and two bispecific antibodies (BsAb-1 and BsAb-2) dedicated to research work.

2.3.2 Cell Culture Maintenance

Routine maintenance involved the culture of cells in vented Erlenmeyer flasks (Corning) using CD-CHO medium (Thermo Fisher Scientific) supplemented with 50 mM L-Methionine sulfoximine (MSX, Sigma-Aldrich). The cell culture volumes used were 20-25% of Erlenmeyer flask total volume. Flasks were incubated at a temperature of 37 °C, in 5% (v/v) CO_2, and shaken at 140 rpm. Cells were subcultured at a density of 0.3 x 106 cells/mL on a 3 to 4 days schedule to ensure the maintenance of exponential growth. To minimise genetic drift, cells were subcultured up to a maximum of 15 passages. The average cell viability, cell density, and diameter were determined by a ViCell viability analyser (Beckman-Coulter).

2.3.3 Cryopreservation, Cell Bank Generation and Revival

Recombinant GS-CHO cells were frozen and revived following standardised protocols to ensure consistent and successful recovery of the cells after storage in liquid nitrogen. Master and working cell banks were created for the cell lines received from AstraZeneca. The generation of cell banks consisted of cell pelleting three days after subculture (mid-exponential phase) by centrifugation at 130 x g for 8 minutes and resuspension at a concentration of 1 x 10E+7 cells/mL in CD-CHO media containing 10% DMSO (Sigma-Aldrich). Aliquots of 1.5 mL were assorted into NUNC cryovials (Thermo Fisher Scientific) and stored in "Mr Frosty" containers (Thermo Fisher Scientific), filled with 100% isopropanol, at -80 °C overnight to allow gradual freezing of cell solutions. Cryovials were then transferred to a liquid nitrogen freezer (-196 °C) for long-term storage. Cell revival from liquid nitrogen storage was carried out by thawing at 37 °C and subsequent addition of 30 mL of pre-warmed non-supplemented CD-CHO media to the cell solution. After determination of viability and viable cell density (VCD), cells were finally seeded with 25 mL CD-CHO/MSX media at a concentration of 0.3 x 10E+6 cells/mL, in a 125 mL Erlenmeyer flask. These cells were labelled "Day 0" and were subcultured two days after the first passage and subsequently on a 3- to 4-day regime. Cells were acclimatised to these conditions for four subcultures before being used for any experimental work.

2.3.4 Shake-Flasks Fed-Batch Overgrows of CHO Cells

All the fed-batch overgrows were set up 3 days post-subculture and seeded at a density of 0.7 x 10E+6 cells/mL in CD-CHO media supplemented with AstraZeneca proprietary in-house feed. Cells were counted on a ViCell viability analyser on the day of seeding to check the variation in seeding between cultures when required. Subsequently, cells were sampled on a 2-day regime and all ViCell measurements were carried out with a 1:4 dilution. Additional feeding was supplemented on the third day from the start of the overgrow and carried on a 2-day schedule. Metabolites and glucose consumption analysis were carried out using a YSI 2950D Biochemistry Analyzer (YSI Life Sciences). For this assay, 200 µL of cell culture was aliquoted and centrifuged at 4000 g before analysis. When the glucose concentration was below 10 g/L, an in-house glucose supplement was added to feedback to 10 g/L. Samples for titer analysis were taken from day 7 until the end of the culture.

2.3.5 Harvesting

At the end of the overgrowth, cell culture supernatants were harvested by centrifugation at 2500 rpm for 90 min and filtered with Nalgene™ Rapid-Flow™ Sterile Disposable Filter Units with a 0.2 µm pore size PES Membrane (Thermo Fisher Scientific).

2.4 Recombinant Protein Quantification

2.4.1 Titre Analysis by Analytical Protein-A Affinity Chromatography

High-throughput analytical Protein-A affinity chromatography was carried out on an Agilent 1200 HPLC system (Agilent Technologies) equipped with a degasser, binary pump, well plate autosampler, column oven, UV detector, and Agilent ChemStation software. The separation was performed using an analytical HPLC column packed with POROS™ A functionalised beads with 20 µm particle size, 2.1 mm x 30 mm (ID x L), and 0.1 mL bed volume (Applied Biosystems, Inc.) and HPLC grade water (Merk Group Ltd.). The mobile phase was prepared using sodium phosphate, sodium chloride, hydrochloric acid, and sodium hydroxide purchased from Sigma-Aldrich. Buffer A was composed of 10 mM sodium phosphate and 150 mM sodium chloride at pH 7.2 whereas buffer B was composed of 12 mM hydrochloric acid and 150 mM sodium chloride at pH 2.0. All buffers were filtered with Nalgene™ Rapid-Flow™ Sterile Disposable Filter Units with a 0.2 µm pore size PES Membrane (Thermo Fisher Scientific). Protein concentration was extrapolated from molecule-specific standard curves generated from purified material in the range 10 mg/L – 10 g/L.

2.4.2 UV/Vis Absorption Spectroscopy

UV/Vis absorption measurements were collected using the Stunner (Unchained Labs) and the DropSense 96 (Trinean). Each plate was loaded with 2-3 µL of sample and measured immediately by the spectrophotometer.

2.5 Equations

2.5.1 Chromatography Peak Analysis

Detailed below are the equations used for chromatography peak analysis.

Tailing factor or Symmetry factor

$$T_S = \frac{\omega_{0.05}}{2f} \quad (2.5.1.1)$$

Tailing factor (USP) or Symmetry factor (EP, BP, JP), where ω is the peak width at 5% peak height, and *f* is the distance from the peak apex to the leading edge of the peak measured at 5% of the peak height.

Resolution

$$Rs = \frac{(2.35/2)(t_{R1} - t_{R2})}{\omega_1 + \omega_2} \quad (2.5.1.2)$$

Resolution (EP) where, t_{R1} and t_{R2} are the retention time and $\omega_1$and ω_2 are the widths of the first peak, and second peaks, respectively.

Experimental Peak Capacity (ePC)

$$ePC = \frac{t_{Rz} - t_{Ra}}{\omega} \quad (2.5.1.3)$$

Experimental peak capacity (ePC), where t_{Rz} is the retention time of the last peak in the chromatogram, t_{Ra} is the retention time of the last peak in the chromatogram, and ω is the peak width of a reference peak in the chromatogram.

2.5.2 Method Assessment

Proportional protein load (PPL)

$$PPL = \frac{\mu(A_1)}{\mu(A_{total})}\ x\ PL\ (\mu g) \quad (2.5.2.4)$$

Proportional protein load (PPL), where $\mu(A_1)$ is the mean of the target peak area, $\mu(A_{total})$ is the mean total peak area of all the peaks in a chromatogram, and PL is the protein load.

Limit of quantification (LOQ)

$$\text{LOQ } (\mu g) = \frac{10 \text{ x } \sigma}{S} \quad (2.5.2.5)$$

Limit of quantification (LOQ), where σ is the standard deviation amongst the replicates at a specific level of the linearity study, and S is the slope of the calibration curve.

Per cent limit of quantification

$$\text{LOQ } (\%) = \frac{\text{LOQ } (\mu g)}{PL\ (\mu g)}\ x\ 100 \quad (2.5.2.6)$$

Per cent limit of quantification (LOQ %), where LOQ is the method LOQ in μg, and PL is the protein load in μg.

Limit of Detection (LOD)

$$\text{LOD} = \frac{LOQ}{3} \quad (2.5.2.7)$$

2.6 Statistics

2.6.1 Actual-by-Predicted Plot

The actual-by-predicted plot is a scatter plot displaying the observed response (x) on the abscissa *vs.* those predicted (Y) by the model on the ordinate. The horizontal blue line corresponds to the null hypothesis (the response does not depend on the factors) and the slanted red line to the alternative hypothesis (the response depends on the factors). The 95% confidence interval is indicated by the red shading region. If the horizontal blue line is contained within the red shaded region then the model is not significant at the alfa level 0.05. Conversely, if the blue line is not contained within the red region, the model is significant at the same alfa level. The plot was also used in this manuscript to determine the model "lack of fit". When unbiased, a prediction should produce estimates that agree with the observed values on average. Thus, the red line should go through the middle of the data points. On the other hand, the data points generated by a biased model will deviate from the line. The goodness of fit in the actual-by-predicted plot was evaluated in terms of coefficient of determination (R^2) and root mean square error (RMSE), whilst the model significance is given by the p-value.

2.6.2 Effect Summary Report

The model effects correspond to all the factors and their interactions investigated by the model. The effect summary reports presented in this manuscript list all the effects estimated by models that contained more than one effect. Each model effect was reported together with its false discovery rate -log10(p-value) (FDR LogWorth) and FDR p-value. The FDR LogWorth transformation adjusted the p-value to display a scale of graphing, where values that exceeded 2 (normally indicated as a blue line) were significant at the 0.01 level. The bar chart of the FDR LogWorth displays dashed vertical lines at integer values. The FDR was calculated using the Benjamini-Hochberg technique (Benjamini 1995).

2.6.3 Parameter Estimates Table

The model parameter estimates are shown for each model parameter together with the t-test results for hypothesis equals to zero. The "*Term"* column corresponds to the estimated parameter with the intercept always reported as the first term. The estimates of the model coefficients of each term are reported under "*Estimate*". The sign of the coefficient indicates whether the correlation is positive (+) or negative (-), whilst the coefficient value represents how much the mean of the dependent variable (Y) varies given a one-unit shift in the independent variable (x_n) while holding the other variable constant. The standard error of the estimated parameters is reported under "*Std Error"* and computed using equation (2.6.3.8). The t-test results are listed under "*t Ratio"* and reported as the ratio of the estimates to their respective standard error given the t Ratio having a Student's t-distribution under the null hypothesis as per (2.6.3.9); where $\bar{x}$ is the sample mean, μ_0 is the population mean, s is the standard deviation, and $\sqrt{n}$ is the square root of the sample size. The 'Prob>|t|' column lists the p-value of the two-tailed hypothesis test.

Standard Error (SE)

$$SE = \sigma/\sqrt{n} \tag{2.6.3.8}$$

t Ratio

$$t = \frac{\bar{x} - \mu_0}{s/\sqrt{n}} \tag{2.6.3.9}$$

2.6.4 Prediction Profiler

The prediction profiler was used to display the conditional relationship between the response (Y) and a given predictor (X), given the level selected on the other predictors (X_1, X_2, X_3, X_n, etc.). The graph provides a visual representation of the interactions between the variables and how the response is dependent on them.

2.6.5 Desirability Function

The desirability function approach was used for optimisation and the identification of the operating conditions (factors setting in a DoE model) that provide the "most desirable" response. The desirability function, $d_i(Y_i)$, assigns a value from 0 to 1 for each response, $Y_i(x)$, with $d_i(Y_i) = 0$ representing the most undesirable value and $d_i(Y_i) = 1$

corresponding to the most desirable response. The geometric mean is used to combine the individual response desirabilities to obtain overall desirability. Different desirability functions can be used depending on whether the response, $Y_i(x)$, is to be maximised, minimised or assigned to a target value. The type of desirability function used in this manuscript was the one proposed by Derringer and Suich (1980): let L_i, U_i, and T_i be the lower, upper, and target values desired for response i, where $L_i < T_i < U_i$, the desirability function of i is:

Desirability function

$$\mathrm{d}(\hat{Y}_i) = \begin{cases} O & if\ \ \hat{Y}_i(x) < L_i \\ \left(\frac{\hat{Y}_{(x)}-L_i}{T_i-L_i}\right)^s & if\ \ L_i \leq \hat{Y}_i(x) \leq T_i \\ \left(\frac{\hat{Y}_{(X)}-U_i}{T\mathrm{i}-v_i}\right)^t & if\ \ T_i \leq \hat{Y}_i(x) \leq U_i \\ 0 & if\ \ \hat{Y}_i(x) > U_i \end{cases} \qquad (2.6.5.10)$$

Where the exponents *s* and *t* indicate the importance of each target value.

This page was intentionally left blank

Chapter 3

Part A: High-throughput platform workflow for the purification and aggregation analysis of mAbs and BsAbs

3.1 Abstract

Scale-down cell culture systems such as shaken deep-well plates (DWPs) offer a valuable approach in high-throughput process development (HTPD) for screening several clones and process conditions to ultimately reduce costs and accelerate cell line development (CLD). Due to the small cell culture volume and low expression titres, the selection of both clone and process conditions is often limited by cell productivity. Product quality (PQ) analysis is generally carried out at a later stage when the titre levels are high enough to allow sufficient material for analytical testing. Purification of the therapeutic proteins from the host cell culture fluid (HCCF) is often required before analytical characterisation. Protein aggregation is a critical quality attribute (CQA) of monoclonal antibodies (mAbs) and bispecific antibodies (BsAbs), compromising the safety and efficacy of the protein. Size-exclusion chromatography (SEC) is the industry standard analytical methodology for the analysis of aggregates. However, its implementation as a highly sensitive small-scale analytical tool in the biopharmaceutical industry has been hampered by the considerable drop in resolution (Rs) resulting from the use of narrow ID columns. Here is presented the development of a fully automated platform workflow for the purification of mAbs and BsAbs expressed in 96-DWP cell cultures, combined with rapid small-scale SEC analysis with sub-2 μg sensitivity. Protein purification by resin-filled pipette tip columns was successfully automated on a robotic liquid handler for the parallel processing of 96 samples at a time. At-line coupling of SEC on a 2.1 mm ID column enabled highly sensitive characterisation of protein aggregates with a 3.5 min run time per injection. The entire workflow was designed to apply to mAbs and mAb-like next-generation biopharmaceuticals, empowering the CLD process with an analytical ranking tool for clone selection as described in Chapter 6.

3.2 Introduction

As previously mentioned (Chapter 1, Section 1.1.3), mAbs continue to dominate the biopharmaceutical market whilst next-generation biopharmaceuticals, such as BsAbs, promise to revolutionise tumour immunotherapy (Reichert, 2019; Kontermann and Brinkmann, 2015). Cell line development and engineering (CLD&E) are the first steps of biopharmaceutical process development and aim to generate high-producing clones that express the product of interest with the desirable PQ (Tihanyi and Nyitray, 2021). Scale-down cell culture systems, such as shaken DWPs have successfully been employed in HTPD for clone selection (Cartwright et al., 2020) and optimisation of the media and supplements composition (Sokolov et al., 2017). This approach enables the execution of large screening experiments and has proven advantageous in reducing the time and costs for CLD.

Biopharmaceutical process development relies on analytical methods at all stages of a product life cycle to ensure the entrance of safe and efficacious drugs to market. However, the implementation of analytical testing to small-scale cell culture systems is hampered by the low expression titres and limited sample volume available for analysis. Thus, the selection of both clones and process conditions during the very early stages of CLD is often driven by expression titre, whilst PQ data are introduced at a later stage. Microfluidics-based platforms such as LabChip GXII (PerkinElmer) have successfully been applied for the HT analysis of protein size, purity, and glycans (Gerster et al., 2016; Scheller, 2021). However, chip-based techniques use denaturing conditions for the analysis and when it comes to sizing large biomolecules, they lack sufficient Rs for the separation of high-molecular-weight species (HMWS). Therefore, aggregates analysis is often carried out by size-exclusion chromatography (SEC) (Garripelli, Wu, and Gupta, 2020). Despite the great advancements in SEC column technology for UHPLC operations, the use of small-scale ID columns has been limited by the poor resolving power of this mode of chromatography (3.3.2.1). The use of large ID columns may hamper the sensitivity of SEC methods thus, their application for the analysis of low concentrated samples.

Another challenge of developing analytical methods to support biopharmaceutical development is their easiness of operation and flexibility of application to a variety of molecular formats. Because HT tools are often expected to be used for routine testing, they must be simple, robust and easy to perform by non-expert scientists. Moreover, they should

provide a platform approach for a defined class of molecules thus, minimising the need for additional method development.

Part A of this chapter presents the development of a high-throughput (HT) analytical platform workflow integrating the purification of mAbs and BsAbs expressed in 96-DWP cell cultures systems with aggregation analysis. This study aimed to design an analytical workflow suitable to work at microscales and providing with PQ data with minimal sample requirements. The analytical procedure was destined to be implemented as a HT routine testing tool to support CLD. Therefore, the choice of the technology used for both purification and aggregation analysis was driven by their ease of operations and potential for automation. Protein-A resin-filled pipette tips were adopted due to their feasibility in processing small cell culture volumes providing purified and enriched material for analytical testing. Robotic liquid handling enabled the automation and parallel purification of 96 samples at a time. The development of a rapid small-scale SEC method on a 2.1 mm ID column allowed for aggregation analysis with sub-µg sensitivity and automated processing of a 96-DWP on an LC system. This established the development of a HT engine to link PQ to cell engineering strategies to help guide the CLD process and maximise efficiency. Application of the method is described in Chapter 6.

3.3 Results and Discussions

3.3.1 A Fully Automated Platform Method for Small Scale Purification mAbs and BsAbs by PhyTip Columns

3.3.1.1 Overview

This experiment aimed to develop a fully automated analytical platform to enable high yield purification of mAbs and BsAbs expressed in small scale cell culture systems. The method was designed to be suitable for the purification of 300 μL HCCF in 96-DWPs. Resin-filled pipette-tip technology for affinity chromatography was implemented as a purification tool in this research due to the established superior capability in handling low-volume samples (< 1 mL) over other commercial products (Evans et al., 2017). Moreover, this methodology is amenable to automated workflows and is flexible for application to a plethora of molecules and cell culture scales thanks to the variety of resin chemistries and tip volumes available (Matte, 2020). PhyTip columns (PhyNexus Inc.) are an example of commercially available resin-filled pipette-tips suitable for HT applications and designed for parallel operation on robotic liquid handlers for automated laboratory workflows (Tecan Group Ltd., 2010). Protein purification by PhyTip columns is governed by the fundamental principles of Dual Flow Chromatography (DFC) (PhyNexus Inc.), characterised by a controlled bidirectional flow of sample and mobile phase travelling in and out/back and forth in all the steps of the process including sample loading (capture), washing, and elution (Bonn, 2017). This is fundamentally different from traditional flow-through chromatography where samples and mobile phases are pumped in and out of the column unidirectionally. The physical and mechanical properties of the DFC columns differ from those employed for flow-through chromatography to facilitate the control of the fluids through the column. Likewise, the control of chromatographic selectivity is also different. The time for interaction between the protein and the resin plays a critical role to maximise both protein binding and final recovery. In DFC, this can be controlled by adjusting the volume of the fluids processed during each aspirate/dispense cycle (processing volume), the number of cycles, and the flow rate (F) in each purification step. In this context, the use of a programmable robotic system was key for controlling the F of liquid aspiration and dispensing to modulate the time of interaction of the target protein with the resin bed to maximise sample recovery. The robotic arm was also

required for positioning and holding the pipette-tip at adequate height from the well bottom to facilitate the bidirectional flow. Figure 3.1 illustrates the mechanism of DFC applied to protein purification.

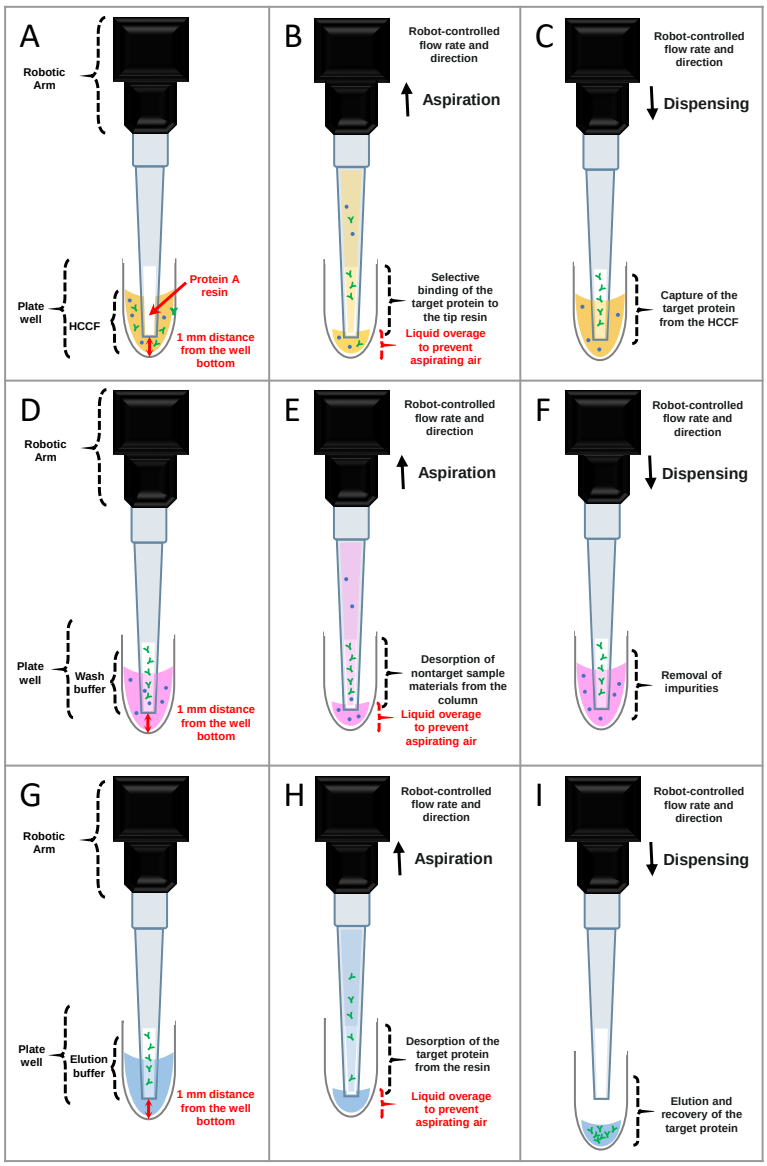

Figure 3.1 Schematic representation of DFC mechanism on resin-filled pipette-tips. A) The pipette-tip packed with protein A resin is dipped into the HCCF containing the expressed biopharmaceutical together with a mixture of host cell proteins (HCPs). The tip is positioned at 1 mm height from the bottom of the well to facilitate the continuous in/out flow. B) The robotic arm is used to aspirate the HCCF with a controlled F, whilst the protein of interest binds selectively to the protein A resin bed at the tip end. Liquid overage avoids the entrance of air into the system whilst aspirating. After aspiration, the liquid is held for a set time before being dispensed. C) The robotic arm dispenses the liquid out of the tip at a controlled F whilst the target protein remains bound to the resin. D) The pipette tip is dipped into the wash buffer solution. E) Aspiration of the wash buffer and desorption of the nontarget sample materials from the resin. F) Liquid dispensing and removal of the HCCP impurities. G) The pipette-tip resin binding the target protein is immersed into the elution buffer. H) The elution buffer is aspirated and (I) dispensed causing the target protein to completely desorb from the resin bed and finally being recovered. The aspirate/dispense cycles during the capture, wash and elution steps can be repeated several times to maximise the protein binding.

Initial work demonstrating the application of the PhyTip columns was performed using clarified supernatants of a CHO cell line expressing a mAb (IgG1, κ). The SDS-PAGE gel run under non-reducing conditions (Figure 3.2) demonstrated the successful purification of the mAb from HCCF by PhyTip methodology. The intact mAb was selectively bound to the resin during the capture step (Figure 3.2, 1) whilst the other HCPs present in the HCCF, the free mAb heavy chain (HC) and light chain (LC) were left unbound (Figure 3.2, 2). Successively, 2 washing steps were performed to release any impurity that might have been non-specifically bound to the column (Figure 3.2, 3 and 4). Lastly, the intact mAb was successfully eluted and enriched in the final step. More information on the buffers used was reported in Chapter 2, Section 2.1.1).

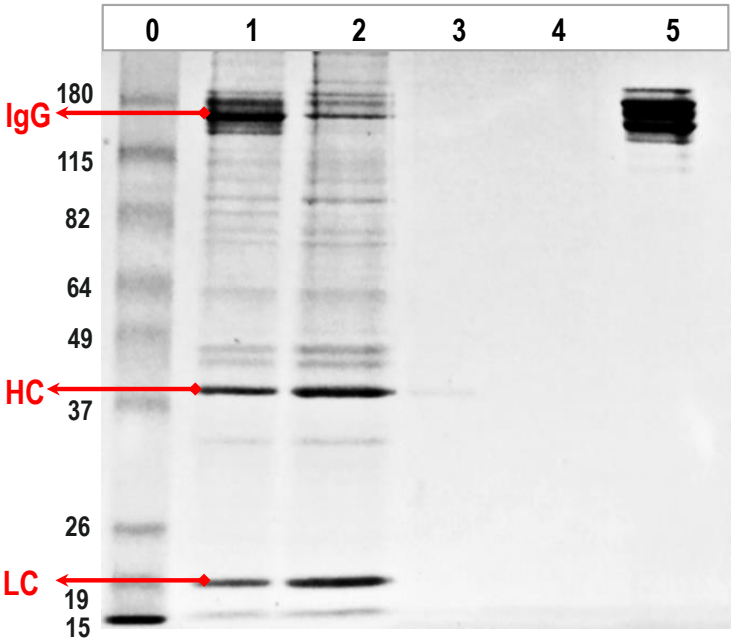

Figure 3.2 Non-reducing SDS-PAGE gel electrophoretogram of the purification of a mAb from the cell culture supernatant.
Non-reducing SDS-PAGE gel electrophoretogram showing the steps involved in the PhyTip purification methodology: 0) Protein ladder; 1) 15 µL loading of cell culture supernatants from a cell line expressing mAb-1; 2) 15 µL loading of the supernatants unbound after the capture step; 3 and 4) 15 µL loading of the sample left unbound after the washing steps; 5) 5 µL loading of the purified mAb recovered from the affinity resin.

During early-stage CLD, expression titres are often scarce. This is particularly accentuated when both transient expression and microscale bioreactors systems such as 24- and 96-DWPs are used. Desirable protein recovery achieved by standard HT purification methodologies is usually in the range of 70-90%. Maximising the sample recovery during

purification is key for enabling successive analytical testing. Thus, the proposed DoE strategy was focused on the identification and subsequent optimisation of the purification process parameters that enhanced protein recovery. Two model molecules, mAb-1 and BsAb-1, were selected as being representative of each molecule class and used throughout method development. A flexible script was written by AstraZeneca to aid the execution of the DoEs on the Tecan robotic liquid handler. Further description of the equipment and chemicals used for the PhyTip purification was given in Section 2.2.3.

3.3.1.2 DoE1: Screening DoE

Despite the apparent ease of operating the PhyTip affinity purification, several factors may impact the total sample recovery. Based on the fundamental understanding of the DFC principles, the main effects screening design (MESD) was used to evaluate which process parameters during the capture, wash and elution steps most importantly impact on the sample recovery. The process parameters studied for each purification step were the number of aspirating/dispensing cycles and F. Additionally, the volume of elution buffer was included as a factor in the MESD since, in theory, larger processing volumes increase the time of interaction of the protein with the affinity resin. To generate a consistent starting material for method development that would be representative of HCCF, the samples of mAb-1 and BsAb-1 were diluted in cell culture media in bulk at a concentration of 2 mg/mL. Based on the standard 96-DWP cell culture scale, the sample volume at the start of the purification was 300 µL. Thus, the initial PhyTip column loading was at ~75% of the resin capacity, this being the theoretical capacity of a 20 µL resin bed at ~800 µg. Analytical Protein A chromatography was performed to verify the sample concentration before purification to allow accurate estimations of the protein per cent recovery (%R). The processing volumes were kept constant at 160 µL for all the steps except during the elution where it was varied from 80-120 µL according to the MESD. A 20% volume overage was introduced in all the wells to avoid the aspiration of air in the system. The final sample concentration was calculated by UV absorbance at 280 nm and used to address the %R. The factors evaluated and analysis conditions are summarised in Appendix A, Table 9.1. The MESD comprised 16 treatments analysed in duplicate, resulting in 32 samples in total. Linear regression analysis was used to build an empirical model to identify the factors that most significantly correlate with an improved %R. The model demonstrated a good fit with coefficients of determination were $R^2 \geq 0.85$ and p-value ≤ 0.05 for both molecules (Appendix A, Figure

9.1). As shown in Table 3.1, both the number of capture cycles and F were statistically significant for the %R of both molecules, with the final elution volume also significant for BsAb-1.

Table 3.1 Summary of estimates of the PhyTip purification MESD model parameters with t-test results

mAb-1 Parameter Estimates				
Term	**Estimate**	**Std Error**	**t Ratio**	**Prob>|t|**
Intercept	16.89	1.67	10.09	<.0001*
Capture cycles (4,15)	5.56	1.67	3.32	0.0031*
Capture F (μL/sec)(4,16)	-3.63	1.67	-2.17	0.0410*
Wash1 cycles (1,3)	2.37	1.67	1.42	0.1701
Wash1 F (μL/sec)(4,16)	-2.24	1.67	-1.34	0.1949
Wash2 cycles (1,3)	-0.31	1.67	-0.18	0.8556
Wash2 (μL/sec)(4,16)	-2.84	1.67	-1.70	0.1037
Elution cycles (4,15)	-2.28	1.67	-1.36	0.1877
Elution F (μL/sec)(4,16)	-0.04	1.67	-0.02	0.9816
Final Elution Volume (μL)(80,120)	0.19	1.67	0.11	0.9115
BsAb-1 Parameter Estimates				
Term	**Estimate**	**Std Error**	**t Ratio**	**Prob>|t|**
Intercept	37.54	1.27	29.57	<.0001*
Capture cycles (4,15)	8.90	1.27	7.01	<.0001*
Capture F (μL/sec)(4,16)	-4.62	1.27	-3.64	0.0014*
Wash1 cycles (1,3)	-0.54	1.27	-0.42	0.6750
Wash1 F (μL/sec)(4,16)	-0.76	1.27	-0.60	0.5574
Wash2 cycles (1,3)	1.79	1.27	1.41	0.1720
Wash2 F (μL/sec)(4,16)	0.36	1.27	0.29	0.7773
Elution cycles (4,15)	-0.09	1.27	-0.07	0.9465
Elution F (μL/sec)(4,16)	1.31	1.27	1.03	0.3124
Final Elution Volume (μL)(80,120)	4.68	1.27	3.69	0.0013*

* = factors found to be significant with a probability of $p \leq 0.05$

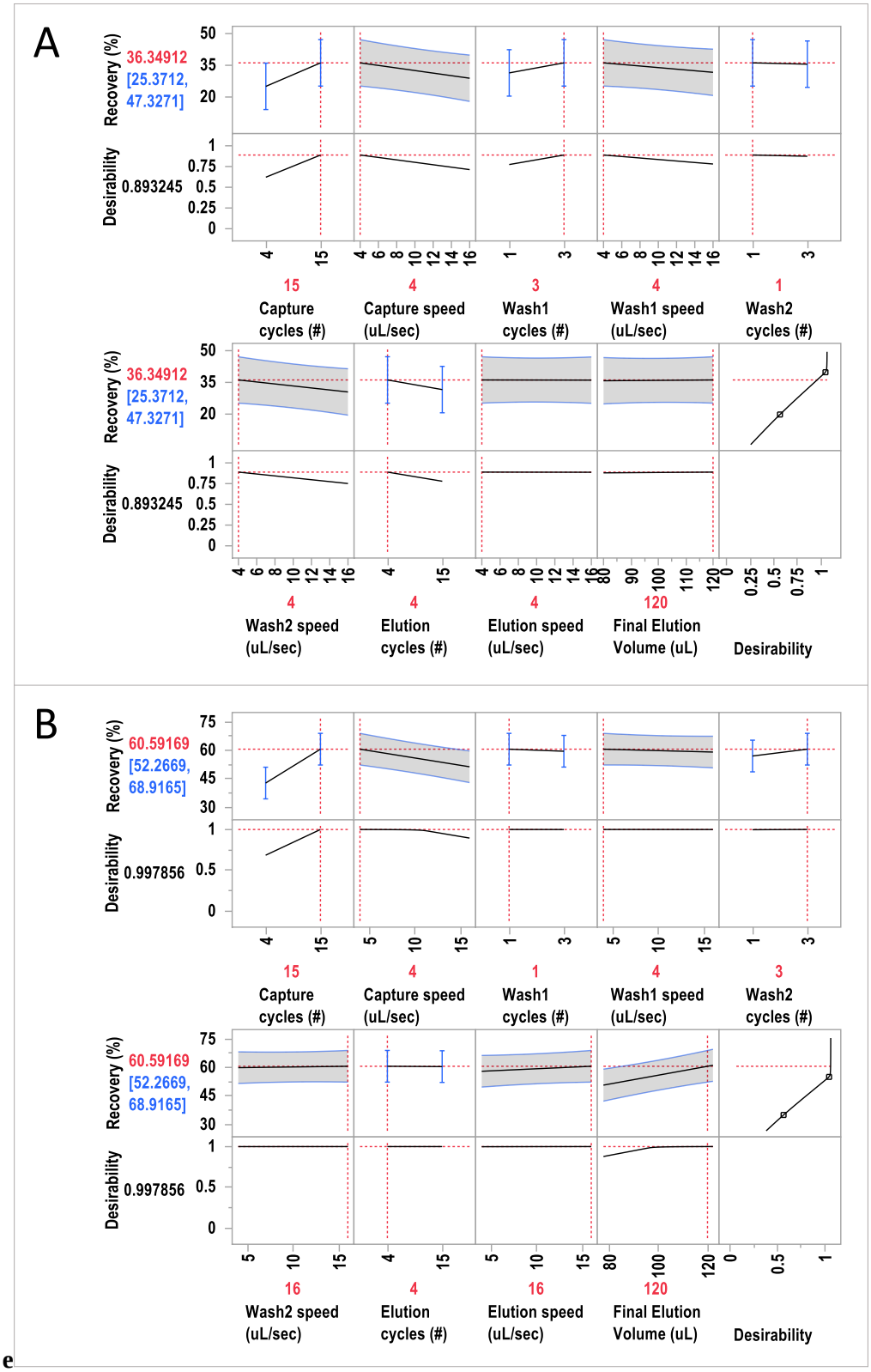

e

Figure 3.3 PhyTip purification MESD prediction profiler.

MESD model prediction profiler for (A) mAb-1 and (B) BsAb-1, displaying the %R variation concerning changes of the factors under investigation. The desirability function (Appendix A, Equation 9.1) was computed to identify the factor settings that maximised sample recovery and display the response predictions.

The model desirability function (see Appendix A, Equation 9.1) was used to find the optimal conditions to maximise the %R for both molecules. As displayed by the model prediction profiler (Figure 3.3), increasing the number of capture cycles and decreasing the F maximised the %R of both the molecules. Likewise, greater elution volumes improved the %R of BsAb-1 whilst no significant effect was observed on mAb-1. Nevertheless, the model estimates for maximum %R were ~40% and ~60%R for mAb-1 and BsAb-1, respectively, which was still far from the desirable 70-90% range. Varying the number of cycles and F during the washing steps didn't have a significant effect, however, greater %R for both molecules were obtained at low F (4 µL/sec). To minimise the purification time and maintain a desirable %R, the washing steps parameters were optimised to 1 cycle at 4 µL/sec whilst the other parameters were subjected to further optimisation to improve %R.

3.3.1.3 DoE2: Central Composite Design for PhyTip purification Method Optimisation

A Box-Wilson central composite design (CCD) was used for optimising the number of capture cycles, F and final elution volume to maximise %R. As shown in Figure 3.4, the CCD is a type of DoE characterised by a factorial or fractional factorial design with centre points and axial points to estimate the presence of curvature. For these characteristics, the CCD is generally used in response surface methodology (RSM) for optimisation experiments.

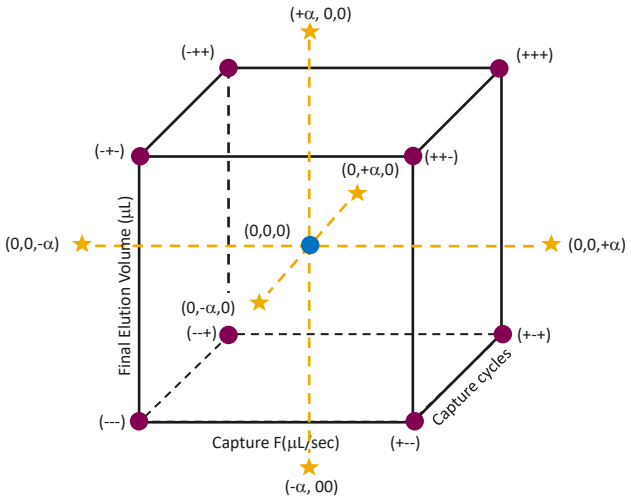

Figure 3.4 Box-Wilson CCD points representation on a cube.
The axial points (yellow stars) are used to augment the centre points (blue circle) to allow the estimation of curvature. The distance from the centre of the design space to a factorial point (purple circle) is ± 1 unit for each factor, whilst the distance from the centre of the design space to a star point is ± α.

The MESD served to identify the factors that most significantly affect the %R as well as their range of investigation. Based on the results of the MESD (Figure 3.3, Table 3.1) the range of investigation of the number and F of the capture cycles and the elution volume were varied, whilst the other method parameters were kept constant as previously mentioned (Appendix A, Table 9.1). Linear regression analysis was used to generate an empirical model for each molecule to study the relationship between the factors under investigation and the %R. The results showed that both models had a good fit with $R^2 \geq 0.85$ (Appendix A, Figure 9.2). Table 3.2 reports the main effects and second-order interactions explored by the model together with a summary of the model parameter estimates with respective t-test results. A desirability function (Appendix A, Equation 9.2) was computed to obtain optimal factor levels that maximised the %R. The prediction profilers displayed the model estimates with the factors set to optimal values as obtained by the maximise desirability function (Figure 3.5).

Table 3.2 Summary of the estimates of the PhyTip purification CCD model parameters with t-test results

mAb-1 Parameter Estimates				
Term	**Estimate**	**Std Error**	**t Ratio**	**Prob>|t|**
Intercept	28.59	4.39	6.52	<.0001*
Capture cycles(8,20)	4.69	2.58	1.82	0.0844
F(ul/sec)(2,4)	-0.45	2.58	-0.17	0.8637
Elution Volume (uL)(80,160)	10.02	2.58	3.88	0.0009*
Capture cycles*F(ul/sec)	-2.21	2.88	-0.77	0.4523
Capture cycles*Elution Volume (uL)	-0.38	2.88	-0.13	0.8968
F(ul/sec)*Elution Volume (uL)	-2.93	2.88	-1.02	0.3219
Capture cycles*Capture cycles	6.38	5.09	1.25	0.2241
F(ul/sec)*F(ul/sec)	-1.17	5.09	-0.23	0.8199
Elution Volume (uL)*Elution Volume (uL)	-3.35	5.09	-0.66	0.5173
BsAb-1 Parameter Estimates				
Term	**Estimate**	**Std Error**	**t Ratio**	**Prob>|t|**
Intercept	50.03	4.31	11.62	<.0001*
Capture cycles(8,20)	9.10	2.53	3.59	0.0018*
F(ul/sec)(2,4)	-3.39	2.53	-1.34	0.1963
Elution Volume (uL)(80,160)	6.75	2.53	2.67	0.0149*
Capture cycles*F(ul/sec)	6.54	2.83	2.31	0.0317*
Capture cycles*Elution Volume (uL)	0.88	2.83	0.31	0.7597
F(ul/sec)*Elution Volume (uL)	-0.97	2.83	-0.34	0.7356
Capture cycles*Capture cycles	-2.76	5.00	-0.55	0.5871
F(ul/sec)*F(ul/sec)	-11.32	5.00	-2.27	0.0347*
Elution Volume (uL)*Elution Volume (uL)	1.20	5.00	0.24	0.8126

* = factors found to be significant with a probability of $p \leq 0.05$

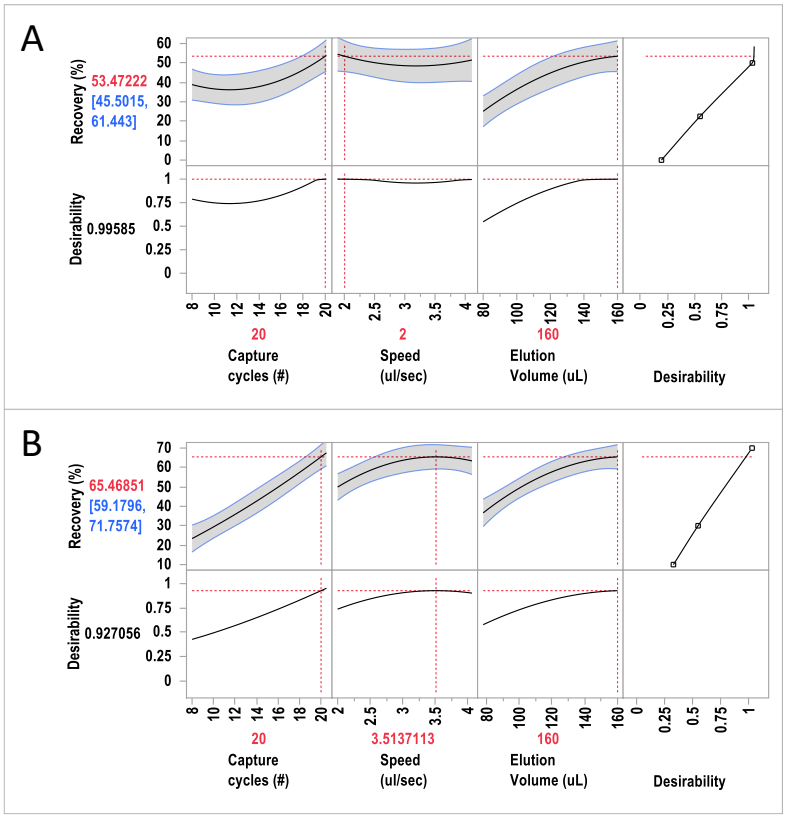

Figure 3.5 PhyTip purification CCD prediction profiler.
A) mAb-1 and B) BsAb-1 model prediction profiler displaying the optimal CCD factor settings to obtain the maximum %R as estimated by the maximise desirability function.

These results were consistent with the observations from the MESD (Figure 3.3) and showed that increasing the number of capture cycles and elution volume as well as decreasing the capture F improved the %R in both molecules. Optimal capture F for BsAbs was identified at 3 µL/sec whilst the %R for mAb-1 was greater at 2 µL/sec. The number of capture cycles and the elution volume were optimised for both molecules to 20 cycles and 160 µL, respectively. Noteworthy, the significant factors identified by the BsAb-1 model were the first-order interaction capture cycles, elution volume, the second-order interactions Capture cycles*F, and the F*F quadratic effect, whilst the only significant factor of the mAb-1 CCD model was the elution volume (Table 3.2). The results of this experiment highlighted the different dependencies of the two molecules in response to the process parameters. Moreover, the scarce %R obtained for both molecules led to the hypothesis that this may be more strongly influenced by a process factor that was not explored in the DoE models. Although the maximum %R obtained by the CCD was improved in comparison to the

MESD, the estimated values were still lower than sought, namely ~50% and ~65%R *vs.* for mAb-1 and BsAb-1, respectively (Figure 3.5). Based on the information captured from both DoEs as well as from process knowledge, it was deduced that the nature of the elution buffer may significantly impact the final %R. Hence, an elution buffer composed of 0.1 M glycine hydrochloride, pH 2.6 (Gly·HCl-2.6) was evaluated and compared to the previously used acetate buffer (AcOOH-3.6). The two elution buffers were evaluated by purifying mAb-1 and BsAb-1 in duplicate using the optimised method parameters as reported in Table 3.3. The %R achieved for both molecules when using AcOOH-3.6 were ~50% and ~55% for mAb-1 and BsAb-1, respectively, confirming the CCD model estimates. However, by using the Gly·HCl-2.6 buffer, the %R reached ~90% and ~70% for mAb-1 and BsAb-1, respectively. This experiment confirmed that the nature of the elution buffer was strongly affecting the %R in both molecules and the lower pH buffer improved protein recovery. Nevertheless, it is well established in the literature that the chemical properties of the buffers used during purification may affect PQ with major emphasis on the generation of size variants. The preservation of the physicochemical properties of a molecule during the purification is generally more important than the final yield. Aggregation analysis by HT SEC (Section 3.3.2) was carried out to assess the impact of the type of elution buffer on the final PQ. Figure 3.6 showed the SEC profiles of mAb-1 and BsAb-1 purified by AcOOH-3.6 and GlyHCl-2.6 buffers overlaid against their respective reference standard (RS). An increase in mAb-1 HMWS impurities was observed as a consequence of using the AcOOH-3.6 buffer. However, the mAb-1 SEC profile overlayed perfectly to its RS when GlyHCl-2.6 was employed. Conversely, the SEC profile of BsAb-1 was not impacted by the use of the two buffers.

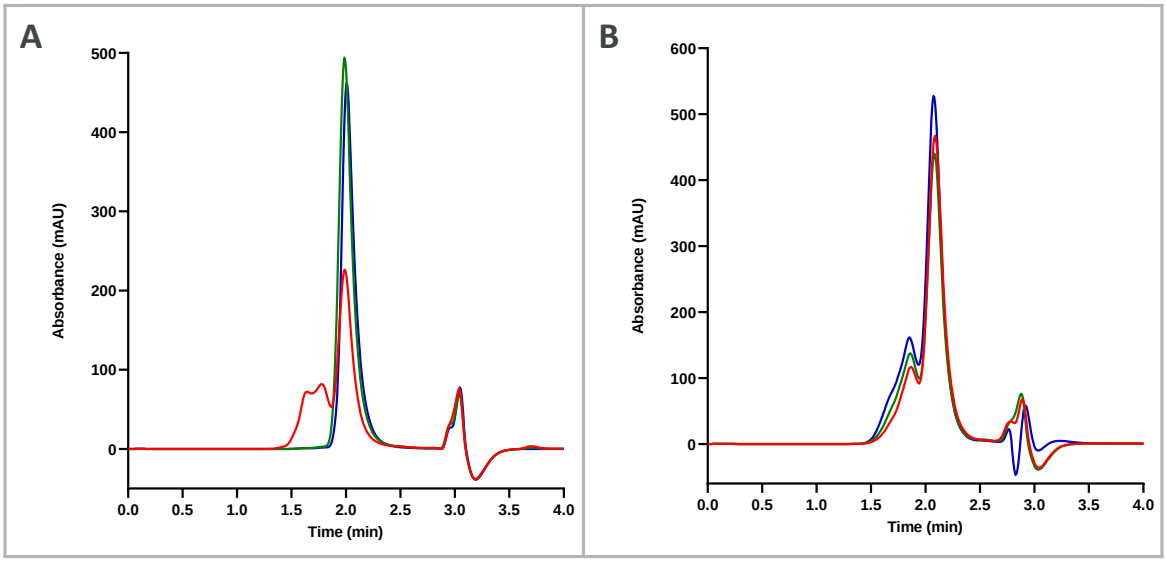

Figure 3.6 Assessment of the effect of different elution buffers on PQ.
SEC chromatograms of (mAb-1) and BsAb-1 (B) purified using AcOOH-3.6 (red) and GlyHCl-2.6 (green) as elution buffers overlaid against their RS (blue). The SEC method conditions used for the analysis are summarised in Table 3.7.

This experiment underlined the complexity of the purification process and demonstrated that fine-tuning method conditions is necessary to maximise the %R. Despite certain factors influencing the purification yield may be molecule-specific and require case-by-case optimisation, platform methods aim to address specific classes of molecules rather than individual candidates. The final optimised method parameters are reported in Table 3.3.

Table 3.3 Optimised PhyTip purification method

PhyTip Process Parameters
Equilibration cycles: 2 x 15
Equilibration F: 8 µL/sec
Equilibration processing volume: 160 µL
Capture cycles (20)
Capture F (3 µL/sec)
Wash1 cycles (1)
Wash1 F (4 µL/sec)
Wash2 cycles (1)
Wash2 F (4 µL/sec)
Elution cycles (4)
Elution F (16 µL/sec)
Final Elution Volume (160 µL)
Purification Buffers
Equilibration and Wash1 buffer: DPBS
Wash2 buffer: 25 mM acetate, 120 mM NaCl, pH 5.5
Elution buffer: 0.1 M glycine HCl, pH 2.6

3.3.1.4 Method Assessment

One of the key aspects of platform methods is their fitness for routine use therefore, their consistent performance has to be thoroughly evaluated during method development. Method assessment was carried out using both mAb-1 and BsAb-1 as reported in Table 3.4. The repeatability study was conducted by monitoring the %R coefficient of variation (CV) over 6 replicates. A 5-levels linearity study was performed in duplicate over a column loading range of 70-900 µg, corresponding to ~10-110% of the resin capacity. Linear regression analysis of the column loading (µg) *vs.* the protein recovery (µg) was performed for mAb-1 and BsAb-1 separately and confirmed $R^2 \geq 0.99$ (Figure 3.7). The linearity study enabled us to determine the column loading range that allowed for consistent recovery (Figure 3.7, B). The average %R obtained across the column loading range investigated was 80% and 85% for BsAb-1 and mAb-1 with CV < 20% (Appendix A, Table 9.3). This experiment demonstrated that the optimised PhyTip-purification method achieved a consistent %R of 83% across mAb and BsAb samples with various levels of concentrations.

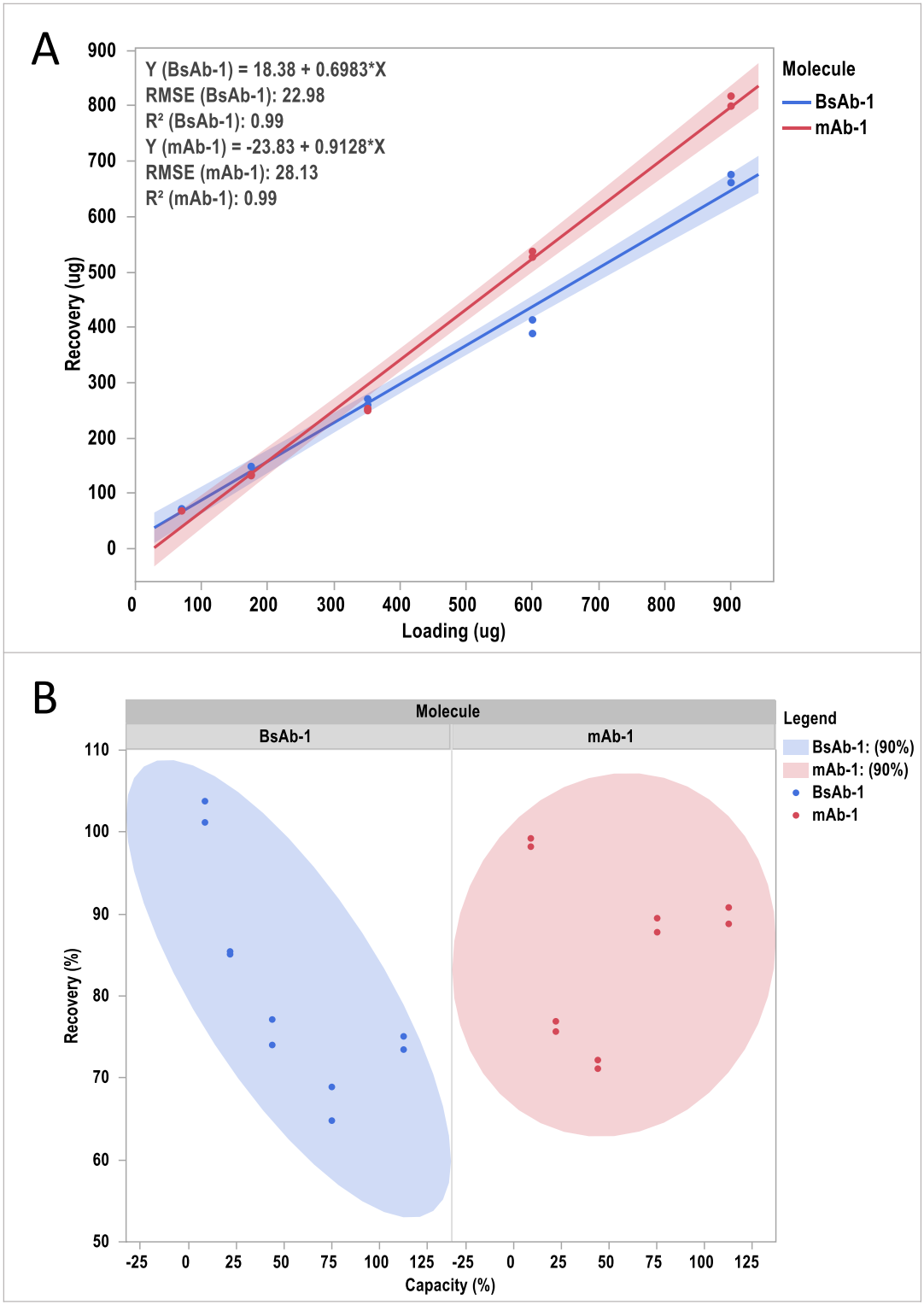

Figure 3.7 PhyTip linearity and column loading range.

A) 5-level linearity study assessed 70, 175, 350, 600, 900 µg column loads. Linear regression analysis performed to study the relationship between column loading (µg) and recovery (µg) confirmed R^2 = 0.99 for both molecules and RMSE = 22.98 and 28.13 for BsAb-1 (blue) and mAb-1 (red), respectively. B) Bivariate normal density ellipse displaying the range of BsAb-1 (blue) and mAb-1 (red) %R obtained *vs.* the PhyTip loads expressed as column % capacity. The %R ranges were 69-104% and 72-99% for BsAb-1 and mAb-1, respectively.

The assessment of the sample stability was aimed to evaluate whether the purification process affected the size variants profile. The mAb-1 reference standard (RS) and BsAb-1 reference material (RM) size variants profiles were analysed before and after purification (n=3) by two different SEC methods for each molecule (Appendix A, Table 9.5). T-test confirmed that the size variants profile analysed by each method did not vary significantly (p-value < 0.05) before and after purification (Appendix A, Table 9.4). The suitability-for-use of the PhyTip-based method for the purification of samples containing various levels of HMWS impurities was confirmed by blending a heat-stressed sample of mAb-1 with its RS at different ratios (0%, 35%, 65%, and 100%). As expected, the change in %HMWS across the sample set was linear (Figure 3.8). The samples were processed in duplicate by PhyTip purification followed by HT SEC analysis for evaluating the changes in the aggregation profile. As expected, the %HMWS varied linearly (R^2 = 0.96) across the samples and the %HMWS CVs of the sample replicates of each level (% of stressed sample spike) were <10%.

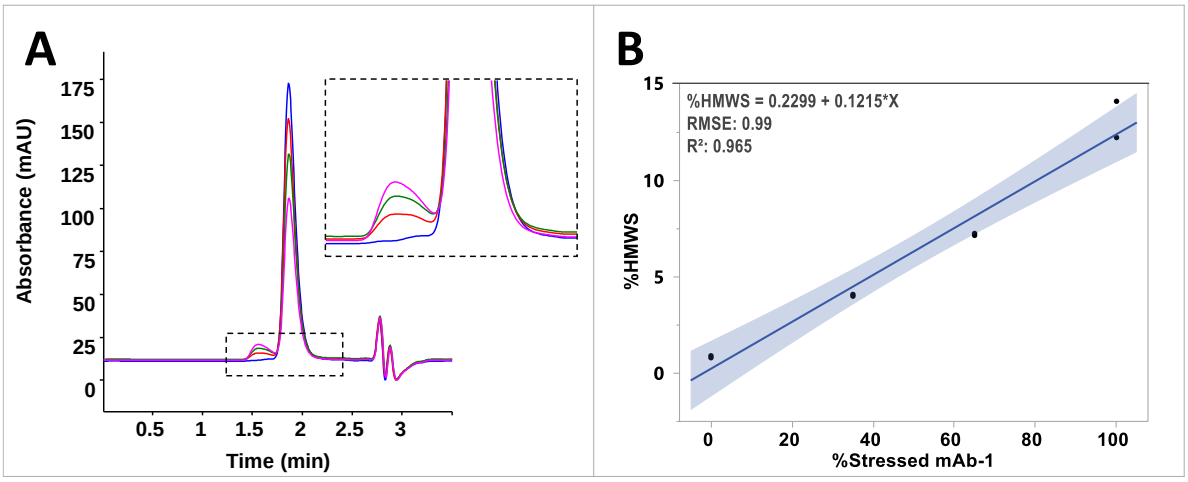

Figure 3.8 Assessment of the PhyTip purification method suitability for use.
A) Chromatograms overlays of mAb-1 sample blends analysed by HT SEC containing 0% (blue), 35% (red), 65% (green), and 100% (pink) of mAb-1 stressed sample spiked into the RS. The sample was stressed by exposing the RS to 70 °C for 60 min to induce the formation of HMWS. B) Linear regression analysis of the %HMWS present in the sample blend analysed by HT SEC.

The method assessment study confirmed that the proposed PhyTip purification method was fit for processing as little as 300 µL of cell culture supernatants in 96-DWP achieving 80 ± 5 %R within 70-900 µg column loading range and providing 160 µL of purified product for following downstream analytical characterisation. Further assessment of the method fitness-for-purpose demonstrated that the HMWS profile of the molecule of interest was not compromised by the purification conditions. The application of the PhyTip-based method for the purification of samples containing various levels of HMWS impurities was demonstrated.

Table 3.4 PhyTip purification method assessment results.

Parameter	Target Expectation	Results
Precision (Repeatability)	No more than 20% CV in %R amongst the replicates (n=6).	mAb-1 %R CV = 0.50 BsAb-1 %R CV = 2.08
Linearity	$R^2 \geq 0.85$ for %R *vs*. column load expressed as PhyTip column %capacity.	mAb-1: $R^2 = 0.99$ BsAb-1: $R^2 = 0.99$ (Figure 3.7, A)
Column loading range	%R ≥ 70% with CV ≤ 20%	~10-110% column capacity 83 %R, CV = 14% (Figure 3.7, B; Appendix A, Table 9.3)
Sample stability	T-test showing no significant changes (p-value, 0.05) in the size variants profile before and after purification.	T-test p-value < 0.05 in all the conditions tested (Appendix A, Table 9.4)
Suitability-for-use	Linear variation of %HMWS impurities ($R^2 \geq 0.85$ for the HMWS peak) and %HMWS CV < 10% amongst the replicates.	$R^2 = 0.96$; %HMWS CV <10% (Figure 3.6)

3.3.2 Fast and Sensitive Aggregation Analysis by Size-Exclusion Chromatography

3.3.2.1 Overview

SEC is a straightforward approach for the analysis of size variants in biopharmaceuticals. Compared to other modes of chromatography such as IEX, HILIC, and RP, SEC method development is driven by the optimisation of only a few factors, predominantly the column chemistry and mobile phase composition. Nevertheless, this advantage comes with a limited number of measures that can be implemented to improve the separation regardless of its final application. Due to the non-retentive nature of SEC separations, the expected peak volume is low and severely affected by the system dispersion occurring as a consequence of the extra-column dead volume (V_{ec}). The minimisation of the V_{ec} is, therefore, of paramount importance to achieve optimal size variants separation by SEC. Sources of V_{ec} are the injection volume, the fluidic path of the LC system to the column inlet and from the column outlet to the detector including the flow cell, as well as all the connections embedded therein. The use of large ID columns compensates for the loss of efficiency due to the considerable dispersion occurring in classical HPLC systems. Nevertheless, recent technological advancements have brought the implementation of ultra-high-performance size exclusion chromatography (UHP-SEC) columns characterised by decreased column volumes and particle size that, together with the increased mechanical resistance to high pressure, improve the analysis throughput whilst still maintaining a desirable Rs. The ordinary dimensions of modern UHP-SEC columns are 4.6 mm x 150 mm ID x L (internal diameter x length) packed with sub-2 µm particles. This column format enables faster separations than those obtained by the standard HPLC columns with 7.8 mm ID x 300 mm L, and 3-5 µm particles without substantial compromise of the analysis Rs. Along these lines, UHPLC systems were optimised to have low V_{ec} (< 10 µL) to compensate for the band broadening effect resulting from the use of small ID columns. Modern UHPLC setups with sub-2 µm particle columns provide a 2-5 fold decrease in plate height and a 2-4 fold boost in analysis speed (Fekete et al., 2013; Yang et al., 2015; Goyon et al., 2018). However, there is little evidence of the use of SEC columns with < 4.6 mm ID. Small-scale chromatography columns such as capillary SEC columns coupled to fluoresce detection prove promising for enhancing sensitivity (Rea, Moreno, et al., 2012; Rea, Lou, et al., 2012).

Despite reductions in column ID being a common practice for improving method sensitivity, this might not be the best approach for SEC since the reduction of the column ID produces larger band heights with a detrimental effect on peak Rs. Thus, the implementation of small-scale SEC in the biopharma community has so far been limited. Furthermore, small-scale SEC columns are difficult to pack due to the poor resistance to packing pressure of the small scale highly porous material. Up to date, < 1 mm ID SEC columns are not commercially available or only available as custom-packed products. The lack of both the availability of such column formats and manufacturing QC consequent to custom-packing procedures hamper the implementation of small-scale SEC in the industry for supporting platform testing.

Aiming to develop a SEC-based ranking tool for clone selection during early-stage product development, the 2.1 mm ID column format was found to be a suitable compromise between the peak Rs and sensitivity required in comparison to traditional 4.6 mm ID SEC columns. This study presents the development of a platform HT SEC method using 2.1 mm ID columns for the analysis of mAbs and BsAbs aggregates expressed in CHO cells cultured in 96-DWPs.

3.3.2.2 DoE-Assisted Method Development for mAbs and BsAbs HMWS Analysis

The development of a platform HT SEC method for monitoring aggregation in mAbs and BsAbs was achieved by using a DoE approach. The molecules chosen as models for method development were mAb-1 and mAb-2 (both IgG1, κ), and BsAb-1 (a BIS5 antibody format). For generating samples suitable for method development, the two mAbs containing >99% main product were stressed at 70 °C for 60 min which induced the formation of ~17% and ~3% HMWS impurities in mAb-1 and mAb-2, respectively analysed by the AstraZeneca benchmark SEC method for QC testing (AZ SEC SOP) (Appendix A, Figure 9.3 A and B). A CAT-S CHO stable clone fed-batch overgrow expressing BsAb-1 (Chapter 2, Section 2.3) was cultured to obtain the BsAb RM used for method development. The HCCF was purified in bulk by Protein-A chromatography to generate homogeneous material for analytical method development. Aggregation analysis by AZ SEC SOP confirmed that the BsAb-1 RM contained 35% HMWS impurities (Appendix A, Figure 9.3, C). Therefore, no further stress conditions were applied to induce aggregation. SEC analysis of all the sample models was

performed using the AZ SEC SOP for the accurate quantitation of the HMWS impurities. This provided an indicative %HMWS target level to match by the HT SEC method.

The DoE approach used for method development involved the use of a multi-factorial, two-level MESD, which served for selecting the most influential factors that significantly impacted the separation of the 2 mAb candidates. For this study, F, injection volume, NaCl concentration and column chemistry were selected as factors to screen (Appendix A, Table 9.6). In respect to the column chemistry, two types of columns were assessed, the Waters and the Sepax columns, both of equal dimensions, 2.1 x 150 mm ID x L (Chapter 2, Section 2.1.4, Table 2.1). The former was packed with ethylene-bridged hybrid (BEH) diol-coated spherical particles with 1.7 μm diameter and 200 Å pore size particles, whilst the latter was characterised by a lay-down monolayer hydrophilic film bonded to spherical silica particles of 1.8 μm diameter and 300 Å pore size. More information on the packing chemistry is proprietary to the manufacturers and, therefore, not provided herein. Other variables such as sample pH and concentration were not taken into consideration for further optimisation since these parameters are strictly dependent on the process conditions upstream of the analysis. To ease the workflow and maintain the throughput, steps such as buffer exchange and sample concentration normalisation were not evaluated herein. Along these lines, the mobile phase Na_3PO_4 buffer concentration was also fixed at 50 mM. Owing to the importance of method sensitivity for its final application, multi-wavelength monitoring of the UV absorbance at both 210 and 280 nm was selected since the former was reported to improve method sensitivity (Rea, Moreno, et al., 2012), although the latter may be necessary to specifically discriminate large proteins. The buffer and the column temperature were kept constant at pH 6.8 and 25 °C as per standard operating procedures (SOP) previously optimised within the company for this class of molecules. The quality of the separation was assessed through the calculation of the tailing factor (Ts) of the main product peak, and the Rs between the main product and HMWS peak. These parameters were chosen as the DoE responses (Appendix A, Table 9.6). For a better understanding of how the factors examined in the DoE influenced the separation efficiency, linear regression analysis was used to build an empirical model for each response separately (Appendix A, Figure 9.4). As evidenced in Table 3.5, all the factors were predicted to have a statistically significant impact on the separation efficiency (p-value ≤ 0.05) with the main contributor being the NaCl concentration. The DoE model showed that a minimum of 100 mM NaCl was necessary for resolving the HMWS from the main product peak. However, further improvements of the chromatographic separation were

attained when using a NaCl concentration of 200 mM. Additional considerations on the final method conditions selected as a result of this experiment are discussed below.

Table 3.5 Effect summary report of the HT SEC MESD model estimates.

Source	FDR LogWorth		FDR PValue
NaCl (mM)(5,200)	6.350		0.00000
InjectionVolume (uL)(0.5,10)	1.969		0.01073
Column	1.875		0.01333
F (mL/min)(0.05,0.15)	1.274		0.05317

The model prediction profiler (Figure 3.9) displayed how the Ts, %HMWS and Rs varied depending on changes in the method conditions which impacted each of the responses significantly. The model estimates were reported as predicted by the desirability function (Appendix A, Equation 9.3). This enabled the identification of the optimal method conditions that led to values of Ts and %HMWS close to 1 and 17%, respectively as well as an increase in the Rs between the HMWS and main product peaks. All the MESD responses were significantly influenced by the concentration of NaCl and the F (Figure 3.9 A, B, and C). In SEC separations, T_s is usually a sign of protein-stationary phase interactions, hence the addition of salting-out agents such as NaCl to shield the protein hydrophobic regions minimises the secondary interactions with the column. Furthermore, these experiments demonstrated that higher F improved peak shape by reducing peak width and distortion as well as playing a part in minimising the secondary interactions. The Rs between the main product and HMWS peaks was also positively influenced by mobile phases containing 200 mM NaCl. Interestingly, lower F improved the Rs values, however, this effect was not as strong as the contribution given by the NaCl concentration as evidenced by the lower slope displayed by the prediction profiler (Figure 3.9, C). Noteworthy, higher F reduced analysis time which is key for HT applications, thus F was optimised to 0.15 mL/min according to the column backpressure limit. Moreover, the Waters column enabled an overall greater performance than the Sepax column for both mAb models, hence it was selected as the optimal stationary phase for this method. Lastly, low injection volumes had a positive effect on the Rs. This provided a first estimate of the method sensitivity and dynamic range for samples containing 3-17% HMWS impurities. However, further considerations on the

injection volume limit and its impact on peak broadening will be discussed in Section 3.3.2.4. The conditions estimated by the MESD were sufficient to obtain a desirable separation between HMWS impurities and main product peak in both mAbs models thus, no further optimisation was undertaken. The final optimised method is reported in Table 3.7 which underwent method assessment to evaluate its suitability for application to the analysis of the HMWS impurities in mAbs and BsAbs samples (see Section 3.3.2.4).

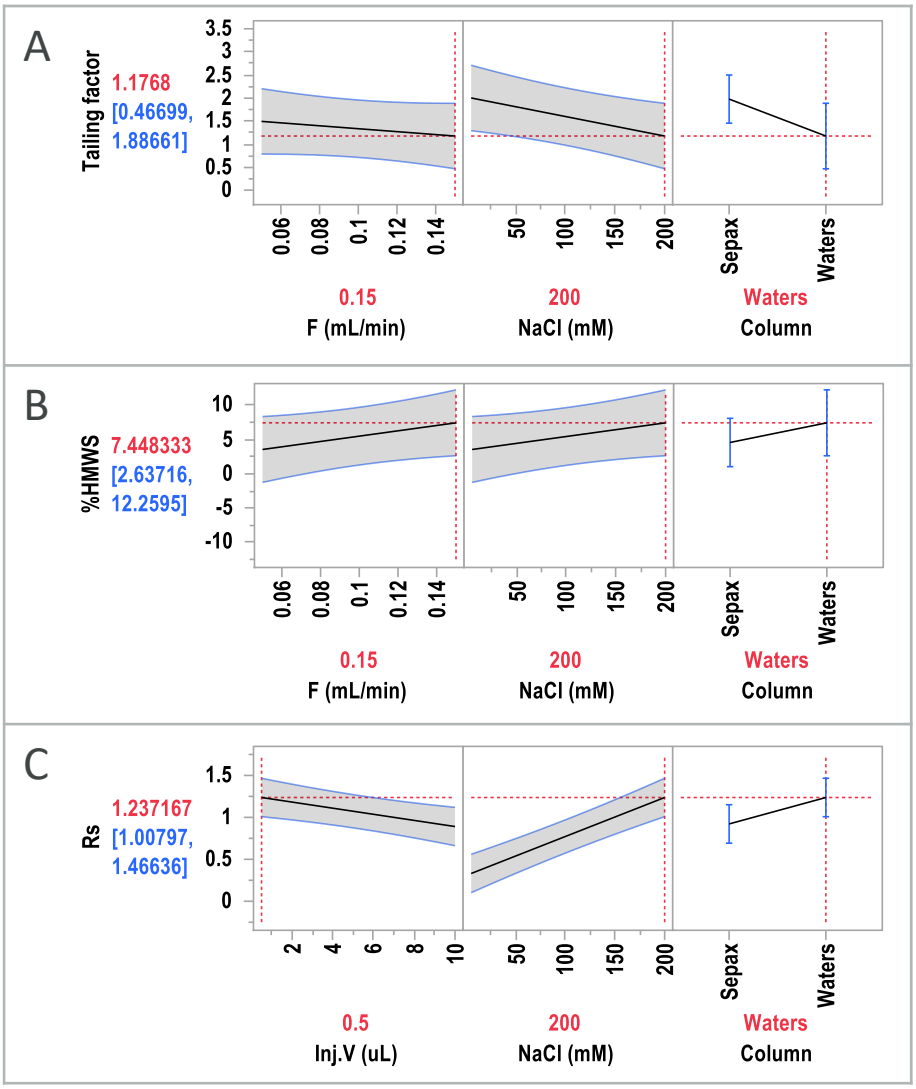

Figure 3.9 HT SEC MESD prediction profiler.

Model prediction profilers for all the MESD responses with factor values estimated at the maximum of the desirability function. A) Ts varied significantly in relation to F, NaCl concentration and was closer to its target value (1 ± 0.2) at higher F, and NaCl and by using the Waters column. B) %HMWS was set to a target match of 17% and was significantly influenced by F, NaCl and column type. Higher values of F and NaCl along with the Waters column enabled HMWS quantitation closer to its target value. C) The model was set to maximise the Rs and was significantly influenced by the injection volume (Inj. V), the concentration of NaCl and the column type. Maximum Rs value was achieved by decreasing the Inj. V, increasing concentrations of NaCl, and by using the Waters column.

3.3.2.3 Method Development Considerations for BsAbs Models

Bispecific antibodies are larger than mAbs and usually prone to generating a higher extent of aggregation (Manikwar, Hari, et al., 2020). The causes of HMWS formation are diverse and often unknown due to the multifaceted possible aggregation pathways. Therefore, several strategies are often attempted to tackle this problem from different angles and HTS experiments are frequently adopted. HT size profiling of large biomolecules is hampered by the size of the aggregates and the great extent of the HMWS impurities expected in BsAbs samples may challenge the method resolving power. Therefore, further investigations on the HT SEC method development were undertaken with the aim to maximise the separation efficiency for BsAbs candidates. A full factorial design (FFD) DoE was carried out to optimise the method conditions for the BsAb-1 model. Based on the result of the MESD, the mobile phase ionic strength proved to be the most significant factor impacting the separation efficiency (Table 3.6). Moreover, several published studies testified to the influence of column chemistry in SEC separations and the importance of column selection for specific classes of molecules (Goyon, Beck, et al., 2017; Uliyanchenko, Schoenmakers, and Wal, 2011; Popovici and Schoenmakers, 2005; Fekete et al., 2014; Goyon, D'Atri, et al., 2017; Fekete et al., 2018). In this study, the DoE approach was focused on both the optimisation of the mobile phase composition in respect of Na_3PO_4 buffer and NaCl concentrations, alongside the evaluation of three columns of equal dimensions (2.1 mm ID x 150 mm L) but with different packing chemistries. The column chemistries of the Waters and Sepax columns were previously described (see Section 3.3.2.2). Additionally, a third column manufactured by Agilent was also evaluated. This column is characterised by a highly hydrophilic stationary phase composed of sugar-coated silica particles with 1.9 µm diameter and 300 Å pore size. The other parameters were kept consistent as reported in Appendix A, Table 9.7. The quality of the separation was evaluated in terms of peak Rs and %HMWS. The latter was set to match the quantitative data obtained by the AZ SEC SOP (Appendix A, Figure 9.3, C).

A linear regression analysis was used to build an empirical model for each response and study how the %HMWS and the peak Rs varied in relation to the mobile phase ionic strength and column chemistry (Appendix A, Figure 9.5). The summary of the model effects is reported in Table 3.6. Interestingly, none of the model factors and interactions had a significant effect on the Rs between the main product and HMWS peaks. However, the

effects on the Rs between HMWS H1 and H2 (Rs(H1/H2) (Figure 3.10) were significant, hence the Rs(H1/H2) was used as a parameter to evaluate the efficiency of the separation.

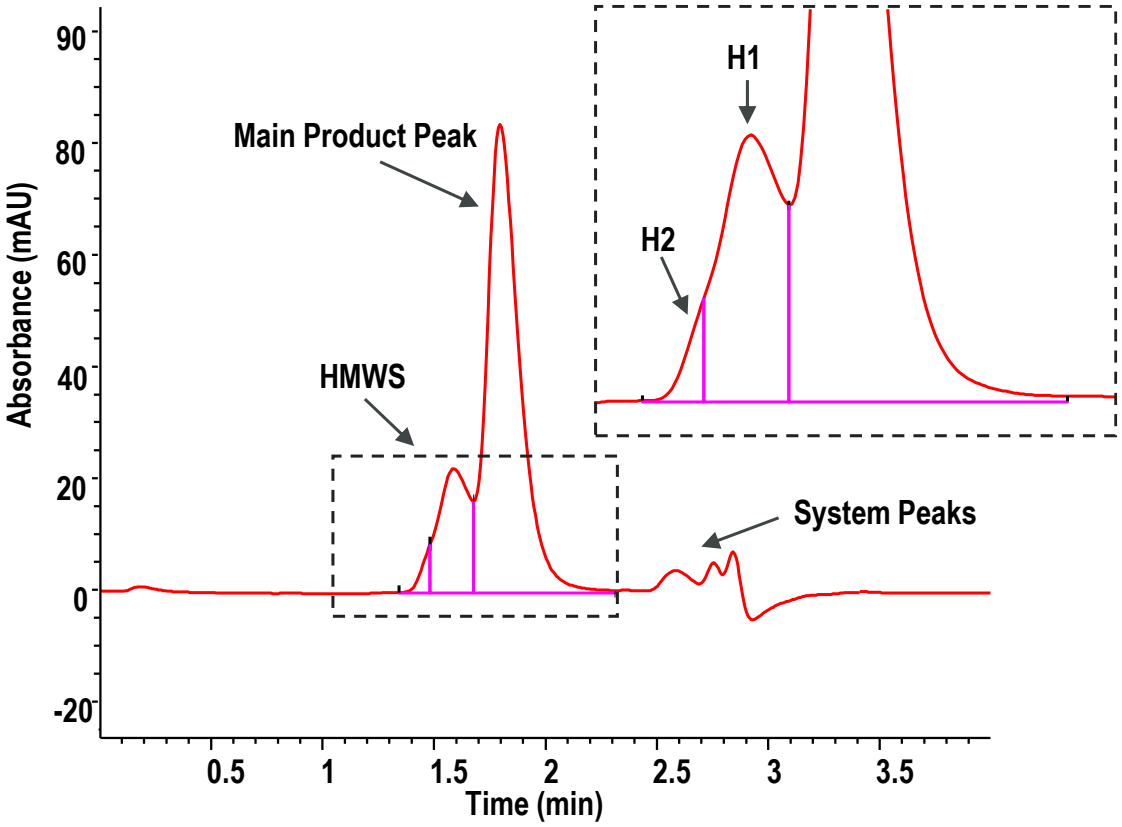

Figure 3.10 BsAb-1 size variants profile of BsAb-1 with peak assignment details. Chromatogram of BsAb-1 analysed by HT SEC displaying the separation between the HMWS, the main product peak and system peaks. The zoomed area illustrates the HMWS H1/H2 shoulder. The sample concentration was diluted to 5 mg/mL before analysis and the injection volume was 1 µL. Further method details conditions are described in Table 3.7.

It is worth considering that further improvements in the Rs between HMWS (H2 and H1) and main product peak were limited by the poor resolving power of the SEC separation, accentuated by the use of a narrow ID column. Further attempts at increasing the Rs of the method may be focused on reducing the instrument V_{ec} by optimising the fluidics path. This would entail reducing the length and diameter of the capillary tubing and optimising the fittings as well as replacing the instrument parts to lower the internal dispersion volume. Due to the complexity and resources required for such a procedure, this was not included in the scope. Despite the instrument limitation, the HMWS/main product Rs values were considered fit-for-purpose hence, the method development moved forward.

Table 3.6 BsAbs HT SEC method development DoE effect summary

Source	FDR LogWorth		FDR PValue	
Na_3PO_4 (mM)*[NaCl] (mM)	4.151		0.00007	
Na_3PO_4 (mM)(50,200)	4.151		0.00007	^
NaCl (mM)(0,200)	1.813		0.01538	^
NaCl (mM)*Column	0.625		0.23698	
Na_3PO_4 (mM)*Column	0.409		0.39030	
Column	0.409		0.39030	^

Not surprisingly, the mobile phase ionic strength generated by the concentration of both Na_3PO_4 buffer and NaCl was the most significant factor influencing the separation efficiency. These results were consistent with the previous analysis (see Section 3.3.2.2). The DoE model prediction profiler (Figure 3.11) estimated that the mobile phase composed of 50 mM Na_3PO_4 buffer and 200 mM NaCl column maximised the Rs(H1/H2). Moreover, the HMWS quantitation achieved by using the Waters column was closer to the one provided by the AZ SEC SOP in comparison to the Agilent and Sepax columns. Noteworthy, the Rs between HMWS and monomer peak of BsAb-1 was improved when using either the Sepax or the Agilent columns. This may be explained by the larger pore size of these columns (300 Å) in comparison to the Waters column (200 Å) allowing for better separation of the BsAb-1 HMWS. Nevertheless, it is worth considering that the improved Rs may also be the result of the lower HMWS area obtained by both Agilent and Sepax, which in turn compromised the quantitation of the HMWS impurities. Therefore, the Waters column was selected as the optimal stationary phase for the present method.

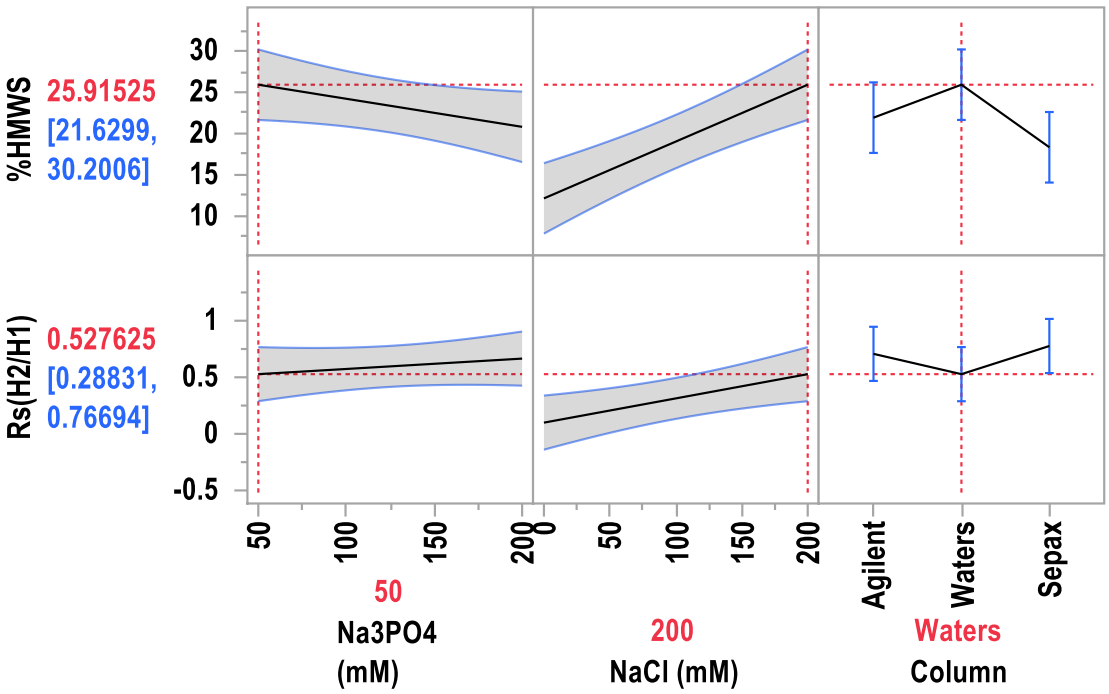

Figure 3.11 FFD model prediction profiler for BsAbs method development.
2x2x3 FFD model prediction profiler at the maximum of the desirability function. The ionic strength mobile phase was reported in terms of the concentration of Na_3PO_4 and NaCl, both in the range 50-200 mM. The effect of the stationary phase chemistry was assessed by the use of three different columns manufactured by Agilent, Waters and Sepax. The %HMWS with target match = 35% was improved by the use of increasing concentrations of NaCl and by using the Waters column. Conversely, the Rs(H1/H2) and was enhanced by decreasing the concentration of Na_3PO_4 and by using the Sepax column.

This experiment confirmed that the method conditions previously selected for mAbs can also successfully be adopted for the analysis of BsAbs candidates. The present analytical tool was proposed as a platform HT SEC method for supporting the analysis of HMWS impurities in both mAbs and BsAbs, designated to be applied as a ranking tool for drug candidate and clone selection in early drug development.

3.3.2.4 Method Optimisation and Throughput Evaluations

To ensure the suitability of the HT SEC method as fit-for-purpose to support in-process development sample testing further optimisation was performed. During early-stage CLD, the expression titres are often low and the samples are poorly concentrated even after purification. As previously mentioned, large injection volumes result in an increased V_{ec} affecting SEC separations, especially when small ID columns are adopted. Therefore, it is important to identify the injection volume range before qualifying the method. To evaluate the optimal injection volume range, samples with different concentrations were prepared in duplicates and injected by varying the injection volume (0.8-18.5 µL) to maintain an equivalent mass loaded on the column (5 µg). As shown in Figure 3.12, increased injection volume resulted in the alteration of the SEC profile. The injection of 18.5 µL resulted in larger peak width (reported as peak width at half height (ω_h) and distortion (Ts) of the main product peak, as evinced by the appearance of a right shoulder (Figure 3.12, C). The Rs between HMWS and main product peak was also compromised and the smaller peak-to-valley ratio (p/v) observed may be the result of the extensive band broadening effect as a consequence of increased V_{ec}. Moreover, the considerable drop in peak area may result as a consequence of the extensive band broadening. This experiment enabled the identification of a suitable injection volume range. Conversely, keeping the injection volume constant (10 µL) and varying the column loading both within the range limits did not affect the SEC profile as displayed in Figure 3.13. This, together with the linearity study, served to estimate the column loading range of the method (2-15 µg).

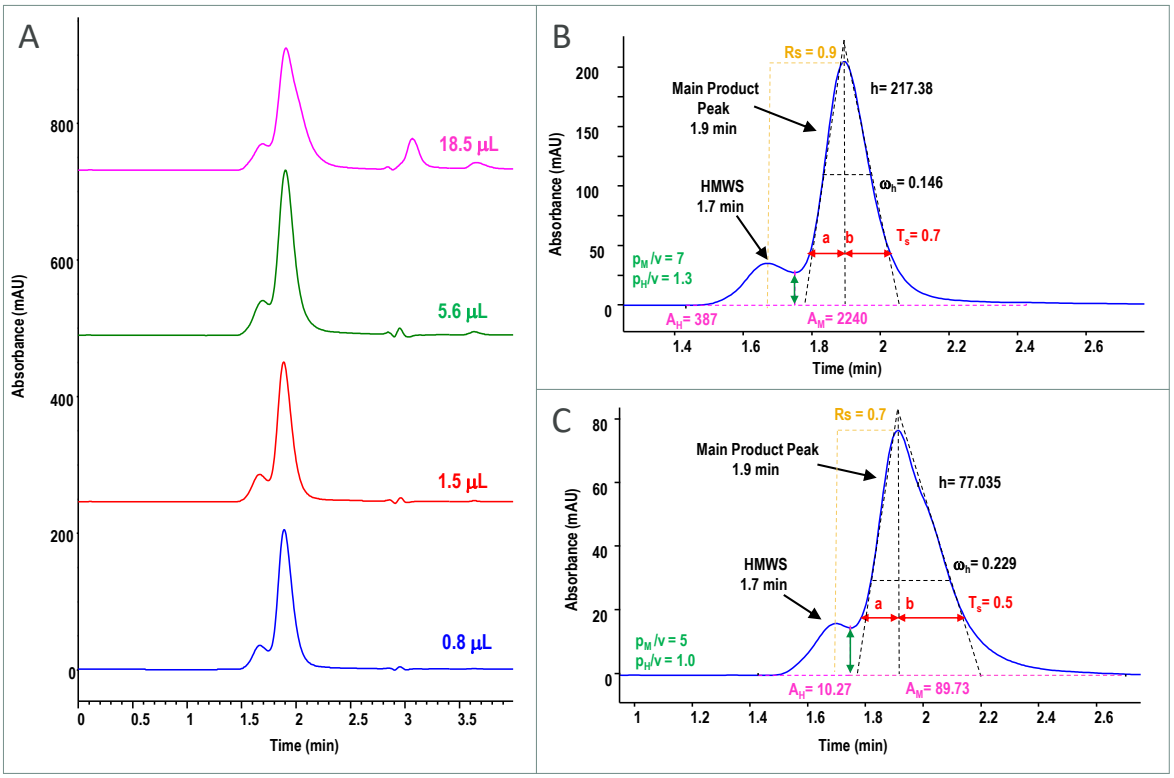

Figure 3.12 Evaluation of the HT SEC method optimal injection volume range.
A) BsAb-1 samples with concentrations 0.27, 0.89, 3.33, and 6.25 mg/mL were prepared in duplicates and analysed by HT SEC, keeping the column loading constant to 5 µg by adjusting the injection volume to 18.5 µL (pink), 5.6 µL (green), 1.5 µL (red), and 0.8 µL (blue), respectively. Peak distortion was observed when analysing the samples with a concentration of 0.23 mg/mL by injecting 18.5 µL. B) Peak analysis of the chromatograms obtained when injecting 0.8 µL. The Rs between HMWS and main product peak was 0.9, the peak-to-valley ratio of the HMWS (p_H/v) and main product peak (p_M/v) were 7 and 1.3, respectively; the peak area of the HMWS (A_H) and main product peak (A_M) were 387 and 2240, respectively; the main product peak height, (h), width at half height (ω_h), and Ts were 217.38, 0.146, and 0.7, respectively. C) Peak analysis of the chromatograms obtained when injecting 18.5 µL and displaying Rs between HMWS and main product peak as 0.7, the peak-to-valley ratio of the HMWS (p_H/v) and main product peak (p_M/v) as 5 and 1.0, respectively; the peak area of the HMWS (A_H) and main product peak (A_M) as 10.27 and 89.73, respectively; the main product peak height, (h), width at half height (ω_h), and Ts = 77.035, 0.229 min, and 0.5, respectively.

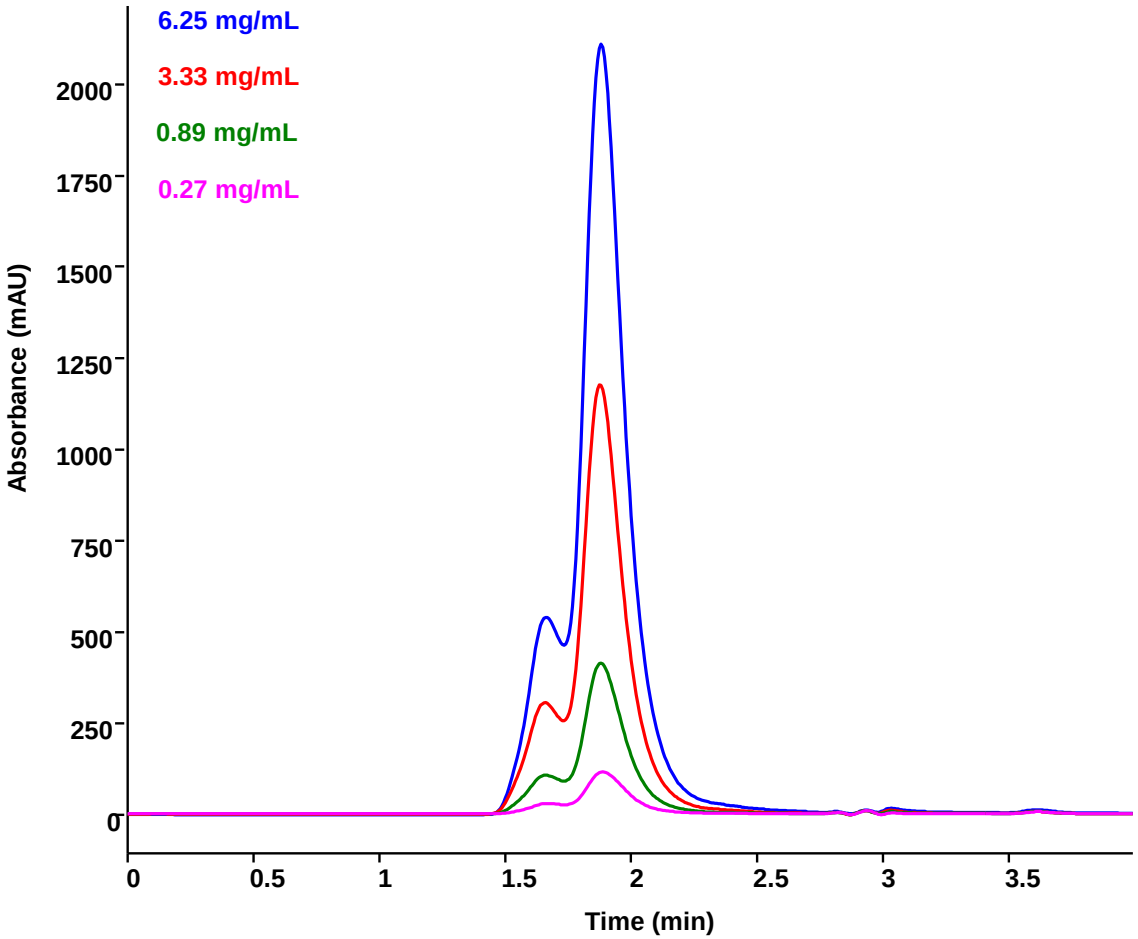

Figure 3.13 Overlay of 10 µL injection of samples with different concentrations.
BsAb-1 samples with concentrations 0.27 (pink), 0.89 (green), 3.33 (red), and 6.25 (blue) mg/mL were prepared in duplicates and analysed by HT SEC, keeping the injection volume constant to 10 µL.

To increase the throughput, the overlapped injections option was chosen as the default instrument setting. This enabled ~0.7 min time gain per injection without compromising the separation efficiency and method repeatability (Appendix A, Table 9.8). Injection overlapping allows the instrument to prepare for the next injection before the completion of the previous. This way, the next injection starts right at the end of the previous run bypassing the time spent by the instrument to prepare for the next injection. This maximises the instrument capabilities for higher throughput applications. The total run time of the HT SEC method from injection to data acquisition was 3.5 min enabling the analysis of a 96-DWP in 5.6 hours. A summary of the optimised HT SEC method is reported in Table 3.7.

.

Table 3.7 HT SEC method

HT SEC Method	
Column	Waters ACQUITY UPLC Protein BEH SEC Column, 200Å, 1.7 µm, 2.1 mm X 150 mm
Mobile phase	50 mM NaH_2PO4/Na_2HPO_4, 200 mM NaCl, pH 6.8
F	0.15 mL/min
Temperature	25℃
Injection Volume	0.5-10 µL
Column loading range	2-15 µg
UV	210 nm, 280 nm

3.3.2.5 Method Assessment

Method assessment was performed to qualify the HT SEC method for its intended use. Table 3.8 outlines the qualification parameter, target expectations, and results from this study. The method specificity was assessed by comparing the UV profile of a sample containing mAb against those obtained by injecting 20 µL of process buffers (Appendix A,

Figure 9.6). Precision was assessed in terms of repeatability, evaluated by calculating the CV of the main product and HMWS peaks retention times and relative peak areas over the 6 replicates of heat-stressed mAb-1 and mAb-2. The sample concentration was diluted to 1 mg/mL before analysis and the injection volume was kept constant to 5 µL (Appendix A, Figure 9.7). The stability-indicating capability of the method was assessed by comparing the UV profiles of stressed samples against the mAb-1 RS and BsAb-1 DS (Appendix A, Figure 9.8). A linearity study was performed for each molecule which involved the assessment of 5 concentration levels, each analysed in triplicate. The sample concentration for BsAb-1 were 0.2, 0.4, 0.8, 1.7, and 2.5 mg/mL with an injection volume of 10 µL, whilst sample concentrations for mAb-1 and mAb-2 were 10, 8, 4, 2, and 1 mg/mL with an injection volume of 0.1 µL. This evaluated the method linearity at the extremes of the injection volume range, over a range of concentrations, and different molecules. Linear regression analysis confirmed a linear response of the variation of HMWS and main product peak area against the sample concentration (Appendix A, Figure 9.9). Accuracy was inferred by the linearity study of each molecule and involved determining the difference between the mean of HMWS and main product peak %area of the sample replicates of each level (n=3) and the grand mean (n=15). The data reported in Appendix A Table 9.9 demonstrated the accuracy of the method. The method limit of detection (LOD) and limit of quantification (LOQ) were inferred from the calibration curve of BsAb-1 used for the linearity study calculated for the

HMWS peak as described in (Chapter 2, Section 2.5, Equations (2.5.2.7) and (2.5.2.6), respectively). Linear regression analysis of the peak area *vs.* the proportional protein load (µg) was performed to determine the LOQ and subsequently the LOD (Appendix A, Figure 9.10).

Table 3.8 HT SEC method assessment results.

Parameter	Target Expectation	Qualification Results
Injection Volume range	Comparable peak shape and no peak distortion observed (n=2)	0.1-10 µL (Appendix A, Figure 9.9).
Column loading range	Consistent %HMWS with S/N ratio >10	2-15 µg (Appendix A, Figure 9.9).
Specificity	No interfering peaks between the sample and the in-process buffer LC traces.	No interfering peaks from mobile phases and formulation buffer at the retention times of the RS peaks were observed (Appendix A, Figure 9.6).
Stability-indicating	Observe changes in the RS peak profile	Changes Observed (Appendix A, Figure 9.8).
Repeatability	No more than 10% CV for both the main product peak and HMWS peak retention time (RT) and areas (A) over the replicates (n=6).	mAb-1 main product peak RT CV = 0.1, area CV = 1.81%, HMWS RT CV = 0.19, area CV = 8.86; mAb-2 main product peak RT CV 0.07, area CV = 0.05, HMWS peak RT CV = 0.09, area CV = 1.73 (Appendix A, Figure 9.7).
Linearity	$R^2 \geq 0.950$ for reference peak area linearity (5 concentration levels, n=3 technical replicates)	Main product: $R^2 = 0.99$ HMWS: $R^2 = 0.99$ (Appendix A, Figure 9.9).
Accuracy (inferred from all the levels in the linearity study.	CV ≤ 20% between the mean of %HMWS of each linearity level of the molecule(s) in examine (n=3 x 5 x 3 molecules) and the grand mean (total n=15 x 3).	BsAb-1 %HMWS CV = 4.92%; mAb-1 %HMWS CV ≤ 11.84%; mAb-2 %HMWS CV ≤ 9.09% (Appendix A, Table 9.9)
LOQ	The CV of the reference peak at each concentration level must be ≤ 20%. $R^2 \geq 0.95$ for reference peak area *vs.* the protein load. Results reported as % of the total peak area	LOQ BsAb-1 HMWS = 4.6% (2.3 µg)
LOD	Results reported as % of the total peak area	LOD BsAb-1 HMWS = 1.55% (0.77 µg)

3.3.3 Proof-of-Concept Application of the HTSEC Method

The proposed analytical method was developed for application in early-stage product development as a ranking tool for clone selection based on the total %HMWS impurities present in the samples. To demonstrate the capability of the method to discriminate amongst samples with different levels of HMWS, samples containing various degrees of aggregates were generated artificially. For this proof-of-concept experiment, BsAb-1, BsAb-2, and mAb-1 were chosen as models of the BsAbs and mAbs classes. SEC analysis by the AZ SEC SOP method demonstrated that the %HMWS of BsAb-1 and BsAb-2 were ~35% and ~22%, respectively whilst mAb-1 showed ~17% HMWS after heat-stress at 70 °C for 1 hour. Subsequently, the HMWS and main product peak fractions were collected and blended at different ratios to generate samples with various levels of HMWS impurities. The samples were analysed by HT SEC and the results are shown in Figure 3.14. Linear regression confirmed that the HMWS peak area measured by HT SEC varied linearly in response to the %HWMS spiked (Appendix A, Figure 9.11). This evidenced that the method was suitable to distinguish from samples with low and high %HMWS and could therefore be adopted as a ranking tool in clone selection (see Chapter 6).

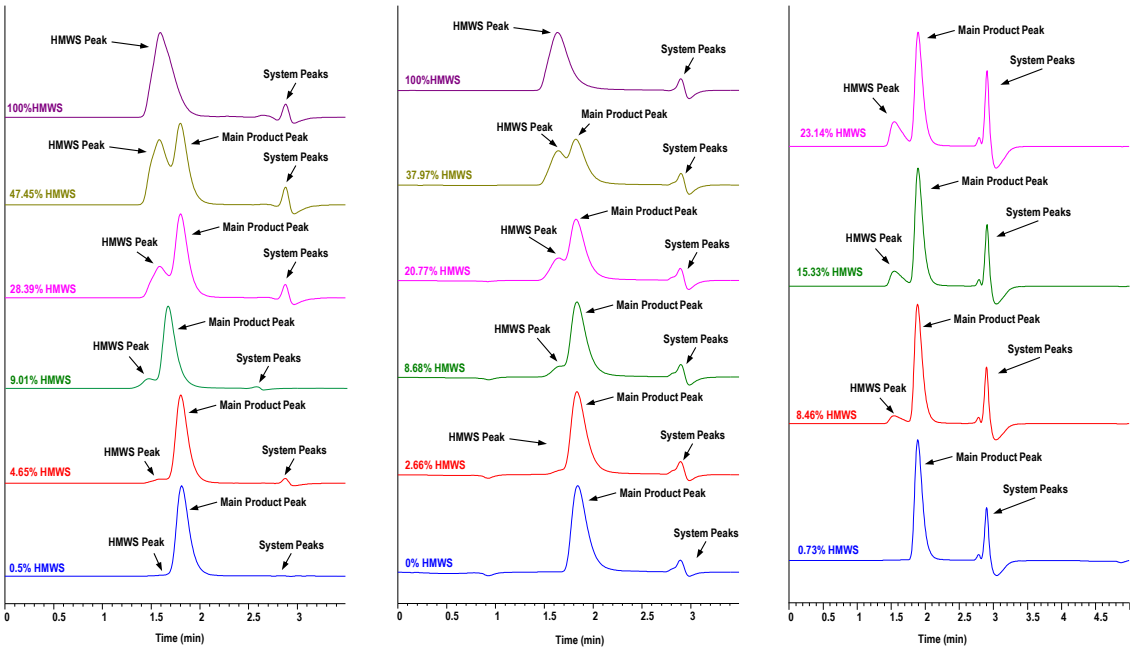

Figure 3.14 HT SEC of samples with various degrees of HMWS impurities.

HT SEC stacked chromatograms of A) BsAb-1, B) BsAb-2, and C) mAb-1 blends showing the presence of different levels of HMWS impurities. To generate the BsAb-1 and BsAb-2 sample blends, the HMWS fraction was spiked into the main product peak fraction to form samples containing 0% (blue), 10% (red), 20% (green),40% (pink), 60% (gold), and 100% HMWS whereas the mAb-1 blends were constituted by 0% (blue), 35% (red), 65% (green), and 100% (purple) stressed material spiked into the RS. The samples were diluted to 1 mg/mL prior to analysis by HT SEC with an injection volume of 5 µL.

This page was intentionally left blank

Part B: DoE-Assisted Method Development for the Analysis of mAb Charge Variants by Cation Exchange Chromatography

3.4 Abstract

Cation-exchange chromatography (CEX) is the industry gold standard for the analysis of biopharmaceuticals charge variants. However, the development of CEX methods in a time and resource-efficient manner constitutes a bottleneck in protein characterisation. CEX separations are complex and governed by multiple factors such as column chemistry, gradient type, flow rate, mobile phase composition and pH. Several scientific publications have proven the successful application of design-of-experiment (DoE) in chromatography method development. Nevertheless, performing DoEs with a large number of factors may be challenging, time-consuming and expensive. This work illustrates the use of a split-DoE approach to aid the development of a CEX method for the analysis of the charge variants profile of a mAb candidate. Analytical method development was intended to provide a high-throughput (HT) CEX method to support charge variants analysis with minimal sample and time requirements. The split-DoE approach is based on fundamental knowledge of the CEX separation mechanism and aims to reduce the number of experimental runs whilst exploring a wide experimental space. Regression modelling was used to study the effect of both individual process parameters and their interactions on the separation efficiency to ultimately identify the optimal method conditions. This study provides an efficient workflow for leveraging the development of CEX methods.

3.5 Introduction

Salt-based linear gradients are considered the gold standard in CEX method development providing high charge variants resolution and desirable method robustness (Guillarme, Fekete, and Beck, 2015). However, several scientific studies have focused on evaluating the use of pH gradients and reported the successful application in the analysis of therapeutic proteins charge variants (Füssl, Trappe, et al., 2018; Leblanc et al., 2017). The separation mechanism of CEX is inherently complex and influenced by several factors such as column chemistry, mobile phase composition, pH, type and shape of gradient often requiring optimisation for each protein drug candidate (Rea et al., 2011; Fekete, Beck, Veuthey, et al., 2015). Moreover, CEX separation mechanisms can be influenced by the type of molecule and its pI in solution, thus requiring case-by-case optimisation (Farsang et al., 2019; Murisier, Farsang, et al., 2019; Fekete, Beck, Veuthey, et al., 2015; Farsang et al., 2020). Therefore, the development of CEX methods in a time and cost-efficient way constitutes a bottleneck in protein characterisation, especially when platform methods are not fit-for-purpose.

DoE approaches have proven valuable tools for chromatography method development enabling the investigation of several factors simultaneously to finally achieve the desired separation (Kumar et al., 2018). The split-DoE approach presented in this chapter was based on fundamental knowledge of the CEX separation mechanism and was used to aid method development by reducing the number of experiments required to study multiple factors at a time and their dependencies. An example of a split-DoE strategy was previously described by Shekhawat et al. to support the development of chromatographic methods used in protein purification (Shekhawat et al. 2019). The method presented herein used a salt-based linear-gradient coupled to DAD detection for charge variants profiling of mAb-1 under native conditions. Similar to what was previously described by Shekhawat, a first DoE (DoE1) was used to investigate the factors that were expected to influence the separation most significantly, whilst a second DoE (DoE2) served to fine-tune other factors that were likely to affect the separation but were also dependent on the choice of the process parameters screened in DoE1. Precisely, DoE1 served to select the column and the mobile phase pH, whereas DoE2 was used to optimise the gradient, the buffer ionic strength, and the flow rate (F). The separation efficiency was evaluated in terms of experimental peak capacity (ePC) which was used as a response for both the DoEs (Chapter 2, Section, 2.5, Equation (2.5.1.3)).

Moreover, the resolution (Rs) between the main species peak (M) and the first basic peak (B1) was monitored as a response in DoE2. Other parameters such as g_t, column temperature, UV absorbance, injection volume, and column loading were kept constant throughout the method development as reported in Appendix A, Table 9.10. Moreover, the CEX method was implemented as a HT analytical tool, therefore it was designed to require minimal sample and time for analysis.

This study aimed to provide an efficient platform analytical workflow for CEX method development. The workflow was applied to generate a HT CEX method for the analysis of the charge variants of a mAb candidate.

3.5.1 DoE1: 4X2 Factorial Design

DoE1 is a full factorial design (FFD), a type of DoE that estimates a first-degree polynomial model and is used to gather information about all possible interactions. The size of an FFD depends on the number of factors (n) and the levels of the factors (L) under investigation which defines the number of experimental treatments (L^n). In comparison to screening designs, FFDs are large, thus, more efficiently adopted when a small number of factors are studied. The design presented here is a 4x2 factorial design, characterised by 2 factors, column and pH, of which the former is a 4 level categorical factor (4 columns) and the latter is a 2 levels continuous factor (pH 5.5 and 6.5). Moreover, a centre point was added for each categorical factor, to gather the data at the middle point of the pH range for each column as well as increasing the model strength resulting in 12 experiments in total.

Figure 3.15 illustrates the spatial representation of DoE1. CEX separations are often characterised by multiple charge variant peaks, however, it is generally impractical to achieve significant Rs for all peaks of interest whilst maintaining a desirable analysis throughput. Thus, the separation power of the chromatographic method was evaluated in terms of ePC rather than peak Rs. The ePC was chosen as a response in the DoE used for method development.

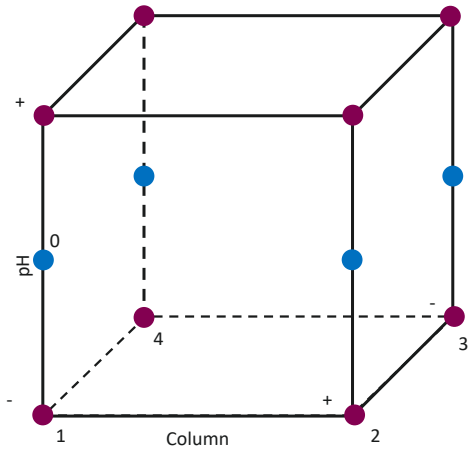

Figure 3.15 Visualisation of the DoE1 data points on a cube.
Experimental space of the 4x2 FFD under investigation displaying factorial points (purple) and the centre points (blue) on a cube. The column is a categorical factor with 4 levels (1-4) corresponding to the Agilent, Phenomenex, Sepax, and Waters columns; the mobile phase pH is a numerical continuous factor with 2 levels (+/-) corresponding to Na_3PO_4 buffer pH 5.5 and pH 6.5. The centre points correspond to the middle point of the pH range (6.0) added for each column.

To develop a HT CEX separation fit for supporting charge variants analysis of biopharmaceuticals expressed in small scale cell culture systems, the final method must also be fast and sensitive. Hence, four columns with equal dimensions (2.1 mm ID x 50 mm L) but different chemistries and packing properties were evaluated as reported in (Chapter 2, Section 2.1.4, Table 2.1). The relatively short column length enabled the use of fast gradient time (g_t) 10-15 min for separating the mAb charge variants. Each column was packed with a stationary phase made from non-porous (np) particles coated with hydrophilic polymers with a buffering capacity of 2-12 pH range. The hydrophilic polymer coating of each column was functionalised with different cation exchange ligands. The column purchased by Agilent and Waters bore a strong cation-exchanger (SCX) ligand (sulfonic group), whereas the stationary phase of the columns provided by Phenomenex and Sepax contained a weak cation-exchanger (WCX) (weakly acidic moieties such as carboxylic acid groups). Noteworthy, the columns particles had different diameters (dp) (Sepax 1.7 µm, Waters 3 µm, Agilent 5 µm, and Phenomenex 6 µm dp). It is well established that the chemical nature of the column ion exchanger, the ligand density as well as particle size can significantly influence the retention mechanism of large biomolecules in CEX (Murisier, Farsang, et al., 2019).

Since the net charge of a molecule is strongly affected by the pH, a common practice in CEX is to use mobile phases with a pH that is two values higher or lower than the analyte pI to

ensure the presence of a superficial charge. The pI of mAb-1, measured both in-silico by GPMAW and experimentally by cIEF analysis, was 9.2. Hence, the choice of a buffer system (Na_3PO_4 buffer) that covered the pH range of 5.5-6.5 was most suitable to enable the formation of a net positive superficial charge. For the reasons outlined above, the stationary phase chemical properties, structure and morphology as well as the mobile phase pH were selected for DoE1. A generic linear-gradient ramping from 40 mM to 500 mM NaCl in 15 min was applied at a flow rate of 0.17 mL/min.

Linear regression analysis was adopted to build on an empirical model to identify the best stationary phase amongst the four columns screened (Agilent, Waters, Sepax and Phenomenex) together with the optimal mobile phase pH in range 5.5-6.5. The model obtained with ePC as a response was statistically significant with p-values < 0.05 and coefficient of determinations $R^2 > 0.85$ (Appendix A, Figure 9.12). The colour-coded heat map in Figure 3.16 showed the variation of the ePC response obtained from each column *vs.* the mobile phase pH investigated. The results showed that all the columns achieved higher ePC values at pH 6.5 however, the Phenomenex column demonstrated greater separation efficiencies (29.38 ePC) in comparison to the other columns. This can be visualised by overlaying the mAb-1 CEX traces obtained from each column when using a mobile phase with pH 6.5 (Figure 3.17, A). The data showed that the Sepax column achieved lower ePC (12.25) than the Waters column and Agilent column (12.41 and 16.77, respectively).

This experiment demonstrated that when comparing mobile phases with equal ionic strength and flow rate, the separation efficiency appeared to be improved by the nature of the weak ion exchange ligand as well as the larger particle size of the Phenomenex column. Therefore, the Phenomenex column and the mobile phase pH 6.5 were identified as optimal to achieve high-resolution separation of mAb-1 charge variants.

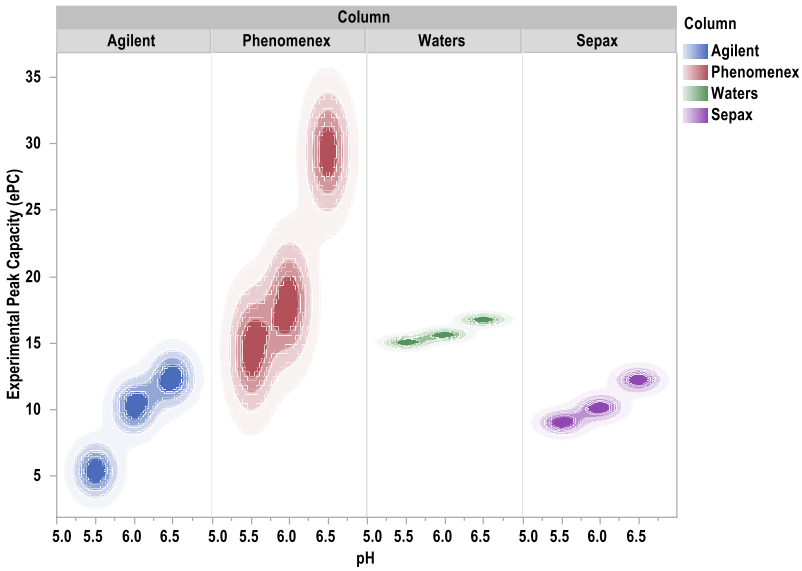

Figure 3.16 DoE1 heatmap of the ePC response in relation to the column chemistry and mobile phase pH.

The heatmap displaying the variation of the ePC in response to the mobile phase pH and the column chemistry under investigation, Agilent (blue), Phenomenex (red), Waters (green), and Sepax (purple).

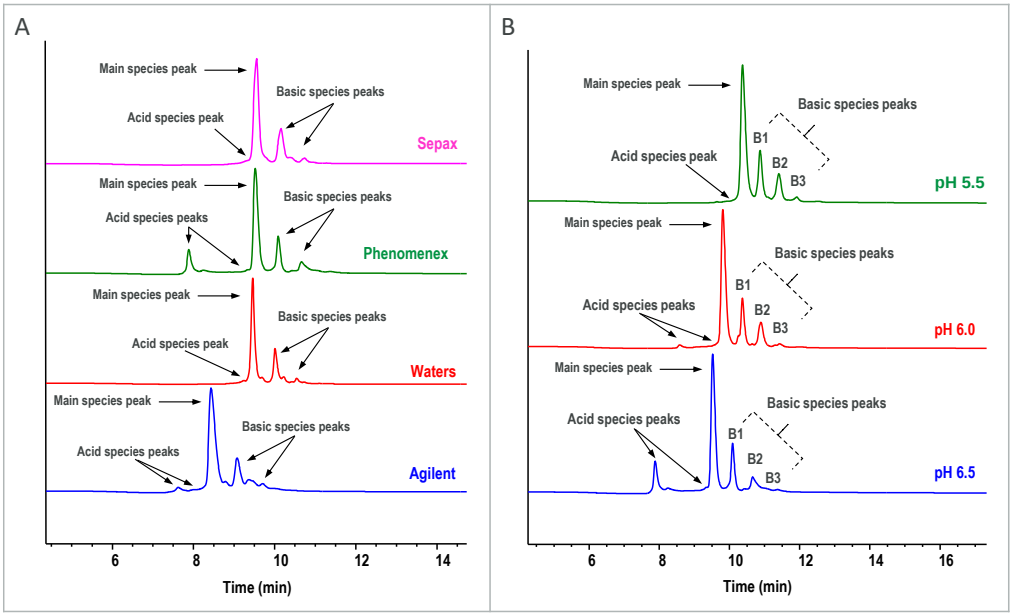

Figure 3.17 CEX charge variants profile of mAb-1 by using different column chemistries and mobile phase chromatograms.

Comparison of the mAb-1 charge variants profile obtained with the Agilent (blue), Waters (red), Phenomenex (green), and Sepax (pink) columns and a mobile phase of pH 6.5. B) Comparison of mAb-1 charge variants profile obtained with the Phenomenex column when using mobile phases of pH 6.5 (blue), 6.0 (red), and 5.5 (green). The sample was diluted to 1 mg/mL before analysis and the injection volume was kept constant at 5 µL. The method used a linear gradient ramping from 40 mM to 500 mM NaCl in 15 min, 0.17 mL/min F, 25 °C column temperature, 280 nm UV detection. Before each DoE1 treatment, column equilibration was achieved by flushing with 20 column volumes of the mobile phase composition at the start of the gradient. The column was conditioned with a blank injection before analysis of the sample.

3.5.2 DoE2: Box-Behnken Design

The design chosen for DoE2 was a Box-Behnken design (BBD), a type of response surface design generally used for optimising the response variables investigated. As shown in Figure 3.18, the BBD requires three levels and each treatment combination at the midpoint of the cube edges and the centre. This type of DoE model was considered suitable for optimising the F, gradient steepness, and mobile phase ionic strength to ultimately achieve the most desirable separation of mAb-1 charge variants. The quality of the separation was evaluated in terms of ePC and Rs between the main species peak and the first basic variants peak ($Rs_{(M/B1)}$) (Figure 3.17, B). The BBD comprised a total of 15 experimental treatments.

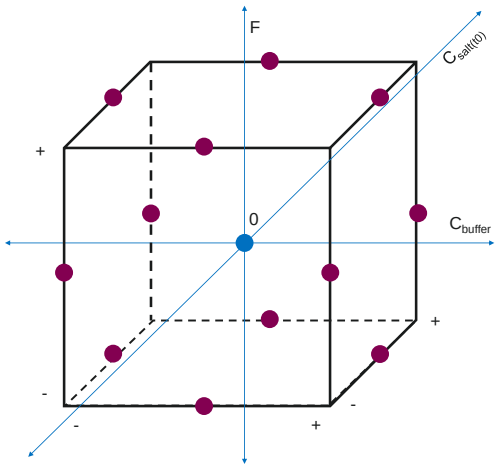

Figure 3.18 Visualisation of the data points of the DoE2 on a cube.
Experimental design space of the BBD on a cube displaying the factors under investigation, the factorial points (purple) and the centre points (blue). All the factors, namely flow rate (F), NaCl concentration at the start of the gradient ($C_{salt(t0)}$), and buffer concentration (C_{buffer}) were numerical and continuous with 3 levels (+, 0, and -) corresponding to the maximum, medium and minimum points of their range examined: F (0.13, 0.17 and 0.21 mL/min), $C_{salt(t0)}$ (0 40, 80 mM), C_{buffer} (10, 20, 30 mM). The ePC and $Rs_{(M/B1)}$-were chosen as model responses to evaluate the quality of the chromatographic separation.

Linear regression analysis was used to build an empirical model to study how the ePC and $Rs_{(M/B1)}$ varied in relation to the DoE2 factors under investigation. The model was statistically significant with p-values <0.05 and $R^2 > 0.85$ (Appendix A, Figure 9.13). Table 3.9 summarised all the model effects and their dependency on the separation efficiency evaluated as a function of both the ePC and $Rs_{(M/B1)}$. The C_{buffer}, $C_{salt(t0)}$, and F main effects were significant (p-value < 0.05) together with the C_{buffer}*$C_{buffer,}$ and F*F quadratic effects. The quadratic effects indicate the presence of curvature, thus, a range of C_{buffer} and F values

that allow for optimal ePC and $Rs_{(M/B1)}$. Moreover, the first-order interaction C_{buffer}*$C_{salt(t0)}$ was also considerable (p-value 0.09). When studying the model parameter estimates for each response (Appendix A, Table 9.12), it is clear that all the factors main effects significantly impacted both ePC and $Rs_{(M/B1)}$. However, the F*F quadratic effect was significant for the ePC and not for the $Rs_{(M/B1)}$, whilst the C_{buffer}*C_{buffer} quadratic effect and C_{buffer}*$C_{salt(t0)}$ first-order interaction were significant for the $Rs_{(M/B1)}$ and not for the ePC. This study demonstrated that the overall efficiency of the chromatographic separation was optimal at a particular F, C_{buffer}, and $C_{salt(t0)}$.

Table 3.9 Summary of the DoE2 model parameters effects.

Source	FDR LogWorth		FDR PValue
F (mL/min)(0.13,0.21)	2.746		0.00179
C_{buffer} [mM](10,30)	2.206		0.00622
C_{salt} [mM](0,80)	1.884		0.01307
C_{buffer} [mM]*C_{buffer} [mM]	1.547		0.02837
F (mL/min)*F (mL/min)	1.505		0.03129
C_{buffer} [mM]*C_{salt} [mM]	1.038		0.09161
C_{salt} [mM]*F (mL/min)	0.462		0.34491
C_{buffer} [mM]*F (mL/min)	0.220		0.60305
C_{salt} [mM]*C_{salt} [mM]	0.036		0.91945

The DoE prediction profiler exhibited how the model predictions varied in response to changes of the individual factors (Figure 3.19). A desirability function was used to estimate the factor setting which would maximise both ePC and $Rs_{(M/B1)}$ (Appendix A, Equation 9.5). It was observed that decreasing the C_{buffer} to 10 mM and increasing F to 0.2 mL/min improved the separation of the charge variants. Furthermore, increasing the $C_{salt(t0)}$ improved both ePC and $Rs_{(M/B1)}$ linearly, implying that shallower gradients improved the separation efficiency. However, it is worth noting that in CEX separations increasing the mobile phase C_{salt} causes the analyte to elute, therefore, the $C_{salt(t0)}$ must be low enough to permit binding of the analyte to the stationary phase. The optimised method conditions are summarised in Table 3.10.

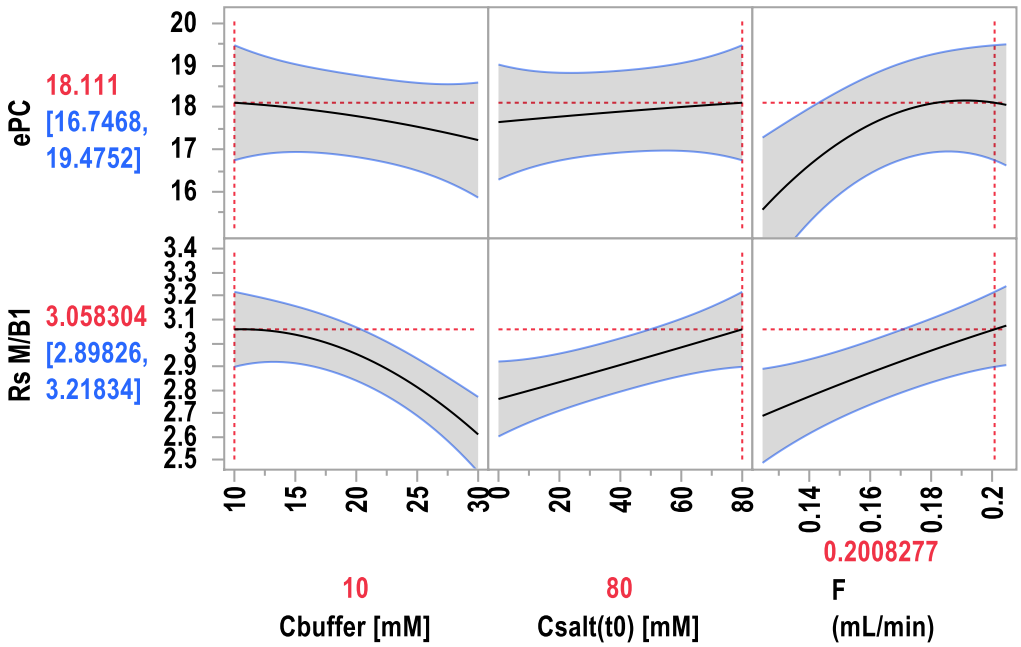

Figure 3.19 HT CEX DoE2 prediction profiler.

HT CEX DoE2 model prediction profiler displaying how the BBD responses ePC and $Rs_{(M/B1)}$ vary in response to changes in factors C_{buffer}, $C_{salt(t0)}$, and F. The relationship between ePC and $Rs_{(M/B1)}$ with changes in C_{buffer} in the range 10-30 mM shows a curvature in the C_{buffer} lower range. Increasing $C_{salt(t0)}$ in the range 10-80 mM improved both ePC and $Rs_{(M/B1)}$ linearly as did increase the F in the range 0.13-0.21 mL/min where the $Rs_{(M/B1)}$ whilst the ePC showed a curvature in F upper range. The BBD factors were set to the maximum desirability function and the model estimates optimal values of C_{buffer}, $C_{salt(t0)}$ and F as 10 mM, 80 mM, and 0.2 mL/min, respectively.

Table 3.10 Summary of the optimised HT CEX method.

HT CEX Method
Column: Phenomenex: bioZen WCX 2.1 x 50 mm, 6 um, np
Mobile phase: A) 10 mM Na3PO4, 80 mM NaCl; B) 10 mM Na3PO4, 80 mM 1 M NaCl
Gradient: 8-40%B in 0-10 min linear ramp, 40-80%B in 0.1 min, 80%B 2 min hold, 8%B in 0.1, 8%B 3 min hold.
gt: 10 min
F: 0.2 mL/min
Temperature: 25 °C
Injection Volume: 5 µL
Sample concentration: 1 mg/mL
UV: 210 nm, 280 nm

3.5.3 Model Verification and Method Assessment

Method assessment was performed to evaluate whether the HT CEX method was fit to support sample testing. Specificity was assessed by comparing the UV profile of a sample containing mAb-1 against those obtained by injecting 20 µL of process buffers and no interfering peaks were observed (Appendix A, Figure 9.14). Method repeatability was tested by calculating the R_t, $Rs_{(M/B1)}$, and ePC CV of the main species peak and B1 using 5 µL injection of 6 technical replicates of a mAb-1 sample at a concentration of 1 mg/mL. The repeatability test verified the DoE model estimates with average ePC and $Rs_{(M/B1)}$ values of 18.15 and 3.6, respectively (Appendix A, Figure 9.15). A sample of mAb-1 RS was treated to induce chemical oxidation by AAPH in order to assess the method stability-indicating capability (Figure 3.20). The UV profile overlay of mAb-1 RS *vs.* the stressed sample demonstrated that the method was able to identify differences in mAb-1 superficial charge distribution. An 8-levels linearity study was performed as previously described (see Section 3.3.2.5) to assess the linear response of the main species peak area *vs.* the sample concentration as well as to extrapolate the method LOD and LOQ and determine the column loading range. The method LOD and LOQ were defined for the smallest basic species peak in the chromatogram (B3). The method assessment data were reported in Table 3.11.

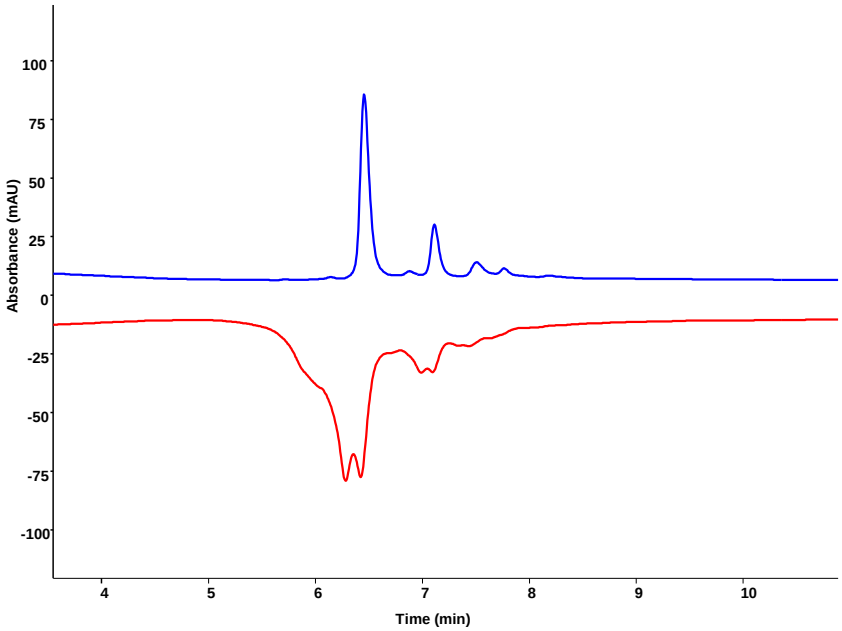

Figure 3.20 HT CEX method stability-indicating capability.
HT-CEX chromatograms mirror-overlay of a mAb-1 sample stressed with AAPH (red) against its RS (blue). Chemical stress was induced by exposure to 1% AAPH for 24 hours at 25 °C and then the sample was buffer-exchanged to remove the stressor. Both RS and the stressed sample were diluted to 1 mg/mL before analysis and the injection volume was 10 µL.

Table 3.11 HT CEX method assessment results.

Parameter	Target Expectation	Qualification Results
Specificity	Buffer profiles	No interfering peaks from mobile phases and formulation buffer at the retention times of the RS peaks (Appendix A, Figure 9.14).
Stability-indicating	Observe the change in the RS peak profile	Changes Observed (Figure 3.20).
Repeatability	No more than 0.5 min retention time (RT) difference between the shortest and longest reference peak retention time across the sample replicates (n=6). NMT 10% CV Rs(M/B1) and ePC across the sample replicates (n=6).	RT_M CV = 0.24; RT_{B1} CV = 0.27; Rs(M/B1) across CV = 3.2; ePC CV = 2.7 (Appendix A, Figure 9.15).
Linearity	$R^2 \geq 0.98$ for the charge variant reference peak area linearity.	Main Species peak: R^2 = 0.99. Basic peak (B1): R^2 = 0.98. (Appendix A, Figure 9.16).
LOD	Linear response of reference peak area *vs.* the protein load (B3) $R^2 \geq 0.95$. Results reported as % of the total peak area.	B3 1.14% (1.7 mg)
LOQ	Results reported as % of the total peak area	B3: 3.4% (5 mg)
Column loading range	Extrapolated from the linearity and LOQ study	5-25 µg

3.6 Conclusions

The present chapter introduced the development of HT tools to support the purification and product quality analysis of mAbs and BsAbs expressed in 96-DWP cell culture systems. Moreover, efficient DoE-based analytical approaches to method development were proposed and implemented.

Part A presented the development of a HT platform workflow for the purification and aggregation analysis of mAbs and BsAbs from shaken 96-DWP cell cultures. The purification method employed Protein-A filled PhyTip columns and was successfully automated on a robotic liquid handler for the parallel processing of 96 samples at a time. Method development aimed to maximise the protein %R to provide sufficient material for following analytical testing in a suitable time for HT operations. DoE-assisted method optimisation helped the identification of optimal purification conditions in a total of 32 experimental runs. The final validated PhyTip-based purification method was fit for the purification of as little as 300 μL of HCCF providing >80%R over a titre range of 200-3000 mg/L in < 2 hours. Post-purification product quality analysis was assessed by HT SEC which confirmed that the PhyTip-based purification method did not alter the size variants profile of the molecule of interest. Method assessment studies confirmed consistency with the requirements of the final application which is the purification of mAbs and BsAbs from 96-DWP cell culture systems. The PhyTip-purification process provided a 96-DWP with 160 μL per well of purified and enriched product to support analytical testing.

A small-scale HT SEC method was developed on 2.1 mm ID columns and provided a rapid analytical tool for aggregation analysis with sub-2 μg sensitivity. The HT SEC method showed some loss in Rs compared to the benchmark SEC method (AZ SEC SOP) however, the HT method allowed the separation and relative quantification of HMWS in a much faster time scale and can therefore be applied as a ranking tool to support early-stage CLD. With 3.5 min analysis time per sample, the HT SEC enabled the processing of a 96-DWP in < 6 hours with a 6-fold throughput gain in comparison to the benchmark SEC method. Moreover, the need for as little as 2 μg of sample per injection provided a 10-fold lower material required for analysis than HT SEC methods performed on 4.6 mm ID columns (AZ HT SEC method).

The entire analytical workflow from HCCF purification to aggregation analysis allowed the processing of a 96-DWP in ~8 hours and demonstrated enough sensitivity to be applied to cell cultures with low expression titres. This analytical workflow was qualified as a suitable HT engine to feedback CLD activities with PQ information to support process development.

Part B of the present chapter presented a split-DoE approach to aid the development of CEX methods for novel therapeutic candidates. Owing to the complexity of CEX separations, method development is often laborious and resource-demanding. The proposed approach aimed to minimise the time and resources required for the development of a CEX fit for HT applications. The split-DoE workflow involved the use of an FFD for selecting the column and mobile phase pH range, followed by a BBD to optimise the method F and gradient steepness. With a total of 27 experimental runs, this approach enabled the screening of 4 columns, mobile phase composition, pH range, and F to optimise a CEX method for the charge variants analysis of a mAb candidate.

Method development was directed to provide a small scale HT CEX method to be employed as a HT tool in process development to support the charge variants analysis of a mAb candidate. The method used a 2.1 mm x 50 mm (ID x L) column and allowed a 15 min separation requiring 5 μg of sample per run. This would lead to the processing of an entire 96-DWP in ~8 hours. The present method can be applied as part of the PhyTip-purification/HT SEC workflow, however, it is limited for use with the specific mAb candidate. Potential implementations of the HT CEX as a platform method can use the proposed split-DoE approach to develop a platform method by extending the procedure to 6-10 candidates from a class of molecules with different pIs. The implementation of the methods developed herein is further discussed in Chapter 6.

This page was intentionally left blank

Chapter 4

Integrating aggregation and charge variants analysis in one single method by heart-cutting 2D SEC-CEX-MS.

4.1 Abstract

Monoclonal antibodies (mAbs) are extremely complex due to the presence of structural modifications resulting from various enzymatic and chemical reactions such as glycosylation, glycation, deamidation, isomerisation, oxidation, aggregation and fragmentation. Analysis of size and charge variants are carried out from the early stages of drug development throughout a product lifetime to investigate degradation pathways and process conditions. This chapter presents the development of a 2D-LC approach combining both size and charge variants profiling of a mAb candidate in a single method. The quantification of aggregates was performed in the first dimension (^{1}D) by SEC, followed by online fraction transfer of the main product peak by a heart-cutting to the second dimension (^{2}D) for charge variants analysis by CEX. Aiming to maximise the information obtained from minimal sample and time required for analysis, a salt-based separation with UV detection was developed for supporting the processing of a large number of samples in compliance with high-throughput (HT) applications. In addition, a mass spectrometry (MS) compatible SEC-CEX separation was developed enabling online identification of charge variants. Accelerated forced degradation and stability studies of a mAb were performed to generate samples with relevant structural modification and thus demonstrate the application of the proposed methodology. This study proved that the ^{1}D SEC was compatible with the ^{2}D CEX and linked size and charge variants analysis in a real-time and efficient manner. To date, this is the first 2D SEC-CEX-UV and SEC-CEX-MS application for intact mAb analysis.

4.2 Introduction

Over the last decade, the value of 2D-LC for the analysis of large molecules has been evidenced by a wide range of publications focusing both on mAbs and next-generation antibody formats (Sarrut et al., 2016; Petersson et al., 2017; Sandra et al., 2017; An et al., 2017; Pirok et al., 2019; Camperi et al., 2021). In a review published in 2021 on multi-dimensional (mD) LC-MS techniques, Camperi stressed the advantage of 2D-LC approaches in hyphenating orthogonal separation modes to enable the analysis of multiple product quality attributes (PQAs) in one single method. The potential of mD-LC in automating sample preparation was previously reviewed by Graf et al. (Graf et al., 2020). The authors reported the works of Bathke, Gstöttner and Goyon as proof of fully automated mD-LC workflows supporting online sample reduction, digestion and separation coupled to MS detection (Bathke et al., 2021; Goyon et al., 2020; Gstöttner et al., 2018). According to both Graf and Camperi, the recently published scientific literature emphasised the suitability of mD-LC for application to HT analytical platforms. This is due to the fact that online fractionation minimises sample loss and accelerates analysis workflows in comparison to offline fraction collection techniques. This is achieved by a modulator that collects a portion of eluents from the ^{1}D and transfers them to the ^{2}D. The device forms the heart of 2D-LC systems and is generally constituted by a valve or ensemble of valves equipped with sampling loops for parking and transferring the fractions of effluent from the ^{1}D to the ^{2}D. Depending on the complexity of the sample and the type of analysis that is desired, several modes of 2D-LC can be selected for online fraction transfer. The fractionation of a limited number of peaks is achieved by LC-LC modes such as heart-cutting, and multiple-heart cutting, whilst LC × LC modes such as selective comprehensive and comprehensive are usually preferred for complex mixtures.

Evidence of the growth of 2D-LC approaches in industry was the scientific publications reporting the implementation of 2D-LC methods for supporting analytical testing. An example is the 2D IEX-SEC method developed by An et al. used to bridge size and charge variants analysis to support mAbs developability studies (An et al., 2017). Online fractionation of IEX peaks using a heart-cutting schedule enabled the analysis of the size variants of each IEX cut minimising sample requirement and analysis time that would be necessary with conventional offline methods. The popularity of 2D-LC has recently gained momentum in PAT to streamline the purification of the target protein from the host cell

culture fluid (HCCF) and structural characterisation analysis in a time-efficient fashion. Industrial applications of 2D-LC methods have been successful in leveraging lead candidate selection, clone selection, process optimisation, and extended characterisation. For instance, Dunn et al. have presented a sub-5 min 2D-LC Protein A-SEC method for measuring titre and aggregation of a target mAb from HCCF (Dunn et al., 2020). Similarly, Williams et al. have demonstrated the implementation of a 2D heart-cutting Protein A-SEC method for automating aggregate analysis to crude in-process samples (Williams et al., 2016). Sandra et al. explored the combination of Protein A to different modes of chromatography such as SEC-UV, IEC-UV and RP-MS to cover the analysis of a range of PQAs (Sandra et al., 2017). Besides the higher resolving power of 2D-LC approaches being particularly beneficial for MS analysis, the presence of concentrated salts and additives in LC mobile phases has serious consequences on MS detection and often hampers the online coupling of the two analytical techniques. In this regard, several examples were reported in the literature demonstrating that online hyphenation of salt-mediated chromatographic separations to MS can be possible when the ^{2}D is used for desalting prior to MS injection (Luo et al., 2017; Petersson et al., 2016). Both Jaag (2021) and Stoll (2015) presented 2D-LC strategies for multi-level characterisation of mAbs charge variants by CEX×RPLC-TOF-MS highlighting the comparability as well as the advantages of the 2D approaches *vs.* the conventional 1D-LC-MS methods (Stoll et al., 2015; Jaag et al., 2021).

Despite the superiority of 2D-LC in addressing large biomolecules characterisation, method development remains challenging with the incompatibility between the two dimensions solvent systems being a frequent limitation (Stoll and Carr, 2017). For instance, peak broadening and distortion can be observed when the properties of the ^{1}D effluent result in low retention of the analyte in the ^{2}D. Another challenge of 2D-LC separations is the partial sample loss and dilution resulting as a consequence of peak fractionation and parking into the 2D-LC valve loops before the transfer to the ^{2}D. This constitutes an issue for the method sensitivity and is particularly accentuated when one peak of the ^{1}D is cut into many (e.g. multiple-heart-cutting) hence, each peak will result in a significant loss in the ^{2}D signal. Therefore, complications regarding the complexity of method development may still hamper the integration of 2D-LC methods to routine analytical workflows. Egeness et al. described various modulation strategies developed for ensuring both the compatibility between chromatographic dimensions and sample enrichment prior to 2D-LC injection (Egeness et al., 2016). The current most popular modulation strategies adopted to overcome mismatches

in mobile-phase composition are the Active Solvent Modulation (ASM) introduced by Stoll et al. and the Stationary-Phase-Assisted Modulation (SPAM) described by Vonk et al. (Stoll et al., 2017; Vonk et al., 2015). The former is obtained by diluting the ^{1}D solvent through an ASM capillary before it reaches the ^{2}D column resulting in the sample focusing at the head of the ^{2}D column and consequent improvement of the resolution (Rs). The latter consists of the use of trapping columns instead of storage loops that retain the analytes whilst the ^{1}D solvent flows through. Upon the valve switching, the ^{2}D solvent enters the trap column and the sharp band of analytes is eluted into the ^{2}D column. The introduction of such technological advancements has favoured the implementation of 2D-LC methods for routine biopharmaceutical analysis (Pirok et al., 2018; Stoll et al., 2017; Vonk et al., 2015; Pirok et al., 2019).

The present study aims to develop a 2D-LC approach for the analysis of mAb multiple quality attributes in a single method by coupling orthogonal modes of chromatography. The combination of orthogonal chromatography modes in a 2D-LC set-up maximises the information obtained from minimal sample consumption and analysis time demonstrating suitability for application to HTPD workflows. Analytical testing for supporting mAbs size and charge variants analysis is pivotal at all stages of drug development, manufacturing and shelf-life. The surface charge diversity of a protein may be indicative of the structural modifications which may translate to different efficacy and immunogenicity and must therefore be tightly controlled. The charge variants profile of a mAb can be used as a fingerprint of its structural heterogeneity throughout the development process. Over the last decades, SEC and IEX have established themselves as gold standard analytical methodologies for the assessment of intact therapeutic protein aggregation and charge variants, respectively. Both techniques do not require laborious sample preparation and their implementation in analytical workflows is usually straightforward. However, peak characterisation remains a challenging task of both SEC and CEX methods often requiring fraction-collection and peak identification by MS. Traditional workflows involve peak fractionation and desalting followed by middle-up or bottom-up analysis such as peptide mapping. Recent studies have demonstrated the benefit of using volatile buffers for hyphenating IEX to MS online for the analysis of mAb charge variants at the intact level (Haberger et al., 2021; Polderdijk et al., 2019; Yan et al., 2018). One of the drawbacks of MS analysis is the overall loss of the method throughput due to the complexity of the procedure requiring expensive equipment and specialised expertise.

This chapter proposes the development of an online 2D SEC-CEX separation for combining the analysis of mAb aggregates and charge variants in a single method. Up to date, there is no evidence in the literature of online 2D SEC-CEX methods developed for supporting biopharmaceuticals PQ analysis in HTPD. Using this novel approach, aggregate analysis was assessed in the ^{1}D by SEC; heart-cutting 2D-LC was used to transfer the main product peak to the ^{2}D for charge variants analysis to separate the charge variants associated with the main product without including the aggregates. The SEC-CEX separation was achieved using both non-volatile buffers with UV detection and volatile buffers for online coupling with ESI-MS detection. The advantages and disadvantages of using MS and the feasibility of native MS analysis were discussed. Finally, the application of both methods to case study samples in support of clone selection (see Chapter 6) and product developability studies were presented. This work demonstrated the versatile application of the present method to various stages of product development and is proposed as an effective analytical tool to be integrated into HTPD workflows.

4.3 Results and Discussion

4.3.1 Heart-cutting 2D SEC-CEX-UV method development, Part A: selection of the ^{1}D SEC conditions for coupling CEX in the ^{2}D

One challenge of the online coupling of SEC to CEX is the incompatibility between the ^{1}D and the ^{2}D mobile phases. SEC separations require high ionic strength mobile phases to limit the non-binding interactions between the analyte and the column stationary phase (Goyon et al., 2018). The mobile phases are usually composed of a mixture of >0.1 M PO_4^{3-} or SO_4^{2-} buffers with the addition of >0.1 M Na/KCl to prevent ionic interactions. Conversely, CEX mobile phases require low-ionic strength (typically <50 mM PO_4^{3-} or MES) buffers. Salt-based gradients in CEX separations start at a low salt concentration to favour the retention of the mAb ions to the cation exchange matrix. By gradually increasing the mobile phase counter ions, the protein ions are displaced from the ion-exchange sites and begin to elute. For this reason, the high salt content of SEC mobile phases may impede the initial binding to the ^{2}D CEX stationary phase resulting in a significant breakthrough of unbound protein. Likewise, low-ionic strength mobile phases (<0.1 M Na/KCl) may not be suitable for SEC.

In the context of this study, the development of the 2D SEC-CEX-UV method focused on finding the optimal conditions that allowed the separation of HMWS impurities in the ^{1}D as well as the binding of the mAb to the ^{2}D stationary phase for charge variants separation. A DoE approach was adopted to identify the optimal SEC conditions that enabled aggregate analysis along with the coupling of CEX in the ^{2}D. A full-factorial DoE was chosen for selecting the optimal SEC column and mobile phase composition. The percentage high-molecular-weight species (%HMWS) and Rs between the main product and HMWS peaks were monitored as DoE responses. More information on the chromatography columns, chemicals and equipment used were shown in (Chapter 2, Section 2.1.4, Table 2.1). Different combinations of Na_3PO_4 and NaCl concentrations in the range 50-200 mM and 0-200 mM, respectively, were assessed. The choice of the concentration range used for the mobile phase was based on previous knowledge of the class of molecules and aimed to maintain their native state without impacting the formation of HMWS impurities and unfolding events. Other chromatographic method parameters were kept constant as reported in Table 4.2. To generate a sample suitable for method development, mAb-1 reference standard (RS) was stressed at 70°C and 300 rpm shaking for 60 min. As previously assessed by a standard

operating procedure (SOP) method developed by AstraZeneca for supporting SEC platform testing (AZ SEC SOP), the heat-stress treatment allowed the formation of ~15-20% HMWS impurities and served to generate a model sample for analytical method development (Appendix B, Figure 10.1). More information on the LC equipment and chemicals used for this analysis can be found in Chapter 2, Section 2.1.2.2. The complete list of the DoE treatments and response values was reported in Appendix B, Table 10.1.

Linear regression analysis was used to build two empirical models to identify the column resin and mobile phase composition that achieved ~15% HMWS and maximised the Rs between the HMWS and main product peaks with minimal salt content. The models obtained for both responses were statistically significant with p-values ≤ 0.05, RMSE < 2, and $R^2 \geq 0.95$ (Appendix B, Figure 10.2).

Table 4.1 DoE factors effects summary.

Source	FDR LogWorth		FDR PValue
Column	10.182		0.00000
[NaCl] (mM)(0,200)	8.960		0.00000
[Na_3PO_4] (mM)*[NaCl] (mM)	7.542		0.00000
[Na_3PO_4] (mM)(50,200)	7.138		0.00000
[NaCl] (mM)*Column	5.259		0.00001
[Na_3PO_4] (mM)*[NaCl] (mM)*Column	4.895		0.00001
[Na_3PO_4] (mM)*Column	3.806		0.00016

All the DoE main effects, second and third-order interactions between column, and concentration of NaCl and Na_3PO_4 in the mobile phase were significant (p-value ≤ 0.05) for both %HMWS and Rs (Table 4.1), indicating that optimal SEC separations were the result of the harmonised interplay of column chemistry and mobile phase composition. The contour plots reported in Figure 4.1 showed the effects of the NaCl and Na_3PO_4 concentration on both the %HMWS and Rs obtained for each column.

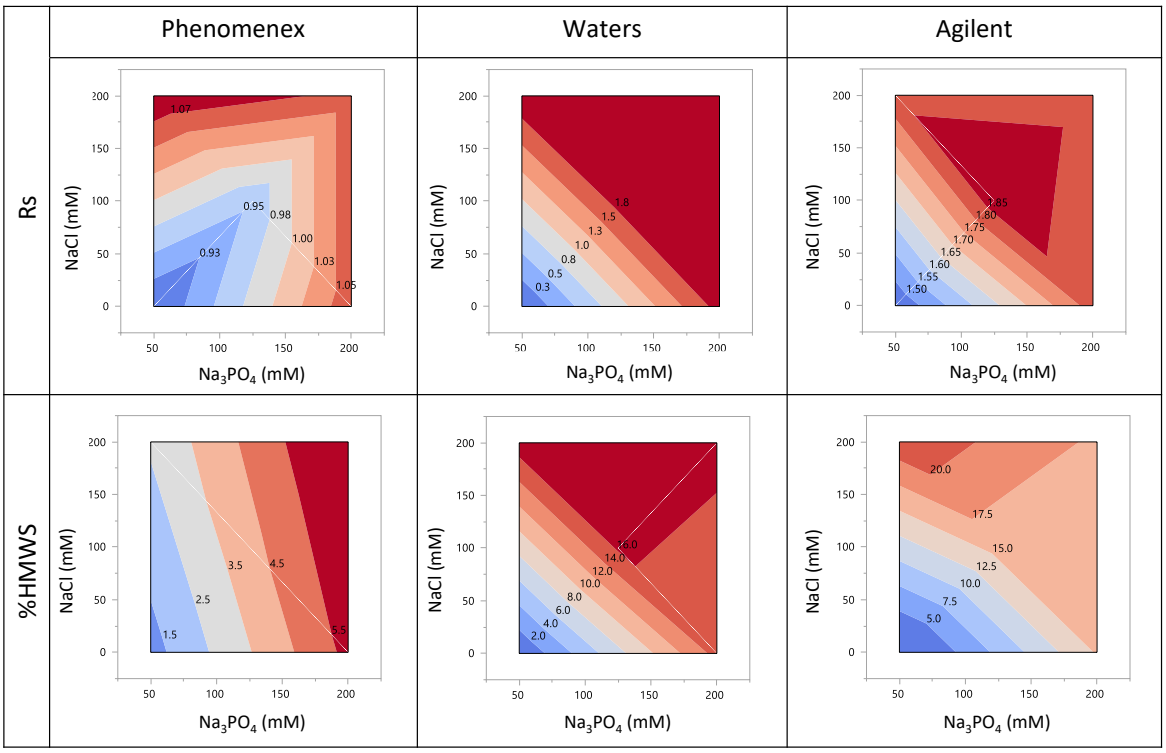

Figure 4.1 Contour plot showing the effect of the mobile phase composition and column chemistry on SEC separation.

The contour plot showed how Rs (top) and %HMWS (bottom) change in response to modifications in mobile phase composition across the three columns. The colour gradient shifts from blue to red shades to indicate low and high response values, respectively. The shaded areas were labelled with the respective values of Rs and %HMWS.

Overall, the separation efficiency improved by increasing the mobile phase ionic strength within the range tested in the DoE. The major contribution was given by the concentration of NaCl since it is a stronger salting-out agent than Na_3PO_4. Improved Rs and optimal values of %HMWS could be achieved with mobile phases composed of > 100 mM NaCl with all the columns. Interestingly, the %HMWS and Rs response values as a consequence of changes in mobile phase composition were different across the three columns. The Rs obtained with the Phenomenex column was lower than both the Agilent and Waters columns with Rs values ≥ 1 achieved only with mobile phases containing >100 mM NaCl. The analysis performed by using the Waters and Agilent columns with mobile phases composed of 125-200 mM Na_3PO_4 and 75-200 mM NaCl, resulted in %HMWS comparable to those achieved by the AZ SEC SOP method (~15%) and Rs > 1.5. However, when compared to Waters and Phenomenex, the Agilent column required lower ionic strength mobile phases to achieve the desirable %HMWS and optimal Rs.

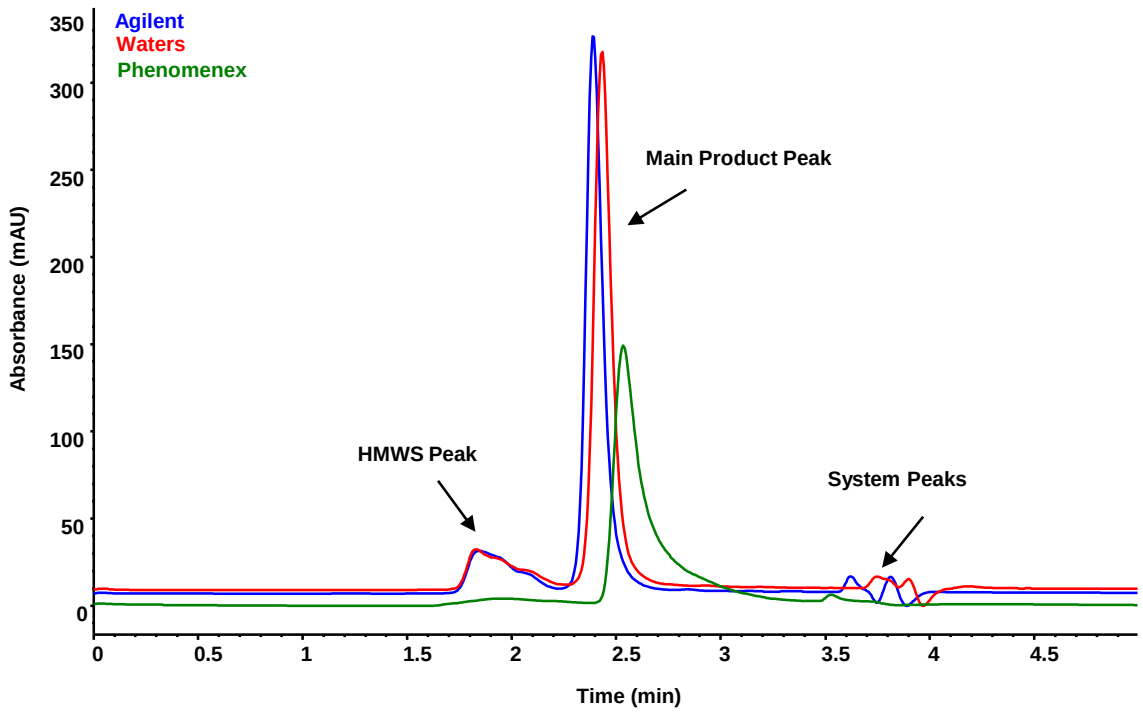

Figure 4.2 Overlay of heat-stressed mAb-1 chromatograms obtained by using the same ionic strength mobile phase across three columns.

SEC chromatograms overlay of the heat-stressed mAb-1 sample analysed using the Phenomenex (green), Waters (red), and Agilent (blue) columns and the mobile phase composed of 200 mM Na_3PO_4, 200 mM NaCl, pH 6.8. The sample was analysed by injecting 10 µL of the same vial across the three columns. The peak total areas obtained from each column were 2487, 2377, and 2290 Agilent, Waters, and Phenomenex, respectively.

Figure 4.2 shows the chromatographic overlay of mAb-1 obtained with the highest ionic strength mobile phase tested. Although the peak total areas obtained from each column were comparable (2487 Agilent, 2377 Waters, 2290 Phenomenex), the Phenomenex column showed extensive peak tailing and poor Rs between HMWS and main product peaks, suggesting the presence of secondary electrostatic interactions between the mAb and the stationary phase. The chromatograms obtained with the Agilent and Waters columns overlayed without major differences.

Since Na^{2+} functions as a counter ion in CEX separations competing with the mAb ions for binding to the stationary phase, gradients starting with high concentrations of NaCl may not be appropriate for CEX applications. This experiment proved that the efficiency of SEC separation was strongly dependent on the column chemistry and suggested that the Phenomenex column may require either higher NaCl concentrations or the addition of organic solvents to the mobile phase to achieve better separations. Nevertheless, neither of these adjustments would be beneficial for coupling CEX in the ^{2}D. Overall, the separation

performance of the Agilent column was less influenced by the concentration of NaCl with the highest separation efficiencies achieved with mobile phases composed of ≥ 100-175 mM Na_3PO_4 buffer.

The DoE prediction profiler reported in Figure 4.3 displayed how %HMWS and Rs changed as a consequence of the variation in the mobile phase concentration of Na_3PO_4 and NaCl across the columns tested. Prediction parameters set for a mobile phase composed of 100 mM Na_3PO_4 showed that the %HMWS predicted for the Agilent was 12.5%, whilst for Waters and Phenomenex columns was 6% and 3%, respectively. Likewise, the Rs between HMWS and main product peak was greater with the Agilent column (Rs = 1.6) than the Waters and Phenomenex (Rs = 0.7 and 0.9, respectively). Therefore, the Agilent column was selected for this application and the DoE model was verified experimentally for this column only (see Section 4.3.1.1).

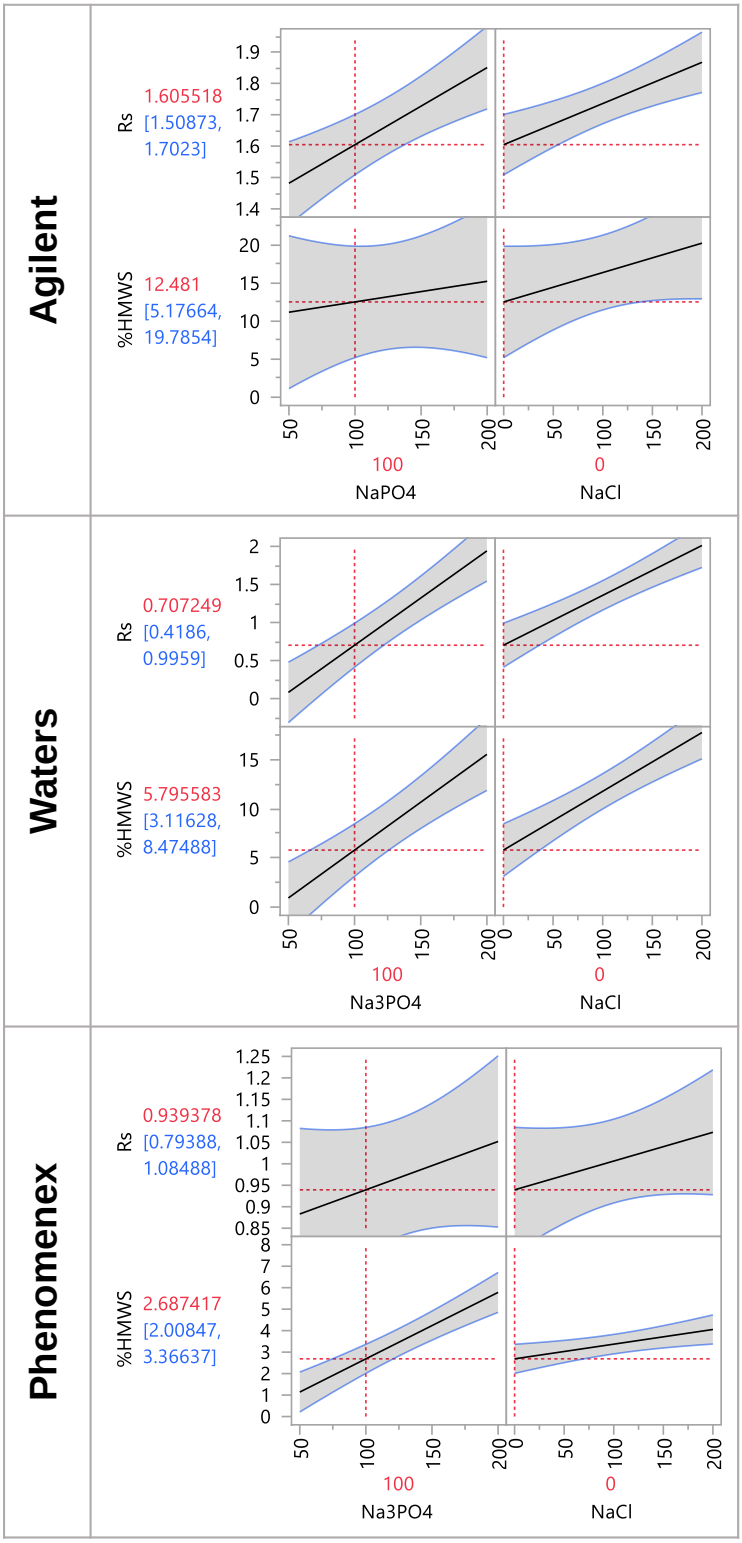

Figure 4.3 DoE prediction profiler for the 2D SEC-CEX-UV method ^{1}D column selection.

The DoE prediction profiler factors were set with fixed values and the response estimates were calculated by the model. The concentration of Na3PO4 buffer and NaCl were set to 100 mM and 0 mM, respectively. The %HMWS (left) and Rs (right) values were calculated separately for each column. The Agilent column (top) was predicted to obtain 12.5% HMWS and 1.6 Rs; the Waters column (middle) was estimated to obtain 5.8% HMWS and 0.7 Rs; the Phenomenex column estimates were 2.7% and 0.9 for HMWS and Rs, respectively.

4.3.1.1 DoE Verification and ^{2}D CEX Coupling by heart-cutting 2D-LC

To verify the DoE model and evaluate the compatibility between the two dimensions, a sample of heat-stressed mAb-1 was analysed in duplicate by using three different ionic strength mobile phases containing 50 mM, 100 mM and 200 mM Na_3PO_4 buffer (Figure 4.5). The ^{2}D CEX separation was performed on the AgilentBio WCX Column, (Chapter 2, Section 2.1.4, Table 2.1). The ^{2}D mobile phase was composed of 25 mM Na_3PO_4, pH 6.0 as buffer A and 25 mM Na_3PO_4, 1 M NaCl, pH 6.0 as buffer B. The mAb-1 main product peak eluting at 2.3 min was transferred to the ^{2}D by an heart-cutting schedule.

The 2D-LC valve configuration for heart-cutting is described in Figure 4.4. The ^{2}D CEX separation was achieved by using a salt-based linear-gradient ramping from 0%B to 48%B in 12 min at 0.2 mL/min flow rate, followed by wash and column equilibration with a total 2D separation time of 20 min.

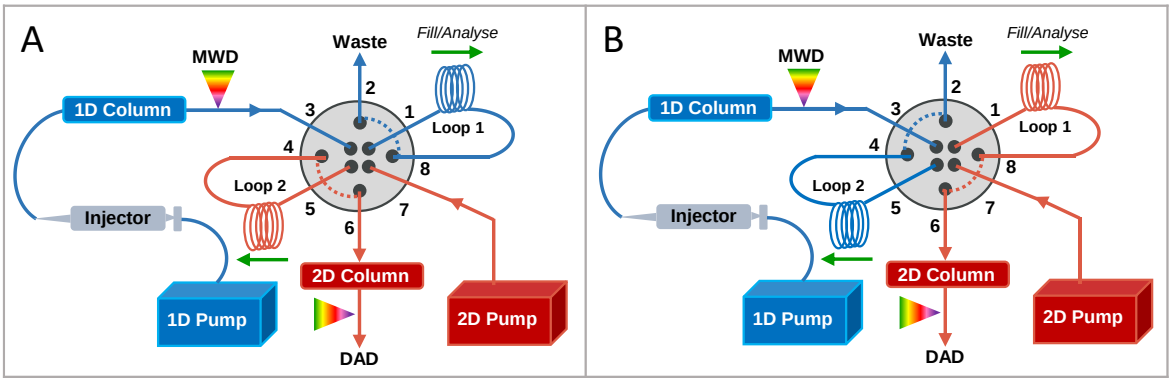

Figure 4.4 Schematic of the 2D-LC system with 2D valve plumbing flow path.
Schematic representation of the 2D-LC system and pumping diagram with the central 2 positions/4 ports 2D-LC valve in concurrent configuration. A) The 2D-LC starts with the valve in position 1 with the ^{1}D effluent passing through loop 1 (blue path). Here the heart-cutting fraction coming from the ^{1}D is parked into sample loop 1. B) Switching valve in position 2 injects the sample in loop 1 into the ^{2}D cycle (red path) whilst loop 2 is filled with the ^{1}D effluent. At the completion of the ^{2}D separation, the valve switches back to position 1 and the contents of loop 2 are injected. The green arrows indicate the concurrent direction of the flow during loop filling and analysis. When loop filling and analysis have opposite flow directions, the valve is set to counter current configurations.

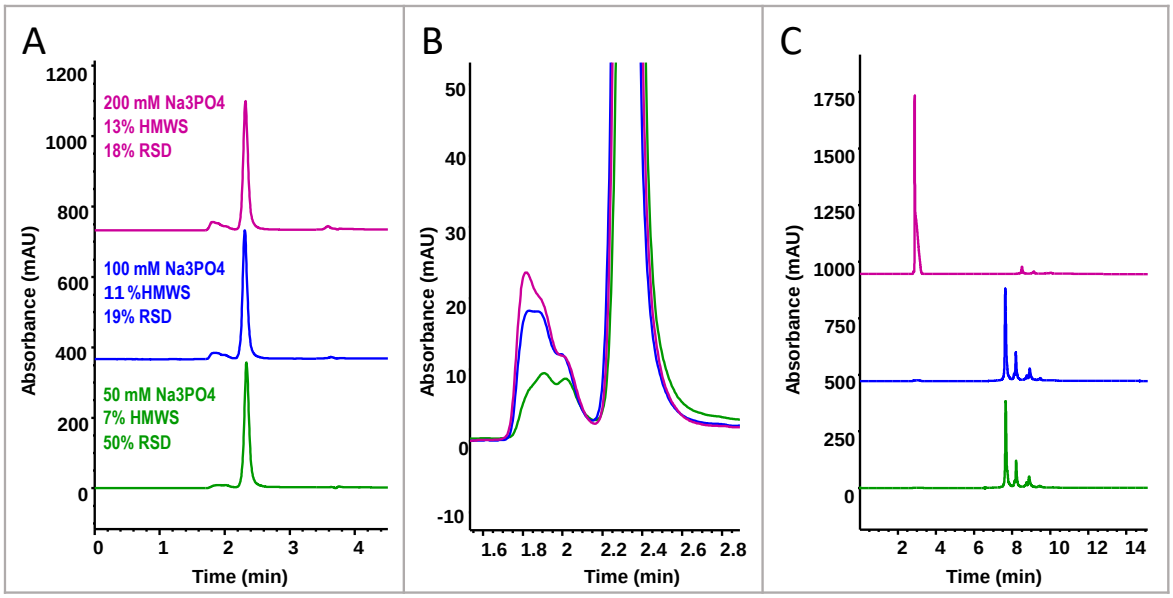

Figure 4.5 DoE verification and evaluation of the ^{1}D SEC mobile phase compatibility with the ^{2}D CEX separation.

Verification of the predictions from the DoE model was performed on the Agilent column for 3 conditions involving the use of mobile phases composed of 50 mM (green), 100 mM (blue), and 200 mM (pink) Na_3PO_4 buffer, pH 6.0. (A). The %HMWS obtained experimentally (B) followed the responses estimated by the model with greater separation efficiency obtained with higher Na_3PO_4 buffer concentrations. The ^{2}D mAb-1 CEX profiles (C) showed that SEC mobile phase ionic strengths >100 mM are not compatible for online coupling of CEX in the ^{2}D.

The data shown in Figure 4.5 (A, B) confirmed that the response values were close to their estimates for the three conditions tested and across the technical replicates. As previously reported by the DoE study, the experimental results confirm that the Agilent column stationary phase chemistry enabled the separation of mAb aggregates without the addition of NaCl. The %HMWS varied across the mobile phase tested, 7.4%, 11.7% and 13.4% using 50, 100 and 200 mM Na_3PO_4 buffer, respectively. The %HMWS acquired by using 50 mM Na_3PO_4 was significantly lower than those obtained with 100-200 mM Na_3PO_4 and showed greater variation across the replicates (Appendix B, Figure 10.3). This study confirmed that ≥100 mM Na_3PO_4 buffers were necessary to minimise protein-stationary phase interactions and improve Rs. Nevertheless, both 50 mM and 100 mM Na_3PO_4 buffer SEC mobile phases enabled the coupling of CEX in the ^{2}D with binding of mAb-1 to the CEX stationary phase. Conversely, the 200 mM Na_3PO_4 mobile phase ionic strength impeded the binding of the protein to the ^{2}D and resulted in an extensive breakthrough. Since the quantitation of HMWS impurities was aimed to match the AZ SEC SOP, the mobile phase composed of 100 mM Na_3PO_4 was chosen as optimal for this application. To assess how the two SEC methods differ in the quantitation of HMWS impurities, 6 technical replicates of a heat-stressed mAb-

1 sample were analysed with both methods. The mean %HMWS was 17% obtained with the AZ SEC SOP and 13% with the SEC-CEX method. A 4% difference in HMWS quantitation was considered acceptable for the final method application.

Other 2D LC-LC modes such as multiple-heart-cutting and high-resolution sampling may be used to profile both the charge variants of HMWS impurities and main product peak separately. High-resolution sampling can also be used to online fraction-transfer portions of the SEC chromatogram for CEX analysis to verify the charge variants and peak purity. However, these setups may not be ideal for HT applications due to the requirement of larger amounts of sample and longer analysis time which would lower the method throughput. Moreover, the increased complexity of the instrument operations of multiple-heart-cutting and High-Resolution sampling over heart-cutting 2D-LC may hamper their implementation for routine testing. The LC × LC modes such as comprehensive 2D-LC can be used to transfer the entire SEC chromatogram to the ^{2}D. However, comprehensive 2D-LC is normally used for improving the resolution of complex sample mixtures and its set-up would require the ^{2}D to be faster than the ^{1}D. Therefore, the implementation of comprehensive 2D-LC in this context may not be straightforward and an heart-cutting 2D-LC approach with a larger sampling volume may be more appropriate. Nevertheless, it is worth considering that the HMWS and LMWS are normally purified from the drug substance and thus it remains a key goal to continue the quality analysis on the main product peak without compromising the workflow efficiency.

The optimised method conditions as reported in Table 4.2 were selected according to the experimental data and statistical evaluation. Figure 4.6. showed the chromatograms obtained from the analysis of a mAb by the 2D heart-cutting SEC-CEX-UV method.

Table 4.2 2D SEC-CEX-UV final method conditions.

Method	2D SEC-CEX-UV
2D Mode	heart-cutting
^{1}D Column	Agilent AdvanceBio SEC 200A 1.9um, 4.6 x 150mm
^{2}D Column	Agilent AgilentBio WCX column 2.1 x 50 mm, 5 um, np
^{1}D Mobile phase	100 mM Na3PO4 buffer, pH 6.0
^{2}D Mobile phase	A: 25 mM Na3PO4, pH 6.0; B: 25 mM Na3PO4, 1M NaCl, pH 6.0
^{1}D Temperature	25 °C
^{2}D Temperature	25 °C
^{1}D Flow rate	0.5 mL/min
^{2}D Flow rate	0.2 mL/min
^{1}D detector	MWD 280 nm, 210 nm
^{2}D detector	DAD 280 nm, 210 nm
Injection Volume	10 uL

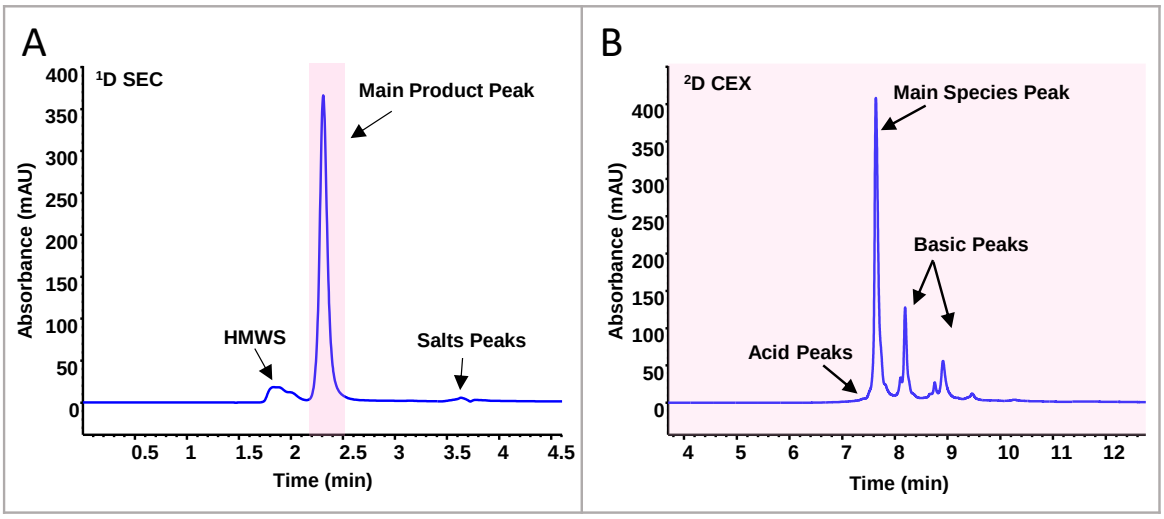

Figure 4.6 2D heart-cutting SEC-CEX-UV analysis of a mAb.
A) ^{1}D SEC MWD profile demonstrating the separation of the aggregates (HMWS) peaks from the main product of a heat-stressed mAb-1 sample. The sample concentration was 1 mg/mL and the injection volume was set to 10 mL. The pink shaded area represents the heart-cutting sampling for online fractionation. Time-based sampling modes with 0.16 min of sampling rate were used to fraction-transfer the main product peak to the ^{2}D. B) ^{2}D CEX DAD charge variants profile of the mAb-1 main product peak fractionated and transferred from the ^{1}D to the ^{2}D column. The mAb-1 charge profile shows the presence of acid and basic species peaks separated from the main peak.

4.3.1.2 2D SEC-CEX-UV Method Assessment

The qualification study aimed to ensure that the 2D SEC-CEX-UV method was fit-for-purpose to support in-process development sample testing. All the information on the method assessment parameters, target expectations and data are summarised in Table 4.3. In this study, method specificity was evaluated for mobile phase and formulation buffer components. All buffers and samples were injected with 10 µL injection volume (Appendix B, Figure 10.4). The addition of 2,2'-azobis(2-amidinopropane) dihydrochloride (AAPH) was used to generate stressed material of mAb-1 for the stability-indicating study. The UV profile of the stressed sample was compared to the reference standard (RS) (Appendix B, Figure 10.5) to show the difference in size and charge variants induced by the chemical stress. Precision was assessed in terms of repeatability over six technical replicates of a sample of mAb-1 RS. The linearity evaluation consisted of 7 levels, each analysed in triplicates, and the injection volume was kept constant at 5 µL. The concentration of the mAb-1 RS dilutions was measured by UV absorbance at 280 nm before injection and corresponded to 9.97, 5.53, 2.76, 1.34, 0.66, 0.3 and 0.15 mg/mL (Appendix B, Figure 10.9). The linearity study defined the linear dynamic range of the method. Method accuracy was inferred from the linearity data. Accuracy was determined by calculating the mean of the %area of all the size and charge variants peaks (%main product, %HMWS, %acid species, %main species, %basic species) for the minimum (3.96 µg), medium (13.8 µg) and maximum (49.85 µg) column loads used in the linearity study. Each of the group mean (n=3) was compared to the grand mean of all the replicate samples analysed in the linearity study (n=15) and the difference between the groups was reported by calculating the coefficient of variation (CV). Limit of detection (LOD) and limit of quantification (LOQ) were inferred from the calibration curve used for the linearity study and calculated for the HMWS peak. The precision and accuracy of each column loading level were calculated. Column loading was expressed as proportional protein load (µg) (Chapter 2, Section 2.5, Equation (2.5.2.4)). Linear regression analysis of the peak area *vs.* the proportional protein load (PPL) (µg) (Appendix B, Figure 10.10) was performed to determine the LOQ and subsequently, the LOD applying the equations reported in Chapter 2, Section 2.5, Equations (2.5.2.6), and (2.5.2.7). The method assessment demonstrated the 2D SEC-CEX-UV suitability for HT profiling of intact mAb size and charge variants and can be applied to PQ assessment during product development.

Table 4.3 2D SEC-CEX-UV method assessment results.

Parameter	Target expectation	Qualification results
Specificity	Buffer profiles	No interfering peaks from mobile phases and formulation buffer at the retention times of the RS peaks (Appendix B, Figure 10.4).
Stability-indicating	Observe changes in the RS peak profile	Changes Observed (Appendix B, Figure 10.5).
Repeatability	No more than 0.5 min retention time difference between the shortest and longest reference peak retention time across the sample replicates (n=6). No more than 10% CV of % reference peak among the replicates (n=6).	^{1}D: main product retention time range: 2.311-2.312 min; %peak CV = 0.8% 2D: Main peak retention time range: 7.6-7.7 min; %peak CV = 1%
Linearity	$R^2 \geq 0.980$ for reference peak area linearity.	^{1}D main product: R^2 = 0.997 ^{1}D HMWS: R2 = 0.994 ^{2}D Main peak: R^2 = 0.998 ^{2}D First basic peak: R^2 = 0.999 (Appendix B, Figure 10.9)
Accuracy (inferred from the low, medium and high sample concentration level used in the linearity study)	CV ≤ 20% between the mean of %main product, %HMWS, %acid species, %main species, and %basic species of each group (n=3 x 3 groups) and the grand mean (total n=15).	%Main product CV≤ 20% %HMWS CV ≤ 20% %Main species CV ≤ 20% %Acid species CV ≤ 20% %Basic species: CV ≤ 20% for all sample groups as reported in Appendix B, Table 10.12
LOQ	The CV of the reference peak of each level must be ≤ 20%. $R^2 \geq 0.95$ for reference peak area *vs.* the protein load. Results reported as % of the total peak area	LOQ HMWS = 48.18% (9.6 μg)
LOD	Results reported as % of the total peak area	LOD HMWS = 24.09% (3.2 μg)

4.3.2 Application of the 2D SEC-CEX-UV Method to Support the Analysis of Size and Charge Variants during mAb-1 Accelerated Forced-Degradation and Stability Study

A forced degradation study is a common practice adopted to elucidate protein structure, assess the degradation pathways upon extreme stress conditions, and ultimately establish structure-function relationships for quality attributes of a drug candidate (Garripelli, Wu, and Gupta, 2020). Depending on the pre-clinical or clinical phases of the drug candidate, the forced degradation study includes varying stress conditions and time window investigated, which can take from days up to several months. In this study, the aim was to demonstrate the potential of the 2D SEC-CEX-UV method for application as a HT analytical tool in conjunction with forced degradation studies.

The stress conditions tested on mAb-1 RS involved low pH, high pH, and chemical oxidation. Low and high pH stress was achieved by adjusting mAb-1 pH to 3.5 with 0.1 M citrate buffer and 8.5 with 0.1 M Trizma HCl/Trizma base buffer, respectively. The samples were incubated at 25 °C and aliquots were taken after 7 days at the end of the incubation time. Chemical oxidation was achieved by exposing mAb-1 to 3% H_2O_2 and 10% AAPH solutions. These chemicals are known to target methionine (Met) and tryptophan (Trp) residues, respectively. However, other amino acids present in the protein sequence may be amenable to oxidative events such as histidine (His) tyrosine (Tyr), and cysteine (Cys). In particular, both H_2O_2 and AAPH are known to oxidise Met residues irreversibly via nucleophilic substitution reactions, whilst Trp residues are modified by peroxyl and alkoxyl radicals via free-radical oxidation generated upon degradation of AAPH (Zheng et al., 2021; Shah et al., 2018; Dion et al., 2018). The mAb-1 degradation pathways resulting from chemical oxidation were monitored over time and aliquots were taken after 1, 3 and 7 days incubation at 25 °C with the respective chemicals. Additionally, an accelerated stability study was done by incubating a mAb-1 RS sample at 37 °C for 30 days. At the end of each time point, the samples were frozen at -80 °C and defrosted all on the same day to allow sample consistency. Buffer exchange was performed prior to analysis for removal of the chemical stressor with the exception of low pH treatment, in which the samples were buffer-exchanged before freezing to avoid precipitation caused by the freeze-thaw cycle at low pH. A t-test was conducted to evaluate the size and charge variants differences between mAb-1 RS and the control sample at the end of the forced degradation study (after 7 days at 25 °C).

These were then compared to the size and charge variants occurring as a consequence of the stress conditions under investigation (Appendix B, Table 10.2). More information on the chemicals used for the sample preparation procedure was given in Chapter 2, Section 2.1.1 2D SEC-CEX-UV.

Table 4.4 2D SEC-CEX-UV PQ analysis of mAb-1 at the start and endpoint of the accelerated forced degradation and stability study.

Treatment	% HMWS	% LMWS	% Main product	%Acid species	%Basic species	%Main species
RS	0	0	100	4.78	38.4	56.80
Control (7 days at 25 °C)	0	0.61	99.39	4.71	39.08	56.21
Low pH (7 days at 25 °C)	0	5.30	94.70	5.70	34.90	59.40
High pH (7 days at 25 °C)	0	1.40	98.60	4.80	33.40	61.80
H_2O_2 stress (7 days at 25 °C)	0.97	20.8	78.23	100	0	0
AAPH stress (7 days at 25 °C)	12.72	6.81	80.48	0	100	0
Accelerated stability (30 days at 37 °C)	0	5.13	95.80	4.16	29.20	66.70

Table 4.4 shows the %area of mAb-1 structural modifications resulting from the stress treatments with aliquots taken at the endpoints of the accelerated forced degradation (7 days) and stability studies (30 days) analysed by 2D SEC-CEX-UV. The RS sample corresponded to the PQ profile of mAb-1 at the start (t_0) of both studies. A mAb-1 RS sample was incubated at 25 °C for 7 days in the absence of stress conditions and used as a control throughout the forced degradation study. The results shown in Table 4.4 revealed the change of mAb-1 PQ profile when exposed to the different stress treatments in a time course of 7 days. Chemical oxidation was responsible for product degradation events resulting in alteration of both the size and charge variants profiles of mAb-1. Figure 4.7 and Figure 4.8 show the change in the PQ profile of mAb-1 over the time frame examined as a result of AAPH and H_2O_2 stress, respectively. Fragmentation occurred as a consequence of both H_2O_2 and AAPH exposure, (20.80% *vs.* 6.81%, respectively). In contrast, aggregation was mostly observed with AAPH rather than H_2O_2 (12.72% *vs.* 0.97%, respectively). As shown in Figure 4.7, 1-day AAPH stress induced the formation of HMWS (A) and LMWS impurities (C) increasing after 3 and 7 days of chemical exposure. The alteration of the surface charge

distribution of mAb-1 main product after 1 day of AAPH treatment was evidenced by the ^{2}D CEX chromatograms (B). This suggested the presence of conformational changes increasing over the timeframe tested. The consequent loss of CEX profile Rs (D) indicated product degradation. Similarly to AAPH, H_2O_2 was responsible for product degradation events resulting in alteration of the size and charge variants increasing over time (see Figure 4.8 C, D). However, the size variants were mainly associated with product fragmentation. The charge variants profile of the main product peak was also visibly different from the RS and presented three main regions. The first region, eluting at a time window corresponding to the RS acidic and main species (4-5), displayed a split peak with a left shoulder. In this specific context, peak splitting may be due to conformational changes resulting in different binding interactions with the stationary phase. The other two regions fell within the RS basic peaks elution time window (6-8) and also resulted in split peaks. This could be representative of closely related conformational modifications occurring as a consequence of Met and possibly Trp oxidation. The overall shift towards the acid region was evident at day 7 and was indicative of the extent of product degradation (Figure 4.8, D).

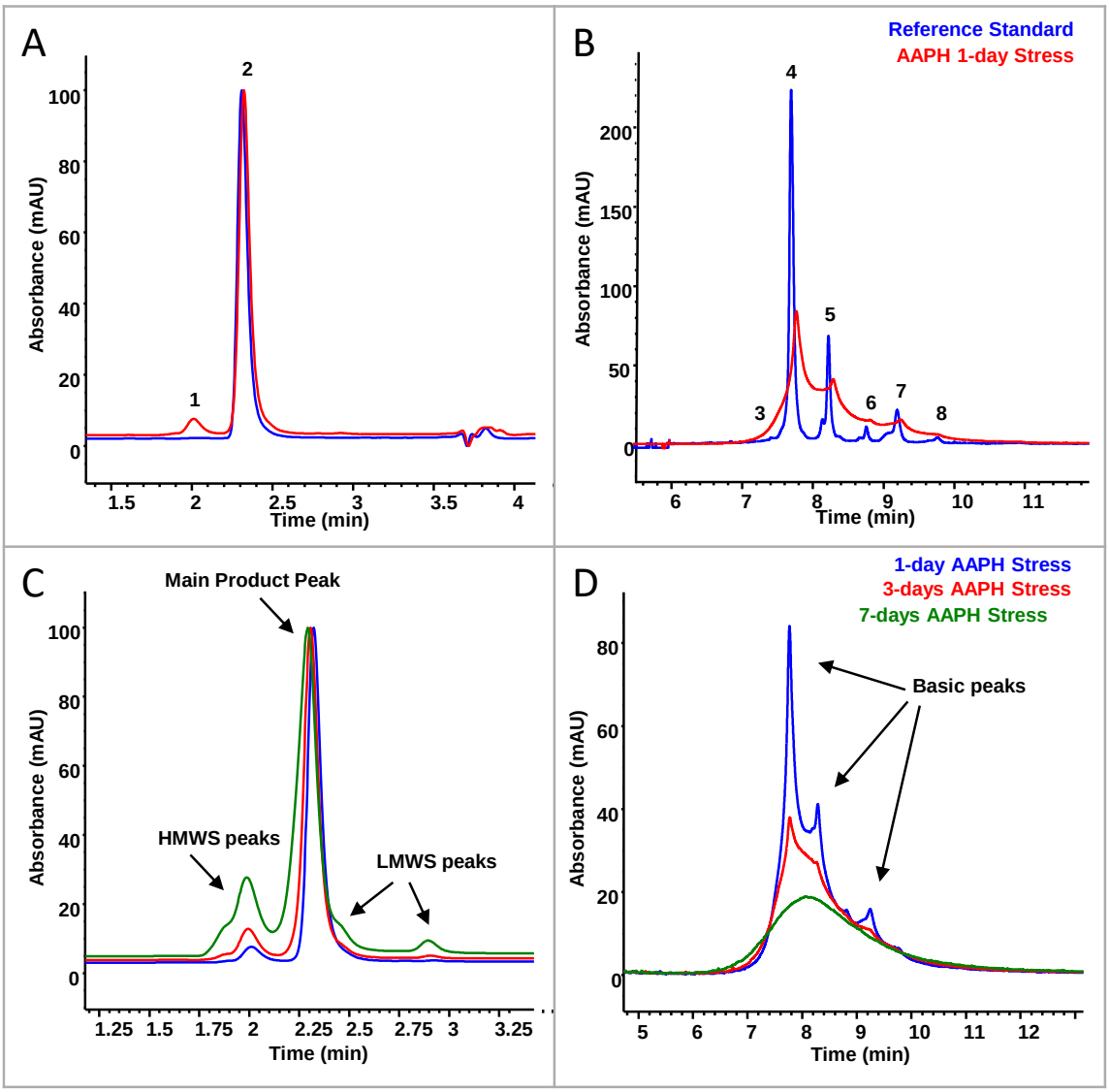

Figure 4.7 Analysis of AAPH stress-induced degradation pathway of mab-1 over time by 2D SEC-CEX-UV.

A) ^{1}D SEC and B) ^{2}D CEX profiles of mAb-1 after 1-day AAPH stress (red) was overlayed against the RS (blue). The AAPH treatment-induced degradation events resulted in increased HMWS impurities (peak 1) (A) and structural modifications of the main product visible as a considerable alteration of the surface charge distribution (peaks 3-8) shown by the CEX profiles. At the bottom, the AAPH stress-induced protein degradation over time was shown for each time point corresponding to aliquots taken after 1 day (blue), 3 days (red), and 7 days (green). The ^{1}D SEC profile (C) showed an increase in %HMWS and %LMWS over time. The ^{2}D CEX profiles overlay (D) revealed the apparent surface charge distribution modifications over time ultimately resulting in the formation of a heterogeneous mixture of charge variants. The stressed sample was diluted to 1 mg/mL before analysis and the injection volume was set to 10 µL.

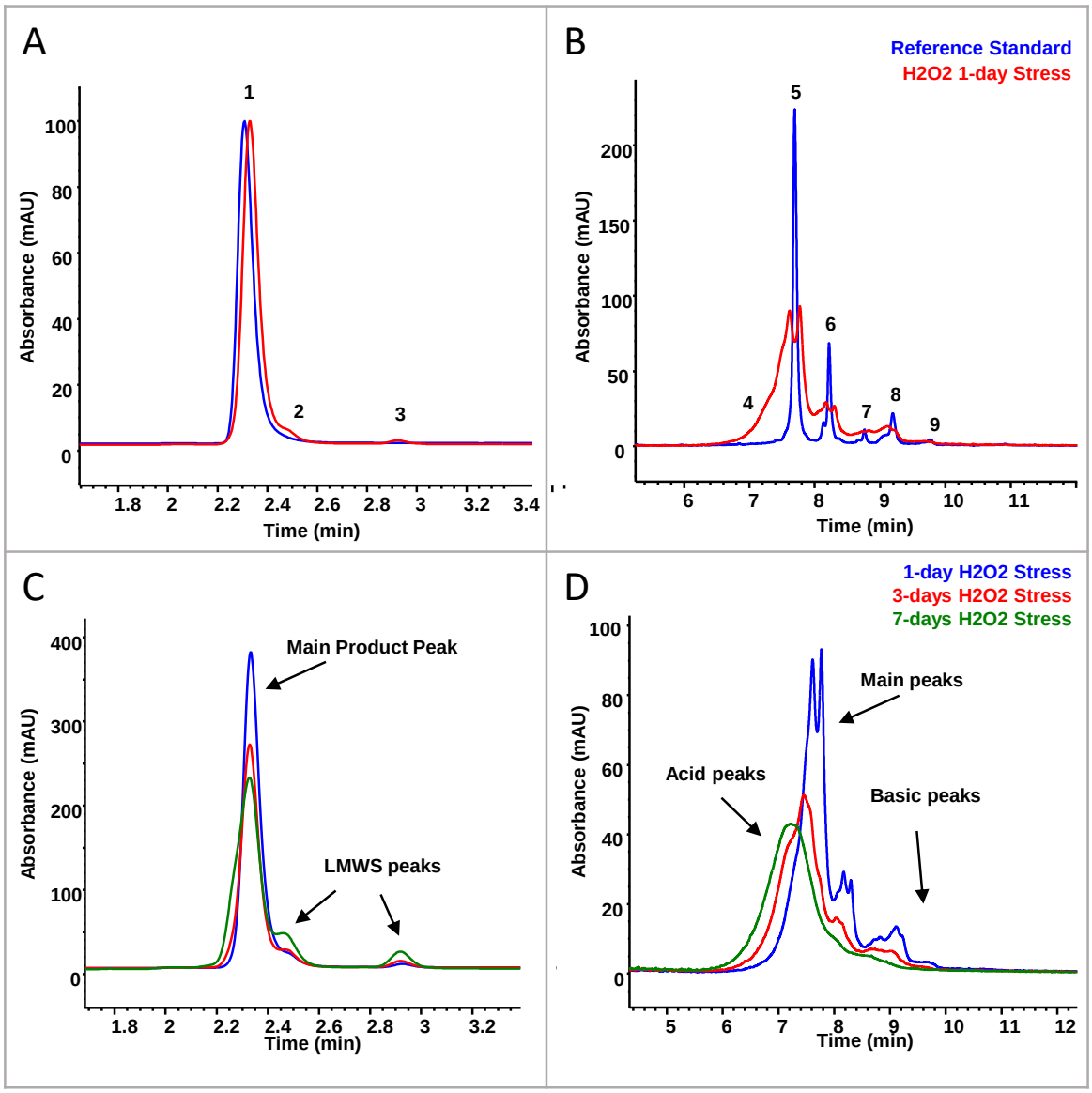

Figure 4.8 Analysis of H_2O_2 stress-induced degradation pathway of mab-1 over time by 2D SEC-CEX-UV.

At the top, 1D SEC (A) and 2D CEX profiles (B) of mAb-1 after 1 day H_2O_2 stress (red) overlayed against the RS (blue). Stress conditions induced the formation of LMWS (peaks 2 and 3) and visible discrepancy of charge variants profiles between the two samples (peaks 4-9). At the bottom, the protein degradation events that occurred over time after 1, 3 and 7 days of H_2O_2 treatment, were displayed for each time point. An increase in mAb-1 %LMWS over time was revealed by the ^{1}D SEC profile (C). The ^{2}D CEX profiles (D) showed the formation of a heterogeneous surface charge distribution resulting in loss of CEX profile Rs with merging of the charge variants in a single peak. The stressed sample was diluted to 1 mg/mL before analysis and the injection volume was set to 10 mL.

Notably, the other stress conditions didn't influence mAb-1 %HMWS which remained < 0.5% suggesting that free-radical oxidative stress induced by AAPH was the main cause of aggregation during the mAb-1 accelerated forced degradation study. In contrast, the LMWS profile varied across all the stress conditions, demonstrating that mAb-1 was more

susceptible to fragmentation rather than aggregation. The degradation rate was observed as a 0.61% significant increase in LMWS after 7 days incubation at 25 °C without the addition of stressors (Appendix B, Figure 10.6 A, Table 10.2). The fragmentation rate induced by low and high pH treatments resulted in ~5% (Appendix B, Figure 10.8 A, Table 10.4) and a 1.4% increase per week (Appendix B, Figure 10.8 C and Table 10.5), respectively. Furthermore, the accelerated stability study confirmed the propensity of mAb-1 to fragment with an increase of ~5% in LMWS whilst no aggregation events were detected (Appendix B, Figure 10.7 A and Table 10.3). The charge variants profile demonstrated that the acidic variants significantly increased by 1% as a result of low pH stress, whilst remaining consistent during high pH stress and accelerated stability study (Appendix B, Figure 10.8 B, Table 10.6, Table 10.7, and Table 10.8). Interestingly the %area of the basic species peak decreased significantly as a consequence of low pH (~3%) and high pH (~5%) stress as well as during the accelerated stability study (~9%) (Appendix B, Figure 10.7 B, D, Figure 10.7 B, Table 10.9, Table 10.10, Table 10.11).

The accelerated forced degradation studies showed that mAb-1 stability was mostly compromised by oxidative stress which led to product degradation resulting in alteration of both the size and charge variants profile. Low and high pH treatments indicated that the molecule was susceptible to fragmentation and the LMWS relative abundance was higher after exposure at high pH. Furthermore, a rise of basic species was observed with low pH stress, whereas high pH stress increased both acidic and basic species. The accelerated forced degradation study confirmed the propensity of the candidate mAb to fragment and indicated the formation of chemical modifications shifting the charge variants profile towards the basic region. This study proved that the 2D SEC-CEX-UV method can provide information on both size and charge variants in a single analysis hence, enhancing the understanding of protein degradation pathways. Furthermore, the method required a limited amount of sample (1.6 µg as per LOQ) and a relatively short run time (20 min per sample) demonstrating its suitability as a HT analytical tool in product development.

Although demonstrating significant advantages over existing 1D-LC approaches, the current 2D approach in conjunction with UV analysis did not provide a detailed characterisation of the protein charge variants peaks. This limits the amount of information provided by conventional analytical workflows used for understanding the protein modifications at the

molecular level involving peak fraction-collection and identification by multi-level MS analysis such as subunit and peptide mapping.

Therefore, further work was performed to enable online hyphenation of the 2D SEC-CEX chromatography with MS detection. The proposed analytical strategy was designed to facilitate peak identifications and validation of the charge variants without the need for offline fractionation and multi-level characterisation.

4.3.3 Part B: Online hyphenation of heart-cutting SEC-CEX-UV to MS detection

4.3.3.1 Overview

The direct coupling of IEX separations to MS has increasingly gained popularity in the pharmaceutical industry as a powerful tool to support biopharmaceutical development (Füssl, Cook et al., 2018; Trappe et al., 2018; Polderdijk et al., 2019; Füssl et al., 2019; Bailey et al., 2018; Haberger et al., 2021; Goyon et al., 2020). Native analysis by IEX-MS has been of particular focus in recent years providing a powerful tool for the analysis of proteins charge variants under physiological conditions and monitoring of multiple quality attributes such as glycosylation, C-terminal Lys clipping and oxidation at the intact level (Füssl et al., 2021; Carillo, Füssl, et al. 2021; Füssl et al. 2020; Kallamvalliillam et al., 2018; Füssl, Cook, Sche, et al. 2018).

The objective of the study presented herein was the coupling of 2D SEC-CEX separation to MS detection for simultaneously monitoring multiple quality attributes at the intact level in one single method. The ^{2}D was coupled to a high-resolution quadrupole-orbitrap (Q-Orbitrap) mass spectrometer capable of achieving accurate and high-definition characterisation of mAbs PTMs. A CEX pH gradient was used to enable the online hyphenation to MS for the assignment of the peak identity. The method was intended to give comparable separation profiles to those obtained with the non-MS compatible mobile phases so that it could serve as a reference for the assignment of the peaks identity. The following sections describe all the steps involved in the development and application of the method to case study samples.

4.3.3.2 Investigation of Suitable Mobile Phase Composition for ^{1}D SEC

The development of the ^{1}D SEC focused on the selection of an MS-compatible mobile phase composition fit for coupling CEX in the ^{2}D. As previously described (see Section 4.3.1), the ^{1}D buffers can affect the ^{2}D separation impeding the online hyphenation of the two modes of chromatography. It is worth considering that although the ^{2}D can function as a desalting step prior to MS detection (Jaag, Shirokikh, and Lämmerhofer, 2021), non-volatile salts from the ^{1}D can affect MS performance by reducing method sensitivity and instrument lifetime. Since the present method was designed to be applied for routine testing in HT settings, both MS sensitivity and instrument lifetime were important parameters to consider. Notably, the improvement of method sensitivity reduces the sample amount required per experiment and, together with extended instrument lifetime, contributes to reduced expenses and time to support analytical testing. Therefore, volatile mobile phase additives were chosen for the optimisation of both chromatography dimensions. A recent study showed the dependence of nature, ionic strength, and pH of SEC eluents on protein-stationary phase interactions, and demonstrated that the use of ammonium acetate at concentrations above 100 mM effectively limited protein retention without inducing denaturation (Ventouri et al., 2020). Although the control of mobile phase ionic strength is difficult to achieve, the effect of the salt concentration and pH on the separation efficiency can be measured. For the purpose of this experiment, ammonium acetate was tested at 100 mM and 200 mM mobile phase concentration and two pH extremes, 5 and 6.8. A sample of mAb-1 was stressed at 70 °C for 30 min to induce < 10% HMWS impurities (Chapter 2, Section 2.1.5) and analysed by SEC using the mobile phase conditions under investigation. For the purpose of this experiment, a content of HMWS < 10% was considered sufficient to evaluate the effect of the mobile phase ionic strength on the SEC separation.

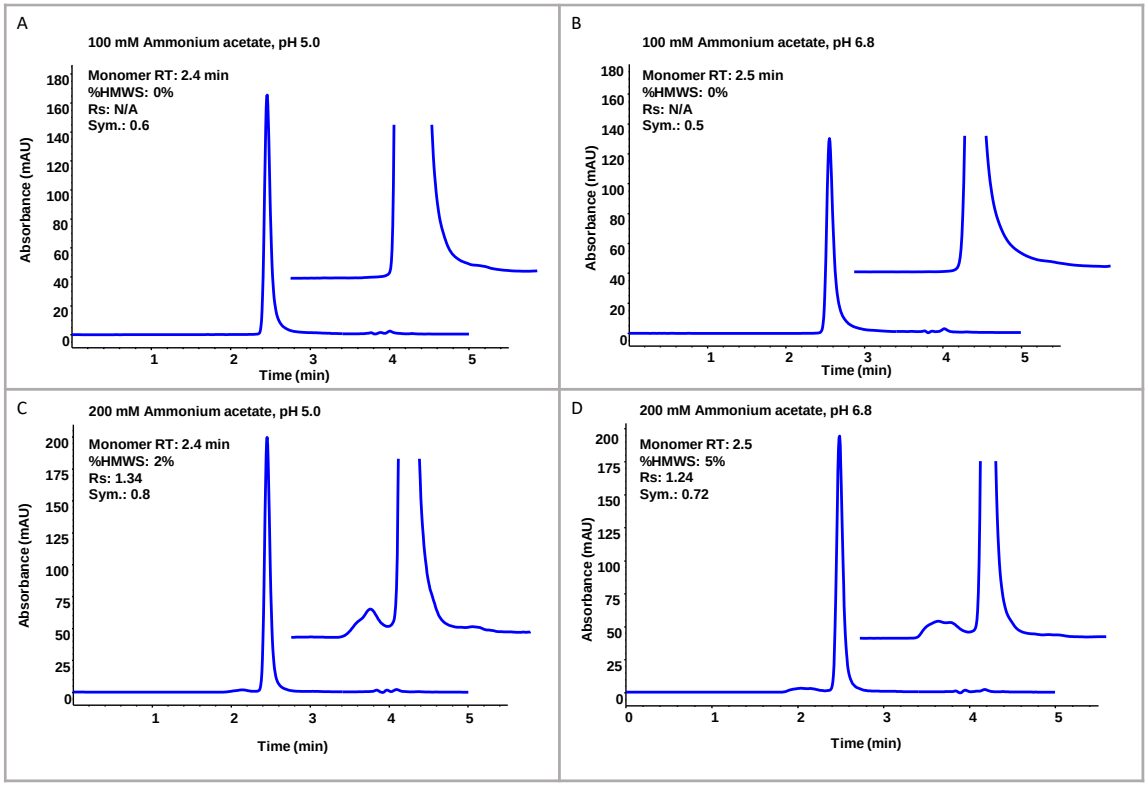

Figure 4.9 Effect of buffer ionic strength and pH on the ^{1}D SEC separation.
Comparison of the effect of SEC mobile phase ionic strength and pH on the size profiling of a heat-stressed mAb-1 sample. The SEC profiles displayed correspond to a mobile phase composed of 100 mM ammonium acetate, pH 5.0 (A) and pH 6.8 (B) and 200 mM ammonium acetate, pH 5.0 (C) and 6.8 (D). The 1.8-3.1 min time window corresponding to the HMWS and main product peaks elution times was zoomed and displayed at the top-right of each panel. The stressed sample was diluted to 1 mg/mL before analysis and the injection volume was 10 µL.

The use of 100 mM ammonium acetate mobile phases (Figure 4.9 A and B) was insufficient to achieve suitable size separation. Moreover, the extensive peak tailing (Sym. 0.6 in A and 0.5 in B) was a sign of protein-stationary phase interactions. As previously shown by Ventouri, this experiment demonstrated that ammonium acetate ionic strengths above 100 mM help preventing protein secondary interactions and ultimately enable size separation. In agreement with Ventouri's findings, 200 mM ammonium acetate improved the size separation. Furthermore, the use of 200 mM ammonium acetate at pH 5.0 and 6.8 gave different %HMWS (2% and 5%, respectively), which may suggest pH dependency on the separation, indicating that pH effects were more important when working at low concentrations (Figure 4.9, C and D). In this analysis, pH 5.0 may be too far from the protein pI, resulting in increased protein-stationary phase ion-exchange interactions, and underestimating the %HMWS (Golovchenko et al., 1992; Fekete et al., 2014). Another explanation of this phenomenon may lead to speculate on different protein conformation in

solution altering the hydrodynamic radii of the protein molecules and ultimately resulting in different size variant profiles observed by SEC.

For MS compatibility, the ^{1}D SEC mobile phase was composed of 200 mM ammonium acetate; the buffer pH was chosen as 6.0 in compliance with the AstraZeneca platform formulation buffers optimised for mAbs. The separation followed the same instrument settings as previously described with heart-cutting sampling and transfer of the mAb-1 main product peak to the ^{2}D (Figure 4.4).

4.3.3.3 ^{2}D CEX Coupling with heart-cutting 2D-LC

Recent studies reported the successful coupling of SCX stationary phases and low ionic strength pH gradients to HR-MS for the analysis of mAbs charge variants (Füssl et al., 2018; Yan et al., 2018). Common practises for online IEX-MS hyphenation adopt pH-gradient based separations to overcome the use of salty buffers which would impede the MS detection. A generic IEX pH gradient is created by varying the pH of the eluent as a function of time at constant ionic strength. Aiming to minimise the variations that may arise from buffer preparation procedures, commercially available columns and buffers were selected for this application. Namely, the Waters IEX-MS platform BioResolve SCX mAb 2.1 x 50 mm column and the IonHance CX-MS buffer system (A and B buffers), assumed to provide a linear pH response from pH 5.0 to 8.5 (Table 4.5).

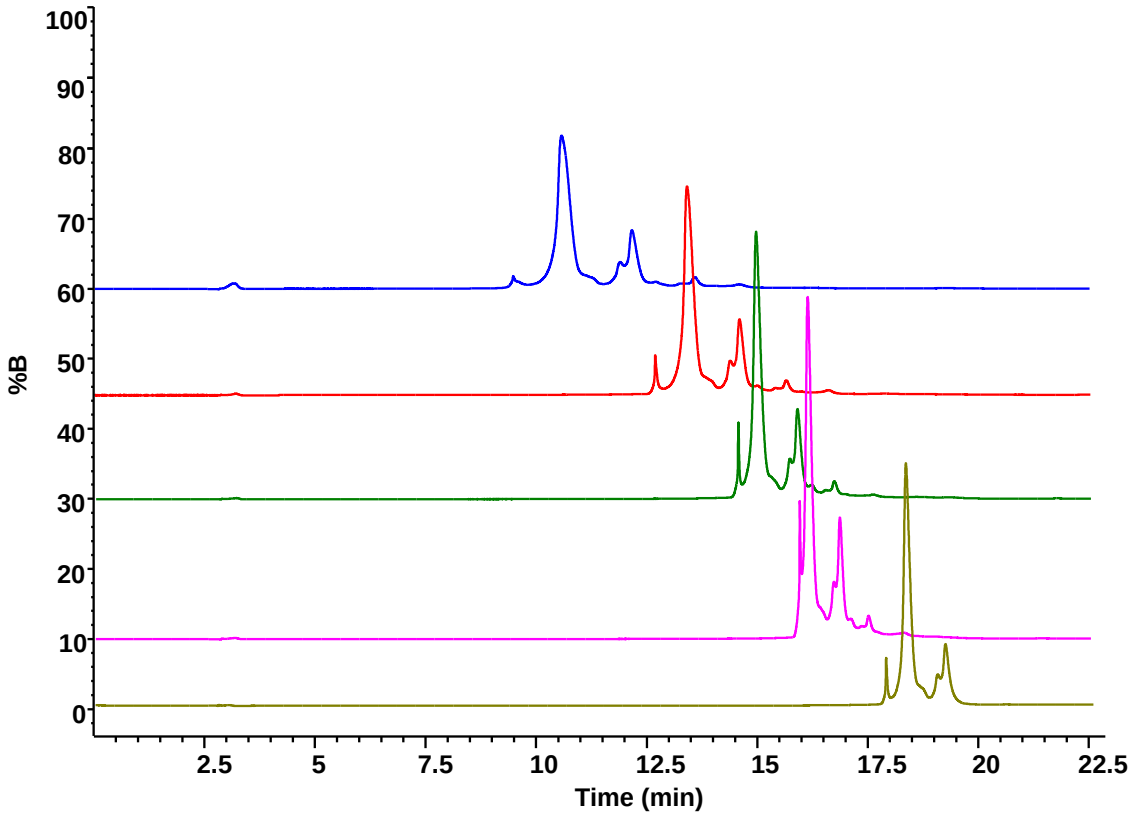

Figure 4.10 ^{2}D CEX gradient slope optimisation.
Cation-exchange chromatograms of the mAb-1 main product fraction transferred to the ^{2}D by heart-cutting 2D-LC. The x-axis represents the gradient time and the y-axis displays the %B (IonHance CX-MS B) utilised for optimising the gradient slope and achieving a desirable charge variants separation. The initial sample corresponded to a 10 µL injection of heat-stressed mAb-1 diluted with water at a concentration of 1 mg/mL prior to analysis.

Heart-cutting 2D-LC was used for the online collection of the mAb main product peak and subsequent transfer to the ^{2}D. The heart-cutting time and sampling time were kept as described in Section 4.3.1 since no significant retention time shift or peak broadening was observed in comparison to the non-MS compatible SEC method (Figure 4.12). The gradient slope was optimised for mAb-1 by varying the %B at the start (t_0) whilst maintaining the gradient time constant. The %B at t_0 was increased from 2% to 60% until acceptable charge variants separation was achieved and no breakthrough was observed. As shown in Figure 4.10, steep gradients with %B starting between 2-30% and ramping to 100% B in 14 min were not suitable, since the mAb-1 peaks were eluting during the wash and equilibration time window (17.5-22.5 min). Improved separation efficiency was accomplished with a shallow gradient starting from 60% B. The complete list of method parameters is summarised in Table 4.5.

4.3.3.4 Online Hyphenation to HR-MS

In this research, a Q-Orbitrap MS was selected for achieving high-resolution characterisation of the mAb charge variants at the intact level. The capillary temperature, AGC target, Rs, and micro-scans were chosen according to data obtained from previous studies and kept consistent throughout method development (details were reported in Figure 4.11). To evaluate the optimal instrument setting for native analysis, the in-source CID was tested at 50 eV increments over a range of 100-200 eV. A sample of mAb-1 was injected in triplicate for each in-source CID setting (100 eV, 150 eV, and 200 eV) and the data were compared as reported in (Figure 4.11).

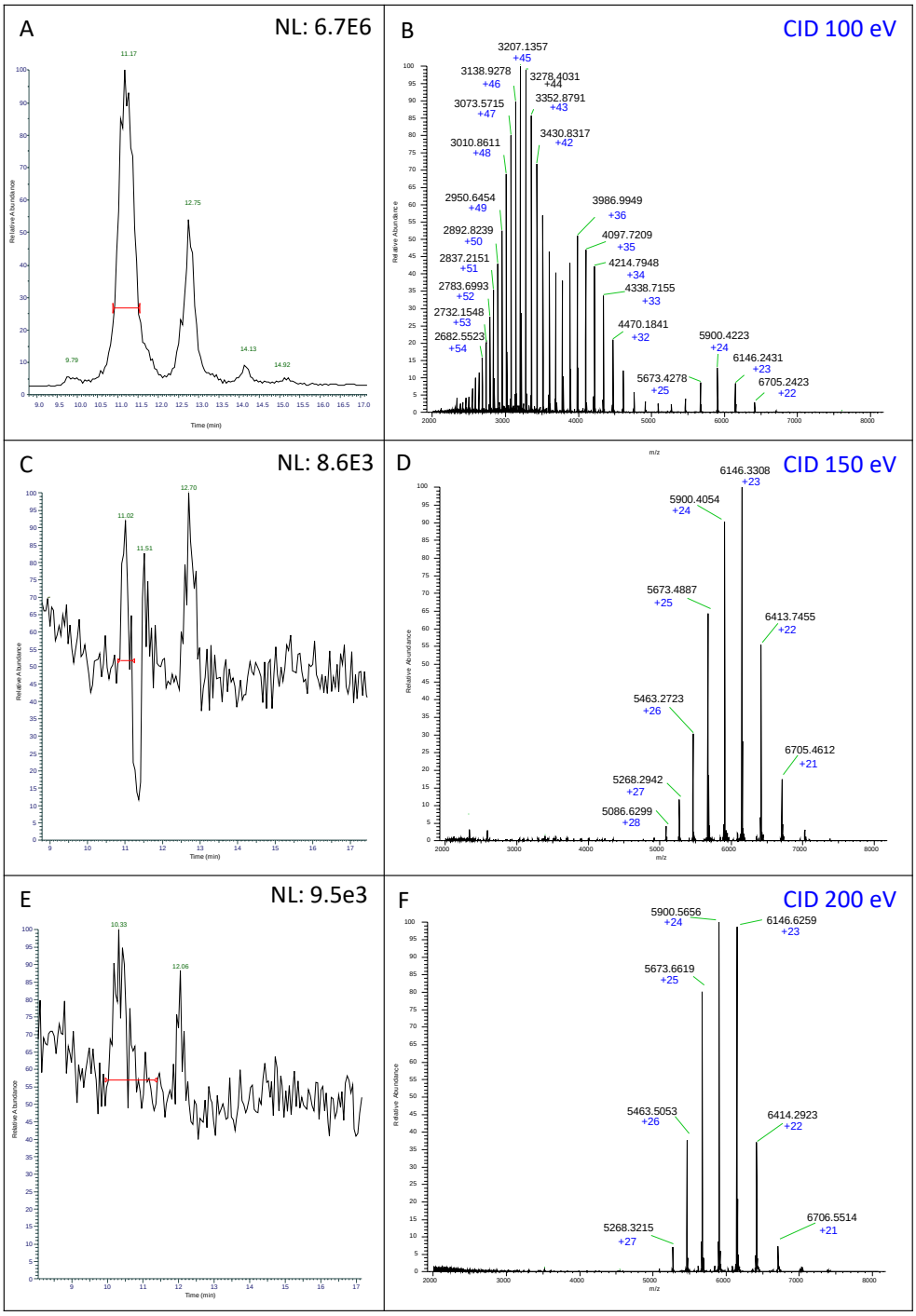

Figure 4.11 Intact mAb-1 Analysis under denaturing and native conditions with increasing in-source CID setting.

The spectra were ordered starting with the lowest CID at the top. The TIC profiles were reported on the left (A, C, E). The source spectra of the main peak eluting at 11.17 min were displayed on the right (B, D, F). Intact mass analysis of mAb-1 was accomplished under denaturing (B) and native conditions (D and F) by modifying the in-source CID from 100 eV to 200 eV. The TIC main peak eluting at 11.17 min (A) was taken as a reference point and compared with the mAb-1 native-like traces (B and C). The base peak of the denaturing spectrum was 6.7 x 10^6 in contrast with the base peak of the native spectra, which were 8.6 x 10^6 and 9.5 x 10^3, respectively.

The degree of multiple charging in the ESI spectra can reflect the physical conformation of the protein in the solution. Indeed, compared to their denatured counterparts, the globular nature of folded proteins offers less solvent accessible residues, resulting in smaller collisional cross-sections and referred to as a native-like state. The ESI-MS spectrum of mAb-1 acquired with 100 eV in-source CID (Figure 4.11 A) exhibited the profile of a partially denatured version of the molecule in the gas phase. By looking at the source spectra displayed in Figure 4.11 A, different charge state distributions could be observed. The narrowly spaced charge envelop distribution at the left showed high protein charge states from 54+ to 42+ with an apex intensity at 45+ which may correspond to the fully denatured ESI-MS spectra of mAb-1. The charge envelope with an apex at 36+ may indicate partially denatured ESI-MS spectra whilst, at the far right, the low-intensity narrow charge envelope with an apex at 24+ showed a native-like charge distribution. Similarly to the latter, the mAb spectra acquired with 150 and 200 eV in-source CID (Figure 4.11 B, C), displayed the signature profile of a native molecule in the gas phase. The widely spaced charge envelope distribution with lower charge states from 28+ to 22+, and apex intensity at 23+, indicated that mAb-1 maintained its physiological conformation. The nearly 3-fold discrepancy in the number of charge states of mAb-1 denatured and native spectra denoted a substantial difference in the structure of the ions. These results were consistent with the previous analysis of mAbs under native conditions (Scheffler et al., 2016).

Nonetheless, the fewer charge states associated with mAb-1 native-like ESI-MS analysis affected the method sensitivity. A significant drop in signal intensity was observed at 150 and 200 eV compared to 100 eV (Figure 4.11). Data from this experiment are evidence of the dependency of the rate of ion decay within a Q-Orbitrap analyser on the protein collisional cross-section. Ion dephasing, fragmentation during injection and metastable decay during detection are all possible reasons for the drop in signal during native MS acquisition. Considering the sensitivity constraints of the native analysis and the final application of the present method, the subsequent experiments were carried out under denaturing conditions. The final 2D SEC-CEX-UV-MS details were reported in Table 4.5.

.

Table 4.5 2D-LC SEC-CEX-UV-MS final method conditions.

Method	**2D SEC-CEX-UV-MS**
2D Mode	heart-cutting
^{1}D Column	Agilent AdvanceBio SEC 200A 1.9um, 4.6 x 150mm
^{2}D Column	Waters SCX BioResolve column 2.1 x 50 mm, 3 um, np
^{1}D Mobile phase	200 mM ammonium acetate, pH 6.0
^{2}D Mobile phase	A: IonHance CX-MS A; B: IonHance CX-MS B
^{1}D Temperature	25 °C
^{2}D Temperature	25 °C
^{1}D Flow rate	0.5 mL/min
^{2}D Flow rate	0.2 mL/min
^{1}D Detector	MWD 280 nm, 210 nm
^{2}D Detector	DAD 280 nm, 210 nm
Injection volume	20 uL
HR-MS	Quadrupole-orbitrap mass spectrometer
Ionisation	ESI
In-source CID	100 eV
Capillary temperature	250 °C
Micro-scans	10
Resolution	15,000
AGC target	3e6
Scan range	2000-8000 m/z
Processing parameters	
Source Spectra Method	Average over selected retention time
m/z Range	3,000.0000-6,500.0000
Chromatogram Trace Type	TIC
Deconvolution Algorithm	ReSpect
Output Mass Range	10,000-200,000
Charge State Range	10-100
Minimum Adjacent Charges	6-10
Target Mass	142,000.0000

4.3.4 SEC-CEX-UV-MS Characterisation of mAb-1 Structural Modifications Resulting from Accelerated Forced Degradation and Stability Study

The following section illustrates the application of the 2D SEC-CEX-UV-MS for supporting mAb-1 accelerated forced degradation and stability study. Further considerations on the use of the 2D SEC-CEX approach with and without MS hyphenation were addressed. The set of samples deriving from mAb-1 accelerated forced degradation and stability study was analysed by 2D SEC-CEX-UV-MS. Data from UV detection are reported in Table 4.6.

Table 4.6 2D SEC-CEX-UV-MS PQ analysis of mAb-1 at the start and endpoint of the accelerated forced degradation and stability study.

Treatment	% HMWS	% LMWS	% Main product	%Acidic species	%Basic species	%Main species
RS	0.43	1.82	97.8	3.29	31.6	65.2
Control (7 days at 25 °C)	0.38	1.76	97.9	3.09	30.7	66.3
Low pH (7 days at 25 °C)	0.5	2.11	97.4	3.53	27.5	69
High pH (7 days at 25 °C)	0.41	1.8	97.8	2.87	24.7	72
H_2O_2 stress (7 days at 25 °C)	1.49	19.49	79.02	100	0	0
AAPH stress (7 days at 25 °C)	23.3	3.49	73.2	100	0	0
Accelerated stability (30 days at 37 °C)	0.39	2.1	97.5	3.92	19.5	76.6

The UV profiles of both size and charge variants were comparable to the ones obtained with the salt-based SEC-CEX separation as reported in Section 4.3.2. Online fractionation by heart-cutting 2D-LC resulted in the injection of the main product peak from the ^{1}D to the ^{2}D for CEX separation. Mass spectra deconvolution revealed that the charge variants peaks arising from the mAb-1 RS analysis were mainly due to glycosylation heterogeneity and conformational changes resulting from different oxidation species (Figure 4.12). All the glycoforms and oxidated species observed in the RS were confirmed in the samples handled in low and high pH as well as after the stability stress. Reduced peptide mapping (RPM) analysis performed in AstraZeneca by Dr Lydia Dewis demonstrated a small (<5%) increase in deamidation and succinimide formation as a result of low and high pH treatment. However, the Rs of the 2D SEC-CEX-MS method was insufficient to detect such

modifications. The moderate variation of the charge variants profile may indicate an initial protein unfolding which may have altered the mAb-stationary phase interactions. More interestingly, chemical oxidation induced major changes in the charge variants profile resulting in a gradual loss of the surface charge distribution over time (Figure 4.13, Figure 4.14). Over the time points, the entire CEX profiles of the oxidised mAb shifted towards the lower retention time region. This was consistent with previous observations demonstrating that oxidised species may result in earlier eluting peaks (Sokolowska et al., 2017; Yang et al., 2017; Shi et al., 2020). Mass spectra deconvolution provided the intact molecular weights of the separated charge variants and revealed the presence of heterogeneous oxidised species as a result of AAPH and H_2O_2 stress. Oxidation of Trp and Met by AAPH and H_2O_2 are known to induce higher-order structural (HOS) changes which can, in turn, affect the CEX profile of the molecule (Barnett et al., 2019). It is worth considering the susceptibility of mAb-1 to fragment and how chemical oxidation promoted fragmentation mechanisms. Notably, the mass spectra of H_2O_2 stressed samples were characterised by the presence of two ion distributions areas, falling within the 1000-3500 m/z and the 4000-6500 m/z ranges (Figure 4.13). Deconvoluted mass spectra revealed that the ion distributions corresponded to fragments with masses of 23238 Da and 124442 Da, corresponding to the Fab portion of the mAb and its complementary heavily oxidated fragment, respectively. The 23238 Da mass corresponded to the fragment extending from Cys^{230} and the Gln^{13} of the heart-cutting bearing 2 oxidation sites (presumably Met^{34} and Met^{83}). This may be the result of the H_2O_2-mediated radical cleavage of the first interchain disulphide bond in the hinge region with subsequent formation of sulfenic acid (Cys^{230}-SOH) on one Cys and a thiyl radical on the other (Cys^{231} -S$^{\cdot}$) along with the breakage of the peptide bond between Val^{12} and Gln^{13} and loss of an H_2O molecule on one side of the fragment (Val^{12}). The mAb hinge cleavage mediated by hydroxyl radical reaction mechanism was previously described (Yan et al., 2009). Interestingly, the Fab ion distribution was seen from the start to the end of the mAb TIC trace suggesting that the fragment may have slow interaction kinetics with the CEX stationary phase. The complementary heavily oxidated fragment of 124442 Da eluted at 10.8 min. Highly heterogeneous intact molecules were observed eluting at 11.5 min with mass in the range 147583 – 147749 corresponding to species bearing multiple oxidation sites (Figure 4.13).

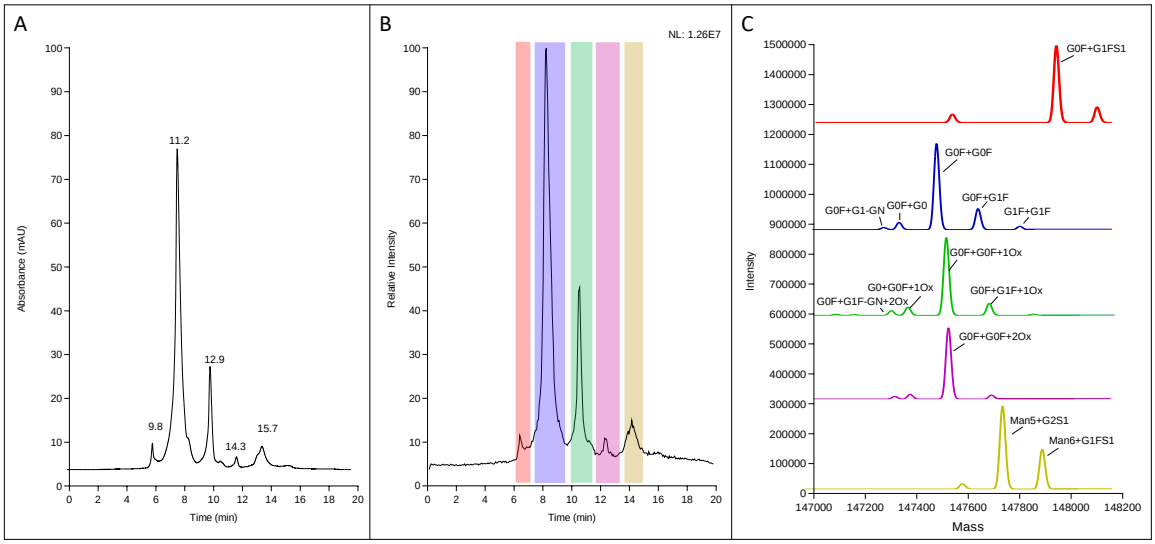

Figure 4.12 mAb-1 RS charge variants peak identification by 2D SEC-CEX-UV-MS.
A) 2D CEX UV profile of mAb-1 RS charge variants; B) TIC of mAb-1 RS charge variants separated by 2D CEX. The charge variants peaks are colour coded depending on their different retention time: 9.8 min (red), 11.2 min (blue), 12.9 min (green), 14.3 min (pink), 15.7 min (gold); C) deconvoluted mass spectra with peak assignment of all the TIC charge variants peaks matched by colour: 9.8 min peak (red) corresponds to G0F+G1FS1; 11.2 min (blue) corresponds to G0F+G1-GN, G0F+G0, G0F+G0F G0F+01F, G1F+G1F; 12.9 min (green), corresponds to G0F+G1F-GN+2Ox, G0+G0F+1Ox, G0F+G0F+1Ox, G0F+G1F+1Ox; 14.3 min (pink) corresponds to G0F+G0F+2Ox; 15.7 min (gold) corresponds to Man5+G2S1, Man6+G1FS1.

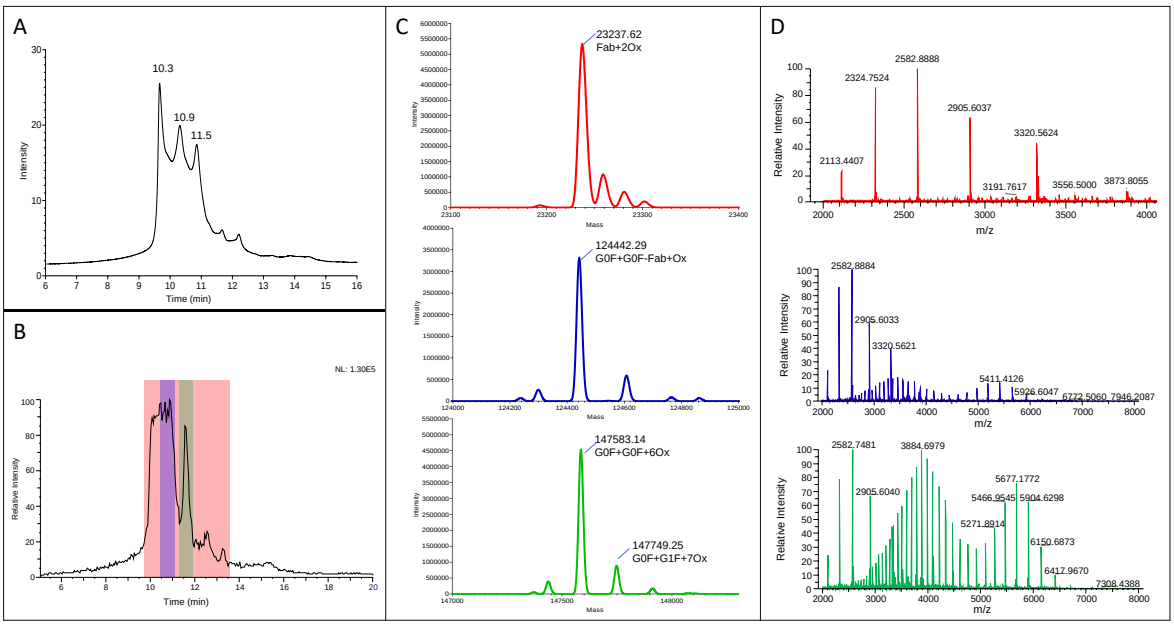

Figure 4.13 H_2O_2-stressed mAb-1 charge variants peak identification by 2D SEC-CEX-UV-MS.
A) ^{2}D CEX UV profile of mAb-1 charge variants after 1-day stress by H_2O_2; B) ^{2}D CEX separated charge variants BPC of H_2O_2-stressed mAb-1. The charge variants peaks colour coded depending on their retention times: 10.3 min (red), 10.9 min (blue), 11.5 min (green); C) deconvoluted mass spectra with the assignment of all the TIC charge variants peaks matched by colour: 10.3 min (red)

corresponded to the Fab fragment; 10.9 min (blue) corresponded to G0F+G0F-Fab+5Ox; 11.5 min (green) corresponded to G0F+G0F+6Ox and G0F+G1F+7Ox; D) colour-coded mass spectra.

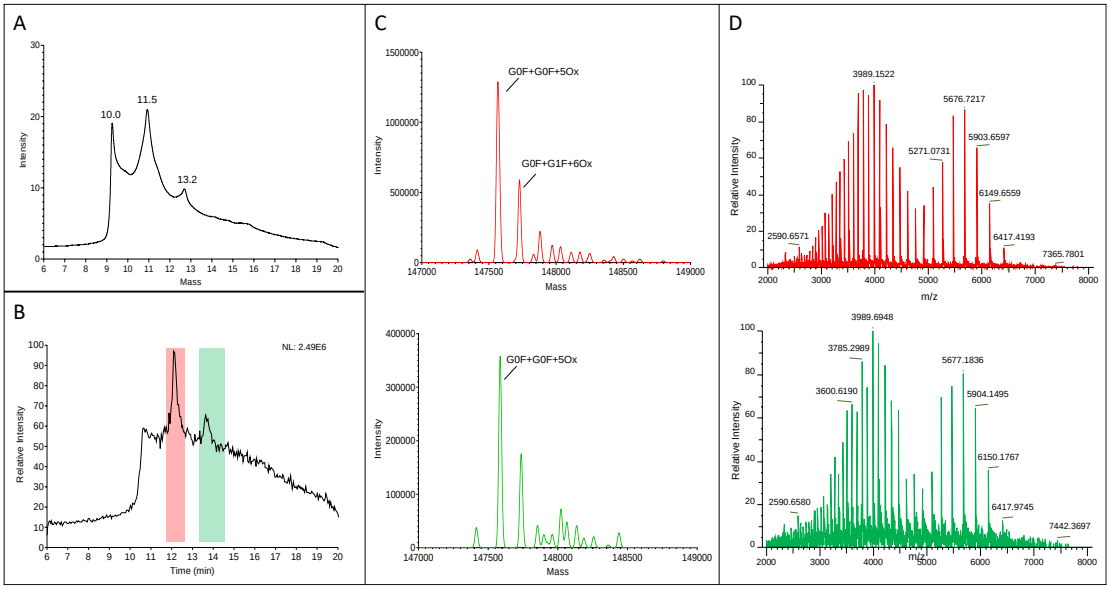

Figure 4.14 AAPH-stressed mAb-1 charge variants peak identification by 2D SEC-CEX-UV-MS.

A) ^{2}D CEX UV profile of mAb-1 charge variants after 1-day stress by AAPH; B) ^{2}D CEX separated charge variants TIC of AAPH-stressed mAb-1. The charge variants peaks are colour coded depending on their retention times: 11.5 min (red), 13.2 min (green); C) deconvoluted mass spectra with the assignment of all the TIC charge variants peaks matched by colour: 11.5 min (red) corresponded to G0F+G0F+5Ox and G0F+G1F+5Ox; 13.2 min (green) corresponded to G0F+G0F+5Ox; D) colour-coded peaks mass spectra. These results demonstrated the susceptibility of mAb-1 to chemical oxidation and were consistent with the previous SEC-CEX-UV analysis in addressing mAb-1 degradation pathways. Moreover, MS hyphenation enabled the identification of the charge variants peaks providing important further insight into mAb-1 glycosylation heterogeneity, oxidation, and fragmentation mechanisms that were not possible using SEC CEX UV analysis.

Data from AZ SOP RPM analysis confirmed the oxidation of Met and Trp residues as a result of both AAPH and H_2O_2 treatment. It should be noted that the SEC-CEX-MS method was unable to achieve site-specific structural information of charge modification as well as identifying the presence of deamidated species that were detected by AZ SOP RPM (data not shown). Baseline Rs of all mAb-1 glycoforms was not accomplished by CEX meaning that the UV detection was not exhaustive of the complete glycoprofile. Glycoforms assignment was achieved by deconvoluting the mass spectra throughout the entire peak profile and all the glycans identified were reported. Intact CEX-MS analysis enabled the assignment of all the glycoforms identified by the AZ SOP 2-AB method for glycan analysis (performed by Davide Di Girolamo, AstraZeneca, data not shown) but could not discriminate between G1F(α-1,3) and G1F(α-1-6) species. Nevertheless, the 2D SEC-CEX-

UV-MS enabled the identification of mAb hinge cleavage mediated by hydroxyl radical reaction which couldn't be accomplished by the AZ SOP RPM analysis. Orthogonal analytical tools to confirm the H_2O_2-mediated fragmentation mechanism could be non-reduced peptide mapping (NRPM) as well as reduced intact mass analysis by RP-LC-MS.

The 2D SEC-CEX-UV-MS method presented here can complement the current methodologies for intact mass analysis and provides the advantage of monitoring multiple-quality attributes in one single method with minimal resources required. The level of information given by the 2D SEC-CEX-UV-MS method for the analysis of mAb-1 accelerated forced degradation and stability study provided further insights for its application and confirmed the suitability in HT analytical workflows.

4.4 Conclusions

Molecular size and charge variants analysis are an integral part of the quality control strategies of therapeutic antibodies. SEC and CEX are the industry-standard methodologies for the qualitative and quantitative analysis of protein aggregates and charge variants, respectively and are compliant with regulatory guidelines (Kristina et al., 2016; Ph. Eur. 10.0, 2020; ICH Q6B, 1999). Traditional analytical workflows using 1D-LC approaches and orthogonal MS characterisation are often time-consuming and require a considerable amount of sample material. Due to their low throughput and complexity of operations, their implementation in early-stage product development is limited. This chapter demonstrates the development of a fully automated approach integrating size and charge variants characterisation in one single method by 2D-LC. The procedure involved the use of SEC in the ^{1}D to separate and quantify mAb HMWS impurities; the main product peak was then fraction-transferred with a heart-cutting schedule to the ^{2}D for charge variants profiling by CEX. The charge variants analysis was therefore respective to the main product peak only and allowed to isolate the structural changes relative to the main product separately from the size variants. Since the HMWS and LMWS impurities are normally purified from the from the main product, using a heart-cutting for transferring the peak to the ^{2}D allows to selectively characterise the charge variants of the main product.

Method development focused on the establishment of SEC-CEX separations for a mAb candidate using UV detection only as well as online MS hyphenation. The former involved the use of non-volatile mobile phases in both dimensions with CEX separation achieved by a salt-based gradient. The latter used volatile mobile phases in both dimensions with CEX separation achieved using a pH-gradient for coupling the ^{2}D CEX online with MS. Accelerated forced degradation and stability study of a mAb sample was performed to demonstrate the suitability of the methods for their intended application. The salt-based SEC-CEX-UV analysis enabled the quantitation of the size and charge variants with a suitable throughput. Method validation demonstrated that quantitation of the HMWS could be achieved by injecting as little as ~10 μg of sample (9.6 μg LOQ) and the total analysis time was 20 min per sample. An automated data processing workflow was created to accelerate the processing of a large number of samples and involved the integration of OpenLab Intelligent Reporting on ChemStation with a Python script. In this proof-of-concept study, the 2D online hyphenation of SEC to CEX was successfully applied to study

a mAb degradation pathway. Size variants were analysed by SEC in the ^{1}D, and the main product peak was fraction-transferred to the ^{2}D with an heart-cutting schedule for charge variants analysis by CEX. The CEX salt-based linear-gradient coupled to UV detection served for the profiling of charge variants and provided a fast and sensitive method suitable for HT analysis of a large number of samples with minimal sample requirement. The overall analysis time (without considering blanks and system suitability) was 8 hours with a column loading of 10 μg per injection. Here, it is important to mention that the SEC-CEX-UV method integrated with automated data processing script can provide data for ~70 samples in 24 h. Besides the increase in throughput against the standard 1D-LC approaches, the 2D SEC-CEX-UV method doesn't come without limitations. Firstly, the absolute quantitation of HMWS impurities by SEC was compromised due to solvent incompatibility between the two dimensions. Data showed that lowering the ^{1}D SEC ionic strength, which was necessary to ensure compatibility with the CEX, resulted in a 4% agreement of the HMWS quantitation against the benchmark SEC method used in AstraZeneca. Solvent incompatibility between the two dimensions may be overcome by the use of an ASM valve or by SPAM. Despite a 4% underestimation of HMWS quantitation may compromise the application of the method for late-stage development and manufacturing QC testing, its use in early-stage development is fit-for-purpose. Particularly, the present method is suited to be applied as a ranking tool during clone selection and process optimisation.

Charge variants peak characterisation couldn't be achieved without downstream analysis using MS. For this reason, an SEC-CEX separation using volatile buffers was developed for the online coupling to MS detection. MS analysis confirmed that mAb charge variants were due to glycoforms and oxidated species. Moreover, the susceptibility of the mAb to H_2O_2-mediated fragmentation via a hydroxyl radical reaction mechanism was identified. The UV traces obtained with the MS-compatible method were comparable to the salt-based SEC-CEX-UV method and the run time was 22 min. However, the Rs of intact MS analysis was not enough to detect deamidation with appropriate mass accuracy. Peptide-mapping analysis was performed to confirm mAb-1 quality attributes. Nevertheless, MS hyphenation enhanced the PQ information gathered in one analysis, enabled charge variants peak characterisation at the intact level and provided a deeper understanding of mAb-1 PQAs and degradation pathways under stress conditions.

Despite the advantages of MS hyphenation, this resulted in a decrease in sensitivity and throughput. To attain adequate MS signal a larger amount of sample (20 μg) was necessary.

Furthermore, besides the similar analysis time, MS data analysis was lengthy and manual processing was required. Therefore, the implementation of the SEC-CEX-MS method to HT workflows may be hampered by the overall reduction in throughput as well as the need for sophisticated equipment and expert scientists.

This study presented the hyphenation of SEC and CEX by 2D-LC to combine size and charge variants analysis in one single method maximising the PQ information obtained with minimal resources. Data demonstrated the benefit of the novel approach in providing fully automated instrument operations and data processing with little sample and time requirements for the analysis, in line with the HTPD framework. Online hyphenation to MS detection provided accurate characterisation of mAbs quality attributes at the molecular level.

This page was intentionally left blank

Chapter 5

Targeted mass spectrometry for aggregates assessment in a MAM workflow

5.1 Abstract

Bispecific antibodies are a promising growing class of biopharmaceuticals and have proven advantageous for the treatment of cancer. However, the complex structure and propensity to aggregate have hindered their entrance to the market. Consequently, more efficient analytical characterisation is necessary to drive product development and meet regulatory approval. Targeted mass spectrometry (MS) approaches such as multiple reaction monitoring (MRM) can be used to develop multi-attribute methods (MAM) that enable the quantitative analysis of multiple quality attributes of a drug candidate during development. The MAM methodology has emerged as a powerful tool in high-throughput process development (HTPD) activities where gathering a large amount of product and process information in a time and cost-efficient fashion is key to speed the entrance of new drugs to market. Nevertheless, the current MAM methods are generally based on the proteolytic cleavage of reduced and denatured peptides thus, fail to provide information on protein aggregation. Moreover, these methods combine high-resolution mass spectrometers with sophisticated data analysis software, hampering the overall analysis throughput. This study demonstrates the development of an MRM-based method to analyse aggregation of a bispecific antibody candidate (BsAb-1) by the assessment of cysteine (Cys) modified peptides. The MRM methodology is used to specifically target peptides involved in BsAb-1 aggregates formation and monitoring other PQAs such as C-terminal lysine (Lys) clipping, glycosylation, and deamidation. This proof-of-concept experiment proposes the use of a MRM-based MAM approach to comprehensively support quality analysis of a BsAbs candidate during the product development life cycle.

5.2 Introduction

Bispecific antibodies (BsAbs) have emerged as promising medicines in oncology thanks to their dual-target specificity (Brinkmann and Kontermann, 2021; Weidanz, 2021; Reichert, 2019; Krishnamurthy and Jimeno, 2018). Advancements in protein engineering and antibody biology led to the development of over 100 BsAb formats (Reichert, 2019). However, their complex structural architecture presents challenges in product development and has hindered their entrance to market (Suurs et al., 2019; Krishnamurthy and Jimeno, 2018; Nagorsen et al., 2012). One of the main challenges of BsAbs development is manufacturing a product with a consistent purity profile. Disulphide bonds play a critical role in this process; indeed, cysteine (Cys) bridges are often inserted as flexible linkers to connect the two antigen-binding sites (e.g. Blincyto) (Nagorsen et al., 2012) as well as for maintaining the biochemical stability of the molecule (Cao et al., 2018). In this regard, the structure of BsAbs that present an appended single-chain variable fragment (scFv) functioning as a second binding site is often stabilised by engineered disulphide bonds (Yu et al. 2021; Schmiedl, Breitling, and Du, 2000). Although introduced to improve the stability and binding of the molecule, these protein engineering strategies may lead to undesirable consequences such as low expression titres and expression inconsistency (Cao et al., 2018; Ding et al., 2021).

The subject of this study was a symmetric IgG-like BsAb with an appended scFv tethered within the CH3 domain (BsAb-1). As shown in Figure 5.1, an additional engineered disulphide bond was introduced between the light chain variable (VL) and heavy chain variable (VH) domains of the scFv to improve its biochemical stability. However, thorough characterisation studies previously performed in AstraZeneca demonstrated that the formation of the high-molecular-weight species (HMWS) impurities was linked to unfolding mechanisms causing the scFv engineered disulphide bond to remain opened (Cao et al., 2018). Precisely, BsAb-1 size variants characterisation by intact, subunit mass analysis and non-reduced peptide mapping demonstrated that the scFv engineered disulphide bond was opened in the monomer variant and both Cys residues (Cys442 and Cys640) were capped. The capping occurred by either cysteinylation (+119 Da) or glutathionylation (+305 Da) preventing the correct formation of the scFv engineered disulphide bond. This led to the formation of a mixture of molecular masses with +119 Da for cysteinylation or +305 Da for glutathionylation. Moreover, it was deduced that the opened scFv engineered disulphide bond induced the formation of head-to-tail dimers by the intermolecular connection of the

Cys442 of one molecule with the Cys640 of another molecule (Cao et al., 2018). The data supported the theory of a link between reduced Cys bridges and molecule unfolding mechanisms leading to the formation of HMWS impurities.

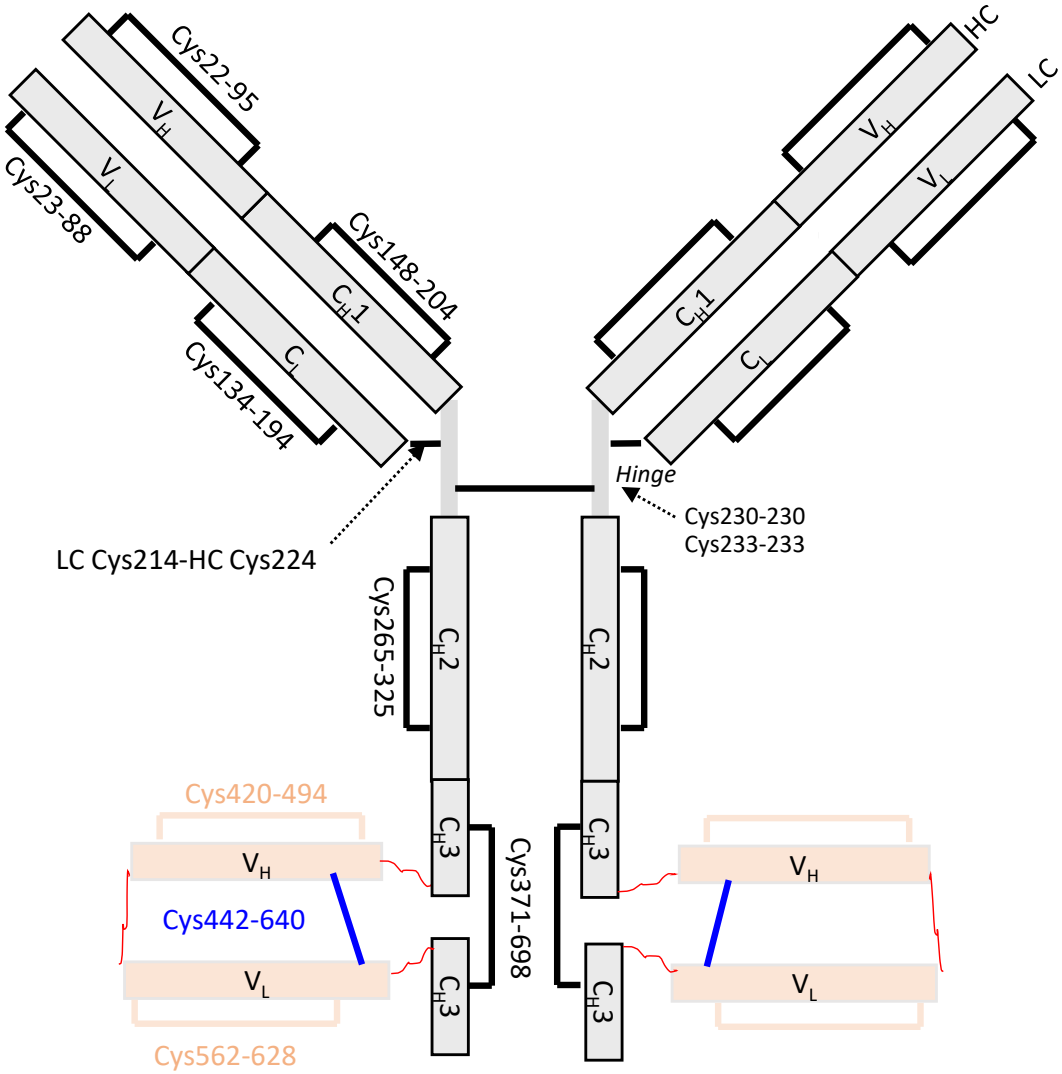

Figure 5.1 Schematic representation of BsAb-1 molecular structure and disulphide bond linkage.

The IgG-like backbone with the respective endogenous disulphide bonds (Cys371-Cys698, Cys265-Cys325, Cys 230-Cys230, Cys233-Cys233, Cys214-Cys224, Cys148-Cys204, Cys23-88, and Cys22-95) was depicted in grey. The scFv fraction appended within the CH3 domain with the two endogenous disulphide bonds (Cys420-Cys494, and Cys562-Cys628) was coloured in pink whilst the engineered stabilising bond (Cys442-Cys640) was shown in blue.

Liquid chromatography-tandem mass spectrometry (LC-MS/MS) analytical approaches provide protein structural information specific to amino acid residues. In this context, the MRM technique, performed on triple quadrupole (QqQ) mass spectrometers, is known to be

highly specific and sensitive due to the targeted monitoring of defined m/z values at the MS1 and MS2; also it is employed for accurate quantitation of protein and peptides (Mörtstedt et al., 2020). Current debates in the regulatory landscape have highlighted compliance of MAM in implementing FDA QbD approach and its implementation in a QC environment (U.S. FDA 2019; Rogers et al. 2018). Analysis by MAM is capable of identifying and quantitating multiple types of modifications in one single analysis, becoming increasingly popular in the biopharmaceutical industry as a tool to support the development life cycle of biotherapeutic proteins (Rogers et al. 2018). A key advantage of the MAM methodology over profile-based chromatography and electrophoretic techniques is the ability to accurately identify residue-specific modifications. Although conventional MAM uses HRMS instrumentations, a MRM approach would generate less complex data in comparison to HRMS allowing for a simpler workflow and greater throughput whilst providing sensitive and residue-specific information.

This study aimed to develop an MRM-based MAM approach to target the Cys modified peptides resulting from protein expression and aberrant protein folding which may lead to protein aggregation (HMWS) in the host cell culture fluid (HCCF). Furthermore, other PQAs were also integrated to develop an analytical workflow that could comprehensively support the analysis of BsAb-1 during development whilst minimising the need for orthogonal analytical testing.

In practice, BsAb-1 Cys modifications can be identified and quantified by MRM, therefore, the key research question of this study was to address whether the MRM methodology could be used to quantify the HMWS impurities present in BsAb-1 samples. In addition, further characterisation was performed to identify other BsAb-1 PTMs and define which of them were important to monitor during development. Subsequently, the data acquired from the initial analytical characterisation were used to build the MAM method. The proposed targeted approach was intended to be implemented in stages of development when substantial analytical information on a specific drug candidate is gathered and the PQAs are defined. The final method was aimed to be applied as a HT analytical tool to aid clone selection and process optimisation. Sensitivity and runtime were optimised for supporting the analysis of 48 samples at a time as per standard ambr® runs. Although this setup required a lower throughput than the methods previously presented for 96-DWP screening experiments (Chapter 3), it provided greater analytical information on the molecule PQAs with the specificity of MS detection. To increase the method throughput, sample preparation

was automated on a robotic liquid handler enabling the processing of 48 samples in parallel. Likewise, data analysis was leveraged by the use of an automated data processing workflow. The automation of the analytical workflow provided a significant increase in the method throughput enabling its application as a comprehensive analytical tool for the characterisation of BsAb-1 PQAs in HTPD.

5.3 Results and Discussions

5.3.1 Analytical Discovery of BsAb-1 Quality Attributes

5.3.1.1 EThcD-Assisted Non-reduced Peptide Mapping Analysis of BsAb-1 Fractions Separated by SEC

A substantial percentage of BsAb-1 HMWS impurities ~30% was observed by SEC analysis. Enriched fractions of HMWS and main product peaks as well as their purity analysis were obtained by SEC and named fractions 1 and 2, respectively (Appendix C, Figure 11.1). Non-reduced peptide mapping (NRPM) was used to assign the status of the Cys residues within each BsAb-1 fraction. To verify the presence of non-native disulphide bonds, sample preparation procedures were conducted both under conditions that maintain the native arrangement of disulphide bonds as well as inducing scrambling. The samples were divided into group A, group B and group C all comprising of fractions 1 and 2 and prepared as shown in Table 5.1. Tandem mass spectra were acquired with EThcD fragmentation to cleave the interchain disulphide bonds and reveal the modification status of the Cys residues. Retention time shifts were observed in the peptide maps of group A samples therefore, all the peaks were confirmed by high-resolution MS (HRMS) and fragmentation data. Peptide assignment was achieved by comparing the m/z of the observed ions in the MS spectra against all theoretical ions of the possible disulphide bonded peptides combinations calculated by in-silico prediction of the monoisotopic mass of the digested peptides. Peptides containing free Cys were searched with a mass addition corresponding to the alkylated species. EThcD-assisted NRPM analysis of BsAb-1 fractions confirmed the presence of 8 out of the 12 theoretical disulphide bonds (Figure 5.2; Appendix C, Figure 11.2; Figure 11.3; Figure 11.4; Figure 11.5; Figure 11.6; Figure 11.7). To further validate BsAb-1 disulphide bonds, the non-reduced peptide map was compared to the corresponding reduced peptide map. No unexpected disulphide bond was observed confirming that no scrambling had occurred. The MS1 and MS2 spectra of the peptides involved in the engineered stabilising disulphide bond were observed in both fractions eluting at 53.52 min and 52.48 min in fractions 1 and 2, respectively (Figure 5.2).

Table 5.1 Sample groups used for BsAb-1 disulphide bonds mapping.

Group A	Samples were alkylated, denatured and digested. This treatment preserved the native arrangement of the disulphide bonds.
Group B	Samples were denatured, alkylated and digested. This treatment induced the formation of non-native disulphide bonds.
Group C	The samples were alkylated, denatured, digested, and finally reduced before injection. This was done to confirm the presence of the disulphide bonds since peptides containing the Cys residues linked by disulphide bonds will be present only in Group A (non-reduced peptide map), and absent or low abundant in group C (reduced peptide map).

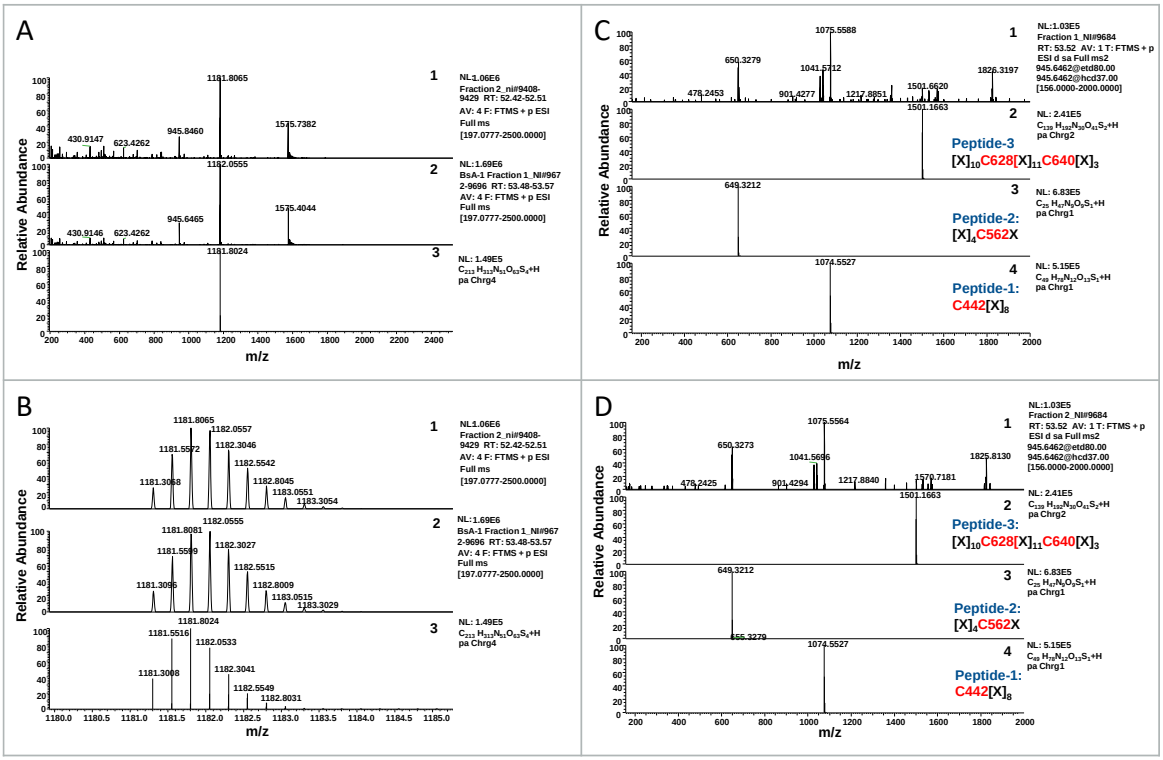

Figure 5.2 EThcD-assisted MS and MS/MS spectra of the scFv tripeptide in BsAb-1 SEC fractions.

A) Full MS spectra of the scFv tripeptide observed in the SEC fraction 1 (1) and fraction 2 (2) with $[M+3H]^{+3}$ (1574 m/z), M+4 (1181 m/z), and $[M+5H]^{+5}$ (945 m/z) species detected in both fractions and $[M+4H]^{+4}$ matching the theoretical m/z value (3); B) Zoom of the isotopic charge distribution of $[M+4H]^{+4}$ matching the theoretical m/z; C, and D) EThcD MS/MS spectra showing the fragments of the three peptides constituting the scFv tripeptide of both fractions observed in fraction 1 and 2, respectively (1). As a result of EThcD fragmentation, peptide-3 (2), peptide-2 (3), and peptide-(3) were detected confirming the presence of the native engineered stabilising disulphide bond in both SEC fractions.

Due to the specificity of the trypsin cleavage at Lys and Arg residues, the engineered stabilising disulphide bond was seen as part of a tripeptide species comprising of peptide-1, peptide-2 and peptide-3, and referred to as scFv tripeptide in this manuscript. Particularly, the native organisation of the scFv tripeptide disulphide bonds comprised Cys442 in peptide-1 binding to Cys640 in peptide-3; the latter peptide also contained Cys628 linked to Cys526 in peptide-2 (Figure 5.3).

To look for Cys modifications in the scFv tripeptide, the MS2 extracted ion chromatograms (XIC) of the peptides fragments were searched to identify all the species containing the fragments bearing Cys442, Cys526, Cys628 and Cys640. Interestingly, the MS2 XIC of the peptide-3 $[M+2H]^{2+}$fragment (1501.67 m/z) showed the presence of peaks eluting at 48.4 min and 48.75 min (Figure 5.4, A) corresponding to glutathionylation and cysteinylation of Cys640, respectively (Figure 5.5). Likewise, the XIC of peptide-1 $[M+1H]^{1+}$ (1705.56 m/z) peaks eluting at 34.82 min and 35.05 min (Figure 5.4, B) were confirmed at the MS2 level as cysteinylation and glutathionylation of Cys442, respectively (Figure 5.6). The observed masses of both parent ions and in-source fragments matched their respective theoretical values, confirming peak identification. Such modifications were not found in fraction 2. Moreover, no modifications of peptide-3 were observed. The data were consistent with the observations previously presented by Cao suggesting that the incorrect folding of the protein exposed the Cys442 and Cys640 residues to react with the Cys and GSH present in the media or with the respective Cys442/Cys640 from another molecule to form head-to-tail dimers (Cao et al., 2018). These observations led to the hypothesis of a correlation between the modifications occurring on Cys442 and Cys640 with the amount of HMWS forming in BsAb-1 samples. The following section of this chapter will investigate the development and application of an MRM for targeting Cys442/Cys640 modifications and correlate their relative quantification to the %HMWS present in BsAb-1 samples.

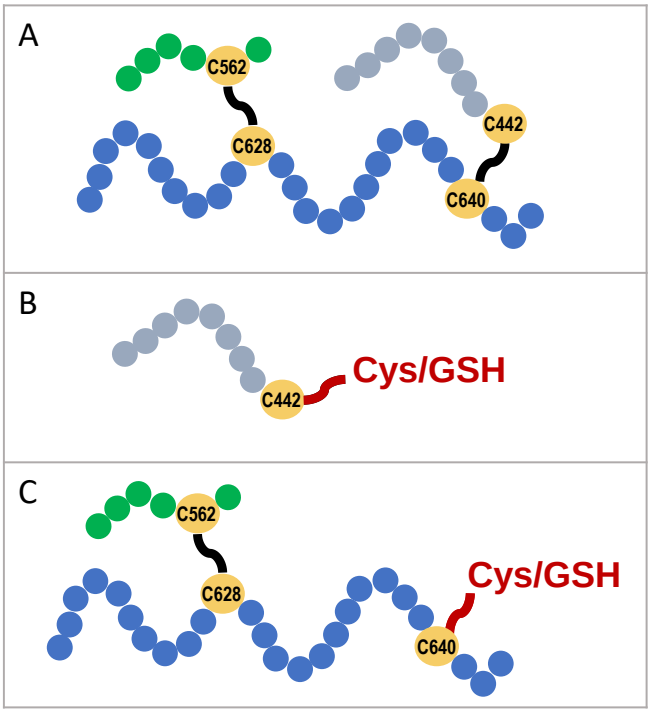

Figure 5.3 Schematic representation of the scFv tripeptide disulphide bonds and site-specific modifications.

A) Unmodified scFv tripeptide comprising of peptide-1 (grey) bearing Cys442 linked to Cys640 of peptide-3 (blue) and constituting the engineered stabilising disulphide bond; peptide-2 bearing Cys562 linked to Cys628 on peptide-3. B and C) Site-specific cysteinylation and glutathionylation on Cys442 and Cys640, respectively, leading to the formation of peptide-1 and the dipeptide composed of peptide-2 and 3.

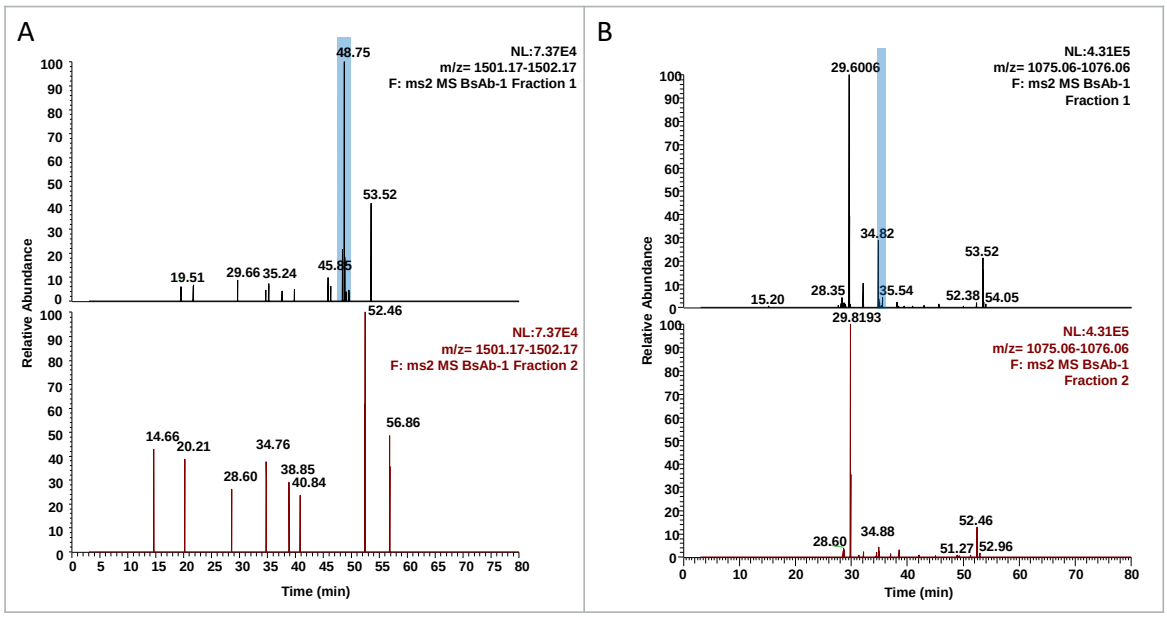

Figure 5.4 XIC of peptide-3 $[M+2H]^{2+}$ (1501 m/z) and peptide-1 $[M+1H]^{1+}$ (1075 m/z).

A) XIC of peptide-3 $[M+2H]^{2+}$ (1501 m/z) eluting at 48.75 min and B) XIC of peptide-1 $[M+1H]^{1+}$ (1075 m/z) eluting at 34.82 min both observed in fraction 1 (top) but not in fraction 2 (bottom).

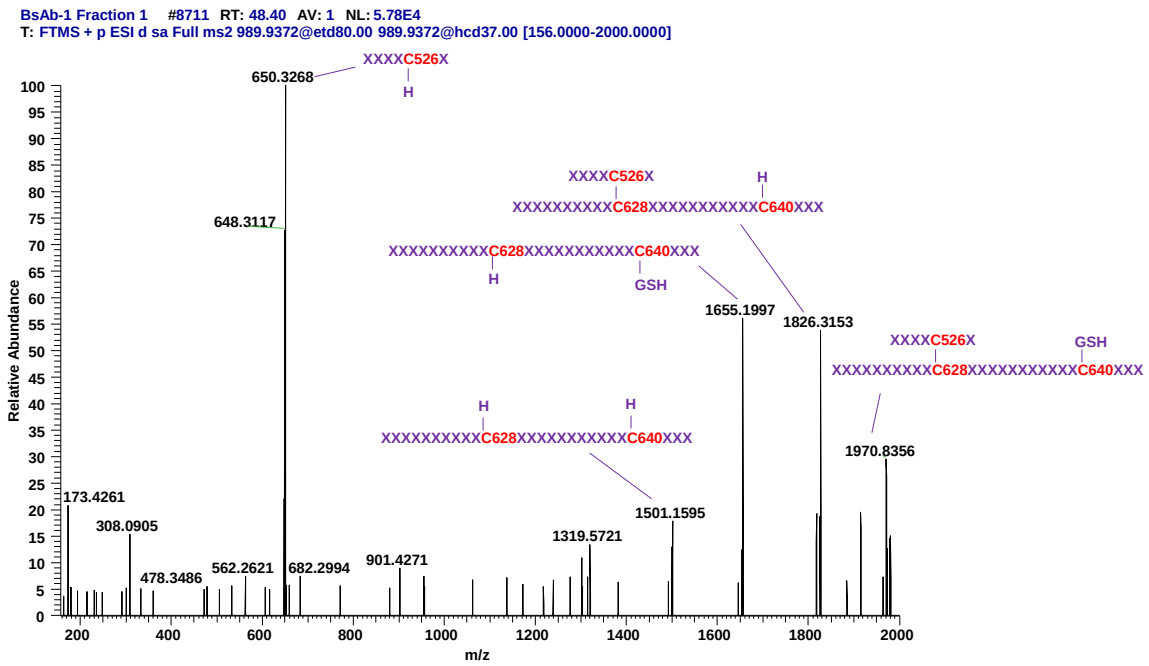

Figure 5.5 EThcD MS/MS spectra of glutathionylation on Cys640 observed in fraction 1.

The MS2 of 989.9372 m/z precursor ion fragmented by EThcD showed the presence of 1970 m/z, and 1655 m/z corresponding to glutathionylation of Cys640 with the disulphide bond Cys628-Cys526 in the intact and reduced status, respectively. Other fragments identified were 650 m/z, 1501 m/z, and 1826 m/z corresponding to reduced peptide-2, reduced peptide-3 and peptide-2 and 3 linked via Cys526-Cys628 disulphide bond with reduced Cys640, respectively.

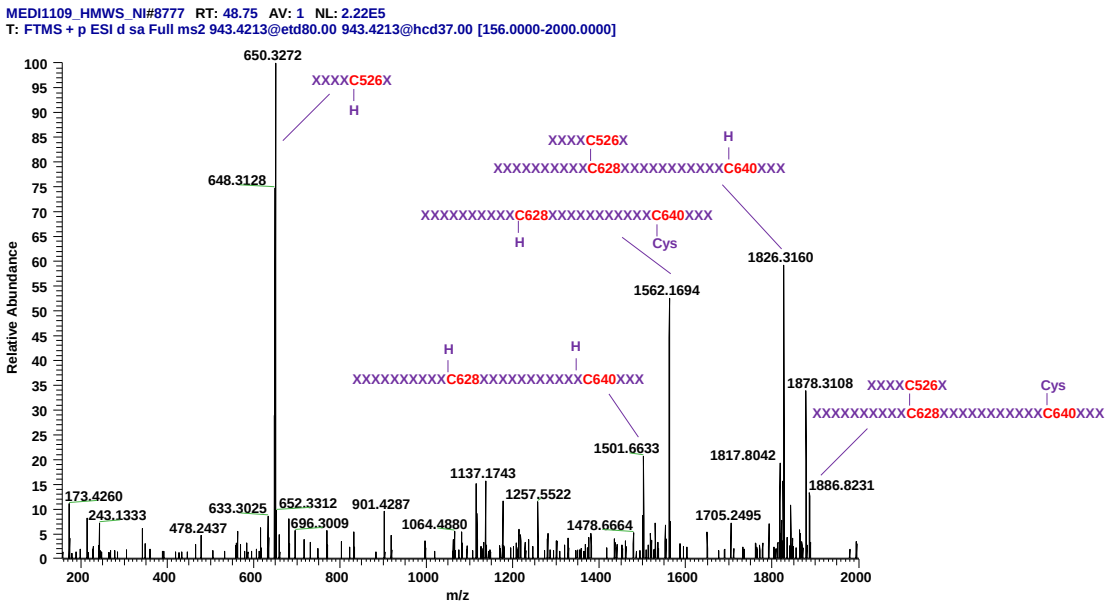

Figure 5.6 EThcD MS/MS spectra of cysteinylation on Cys640 observed in fraction 1.

The MS2 of 943.4213 m/z precursor ion fragmented by EThcD displaying the presence of 1886 m/z, and 1562 m/z corresponding to cysteinylation of Cys640 with the Cys628-Cys526 disulphide bond in the intact and reduced status, respectively. Other fragments identified were 650 m/z, 1501 m /z, and 1826 m/z corresponding to reduced peptide-2, reduced peptide-3 and peptide-2 and 3 linked via Cys526-Cys628 disulphide bond with reduced Cys640, respectively.

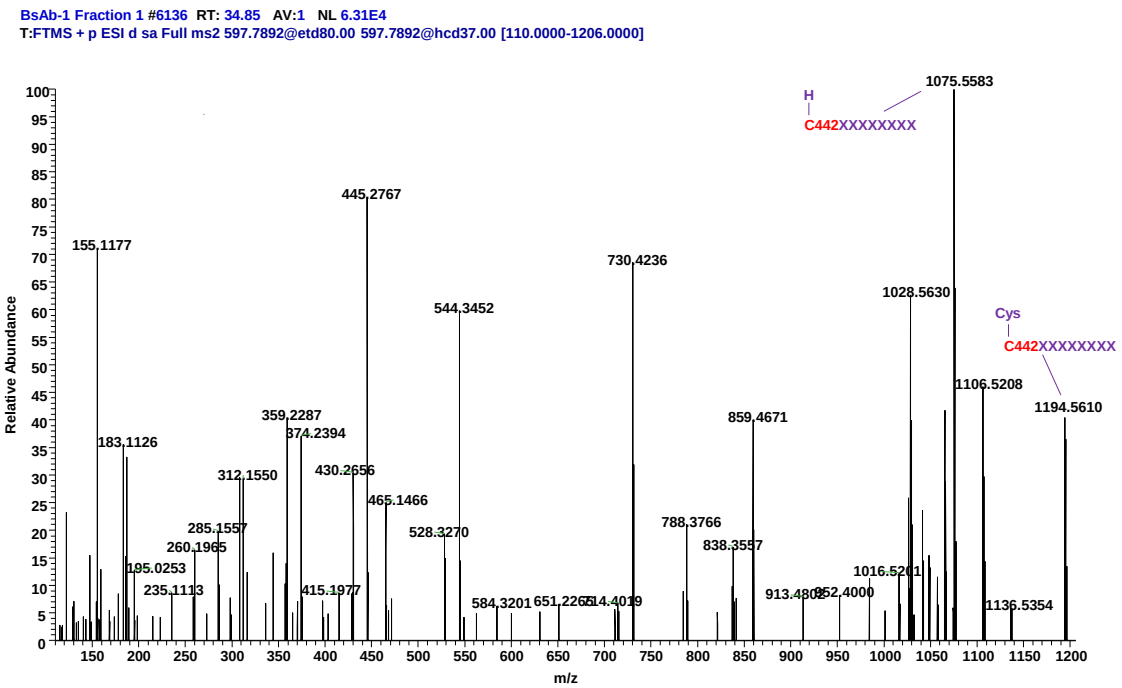

Figure 5.7 EThcD MS/MS spectra of glutathionylation on Cys442 observed in fraction 1.

The MS2 of 597.78 m/z precursor ion fragmented by EThcD displaying the presence of 1194.56 m/z corresponding to cysteinylation of Cys442. The reduced peptide-1 fragment with 1075 m/z $[M+1H]^{1+}$ was also identified.

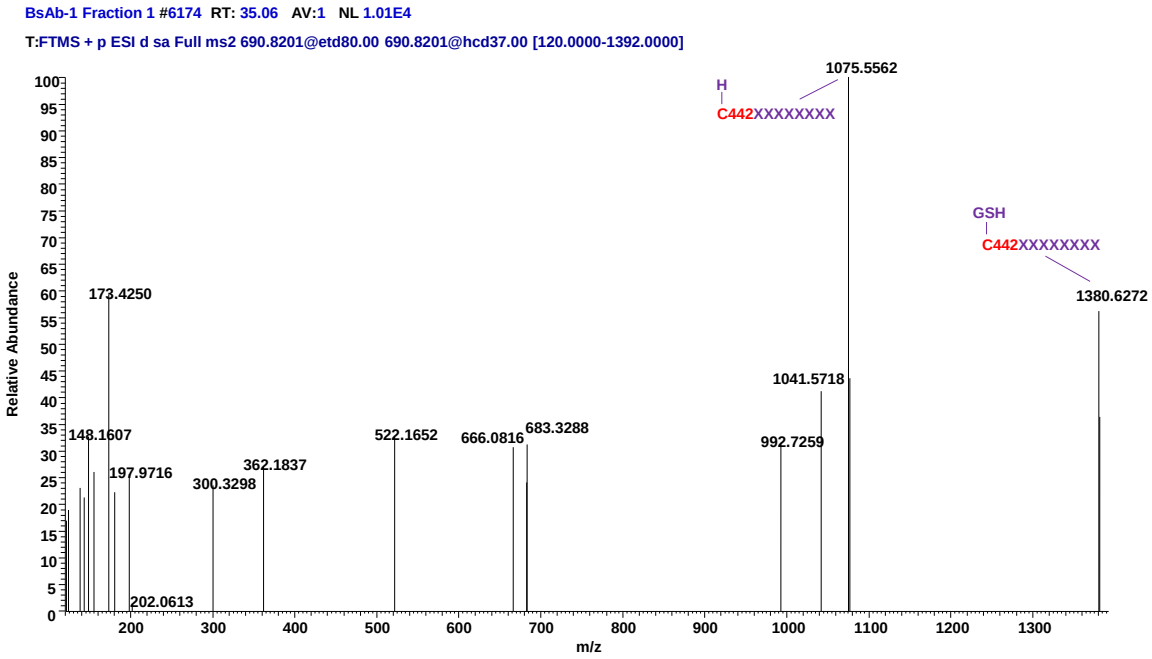

Figure 5.8 EThcD MS/MS spectra of cysteinylation on Cys442 observed in fraction 1.

The MS2 of 690.82 m/z precursor ion fragmented by EThcD displaying the presence of 1380.64 m/z corresponding to glutathionylation of Cys442. The reduced peptide-1 fragment with 1075 m/z $[M+1H]^{1+}$ was also identified.

5.3.1.2 Reduced Peptide Mapping for Protein Characterisation

Aiming to develop an analytical strategy that produced targeted information on BsAb-1 quality attributes, thorough characterisation analysis was necessary to identify the sequence liabilities and PTMs of this specific therapeutic candidate. Reduced peptide mapping (RPM) was performed for confirming the BsAb-1 primary sequence and determining the site-specific post-translational modifications (PTMs) to monitor by MRM. These were C-terminal Lys retention, deamidation of Asn54, Asn365 and Asn662, oxidation of Met256 and Met481, and glycosylation of Asn301 with 6 identified glycoforms namely, A1G0, A1G0F, A1G1F, A2G0F, Man3 and Man5.

Together with the NRPM, RPM analysis enabled the identification of 9 different peptide sequences that could present potential liabilities to product quality. These data served as a basis to build the MAM as described in the next section.

5.3.2 Development of the Multi-Attribute Method

The present method was designed to cover the quantitative analysis of glycosylation, deamidation, oxidation, C-terminal Lys clipping, Cys modifications, and including aggregation occurring in BsAb-1 generated from medium-throughput cell culture experiments during product development such as ambr® runs (48 samples at a time). As previously described, aberrant protein folding events may cause the exposure of free Cys442 and Cys640 residues to react with other Cys leading to the formation of Cys modifications resulting in aggregation and HMWS. Hence, the main challenge of this research was to investigate the presence of a correlation between the Cys modifications and the HMWS present in the sample to successively build a statistical model for inferring the quantitation of HMWS based on the Cys modifications.

Previous discovery analysis of BsAb-1 identified 9 peptides with PTMs accounting for product quality liability to target by MRM (see Section 5.3.1). Each quality attribute was analysed by monitoring the unmodified *vs.* the modified peptide sequence. Sample preparation and chromatography conditions were optimised from the AZ SOP for NRPM (see Chapter 2, Section 2.1.4.4). Particularly, the sample preparation protocol was automated on a robotic liquid handler for improving method throughput and consistency over a large number of samples. More information on the automation of the sample preparation protocol was addressed in the following section of this chapter (see Section 5.3.2.1).

To obtain robust and quantitative MS/MS analysis, a QqQ mass spectrometer was selected and operated in Multiple Reaction Monitoring (MRM) mode (for further information on method development see Chapter 2, Section 2.1.4.4). A Python-JMP integrated script was developed to automate the data processing and ease the handling of large datasets.

As a proof-of-concept, a sample of BsAb-1 was analysed in triplicate and the data acquired are displayed in Figure 5.9. Data showed that the simultaneous identification and quantitation of BsAb-1 QAs were successfully achieved by the MRM-based MAM.

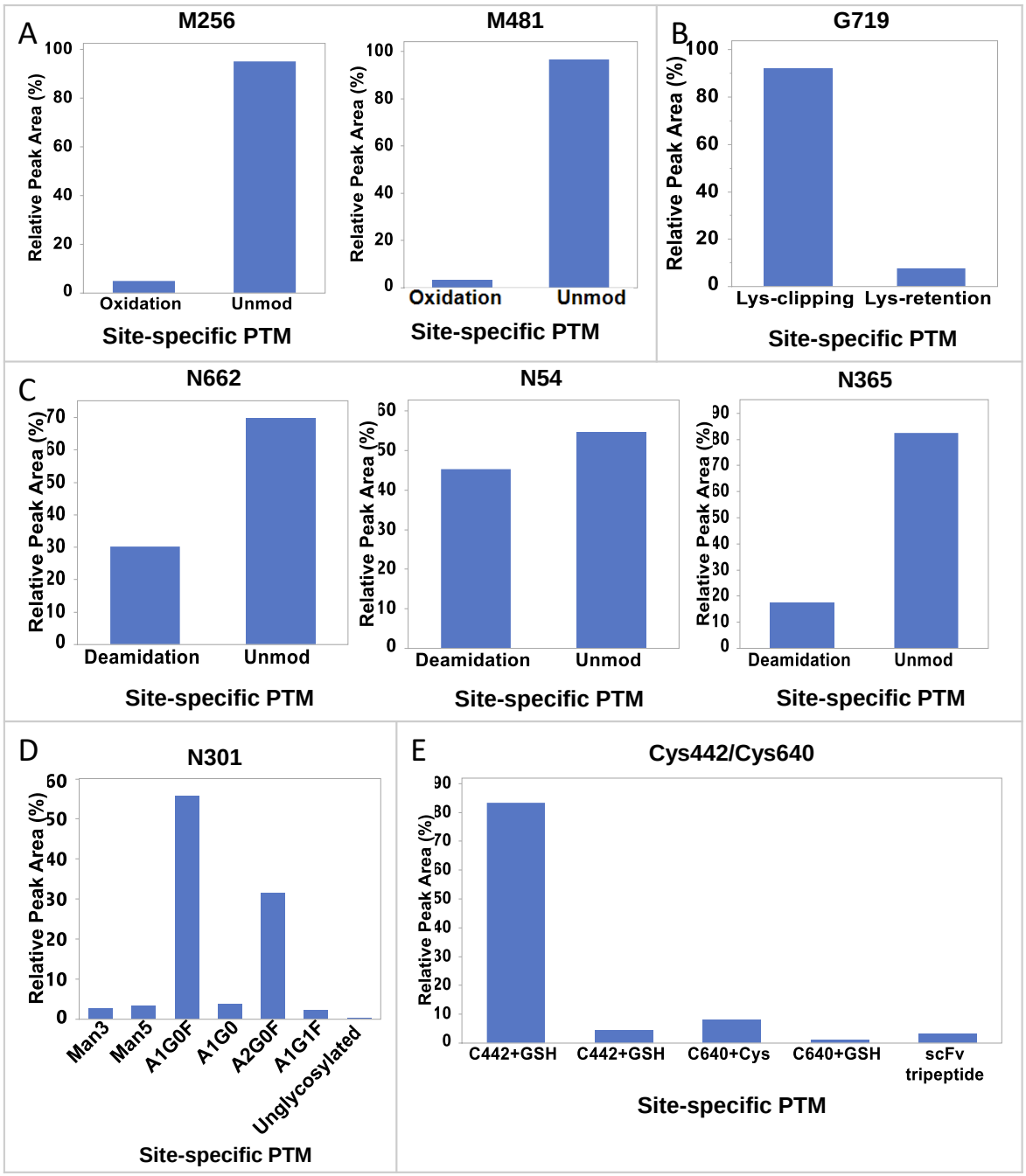

Figure 5.9 MAM analysis of BsAb-1: proof-of-concept of targeted PTMs monitoring.
Bar chart representing the relative quantification of modified peptides against the unmodified (Unmod) species. A) Oxidation of M256 and M481; B) C-terminal Lys processing; C) Deamidation of N662, N365 and N54; D) Glycosylation displaying the relative quantification of Man3, Man5, A1G0F, A1G0, A2G0F, and A1G1F; E) Cys-modifications including glutathionylation and cysteinylation of Cys442 and Cys640 as well as the unmodified peptide.

5.3.2.1 *Correlating HMWS from Cys Modifications*

Findings from the NRPM analysis of BsAb-1 fractions revealed the presence of Cys modifications in fraction 1 containing HMWS impurities (see Section 5.3.1). Along with the findings from Cao et al., this study demonstrated that modifications of Cys442 and Cys640 were responsible for the formation of HMWS in this specific therapeutic candidate. The study proposed herein aimed to address whether the relative quantitation of Cys modifications by MRM can be used to quantitate the %HMWS impurities present in the sample. The following proof-of-concept experiment was part of method development and used to investigate the method application for the analysis of BsAb-1 RM samples with known %HMWS.

Firstly, samples with different levels of HMWS, samples of the BsAb-1 SEC fractions 1 and 2 were blended at different ratios, namely 0%, 10%, 20%, 40% and 60% of fraction 1 (HMWS) spiked into fraction 2 (main product peak). Subsequently, the samples were divided into 8 replicates to generate an adequate sample size for evaluating the presence of a correlation between Cys modifications and HMWS impurities. Finally, the samples were analysed by MAM and the relative abundance of cysteinylation of Cys442, Cys640 and the unmodified scFv tripeptide were displayed in Figure 5.10.

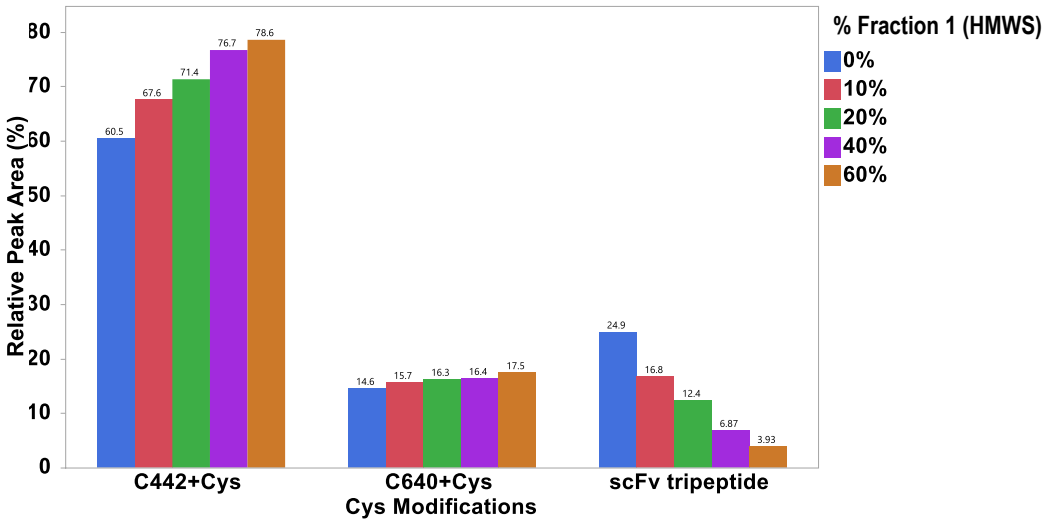

Figure 5.10 Quantitative analysis of BsAb-1 Cys modifications by MAM.
Bar chart depicting the relative abundance of Cys modifications analysed in the BsAb-1 sample blends by MAM, namely cysteinylation of Cys442 (C442+Cys) and Cys640 (C640+Cys) and the unmodified scFv tripeptide. The blends were prepared by normalising the fractions concentration to 1 mg/mL and spiking fraction 1 into fraction 2 at different ratios, namely 0% (blue), 10% (red), 20% (green), 40% (purple), 60% (orange).

The MAM analysis revealed that the relative abundance of cysteinylated species increased proportionally to the %fraction 1 spiked into the sample whereas the levels of unmodified scFv tripeptide decreased proportionally (Figure 5.10). This experiment confirmed that the MRM-based MAM was capable of discriminating between samples containing different levels of Cys modifications.

Multivariate analysis (MVA) was used to investigate the presence of a correlation between the Cys modifications and assessing their relevance to changes in the content of HMWS (Figure 5.11). Both cysteinylation of Cys442 and Cys640 were positively correlated with the %fraction 1 spiked in the sample, whilst the scFv tripeptide was negatively correlated. The correlation between cysteinylation at Cys442 and the scFv tripeptide with the %HMWS was strong (0.8781 and -0.8884, respectively) and significant (p-value <0.0001). Differently, cysteinylation of Cys640 showed a weak positive (0.3804) although significant (p-value = 0.0155) correlation with the %HMWS. Another aspect to take into consideration is that the Cys modifications are correlated with one another. Particularly, cysteinylation of Cys442 was strongly, negatively (-0.9582), and significantly (p-value <0.0001) correlated with the scFv tripeptide whilst non correlated with Cys640 (0.2523, p-value = 0.1163). Interestingly, Cys640 had a stronger negative (-0.5185) significant (p-value = 0.0006) correlation with scFv tripeptide than with the %HMWS (0.3804, p-value = 0.0155).

This may indicate that, in the BsAb-1 RM model sample, cysteinylation of Cys442 and the scFv tripeptide were the most probable modifications consequent to protein unfolding mechanisms inducing the formation of HMWS.

A

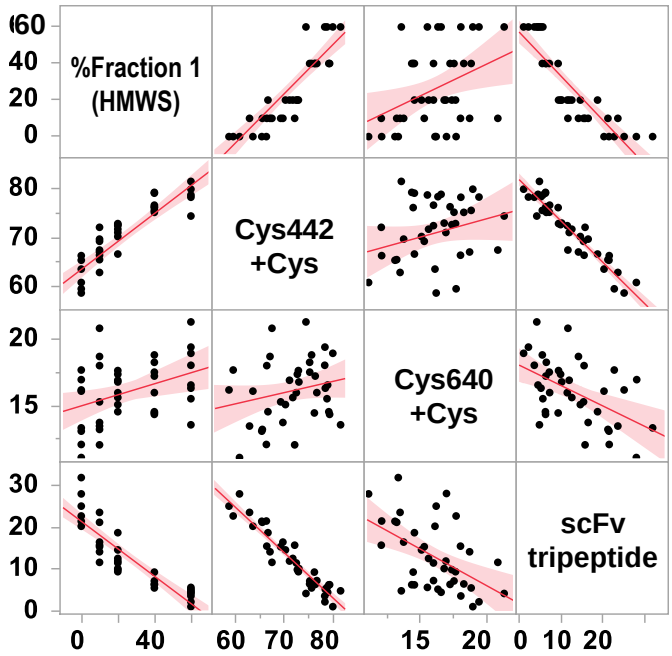

B

Correlation				
	%HMWS	C442 +Cys	C640 +Cys	scFv tripeptide
%HMWS	1.0000	0.8781	0.3804	-0.8884
C442+Cys	0.8781	1.0000	0.2523	-0.9582
C640+Cys	0.3804	0.2523	1.0000	-0.5185
scFv tripeptide	-0.8884	-0.9582	-0.5185	1.0000

C

Correlation Probability				
	%HMWS	C442 +Cys	C640 +Cys	scFv tripeptide
%HMWS	<.0001	<.0001	0.0155	<.0001
C442-Cys	<.0001	<.0001	0.1163	<.0001
C640-Cys	0.0155	0.1163	<.0001	0.0006
scFv tripeptide	<.0001	<.0001	0.0006	<.0001

Figure 5.11 MVA report.

A) Scatter plot matrix showing the relationship between %fraction 1 (HMWS) spiked in the sample (y-axis) and the relative abundance of each Cys modification (x-axis). Linear regression analysis was used to fit the data: the greater is the slope of the line (red), the stronger is the correlation and the direction of the line indicates whether the correlation is positive or negative. B) Correlation matrix reporting the correlation values of each Cys modification *vs.* the %HMWS. Negative correlations were reported in red whilst positive correlations were displayed in blue. A strong correlation was defined as $\geq |0.8|$ as the maximum correlation value is 1. C) probability matrix demonstrating the relevance of each Cys modifications for the %HMWS. The Cys-modifications with p-value < 0.05 are significantly correlated with the content of HMWS impurities in BsAb-1.

Regression analysis was used to study the relationship between Cys modifications and HMWS as well as inferring the relative abundance of HMWS impurities present in the sample. A regression model with L2 regularisation (Ridge regression) was used to infer the %HMWS from the Cys modifications present in the samples (Appendix C, Table 11.4,

Table 11.5). The dataset used for training the model comprised of 8 replicates for each sample group. The %HMWS used for training the model was based on the HT SEC analysis (see Chapter 3, Section 3.3.2) of the sample blends (Figure 5.12, A). Subsequently, a heterogeneous group of samples was used to test the model. This comprised of BsAb-1 drug substance (DS), a sample of BsAb-1 stressed at high pH (HP) by adding 1M Tris pH 8.5, a sample of BsAb-1 stressed at 70 °C for 30 min and 3 replicates of the RM (RM1, RM2 and RM3). All the samples of the test group were analysed in triplicate and the %HMWS predicted by the model was compared with the one obtained by HT SEC.

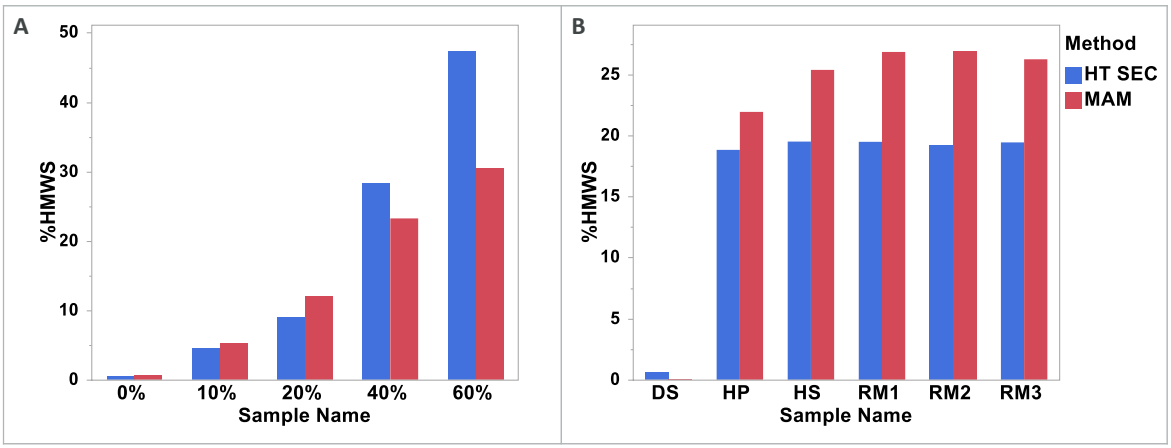

Figure 5.12 Inferring the quantitation of HMWS from Cys modifications by Ridge regression analysis.

Bar chart displaying the %HMWS estimated by the model based on the relative quantification of the Cys modifications monitored by MAM (red) *vs.* the %HMWS analysed by HT SEC (blue). A) Training dataset including 8 technical replicates of the sample blends. B) Testing dataset comprising of the BsAb-1 drug substance (DS), samples stressed with high pH (HP) and heat (HS) and 3 replicates of the RM (RM1, RM2 and RM3).

Figure 5.12, B displays the %HMWS predicted by the model (red) *vs.* the one analysed by HT SEC (blue). Both techniques can discriminate from samples containing various levels of HMWS impurities, and give the same trend. However, the HMWS values measured by MAM and SEC differ significantly from one another. Moreover, the %HMWS predicted by the MAM model was not precise (Appendix Figure 11.11) and showed wide confidence intervals, making it difficult to both accurately quantify and confidently discriminate between the samples with different levels of HMWS impurities. In this regard, a few considerations need to be addressed. Firstly, the low intensity of the scFv tripeptide affected the precision of the MRM method and consequently resulted in high measurement variability of the peptide relative abundance. This may affect the capability of the MAM model to precisely quantitate the amount of HMWS impurities. Similarly, peptides bearing

glutathionylation of Cys442 and Cys640 were below the method LOQ thus they were not included in the model. This may indicate that the model falls short in having all the predictors necessary to truly capture the main feature behind the data. Sensitivity issues may be overcome by either increasing the column loading or modifying the sample preparation procedure. The latter could benefit by either investigating on the use different digestion enzymes such as Lys-C, Glu-C and pepsin as well as different digestion pH, to obtain peptides that better ionise in the ESI source (F. Liu, Breukelen, and Heck 2014; Cui et al. 2019). Proteases such as pepsin can be used to verify reshuffling of disulphide bonds (F. Liu, Breukelen, and Heck 2014; Cui et al. 2019). Mobile phase additives such as formic acid, propionic acid, and TFA at various concentrations could also be investigated to improve the MS signal.

Another factor to take into consideration is that the model predictors are correlated not only with the %HMWS but also with one another, e.g. Cys442 is strongly correlated with the scFv tripeptide. This phenomenon, known as multicollinearity, tends to overinflate the standard errors of the model coefficients making some predictors statistically insignificant when they should be significant. Moreover, the change in one variable produces mutual changes of the correlated variable. Therefore, the model results would be sensitive to small changes in the data and unstable. This may explain why the model prediction accuracy was ultimately affected. Multicollinearity may be overcome by removing the highly correlated variables, linearly combining them in the model as a unique variable or using other modelling tools designed for highly correlated variables such as principal component analysis. Nevertheless, it would be sensible to investigate other statistical approaches if multicollinearity is still present when the method sensitivity is improved to include all the possible predictors in the model (such as the glutathionylated peptides).

Additional considerations concern the features of the training dataset. Indeed, the sample group used for this experiment was suitable for confirming that the method was able to discriminate between samples containing various levels of Cys modifications which also corresponded to different %HMWS. However, this specific sample set may not be suited for building a model that accurately predicts aggregation. Training datasets for obtaining accurate model predictions are generally larger (hundreds of samples) and investigate a wider experimental space involving the use of various conditions. Conversely, the sample group used herein derived from a single stock of BsAb-1 RM with unique characteristics which may not be representative of the same molecule when expressed in culture by means

which alter its aggregation pathway. As an example, if cysteinylation and glutathionylation of Cys442 and Cys640 occurred at different ratios than the ones observed in the BsAb-1 RM, this model would not work as the relationship between Cys modifications and %HMWS would be different. In that case, another model would need to be generated to study how the Cys modifications are related to each other and the %HMWS present in the sample. Therefore, the MAM model described in this study would be suitable for application to quantify the HMWS of BsAb-1 RM only. A more diverse set of samples would be necessary to build a model that could comprehensively quantify the HMWS impurities in BsAb-1 during the various development stages.

The data presented herein suggest that further experimentation is needed to achieve accurate quantitation of BsAb-1 HMWS by MAM. Nevertheless, this work provided a proof-of-concept study demonstrating the potential of the MRM methodology in quantifying BsAbs aggregates and gave a vision to the application of MAM as comprehensive analytical tool to support product development minimising the need for orthogonal testing.

Future experiments would be focused on improving the MS sensitivity of low-intensity peptides, using a larger and more diverse case-study sample to train the model and investigate statistical modelling tools that can capture all the possible features in the data and accurately predict the amount of HMWS present in the sample. Cross-validation of the statistical model would also be required when dealing with a larger dataset and demonstrate the feasibility of the method to be applied for supporting product development.

5.3.3 Development of Automated Sample Preparation

The sample preparation for NRPM is a complex and lengthy procedure. Manual execution can be inconsistent and inconvenient especially for the processing of a large number of samples. Automation enables robust and consistent execution of sample preparation protocols leveraging scientists work and increasing the throughput of analytical workflows (Qian et al., 2021). Nevertheless, the development of automated processes may not be straightforward and often require careful tuning of all the steps. Therefore, it is important to address the comparability of the results with manual procedures and assess the fitness-for-purpose of the automated operation. In this study, the sample preparation for NRPM was automated on a robotic liquid handler to support the processing of a large number of samples and designed for 96-DWP sample handling. Method comparability against the manual

procedure was evaluated based on the quantification of the digested peptide PTMs across 6 sample replicates. To evaluate the robot consistency across the plate, the samples were divided into 3 groups each comprising of 6 replicates and placed at the front, middle and back of the plate constituting a total of 18 replicates for the automated procedure. Moreover, data for evaluating the method repeatability were extrapolated from the comparability study to assess whether the automated procedure would increase method precision. A summary of the comparability study data can be found in Table 5.3 as part of the method assessment.

The PTMs quantification involved 1) the calculation of the qualifier/quantifier ion ratio coefficients of variation (CVs) across the 6 replicates of each sample group (namely manual and automated front, automated middle and automated back), followed by 2) the calculation of each PTM relative peak area based on the %area of the quantifier ion peak of modified peptide *vs.* the unmodified peptide. Data showed that the qualifier/quantifier ions ratio CVs were comparable amongst the sample groups and < 20% (Appendix C, Figure 11.8). The peptide ion transitions corresponding to unglycosylated N301 and glutathionylation of Cys442 and Cys640 were not detected (Appendix C, Figure 11.8). Visual representation of the PTMs quantitation showed a comparable trend between the manual and the automated sample groups (Appendix C, Figure 11.9). ANOVA test demonstrated that the PTMs quantitation between the automated groups (front, middle and back) was not significantly different (Appendix C, Table 11.1) inferring consistency across the plate. T-test for an equal group size of 6 sample replicates verified that the PTMs quantitation obtained by using the manual and the automated sample preparation procedures were not statistically different (Appendix C, Table 11.2). Variability gauge analysis was performed to examine the measurement variation between the two sample preparation procedures. The variability chart (Figure 5.13, Appendix C, Table 11.2) visualises the variability of the site-specific PTM quantitation amongst the sample replicates between the manual and automated processes. With this experiment, we conclude that the two sample preparation procedures were comparable for PTMs quantification and method repeatability. Nevertheless, automation improved method throughput by parallel processing of a large number of samples and allowing walk-away time during sample preparation.

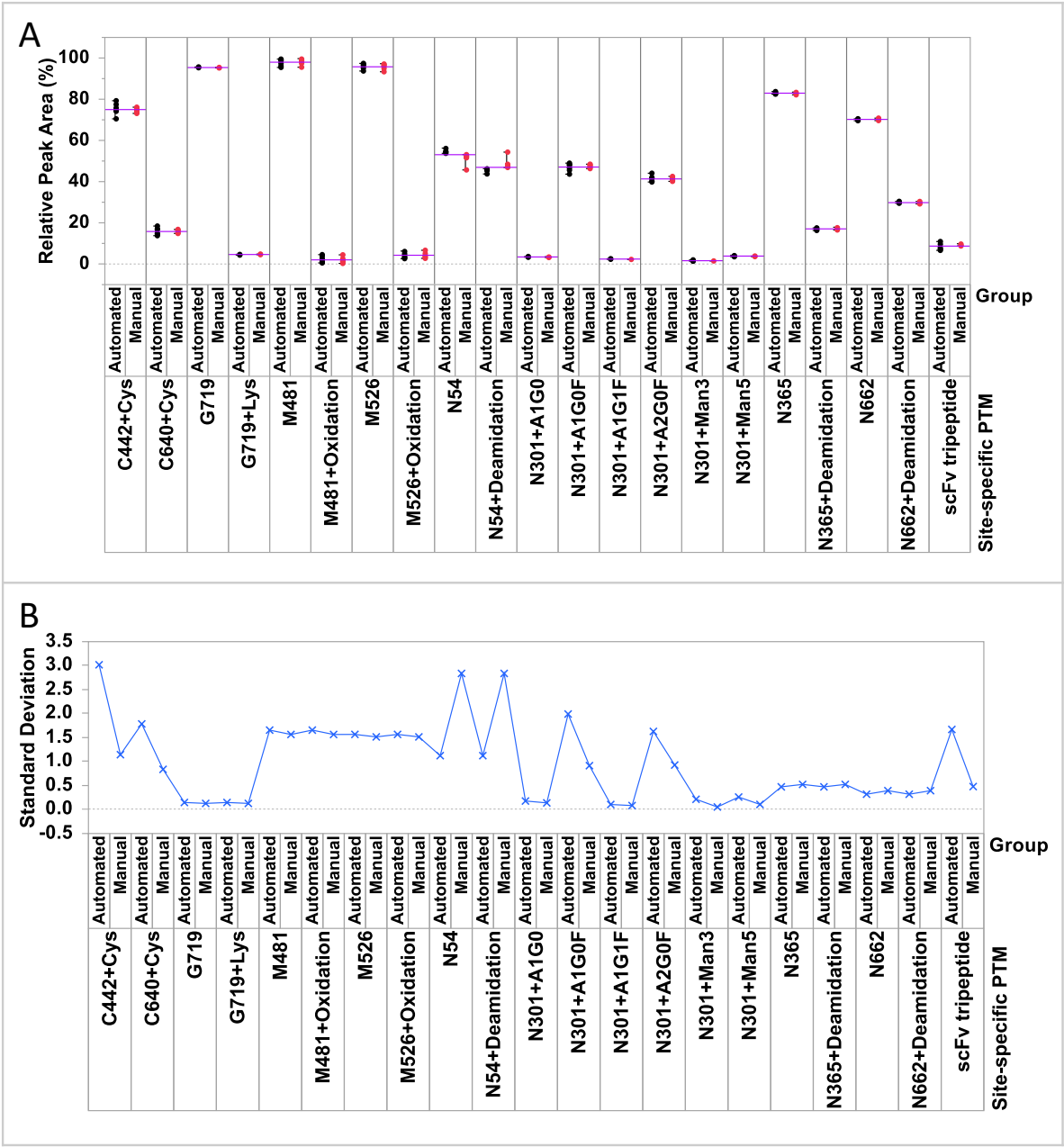

Figure 5.13 Variability gauge chart for site-specific PTMs relative peak area between manual and automated procedures.

A) Variability chart displaying the relative peak area of each site-specific PTM measured for all the group replicates prepared by using the manual (pink dots) and the automated processes (black dots). The purple line indicates the group mean. B) Standard deviation of each site-specific PTM relative peak area compared between the groups. Connecting lines were used to better visualise the fluctuation of the standard deviation across the samples.

5.3.4 MAM Method Assessment

The MAM method was qualified for the relative quantification of BsAb-1 PQAs such as Cys modifications, aggregation, glycosylation, deamidation, oxidation and C-terminal Lys-retention. This study focused on the assessment of sample stability over the time scales of the analysis conditions, method repeatability, and day-to-day reproducibility. The analytical workflow was designed and assessed for supporting the analysis of BsAb-1 expressed in medium-throughput cell culture experiments such as ambr® micro bioreactors setups with up to 48 cultures. The data presented herein were integrated with the comparability study aimed to gauge the suitability of automated operations for sample preparation previously presented in Section 5.3.2.1 (see Figure 5.13).

5.3.4.1 Overtime Sample Stability under Analysis Conditions

To evaluate the overtime stability of the tryptic digested peptides under process conditions before LC-MS injection, 48 replicates of BsAb-1 RM were prepared and analysed in the same plate. A variability gauge study was performed to measure the variation of the PTMs relative peak areas amongst the replicated measurements (Appendix C, Table 11.6). Figure 5.14 provided a visual representation of the variation of the PTMs relative peak areas over time. Whilst glycosylation, deamidation, C-terminal Lys clipping and Cys modifications were consistent (CV < 20%, Appendix C, Table 11.6) it is clear that oxidation of Met481 and Met526 was inconsistent (CV > 20%, Appendix C, Table 11.6) and increased over time. This may be due to the instability of the tryptic digested peptides to oxidative events occurring as a result of sample storage in the NRPM buffer and at 4 °C in the autosampler. This observation testified that oxidation occurred as an artefact of sample preparation and increased over time. Therefore, the present method is not fit for monitoring and correlate oxidation to process engineering strategies.

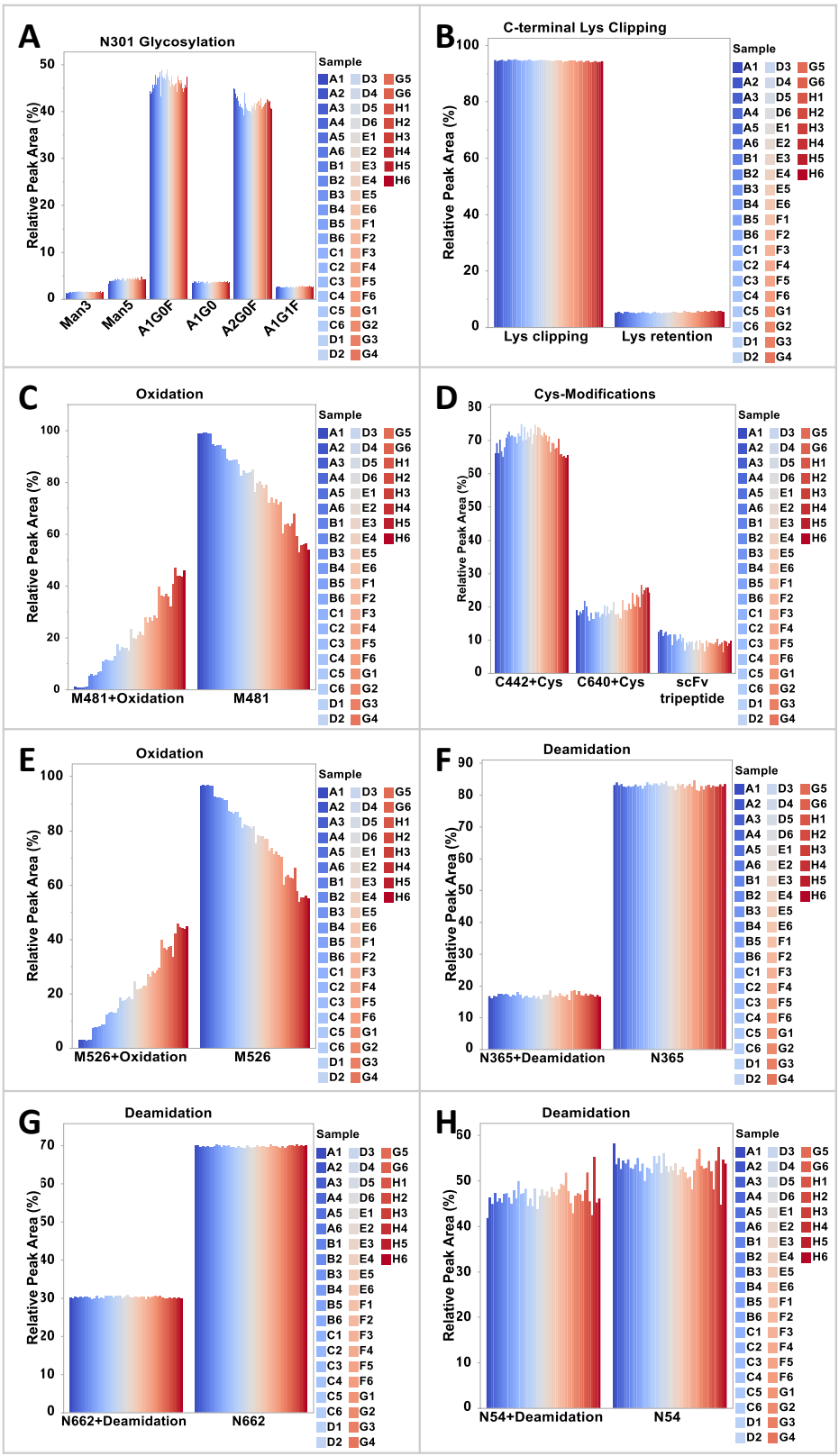

Figure 5.14 Assessment of the overtime sample stability across 48 injections.
Bar chart representing the overtime variation of the BsAb-1 PTMs relative peak area such as A) glycosylation; B) C-terminal Lys processing; C) and E) oxidation; D) Cys-modifications; F, G and H) deamidation. The sample name was reported and colour-coded varying from blue to red shades as a function of injection time.

5.3.4.2 *Day-to-day Reproducibility*

Day-to-day reproducibility was assessed over 6 replicates of BsAb-1 RM prepared and analysed on two different days. A preliminary visualisation of the day-to-day variability was illustrated in Figure 5.15 depicting the average measurement of the BsAb-1 PTMs monitored each day. Because the lines are parallel and there is no crossing, we can conclude that there is no interaction between the measurements taken on the two different days. Interestingly, it was observed that the standard deviations of the PTMs with high-intensity MS signals were greater than the low-intensity peptides (Figure 11.10) meaning that larger MS signal intensity resulted in higher measurement inconsistency. Variability gauge analysis identified site-specific PTM as the main experimental factor contributing to inconsistency in the data whereas the variability resulting from the day of the analysis was minimal (Figure 5.16). This was not surprising since the BsAb-1 PTMs vary from type to type. A random-effect model was fit to understand if the day of the analysis could significantly explain the variability in the data. Fitting a random effect model proved that the contribution of the day-to-day variability was not significant.

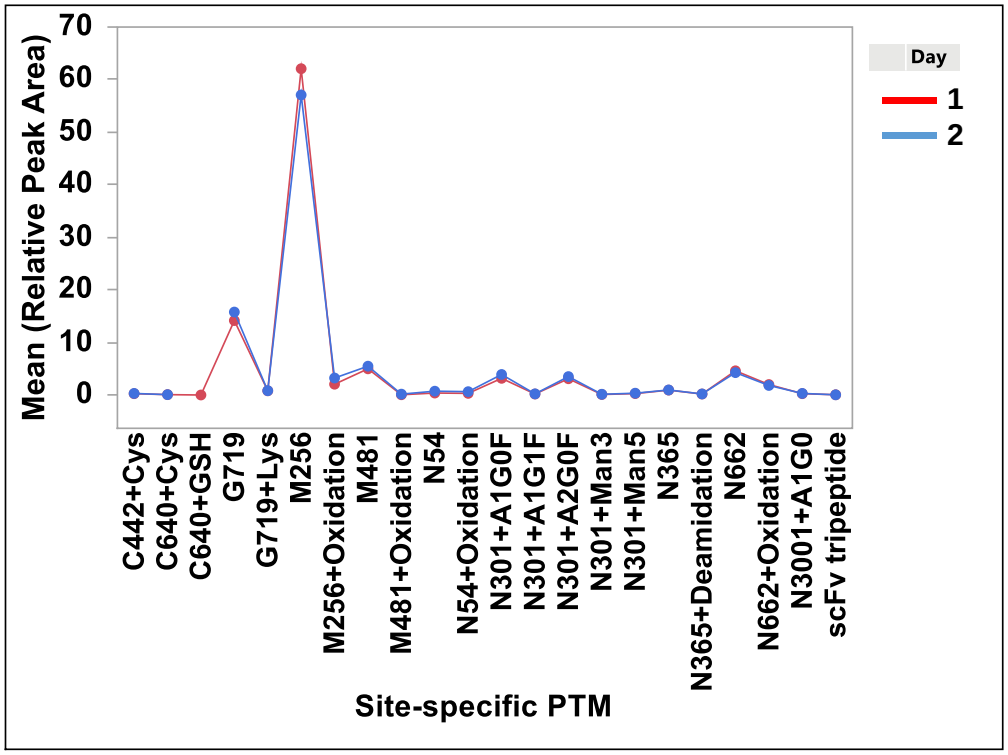

Figure 5.15 Day-to-day reproducibility parallelism plot.
Visual representation of day-to-day variability given by the mean PTMs relative peak area across 6 replicate measurements prepared and analysed on day 1 (red) and day 2 (blue).

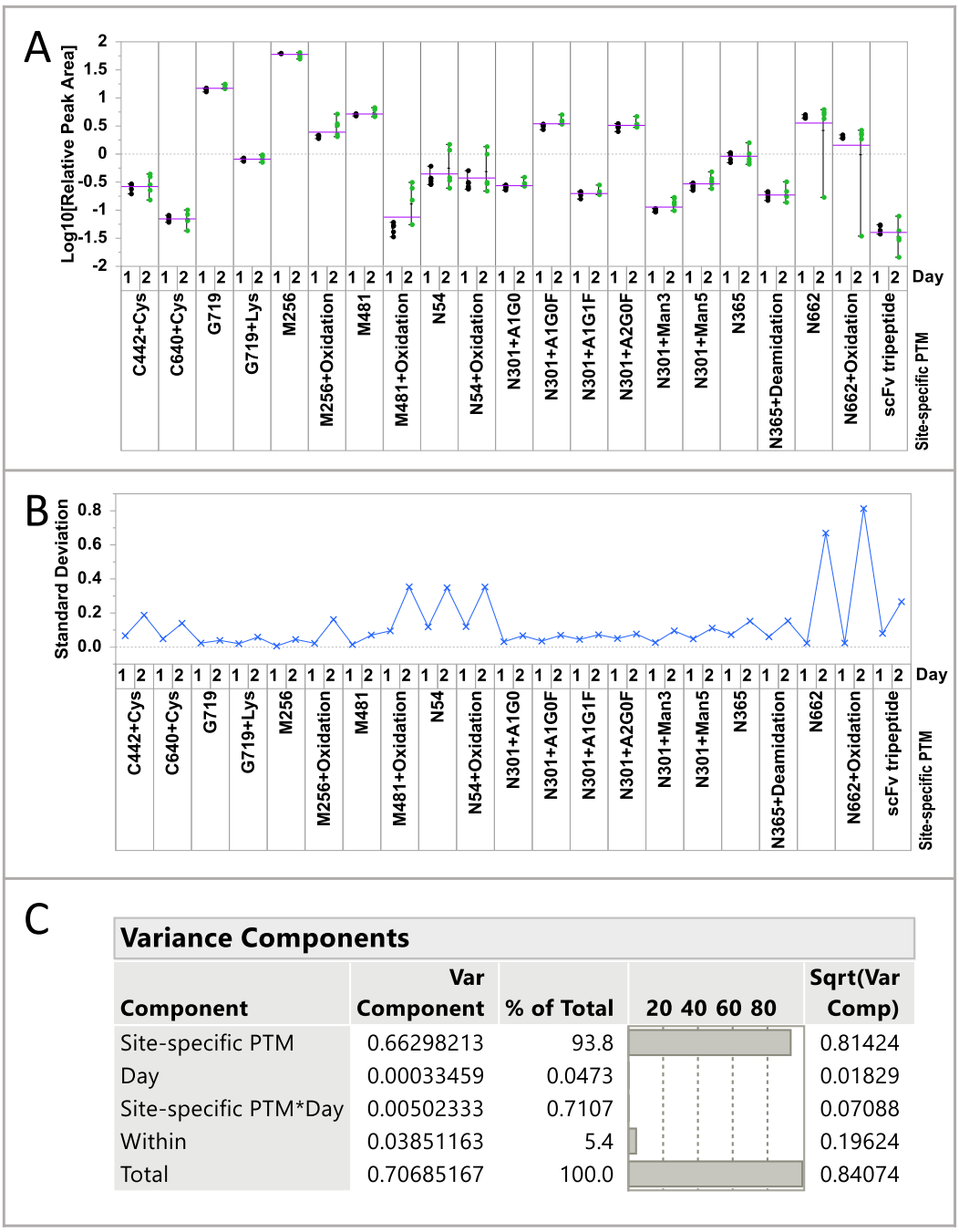

Figure 5.16 Variability gauge charts of day-to-day reproducibility.

A) Variability chart and B) standard deviation chart of the Log_{10} PTMs relative peak area plotted for the 6 replicates prepared and analysed on day 1 and day 2. C) Variance components table summarising the contributions that the experimental factors (days and site-specific PTM) make to the overall variability in the data.

Table 5.2 Random effect model report.

Source	FDR LogWorth	FDR PValue
Site	15.114	0.00000
Day	0.653	0.22248

Model Summary of Fit	
RSquare	0.950482
RSquare Adj	0.945506
Root Mean Square Error	0.19627
Mean of Response	-0.1343
Observations (or Sum Wgts)	231

Random Effect	Var Ratio	Var Component	Std Error	95% Lower	95% Upper	Wald pValue	Pct of Total
Day[Site-specific PTM]	0.129	0.005	0.004	-0.003	0.0126	0.198	11.471
Residual		0.038	0.004	0.032	0.048		88.529
Total		0.043	0.005	0.035	0.055		100.00

5.3.4.3 Method Suitability for the Analysis of in-Process Samples and Stability-Indicating Capability

During early-stage cell line development expression titres may be inconsistent as a result of the engineering strategies applied for process development and optimisation. Moreover, the sample matrix may be different based on whether the molecule is analysed in the host cell culture fluid (HCCF), purification or formulation buffers. The composition of HCCF is highly complex and varies due to the different media and feed compositions chosen for the cell culture. Typical purification buffers for mAbs and BsAb-1 are glycine HCl and sodium acetate with a pH range of 2.5-3.6. Formulations are generally composed of a buffer component such as acetate, histidine, or phosphate that keep the pH between 5.0 and 7.4, together with other excipients such as salts, surfactants, amino acids and antioxidants. The matrix components can affect the performance of analytical methods, hence their suitability to analyse samples with various matrices must be assessed. To evaluate the MAM method suitability for application for the analysis of in-process samples, BsAb-1 was analysed directly from HCCF and purification buffer (glycine HCl, pH 2.6) (post pA $C_{(high)}$) without buffer-exchange and compared with the RM. All the samples were analysed in 6 replicates and the concentration was normalised to 1 mg/mL before sample preparation. To evaluate the suitability of the method to analyse low concentrated samples, the post-pA $C_{(high)}$ sample was diluted to 0.2 mg/mL (post pA $C_{(high)}$) before sample preparation. Moreover, to assess the stability-indicating capability of the method, a sample of BsAb-1 was stressed at 70 °C for 30 min and compared to the RM. The qualifier/quantifier ion ratio CV of the post pA

$C_{(high)}$ sample were > 20% due to low signal intensity. This confirmed that further optimisation must be carried out to apply the present method for the analysis of samples with concentrations < 1 mg/mL. Unglycosylation of Asn301and glutathionylation at Cys442 and Cys640 were not identified (CV > 20%). The scFv tripeptide was not detected in clarified media due to the increased background noise registered in the MS spectra of these samples. The other PTMs qualifier/quantifier ion ratio CVs were comparable amongst the sample groups.

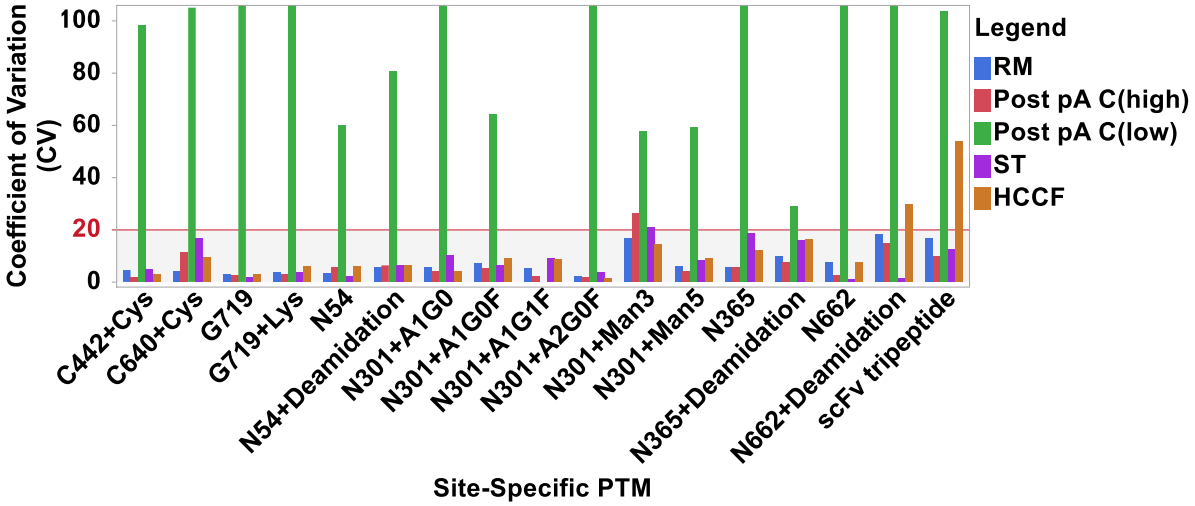

Figure 5.17 Qualifier/quantifier ion ratio CVs for the assessment of method suitability for the analysis of in-process samples and stability-indicating capability.
Bar chart depicting the qualifier/quantifier ion ratio CVs of each PTM monitored by MAM analysis of the BsAb-1 reference material (RM, blue), post-pA $C_{(high)}$ (red), post-pA $C_{(low)}$ (green), stressed material (ST, purple), and HCCF (orange).

Figure 5.18 displayed the relative quantitation of all the site-specific PTMs amongst the sample groups. An increased C-terminal Lys retention was observed in the HCCF ~28% in comparison to the ~5% detected in the other samples. Various levels of Cys modifications amongst the sample groups were quantified. Particularly, cysteinylation of Cys442 was higher in the stressed sample (79.3%) than in the post-pA $C_{(high)}$ and RM (71% and 71.4%, respectively). It is important to notice that cysteinylation of Cys442 was 75.4% in the HCCF but the relative quantitation didn't take into account the scFv tripeptide since this peptide was not detected due to an increase in background noise. The other PTMs were consistent amongst the sample groups.

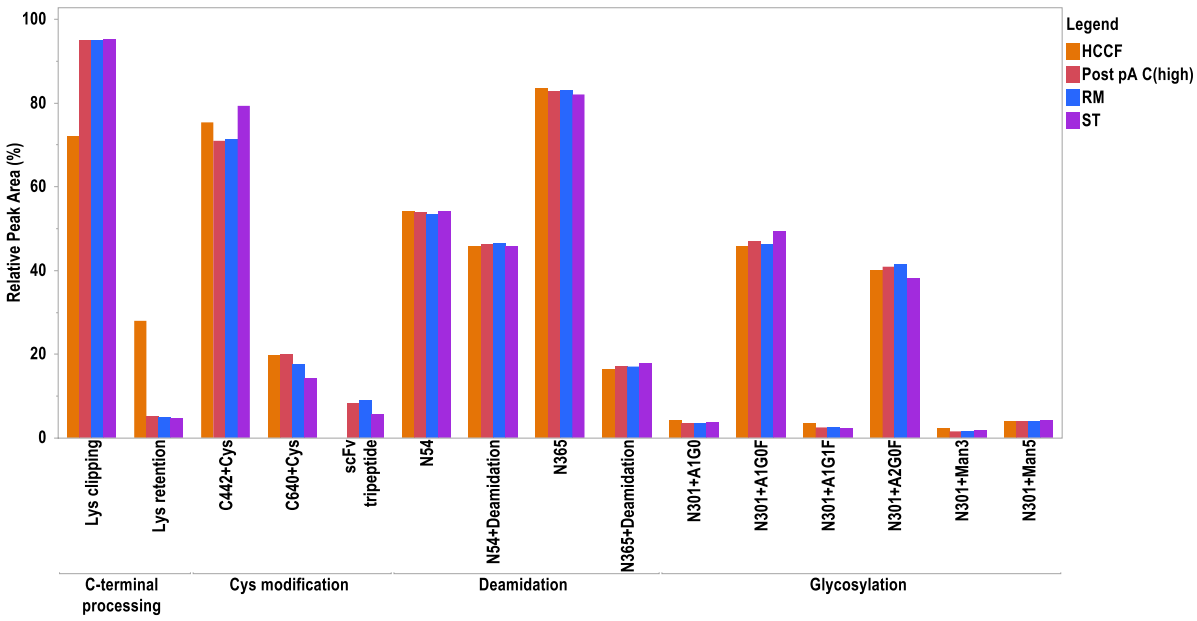

Figure 5.18 PTMs quantitation for the assessment of method suitability for the analysis of in-process samples and stability-indicating capability.

Bar chart illustrating the relative quantification of the site-specific modifications monitored by MAM analysis for the BsAb-1 reference material (RM, blue), post-pA $C_{(high)}$ (red), stressed material (ST, purple), and HCCF (orange). The % area of the modified peptide was plotted against the %area of the unmodified peptide.

The assessment of the analytical workflow was critical to verify the feasibility of the MAM method for the analysis of samples in purification buffer without the need for buffer exchange and highlighted that sample concentration and the increase in MS spectra background noise were limiting factors.

Table 5.3 MAM method assessment results

Parameter	Target Expectation	Qualification results
Comparability Study	The qualifier/quantifier ion ratio CVs of all the transitions monitored in the MAM must be <20% and comparable amongst the groups.	The CVs of the Automated front, middle and back groups were comparable to the manually prepared samples and <20% (Appendix C, Figure 11.8).
	ANOVA test of the automated sample groups showing no significant difference of the PTMs relative peak area amongst the groups.	No significant difference (Appendix C, Figure 11.9; Table 11.1).
	T-test of the manual and automated sample preparation groups showing no significant difference in the PTMs relative peak area between the groups.	No significant difference (Appendix C, Table 11.2).
Precision	The CV of the PTMs quantitation amongst the replicate measurements must be < 20%	PTMs quantitation amongst the sample replicates was <20% except for the oxidation at M481 and M256 (Appendix C, Table 11.3).
Overtime sample stability	The variation of the relative peak area of each PTM monitored within the repeated measurement must have CV < 20%.	All PTMs relative peak areas CV were < 20% except for oxidation at M481 and M256 (Appendix C, Table 11.6).
Day-to-day Reproducibility	The contribution of the day of the analysis on the data variability must be < 10% and not significant (p-value >0.05).	Day variance component = 0.05% and p-value = 0.222 (Figure 5.16, Table 5.2).
Suitability for in-process samples	Quantifier/qualifier ion ratio CV<20%.	Suitable for the analysis of samples in purification and formulation buffers with a concentration of 1 mg/mL
Stability-indicating	Discriminating variation of the PTM profile of stressed samples compared to RM.	The method can discriminate variations of the PTM profile (see Sections 5.3.4.3, 5.3.2.1)

5.4 Conclusions

The success of BsAbs as future medicines for the treatment of cancer requires more efficient analytical methodologies to both drive product development strategies and speed their market access. MAM methods stand out as analytical tools in HTPD for their capability of providing multiple product quality information at the molecular level increasing data and product understanding gathered in a single analysis (Carillo, Sche, et al. 2021). However, current MAM approaches based on targeted LC-MS/MS analysis do not provide information on protein aggregation. This work demonstrated the development of a MAM method based on MRM analysis of non-reduced tryptic peptides to support PQAs analysis of a BsAb candidate, BsAb-1, during its development life cycle. The method was designed to monitor the Cys modifications, glycosylation, deamidation and C-terminal Lys clipping and proved the possibility of quantifying the %HMWS impurities based on BsAb-1 Cys modifications. The choice of the PQAs to monitor and the use of Cys modified peptides to quantitate protein aggregation was achieved based on previous product knowledge gathered from a thorough characterisation analysis. Hence, this method is an example of analytical tools dedicated to addressing the development challenges of a specific drug candidate. The method was designed and validated to support the analysis of 48 samples deriving from cell cultures and trend multiple product quality attributes of the candidate BsAb-1 throughout the cell line development process. This proof-of-concept work demonstrated that MRM analysis of Cys modified peptides can be used to quantify protein aggregation and highlighted the importance of using chemometrics and machine learning to extrapolate meaningful analytical information. The MAM method proved to maximise the product quality information gathered with minimal sample amount, time and orthogonal analytical testing required to support product development.

This page was intentionally left blank

Chapter 6

Hyphenation of the high-throughput analytical platform to cell engineering

6.1 Abstract

High-throughput screening (HTS) approaches are adopted to provide important information for cell line development (CLD). HTS is resource-efficient since it enables the investigation of a wide range of experimental conditions with little sample and time required. However, there are a number of challenges to developing and implementing analytical tools for supporting HTS experiments such as the limited amount of material available for analysis, the large number of samples and the rapid timelines. For these reasons, analytical testing is often postponed to later development stages. This research aimed to bring product quality (PQ) analysis to the fore of CLD and drive clone selection in early-stage process development. In the previous chapters of this thesis, I presented the development of a HT analytical platform involving automated small scale methods for the purification and PQ analysis of therapeutic proteins expressed in small scale cell culture systems. Here the application of the HT analytical workflows to three case studies was demonstrated. In the first case study, little process knowledge is known and the application of the PhyTip-purification/HT SEC workflow to a 96-deep-well shake plate overgrows (SPOG) screen is described. The second case study concerns CLD activities for a molecule of which the product quality attributes (PQAs) were previously characterised. PhyTip-purification/HT SEC/MAM analysis was integrated into 10 mL cell culture bioreactors to understand how CHO cells media supplementation may impact PQ. Finally, the third study describes the application of the PhyTip-purification/2D SEC-CEX-UV workflow to monitor size and charge variants of a mAb to drive clone selection during both 24-deep well plates (DWPs) and 10 mL cell culture screening experiments. Further considerations on how HT analytical workflows can be implemented in early process development to support clone selection are also discussed.

6.2 Introduction

The increasing demand for novel biopharmaceuticals such as monoclonal antibodies (mAbs) and other engineered antibodies has pushed the focus to cost-efficient and fast-turnaround strategies for process development (Qian et al., 2020; Lanter et al., 2020; Petroff et al., 2016). In this regard, high-throughput process development (HTPD) tools such as high-throughput screening (HTS) methods have enabled major scientific breakthroughs in biopharmaceutical process development (Silva, Eppink, and Ottens, 2021). Scale-down bioreactor platforms such as ambr® systems and shaken DWPs have increasingly been implemented in upstream HTPD and demonstrated to significantly shorten development timelines (Manahan et al., 2019). Analytical testing is a key driver of biopharmaceuticals development since chemical and enzymatic modifications of therapeutic proteins pose a risk for drug safety and efficacy and must therefore be monitored throughout a product lifetime. However, the implementation of protein characterisation analysis has been limited by analytical bottlenecks due to the large number of samples and the limited amount of material generated in small-scale cell cultures.

The focus of this research work was the development of HT analytics to drive cell engineering strategies during early-stage biopharmaceuticals development. This chapter demonstrates the application of the analytics described in Chapters 3-5 to case study samples in support of CLD research work conducted at AstraZeneca and the University of Sheffield.

6.3 Results and Discussions

6.3.1 Application of the PhyTip-purification/HT SEC workflow to 96-DWPs CHO cell cultures

A research study conducted in AstraZeneca was aimed to adapt conventional fed-batch CLD screens to the Next-Generation Manufacturing (NGM) platform through mimicking perfusion culture and incorporating adaptive feeding. The study involved the use of a CAT-S host cell line, and a hydrogen peroxide adapted CHO-K1 derived cell line (H_2O_2 host). Both cell line transfectants produced BsAb-1, a difficult-to-express (DTE) bispecific antibody. A HT shake plate overgrows (SPOG) screen was set up to compare the performance of the CHO CAT-S and H_2O_2 host clones when cultured both in standard fed-batch and in presence of a perfusion component. The SPOG screen involved 384 clones cultured in duplicate (768 cultures in total) in 350 μL within shaken 96-DWPs. Cell culture operations for inoculum in 96-DWPs, feed supplementation, media exchange, and sampling were automated on a robotic liquid handler. All the cultures were sampled for measurements of glucose and lactate concentration, titre, viable cell density (VCD), and viability. On day 11, the expression titre range of the cell cultures was 7.64 – 1372.3 mg/L with a mean titre value of 390.46 mg/L and mode of 117.1 mg/L, corresponding to ~78 μg average and ~23 μg mode of product in 200 μL of host cell culture fluid (HCCF) available for analysis. Relevant clones were selected for aggregation analysis and the HCCF containing the secreted BsAb-1 were harvested and transferred in 4 cleaned 96-DWPs. Subsequently, the volume of the sample was adjusted to 300 μL by adding 100 μL of media to each well to prevent the entrance of air during the purification process. Finally, all the 96-DWP were processed by PhyTip-purification/HT SEC in series. Figure 6.1 illustrates a schematic of the PhyTip-purification/HT SEC workflow from start to data analysis. Further details on the analytical methods used were reported in Chapter 3, Part A.

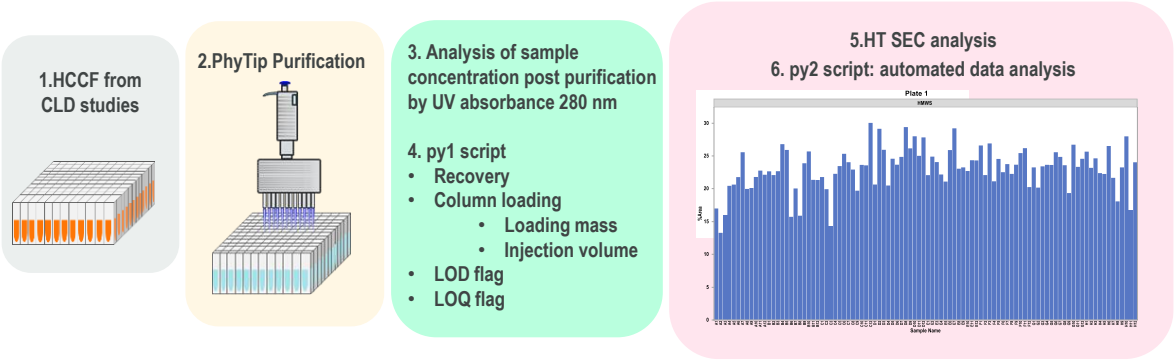

Figure 6.1 Schematics of the PhyTip-purification/HT SEC workflow

1) A volume of 300 µL of HCCF containing the expressed molecule is harvested and placed in a cleaned 96-DWP. 2) The 96-DWP is purified by PhyTip purification, consisting of the capturing of the targeted molecule from the HCCF, washing of impurities that may be bound to the PhyTip resin, and final elution of 160 µL of the molecule of interest with high concentration. 3) The sample concentration post purification is measured by absorbance at 280 nm and the py1 script is run for monitoring of sample recovery, calculating the injection volume required for consistent column loading during the analysis and flagging the sample with concentration below the method LOD and LOQ. 5) Subsequently, the samples are analysed by HT SEC. 6) Finally, the py2 script is run for data analysis and reporting.

Firstly, PhyTip purification was performed to purify the BsAb-1 from the HCCF and generate sufficient material for aggregation analysis. The PhyTip purification method was integrated with a custom Python script (py1) that was written to automate the calculation of the %R to monitor the purification performance throughout the process, adjust the injection volume to obtain a consistent column loading of 5 µg, and flag the samples with concentration below the method LOD and LOQ. The py1 script introduced a process control element for monitoring and feeding back PQ data analysis. Table 12.1 in Appendix D shows an example of the py1 script output table.

Following PhyTip purification, the 96-DWP was loaded into an LC system autosampler for HT SEC analysis. A blank injection, SST and a control sample were added at the start and end of each 96-DWP analysis sequence to check the system performance during the HT SEC analysis. Therefore, each 96-DWP HT SEC run counted a total of 102 samples resulting in sub-6 hours of analysis time per plate. Processing one 96-DWP by PhyTip purification took ~8 hours in total, thus, 384 samples were processed within 32 hours. The sensitivity of the HT SEC method enabled the quantitation of aggregates using < 5 µg of product. Therefore, PQ information was obtained for samples with expression titres < 200 mg/L and culture volume ~200 µL. Around 100 µL were left for each sample post-SEC analysis which could

potentially be utilised for further analytical testing. Likewise, the cell pellet and the post-PhyTip purification unbound fraction of the HCCF could be used for further analysis.

HT SEC data analysis and final report generation involved various steps. Firstly, preliminary data investigation consisted of the visualisation and interpretation of each chromatogram. This functioned as the basis to build a custom peak table report for each sample in OpenLab Intelligent Reporting. This script is integrated with a Python-JMP combined script (py2) for the final data analysis, visualisation, and reporting. This involved the calculation of the proportion of the total fraction of HMWS to the total species detected in a chromatogram, expressed as a percentage (%HMWS). The data were finally visualised in a bar chart displaying the %HMWS peak against the sample name, which in this specific case, corresponded to the 96-DWP position. Automation of the data analysis workflow allowed the processing of 384 samples of data in a single click. Figure 6.2. shows the results of the PhyTip purification/HT SEC workflow applied for the processing of the shake-plate overgrowth (SPOG) screen.

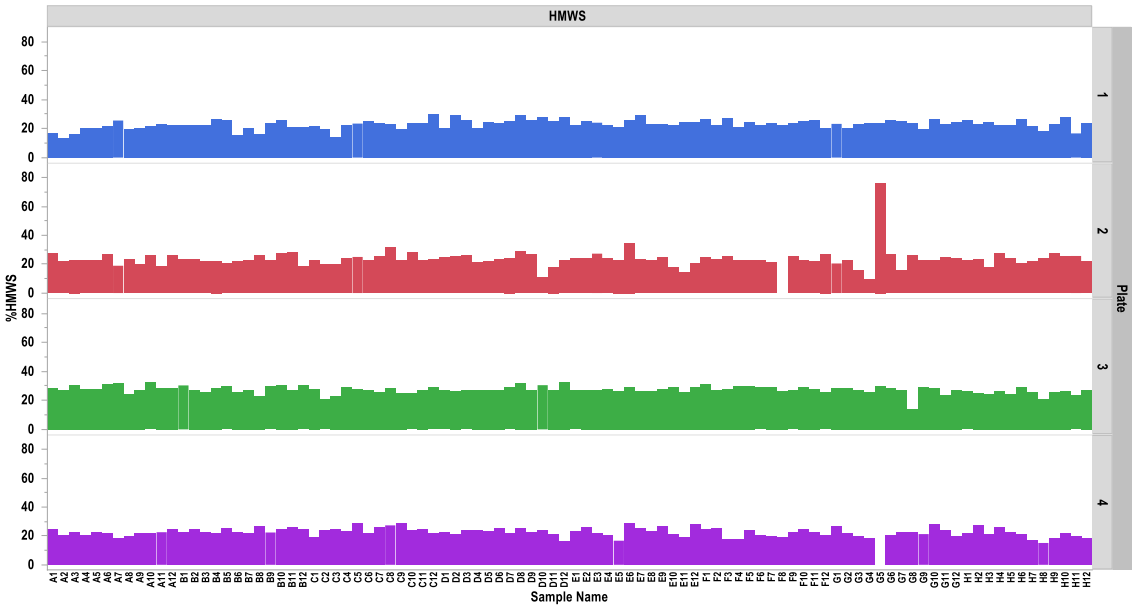

Figure 6.2 Visual representation of the %HMWS in each 96-DWP analysed during the SPOG screen.

The bar chart displays the %HMWS impurities present in 96-DWP analysed in the SPOG screen. The %HMWS range of plate 1 (blue) varied from 13.3% to 30%, with mean and median values of 23%; The %HMWS range of plate 2 (red) varied from 9.3% to 76%, with mean and median values of 23.4 and 22.9, respectively%. The concentration of sample F8 was below the method LOD, thus no data were acquired. The %HMWS range of plate 3 (green) varied from 14.2% to 32.7%, with mean and median values of 27.4 and 27.3, respectively. The %HMWS range of plate 4 (purple) varied from 15.2% to 29.1%, with mean and median values of 22.6 and 22.4, respectively. The concentration of sample G5 was below the method LOD, thus no data were acquired.

The results from this HT study show that the average BsAb-1 HMWS levels of the CAT-S and H_2O_2 clones were 23.2 ±3.3 % and 22.8± 3.7 %, respectively, demonstrating that the average aggregation levels of the expressed protein remained consistent between the two cell lines. Interestingly, the two cell lines seemed to perform differently in response to the introduction of a perfusion component. The %HMWS of BsAb-1 expressed in the CAT-S clones was significantly ($p<0.001$) higher, 26.9 ± 2.8 % average, when cultured in the presence of a perfusion component, whilst the H_2O_2 clones were 22.2 ± 2.9 % average. Indeed, whilst the levels of aggregation significantly dropped for the CAT-S cell line as a consequence of the introduction of the perfusion component, those expressed by the H_2O_2 host remained unvaried. Furthermore, when all clones were ranked on aggregation in both the fed-batch and perfusion conditions, no significant correlation was found between the rankings (data not shown as proprietary of AstraZeneca). These data suggested that the H_2O_2 host was overall a better expression system than the CAT-S host, however, the aggregation level of BsAb-1 were not substantially influenced by the cell engineering strategy under

investigation. Therefore, different cell engineering approaches will have to be investigated to alleviate aggregation in this BsAb model.

This study demonstrated the application of the PhyTip purification/HT SEC workflow as a ranking tool for clone selection providing quantitative analysis of protein aggregation in a time and resource-efficient fashion. The processing of 384 cultures was accomplished within 32 hours with minimal sample consumption (< 5 μg of protein per sample). One caveat of the HT SEC method is the low resolution of the size variants. Indeed, aggregates of different sizes cannot the observed, thus it was impossible to discriminate how heterogeneous the HMWS expressed by the clones were, namely dimers, trimers or different sized species were not separated. Moreover, the poor resolution also hampered the method accuracy in quantifying the HMWS since the main product and HMWS peaks are not baseline resolved so accurate peak integration is impeded. Therefore, absolute quantification of the HMWS expressed from each clone could not be achieved nor could the %HMWS be compared with those obtained by benchmark SEC methods used in quality control (QC).

Nevertheless, this study proved that the HT SEC method was fit for use as a ranking tool for supporting HTS experiments during early-stage cell line development providing relative quantitation analysis of BsAb-1 HMWS with remarkable analysis throughput. Together with tire data, HT SEC analysis helped to improve understanding and will drive future research strategies for the development of cell lines for BsAbs.

6.3.2 Application of the PhyTip purification/HT SEC/MAM workflow to understand the effect of small molecule-enriched media on the product quality of CHO-expressed bispecific antibodies

Cell engineering research conducted in AstraZeneca investigated the use of a group of small-molecule compounds added to the cell culture feeds to reduce intracellular aggregation of CHO-expressed BsAbs. A 14-day fed-batch overgrowth was set up in 10 mL cultiflasks to screen 18 conditions involving the addition of the small-molecule drugs to the CHO feeds individually and in combinations. A control sample (CLD Control) was also added corresponding to a cell line expressing BsAb-1 transfected with the same vector as all the other cultures but cultured in AstraZeneca proprietary standard media and feed composition. Each condition was repeated in triplicate, resulting in a total of 57 cultures. Glucose and lactate concentration, VCD, and viability were monitored throughout the overgrowth. On days 7, 9, 11, and 14 the cultures were sampled for titre analysis whilst PQ analysis was carried out for the day 9 and 14 samples.

The expression titre ranges were 730 – 1500 mg/L and 1100 – 3400 mg/L on days 9 and 14, respectively. The HCCF was harvested and clarified by centrifugation and 1 mL of the total volume was loaded into a 96-DWP for PhyTip purification. A sample of BsAb-1 reference material (RM) was diluted to 2 mg/mL into cell culture media, spiked into the purification plate and used as a control throughout the purification process (Purification Control). The py1 script was run to evaluate the purification performance and adjust the injection volume for each sample before analysis as described above (6.3.1).

The purified plate was then loaded into the LC system for HT SEC analysis. As previously described, blank, SST and control samples (HTSEC Control) were included in the analysis sequence to check the system performance during data acquisition. Data analysis was performed as described earlier (6.3.1). The same procedure was carried out for the samples harvested on day 14 and all the levels of HMWS resulting from each condition were reported in Figure 6.3.

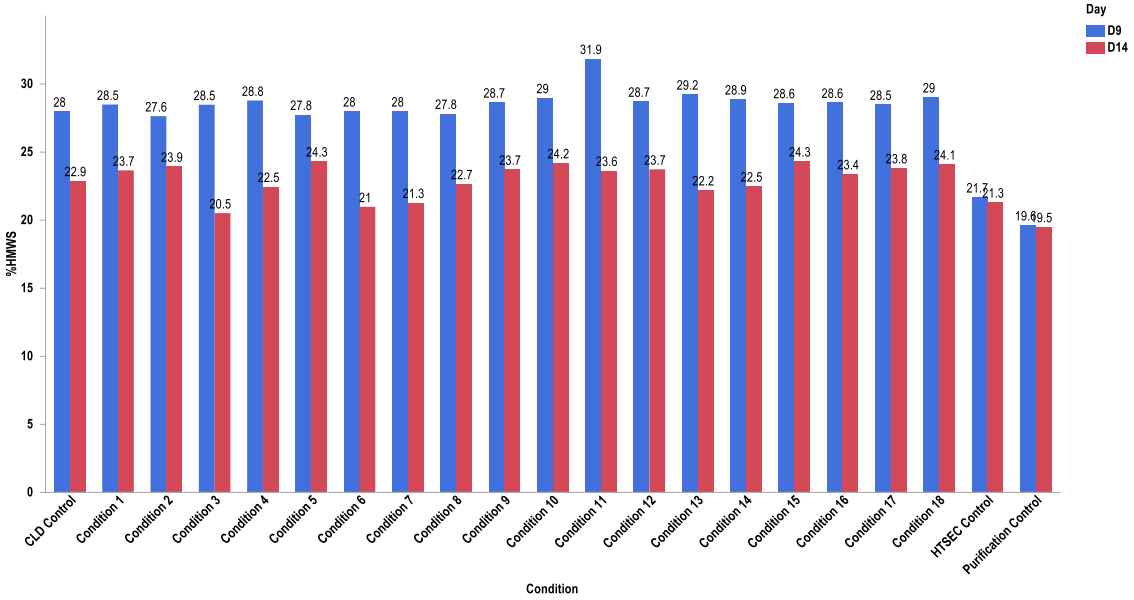

Figure 6.3 Effect of the cell culture conditions under investigation on the %HMWS impurities analysed in samples harvested on day 9 and day 14 of the overgrowth.
Bar chart displaying the mean and standard deviation of the %HMWS analysed across three biological replicates for all the cell culture conditions tested. All the cell engineering conditions were numbered from 1 to 18 and the %area of the HMWS impurities detected on day 9 (blue) and day 14 (red) were reported for each of them.

The results show that the levels of HMWS analysed on day 9 varied from 27% to 36% amongst the experimental conditions. Interestingly, on day 14 the %HMWS dropped to 20-25% in all the cell culture conditions including the CLD Control. T-test analysis confirmed that the drop in HMWS between day 9 and day 14 was significant (p-value <0.05) (Appendix D, Figure 12.1). ANOVA demonstrated that on day 9 the %HMWS was comparable amongst the experimental conditions (Appendix D, Figure 12.2) whilst on day 14 significant differences were observed with conditions 3, 4, 6 and 7 showing %HMWS below the average (~21% *vs.* ~23.5% average) (Appendix D, Figure 12.3). The findings from HT SEC analysis suggested that variations in the levels of HMWS were mostly observed over the cell culture time rather than as a direct consequence of the small-molecule drugs spiked into the media.

For a more in-depth understanding of the impact of the cell culture conditions on the PQ profile, further analytical testing by MS was carried out. The 96-DWPs were buffer exchanged in AstraZeneca proprietary platform formulation buffer and successively analysed by the multi-attribute method (MAM) developed as described in Chapter 5.

The MAM method provided a targeted approach for the assessment of BsAb-1 aggregation based on Cys modifications and simultaneous monitoring of product quality attributes (PQAs) such as glycosylation, deamidation, and C-terminal Lys processing. The PQAs and their amino acid sites were previously identified by peptide mapping analysis as reported in Chapter 5, Section 5.3.1. After data acquisition, an automated data analysis workflow was implemented to ease the processing of a large number of samples. The data analysis workflow involved a first data screen by Skyline MS software for the visualisation of the samples TIC and the generation of a custom peak table. Successively, the Skyline peak table was imported in a Python-JMP integrated script (py3) calculating 1) the peptides quantifier/qualifier ion ratio CVs for each sample replicate against the MAM control sample and 2) the relative peak area of the modified peptides *vs.* the respective unmodified peptides. Finally, the data were visualised in a bar chart reporting the replicates mean and standard deviation of the relative peak area of the modified peptides *vs.* the respective unmodified peptides across all the experimental conditions. The data shown in Figure 6.4-Figure 6.7 show the data of the BsAb-1 PQA monitored by MAM on both days 9 and 14, namely C-terminal Lys processing, deamidation, glycosylation and Cys modifications.

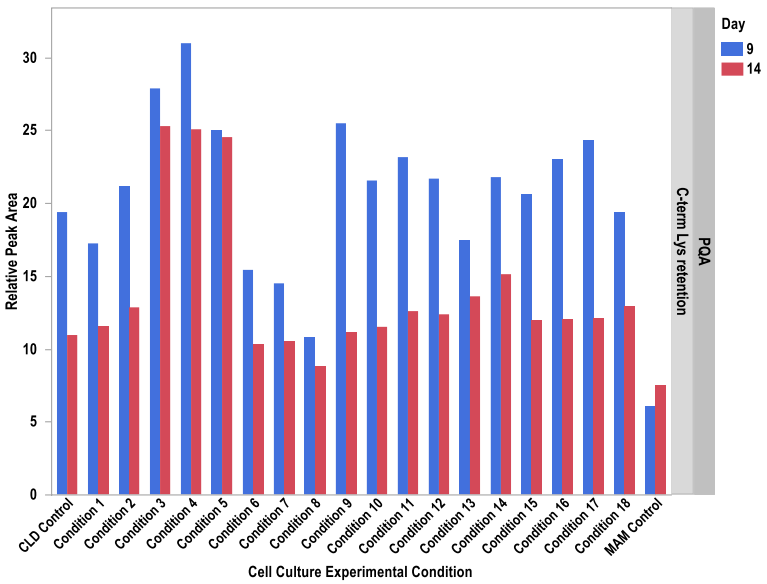

Figure 6.4 Effect of the cell culture experimental conditions on BsAb-1 C-terminal retention on days 9 and 14 of the overgrow analysed by MAM.
Bar chart displaying the % C-terminal Lys retention for the 18 experimental conditions tested on day 9 (blue) and day 14 (red) including the CLD Control and MAM Control samples.

C-terminal Lys processing exhibited a similar trend on days 9 and 14 and the %Lys retention was significantly different amongst the 18 conditions (Appendix D, Figure 12.4 and Figure 12.5, respectively). On day 9, the lowest %Lys retention was reported in condition 8 (10.8%) followed by conditions 6 and 7 (15.4% and 14.5%, respectively) whilst conditions 3, 4, and 5 showed the highest values (27.9%, 31%, and 25%, respectively. The level of C-terminal Lys retention dropped significantly from day 9 to day 14 with average values falling from ~20% to ~13.5%, respectively (Appendix D, Figure 12.6). Conditions 6, 7 and 8 remained the ones with the lowest (10.5%, 10.3%, and 8.8%, respectively) and conditions 3, 4, and 5 with the highest values of %Lys retention (25.3%, 25.1% and 24.6%, respectively).

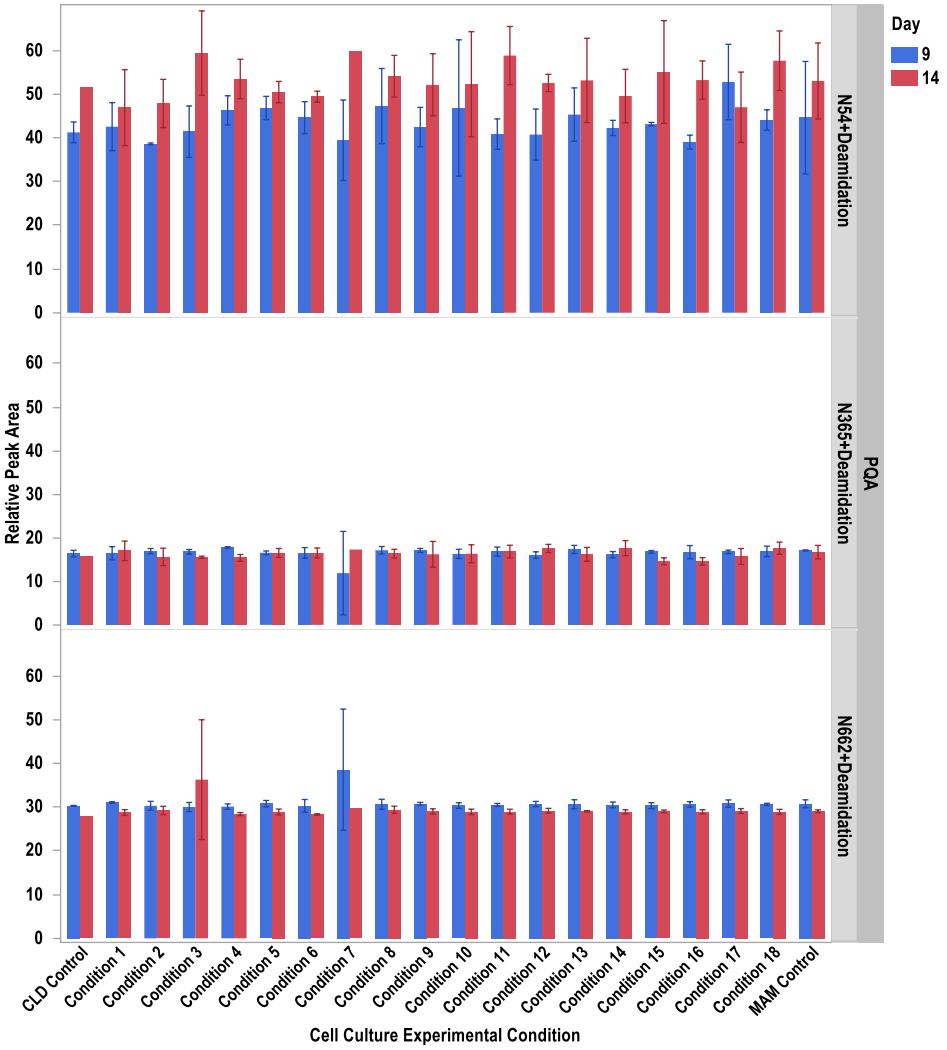

Figure 6.5 Effect of the cell culture experimental conditions on BsAb-1 deamidation on days 9 and 14 of the overgrow analysed by MAM.

Bar chart displaying the % peak area of the peptide bearing deamidation of Asn54 (top), Asn365 (middle) and Asn662 (bottom) across the 18 experimental conditions tested on day 9 (blue) and 14 (red) including the CLD Control and MAM Control samples.

No significant difference in deamidation of Asn54, Asn365 and Asn662 residues was observed as a consequence of the experimental conditions studied herein (Appendix D Figure 12.11, Figure 12.12 Figure 12.14, Figure 12.15, Figure 12.17, and Figure 12.18, respectively). However, a significant overall increase in Asn54 deamidation was observed over time from day 9 to day 14 (Appendix D, Figure 12.13) whilst deamidation in Asn662 decreased (Appendix D, Figure 12.19). Conversely, deamidation in Asn365 was comparable on both days although the spread of the data on day 14 was significantly higher than on day 9 (Appendix D, Figure 12.16).

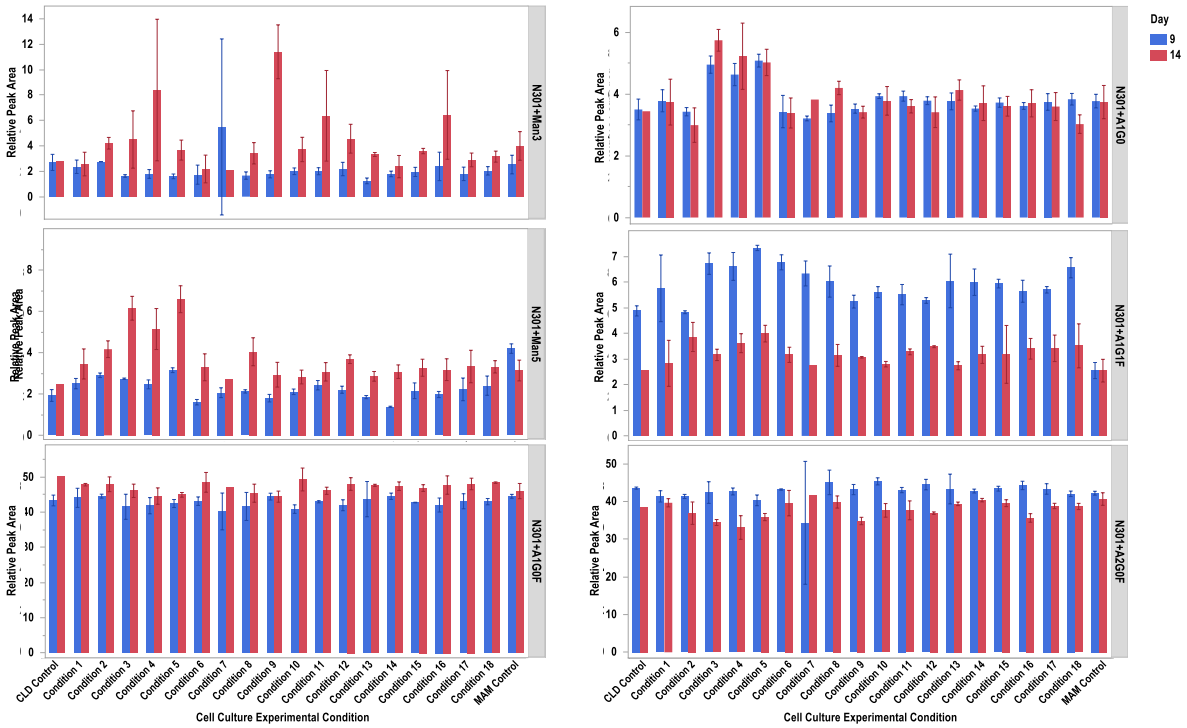

Figure 6.6 Effect of the cell culture experimental conditions on BsAb-1 glycosylation on days 9 and 14 of the overgrow analysed by MAM.

Bar chart displaying the comparison of the %peak area of the Asn301glycoforms Man3, Man5, A1G0F, A1G0, A2G0F, and A1G1F across the 18 experimental conditions on day 9 (blue) and 14 (red) including the CLD Control and MAM Control samples.

As shown in Figure 6.6, on day 9, A1G0F (monoantennary) and A2G0F (biantennary) were the predominant glycoforms followed by A1G1F, A1G0, Man5 and Man3, respectively; and the trend was consistent across the 18 experimental conditions. On day 14, the monoantennary A1G0F was the main species across all the glycoforms followed by the biantennary species. Furthermore, the levels of A1G1F, A1G0, and Man5 remained constant across all the sample conditions whilst Man 3 was higher in conditions 9 and 16. This underlined a slight change in the glycosylation profile over time.

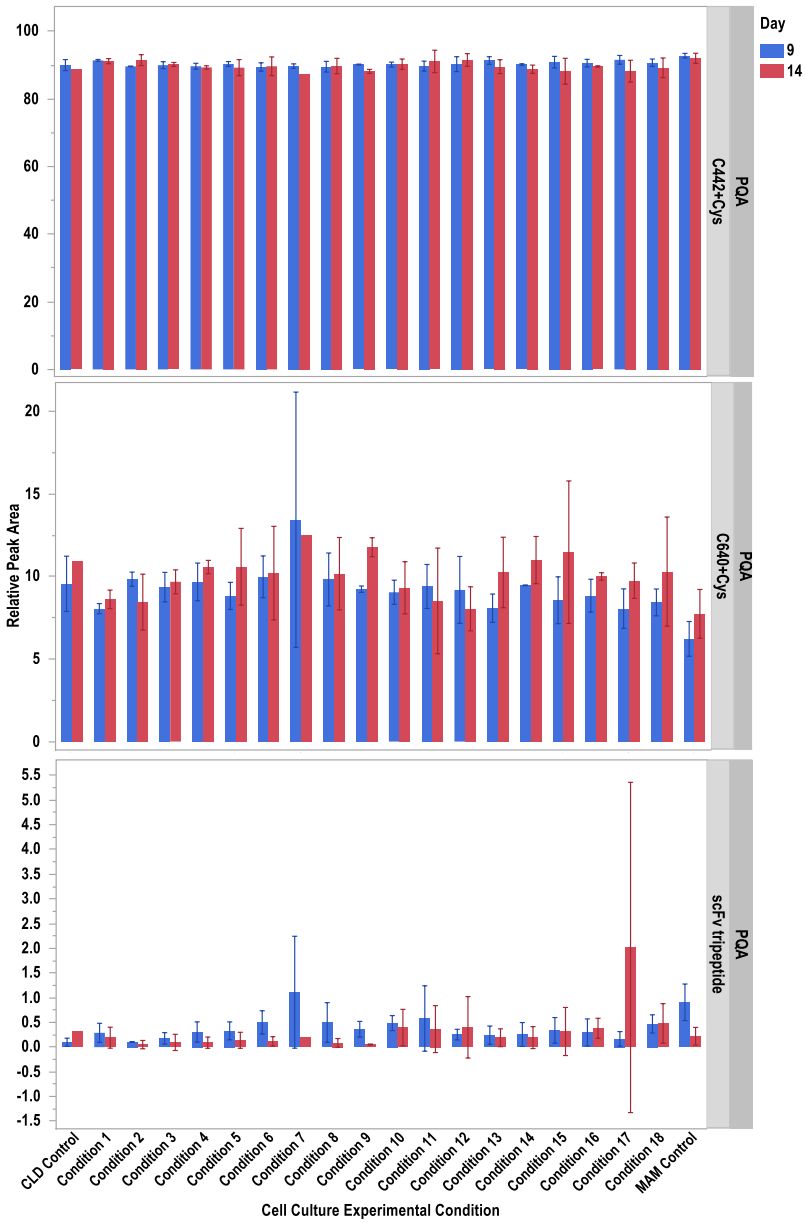

Figure 6.7 Effect of the cell culture experimental conditions on BsAb-1 Cys modifications on days 9 and 14 of the overgrow analysed by MAM.
Bar chart illustrating the % cysteinylation on Cys442 (blue), Cys640 (red) and the % unmodified scFv tripeptide (green) detected for the 18 experimental conditions tested including the CLD Control and MAM Control samples on day 9 (top) and 14 (bottom).

As depicted in Figure 6.7, the levels of Cys modifications remained consistent on both days across the 18 experimental conditions with average values of cysteinylation on Cys442 and Cys640 being ~90% and ~9%, respectively, whilst the %scFv tripeptide remained < 2%. As discussed in Chapter 5, Section 5.3.2.1 of this thesis, BsAb-1 Cys modifications were correlated to the amount of HMWS. Figure 6.8 showed the %HMWS estimated by the MAM model based on the Cys modifications targeted by multiple reaction monitoring (MRM). No

significant difference in the levels of HMWS was observed across the 18 experimental conditions (Appendix D, Figure 12.8 and Figure 12.8 for days 9 and 14, respectively) and between the two days (Appendix D, Figure 12.10). Figure 6.9 compared the quantitation data of the HMWS obtained by HT SEC and MAM. It is evident that the quantitation data were different between the two methods, however, no significant difference in the trend of %HMWS between the two methods was observed (Figure 6.9). Additionally, the HT SEC method was more precise than the MAM, as shown by the standard deviation of the replicate measurements. Unlike MAM, HT SEC analysis was able to detect small changes in the %HMWS. More detailed limitations of the MRM-based quantitation of HMWS were discussed in Chapter 5, Section 5.3.2.1.

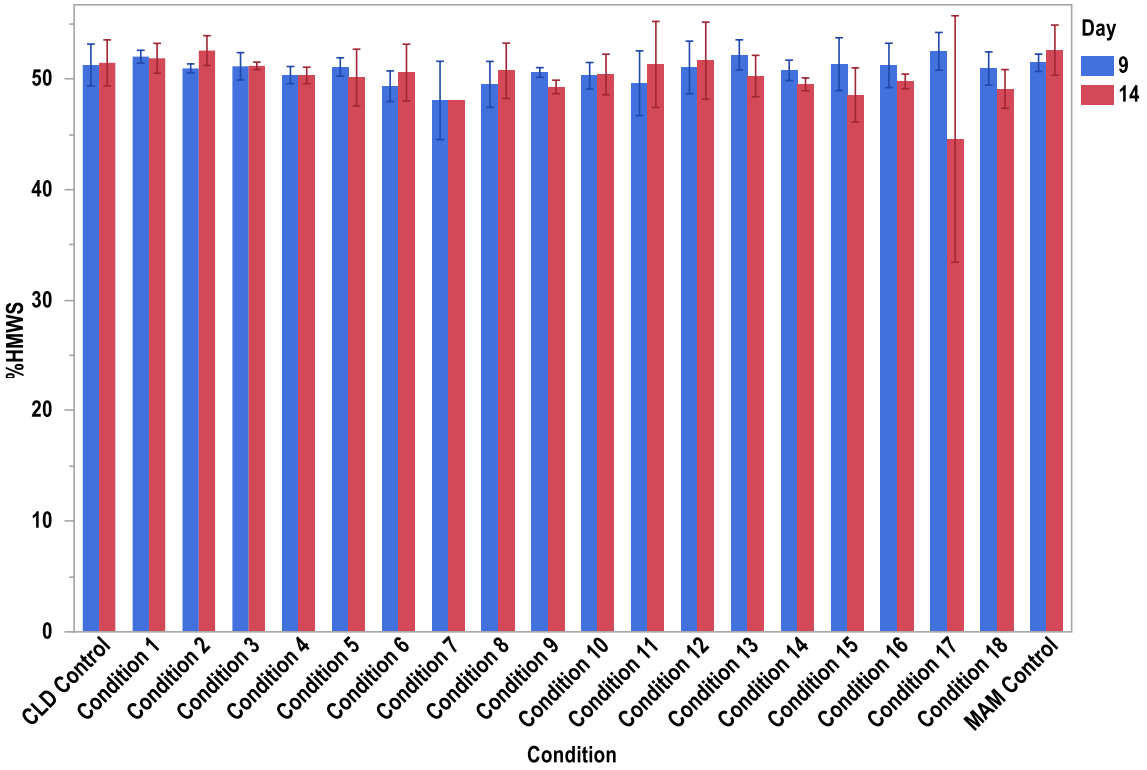

Figure 6.8 HMWS quantitation by MRM.
Bar chart displaying the %HMWS predicted by the MAM model based on the levels of Cys modifications measured by MRM across the 18 experimental conditions on day 9 (blue) and 14 (red).

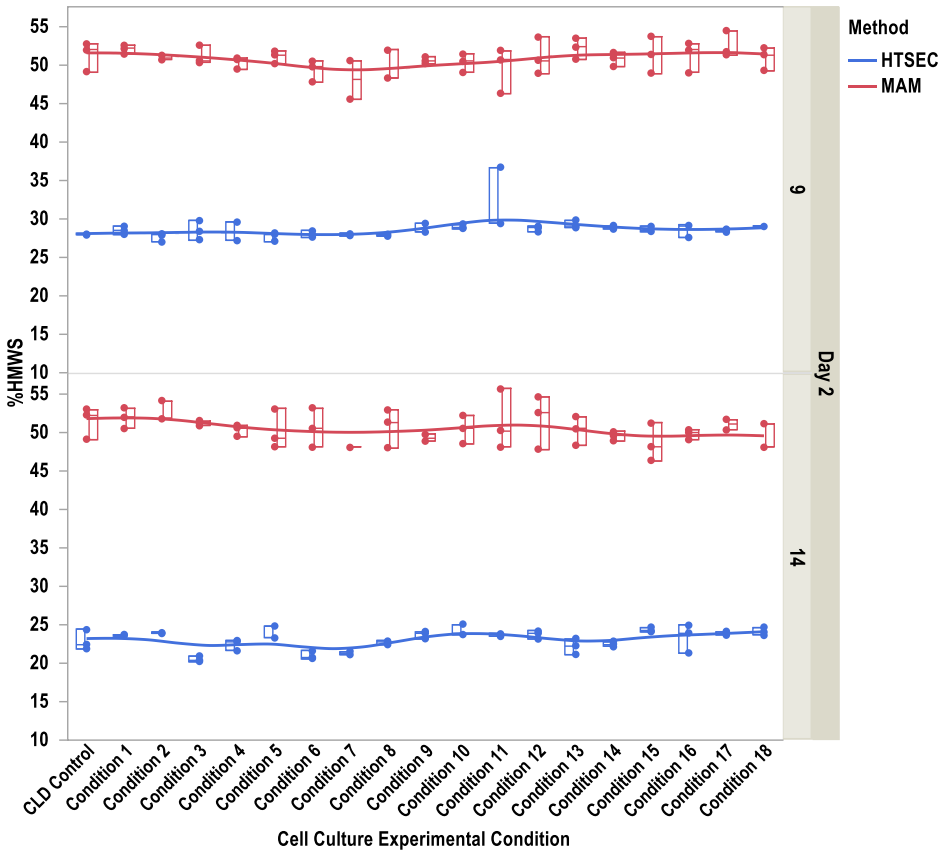

Figure 6.9 Comparison of the HMWS quantitation data analysed by MAM and HT SEC.

Comparison of the HT SEC (blue) and MAM (red) HMWS quantitation data of all the samples of the 18 cell culture experimental conditions analysed on day 9 (top) and day 14 (bottom) of the overgrowth. The smooth curve through data was depicted for each group of samples to visualise the trend across the data points. The variability across the measurement replicates was represented by a boxplot.

Overall, data from both HT SEC and MAM were able to detect small changes in BsAb-1 %HMWS amongst the samples. Most importantly, the PQ analysis by MAM demonstrated that the cell culture conditions under investigation did not significantly impact PQ, rather significant changes were observed over the culture time. C-terminal Lys processing was the most variable PQA with conditions 3, 4, and 5 reporting the highest and conditions 6, 7, and 8 the lowest values of Lys retention, both dropping significantly over time. Similarly, deamidation of Asn54 increased significantly from day 9 to day 14 whilst deamidation of Asn662 decreased. The glycosylation profile was also different between the two days although A1G0F and A2G0F remained the predominant species. An increase in Man3 was observed on day 14 for conditions 9 and 16. With respect to aggregation, HT SEC analysis reported a significant shift between days 9 and 14 which was not observed by MRM. This

was probably because the difference in %HMWS was too small to be detected by MRM. Nevertheless, the MAM analysis proposed a way to maximise the amount of information that can be obtained in one method whilst minimising the analysis time and sample that may be required if each of the BsAbs-1 PQAs were analysed by multiple analyses. The findings from PQ analysis suggested that the hypothesis of the cell culture strategy investigated herein was not confirmed whilst also providing new insights for future CLD experiments. The hyphenation of PQ analysis to early CLD activities diverted the engineering strategies before utilising resources on larger-scale experiments. This enabled a reduction in cost and time that would have been required if the hypothesis was taken forward due to the lack of PQ data.

6.3.3 Understanding the effect of targeted gene expression strategies on CHO-expressed mAbs product quality by the PhyTip-purification/2D SEC-CEX-UV analytical workflow

A research study carried out at the University of Sheffield investigated the use of targeted gene expression strategies in CHO cells for mAb production and their effect on titre and PQ. Firstly, 17 different experimental conditions involving the knockdown and overexpression of targeted genes were screened in triplicate in 24-DWP cell cultures. At the end of the fed-batch overgrow, the 24-DWPs were harvested and the HCCF was used for titre analysis by Protein A chromatography carried out in the department of Bioprocess Analytics at AstraZeneca, Cambridge (data not shown). Subsequently, the product quality of the mAbs expressed by the different clones was analysed by PhyTip purification of the product of interest from the remaining HCCF, followed by size and charge variants analysis by 2D SEC-CEX-UV as previously developed in Chapter 3 and 4, respectively. Data analysis was carried out as previously described (6.3.1). Relative quantification of the size and charge variants involved the calculation of the proportion of each size or charge variant, as compared to the total species detected in a chromatogram expressed as a percentage of the total peak areas. As displayed in Figure 6.10, the main size variants detected in mAb-1 samples were low molecular weight species (LMWS) in the range 0.6-6%. The genetic engineering manipulation did not induce aggregation and the high molecular weight species (HMWS) remained constant at < 0.3%. The acidic and basic charge variance species

remained in the range 0.6-2.8% and 42-54%, respectively without significant difference across all conditions.

Overall, no significant difference in either size and charge variants were observed as a consequence of targeted gene expression engineering. Thus, clone selection was driven by the expression titres (data not shown) and the three best high producing CHO CAT-S clones were scaled up to 10 mL cell cultures. At the end of the scaled-up fed-batch overgrow, the same analytical workflow was applied to evaluate whether both the cell engineering approaches and the cell culture scale affected PQ. As shown in Figure 6.11, the levels of LMWS were in the range 0.44-7.82% whereas the acid and basic variants were 1.24-4.14% and 36-63.2%, respectively again no aggregation was detected.

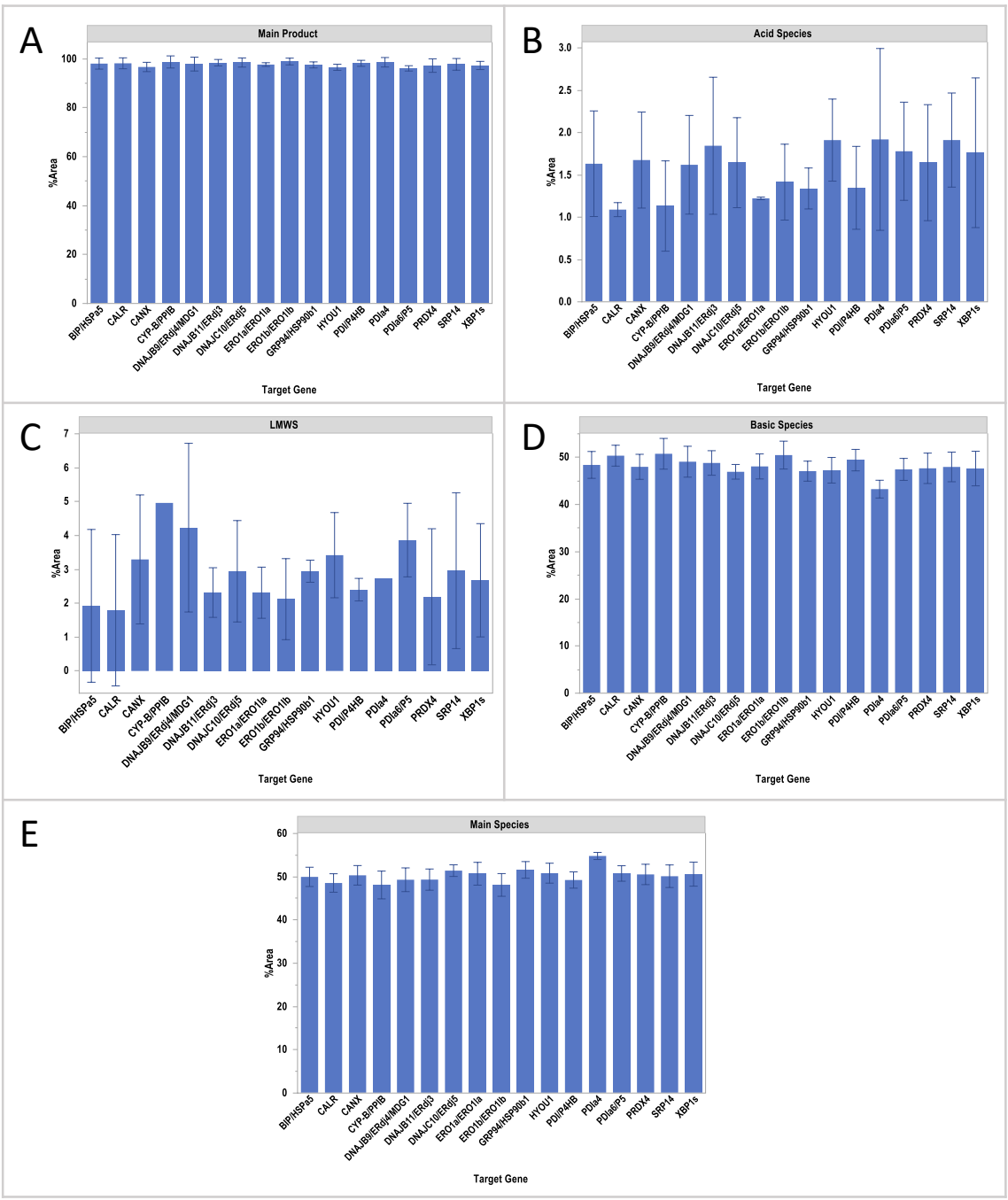

Figure 6.10 Size and charge variants profile of mAb-1 samples in the 24-DWP screen

Bar chart representing the mean and standard deviation of the % area of each species calculated across three biological replicates and displayed against the targeted effector gene. The %area of the main product peak (A) and %LMWS (C) was relative to the size variants whilst the % acid species (B), %basic species (D), and %main species (E) corresponded to the charge variants detected for the mAb-1 samples in the 24-DWP screen.

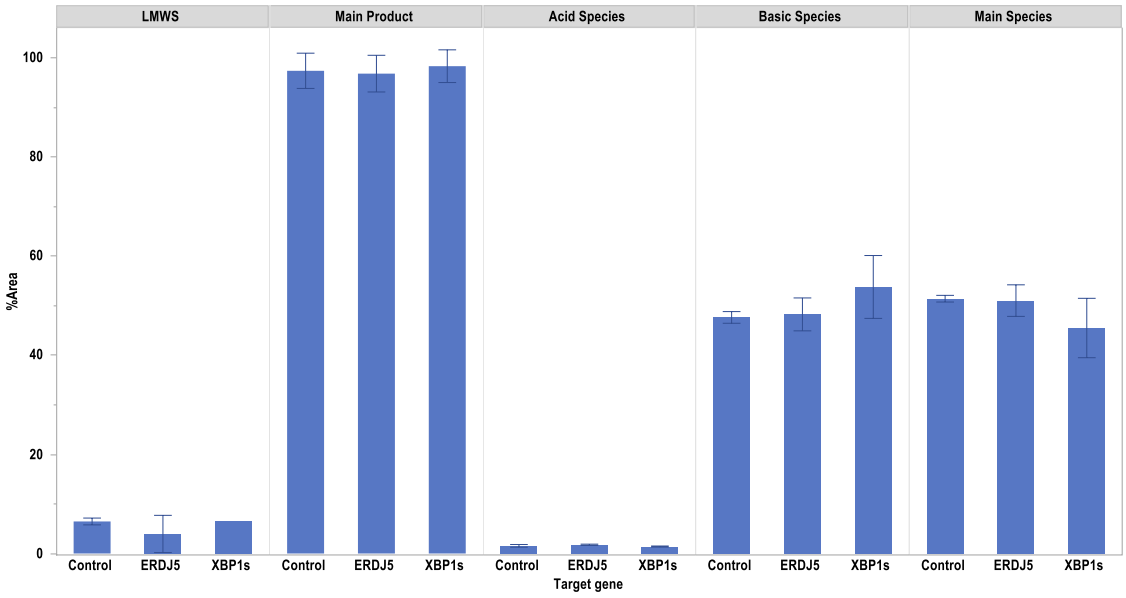

Figure 6.11 Size and charge variants of mAb-1 in the 10 mL culti-flasks experiment
Bar chart representing the mean and standard deviation of the % area of each size and charge variant species calculated across three biological replicates and displayed against the target gene of interest. The Control sample corresponded to cells transfected with a vector having the same backbone as the vectors containing the effector genes but without any gene in it. This was used to control how the transfection process impacted the expression of mAb-1. The %area of the main product peak and %LMWS were the size variants, whilst the % acid species, %basic species, and %main species corresponded to the charge variants detected for the mAb-1 samples in the 10 mL culti-flask experiment.

PQ analysis confirmed that the mAb size and charge variants profile did not change as a consequence of the gene expression manipulations across the two cell culture scales tested in this experiment. This was expected since previous research work carried out in AstraZeneca demonstrated that mAb-1 was particularly stable under standard cell culture conditions (data not shown as proprietary of AstraZeneca archive). This was also confirmed in the accelerated forced degradation and stability study presented in Chapter 4, Section 4.3.2. Indeed, it was observed that mAb-1 had a low tendency to aggregate whilst being more prone to fragment as a consequence of the stress conditions under examination. However, SEC may not be the best method to employ for fragmentation analysis. The industry gold standard for protein fragmentation analysis is capillary gel electrophoresis (CGE) providing higher resolving power of LMWS in comparison to SEC. Thus, the present method may not be accurate to assess the content of LMWS in this study. Nevertheless, the results from this experiment demonstrated that the PhyTip purification/2D SEC-CEX-UV workflow could successfully support the analysis of both screens comprising of a total of 60 samples within 24 hours.

Like the MAM, the 2D SEC-CEX-UV method covered the analysis of multiple quality attributes in one single method, minimising time and sample requirements for analytical testing. Size and charge variants analysis was achieved with less than 10 μg of protein per injection. Selective fractionation of the main product peak in the SEC chromatogram was achieved in a fully automated fashion reducing time and the amount of sample that would have been required with a benchmark 1D-LC approach using offline fractionation.

In contrast to MAM studies, the 2D SEC-CEX-UV was unable to provide information on mAb charge variants at the molecular level unless they had previously been characterised by MS (see Chapter 4, Section 4.3.4). Since the mAb-1 charge variants were characterised by the 2D SEC-CEX-MS method as reported in chapter 4, the nature of the charge variants peaks separated by the UV-based 2D SEC-CEX method was known to derive from glycoforms and oxidated species. Thus, we could infer that the cell engineering strategy under investigation did not alter the glycosylation and oxidation profile of the molecule. The HT workflow presented herein provided data relevant for clone selection with time and sample requirements compatible with CLD activities.

6.4 Conclusions

The present chapter demonstrated the application of the HT analytics developed in this research project to real-world samples. Three case studies were presented, each describing different scenarios that may be encountered as part of the CLD process. The first case study described a situation in which little process and product knowledge was gathered a priori. A large HTS experiment consisting of a 96-well SPOG screen was conducted to interrogate a broad space of investigation. The PhyTip purification/HT SEC workflow was applied to rank 384 clones based on the aggregation levels of BsAb-1, a DTE bispecific antibody with a high tendency to aggregate. The determination of the BsAb-1 aggregation from 384 cultures with titres in the range of 7.64-1372.3 mg/L was successfully achieved in 32 hours. Although the cell culture conditions investigated in this study did not significantly alter the aggregation of BsAb-1, the HT SEC method was able to determine small changes in the aggregation levels. This helped clone selection, improved process understanding and gathered insights on the BsAb-1 aggregation mechanism.

The second case study presented a situation in which both product and process knowledge had been previously gathered. A PhyTip purification/HT SEC/MAM workflow was used to investigate the use of small molecule drugs as media supplements and their potential effect on titre and PQ of BsAb-1. A scaled-up screening experiment in 10 mL cell cultures was set up to test the clones selected in the previous experiment. Cell culture volume and expression titres were sufficient to run more in-depth analytical testing in comparison to the one presented in the first case study. Aggregation data were provided by both HT SEC and MAM, however, HT SEC demonstrated higher sensitivity and precision in identifying small variations in the aggregation levels. Nevertheless, MAM analysis complemented HT SEC data, providing the site-specific determination of BsAb-1 deamidation, glycosylation, Cys modifications, and C-terminal Lys retention in a single method for all the clones tested. Analytical testing indicated that major variations of BsAb-1 PQ were observed over time rather than as a consequence of the cell culture conditions tested.

The third case study demonstrated the application of the PhyTip purification/2D SEC-CEX-UV workflow to support clone selection during both 24-DWP screening and a scaled-up HTS experiment in 10 mL cell cultures. Cell engineering strategies focused on studying the role of effector genes in the productivity and PQ profile of mAb-1 expressed in CHO cells. The analytical workflow provided information on both size and charge variants of mAb-1

expressed by the different clones supporting both the 24-DWP and 10 mL cell culture screens enabling the analysis of 60 samples in ~24 hours.

In conjunction with all the analytical workflows, automated data analysis pipelines enabled the processing and reporting of the data from a large number of samples providing PQ information to feedback to CLD in a time-efficient fashion.

The studies presented herein demonstrated the successful application of the HT analytical methods developed in this research project to real case studies. The information provided by analytical testing aided clone selection, improved process understanding and provided insights on future experiments for CLD. Particularly, the outcomes of this study revealed that the introduction of analytical testing during the early stage of CLD, in support of small scale HTS experiments, was fundamental to identify process conditions that did not work or did not alter PQ before scaling up. This ultimately helped to minimise both the time and costs of product development.

Despite the advantages brought by the application of HT analytics to CLD, considerations needs to be made when implementing the HT methods in industry in support of HTS. Firstly, all the methods developed in this project lack the resolving power of benchmark QC methods and provide a relative quantitation of PQAs rather than absolute quantitative data. Consequently, these methods can only be used in early product development but would not be fit for later-stage development due to regulatory issues. Although the data obtained by the HT methods can be substantially different from those obtained by the benchmark methods, the trend is comparable conforming their relevance as powerful analytical tools in early development stages. Interestingly, the throughput of the methods applied in this study was inversely proportional to the amount of information gathered by each method. Indeed, the analytical throughput of both MAM and the 2D SEX-CEX-UV methods was overall lower than the HT SEC method since they required a larger sample amount (100 μg and 20 μg *vs.* 2 μg, respectively) and time (30 min and 20 min *vs.* 3.5 min, respectively) per analysis. Despite MS being a burden to the experimental throughput, it provided significant improvement on the depth of the PQ information. Automation of both experimental procedure and data analysis was of paramount importance to increase the throughput capability. Although, data interpretation from an expert scientist was still required, automation of data processing allowed for faster analysis turnaround for hundreds of samples. Overall, the outcome of this work demonstrate the relevance of these methods for

application to industrial analytical workstream. Industrial applications would favour next generation manufacturing as well as discovery research where greater throughout is required for investigating a wide design space. The methods comply with the QbD approach by contributing to building a process aimed at understanding product quality and delivering the product with a desirable quality since early stage development.

This page was intentionally left blank

Chapter 7

Concluding Remarks and Future Work

This research work was focused on the miniaturisation, parallelisation and automation of low throughput industrial methods for protein characterisation and the generation of flexible analytical workstreams for supporting clone selection during early product development as illustrated in Figure 7.1. This chapter provides the reader with a summary of the findings, the concluding impact of this research and future work.

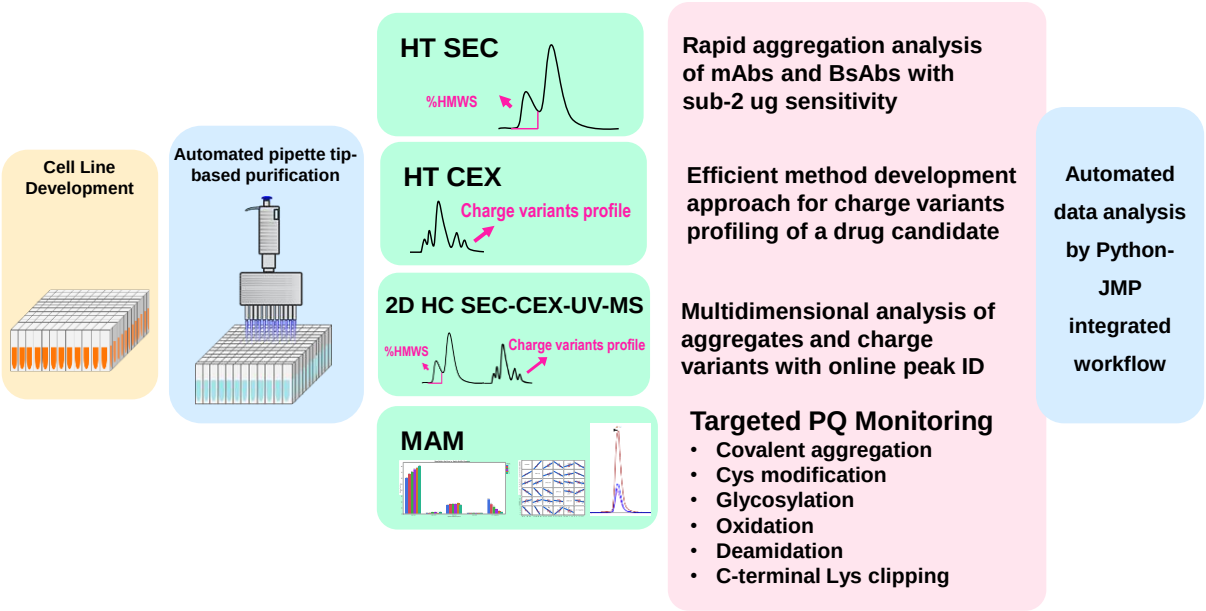

Figure 7.1 Schematics of the HT Analytical Platform.

7.1 One-dimensional chromatography methods for flexible high-throughput purification and characterisation of mAbs and BsAbs

The miniaturisation of affinity chromatography into resin-filled pipette-tips columns empowered the parallel and fully automated purification of proteins from small-scale cell cultures such as 96-DWP (Chapter 3 Part A and Chapter 6). This technology offers a high degree of flexibility to a wide range of molecules thanks to the variety of commercially available resins. As part of this work, method development consisted of the application of the PhyTip methodology in combination with a robotic liquid handler (Tecan) for the purification of mAbs and BsAbs. Validation experiments confirmed that the method achieved the processing of a full 96-DWP containing 300 μL of HCCF per well in less than 2 hours with minimal sample requirement. Most importantly, this purification methodology enabled the handling of low volumes typical of 384/96-DWPs and elution in small volumes at high concentration, therefore, compatible with further downstream analysis with no need for sample manipulation. This provided sufficient material with an adequate level of purity for analytical characterisation during clone selection and process development activities. Purification conditions were compatible with both aggregation and charge variants analysis by SEC and CEX methods, respectively. Based on the analytical tests performed in this study, the PhyTip purification method did not alter the quality profile of the molecules investigated. Although the buffers used for small and large scale purification are the same, the implementation of the PhyTip purification method in industry would require a thorough investigation of its effect on PQ in comparison to the benchmark affinity chromatography procedure. This would involve the execution of further analysis before and after PhyTip purification such as intact mass analysis of non-reduced, reduced glycosylated and deglycosylated proteins, peptide mapping, benchmark SEC, cIEF, DLS, etc. Furthermore, comparability studies will have to be performed to evaluate differences and similarities in both performance and costs with the larger scale SPE or affinity-chromatography industry-standard purification methods. Thorough characterisation analysis and comparability assessment would provide a better understanding of the feasibility of this method for applications to industrial process development activities that are beyond the scope of this project.

SEC is the industry gold standard analytical methodology for the analysis of protein aggregates. One of the main advantages of SEC is the ability to analyse proteins in their native state without sample preparation. Whilst the current HT SEC methods are based on 4.6 mm ID columns, findings from this research work demonstrated that the miniaturisation of SEC methods on 2.1 mm ID columns achieved suitable resolution and substantial gain in sensitivity and speed. The HT SEC method developed to support HTS experiments for CLD activities provided aggregation data in 3.5 min per injection and sub-2 μg sensitivity resulting in 6-fold faster run time requiring 125-fold less material per injection than the benchmark SEC method. The HT SEC method can be easily implemented as a HT tool in laboratories equipped with an LC system for the processing of large sample sequences in an automated fashion. Column technologies have been developed for application to various classes of molecules based on their hydrodynamic radii allowing the establishment of platform approaches.

One caveat is the need for purified samples since the injection of HCCF would compromise the separation as well as the instrument performance. Therefore, the HT SEC method was combined offline with the PhyTip purification. This research work presented the development of a novel PhyTip purification/HT SEC workflow applied as a platform approach providing mAb and BsAb aggregation data to drive CLD activities (see Chapter 6). The HT analytical workflow enabled the analysis of 384 samples from 4 x 96-DWPs cell culture in 32 hours. Despite the successful application of this analytical workflow as a ranking tool in early development activities, it is important to consider that lower throughput SEC methods may provide different %HMWS data due to their greater resolving power. However, the trend across the sample should remain the same between the different SEC scales. This observation reiterates the importance of performing comparability studies in case such workflows were to be implemented in an industrial setting.

The analysis of the charge variants profiles of protein therapeutics provides clustered information on their PTMs and chemical modifications affecting their microheterogeneity and thereby their PQAs (Sissolak et al., 2019; Füssl et al., 2018). Therefore, charge variants analysis is monitored from the early development of a product (Sissolak et al., 2019, Garripelli, Wu, and Gupta, 2020). Chapter 3 Part B, presented the development of a HT CEX method aided by a Split-DoE approach for supporting the analysis of the surface charge distribution of mAbs during early CLD activities. The Split-DoE-assisted method development approach involved a fractional factorial DoE for optimising the variables that

most significantly affect CEX separation, i.e. column and mobile phase pH. Subsequently, a response surface design was used to optimise the flow rate and gradient steepness for achieving adequate separation of mAb-1 charge variants. Overall, 27 runs were sufficient to screen 4 columns, mobile phase pH range, flow rate and gradient steepness to ultimately develop a HT CEX fit for HT applications. The Split-DoE approach offered a flexible and efficient workflow for the development of IEX methods.

It is worth considering that, as opposed to PhyTip purification and HT SEC methods, the HT CEX method was specific for mAb-1. Its suitability for analysing other drug candidates will have to be assessed as it is strongly dependent on the superficial charge of the molecule of interest. Nevertheless, the Split-DoE workflow can be used for the development of a platform CEX method fit for HT analysis. This would require the use of 6-10 candidates from a class of molecules covering a wide range of pIs. The use of DoE and other chemometric tools is a growing practice in chromatography method development as particularly apt for a changing scientific and regulatory scenario that puts process understanding at the centre of biopharmaceutical development (Ganorkar 2017; Joshi, Kumar, and Rathore, 2017; Sahu et al., 2018; Leweke and von Lieres, 2018). Ganorkar remarked that chromatography method development can be time-consuming and subjective thus, chemometric approaches can minimise complexity providing a 360° view of all the factors affecting chromatographic efficiency and ultimately accelerate the timeline of drug development (Ganorkar, 2017). All the methods presented in Chapter 3 were developed by using DoE, thus demonstrating how to flexibly structure the experimental work based on the time, sample and resources available with enough statistical control to maximise the amount of information extracted from the experiments.

7.2 Multiple Attribute Analysis of Therapeutic Proteins using LC-MS methods

Unlike 1D-LC, 2D-LC methods allow the determination of multiple quality attributes within the same run and instrument setup. Whilst the analysis of mAb size and charge variants would be performed separately when using the HT SEC and HT CEX methods, the 2D SEC-CEX-UV separation combined both data in a single, fully automated analysis (see Chapter 4). Heart-cutting 2D-LC mode enabled the selective transfer of the main product peak to the ^{2}D for CEX analysis with considerable time and sample saving in comparison to offline procedures. Offline 1D-LC procedures consist of peak fraction collection followed by enrichment, buffer exchange, and reinjection of the sample fractions for further analytical characterisation whilst the 2D-LC automates all these steps within the LC system. Charge variants peak identification was efficiently achieved by online hyphenation of MS. The 2D SEC-CEX-MS method offered a tool to maximise product knowledge during early development. Particularly, the intact protein analysis by 2D SEC-CEX-MS complemented peptide mapping and released glycan analysis for the characterisation of the physicochemical properties of mAb-1 under forced degradation studies. This provided a better understanding of the degradation mechanism occurring to the molecule of interest under H_2O_2 stress which would not be accomplished with peptide mapping alone. Nevertheless, this also underlined the limitations of intact mass analysis in providing a comprehensive picture of the physicochemical properties of proteins and emphasised the need for a range of analytical methods to fully resolve and characterise them. To date, no analytical technology can accurately characterise the full spectrum of protein quality attributes. Therefore, standard industrial analytical workflows require the execution of various testing employing a range of techniques and orthogonal analysis (Staub et al., 2011). It is worth considering that the use of the MS reduced the method throughput considerably. This was not only due to the increased instrumental complexity but also the lengthy data analysis. Indeed, such methodology requires expert scientists for both instrument operation, data handling and interpretation. Additionally, automation of the data processing was hampered by the lack of data analysis tools to interpret MS data. For this reason, the MS-based method was used when in-depth characterisation was needed (Chapter 4) whilst the UV-based separation was employed as a HT tool during clone selection (Chapter 6).

The MAM method (Chapter 5) consisting of the MRM analysis of non-reduced tryptic peptides, is an example of another analytical tool that can be used to maximise the amount of PQ data obtained from a single analysis. The method targeted peptides bearing predetermined PTMs at specific amino acid sites, namely glycosylation, deamidation, C-terminal Lys retention and Cys modifications. Most interestingly, this proof-of-concept work demonstrated the use of chemometric tools and machine learning combined with MRM to quantify HWMS impurities of a BsAb candidate by targeting Cys modifications. As described in Chapter 6, Section 6.3.2, its successful application as a ranking tool in small scale CLD HTS experiments proved how analytical chemistry, chemometrics, and machine learning can be integrated to maximise understanding of the principles governing biopharmaceutical production by extrapolating meaningful data from chemical experiments. Hence, it could conceivably be hypothesised that MAM could provide a unique tool to comprehensively support analytical testing during dedicated development activities. This would minimise the need for orthogonal analytical testing, again reducing the time, sample, costs and other resources necessary for biopharmaceutical development.

The main drawback of this method is that it was designed for a specific drug candidate thus, it cannot be applied for the analysis of another molecule. In theory, the same approach could be used to build a MAM method for a group of BsAbs sharing the same aggregation pathway and aminoacidic sequence of the peptides bearing the targeted modifications. Additionally, MRM analysis can only monitor fixed quality attributes thus, modifications different from the ones predefined in the method will not be identified, meaning that some PQ information might be missed. Therefore, the MAM method as presented in Chapter 5 is fit to be applied during R&D activities of a lead candidate after thorough analytical characterisation and sufficient product knowledge have been gathered to define the molecule CQAs.

7.3 Future Work

Future work will involve the transfer of the PhyTip purification/HT SEC workflow to the analytical laboratories in AstraZeneca for the implementation of this technology as part of the analytical workstream to support the company pipelines. Both the PhyTip purification and HT SEC methods were transferred to the Bioprocess Analytics team (BPA) in AstraZeneca and are currently being validated. Next, the automated data processing tool will be optimised to be implemented in the LC systems of BPA. Further implementation of the PhyTip purification/HT SEC workflow in the laboratories of both BPA and Analytical Science (AS) teams will require the training of scientists and authoring of the standard operating procedure. Further evaluation of the effect of the PhyTip purification method on PQ will be carried out by purifying 2 mAbs and 2 BsAbs using AstraZeneca purification platform buffers followed by benchmark SEC, intact mass analysis of non-reduced, reduced and deglycosylated protein, peptide mapping and cIEF. The same analytical tests will be performed and compared to the AstraZeneca benchmark purification method with the same buffer system. This will enable a direct comparison of the effect of the PhyTip purification procedure on PQ with the existing benchmark purification method.

Owing to the great potential demonstrated by both MAM and 2D SEC-CEX-UV/MS methods for the determination of multiple quality attributes of BsAbs and mAbs, future experiments will need to be carried out to further explore their potential application in the industry. As discussed in Chapter 5 Section 5.3.2.1, the quantitation of BsAb-1 HMWS by MRM analysis of Cys modifications lacked the precision and accuracy necessary to confidently discriminate between the samples with different levels of HMWS impurities. Method optimisation will have to be carried out to improve the signal intensity of low abundance species necessary for building the predictive model such as the scFv tripeptide and glutathionylated peptides. This would require either increasing the column loading or modifying the sample preparation procedure, such as using different digestion enzymes to obtain peptides that ionise better in the ESI source, or mobile phase additives that improve the MS signal. Furthermore, the issues deriving from multicollinearity will need to be overcome by constructing a model comprising of all the possible predictors including the peptides that do not have a strong correlation as well as investigating other predictive modelling tools designed for highly correlated variables such as principal component analysis. Most importantly, the model will need to be built with data deriving from a larger

and more heterogenous dataset, ideally from samples expressed in cell cultures having various aggregation levels. This would provide a more comprehensive and realistic picture of the relationship between BsAb-1 Cys modifications and the levels of aggregation in order to obtain a model that more accurately explains the true features behind the BsAb-1 aggregation mechanism. Cross-validation of the statistical model will be performed to demonstrate the feasibility of the method for its final application in product development. Finally, future experiments could be dedicated to the design of a MAM method for the analysis of a class of BsAbs sharing the same aggregation mechanism extending its application as a platform method. It is worth considering that the use of a quadrupole-orbitrap (Q-Orbitrap) mass spectrometer instead of a triple quadrupole (QqQ) would enable the acquisition of high-resolution mass spectrometry (HRMS) data in HR-full scan mode rather than in selective reaction monitoring (SRM). Indeed, HRMS can be as sensitive and selective in HR-full scan as QqQ in SRM acquisition but would provide a more comprehensive picture of what is in a biological sample by the parallel monitoring (PRM) of all the peptide fragments from a precursor ion, thus maximising the information output of the method. Further, HRMS is more versatile enabling both qualitative and quantitative analysis. If implemented in the company, the MAM method could support a lead candidate selection, production clone selection, production process optimisation, extended characterisation and release stability testing.

With respect to the 2D SEC-CEX-UV-MS, future experiments could be tailored to the application of the method in support of clone selection to a different case study where greater differences in PQ such as aggregates and charge variants are expected. This would demonstrate its ability to detect significant differences in PQ in support of CLD activities as well as developability studies.

7.4 Considerations on the implementation of the High-Throughput Analytical Platform in Industry

With a global view of the analytics developed in this research project, we can recognise that miniaturisation, parallelisation and automation enabled substantial throughput gain of the analytical workstream. However, the maximisation of the PQ data gathered from each method was inversely proportional to the analytical resources required for both the experimental execution and data processing. Despite holding the greatest potential in generating a large amount of data from a single run, performing MAM and 2D SEC-CEX-MS analysis augmented the analytical burden due to the increased instrument complexity, sample, time and costs required. By deconvoluting instrument complexity from 2D SEC-CEX-UV to the 1D-LC methods such as HT SEC and HT CEX, the experimental operation burden was eased and the analytical requirement minimised but at the expense of the amount and depth of PQ data. Similarly, automation was undoubtedly the key enabler for parallel execution of multiple experiments but required sophisticated instrumentations leading to a considerable increase in cost. The use of data analytics tools for data processing offered easier and faster data handling providing a greater understanding and comprehensive view of the outcomes. Nevertheless, the increased analytical complexity for both equipment and data analysis required highly skilled scientists.

The implementation of HT technologies in an industrial setting is hindered by all the aforementioned reasons. Moreover, the studies of method comparability with conventional benchmark procedures must be thoroughly assessed before implementation in routine testing. Likewise, the methods must be validated for use in the industrial workstream and regulatory compliance must be evaluated. The findings from this research work provided a vision towards future industrial analytical technologies (Figure 7.2) highlighting the need for deconvoluting the complexity of the analytical workstream whilst empowering the generation, extraction and analysis of big datasets.

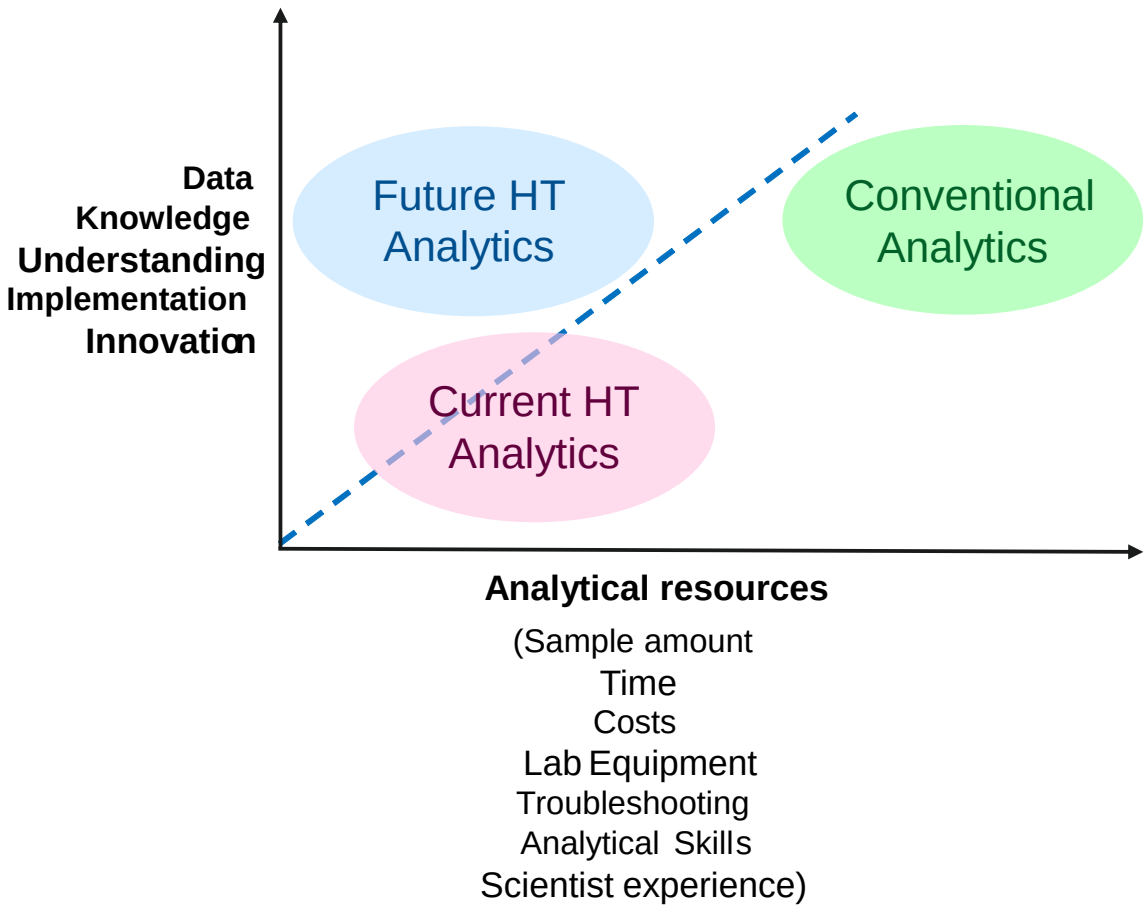

Figure 7.2 A view of the direction of the biopharmaceutical analytics from the current HT and conventional tools towards future technologies.

This page was intentionally left blank

Bibliography

Aggarwal, Saurabh Rob. 2014. “What ’ s Fueling the Biotech Engine — 2012 to 2013.” *Nature Biotechnology* 32 (1): 32–39. https://doi.org/10.1038/nbt1109-987.

Aich, Udayanath, Jude Lakbub, and Aston Liu. 2016a. “State-of-the-Art Technologies for Rapid and High-Throughput Sample Preparation and Analysis of N-Glycans from Antibodies.” *Electrophoresis* 37 (11): 1468–88. https://doi.org/10.1002/elps.201500551..

Alam, Magfur E., Gregory V. Barnett, Thomas R. Slaney, Charles G. Starr, Tapan K. Das, and Peter M. Tessier. 2019. “Deamidation Can Compromise Antibody Colloidal Stability and Enhance Aggregation in a PH-Dependent Manner.” *Molecular Pharmaceutics* 16 (5): 1939–49. https://doi.org/10.1021/acs.molpharmaceut.8b01311.

Alam, Magfur E., Thomas R. Slaney, Lina Wu, Tapan K. Das, Sambit Kar, Gregory V. Barnett, Anthony Leone, and Peter M. Tessier. 2020. “Unique Impacts of Methionine Oxidation, Tryptophan Oxidation, and Asparagine Deamidation on Antibody Stability and Aggregation.” *Journal of Pharmaceutical Sciences* 109 (1): 656–69. https://doi.org/10.1016/j.xphs.2019.10.051.

Alekseychyk, Larysa, Cheng Su, Gerald W. Becker, Michael J. Treuheit, and Vladimir I. Razinkov. 2017a. “High-Throughput Screening and Analysis of Charge Variants of Monoclonal Antibodies in Multiple Formulations.” *SLAS Discovery* 22 (8): 1044–52. https://doi.org/10.1177/2472555217711666.

Alekseychyk, Larysa, Cheng Su, Gerald W Becker, Michael J Treuheit, and Vladimir I Razinkov. 2017b. “High-Throughput Screening and Analysis of Charge Variants of Monoclonal Antibodies in Multiple Formulations.” *SLAS Discovery* 22 (8): 1044–52. https://doi.org/10.1177/2472555217711666.

Alzahrani, Rihana. 2020. “Biopharmaceutical Revolution in Saudi Arabia: Progress and Development.” *Journal of Pharmaceutical Innovation* 2020 (January): 1–14. https://doi.org/doi.org/10.1007/s12247-020-09429-1.

Amanullah, Ashraf, Jose Manuel Otero, Mark Mikola, Amy Hsu, Jinyou Zhang, John Aunins, H. Brett Schreyer, James A. Hope, and A. Peter Russo. 2010. “Novel Micro-

Bioreactor High Throughput Technology for Cell Culture Process Development: Reproducibility and Scalability Assessment of Fed-Batch CHO Cultures." *Biotechnology and Bioengineering* 106 (1): n/a-n/a. https://doi.org/10.1002/bit.22664.

Ambrogelly, Alexandre, Stephen Gozo, Amit Katiyar, Shara Dellatore, Yune Kune, Ram Bhat, Joanne Sun, et al. 2018. "Analytical Comparability Study of Recombinant Monoclonal Antibody Therapeutics." *MAbs* 10 (4): 513–38. https://doi.org/10.1080/19420862.2018.1438797.

An, Y., S. Verma, Y. Chen, S. Yu, Y. Zhang, S. Kelner, S. Mengisen, D. Richardson, and Z. Chen. 2017. "Forced Degradation Study of Monoclonal Antibody Using Two-Dimensional Liquid Chromatography." *Journal of Chromatography Separation Techniques* 8 (3): 1–7. https://doi.org/10.4172/2157-7064.1000365.

Arnold, James N., Mark R. Wormald, Robert B. Sim, Pauline M. Rudd, and Raymond A. Dwek. 2007. "The Impact of Glycosylation on the Biological Function and Structure of Human Immunoglobulins." *Annual Review of Immunology* 25 (1): 21–50. https://doi.org/10.1146/annurev.immunol.25.022106.141702.

Arora, Sushrut, Vikas Saxena, and B. Vijayalakshmi Ayyar. 2017. "Affinity Chromatography: A Versatile Technique for Antibody Purification." *Methods* 116 (December): 84–94. https://doi.org/10.1016/j.ymeth.2016.12.010.

Arosio, Paolo, Giuliano Barolo, Thomas Müller-Späth, Hua Wu, and Massimo Morbidelli. 2011. "Aggregation Stability of a Monoclonal Antibody during Downstream Processing." *Pharmaceutical Research* 28 (8): 1884–94. https://doi.org/10.1007/s11095-011-0416-7.

Bailey, Aaron O., Guanghui Han, Wilson Phung, Paul Gazis, Jennifer Sutton, Jonathan L. Josephs, and Wendy Sandoval. 2018. "Charge Variant Native Mass Spectrometry Benefits Mass Precision and Dynamic Range of Monoclonal Antibody Intact Mass Analysis." *MAbs* 10 (8): 1214–25. https://doi.org/10.1080/19420862.2018.1521131.

Bakhtiar, Ray. 2012. "Therapeutic Recombinant Monoclonal Antibodies." *Journal of Chemical Education* 89 (12): 1537–42. https://doi.org/10.1021/ed200392h.

Balcerek, Julita, Marta Bednarek, and Tomasz D Sobie. 2021. "Toward Shortened the Time-to-Market for Biopharmaceutical Proteins : Improved Fab Protein Expression Stability Using the Cre / Lox System in a Multi-Use Clonal Cell Line." *Journal of*

Pharmaceutical Sciences 110 (2): 946–51. https://doi.org/10.1016/j.xphs.2020.10.005.

Barnett, Gregory V, Gurusamy Balakrishnan, Naresh Chennamsetty, Laurel Hoffman, Jacob Bongers, Li Tao, Yunping Huang, et al. 2019. "Probing the Tryptophan Environment in Therapeutic Proteins : Implications for Higher Order Structure on Tryptophan Oxidation." *Journal of Pharmaceutical Sciences* 108 (6): 1944–52. https://doi.org/10.1016/j.xphs.2018.12.027.

Bathke, Anja, Christian Bell, Christoph Gstöttner, and Robert Kopf. 2021. "Rapid Online Characterization and Reduction of Protein Modifications Using Fully Automated Two-Dimensional High Performance Liquid Chromatography – Mass Spectrometry." *LCGC Europe* 31 (1): 1–11.

Batra, Jyoti, and Anurag S. Rathore. 2016. "Glycosylation of Monoclonal Antibody Products: Current Status and Future Prospects." *Biotechnology Progress* 32 (5): 1091–1102. https://doi.org/10.1002/btpr.2366.

Baumann, Pascal, and Jürgen Hubbuch. 2017. "Downstream Process Development Strategies for Effective Bioprocesses: Trends, Progress, and Combinatorial Approaches." *Engineering in Life Sciences* 17 (11): 1142–58. https://doi.org/10.1002/elsc.201600033.

Beck, Alain, Sarah Sanglier-Cianférani, and Alain Van Dorsselaer. 2012. "Biosimilar, Biobetter, and next Generation Antibody Characterization by Mass Spectrometry." *Analytical Chemistry* 84 (11): 4637–46. https://doi.org/10.1021/ac3002885.

Benjamini, Yoav. 1995. "Controlling The False Discovery Rate - A Practical And Powerful Approach To Multiple Testing." *Journal of the Royal Statistical* 57 (1): 289–300. https://doi.org/10.2307/2346101.

Berger, Scott, and Joe Fredette. 2017. "Mass Spectrometry in Late Development and QC: Practical Considerations for Multi-Attribute Monitoring and Beyond." *LC/GC The Column* 13 (9): 9–13. http://www.chromatographyonline.com/mass-spectrometry-late-development-and-qc-practical-considerations-multi-attribute-monitoring-and-be?pageID=4.

Berkowitz, Steven A., John R. Engen, Jeffrey R. Mazzeo, and Graham B. Jones. 2012. "Analytical Tools for Characterizing Biopharmaceuticals and the Implications for Biosimilars." *Nature Reviews Drug Discovery* 11 (July): 527–40.

https://doi.org/10.1038/nrd3746.

Bhambure, Rahul, Kaushal Kumar, and Anurag S. Rathore. 2011. “High-Throughput Process Development for Biopharmaceutical Drug Substances.” *Trends in Biotechnology* 29 (3): 127–35. https://doi.org/10.1016/j.tibtech.2010.12.001.

Bhat, Alangar Ishwara, and Govind Pratap Rao. 2020. *Characterization of Plant Viruses*. New York: Humana Press. https://link.springer.com/book/10.1007/978-1-0716-0334-5.

Blanchard, Veronique, Xi Liu, Susann Eigel, Matthias Kaup, Silke Rieck, Sabina Janciauskiene, Volker Sandig, et al. 2011. “N-Glycosylation and Biological Activity of Recombinant Human Alpha1-Antitrypsin Expressed in a Novel Human Neuronal Cell Line.” *Biotechnolgy and Bioengineering* 108 (9): 2118–2128. https://doi.org/10.1002/bit.23158.

Bonn, Guenther and Douglas T. Gjerde. 2017. “Dual Flow Chromatography.” *LCGC Europe* 30 (8): 404–11. http://www.chromatographyonline.com/dual-flow-chromatography?pageID=2.

Brekke, Ole Henrik, and Inger Sandlie. 2003. “Therapeutic Antibodies for Human Diseases at the Dawn of the Twenty-First Century.” *Nature Reviews Drug Discovery* 2 (1): 52–62. https://doi.org/10.1038/nrd984.

Brinkmann, Ulrich, and Roland E. Kontermann. 2017. “The Making of Bispecific Antibodies.” *MAbs* 9 (2): 182–212. https://doi.org/10.1080/19420862.2016.1268307.

Brinkmann, Ulrich, and Roland E Kontermann. 2021. “Bispecific Antibodies.” *Science* 372 (6545): 916–18.

Brunner, Matthias, Jens Fricke, Paul Kroll, and Christoph Herwig. 2017. “Investigation of the Interactions of Critical Scale-up Parameters (PH, PO2 and PCO2) on CHO Batch Performance and Critical Quality Attributes.” *Bioprocess and Biosystems Engineering* 40 (2): 251–63. https://doi.org/10.1007/s00449-016-1693-7.

Budge, James D, Tanya J Knight, Jane Povey, Joanne Roobol, Ian R Brown, Gurdeep Singh, Andrew Dean, et al. 2020. “Engineering of Chinese Hamster Ovary Cell Lipid Metabolism Results in an Expanded ER and Enhanced Recombinant Biotherapeutic Protein Production.” *Metabolic Engineering* 57 (December 2019): 203–16. https://doi.org/10.1016/j.ymben.2019.11.007.

Buettner, Alexander, Maria Maier, Lea Bonnington, Patrick Bulau, and Dietmar Reusch. 2020. “Multi-Attribute Monitoring of Complex Erythropoetin Beta Glycosylation by GluC Liquid Chromatography − Mass Spectrometry Peptide Mapping.” *Anal. Chem.* 92 (May): 7574–80. https://doi.org/10.1021/acs.analchem.0c00124.

Büttner, Alexander, Dietmar Reusch, Guusje Van Schaick, Christoph Gst, Manfred Wuhrer, and Elena Domínguez-vega. 2021. “Analytica Chimica Acta Anion Exchange Chromatography e Mass Spectrometry for Monitoring Multiple Quality Attributes of Erythropoietin Biopharmaceuticals.” *Analytica Chimica Acta* 1143 (Novermber): 166–72. https://doi.org/10.1016/j.aca.2020.11.027.

Byrne, Hannah, and Oscar Swindley. 2020. “Automated, Rapid & Reproducible Measurement of Immunoglobulin G Using Opentrons OT-2 Liquid Handling Robot and Valita®TITER and Valita®TITER Plus, Application Note.” The University Of Sheffield, Opentrons, Valitacell.

Camperi, Julien, Alexandre Goyon, Davy Guillarme, Kelly Zhang, and Cinzia Stella. 2021. “Multi-Dimensional LC-MS: The next Generation Characterization of Antibody-Based Therapeutics by Unified Online Bottom-up, Middle-up and Intact Approaches.” *Analyst* 146 (1): 1–23. https://doi.org/10.1039/d0an01963a.

Cao, Mingyan, Chunlei Wang, Wai Keen, Dana Motabar, Jihong Wang, and Elizabeth Christian. 2018. “Characterization and Analysis of ScFv-IgG Bispecific Antibody Size Variants.” *MAbs* 10 (8): 1236–47. https://doi.org/10.1080/19420862.2018.1505398.

Carillo, Sara, Florian Füssl, Jennifer Sutton, Paul Gazis, Ken Cook, Silvia Mill, Kai Scheffler, and Jonathan Bones. 2021. “Optimisation of the Use of Sliding Window Deconvolution for Comprehensive Characterisation of Trastuzumab and Adalimumab Charge Variants by Native High Resolution Mass Spectrometry.” *European Journal of Pharmaceutics and Biopharmaceutics* 158 (November): 83–95. https://doi.org/10.1016/j.ejpb.2020.11.006.

Carillo, Sara, Craig Jakes, and Jonathan Bones. 2020. “In-Depth Analysis of Monoclonal Antibodies Using Microfluidic Capillary Electrophoresis and Native Mass Spectrometry.” *Journal of Pharmaceutical and Biomedical Analysis* 185 (February): 113218.

Carillo, Sara, Kai Sche, Izabela Zaborowska, Jonathan Bones, Craig Jakes, and Silvia Milla.

2021. “Tracking the Behavior of Monoclonal Antibody Product Quality Attributes Using a Multi-Attribute Method Work Fl Ow.” *Journal of the American Society for Mass Spectrometry* 32 (8): 1998–2012. https://doi.org/10.1021/jasms.0c00432.

Carter, Paul J. 2011. “Introduction to Current and Future Protein Therapeutics: A Protein Engineering Perspective.” *Experimental Cell Research* 317 (9): 1261–69. https://doi.org/10.1016/j.yexcr.2011.02.013.

Cartwright, Joseph F., Karin Anderson, Joseph Longworth, Philip Lobb, and David C. James. 2018. “Highly Sensitive Detection of Mutations in CHO Cell Recombinant DNA Using Multi-Parallel Single Molecule Real-Time DNA Sequencing.” *Biotechnology and Bioengineering* 115 (6): 1485–98. https://doi.org/10.1002/bit.26561.

Cartwright, Joseph F, Claire L Arnall, Yash D Patel, Nicholas O W Barber, Clare S Lovelady, Guglielmo Rosignoli, Claire L Harris, et al. 2020. “A Platform for Context-Specific Genetic Engineering of Recombinant Protein Production by CHO Cells.” *Journal of Biotechnology* 312 (September 2019): 11–22. https://doi.org/10.1016/j.jbiotec.2020.02.012.

Chakrabarti, Anirikh, Aaron W. Chen, and Jeffrey D. Varner. 2011. “A Review of the Mammalian Unfolded Protein Response.” *Biotechnology and Bioengineering* 108 (12): 2777–93. https://doi.org/10.1002/bit.23282.

Chang, Michelle M., Leonid Gaidukov, Giyoung Jung, Wen Allen Tseng, John J. Scarcelli, Richard Cornell, Jeffrey K. Marshall, et al. 2019. “Small-Molecule Control of Antibody N-Glycosylation in Engineered Mammalian Cells.” *Nature Chemical Biology* 15 (7): 730–36. https://doi.org/10.1038/s41589-019-0288-4.

Chen, Zhi, Ming Zeng, Sung Joo Park, Gurusamy Balakrishnan, Kaimeng Zhou, Duohai Pan, and Tapan K. Das. 2020. “Bridging Size and Charge Variants of a Therapeutic Monoclonal Antibody by Two-Dimensional Liquid Chromatography.” *Journal of Pharmaceutical and Biomedical Analysis* 183 (May): 113178. https://doi.org/10.1016/j.jpba.2020.113178.

Chennamsetty, Naresh, Vladimir Voynov, Veysel Kayser, Bernhard Helk, and Bernhardt L Trout. 2009. “Design of Therapeutic Proteins with Enhanced Stability.” *PNAS* 106 (29): 11937–11942.

———. 2010. “Prediction of Aggregation Prone Regions of Therapeutic Proteins.” *Journal of Physical Chemitry* 114 (19): 6614–24.

Chhatre, Sunil, Daniel G. Bracewell, and Nigel J. Titchener-Hooker. 2009. “A Microscale Approach for Predicting the Performance of Chromatography Columns Used to Recover Therapeutic Polyclonal Antibodies.” *Journal of Chromatography A* 1216 (45): 7806–15. https://doi.org/10.1016/j.chroma.2009.09.038.

Chi, Bertie, Christel Veyssier, Toyin Kasali, Faisal Uddin, and Christopher A. Sellick. 2020. “At-Line High Throughput Site-Specific Glycan Profiling Using Targeted Mass Spectrometry.” *Biotechnology Reports* 25 (January): 1–9. https://doi.org/10.1016/j.btre.2020.e00424.

Christian, Gary D. 2005. “What Analytical Chemists Do: A Personal Perspective * Qualitative Analysis Is What . Quantitative Analysis Is How.” *Science* 32 (2): 81–92.

Chung, Christine H., Beloo Mirakhur, Emily Chan, Quynh-Thu Le, Jordan Berlin, Michael Morse, Barbara A. Murphy, et al. 2008. “NIH Public Access.” *The New England Journal of Medicine* 358 (11): 1109–17. https://doi.org/10.1056/NEJMoa074943.

Chung, Hyo Helen, Lynette Buck, Kristi Daris, Brent Welborn, Quanzhou Luo, and Jette Wypych. 2018. “Investigation of the Free Heavy Chain Homodimers of a Monoclonal Antibody.” *Biotechnology Progress* 34 (3): 738–45. https://doi.org/10.1002/btpr.2611.

Chung, Stanley, Jun Tian, Zhijun Tan, Jie Chen, Jongchan Lee, Michael Borys, and Zheng Jian. 2018. “Industrial Bioprocessing Perspectives on Managing Therapeutic Protein Charge Variant Profiles.” *Biotechnolgy and Bioengineering* 115 (7): 1646–65. https://doi.org/10.1002/bit.26587.

Chung, Stanley, Jun Tian, Zhijun Tan, Jie Chen, Na Zhang, Yunping Huang, Erik Vandermark, Jongchan Lee, Michael Borys, and Zheng Jian Li. 2019. “Modulating Cell Culture Oxidative Stress Reduces Protein Glycation and Acidic Charge Variant Formation.” *MAbs* 11 (1): 205–16. https://doi.org/10.1080/19420862.2018.1537533.

Courtois, Fabienne, Neeraj J Agrawal, Timothy M Lauer, Bernhardt L Trout, Fabienne Courtois, Neeraj J Agrawal, Timothy M Lauer, and Bernhardt L Trout. 2016. “Rational Design of Therapeutic MAbs against Aggregation through Protein Engineering and Incorporation of Glycosylation Motifs Applied to Bevacizumab Rational Design of Therapeutic MAbs against Aggregation through Protein Engineering and Incorporation

of G." *MAbs* 0862 (1): 99–112. https://doi.org/10.1080/19420862.2015.1112477.

Cox Gad, Shayne. 2007. *Handbook of Pharmaceutical Biotechnology*. Hoboken, New Jersey: John Wiley & Sons, Inc. https://doi.org/10.1002/9780470117118.

Craik, David J, David P Fairlie, Spiros Liras, and David Price. 2013. "The Future of Peptide-Based Drugs." *Chemical Biology & Drug Design* 81 (1): 136–47. https://doi.org/10.1111/cbdd.12055.

Cromwell, Mary E. M., Eric Hilario, and Fred Jacobson. 2006. "Protein Aggregation and Bioprocessing." *The AAPS Journal* 8 (3): E572–E579. https://doi.org/10.1208/aapsj080366.

Crunkhorn, Sarah. 2014. "Genentech Dives Deeper into the next Wave of Cancer Immunotherapies." *Nature Publishing Group* 13 (December): 2014. https://doi.org/10.1038/nrd4502.

Cui, Chuanlong, Tong Liu, Tong Chena, Johanna Lua, Ian Casarena, Diogo Borges Limab, Paulo Costa Carvalhoc, Annie Beuved, and Hong Li. 2019. "Comprehensive Identification of Protein Disulfide Bonds with Pepsin/Trypsin Digestion, Orbitrap HCD and Spectrum Identification Machine Chuanlong." *Proteomics* 198 (April): 78–86. https://doi.org/10.1016/j.jprot.2018.12.010.Comprehensive.

Dai, Jun, Jared Lamp, Qiangwei Xia, and Yingru Zhang. 2018. "Capillary Isoelectric Focusing-Mass Spectrometry Method for the Separation and Online Characterization of Intact Monoclonal Antibody Charge Variants." *Analytical Chemistry* 90 (3): 2246–54. https://doi.org/10.1021/acs.analchem.7b04608.

Daramola, Olalekan, Jessica Stevenson, Greg Dean, Diane Hatton, Gary Pettman, and William Holmes. 2013. "A High-Yielding CHO Transient System : Coexpression of Genes Encoding EBNA-1 and GS Enhances Transient Protein Expression." *American Institute of Chemical Engineers* 30 (1): 132–41. https://doi.org/10.1002/btpr.1809.

Das, Tapan K., Linda O. Narhi, Alavattam Sreedhara, Tim Menzen, Christoph Grapentin, Danny K. Chou, Valentyn Antochshuk, and Vasco Filipe. 2020. "Stress Factors in MAb Drug Substance Production Processes: Critical Assessment of Impact on Product Quality and Control Strategy." *Journal of Pharmaceutical Sciences* 109 (1): 116–33. https://doi.org/10.1016/j.xphs.2019.09.023.

Davies, Sarah L, Clare S Lovelady, Rhian K Grainger, Andrew J Racher, Robert J Young,

and David C James. 2013. “Functional Heterogeneity and Heritability in CHO Cell Populations.” *Biotechnology and Bioengineering* 110 (1): 260–74. https://doi.org/10.1002/bit.24621.

Deribe, Yonathan Lissanu, Tony Pawson, and Ivan Dikic. 2010. “Post-Translational Modifications in Signal Integration.” *Nature Structural & Molecular Biology* 17 (6): 666–72. https://doi.org/10.1038/nsmb.1842.

Diederich, Patrick, Sigrid K. Hansen, Stefan A. Oelmeier, Bianca Stolzenberger, and Jürgen Hubbuch. 2011. “A Sub-Two Minutes Method for Monoclonal Antibody-Aggregate Quantification Using Parallel Interlaced Size Exclusion High Performance Liquid Chromatography.” *Journal of Chromatography A* 1218 (50): 9010–18. https://doi.org/10.1016/j.chroma.2011.09.086.

DiMasi, Joseph A., Henry G. Grabowski, and Ronald W. Hansen. 2016. “Innovation in the Pharmaceutical Industry: New Estimates of R&D Costs.” *Journal of Health Economics* 47 (February): 20–33. https://doi.org/10.1016/j.jhealeco.2016.01.012.

Dimitrov, Dimiter S. 2012. *Therapeutic Proteins*. Edited by Vladimir Voynov and Justin A. Caravella. *Methods in Molecular Biology*. Vol. 899. London: Human Press. https://doi.org/10.1007/978-1-61779-921-1_9.

Ding, Mingjian, Li Shen, Liang Xiao, Xiaohui Liu, and Jianzhong Hu. 2021. “A Cell Line Development Strategy to Improve a Bispecific Antibody Expression Purity in CHO Cells.” *Biochemical Engineering Journal* 166 (November 2020): 107857. https://doi.org/10.1016/j.bej.2020.107857.

Dion, Michelle Z, Y John Wang, Daniel Bregante, Wayman Chan, Nisana Andersen, Amy Hilderbrand, Danielle Leiske, and Cleo M Salisbury. 2018. “The Use of a 2,2 ’-Azobis (2-Amidinopropane) Dihydrochloride Stress Model as an Indicator of Oxidation Susceptibility for Monoclonal Antibodies.” *Journal of Pharmaceutical Sciences* 107 (2): 550–58. https://doi.org/10.1016/j.xphs.2017.09.022.

Dong, Jia, Nicole Migliore, Steven J. Mehrman, John Cunningham, Michael J. Lewis, and Ping Hu. 2016. “High-Throughput, Automated Protein A Purification Platform with Multiattribute LC-MS Analysis for Advanced Cell Culture Process Monitoring.” *Analytical Chemistry* 88 (17): 8673–79. https://doi.org/10.1021/acs.analchem.6b01956.

Dotz, Viktoria, Rob Haselberg, Archana Shubhakar, Radoslaw P Kozak, David Falck, Yoann Rombouts, Dietmar Reusch, Govert W Somsen, Daryl L Fernandes, and Manfred Wuhrer. 2015. "Mass Spectrometry for Glycosylation Analysis of Biopharmaceuticals." *Trends in Analytical Chemistry* 73: 1–9. https://doi.org/10.1016/j.trac.2015.04.024.

Du, Yi, Alison Walsh, Robin Ehrick, Wei Xu, Kimberly May, Hongcheng Liu, Yi Du, et al. 2012. "Chromatographic Analysis of the Acidic and Basic Species of Recombinant Monoclonal Antibodies" 862 (5): 578–85. https://doi.org/10.4161/mabs.21328.

Du, Zhimei, David Treiber, Rebecca E. Mccoy, Amanda K. Miller, Mei Han, Feng He, Sarah Domnitz, Carole Heath, and Pranhitha Reddy. 2013. "Non-Invasive UPR Monitoring System and Its Applications in CHO Production Cultures." *Biotechnology and Bioengineering* 110 (8): 2184–94. https://doi.org/10.1002/bit.24877.

Duan, Guangyou, and Dirk Walther. 2015. "The Roles of Post-Translational Modifications in the Context of Protein Interaction Networks." *PLoS Computational Biology* 11 (2): 1–23. https://doi.org/10.1371/journal.pcbi.1004049.

Dumont, Jennifer, Don Euwart, Baisong Mei, Scott Estes, Rashmi Kshirsagar, Jennifer Dumont, Don Euwart, et al. 2015. "Human Cell Lines for Biopharmaceutical Manufacturing: History, Status, and Future Perspectives." *Critical Reviwes in Biotechnology* 36 (6): 1110–22. https://doi.org/10.3109/07388551.2015.1084266.

Dunn, Zachary D, Jayesh Desai, Gabriel M Leme, Dwight R Stoll, and Douglas D Richardson. 2020. "Rapid Two-Dimensional Protein-A Size Exclusion Chromatography of Monoclonal Antibodies for Titer and Aggregation Measurements from Harvested Cell Culture Fluid Samples." *MAbs* 12 (1): 1–11. https://doi.org/10.1080/19420862.2019.1702263.

Ebo, Jessica S, Nicolas Guthertz, Sheena E Radford, and David J Brockwell. 2020. "ScienceDirect Using Protein Engineering to Understand and Modulate Aggregation." *Current Opinion in Structural Biology* 60 (February): 157–66. https://doi.org/10.1016/j.sbi.2020.01.005.

Ecker, Dawn M, Susan Dana Jones, Howard L Levine, Dawn M Ecker, Susan Dana Jones, and Howard L Levine. 2015. "The Therapeutic Monoclonal Antibody Market." *MAbs* 7 (1): 9–14. https://doi.org/10.4161/19420862.2015.989042.

Egeness, Mari J, Michael C Breadmore, Emily F Hilder, Robert A Shellie, and Australian Centre. 2016. “The Modulator in Comprehensive Two- Dimensional Liquid Chromatography.” *LCGC Europe* 5 (May): 268−276.

Ehkirch, Anthony, Oscar Hernandez-Alba, Olivier Colas, Alain Beck, Davy Guillarme, and Sarah Cianférani. 2018. “Hyphenation of Size Exclusion Chromatography to Native Ion Mobility Mass Spectrometry for the Analytical Characterization of Therapeutic Antibodies and Related Products.” *Journal of Chromatography B* 1086 (June): 176–83. https://doi.org/10.1016/J.JCHROMB.2018.04.010.

Elich, Thomas, Elizabeth Goodrich, Herb Lutz, and Ushma Mehta. 2019. “Investigating the Combination of Single-Pass Tangential Flow Filtration and Anion Exchange Chromatography for Intensified MAb Polishing.” *Biotechnology Progress* 35 (5). https://doi.org/10.1002/btpr.2862.

Evans, James B., and Basharut A. Syed. 2014. “Next-Generation Antibodies.” *Nature Reviews Drug Discovery* 13 (6): 413–14. https://doi.org/10.1038/nrd4255.

Evans, Steven T., Kevin D. Stewart, Chris Afdahl, Rohan Patel, and Kelcy J. Newell. 2017a. “Optimization of a Micro-Scale, High Throughput Process Development Tool and the Demonstration of Comparable Process Performance and Product Quality with Biopharmaceutical Manufacturing Processes.” *Journal of Chromatography A* 1506: 73–81. https://doi.org/10.1016/j.chroma.2017.05.041.

Fanayan, Susan, Marina Hincapie, and William S Hancock. 2012. “Using Lectins to Harvest the Plasma/Serum Glycoproteome.” *Electrophoresis* 33 (March): 1746–54. https://doi.org/10.1002/elps.201100567.

Farsang, Evelin, Krisztián Horváth, Alain Beck, Qi Wang, Matthew Lauber, Davy Guillarme, and Szabolcs Fekete. 2020. “Impact of the Column on Effluent PH in Cation Exchange PH Gradient Chromatography, a Practical Study.” *Journal of Chromatography A* 1626 (June): 461350. https://doi.org/10.1016/j.chroma.2020.461350.

Farsang, Evelin, Amarande Murisier, Krisztián Horváth, Alain Beck, Róbert Kormány, Davy Guillarme, and Szabolcs Fekete. 2019. “Tuning Selectivity in Cation-Exchange Chromatography Applied for Monoclonal Antibody Separations , Part 1 : Alternative Mobile Phases and Fine Tuning of the Separation.” *Journal of Pharmaceutical and*

Biomedical Analysis 168 (2019): 138–47. https://doi.org/10.1016/j.jpba.2019.02.024.

FDA. 2004. "Pharmaceutical CGMPs for the 21s Century - A Risk-Based Approach." *Food and Drug Administration*. http://www.fda.gov/Drugs/DevelopmentApprovalProcess/Manufacturing/QuestionsandAnswersonCurrentGoodManufacturingPracticescGMPforDrugs/UCM071836.

Feidl, Fabian, Sebastian Vogg, Moritz Wolf, Matevz Podobnik, Caterina Ruggeri, Nicole Ulmer, Ruben Wälchli, et al. 2020. "Process-Wide Control and Automation of an Integrated Continuous Manufacturing Platform for Antibodies." *Biotechnology and Bioengineering* 117 (5): 1367–80. https://doi.org/10.1002/bit.27296.

Fekete, Szabolcs, Alain Beck, Jeno Fekete, and Davy Guillarme. 2015a. "Method Development for the Separation of Monoclonal Antibody Charge Variants in Cation Exchange Chromatography, Part I: Salt Gradient." *Journal of Pharmaceutical and Biomedical Analysis* 102 (September): 282–89. https://doi.org/10.1016/j.jpba.2014.09.032.

Fekete, Szabolcs, Alain Beck, and Davy Guillarme. 2015a. "Analysis Characterization of Cation Exchanger Stationary Phases Applied for the Separations of Therapeutic Monoclonal Antibodies." *Journal of Pharmaceutical and Biomedical Analysis* 111 (July): 169–76. https://doi.org/10.1016/j.jpba.2015.03.041.

Fekete, Szabolcs, Alain Beck, Jean Luc Veuthey, and Davy Guillarme. 2014. "Theory and Practice of Size Exclusion Chromatography for the Analysis of Protein Aggregates." *Journal of Pharmaceutical and Biomedical Analysis* 101: 161–73. https://doi.org/10.1016/j.jpba.2014.04.011.

Fekete, Szabolcs, Alexandre Goyon, Jean-luc Veuthey, and Davy Guillarme. 2018. "Size Exclusion Chromatography of Protein Biopharmaceuticals: Past , Present and Future." *American Pharmaceutical Review*.

Fekete, Szabolcs, Ganzler Katalin, and Davy Guillarme. 2013. "Critical Evaluation of Fast Size Exclusion Chromatographic Separations of Protein Aggregates, Applying Sub-2μm Particles." *Journal of Pharmaceutical and Biomedical Analysis* 78–79 (May): 14149. https://doi.org/https://doi.org/10.1016/j.jpba.2013.02.013.

Fenn, John B, Matrhias Mann, Chin K A I Meng, Shek Fu Wong, and Craig M Whitehouse. 1989. "Electrospray Ionization for Mass Spectrometry of Large Biomolecules." *Science*

246 (October): 64–70.

Fischer, Simon, René Handrick, and Kerstin Otte. 2015. “The Art of CHO Cell Engineering: A Comprehensive Retrospect and Future Perspectives.” *Biotechnology Advances* 33 (8): 1878–96. https://doi.org/10.1016/j.biotechadv.2015.10.015.

Floris, Patrick, Noemí Dorival-García, Graham Lewis, Graham Josland, Daniel Merriman, and Jonathan Bones. 2020. “Real-Time Characterization of Mammalian Cell Culture Bioprocesses by Magnetic Sector MS.” *Analytical Methods* 12 (46): 5601–12. https://doi.org/10.1039/d0ay01563f.

Fourn, Valérie Le, Pierre Alain Girod, Montse Buceta, Alexandre Regamey, and Nicolas Mermod. 2014. “CHO Cell Engineering to Prevent Polypeptide Aggregation and Improve Therapeutic Protein Secretion.” *Metabolic Engineering* 21: 91–102. https://doi.org/10.1016/j.ymben.2012.12.003.

Frye, Christopher, Rohini Deshpande, Scott Estes, Kathy Francissen, John Joly, Anthony Lubiniecki, Trent Munro, Reb Russell, Tongtong Wang, and Karin Anderson. 2016. “Industry View on the Relative Importance of ‘Clonality’ of Biopharmaceutical-Producing Cell Lines.” *Biologicals* 44 (2): 117–22. https://doi.org/10.1016/j.biologicals.2016.01.001.

Füssl, Florian, Ken Cook, Kai Sche, Amy Farrell, Stefan Mittermayr, and Jonathan Bones. 2018. “Charge Variant Analysis of Monoclonal Antibodies Using Direct Coupled PH Gradient Cation Exchange Chromatography to High- Resolution Native Mass Spectrometry.” *Analytical Chemistry* 90 (March): 4669−4676. https://doi.org/10.1021/acs.analchem.7b05241.

Füssl, Florian, Ken Cook, Kai Scheffler, Amy Farrell, Stefan Mittermayr, and Jonathan Bones. 2018. “Charge Variant Analysis of Monoclonal Antibodies Using Direct Coupled PH Gradient Cation Exchange Chromatography to High-Resolution Native Mass Spectrometry.” *Analytical Chemistry* 90 (7): 4669–76. https://doi.org/10.1021/acs.analchem.7b05241.

Füssl, Florian, Lisa Strasser, Sara Carillo, and Jonathan Bones. 2021. “Native LC – MS for Capturing Quality Attributes of Biopharmaceuticals on the Intact Protein Level.” *Current Opinion in Biotechnology* 71 (October): 32–40. https://doi.org/10.1016/j.copbio.2021.05.008.

Füssl, Florian, Anne Trappe, Sara Carillo, Craig Jakes, and Jonathan Bones. 2020. "Comparative Elucidation of Cetuximab Heterogeneity on the IntactProtein Level by Cation Exchange Chromatography and CapillaryElectrophoresis Coupled to Mass Spectrometry." *Analytical Chemistry* 92 (7): 5431–38.

Füssl, Florian, Anne Trappe, Ken Cook, Kai Scheffler, and Oliver Fitzgerald. 2019. "Comprehensive Characterisation of the Heterogeneity of Adalimumab via Charge Variant Analysis Hyphenated On-Line to Native High Resolution Orbitrap Mass Spectrometry." *MAbs* 11 (1): 116–28. https://doi.org/10.1080/19420862.2018.1531664.

Füssl, Florian, Anne Trappe, Ken Cook, Kai Scheffler, Oliver Fitzgerald, and Jonathan Bones. 2018. "Comprehensive Characterisation of the Heterogeneity of Adalimumab via Charge Variant Analysis Hyphenated On-Line to Native High Resolution Orbitrap Mass Spectrometry." *MAbs* 11 (1): 1–13. https://doi.org/10.1080/19420862.2018.1531664.

Galleguillos, Sarah N., David Ruckerbauer, Matthias P. Gerstl, Nicole Borth, Michael Hanscho, and Jürgen Zanghellini. 2017. "What Can Mathematical Modelling Say about CHO Metabolism and Protein Glycosylation?" *Computational and Structural Biotechnology Journal* 15 (January): 212–21. https://doi.org/10.1016/j.csbj.2017.01.005.

Gangadharan, Nishanthi, Richard Turner, Ray Field, Stephen G. Oliver, Nigel Slater, and Duygu Dikicioglu. 2019. "Metaheuristic Approaches in Biopharmaceutical Process Development Data Analysis." *Bioprocess and Biosystems Engineering* 42 (9): 1399–1408. https://doi.org/10.1007/s00449-019-02147-0.

Ganorkar, Saurabh B. 2017. "Design of Experiments in Liquid Chromatography (HPLC) Analysis of Pharmaceuticals: Analytics, Applications, Implications and Future Prospects." *Reviews in Analytical Chemistry* 36 (3): 1–43. https://doi.org/10.1515/revac-2016-0025.

Garripelli, Vivek Kumar, Zhen Wu, and Supriya Gupta. 2020. "Developability Assessment for Monoclonal Antibody Drug Candidates." *Pharmaceutical Development and Technology* 26 (1): 11–20.

Gaza-bulseco, Georgeen, Ashley Bulseco, Chris Chumsae, and Hongcheng Liu. 2008.

"Characterization of the Glycosylation State of a Recombinant Monoclonal Antibody Using Weak Cation Exchange Chromatography and Mass Spectrometry." *Journal of Chromatography B* 862 (December): 155–60. https://doi.org/10.1016/j.jchromb.2007.12.001.

Gerster, Anja, Ilse Villmann, Nico Verlinden, and Brian Gerwe. 2016. "High-Throughput Evaluation of Product Quality in Cell Line Generation and Upstream Process Development." *Application Note - PerkinElmer*.

Glassey, Jarka, Krist V Gernaey, Christoph Clemens, Torsten W Schulz, Rui Oliveira, Gerald Striedner, and Carl-Fredrik Mandenius. 2011. "Process Analytical Technology (PAT) for Biopharmaceuticals." *Biotechnology Journal* 6 (4): 369–77. https://doi.org/10.1002/biot.201000356.

Goldberg, Deborah S., Rachael A. Lewus, Reza Esfandiary, David C. Farkas, Neil Mody, Katrina J. Day, Priyanka Mallik, Malgorzata B. Tracka, Smita K. Sealey, and Hardeep S. Samra. 2017. "Utility of High Throughput Screening Techniques to Predict Stability of Monoclonal Antibody Formulations During Early Stage Development." *Journal of Pharmaceutical Sciences* 106 (8): 1971–77. https://doi.org/10.1016/j.xphs.2017.04.039.

Golovchenko, Nikolai P, Irina A Kataeva, and Vasily K Akimenko. 1992. "Analysis of PH-Dependent Filtration Medium Protein Interactions with Gel." *Journal of Chromatography* 591 (1–2): 121–28.

Gomez, Natalia, Hedieh Barkhordarian, Jonathan Lull, Joon Huh, Pavan GhattyVenkataKrishna, and Xin Zhang. 2019. "Perfusion CHO Cell Culture Applied to Lower Aggregation and Increase Volumetric Productivity for a Bispecific Recombinant Protein." *Journal of Biotechnology* 304 (October): 70–77.

Gomez, Natalia, Jonathan Lull, Xiaorui Yang, Yan Wang, Xin Zhang, Agatha Wieczorek, John Harrahy, et al. 2020. "Improving Product Quality and Productivity of Bispecific Molecules through the Application of Continuous Perfusion Principles." *Biotechnology Progress*, no. November 2019: 1–10. https://doi.org/10.1002/btpr.2973.

Gomez, Natalia, Jayashree Subramanian, Jun Ouyang, Mary D.H. Nguyen, Matthew Hutchinson, Vikas K. Sharma, Andy A. Lin, and Inn H. Yuk. 2012. "Culture Temperature Modulates Aggregation of Recombinant Antibody in Cho Cells."

Biotechnology and Bioengineering 109 (1): 125–36. https://doi.org/10.1002/bit.23288.

Goudar, Chetan, Kevin McFarland, and Michael Betenbaugh. 2018. "Editorial Overview: Latest Advances and Current Challenges in Biomanufacturing." *Current Opinion in Chemical Engineering* 22 (December): 1–3. https://doi.org/10.1016/j.coche.2018.12.002.

Goyon, Alexandre, Alain Beck, Olivier Colas, Koen Sandra, Davy Guillarme, and Szabolcs Fekete. 2017a. "Evaluation of Size Exclusion Chromatography Columns Packed with Sub-3 Mm Particles for the Analysis of Biopharmaceutical Proteins." *Journal of Chromatography A* 1498: 80–89. https://doi.org/10.1016/j.chroma.2016.11.056.

Goyon, Alexandre, Valentina D'Atri, Olivier Colas, Szabolcs Fekete, Alain Beck, and Davy Guillarme. 2017a. "Characterization of 30 Therapeutic Antibodies and Related Products by Size Exclusion Chromatography: Feasibility Assessment for Future Mass Spectrometry Hyphenation." *Journal of Chromatography B: Analytical Technologies in the Biomedical and Life Sciences* 1065–1066 (August): 35–43. https://doi.org/10.1016/j.jchromb.2017.09.027.

Goyon, Alexandre, Lu Dai, Tao Chen, Bingchuan Wei, Feng Yang, Nisana Andersen, Robert Kopf, et al. 2020. "From Proof of Concept to the Routine Use of an Automated and Robust Multi-Dimensional Liquid Chromatography Mass Spectrometry Workflow Applied for the Charge Variant Characterization of Therapeutic Antibodies." *Journal of Chromatography A* 1615: 460740. https://doi.org/10.1016/j.chroma.2019.460740.

Goyon, Alexandre, Melissa Exco, Marie-claire Janin-bussat, Balazs Bobaly, Szabolcs Fekete, Davy Guillarme, and Alain Beck. 2017c. "Determination of Isoelectric Points and Relative Charge Variants of 23 Therapeutic Monoclonal Antibodies" 1066 (September): 119–28. https://doi.org/10.1016/j.jchromb.2017.09.033.

Goyon, Alexandre, Szabolcs Fekete, Alain Beck, Jean Luc Veuthey, and Davy Guillarme. 2018. "Unraveling the Mysteries of Modern Size Exclusion Chromatography - the Way to Achieve Confident Characterization of Therapeutic Proteins." *Journal of Chromatography B* 1092 (June): 368–78. https://doi.org/10.1016/j.jchromb.2018.06.029.

Goyon, Alexandre, Luca Sciascera, Adrian Clarke, Davy Guillarme, and Reinhard Pell. 2018. "Extending the Limits of Size Exclusion Chromatography: Simultaneous

Separation of Free Payloads and Related Species from Antibody Drug Conjugates and Their Aggregates." *Journal of Chromatography A* 1539: 19–29. https://doi.org/10.1016/j.chroma.2018.01.039.

Graf, Tobias, Katrin Heinrich, Ingrid Grunert, Harald Wegele, Markus Haberger, Patrick Bulau, and Michael Leiss. 2020. "Recent Advances in LC–MS Based Characterization of Protein-Based Bio-Therapeutics – Mastering Analytical Challenges Posed by the Increasing Format Complexity." *Journal of Pharmaceutical and Biomedical Analysis2* 186 (July): 113251.

Graham, Ryan J., Hemlata Bhatia, and Seongkyu Yoon. 2019a. "Consequences of Trace Metal Variability and Supplementation on Chinese Hamster Ovary (CHO) Cell Culture Performance: A Review of Key Mechanisms and Considerations." *Biotechnology and Bioengineering* 116 (12): 3446–56. https://doi.org/10.1002/bit.27140.

Graham, Ryan J, Hemlata Bhatia, and Seongkyu Yoon. 2019b. "Consequences of Trace Metal Variability and Supplementation on Chinese Hamster Ovary (CHO) Cell Culture Performance : A Review of Key Mechanisms and Considerations." *Biotechnology and Bioengineering* 116 (12): 3446–56. https://doi.org/10.1002/bit.27140.

Grainger, Rhian K., and David C. James. 2013. "CHO Cell Line Specific Prediction and Control of Recombinant Monoclonal Antibody N-Glycosylation." *Biotechnology and Bioengineering* 110 (11): 2970–83. https://doi.org/10.1002/bit.24959.

Gramer, Michael J., Jackie J. Eckblad, Ruth Donahue, Joseph Brown, Carrie Shultz, Kent Vickerman, Patrick Priem, Ewald T.J. van den Bremer, Jolanda Gerritsen, and Patrick H.C. van Berkel. 2011. "Modulation of Antibody Galactosylation through Feeding of Uridine, Manganese Chloride, and Galactose." *Biotechnology and Bioengineering* 108 (7): 1591–1602. https://doi.org/10.1002/bit.23075.

Greer, Eric L., and Yang Shi. 2012. "Histone Methylation: A Dynamic Mark in Health, Disease and Inheritance." *Nature Reviews Genetics* 13 (5): 343–57. https://doi.org/10.1038/nrg3173.

Gronemeyer, Petra, Reinhard Ditz, and Jochen Strube. 2014. "Trends in Upstream and Downstream Process Development for Antibody Manufacturing." *Bioengineering* 1 (4): 188–212. https://doi.org/10.3390/bioengineering1040188.

Gstöttner, Christoph, Denis Klemm, Markus Haberger, Anja Bathke, Harald Wegele, Christian Bell, and Robert Kopf. 2018. “Fast and Automated Characterization of Antibody Variants with 4D HPLC/MS.” *Analytical Chemistry* 90 (3): 2119–25. https://doi.org/10.1021/acs.analchem.7b04372.

Guerra, André, Moritz von Stosch, and Jarka Glassey. 2019. “Toward Biotherapeutic Product Real-Time Quality Monitoring.” *Critical Reviews in Biotechnology* 39 (3): 289–305. https://doi.org/10.1080/07388551.2018.1524362.

Guillarme, Davy, Szabolcs Fekete, and Alain Beck. 2015. “Method Development for the Separation of Monoclonal Antibody Charge Variants in Cation Exchange Chromatography , Part II : PH Gradient Approach.” *Journal of Pharmaceutical and Biomedical Analysis* 102 (2015): 282–89. https://doi.org/10.1016/j.jpba.2014.09.032.

Guttman, Miklos, Neal N. Padte, Yaoxing Huang, Jian Yu, Gabriel J. Rocklin, Brian D. Weitzner, Michele Scian, David D. Ho, and Kelly K. Lee. 2020. “The Influence of Proline Isomerization on Potency and Stability of Anti-HIV Antibody 10E8.” *Scientific Reports* 10 (August): 14313.

Haberger, Markus, Anna-katharina Heidenreich, Michaela Hook, Ju Fichtl, Rainer Lang, Florian Cymer, Mahdi Adibzadeh, et al. 2021. “Multiattribute Monitoring of Antibody Charge Variants by Cation- Exchange Chromatography Coupled to Native Mass Spectrometry.” *Jounal of the American Society for Mass Spectrometry* 32 (4): 832–1141. https://doi.org/https://dx.doi.org/10.1021/jasms.0c00446.

Hailong Liu, Weicheng Ren, Li Zong, Jinliang Zhang, Yingwu Wang. 2019. “Characterization of Recombinant Monoclonal Antibody Charge Variants Using WCX Chromatography, IcIEF and LC/MS.” *Analytical Biochemistry* 564–565 (January): 1–12.

Hajba, Laszlo, Eszter Csanky, and Andras Guttman. 2016. “Liquid Phase Separation Methods for N-Glycosylation Analysis of Glycoproteins of Biomedical and Biopharmaceutical Interest. A Critical Review.” *Analytica Chimica Acta* 943 (August): 8–16. https://doi.org/10.1016/j.aca.2016.08.035.

Ham, Renske M T, Jarno Hoekman, Anke M Hövels, Andre W Broekmans, Hubert G M Leufkens, and Olaf H Klungel. 2018. “Challenges in Advanced Therapy Medicinal Product Development : A Survey among Companies in Europe.” *Molecular Therapy:*

Methods & Clinical Development 11 (December): 121–30. https://doi.org/10.1016/j.omtm.2018.10.003.

Hansen, Henning Gram, Nuša Pristovšek, Helene Faustrup Kildegaard, and Gyun Min Lee. 2017. "Improving the Secretory Capacity of Chinese Hamster Ovary Cells by Ectopic Expression of Effector Genes: Lessons Learned and Future Directions." *Biotechnology Advances* 35 (1): 64–76. https://doi.org/10.1016/j.biotechadv.2016.11.008.

Havenga, MJ, L Holterman, and I Melis. 2008. "Free Transient Protein Production System Based on Adenoviral Vector and PER.C6 Technology: High Yield and Preserved Bioactivity." *Biotechnolgy and BioengineeringBioeng* 100 (2): 273–283. https://doi.org/10.1002/bit.21757.

Hemmerich, Johannes, Stephan Noack, Wolfgang Wiechert, and Marco Oldiges. 2018. "Microbioreactor Systems for Accelerated Bioprocess Development." *Biotechnology Journal* 13 (4): 1–9. https://doi.org/10.1002/biot.201700141.

Hernandez, By Randi. 2015. "Top Trends in Biopharmaceutical Manufacturing: 2015." *Pharmaceutical Technology* 39 (6): 1–4.

Herring, Chris, Jennifer Ji, and Claudia Richter. 2019. "A Novel Microchip-Based Imaged CIEF-MS System for Comprehensive Characterization and Identification of Biopharmaceutical." *Electrophoresis* 40 (23–24): 3084–91. https://doi.org/10.1002/elps.201900325.

Herring, Chris, and Claudia Richter. 2019. "A Novel Microchip - Based Imaged CIEF - MS System for Comprehensive Characterization and Identification of Biopharmaceutical Charge Variants A Novel Microchip-Based Imaged CIEF-MS System for Comprehensive Characterization and Identification of Biopharmace." *Electrophoresis* 40 (23–24): 3084–91. https://doi.org/10.1002/elps.201900325.

Higel, Fabian, Andreas Seidl, Fritz Sörgel, and Wolfgang Friess. 2016. "N-Glycosylation Heterogeneity and the Influence on Structure, Function and Pharmacokinetics of Monoclonal Antibodies and Fc Fusion Proteins." *European Journal of Pharmaceutics and Biopharmaceutics* 100 (January): 94–100. https://doi.org/10.1016/j.ejpb.2016.01.005.

Ho, Steven C.L., Esther Y.C. Koh, Miranda van Beers, Monika Mueller, Corrine Wan, Gavin Teo, Zhiwei Song, Yen Wah Tong, Muriel Bardor, and Yuansheng Yang. 2013.

"Control of IgG LC: HC Ratio in Stably Transfected CHO Cells and Study of the Impact on Expression, Aggregation, Glycosylation and Conformational Stability." *Journal of Biotechnology* 165 (3–4): 157–66. https://doi.org/10.1016/j.jbiotec.2013.03.019.

Hong, Jong Kwang, Meiyappan Lakshmanan, Chetan Goudar, and Dong Yup Lee. 2018. "Towards next Generation CHO Cell Line Development and Engineering by Systems Approaches." *Current Opinion in Chemical Engineering* 22 (December): 1–10. https://doi.org/10.1016/j.coche.2018.08.002.

Hong, Jong Kwang, Hock Chuan Yeo, Meiyappan Lakshmanan, Sung hyuk Han, Hyun Myoung Cha, Muri Han, and Dong Yup Lee. 2020. "In Silico Model-Based Characterization of Metabolic Response to Harsh Sparging Stress in Fed-Batch CHO Cell Cultures." *Journal of Biotechnology* 308 (November): 10–20. https://doi.org/10.1016/j.jbiotec.2019.11.011.

Hong, Paula, Stephan Koza, and Edouard S.P. Bouvier. 2012. "Size-Exclusion Chromatography for the Analysis of Protein Biotherapeutics and Their Aggregates." *Journal of Liquid Chromatography and Related Technologies* 35 (20): 2923–50. https://doi.org/10.1080/10826076.2012.743724.

Hu, Wei-Shou. 2020. *Cell Culture Bioprocess Engineering*. Second Edi. Taylor & Francis Group. https://lccn.loc.gov/2019047452.

Hu, Wei Shou, Gargi Seth, Sadettin Ozturk, and Chun Zhang. 2012. *Cell Culture Bioprocess Engineering*. *PhD Proposal*. Minneapolis: University of Minnesota. https://doi.org/10.1017/CBO9781107415324.004.

Hu, Zhilan, Danming Tang, Shahram Misaghi, Guoying Jiang, Christopher Yu, Mandy Yim, David Shaw, Brad Snedecor, Michael W. Laird, and Amy Shen. 2017. "Evaluation of Heavy Chain C-Terminal Deletions on Productivity and Product Quality of Monoclonal Antibodies in Chinese Hamster Ovary (CHO) Cells." *Biotechnology Progress* 33 (3): 786–94. https://doi.org/10.1002/btpr.2444.

Huang, Yao-ming, Weiwei Hu, Eddie Rustandi, Kevin Chang, Helena Yusuf-makagiansar, and Thomas Ryll. 2010. "Maximizing Productivity of CHO Cell-Based Fed-Batch Culture Using Chemically Defined Media Conditions and Typical Manufacturing Equipment." *Analytical Chemistry* 26 (5): 1400–1410.

https://doi.org/10.1002/btpr.436.

Ibrahim, Thiago, Claudia A S Araujo, Thiago Ibrahim, and Claudia A S Araujo. 2021. "Biopharmaceutical Supply Chain Challenges in Developing Countries: An Exploratory Analysis Exploratory Analysis." *Supply Chain Forum: An International Journal* 22 (2): 1–16. https://doi.org/10.1080/16258312.2021.1936152.

ICH-Q8(R2). 2009. "ICH Guideline Q8 (R2) on Pharmaceutical Development EMA/CHMP/ICH/167068/2004." https://www.ema.europa.eu/en/documents/scientific-guideline/international-conference-harmonisation-technical-requirements-registration-pharmaceuticals-human-use_en-11.pdf.

ICH. 2009. "Pharmaceutical Development Q8." *ICH Harmonised Tripartite Guideline* Q8 (R2): 1–28.

Isett, Kevin, Hugh George, Wayne Herber, and Ashraf Amanullah. 2007. "Twenty-Four-Well Plate Miniature Bioreactor High-Throughput System: Assessment for Microbial Cultivations." *Biotechnolgy and Bioengineering* 98 (5): 1017–28. https://doi.org/10.1002/bit.

Jaag, Simon, Marina Shirokikh, and Michael Lämmerhofer. 2021a. "Charge Variant Analysis of Protein-Based Biopharmaceuticals Using Two-Dimensional Liquid Chromatography Hyphenated to Mass Spectrometry." *Journal of Chromatography A* 1636 (December): 461786.

Jameel, Feroz, John W Skoug, and Robert R Nesbitt. 2020. *Development of Biopharmaceutical Drug-Device Products*. Vol. 35. Cham, Switzerland: AAPS Advances in the Pharmaceutical Sciences. https://doi.org/10.1007/978-3-030-31415-6.

Jansen, Bas Cornelis, Lise Hafkenscheid, Albert Bondt, Richard Andrew Gardner, Jenifer Lynn Hendel, Manfred Wuhrer, and Daniel Ian Richard Spencer. 2018. "HappyTools: A Software for High-Throughput HPLC Data Processing and Quantitation." *PLoS ONE* 13 (7): 1–14. https://doi.org/10.1371/journal.pone.0200280.

Jarasch, Alexander, Hans Koll, Joerg T. Regula, Martin Bader, Apollon Papadimitriou, and Hubert Kettenberger. 2015. "Developability Assessment during the Selection of Novel Therapeutic Antibodies." *Journal of Pharmaceutical Sciences* 104 (6): 1885–98. https://doi.org/10.1002/jps.24430.

Jefferis, Roy. 2012a. “Isotype and Glycoform Selection for Antibody Therapeutics.” *Archives of Biochemistry and Biophysics* 526 (2): 159–66. https://doi.org/10.1016/j.abb.2012.03.021.

Jesus, Maria J. De, Philippe Girard, Michaela Bourgeois, Gwendoline Baumgartner, Barbara Jacko, Hanspeter Amstutz, and Florian M. Wurm. 2004. “TubeSpin Satellites: A Fast Track Approach for Process Development with Animal Cells Using Shaking Technology.” *Biochemical Engineering Journal* 17 (3): 217–23. https://doi.org/10.1016/S1369-703X(03)00180-3.

Jiang, Hanxiao, Andrew A Horwitz, Chapman Wright, Anna Tai, Elizabeth A Znameroski, Benjamin S Bower, Darren Platt, et al. 2019. “Challenging the Workhorse: Comparative Analysis of Eukaryotic Micro-Organisms for Expressing Monoclonal Antibodies.” *Biotechnology and Bioengineering* 116 (November): 1449–62. https://doi.org/10.1002/bit.26951.

Jing, Ying, Michael Borys, Samiksha Nayak, Susan Egan, Yueming Qian, Shih Hsie Pan, and Zheng Jian Li. 2012a. “Identification of Cell Culture Conditions to Control Protein Aggregation of IgG Fusion Proteins Expressed in Chinese Hamster Ovary Cells.” *Process Biochemistry* 47 (1): 69–75. https://doi.org/10.1016/j.procbio.2011.10.009.

Joelsson, Daniel, Phil Moravec, Matthew Troutman, Joseph Pigeon, and Pete DePhillips. 2008. “Optimizing ELISAs for Precision and Robustness Using Laboratory Automation and Statistical Design of Experiments.” *Journal of Immunological Methods* 337 (1): 35–41. https://doi.org/10.1016/j.jim.2008.05.012.

Johari, Yusuf B;, Scott D.; Estes, S. Christina; Alves, S. Marty Sinacore, and David C. James. 2015. “Integrated Cell and Process Engineering for Improved Transient Production of a ‘‘ Difficult-to-Express ‘‘ Fusion Protein by CHO Cells.” *Biotechnolgy and Bioengineering* 112 (12): 2527–42. https://doi.org/10.1002/bit.25687.

Jonnalagadda, Kanvasri N., Lam Raga A. Markely, Bing Guan, Christina Alves, and Shashi Prajapati. 2016. “High-Throughput Sialylation Measurement Using Lectins on an Octet Platform for Clone Screening.” *Analytical Methods* 8 (39): 7193–98. https://doi.org/10.1039/c6ay01703g.

Joshi, Varsha, Vijesh Kumar, and Anurag S. Rathore. 2015. “Rapid Analysis of Charge Variants of Monoclonal Antibodies Using Non-Linear Salt Gradient in Cation-

Exchange High Performance Liquid Chromatography." *Journal of Chromatography A* 1406 (June): 175–85. https://doi.org/10.1016/j.chroma.2015.06.015.

Joshi, Varsha S, Vijesh Kumar, and Anurag S Rathore. 2017. "Optimization of Ion Exchange Sigmoidal Gradients Using Hybrid Models : Implementation of Quality by Design in Analytical Method Development." *Journal of Chromatography A* 1491 (March): 145–52. https://doi.org/10.1016/j.chroma.2017.02.058.

Kahle, Julia, and W Hermann. 2018. "Determination of Protein Charge Variants with (Imaged) Capillary Isoelectric Focusing and Capillary Zone Electrophoresis." *Electrophoresis* 39 (20): 2492–2511. https://doi.org/10.1002/elps.201800079.

Kallamvalliillam, Praveen, Pradeep G Kabadi, Chethan Gejjalagere, Malini Subbarao, Harish V Pai, Laxmi Adhikary, and Dinesh V Palanivelu. 2018. "Identification and Quantification of Product-Related Quality Attributes in Bio- Therapeutic Monoclonal Antibody via a Simple , and Robust Cation-Exchange HPLC Method Compatible with Direct Online Detection of UV and Native ESI- QTOF-MS Analysis." *Journal of Chromatography B* 1102–1103 (July): 83–95. https://doi.org/10.1016/j.jchromb.2018.10.019.

Kaplon, Hélène, Mrinalini Muralidharan, Zita Schneider, Janice M Reichert, Hélène Kaplon, Mrinalini Muralidharan, Zita Schneider, et al. 2020. "Antibodies to Watch in 2020." *MAbs* 12 (1): 1–24. https://doi.org/10.1080/19420862.2019.1703531.

Keser, Toma, Tamara Pavic, Gordan Lauc, and Olga Gornik. 2018. "Comparison of 2-Aminobenzamide, Procainamide and RapiFluor-MS as Derivatizing Agents for High-Throughput HILIC-UPLC-FLR-MS N-Glycan Analysis." *Frontiers in Chemistry* 6 (July): 1–12. https://doi.org/10.3389/fchem.2018.00324.

Kesik-brodacka, Malgorzata. 2018. "Progress in Biopharmaceutical Development." *Biotechnology and Applied Biochemistry* 65 (3): 306–22. https://doi.org/10.1002/bab.1617.

Khan, Suliman, Muhammad Wajid Ullah, Rabeea Siddique, Ghulam Nabi, Sehrish Manan, Muhammad Yousaf, and Hongwei Hou. 2016. "Role of Recombinant DNA Technology to Improve Life." *International Journal of Genomics* 2016 (December): 2405954. https://doi.org/10.1155/2016/2405954.

Kimzey, Michael, Zoltan Szabo, Vaishali Sharma, Alexander Gyenes, Samnang Tep, Adele

Taylor, Aled Jones, Justin Hyche, Ted Haxo, and Sergey Vlasenko. 2015. "Development of an Instant Glycan Labeling Dye for High Throughput Analysis by Mass Spectrometry." *ProZyme Technical Note*. https://www.europa-bioproducts.com/pdf/IPC_Glycan-Labeling- Dye-2015_handout_v3_r2.pdf.

Kiss, Bob, and Uwe Gottschalk. 2018. *New Bioprocessing Strategies: Development and Manufacturing of Recombinant Antibodies and Proteins*. Edited by Bob Kiss, Uwe Gottschalk, and Michael Pohlscheidt. Cham, Switzerland: Springer International Publishing AG. https://doi.org/10.1007/978-3-319-97110-0.

Ko, Peggy, Shahram Misaghi, Zhilan Hu, Dejin Zhan, Joni Tsukuda, Mandy Yim, Mark Sanford, et al. 2018. "Probing the Importance of Clonality: Single Cell Subcloning of Clonally Derived CHO Cell Lines Yields Widely Diverse Clones Differing in Growth, Productivity, and Product Quality." *Biotechnology Progress* 34 (3): 624–34. https://doi.org/10.1002/btpr.2594.

Kober, Lars, Christoph Zehe, and Juergen Bode. 2012. "Development of a Novel Er Stress Based Selection System for the Isolation of Highly Productive Clones." *Biotechnology and Bioengineering* 109 (10): 2599–2611. https://doi.org/10.1002/bit.24527.

Koen, Sandra, Mieke Steenbeke, Isabel Vandenheede, Gerd Vanhoenacker, and Sandra Pat. 2017. "The Versatility of Heart-Cutting and Comprehensive Two-Dimensional Liquid Chromatography in Monoclonal Antibody Clone Selection." *Journal of Chromatography A* 1523 (June): 283–92. https://doi.org/10.1016/j.chroma.2017.06.052.

Koen, Sandra, Isabel Vandenheede, and Sandra Pat. 2014. "Modern Chromatographic and Mass Spectrometric Techniques for Protein Biopharmaceutical Characterization." *Journal of Chromatography A* 1335 (December): 81–103. https://doi.org/10.1016/j.chroma.2013.11.057.

Konstantinidis, Spyridon, Simyee Kong, and Nigel Titchener-Hooker. 2013. "Identifying Analytics for High Throughput Bioprocess Development Studies." *Biotechnology and Bioengineering* 110 (7): 1924–35. https://doi.org/10.1002/bit.24850.

Kontermann, Roland E., and Ulrich Brinkmann. 2015. "Bispecific Antibodies." *Drug Discovery Today* 20 (7): 838–47. https://doi.org/10.1016/j.drudis.2015.02.008.

Krishnamurthy, Anuradha, and Antonio Jimeno. 2018. "Bispecific Antibodies for Cancer

Therapy: A Review." *Pharmacology and Therapeutics* 185 (December): 122–34. https://doi.org/10.1016/j.pharmthera.2017.12.002.

Kroll, Paul, Alexandra Hofer, Sophia Ulonska, Julian Kager, and Christoph Herwig. 2017. "Model-Based Methods in the Biopharmaceutical Process Lifecycle." *Pharmaceutical Research* 34 (12): 2596–2613. https://doi.org/10.1007/s11095-017-2308-y.

Kumar, Kotta Kranthi. 2019. "Importance of Critical Quality Attributes in Biopharmaceuticals Development" 10 (June): 29–33. https://doi.org/10.5958/2321-5844.2019.00007.4.

Kumar, Prafulla, Nageswara Rao, Teresa Cecchi, Suryakanta Swain, Chandra Sekhar, and Jagadeesh Panda. 2018. "An Overview of Experimental Designs in HPLC Method Development and Validation." *Journal of Pharmaceutical and Biomedical Analysis* 147 (May): 590–611. https://doi.org/10.1016/j.jpba.2017.05.006.

Kumar, Vijesh, Samuel Leweke, Eric von Lieres, and Anurag S. Rathore. 2015. "Mechanistic Modeling of Ion-Exchange Process Chromatography of Charge Variants of Monoclonal Antibody Products." *Journal of Chromatography A* 1426 (November): 140–53. https://doi.org/10.1016/j.chroma.2015.11.062.

Kuo, Chih-Chung, Austin WT Chiang, Isaac Shamie, Mojtaba Samoudi, Jahir M Gutierrez, and Nathan E Lewis. 2018. "The Emerging Role of Systems Biology for Engineering Protein Production in CHO Cells." *Current Opinion in Biotechnology* 51: 64–69. https://doi.org/10.1016/j.copbio.2017.11.015.

Kuo, Chih Chung, Austin WT Chiang, Isaac Shamie, Mojtaba Samoudi, Jahir M. Gutierrez, and Nathan E. Lewis. 2018. "The Emerging Role of Systems Biology for Engineering Protein Production in CHO Cells." *Current Opinion in Biotechnology* 51 (December): 64–69. https://doi.org/10.1016/j.copbio.2017.11.015.

Kuriakose, Anshu, Narendra Chirmule, and Pradip Nair. 2016. "Immunogenicity of Biotherapeutics: Causes and Association with Posttranslational Modifications." *Journal of Immunology Research* 2016 (June): 1298473. https://doi.org/10.1155/2016/1298473.

Łącki, Karol M. 2014a. "High Throughput Process Development in Biomanufacturing." *Current Opinion in Chemical Engineering* 6: 25–32. https://doi.org/10.1016/j.coche.2014.08.004.

———. 2014b. “High Throughput Process Development in Biomanufacturing.” *Current Opinion in Chemical Engineering* 6 (September): 25–32. https://doi.org/10.1016/j.coche.2014.08.004.

Lai, Pin-kuang, Amendra Fernando, Theresa K Cloutier, Jonathan S Kingsbury, Yatin Gokarn, Kevin T Halloran, Cesar Calero-rubio, and Bernhardt L Trout. 2021. “Machine Learning Feature Selection for Predicting High Concentration Therapeutic Antibody Aggregation.” *Journal of Pharmaceutical Sciences* 110 (December): 1583–91.

Lakbub, Jude C., Joshua T. Shipman, and Heather Desaire. 2018. “Recent Mass Spectrometry-Based Techniques and Considerations for Disulfide Bond Characterization in Proteins.” *Analytical and Bioanalytical Chemistry* 410 (10): 2467–84. https://doi.org/10.1007/s00216-017-0772-1.

Lalonde, Marie Eve, and Yves Durocher. 2017. “Therapeutic Glycoprotein Production in Mammalian Cells.” *Journal of Biotechnology* 251 (April): 128–40. https://doi.org/10.1016/j.jbiotec.2017.04.028.

Lamping, S. R., H. Zhang, B. Allen, and P. Ayazi Shamlou. 2003. “Design of a Prototype Miniature Bioreactor for High Throughput Automated Bioprocessing.” *Chemical Engineering Science* 58 (3–6): 747–58. https://doi.org/10.1016/S0009-2509(02)00604-8.

Lanter, Carolina, Malka Lev, Li Cao, and Vakhtang Loladze. 2020. “Rapid Intact Mass Based Multi-Attribute Method in Support of MAb Upstream Process Development.” *Journal of Biotechnology* 314–315 (May): 63–70. https://doi.org/10.1016/j.jbiotec.2020.04.001.

Lauer, Timothy M., Neeraj J. Agrawal, Naresh Chennamsetty, Kamal Egodage, Bernhard Helk, and Bernhardt L. Trout. 2011. “Developability Index: A Rapid in Silico Tool for the Screening of Antibody Aggregation Propensity.” *Journal of Pharmaceutical Sciences* 101 (1): 102–15. https://onlinelibrary.wiley.com/doi/10.1002/jps.22758.

Lazar, Iulia M. 2011. “Recent Advances in the MS Analysis of Glycoproteins : Capillary and Microfluidic Workflows.” *Electrophoresis* 32 (1): 14–29. https://doi.org/10.1002/elps.201000394.

LeBasle, Yoann, Philip Chennell, Nicolas Tokhadze, Alain Astier, and Valerie Sautou. 2020. “Physicochemical Stability of Monoclonal Antibodies: A Review.” *Journal of*

Pharmaceutical Sciences 109 (August): 169–90. https://doi.org/10.1016/j.xphs.2019.08.009.

Leblanc, Y., C. Ramon, N. Bihoreau, and G. Chevreux. 2017. "Charge Variants Characterization of a Monoclonal Antibody by Ion Exchange Chromatography Coupled On-Line to Native Mass Spectrometry: Case Study after a Long-Term Storage at +5 °C." *Journal of Chromatography B: Analytical Technologies in the Biomedical and Life Sciences* 1048 (February): 130–39. https://doi.org/10.1016/j.jchromb.2017.02.017.

Leblanc, Y, N Bihoreau, M Jube, M Andre, Z Tellier, and G Chevreux. 2016. "European Journal of Pharmaceutics and Biopharmaceutics Glycation of Polyclonal IgGs : Effect of Sugar Excipients during Stability Studies." *EUROPEAN JOURNAL OF PHARMACEUTICS AND BIOPHARMACEUTICS* 102 (May): 185–90. https://doi.org/10.1016/j.ejpb.2016.03.016.

Legmann, Rachel, H. Brett Schreyer, Rodney G. Combs, Ellen L. McCormick, A. Peter Russo, and Seth T. Rodgers. 2009. "A Predictive High-Throughput Scale-down Model of Monoclonal Antibody Production in CHO Cells." *Biotechnology and Bioengineering* 104 (6): 1107–20. https://doi.org/10.1002/bit.22474.

Lemmerer, Martin, Anne Serdakowski London, Alexandra Panicucci, Cristina Gutierrez-Vargas, Michael Lihon, and Philippe Dreier. 2013. "Coupled Affinity and Sizing Chromatography: A Novel in-Process Analytical Tool to Measure Titer and Trend Fc-Protein Aggregation." *Journal of Immunological Methods* 393 (1–2): 81–85. https://doi.org/10.1016/j.jim.2013.04.008.

Leoz, Maria Lorna A De, David L Duewer, Adam Fung, Lily Liu, Hoi Kei Yau, Oscar Potter, Gregory O Staples, et al. 2020. "NIST Interlaboratory Study on Glycosylation Analysis of Monoclonal Antibodies : Comparison of Authors NIST Interlaboratory Study on Glycosylation Analysis of Monoclonal Antibodies : Comparison of Results from Diverse Analytical Methods * □." *Molecular & Cellular Proteomics* 19 (January): 11–30.

Leweke, Samuel, and Eric von Lieres. 2018. "Chromatography Analysis and Design Toolkit (CADET)." *Computers and Chemical Engineering* 113: 274–94. https://doi.org/10.1016/j.compchemeng.2018.02.025.

Lewis, Nathan E., Xin Liu, Yuxiang Li, Harish Nagarajan, George Yerganian, Edward O'Brien, Aarash Bordbar, et al. 2013. "Genomic Landscapes of Chinese Hamster Ovary Cell Lines as Revealed by the Cricetulus Griseus Draft Genome." *Nature Biotechnology* 31 (8): 759–67. https://doi.org/10.1038/nbt.2624.

Lim, Lisa P L, Elizabeth Garnsey, Mike Gregory, Lisa P L Lim, Elizabeth Garnsey, and Mike Gregory. 2006. "Product and Process Innovation in Biopharmaceuticals : A New Perspective on Development." *R&D Management* 36 (1): 27–36.

Liu, Fan, Bas Van Breukelen, and Albert J R Heck. 2014. "Facilitating Protein Disulfide Mapping by a Combination of Pepsin Digestion , Electron Transfer Higher Energy Dissociation (EThcD), and a Dedicated Search Algorithm SlinkS * □." *Molecular & Cellular Proteomics* 13 (10): 2776–2786. https://doi.org/10.1074/mcp.O114.039057.

Liu, Hongcheng, and Kimberly May. 2012. "Disulfide Bond Structures of IgG Molecules: Structural Variations, Chemical Modifications and Possible Impacts to Stability and Biological Function." *MAbs* 4 (1): 17–23. https://doi.org/10.4161/mabs.4.1.18347.

Liu, Hongcheng, Gomathinayagam Ponniah, Hui-min Zhang, Alyssa Neill, Nidia Gonzalez-lopez, Rekha Patel, Guilong Cheng, et al. 2014. "In Vitro and in Vivo Modifications of Recombinant and Human IgG Antibodies In Vitro and in Vivo Modi Fi Cations of Recombinant and Human IgG Antibodies." *MAbs* 6 (5): 1145–54. https://doi.org/10.4161/mabs.29883.

Liu, Liming. 2015a. "Antibody Glycosylation and Its Impact on the Pharmacokinetics and Pharmacodynamics of Monoclonal Antibodies and Fc-Fusion Proteins." *Journal of Pharmaceutical Sciences* 104 (6): 1866–84. https://doi.org/10.1002/jps.24444.

Liu, Peiran, Richard Ludwig, and Anthony M Leone. 2019. "Subunit Mass Analysis for Monitoring Multiple Attributes of Monoclonal Antibodies." *Rapid Communications in Mass Spectrometry* 33 (August 2018): 31–40. https://doi.org/10.1002/rcm.8301.

Liu, Songsong, Spyridon Gerontas, David Gruber, Richard Turner, Nigel J. Titchener-Hooker, and Lazaros G. Papageorgiou. 2017. "Optimization-Based Framework for Resin Selection Strategies in Biopharmaceutical Purification Process Development." *Biotechnology Progress* 33 (4): 1116–26. https://doi.org/10.1002/btpr.2479.

Lonardo, Amedeo, and Enrica Baldelli. 2020. "Methodological Tools for Exploring Novel Biopharmaceutical Approaches to the Metabolic Syndrome and Related Disorders."

Diabetes Therapy 11 (4): 773–77. https://doi.org/10.1007/s13300-020-00794-1.

Lu, Ruei-min, Yu-chyi Hwang, I-ju Liu, Chi-chiu Lee, Han-zen Tsai, Hsin-jung Li, and Han-chung Wu. 2020. "Development of Therapeutic Antibodies for the Treatment of Diseases." *Journal of Biomedical Science* 27 (1): 1–30.

Lumley, James A., Gary Sharman, Thomas Wilkin, Matthew Hirst, Carlos Cobas, and Michael Goebel. 2020. "A KNIME Workflow for Automated Structure Verification." *SLAS Discovery* 25 (8): 950–56. https://doi.org/10.1177/2472555220907091.

Luo, Hao, Wendy Zhong, Jiong Yang, Ping Zhuang, Fanyu Meng, John Caldwell, Bing Mao, and Christopher J. Welch. 2017. "2D-LC as an on-Line Desalting Tool Allowing Peptide Identification Directly from MS Unfriendly HPLC Methods." *Journal of Pharmaceutical and Biomedical Analysis* 137 (April): 139–45.

Luo, Quanzhou, Marisa K. Joubert, Riki Stevenson, Randal R. Ketchem, Linda O. Narhi, and Jette Wypych. 2011. "Chemical Modifications in Therapeutic Protein Aggregates Generated under Different Stress Conditions." *Journal of Biological Chemistry* 286 (28): 25134–44. https://doi.org/10.1074/jbc.M110.160440.

Ma, Fengfei, Fahimeh Raoufi, Marc Andre Bailly, and Laurence Fayadat-dilman. 2020. "Hyphenation of Strong Cation Exchange Chromatography to Native Mass Spectrometry for High Throughput Online Characterization of Charge Heterogeneity of Therapeutic Monoclonal Antibodies." *MAbs* 12 (1): 1–25. https://doi.org/10.1080/19420862.2020.1763762.

Madadkar, Pedram, Umatheny Umatheva, Geoff Hale, Yves Durocher, and Raja Ghosh. 2017. "Ultrafast Separation and Analysis of Monoclonal Antibody Aggregates Using Membrane Chromatography." *Analytical Chemistry* 89 (8): 4716–20. https://doi.org/10.1021/acs.analchem.7b00580.

Malphettes, Laetitia, Yevgeniy Freyvert, Jennifer Chang, Pei Qi Liu, Edmond Chan, Jeffrey C. Miller, Zhe Zhou, et al. 2010. "Highly Efficient Deletion of FUT8 in CHO Cell Lines Using Zinc-Finger Nucleases Yields Cells That Produce Completely Nonfucosylated Antibodies." *Biotechnology and Bioengineering* 106 (5): 774–83. https://doi.org/10.1002/bit.22751.

Manahan, Matthew, Michael Nelson, Jonathan J. Cacciatore, Jessica Weng, Sen Xu, and Jennifer Pollard. 2019. "Scale-down Model Qualification of Ambr® 250 High-

Throughput Mini-Bioreactor System for Two Commercial-Scale MAb Processes." *Biotechnology Progress* 35 (6): 1–13. https://doi.org/10.1002/btpr.2870.

Manikwar, Prakash, Sri Hari, Raju Mulagapati, Srinath Kasturirangan, Khashayar Moez, Godfrey Jonah Rainey, and Brian Lobo. 2020. "Characterization of a Novel Bispecific Antibody With Improved Conformational and Chemical Stability." *Journal of Pharmaceutical Sciences* 109 (1): 220–32. https://doi.org/10.1016/j.xphs.2019.06.025.

Manikwar, Prakash, Sri Hari Raju Mulagapati, Srinath Kasturirangan, Khashayar Moez, Godfrey Jonah Rainey, and Brian Lobo. 2020. "Characterization of a Novel Bispecific Antibody With Improved Conformational and Chemical Stability." *Journal of Pharmaceutical Sciences* 109 (1): 220–32. https://doi.org/10.1016/j.xphs.2019.06.025.

Martin, G. Steven. 2003. "Cell Signaling and Cancer." In *Cancer Cell*, 4:167–74. https://doi.org/10.1016/S1535-6108(03)00216-2.

Masuda, Yumiko, Yuka Ogino, Kozo Yamaichi, Yusuke Takahashi, Koichi Nonaka, and Kaori Wakamatsu. 2020. "The Prevention of an Anomalous Chromatographic Behavior and the Resulting Successful Removal of Viruses from Monoclonal Antibody with an Asymmetric Charge Distribution by Using a Membrane Adsorber in Highly Efficient, Anion-Exchange Chromatography in Flow." *Biotechnology Progress* 36 (3): e2955. https://doi.org/10.1002/btpr.2955.

Matte, Allan. 2020. "Chapter 9 - High-Throughput, Parallelized and Automated Protein Purification for Therapeutic Antibody Development." In *Approaches to the Purification, Analysis and Characterization of Antibody-Based Therapeutics*, 181–98. Montreal, QC, Canada: Elsevier Ltd. https://doi.org/10.1016/B978-0-08-103019-6.00009-6.

Mergener, Michael A. 2021. "Biotechnology and Drugs." In *Chapter 22 - Journal of the American Association for Medical Transcription*, 397–415. Philadelphia, USA: Elsevier Ltd. https://doi.org/10.1016/b978-0-12-820007-0.00022-2.

Millán-Martín, Silvia, Craig Jakes, Sara Carillo, Tom Buchanan, Marc Guender, Dan Bach Kristensen, Trine Meiborg Sloth, Martin Ørgaard, Ken Cook, and Jonathan Bones. 2020. "Inter-Laboratory Study of an Optimised Peptide Mapping Workflow Using Automated Trypsin Digestion for Monitoring Monoclonal Antibody Product Quality Attributes." *Analytical and Bioanalytical Chemistry* 412 (25): 6833–48.

https://doi.org/10.1007/s00216-020-02809-z.

Mimura, Yusuke, Toshihiko Katoh, Radka Saldova, Roisin O'Flaherty, Tomonori Izumi, Yuka Mimura-Kimura, Toshiaki Utsunomiya, et al. 2018. "Glycosylation Engineering of Therapeutic IgG Antibodies: Challenges for the Safety, Functionality and Efficacy." *Protein and Cell* 9 (1): 47–62. https://doi.org/10.1007/s13238-017-0433-3.

Mohs, Richard C., and Nigel H. Greig. 2017. "Drug Discovery and Development: Role of Basic Biological Research." *Alzheimer's and Dementia: Translational Research and Clinical Interventions* 3 (4): 651–57. https://doi.org/10.1016/j.trci.2017.10.005.

Mörtstedt, Harriet, Åsa Makower, Per Olof Edlund, Katarina Sjöberg, and Agneta Tjernberg. 2020. "Improved Identification of Host Cell Proteins in a Protein Biopharmaceutical by LC–MS/MS Using the ProteoMiner™ Enrichment Kit." *Journal of Pharmaceutical and Biomedical Analysis* 185 (June): 113256. https://doi.org/10.1016/j.jpba.2020.113256.

Moussa, Ehab M., Jainik P. Panchal, Balakrishnan S. Moorthy, Janice S. Blum, Marisa K. Joubert, Linda O. Narhi, and Elizabeth M. Topp. 2016. "Immunogenicity of Therapeutic Protein Aggregates." *Journal of Pharmaceutical Sciences* 105 (2): 417–30. https://doi.org/10.1016/j.xphs.2015.11.002.

Murisier, Amarande, Evelin Farsang, Krisztián Horváth, Matthew Lauber, Alain Beck, Davy Guillarme, and Szabolcs Fekete. 2019. "Tuning Selectivity in Cation-Exchange Chromatography Applied for Monoclonal Antibody Separations, Part 2: Evaluation of Recent Stationary Phases." *Journal of Pharmaceutical and Biomedical Analysis* 172 (May): 320–28. https://doi.org/10.1016/j.jpba.2019.05.011.

Murisier, Amarande, Matthew Lauber, Stephen J. Shiner, Davy Guillarme, and Szabolcs Fekete. 2019. "Practical Considerations on the Particle Size and Permeability of Ion-Exchange Columns Applied to Biopharmaceutical Separations." *Journal of Chromatography A* 1604 (August): 1–10. https://doi.org/10.1016/j.chroma.2019.460487.

Nagorsen, Dirk, Peter Kufer, Patrick A. Baeuerle, and Ralf Bargou. 2012. "Blinatumomab: A Historical Perspective." *Pharmacology and Therapeutics* 136 (3): 334–42. https://doi.org/10.1016/j.pharmthera.2012.07.013.

Newswire. 2016. "Global Biopharmaceuticals Market Expected to Reach $526,008 Million,

by 2025 |CAGR 13.8% - Allied Market Research." Newswire. 2016. https://markets.businessinsider.com/news/stocks/global-biopharmaceuticals-market-expected-to-reach-526-008-million-by-2025-cagr-13-8-allied-market-research-1027370148.

Nuñez-Prado, Natalia, Marta Compte, Seandean Harwood, Ana Álvarez-Méndez, Simon Lykkemark, Laura Sanz, and Luis Álvarez-Vallina. 2015. "The Coming of Age of Engineered Multivalent Antibodies." *Drug Discovery Today* 20 (5): 588–94. https://doi.org/10.1016/j.drudis.2015.02.013.

Ou, Xiaowen, Peng Chen, Xizhi Huang, Shunji Li, and Bi Feng Liu. 2020. "Microfluidic Chip Electrophoresis for Biochemical Analysis." *Journal of Separation Science* 43 (1): 258–70. https://doi.org/10.1002/jssc.201900758.

Oyetayo, Olubukayo Opeyemi, Oscar Méndez-Lucio, Andreas Bender, and Hans Kiefer. 2017. "Towards Understanding Polyol Additive Effects on the PH Shift-Induced Aggregation of a Monoclonal Antibody Using High Throughput Screening and Quantitative Structure-Activity Modeling." *International Journal of Pharmaceutics* 530 (1–2): 165–72. https://doi.org/10.1016/j.ijpharm.2017.07.059.

Ozturk, Sadettin S, and Wei-Shou Hu. 2005. *Cell Culture Technology for Pharmaceutical and Cell-Based Therapies. Cell Culture Technology for Pharmaceutical and Cell-Based Therapies*. Berkeley, CA, USA: Taylor & Francis Group. https://doi.org/10.1201/9780849351068.ch11.

Papathanasiou, Maria M Kontoravdi, Cleo. 2019. "Engineering Challenges in Therapeutic Protein Product and Process Design." *Current Opinion in Chemical Engineering* 27 (March): 81–88. https://doi.org/10.1016/j.coche.2019.11.010.

Papathanasiou, Maria M., Ana L. Quiroga-Campano, Fabian Steinebach, Montaña Elviro, Athanasios Mantalaris, and Efstratios N. Pistikopoulos. 2017. "Advanced Model-Based Control Strategies for the Intensification of Upstream and Downstream Processing in MAb Production." *Biotechnology Progress* 33 (4): 966–88. https://doi.org/10.1002/btpr.2483.

Parr, Maria Kristina, Othman Montacir, and Houda Montacir. 2016a. "Physicochemical Characterization of Biopharmaceuticals." *Journal of Pharmaceutical and Biomedical Analysis* 130: 366–89. https://doi.org/10.1016/j.jpba.2016.05.028.

———. 2016b. “Physicochemical Characterization of Biopharmaceuticals.” *Journal of Pharmaceutical and Biomedical Analysis* 130 (May): 366–89. https://doi.org/10.1016/j.jpba.2016.05.028.

Paul, Albert Jesuran, René Handrick, Sybille Ebert, and Friedemann Hesse. 2017. “Identification of Process Conditions Influencing Protein Aggregation in Chinese Hamster Ovary Cell Culture.” *Biotechnology and Bioengineering* 115 (5): 1173–85. https://doi.org/10.1002/bit.26534.

Paul, Albert Jesuran, Karen Schwab, Nina Prokoph, Elena Haas, René Handrick, and Friedemann Hesse. 2015. “Fluorescence Dye-Based Detection of MAb Aggregates in CHO Culture Supernatants.” *Analytical and Bioanalytical Chemistry* 407 (16): 4849–56. https://doi.org/10.1007/s00216-015-8672-8.

Pauw, Ruben De, Bart Degreef, Harald Ritchie, Sebastiaan Eeltink, Gert Desmet, and Ken Broeckhoven. 2014. “Extending the Limits of Operating Pressure of Narrow-Bore Column Liquid Chromatography Instrumentation.” *Journal of Chromatography A* 1347 (April): 56–62. https://doi.org/10.1016/j.chroma.2014.04.056.

Pereira, Natasha A., Kah Fai Chan, Pao Chun Lin, and Zhiwei Song. 2018. “The ‘Less-Is-More’ in Therapeutic Antibodies: Afucosylated Anti-Cancer Antibodies with Enhanced Antibody-Dependent Cellular Cytotoxicity.” *MAbs* 10 (5): 693–711.

Petersson, Patrik, Kim Haselmann, and Stephan Buckenmaier. 2016a. “Multiple Heart-Cutting Two Dimensional Liquid Chromatography Mass Spectrometry : Towards Real Time Determination of Related Impurities of Bio-Pharmaceuticals in Salt Based Separation Methods.” *Journal of Chromatography A* 1468 (October): 95–101. https://doi.org/10.1016/j.chroma.2016.09.023.

Petroff, Matthew G., Haiying Bao, John P. Welsh, Miranda van Beuningen-de Vaan, Jennifer M. Pollard, David J. Roush, Sunitha Kandula, Peter Machielsen, Nihal Tugcu, and Thomas O. Linden. 2016. “High Throughput Chromatography Strategies for Potential Use in the Formal Process Characterization of a Monoclonal Antibody.” *Biotechnology and Bioengineering* 113 (6): 1273–83. https://doi.org/10.1002/bit.25901.

Pfeuffer, Julianus, Timo Sachsenberg, Oliver Alka, Mathias Walzer, Alexander Fillbrunn, Lars Nilse, Oliver Schilling, Knut Reinert, and Oliver Kohlbacher. 2017. “OpenMS –

A Platform for Reproducible Analysis of Mass Spectrometry Data." *Journal of Biotechnology* 261 (May): 142–48. https://doi.org/10.1016/j.jbiotec.2017.05.016.

Ph.Eur. 10.0. 2020. *European Pharmacopoeia 10th Edition*. Vol. I. Strasbourg: Council of Europe. www.webofpharma.com.

Philippidis, Alex. 2021. "Seven Biopharma Trends to Watch in 2021." *Genetic and Biotechnology News* 4 (1): 1–8.

Philo, John S. 2006. "Is Any Measurement Method Optimal for All Aggregate Sizes and Types?" *The AAPS Journal* 8 (3): E564–71. https://doi.org/10.1208/aapsj080365.

Phung, Wilson, Guanghui Han, Stéphanie G.I. Polderdijk, Michael Dillon, Whitney Shatz, Peter Liu, Bingchuan Wei, et al. 2020. "Data on Charge Separation of Bispecific and Mispaired IgGs Using Native Charge-Variant Mass Spectrometry." *Data in Brief* 30 (March): 105435. https://doi.org/10.1016/j.dib.2020.105435.

Pichon, Chantal, and Federico Perche. 2021. "Design and Delivery of Messenger RNA-Based Vaccines." *Vaccine Strategies* 43 (4): 4–7. https://doi.org/10.1042/bio_2021_151.

Pimenta, Marcela Valente, and Gisele Monteiro. 2019. "The Production of Biopharmaceuticals in Brazil : Current Issues." *Brazilian Journal of Pharmaceutical Sciences* 55 (December): 1–8. https://doi.org/doi.org/10.1590/s2175-97902019000217823.

Pirok, Bob W. J., Dwight R. Stoll, and Peter J. Schoenmakers. 2019. "Recent Developments in Two-Dimensional Liquid Chromatography: Fundamental Improvements for Practical Applications." Review-article. *Analytical Chemistry* 91 (1): 240–63. https://doi.org/10.1021/acs.analchem.8b04841.

Pirok, Bob W.J., Andrea F.G. Gargano, and Peter J. Shoenmakers. 2018. "Optimizing Separations in Online Comprehensive Two-Dimensional Liquid Chromatography." *Journal of Separation Science* 41 (1): 68–98. https://doi.org/10.1002/jssc.201700863.

Plomp, Rosina, Gillian Dekkers, Yoann Rombouts, Remco Visser, Carolien A.M. Koeleman, Guinevere S.M. Kammeijer, Bas C. Jansen, et al. 2015. "Hinge-Region O-Glycosylation of Human Immunoglobulin G3 (IgG3)." *Molecular and Cellular Proteomics* 14 (5): 1373–84. https://doi.org/10.1074/mcp.M114.047381.

Polderdijk, G I, Michael Dillon, Whitney Shatz, Peter Liu, Bingchuan Wei, Pawankumar Suresh, David Fischer, et al. 2019. “Characterization of Bispecific and Mispaired IgGs by Native Charge- Variant Mass Spectrometry.” *International Journal of Mass Spectrometry* 446 (116229): 1–9.

Ponniah, Gomathinayagam, Christine Nowak, Alyssa Neill, and Hongcheng Liu. 2017. “Characterization of Charge Variants of a Monoclonal Antibody Using Weak Anion Exchange Chromatography at Subunit Levels.” *Analytical Biochemistry* 520 (December): 49–57. https://doi.org/10.1016/j.ab.2016.12.017.

Popovici, Simona T., and Peter J. Schoenmakers. 2005. “Fast Size-Exclusion Chromatography—Theoretical and Practical Considerations.” *Journal of Chromatography A* 1099 (1–2): 92–102. https://doi.org/10.1016/J.CHROMA.2005.08.071.

Pörtner, Ralf. 2012. *Animal Cell Biotechnology*. Edited by Ralf Pörtner. *Animal Cell Biotechnology*. 4th ed. New York, USA: Human Press. https://doi.org/10.1016/C2009-0-02458-1.

Pybus, Leon P., Greg Dean, Nathan R. West, Andrew Smith, Olalekan Daramola, Ray Field, Stephen J. Wilkinson, and David C. James. 2014. “Model-Directed Engineering of ‘Difficult-to-Express’ Monoclonal Antibody Production by Chinese Hamster Ovary Cells.” *Biotechnology and Bioengineering* 111 (2): 372–85. https://doi.org/10.1002/bit.25116.

Q6B, ICH. 1999. “ICH Q6B Specifications: Test Procedures and Acceptance Criteria for Biotechnological/Biological Products Step.”

Qian, Chen, Ben Niu, Rod Brian Jimenez, Jihong Wang, and Methal Albarghouthi. 2021. “Fully Automated Peptide Mapping Multi-Attribute Method by Liquid Chromatography – Mass Spectrometry with Robotic Liquid Handling System.” *Journal of Pharmaceutical and Biomedical Analysis* 198 (February): 113988. https://doi.org/10.1016/j.jpba.2021.113988.

Qian, Chen, Ben Niu, Rod Brian Jimenez, Jihong Wang, Methal Albarghouthi, and Xiaoyu Chen. 2020. “Fully Automated Peptide Mapping Protocol for Multi-Attribute Method by Liquid Chromatography–Tandem Mass Spectroscopy with a High-Throughput Robotic Liquid Handling System.” *BioRxiv*.

https://doi.org/10.1101/2020.01.10.902338.

Qian, Jun, Tun Liu, Li Yang, Ann Daus, Richard Crowley, and Qinwei Zhou. 2007. "Structural Characterization of N-Linked Oligosaccharides on Monoclonal Antibody Cetuximab by the Combination of Orthogonal Matrix-Assisted Laser Desorption/Ionization Hybrid Quadrupole-Quadrupole Time-of-Flight Tandem Mass Spectrometry and Sequential Enzy." *Analytical Biochemistry* 364 (1): 8–18. https://doi.org/10.1016/j.ab.2007.01.023.

Qiu, Huawei, Ronnie Wei, Julie Jaworski, Ekaterina Boudanova, Heather Hughes, Scott VanPatten, Anders Lund, et al. 2019. "Engineering an Anti-CD52 Antibody for Enhanced Deamidation Stability." *MAbs* 11 (7): 1266–75. https://doi.org/10.1080/19420862.2019.1631117.

Quan, Cynthia, Emily Alcala, Irena Petkovska, Domenic Matthews, Eleanor Canova-Davis, Ron Taticek, and Stacey Ma. 2008. "A Study in Glycation of a Therapeutic Recombinant Humanized Monoclonal Antibody: Where It Is, How It Got There, and How It Affects Charge-Based Behavior." *Analytical Biochemistry* 373 (2): 179–91. https://doi.org/10.1016/j.ab.2007.09.027.

Quianzon, Celeste C. L., and Issam E. Cheikh. 2012. "History of Current Non-Insulin Medications for Diabetes Mellitus." *Journal of Community Hospital Internal Medicine Perspectives* 2 (3): 19081. https://doi.org/10.3402/jchimp.v2i3.19081.

Rader, Ronald A. 2008. "(Re)Defining Biopharmaceutical." *Nature Publishing Group* 26 (7): 743–51. https://doi.org/doi.org/10.1038/nbt0708-743.

Rameez, Shahid, Sigma S. Mostafa, Christopher Miller, and Abhinav A. Shukla. 2014. "High-Throughput Miniaturized Bioreactors for Cell Culture Process Development: Reproducibility, Scalability, and Control." *Biotechnology Progress* 30 (3): 718–27. https://doi.org/10.1002/btpr.1874.

Rathore, Anurag S., Oscar Fabián Garcia-Aponte, Aydin Golabgir, Bibiana Margarita Vallejo-Diaz, and Christoph Herwig. 2017. "Role of Knowledge Management in Development and Lifecycle Management of Biopharmaceuticals." *Pharmaceutical Research* 34 (2): 243–56. https://doi.org/10.1007/s11095-016-2043-9.

Rathore, Anurag S., Sumit Kumar Singh, and Gunjan Narula. 2016. "Should Charge Variants of Monoclonal Antibody Therapeutics Be Considered Critical Quality

Attributes?" *Electrophoresis* 37 (17–18): 2338–46. https://doi.org/10.1002/elps.201600078.

Rathore, Anurag S, and Ankita Bhargava. 2020. "Biosimilars in Developed Economies: Overview , Status , and Regulatory Considerations." *Regulatory Toxicology and Pharmacology* 110 (November): 1–10. https://doi.org/10.1016/j.yrtph.2019.104525.

Rea, Jennifer C., Yun Lou, Joel Cuzzi, Yuhua Hu, Isabella de Jong, Yajun Jennifer Wang, and Dell Farnan. 2012. "Development of Capillary Size Exclusion Chromatography for the Analysis of Monoclonal Antibody Fragments Extracted from Human Vitreous Humor." *Journal of Chromatography A* 1270 (November): 111–17. https://doi.org/10.1016/j.chroma.2012.10.051.

Rea, Jennifer C., G. Tony Moreno, Yun Lou, and Dell Farnan. 2010. "Validation of a PH Gradient-Based Ion-Exchange Chromatography Method for High-Resolution Monoclonal Antibody Charge Variant Separations." *Journal of Pharmaceutical and Biomedical Analysis* 54 (2): 317–23. https://doi.org/10.1016/j.jpba.2010.08.030.

Rea, Jennifer C., G. Tony Moreno, Lisa Vampola, Yun Lou, Bjorn Van Haan, Guillaume Tremintin, Laura Simmons, Adrian Nava, Yajun Jennifer Wang, and Dell Farnan. 2012. "Capillary Size Exclusion Chromatography with Picogram Sensitivity for Analysis of Monoclonal Antibodies Purified from Harvested Cell Culture Fluid." *Journal of Chromatography A* 1219 (Novemeber): 140–46. https://doi.org/10.1016/j.chroma.2011.11.025.

Rea, Jennifer C, G Tony Moreno, Yun Lou, and Dell Farnan. 2011. "Validation of a PH Gradient-Based Ion-Exchange Chromatography Method for High-Resolution Monoclonal Antibody Charge Variant Separations." *Journal of Pharmaceutical and Biomedical Analysis* 54 (2): 317–23. https://doi.org/10.1016/j.jpba.2010.08.030.

Read, E. K., J. T. Park, R. B. Shah, B. S. Riley, K. A. Brorson, and A. S. Rathore. 2010. "Process Analytical Technology (PAT) for Biopharmaceutical Products: Part I. Concepts and Applications." *Biotechnology and Bioengineering* 105 (2): 276–84. https://doi.org/10.1002/bit.22528.

Read, E. K., R. B. Shah, B. S. Riley, J. T. Park, K. A. Brorson, and A. S. Rathore. 2010. "Process Analytical Technology (PAT) for Biopharmaceutical Products: Part II. Concepts and Applications." *Biotechnology and Bioengineering* 105 (2): 285–95.

https://doi.org/10.1002/bit.22529.

Reason, By Andrew J, Andrew Weiskopf, Anurag S Rathore, and Quality Control. 2018. "Defining Critical Quality Attributes for Monoclonal Antibody Therapeutic Products." *BioPharm International* 27 (7): 1–8.

Redman, Erin A., Nicholas G. Batz, J. Scott Mellors, and J. Michael Ramsey. 2015. "Integrated Microfluidic Capillary Electrophoresis-Electrospray Ionization Devices with Online Ms Detection for the Separation and Characterization of Intact Monoclonal Antibody Variants." *Analytical Chemistry* 87 (4): 2264–72. https://doi.org/10.1021/ac503964j.

Redman, Erin A, J Scott Mellors, Jason A Starkey, and J Michael Ramsey. 2016. "Characterization of Intact Antibody Drug Conjugate Variants Using Micro Fl Uidic Capillary Electrophoresis − Mass Spectrometry." *Analytical Biochemistry* 88 (4): 2220–26. https://doi.org/10.1021/acs.analchem.5b03866.

Reema, Piparia, Ouellette David, W. Blaine Stine, Christine Grinnell, Tarcsa Edit, Radziejewski Czeslaw, and Ivan Correia. 2012. "A High Throughput Capillary Electrophoresis Method to Obtain Pharmacokinetics and Quality Attributes of a Therapeutic Molecule in Circulation." *MAbs* 4 (4): 521–31. https://doi.org/10.4161/mabs.20099.

Reichert, Janice M. 2019. "Bispecific Antibodies: A Mechanistic Review of the Pipeline." *Nature Reviews Drug Discovery* 18 (August): 585–608. https://doi.org/10.1038/s41573-019-0028-1.

Reusch, Dietmar, Markus Haberger, Bernd Maier, Maria Maier, Ronny Kloseck, Boris Zimmermann, Michaela Hook, et al. 2015. "Comparison of Methods for the Analysis of Therapeutic Immunoglobulin G Fc-Glycosylation Profiles - Part 1: Separation-Based Methods." *MAbs* 7 (1): 167–79. https://doi.org/10.4161/19420862.2014.986000.

Reusch, Dietmar, and Max L. Tejada. 2015a. "Fc Glycans of Therapeutic Antibodies as Critical Quality Attributes." *Glycobiology* 25 (12): 1325–34. https://doi.org/10.1093/glycob/cwv065.

Rezaie, Rahim, Anita M Mcgahan, Sarah E Frew, Abdallah S Daar, and Peter A Singer. 2012. "Emergence of Biopharmaceutical Innovators in China , India , Brazil , and South Africa as Global Competitors and Collaborators." *Health Research Policy and Systems*

10 (18): 1–13.

Rita Costa, A., M. Elisa Rodrigues, Mariana Henriques, Joana Azeredo, and Rosário Oliveira. 2010. "Guidelines to Cell Engineering for Monoclonal Antibody Production." *European Journal of Pharmaceutics and Biopharmaceutics* 74 (2): 127–38. https://doi.org/10.1016/j.ejpb.2009.10.002.

Rogers, Richard S., Michael Abernathy, Douglas D. Richardson, Jason C. Rouse, Justin B. Sperry, Patrick Swann, Jette Wypych, Christopher Yu, Li Zang, and Rohini Deshpande. 2018. "A View on the Importance of 'Multi-Attribute Method' for Measuring Purity of Biopharmaceuticals and Improving Overall Control Strategy." *The AAPS Journal* 20 (7): 1–8. https://doi.org/10.1208/s12248-017-0168-3.

Rogers, Richard S., Nancy S. Nightlinger, Brittney Livingston, Phil Campbell, Robert Bailey, and Alain Balland. 2015. "Development of a Quantitative Mass Spectrometry Multi-Attribute Method for Characterization, Quality Control Testing and Disposition of Biologics." *MAbs* 7 (5): 881–90. https://doi.org/10.1080/19420862.2015.1069454.

Rogstad, Sarah, Haoheng Yan, Xiaoshi Wang, David Powers, Kurt Brorson, Bazarragchaa Damdinsuren, and Sau Lee. 2019. "Multi-Attribute Method for Quality Control of Therapeutic Proteins." *Analytical Chemistry* 91 (22): 14170−14177. https://doi.org/10.1021/acs.analchem.9b03808.

Rolinger, Laura, and R Matthias. 2020. "A Critical Review of Recent Trends , and a Future Perspective of Optical Spectroscopy as PAT in Biopharmaceutical Downstream Processing." *Analytical and Bioanalytical Chemistry* 412 (April): 2047–64.

Rosati, Sara, Natalie J. Thompson, Albert J.R. Heck, Sara Rosati, Natalie J. Thompson, and Albert J.R. Heck. 2013. "Tackling the Increasing Complexity of Therapeutic Monoclonal Antibodies with Mass Spectrometry." *Trends in Analytical Chemistry* 48 (July-August): 72–80. https://doi.org/10.1016/j.trac.2013.02.013.

Sahu, Prafulla Kumar, Chandra Sekhar Patro, Jagadeesh Panda, Nageswara Rao Ramisetti, Teresa Cecchi, and Suryakanta Swain. 2018. "An Overview of Experimental Designs in HPLC Method Development and Validation." *Journal of Pharmaceutical and Biomedical Analysis* 147 (May): 590–611. https://doi.org/10.1016/j.jpba.2017.05.006.

Sanchez, A. Carl, Gareth Friedlander, Szabolcs Fekete, Jason Anspach, Dvy Guillarme, Mike Chitty, and Tivadar Farkas. 2013. "Pushing the Performance Limits of Reversed-

Phase Ultra High Performance Liquid Chromatography with 1.3μm Core-Shell Particles." *Journal of Chromatography A* 1311 (August): 90–97. https://doi.org/10.1016/j.chroma.2013.08.065.

Sandner, Viktor, Leon P. Pybus, Graham McCreath, and Jarka Glassey. 2019. "Scale-Down Model Development in Ambr Systems: An Industrial Perspective." *Biotechnology Journal* 14 (4): 1–11. https://doi.org/10.1002/biot.201700766.

Sandra, Koen, Mieke Steenbeke, Isabel Vandenheede, Gerd Vanhoenacker, and Pat Sandra. 2017. "The Versatility of Heart-Cutting and Comprehensive Two-Dimensional Liquid Chromatography in Monoclonal Antibody Clone Selection." *Journal of Chromatography A* 1523 (June): 283–92.

Sangshetti, Jaiprakash N., Mrinmayee Deshpande, Zahid Zaheer, Devanand B. Shinde, and Rohidas Arote. 2017. "Quality by Design Approach: Regulatory Need." *Arabian Journal of Chemistry* 10 (2): S3412–25. https://doi.org/10.1016/j.arabjc.2014.01.025.

Santos, Ana L., and Ariel B. Lindner. 2017. "Protein Posttranslational Modifications: Roles in Aging and Age-Related Disease." *Oxidative Medicine and Cellular Longevity*. https://doi.org/10.1155/2017/5716409.

Sarkis, Miriam, Andrea Bernardi, Nilay Shah, and Maria M. Papathanasiou. 2021. "Decision Support Tools for Next-Generation Vaccines and Advanced Therapy Medicinal Products: Present and Future." *Current Opinion in Chemical Engineering* 32 (May): 100689. https://doi.org/10.1016/j.coche.2021.100689.

Sarrut, Morgan, Amélie Corgier, Szabolcs Fekete, Davy Guillarme, David Lascoux, Marie-claire Janin-bussat, Alain Beck, and Sabine Heinisch. 2016. "Analysis of Antibody-Drug Conjugates by Comprehensive on-Line Two-Dimensional Hydrophobic Interaction Chromatography x Reversed Phase Liquid Chromatography Hyphenated to High Resolution Mass Spectrometry . I − Optimization of Separation Conditions." *Journal of Chromatography B* 1032 (October): 103–11.

Saunders, Janet C, Lydia M Young, Rachel A Mahood, Matthew P Jackson, Charlotte H Revill, Richard J Foster, D Alastair Smith, Alison E Ashcroft, David J Brockwell, and Sheena E Radford. 2016. "An in Vivo Platform for Identifying Inhibitors of Protein Aggregation." *Nature Chemical Biology* 12 (February): 94–104. https://doi.org/10.1038/nchembio.1988.

Schachner, Luis, Guanghui Han, Michael Dillon, Jianhui Zhou, Luke McCarty, Diego Ellerman, Yiyuan Yin, et al. 2016. "Characterization of Chain Pairing Variants of Bispecific IgG Expressed in a Single Host Cell by High-Resolution Native and Denaturing Mass Spectrometry." *Analytical Chemistry* 88 (24): 12122–27. https://doi.org/10.1021/acs.analchem.6b02866.

Schaefer, Cédric, David Clicq, Clémence Lecomte, Alain Merschaert, Edith Norrant, and Frédéric Fotiadu. 2014. "A Process Analytical Technology (PAT) Approach to Control a New API Manufacturing Process: Development, Validation and Implementation." *Talanta* 120 (2014): 114–25. https://doi.org/10.1016/j.talanta.2013.11.072.

Scheffler, Kai, Eugen Damoc, Aaron O. Bailey, and Jonathan Josephs. 2016. "Enabling Mass Spectrometric Analysis of Intact Proteins in Native Conditions on A Hybrid Quadrupole-Orbitrap Mass Spectrometer." *Application Note, Thermo Fisher Scientific*. https://doi.org/10.4161/mabs.26282.

Scheller, Christin. 2021. "A Comparative Study of CE-SDS, SDS-PAGE , and Simple Western — Precision, Repeatability, and Apparent Molecular Mass Shifts by Glycosylation." *Electrophoresis* 42 (14–15): 1521–31. https://doi.org/10.1002/elps.202100068.

Schmidt, Michael, Mathias Hafner, and Christian Frech. 2014. "Modeling of Salt and PH Gradient Elution in Ion-Exchange Chromatography." *Journal of Separation Science* 37 (1–2): 5–13. https://doi.org/10.1002/jssc.201301007.

Schmidt, Peter M., Michael Abdo, Rebecca E. Butcher, Min Yin Yap, Pierre D. Scotney, Melanie L. Ramunno, Genevieve Martin-Roussety, et al. 2016. "A Robust Robotic High-Throughput Antibody Purification Platform." *Journal of Chromatography A* 1455: 9–19. https://doi.org/10.1016/j.chroma.2016.05.076.

Schmiedl, Andreas, Frank Breitling, and Stefan Du. 2000. "Expression of a Bispecific DsFv – DsFv J Antibody Fragment in Escherichia Coli" 13 (10): 725–34.

Scott, Estes, and Mark Melville. 2014. "Mammalian Cell Line Developments in Speed and Efficiency." *Advances in Biochemical Engineering/Biotechnology* 139 (November): 11–33. https://doi.org/10.1007/10.

Sedykh, Sergey, Victor Prinz, Valentina Buneva, and Georgy Nevinsky. 2018. "Bispecific Antibodies: Design, Therapy, Perspectives." *Drug Design, Development and Therapy*

12 (January): 195–208. https://doi.org/10.2147/DDDT.S151282.

Sha, Sha, Cyrus Agarabi, Kurt Brorson, Dong-Yup Lee, and Seongkyu Yoon. 2016. "N-Glycosylation Design and Control of Therapeutic Monoclonal Antibodies." *Trends in Biotechnology* 34 (10): 835–846.

Shah, Dinen D, Jingming Zhang, Ming-ching Hsieh, Shanmuuga Sundaram, Haripada Maity, and Krishna M G Mallela. 2018. "Effect of Peroxide- Versus Alkoxyl-Induced Chemical Oxidation on the Structure , Stability , Aggregation , and Function of a Therapeutic Monoclonal Antibody." *Journal of Pharmaceutical Sciences* 107 (11): 2789–2803. https://doi.org/10.1016/j.xphs.2018.07.024.

Shekhawat, Lalita K., Avinash Godara, Vijesh Kumar, and Anurag S. Rathore. 2019. "Design of Experiments Applications in Bioprocessing: Chromatography Process Development Using Split Design of Experiments." *Biotechnology Progress* 35 (1): 1–17. https://doi.org/10.1002/btpr.2730.

Shi, Rachel Liuqing, Gang Xiao, Thomas M. Dillon, Margaret S. Ricci, and Pavel V. Bondarenko. 2020. "Characterization of Therapeutic Proteins by Cation Exchange Chromatography-Mass Spectrometry and Top-down Analysis." *MAbs* 12 (1): 1–12. https://doi.org/10.1080/19420862.2020.1739825.

Shukla, Abhinav A., Brian Hubbard, Tim Tressel, Sam Guhan, and Duncan Low. 2007. "Downstream Processing of Monoclonal Antibodies-Application of Platform Approaches." *Journal of Chromatography B: Analytical Technologies in the Biomedical and Life Sciences* 848 (1): 28–39. https://doi.org/10.1016/j.jchromb.2006.09.026.

Shukla, Abhinav A, Leslie S Wolfe, Sigma S Mostafa, and Carnley Norman. 2017. "Evolving Trends in MAb Production Processes." *Bioengineering & Translational Medicine*, no. 2: 58–69. https://doi.org/10.1002/btm2.10061.

Siddiqui, Masoom Raza, Zeid A. AlOthman, and Nafisur Rahman. 2017. "Analytical Techniques in Pharmaceutical Analysis: A Review." *Arabian Journal of Chemistry* 10 (April): S1409–21. https://doi.org/10.1016/j.arabjc.2013.04.016.

Silva, Tiago Castanheira, Michel Eppink, and Marcel Ottens. 2021. "Automation and Miniaturization: Enabling Tools for Fast, High-Throughput Process Development in Integrated Countinous Biomanufacturing." *Journal of Chemical Technology and*

Biotechnology 96 (8): 1–11. https://doi.org/10.1002/jctb.6792.

Sissolak, Bernhard, Nico Lingg, Wolfgang Sommeregger, Gerald Striedner, and Karola Vorauer-Uhl. 2019. "Impact of Mammalian Cell Culture Conditions on Monoclonal Antibody Charge Heterogeneity: An Accessory Monitoring Tool for Process Development." *Journal of Industrial Microbiology and Biotechnology* 46 (June): 1167–78. https://doi.org/10.1007/s10295-019-02202-5.

Sissolak, Bernhard, Nico Lingg, Wolfgang Sommeregger, Gerald Striedner, and Karola Vorauer. 2019. "Impact of Mammalian Cell Culture Conditions on Monoclonal Antibody Charge Heterogeneity : An Accessory Monitoring Tool for Process Development." *Journal of Industrial Microbiology & Biotechnology* 46 (8): 1167–78. https://doi.org/10.1007/s10295-019-02202-5.

Sjögren, Jonathan, Fredrik Olsson, and Alain Beck. 2016a. "Rapid and Improved Characterization of Therapeutic Antibodies and Antibody Related Products Using IdeS Digestion and Subunit Analysis." *The Analyst* 141 (11): 3114–25. https://doi.org/10.1039/C6AN00071A.

Sokolov, Michael, Jonathan Ritscher, Nicola Mackinnon, Dominik Rothenh, Gian Thanei, Matthieu Stettler, Jonathan Souquet, Massimo Morbidelli, and Alessandro Butt. 2017. "Robust Factor Selection in Early Cell Culture Process Development for the Production of a Biosimilar Monoclonal Antibody." *Biotechnology Progress* 33 (1): 181–91. https://doi.org/10.1002/btpr.2374.

Sokolowska, Izabela, Jingjie Mo, Jia Dong, Michael J Lewis, and Ping Hu. 2017. "Subunit Mass Analysis for Monitoring Antibody Oxidation." *MAbs* 9 (3): 498–505. https://doi.org/10.1080/19420862.2017.1279773.

Srebalus-Barnes, Catherine A., and Amareth Lim. 2007. "Application of Mass Spectrometry for the Structural Characterisation of Protein Pharmaceuticals." *Mass Spectrometry Reviews* 26 (November): 370–88. https://doi.org/10.1002/mas.

Stamatis, Christos, Stephen Goldrick, David Gruber, Richard Turner, Nigel J. Titchener-Hooker, and Suzanne S. Farid. 2019. "High Throughput Process Development Workflow with Advanced Decision-Support for Antibody Purification." *Journal of Chromatography A* 1596 (July): 104–16. https://doi.org/10.1016/j.chroma.2019.03.005.

Staub, Aline, Davy Guillarme, Julie Schappler, Jean-luc Veuthey, and Serge Rudaz. 2011. "Intact Protein Analysis in the Biopharmaceutical Field." *Journal of Pharmaceutical and Biomedical Analysis* 55 (September): 810–22. https://doi.org/10.1016/j.jpba.2011.01.031.

Stephan, Susanne, and Sonja Krieger. 2017. "High-Resolution Sampling 2D-LC for Pharmaceutical Impurity Analysis Detection of Impurities Hidden Under the API Peak at Relevant Levels." *Agilent Technologies, Inc., Application Note Biotherapeutics and Biosimilars*, no. 5991-8082EN: 1–12.

Stoll, Dwight R., Hayley R. Lhotka, David C. Harmes, Ben Madigan, Jordy J. Hsiao, and Gregory O. Staples. 2019. "High Resolution Two-Dimensional Liquid Chromatography Coupled with Mass Spectrometry for Robust and Sensitive Characterization of Therapeutic Antibodies at the Peptide Level." *Journal of Chromatography B* 1134–1135 (August): 121832. https://doi.org/10.1016/j.jchromb.2019.121832.

Stoll, Dwight R, and Peter W Carr. 2017. "Two-Dimensional Liquid Chromatography: A State of the Art Tutorial." *Anal. Chem.* 89 (1): 519−531. https://doi.org/10.1021/acs.analchem.6b03506.

Stoll, Dwight R, Konstantin Shoykhet, Patrik Petersson, and Stephan Buckenmaier. 2017. "Active Solvent Modulation: A Valve-Based Approach to Improve Separation Compatibility in Two-Dimensional Liquid Chromatography." *Analytical Chemistry* 89 (17): 9260–67. https://doi.org/10.1021/acs.analchem.7b02046.

Stoll, Jeffrey, Kristin C. Pothier, Steve Sapletal, Alasdair Milton, Andrew M. Stephenson, and Jeff Katz. 2021. "Biopharmaceuticals Deal Trends." KPMG. 2021. https://assets.kpmg/content/dam/kpmg/ie/pdf/2021/04/ie-2021-kpmg-biopharmaceuticals-deal-trends-stoll-040521.pdf.

Strand, James, Chi Ting Huang, and Jin Xu. 2013. "Characterization of Fc-Fusion Protein Aggregates Derived from Extracellular Domain Disulfide Bond Rearrangements." *Journal of Pharmaceutical Sciences* 102 (2): 441–53. https://doi.org/10.1002/jps.23421.

Strasser, Lisa, Amy Farrell, Jenny T. C. Ho, Kai Scheffler, Ken Cook, Patrick Pankert, Peter Mowlds, Rosa Viner, Barry L. Karger, and Jonathan Bones7. 2021. "Proteomic

Profiling of IgG1 Producing CHO Cells Using LC/LC-SPS-MS3: The Effects of Bioprocessing Conditions on Productivity and Product Quality." *Frontiers in Bioengineering and Biotechnology* 9 (April): 569045. https://doi.org/10.3389/fbioe.2021.569045.

Strasser, Lisa, Tomos E Morgan, Felipe Guapo, Florian Füssl, Daniel Forsey, Ian Anderson, and Jonathan Bones. 2021. "A Native Mass Spectrometry-Based Assay for Rapid Assessment of the Empty:Full Capsid Ratio in Adeno-Associated Virus Gene Therapy Products." *Analytical Chemistry*.

Suurs, Frans V, Marjolijn N Lub-de Hooge, Elisabeth G E De Vries, Derk Jan, and A De Groot. 2019. "A Review of Bispecific Antibodies and Antibody Constructs in Oncology and Clinical Challenges." *Pharmacology and Therapeutics* 201 (April): 103–19. https://doi.org/10.1016/j.pharmthera.2019.04.006.

Swiech, Kamilla, Virgínia Picanço-castro, and Dimas Tadeu. 2012. "Human Cells: New Platform for Recombinant Therapeutic Protein Production." *Protein Expression and Purification* 84 (1): 147–53. https://doi.org/10.1016/j.pep.2012.04.023.

Szigeti, Marton, Judit Bondar, Douglas Gjerde, Zsolt Keresztessy, Akos Szekrenyes, and Andras Guttman. 2016. "Rapid N -Glycan Release from Glycoproteins Using Immobilized PNGase F Microcolumns." *Journal of Chromatography B* 1032 (February): 139–43. https://doi.org/10.1016/j.jchromb.2016.02.006.

Tecan Group Ltd. 2010. "Application Note: PhyTip ® Columns Processed on the Tecan Freedom EVO ® for Complete Automation of High-Throughput Protein Purification and Sample Preparation."

Tejwani, Vijay, Mikael R. Andersen, Jong Hyun Nam, and Susan T. Sharfstein. 2018. "Glycoengineering in CHO Cells: Advances in Systems Biology." *Biotechnology Journal* 13 (3): 1–16. https://doi.org/10.1002/biot.201700234.

Tihanyi, Borbála, and László Nyitray. 2021. "Recent Advances in CHO Cell Line Development for Recombinant Protein Production." *Drug Discovery Today: Technologies* 35–36 (April): 1–10. https://doi.org/10.1016/j.ddtec.2021.02.003.

Tjio, J. H., and T.T. Puck. 1958. "Genetics of Somatic Mammalian Cells. II. Chromosomal Constitution of Cells in Tissue Culture." *The Journal of Experimental Medicine* 108 (2): 259–68. https://doi.org/10.1084/jem.108.2.259.

Trappe, Anne, Florian Füssl, Sara Carillo, Izabela Zaborowska, Paula Meleady, and Jonathan Bones. 2018a. "Rapid Charge Variant Analysis of Monoclonal Antibodies to Support Lead Candidate Biopharmaceutical Development." *Journal of Chromatography B: Analytical Technologies in the Biomedical and Life Sciences* 1095 (April): 166–76. https://doi.org/10.1016/j.jchromb.2018.07.037.

Treier, Katrin, Sigrid Hansen, Carolin Richter, Patrick Diederich, Jürgen Hubbuch, and Philip Lester. 2012. "High-Throughput Methods for Miniaturization and Automation of Monoclonal Antibody Purification Processes." *Biotechnology Progress* 28 (3): 723–32. https://doi.org/10.1002/btpr.1533.

U.S. FDA. 2019. "Impact Story: Transitioning a Powerful Analytical Tool into Manufacturing to Improve the Quality of Complex Therapeutics." FDA Website. 2019. https://www.fda.gov/drugs/regulatory-science-action/impact-story-transitioning-powerful-analytical-tool-manufacturing-improve-quality-complex?utm_campaign=New CDER Impact Story%3A Transitioning a Powerful Analytical Tool Into Manufacturing to Improve&utm_medium=email&utm_source=Eloqua.

Uliyanchenko, Elena, Peter J Schoenmakers, and Sjoerd Van Der Wal. 2011. "Fast and Efficient Size-Based Separations of Polymers Using Ultra-High-Pressure Liquid Chromatography." *Journal of Chromatography A* 1218 (11): 1509–18. https://doi.org/10.1016/j.chroma.2011.01.053.

Urlaub, Gail, and Lawrence A Chasin. 1980. "Isolation of Chinese Hamster Cell Mutants Deficient in Dihydrofolate Reductase Activity." *Proceedings of the National Academy of Sciences of the United States of America* 77 (7): 4216–20.

US-FDA Center for Drug Evaluation and Research. 2015. "Analytical Procedures and Methods Validation for Drugs and Biologics." *Guidance for Industry*. Rockville (MD). https://doi.org/http://www.ich.org/fileadmin/Public_Web_Site/ICH_Products/Guidelines/Quality/Q2_R1/Step4/Q2_R1__Guideline.pdf.

Váradi, Csaba, Clarence Lew, and András Guttman. 2014. "Rapid Magnetic Bead Based Sample Preparation for Automated and High Throughput N-Glycan Analysis of Therapeutic Antibodies." *Analytical Chemistry* 86 (12): 5682–87. https://doi.org/10.1021/ac501573g.

Vázquez-Rey, María, and Dietmar A. Lang. 2011. “Aggregates in Monoclonal Antibody Manufacturing Processes.” *Biotechnology and Bioengineering* 108 (7): 1494–1508. https://doi.org/10.1002/bit.23155.

Ventouri, Iro K., Daniel B.A. Malheiro, Robert L.C. Voeten, Sander Kok, Maarten Honing, Govert W. Somsen, and Rob Haselberg. 2020. “Probing Protein Denaturation during Size-Exclusion Chromatography Using Native Mass Spectrometry.” *Analytical Chemistry* 92 (6): 4292–4300. https://doi.org/10.1021/acs.analchem.9b04961.

Vlasak, Josef, Marie C. Bussat, Shiyi Wang, Elsa Wagner-Rousset, Mark Schaefer, Christine Klinguer-Hamour, Marc Kirchmeier, Nathalie Corvaïa, Roxana Ionescu, and Alain Beck. 2009. “Identification and Characterization of Asparagine Deamidation in the Light Chain CDR1 of a Humanized IgG1 Antibody.” *Analytical Biochemistry* 392 (2): 145–54. https://doi.org/10.1016/j.ab.2009.05.043.

Vonk, Rudy J, Andrea F G Gargano, Ekaterina Davydova, Henk L Dekker, Sebastiaan Eeltink, Leo J De Koning, and Peter J Schoenmakers. 2015. “Comprehensive Two-Dimensional Liquid Chromatography with Stationary-Phase-Assisted Modulation Coupled to High-Resolution Mass Spectrometry Applied to Proteome Analysis of Saccharomyces Cerevisiae.” *Analytical Chemistry* 87 (10): 5387–94. https://doi.org/10.1021/acs.analchem.5b00708.

Wagner-rousset, Elsa, Szabolcs Fekete, Laura Morel-chevillet, Olivier Colas, Nathalie Corvaïa, Sarah Cianférani, Davy Guillarme, and Alain Beck. 2017. “Development of a Fast Workflow to Screen the Charge Variants of Therapeutic Antibodies.” *Journal of Chromatography A* 1498 (February): 147–54. https://doi.org/10.1016/j.chroma.2017.02.065.

Walsh. 2004. *Biopharmaceuticals: Biochemistry and Biotechnology, 2nd Edition*. *Biochemistry and Molecular Biology Education*. Vol. 32.

Walsh, Gary. 2010. “Biopharmaceutical Benchmarks 2010.” *Nature Biotechnology* 28 (9): 917–24.

Wang, Chunlei, Bhargavi Vemulapalli, Mingyan Cao, Dhanesh Gadre, Jihong Wang, Alan Hunter, Xiangyang Wang, and Dengfeng Liu. 2018. “A Systematic Approach for Analysis and Characterization of Mispairing in Bispecific Antibodies with Asymmetric Architecture.” *MAbs* 10 (8): 1226–35.

https://doi.org/10.1080/19420862.2018.1511198.

Wang, Xiaoling, Sandeep Kumar, and Satish K Singh. 2011. "Disulfide Scrambling in IgG2 Monoclonal Antibodies: Insights from Molecular Dynamics Simulations." *Pharmaceutical Research* 28 (June): 3128–44. https://doi.org/10.1007/s11095-011-0503-9.

Wang, Yi, Xiaojuan Li, Yan-hui Liu, Daisy Richardson, Huijuan Li, and Xiaoyu Yang. 2016. "Simultaneous Monitoring of Oxidation , Deamidation , Isomerization , and Glycosylation of Monoclonal Antibodies by Liquid Chromatography- Mass Spectrometry Method with Ultrafast Tryptic Digestion." *MAbs* 8 (8): 1477–86. https://doi.org/10.1080/19420862.2016.1226715.

Wang, Ziyan, Jianwei Zhu, and Huili Lu. 2020. "Antibody Glycosylation: Impact on Antibody Drug Characteristics and Quality Control." *Applied Microbiology and Biotechnology* 104 (5): 1905–14. https://doi.org/10.1007/s00253-020-10368-7.

Wecksler, Aaron T., Jian Yin, Paula Lee Tao, Bruce Kabakoff, Alavattam Sreedhara, and Galahad Deperalta. 2018. "Photodisruption of the Structurally Conserved Cys-Cys-Trp Triads Leads to Reduction-Resistant Scrambled Intrachain Disulfides in an IgG1 Monoclonal Antibody." *Molecular Pharmaceutics* 15 (4): 1598–1606. https://doi.org/10.1021/acs.molpharmaceut.7b01128.

Weidanz, Jon. 2021. "Targeting Cancer with Bispecific Antibodies." *Science* 371 (6533): 996–98.

Wheeler, Tobias D., Jing Lucy Sun, Sina Pleiner, Holger Geier, Philine Dobberthien, Joey Studts, Rajendra Singh, and Bahram Fathollahi. 2014. "Microchip Zone Electrophoresis for High-Throughput Analysis of Monoclonal Antibody Charge Variants." *Analytical Chemistry* 86 (11): 5416–24. https://doi.org/10.1021/ac500497n.

White, James, D Ph, Erik Miller, and D Ph. 2018. "Characterization of NISTmAb with Microfluidic CE-SDS Using the Protein Clear ™ HR Assay." *Application Note - PerkinElmer*.

Williams, Abasha, Erik K. Read, Cyrus D. Agarabi, Scott Lute, and Kurt A. Brorson. 2017. "Automated 2D-HPLC Method for Characterization of Protein Aggregation with in-Line Fraction Collection Device." *Journal of Chromatography B: Analytical Technologies in the Biomedical and Life Sciences* 1046 (301): 122–30.

https://doi.org/10.1016/j.jchromb.2017.01.021.

Williams, Abasha, Erik K Read, Cyrus D Agarabi, Scott Lute, and Kurt A Brorson. 2016. "Automated 2D-HPLC Method for Characterization of Protein Aggregation with In-Line Fraction Collection Device." *Journal of Chromatography B: Analytical Technologies in the Biomedical and Life Sciences* 1046 (301): 122–130.

Wise, John, Alexandra Grebe de Barron, Andrea Splendiani, Beeta Balali-Mood, Drashtti Vasant, Eric Little, Gaspare Mellino, et al. 2019. "Implementation and Relevance of FAIR Data Principles in Biopharmaceutical R&D." *Drug Discovery Today* 24 (4): 933–38. https://doi.org/10.1016/j.drudis.2019.01.008.

Wurm, Florian M. 2004. "Production of Recombinant Protein Therapeutics in Cultivated Mammalian Cells." *Nature Biotechnology* 22 (11): 1393–98. https://doi.org/10.1038/nbt1026.

Xiaojuan Li, Wei Xu, Yi Wang, Jia Zhao, Yan-Hui Liu, Daisy Richardson, Huijuan Li, Mohammed Shameem, Xiaoyu Yang. 2016. "High Throughput Peptide Mapping Method for Analysis of Site Specific Monoclonal Antibody Oxidation." *Journal of Chromatography A* 1460 (June): 51–60. https://doi.org/10.1016/j.chroma.2016.06.085.

Xiaojuan Li, et al. 2016. "High Throughput Peptide Mapping Method for Analysis of Site Specific Monoclonal Antibody Oxidation." *Journal of Chromatography A* 1460 ((2016)): 51–60. https://doi.org/10.1016/j.chroma.2016.06.085.

Xie, Panpan, Huijie Niu, Xinning Chen, Xintao Zhang, Shiwei Miao, Xiancun Deng, Xuping Liu, Wen Song Tan, Yan Zhou, and Li Fan. 2016. "Elucidating the Effects of PH Shift on IgG1 Monoclonal Antibody Acidic Charge Variant Levels in Chinese Hamster Ovary Cell Cultures." *Applied Microbiology and Biotechnology* 100 (24): 10343–53. https://doi.org/10.1007/s00253-016-7749-4.

Xu, Weichen, Rod Brian Jimenez, Rachel Mowery, Haibin Luo, Mingyan Cao, Nitin Agarwal, Irina Ramos, Xiangyang Wang, and Jihong Wang. 2017. "A Quadrupole Dalton-Based Multi-Attribute Method for Product Characterization, Process Development, and Quality Control of Therapeutic Proteins." *MAbs* 9 (7): 1186–96. https://doi.org/10.1080/19420862.2017.1364326.

Yan, Boxu, Zac Yates, Alain Balland, and Gerd R Kleemann. 2009. "Human IgG1 Hinge Fragmentation as the Result of H2O2 -Mediated Radical Cleavage □." *Journal of*

Biological Chemistry 284 (51): 35390–402. https://doi.org/10.1074/jbc.M109.064147.

Yan, Y., A.P. Liu, S. Wang, T.J. Daly, and N. Li. 2018. "Ultrasensitive Characterization of Charge Heterogeneity of Therapeutic Monoclonal Antibodies Using Strong Cation Exchange Chromatography Coupled to Native Mass Spectrometry." *Analytical Chemistry* 90 (21): 13013–20. https://doi.org/10.1021/acs.analchem.8b03773.

Yang, Renee, Yun Tang, Bing Zhang, Xuemei Lu, Alice Liu, and Yonghua Taylor. 2015. "High Resolution Separation of Recombinant Monoclonal Antibodies by Size-Exclusion Ultra-High Performance Liquid Chromatography." *Journal of Pharmaceutical and Biomedical Analysis* 109 (February): 52–61. https://doi.org/10.1016/j.jpba.2015.02.032.

Yang, Rong, Tushar Jain, Heather Lynaugh, R Paul Nobrega, Xiaojun Lu, Todd Boland, Irina Burnina, et al. 2017. "Rapid Assessment of Oxidation via Middle-down LCMS Correlates with Methionine Side-Chain Solvent-Accessible Surface Area for 121 Clinical Stage Monoclonal Antibodies." *MAbs* 9 (4): 646–53. https://doi.org/10.1080/19420862.2017.1290753.

Yang, Shuang, David Clark, Yang Liu, Shuwei Li, and Hui Zhang. 2017. "High-Throughput Analysis of N-Glycans Using AutoTip via Glycoprotein Immobilization." *Nature Scientific Reports* 7 (10216): 1–11. https://doi.org/10.1038/s41598-017-10487-8.

Yip, Stephanie. 2019. "Top 10 Best-Selling Drugs of 2018 Fund US and EU Pharma R&D." *Informa Pharma Intelligence* 2019 (May): 1–24. file:///C:/Users/kqtd185/Box Sync/Giulia Box folders/Papers/top-10-best-selling-drugs-of-2018-fund-us-and-eu-pharma-rd.pdf.

Yu, Lin, Nan Huang, Liangpeng Ge, Heng Sun, Yuna Fu, Chundong Liu, and Jianhua Wang. 2021. "Structural Design of Tetravalent T-Cell Engaging Bispecific Antibodies : Improve Developability by Engineering Disulfide Bonds." *Journal of Biological Engineering* 15 (18): 1–10.

Yuk, Inn H., Stephen Russell, Yun Tang, Wei Ting Hsu, Jacob B. Mauger, Rigzen P.S. Aulakh, Jun Luo, Martin Gawlitzek, and John C. Joly. 2015. "Effects of Copper on CHO Cells: Cellular Requirements and Product Quality Considerations." *Biotechnology Progress* 31 (1): 226–38. https://doi.org/10.1002/btpr.2004.

Zeitlin, Kevin J. Whaley Larry. 2021. "Emerging Antibody-Based Products for Infectious

Diseases:Planning for Metric Ton Manufacturing." *Human Vaccines and Immunotherapeutics* 17 (7): 1–11.

Zhang, Bing, Justin Jeong, Braydon Burgess, Mansour Jazayri, Yun Tang, and Yonghua Taylor Zhang. 2016. "Development of a Rapid RP-UHPLC–MS Method for Analysis of Modifications in Therapeutic Monoclonal Antibodies." *Journal of Chromatography B* 1032 (October): 172–81. https://doi.org/10.1016/J.JCHROMB.2016.05.017.

Zhang, Hao, Weidong Cui, and Michael L. Gross. 2014. "Mass Spectrometry for the Biophysical Characterization of Therapeutic Monoclonal Antibodies." *FEBS Letters* 588 (2): 308–17. https://doi.org/10.1016/j.febslet.2013.11.027.

Zhang, Jinyou. 2010. "Mammalian Cell Culture for Biopharmaceutical Production." In *Mammalian Cell Culture for Biopharmaceutical Production, Manual of Industrial Microbiology and Biotechnology, Third Edition*, Third Edit, 157–78. Washington, DC, USA: ASM Press. https://doi.org/10.1128/9781555816827.

Zhang, Kerong, and Wuyi Liu. 2020. "The Current Status , Trend , and Development Strategies of Chinese Biopharmaceutical Industry With a Challenging Perspective." *SAGE Open* 10 (1): 1–16. https://doi.org/10.1177/2158244020901529.

Zhang, Lei, Shen Luo, and Baolin Zhang. 2016. "Glycan Analysis of Therapeutic Glycoproteins." *MAbs* 8 (2): 205–15. https://doi.org/10.1080/19420862.2015.1117719.

Zhang, Ximo, Corey E Reed, Robert E Birdsall, Ying Qing Yu, and Weibin Chen. 2020. "High-Throughput Analysis of Fluorescently Labeled N-Glycans Derived from Biotherapeutics Using an Automated LC-MS-Based Solution." *SLAS Technology* 25 (4): 380–87. https://doi.org/10.1177/2472630320922803.

Zhang, Yun, and Jingzhong Guo. 2017. "Characterization and QC of Biopharmaceuticals by MS-Based 'Multi-Attribute Method': Advantages and Challenges." *Bioanalysis* 9 (6): 499–502. https://doi.org/10.4155/bio-2017-0004.

Zhang, Zhongqi, Bhavana Shah, and Xiaoyan Guan. 2019. "Reliable LC-MS Multiattribute Method for Biotherapeutics by Run-Time Response Calibration." Research-article. *Analytical Chemistry* 91 (8): 5252–60. https://doi.org/10.1021/acs.analchem.9b00027.

Zhao, Shimin, Wei Xu, Wenqing Jiang, Wei Yu, Yan Lin, Tengfei Zhang, Jun Yao, et al. 2010. "Regulation of Cellular Metabolism by Protein Lysine Acetylation." *Science* 327 (5968): 1000–1004. https://doi.org/10.1126/science.1179689.

Zheng, Kai, Christopher Bantog, and Robert Bayer. 2011. “The Impact of Glycosylation on Monoclonal Antibody Conformation and Stability.” *MAbs* 3 (6): 568–76. https://doi.org/10.4161/mabs.3.6.17922.

Zheng, Kai, Diya Ren, Y John Wang, Wayne Lilyestrom, Thomas Scherer, Justin K Y Hong, and Junyan A Ji. 2021. “Monoclonal Antibody Aggregation Associated with Free Radical Induced Oxidation.” *Journal of Molecular Sciences* 22 (April): 3952.

This page was intentionally left blank

Appendix

Appendix A

Supplementary information related to Chapter 3

Table 9.1 PhyTip purification method development MESD factors, responses and constant parameters.

MESD Factors	Constant parameters
Capture cycles (4 – 15)	Equilibration processing volume: 160 µL
Capture F (4 – 16 µL/sec)	Equilibration cycles: 2 x 15
Wash1 cycles (1 – 3)	Equilibration F: 8 µL/sec
Wash1 F (4 – 16 µL/sec)	Capture well volume: 300 µL
Wash2 cycles (1 – 3)	Capture processing volume: 160 µL
Wash2 F (4 – 16 µL/sec)	Washing steps well volume: 200 µL
Elution cycles (4 – 15)	Washing processing well-volume:160 µL
Elution F (4 – 16 µL/sec)	PhyTip column loading ~75%
Final Elution Volume (80 – 120 µL)	Equilibration and Wash1 buffer: DPBS
MESD Response	Wash2 buffer: 25 mM acetate, 120 mM NaCl, pH 5.5
%R	Elution buffer: 25 mM acetate pH 3.6

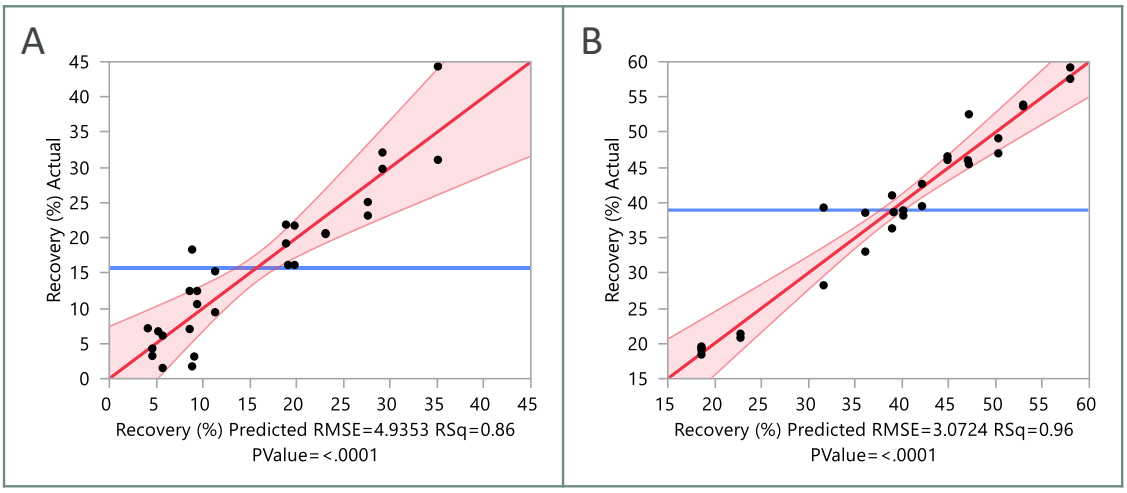

Figure 9.1 PhyTip purification method development MESD actual-by-predicted plot. A) mAb-1 and B) BsAb-1 MESD model actual-by-predicted plot showing the experimental values plotted against the model estimates. The linear function y = x (red) was reported with the confidence intervals (pink) and the mean of the responses (blue). The p-value (<0.0001), R^2 (RSq = 0.86) and RSME (4.9353) were reported and define the model significance and goodness of fit.

$$\text{Desirability}\left(\begin{bmatrix}0\\20\\40\end{bmatrix},\begin{bmatrix}0.066\\0.5\\0.982\end{bmatrix},\text{Recovery (\%)}\hat{}\right) \tag{6.1.A}$$

$$\text{Desirability}\left(\begin{bmatrix}15\\35\\55\end{bmatrix},\begin{bmatrix}0.066\\0.5\\0.982\end{bmatrix},\text{Recovery (\%)}\hat{}\right) \tag{6.1.B}$$

Equation 9.1 PhyTip purification method development MESD models desirability formula of mAb-1 (A) and BsAb-1 (B).

Table 9.2 PhyTip purification CCD factors, responses and constant parameters.

CCD Factors
Capture cycles (8 – 20)
Capture F (2 – 4 µL/sec)
Final Elution Volume (80 – 160 µL)
CCD Response
%R
Constant parameters
Wash1 cycles (1) F (4 µL/sec)
Wash1 F (4 µL/sec)
Wash2 cycles (1), F (4 µL/sec)
Wash2 F (4 µL/sec)
Wash2 cycles (1)
Wash2 F (4 µL/sec)
Elution cycles (4)
Elution F 4 µL/sec

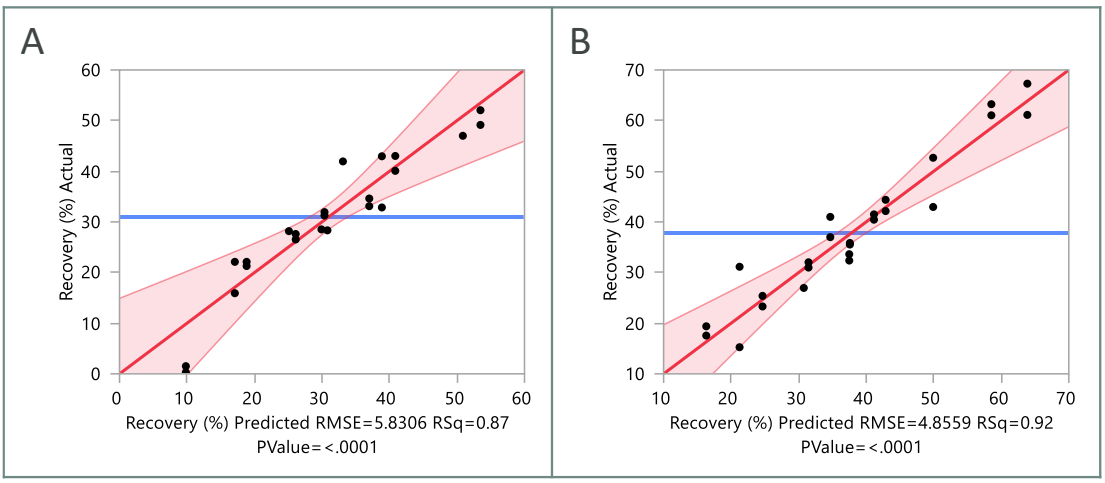

Figure 9.2 PhyTip purification CCD actual-by-predicted plot.

A) mAb-1 and B) BsAb-1 MESD model actual-by-predicted plot showing the experimental values plotted against the model estimates. The linear function y = x (red) was reported with the confidence intervals (pink) and the mean of the responses (blue). The p-value, R^2 and RSME were reported and define the model significance and goodness of fit.

$$\text{Desirability}\left(\begin{bmatrix}0\\22.5\\50\end{bmatrix},\begin{bmatrix}0.144\\0.5\\0.982\end{bmatrix},\text{Recovery (\%)}\right)^{\wedge} \quad (6.2.A)$$

$$\text{Desirability}\left(\begin{bmatrix}10\\30\\70\end{bmatrix},\begin{bmatrix}0.28\\0.5\\0.982\end{bmatrix},\text{Recovery (\%)}\right)^{\wedge} \quad (6.2.B)$$

Equation 9.2 PhyTip purification method development CCD models desirability formula of mAb-1 (A) and BsAb-1 (B).

Table 9.3 Full dataset of the linearity study and determination of the column loading range %R.

Molecule	N	Capacity (%)	Loading (mg/mL)	Loading (ug)	%R	Recovery (ug)	Mean (%R)	Std Dev (%R)	CV (%R)
BsAb-1	1	8.7375	0.233	69.9	103.77	72.535	80.88	13.0248	16.1030
BsAb-1	2	8.7375	0.233	69.9	101.18	70.724	80.88	13.0248	16.1030
mAb-1	1	8.7375	0.233	69.9	98.22	68.65	85.02	10.3421	12.1643
mAb-1	2	8.7375	0.233	69.9	99.23	69.36	85.02	10.3421	12.1643
BsAb-1	1	21.8625	0.583	174.9	85.09	148.82	80.88	13.0248	16.1030
BsAb-1	2	21.8625	0.583	174.9	85.43	149.41	80.88	13.0248	16.1030
mAb-1	1	21.8625	0.583	174.9	76.91	134.51	85.02	10.3421	12.1643
mAb-1	2	21.8625	0.583	174.9	75.66	132.32	85.02	10.3421	12.1643
BsAb-1	1	43.875	1.17	351	77.13	270.72	80.88	13.0248	16.1030
BsAb-1	2	43.875	1.17	351	74.02	259.81	80.88	13.0248	16.1030
mAb-1	1	43.875	1.17	351	71.13	249.66	85.02	10.3421	12.1643
mAb-1	2	43.875	1.17	351	72.18	253.35	85.02	10.3421	12.1643
BsAb-1	1	75	2	600	68.9	413.40	80.88	13.0248	16.1030
BsAb-1	2	75	2	600	64.79	388.74	80.88	13.0248	16.1030
mAb-1	1	75	2	600	89.49	536.94	85.02	10.3421	12.1643
mAb-1	2	75	2	600	87.78	526.68	85.02	10.3421	12.1643
BsAb-1	1	112.5	3	900	75.07	675.63	80.88	13.0248	16.1030
BsAb-1	2	112.5	3	900	73.46	661.14	80.88	13.0248	16.1030
mAb-1	1	112.5	3	900	90.8	817.20	85.02	10.3421	12.1643
mAb-1	2	112.5	3	900	88.8	799.20	85.02	10.3421	12.1643

Table 9.4 T-test of the %HMWS analysed before and after PhyTip purification by SEC for the assessment of the method suitability-for-Use.

The standardised distances between the sample mean and the population mean are described by the t-distribution, here reported for the %HMWS quantified for BsAb-1 by A) HP SEC M1 and B) HT SEC; mAb-1 by C) HP SEC M2 and D) HT SEC.

Molecule: BsAb-1 **Method: HP SEC M1**			
Difference	0.5267	t Ratio	0.483991
Std Err Dif	1.0882	DF	2.017908
Upper CL Dif	5.1691	Prob > |t|	0.6758
Lower CL Dif	-4.1158	Prob > t	0.3379
Confidence	0.95	Prob < t	0.6621

A

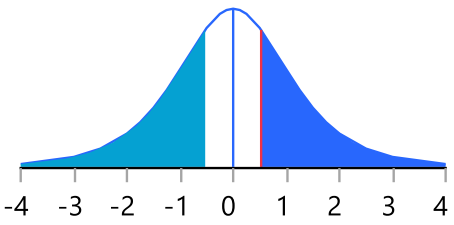

Molecule: BsAb-1 **Method: HT SEC**			
Difference	1.1425	t Ratio	1.405622
Std Err Dif	0.8128	DF	1.1193
Upper CL Dif	9.2000	Prob > |t|	0.3751
Lower CL Dif	-6.9150	Prob > t	0.1876
Confidence	0.95	Prob < t	0.8124

B

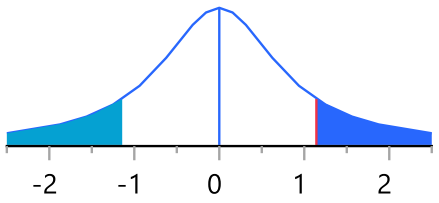

Molecule: mAb-1 **Method: HP SEC M2**			
Difference	0	t Ratio	.
Std Err Dif	0	DF	.
Upper CL Dif	.	Prob > |t|	.
Lower CL Dif	.	Prob > t	.
Confidence	0.95	Prob < t	.

C

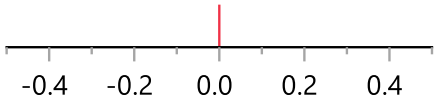

Molecule: mAb-1 **Method: HT SEC**			
Difference	0.0233	t Ratio	0.079638
Std Err Dif	0.2930	DF	2.535421
Upper CL Dif	1.0603	Prob > |t|	0.9424
Lower CL Dif	-1.0136	Prob > t	0.4712
Confidence	0.95	Prob < t	0.5288

D

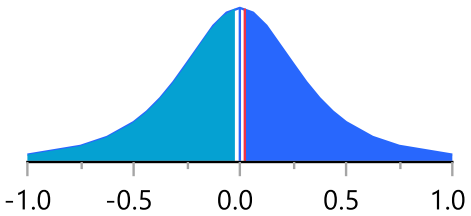

Table 9.5 SEC Methods employed for analysing the %HMWS during the assessment of PhyTip purification suitability-for-Use.

Method Name	Molecule	Conditions
HT SEC	mAb-1 and BsAb-1	See Chaper 3, Table 3.7
HP SEC M1	BsAb-1	Column: Aquity BEH SEC 4.6 x 150 mm, 1.7 µm dp, 200 Å; mobile phase: 50 mM Na_3PO_4, 200 mM NaCl, pH 6.7; Flow rate: 0.5 mL/min; Temperature : 25 °C, Injection volume: 5 µL; Detector: UV, 280 nm.
HP SEC M2	mAb-1	Agilent AdvanceBio SEC 200A 1.9um, 4.6 x 150mm, 100 mM Na_3PO_4, pH 6.0, Flow rate: 0.5 mL/min; Temperature : 25 °C, Injection volume: 5 µL; Detector: UV, 280 nm.

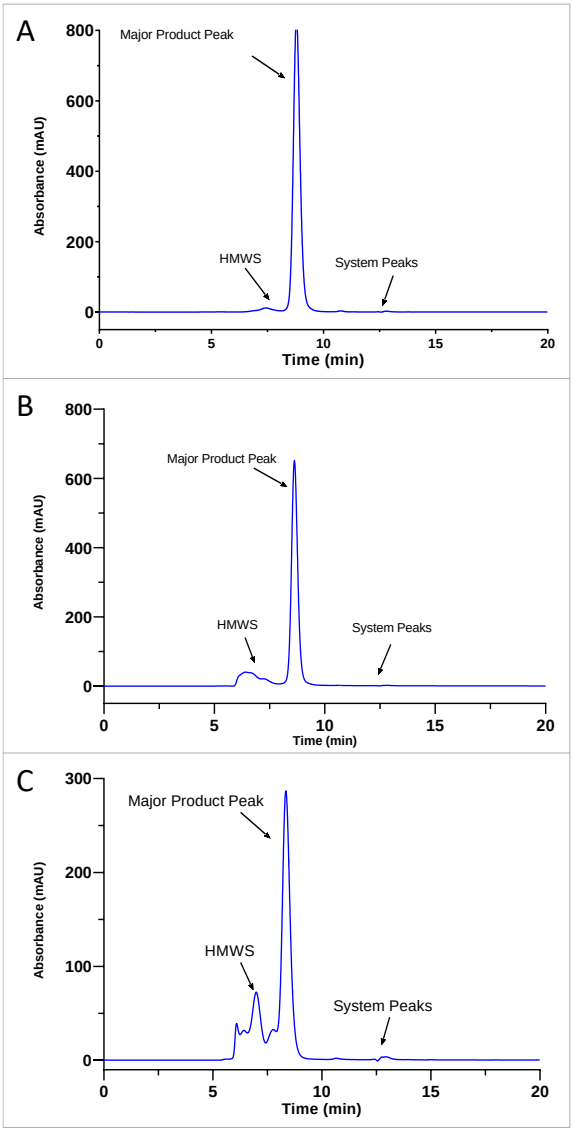

Figure 9.3 Analysis of mAb-1, mAb-2 and BsAb-1 HMWS impurities by AZ SEC SOP. Chromatograms of A) mAb-1, B) mAb-1 and C) BsAb-1 were analysed by the AZ SEC SOP. The HMWS impurities were 3, 17 and 35% for mAb-2, mAb-1 and BsAb-1, respectively.

Table 9.6. List of factors and responses of the MESD for HT SEC method development.

Factors	Responses
Flow rate: 0.05 – 0.15 mL/min	T_s
Injection volume: 0.5 – 10 µL	%HMWS
Salt concentration: 5 – 200 mM	Rs
Column: Waters, Sepax	

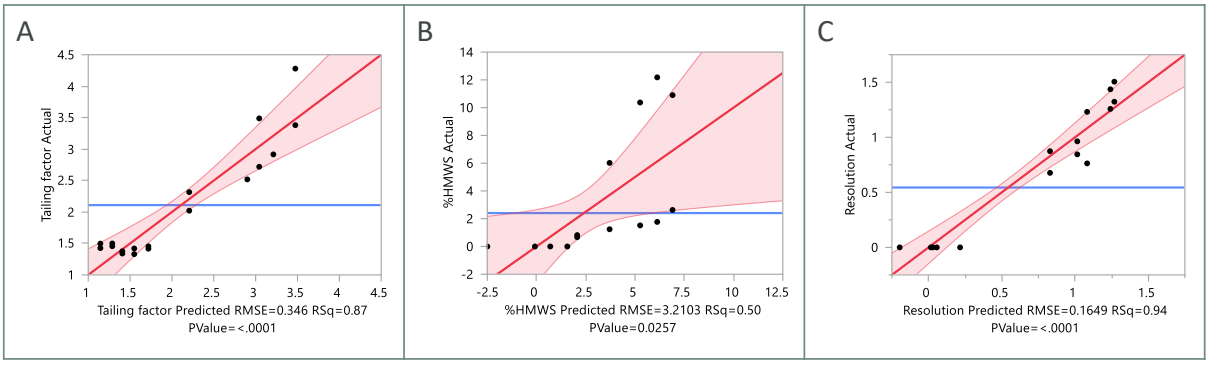

Figure 9.4 HT SEC MESD actual-by-predicted plot for the responses analysed separately.

The model p-value, RMSE, and R^2were reported for all the responses, namely A) Ts p-value < 0.0001, RMSE = 0.346, $R^2 = 0.87$; B) %HMWS p-value < 0.025, RMSE = 3.2103, $R^2 = 0.5$; and C) Rs p-value < 0.0001, RMSE = 0.1649, $R^2 = 0.94$.

(6.3)

$$\text{Exp}\left(\begin{array}{l} 0.2 \bullet \text{Log}\left(\text{Desirability}\left(\begin{bmatrix}0.8\\1\\1.2\end{bmatrix},\begin{bmatrix}0.018\\1\\0.018\end{bmatrix},\text{Tailing factor}\hat{}\right)\right) \\ +0.6 \bullet \text{Log}\left(\text{Desirability}\left(\begin{bmatrix}-2\\6\\14\end{bmatrix},\begin{bmatrix}1\\1\\1\end{bmatrix},\text{\%HMWS}\hat{}\right)\right) \\ +0.2 \bullet \text{Log}\left(\text{Desirability}\left(\begin{bmatrix}1.5\\1.625\\1.75\end{bmatrix},\begin{bmatrix}0.066\\0.5\\0.982\end{bmatrix},\text{Resolution}\hat{}\right)\right) \end{array}\right)$$

Equation 9.3 HT SEC MESD desirability formula.

Table 9.7 List of the 2x2x3 FFD DoE factors, responses and analysis conditions.

Factors
Buffer concentration (50-200 mM Na3PO4 buffer dibasic/monobasic)
NaCl concentration (0-200 mM)
Columns: AdvanceBio SEC 2.1 x 150mm, 1.9 µm, 300Å (Agilent); AQUITY UPLC Protein BEH SEC 2.1x150 mm, 1.7 µm, 200Å (Waters), Unix™-C UHPLC SEC 2.1 x 150, 1.8 µm, 300Å (Sepax)
Responses
Rs
%HMWS
Constant parameters
Sample concentration: 5 mg/mL
Injection Volume: 2 µL
F: 0.15 mL/min
Temperature: 25 °C
Buffer pH: 6.8
UV: 210 nm, 280 nm

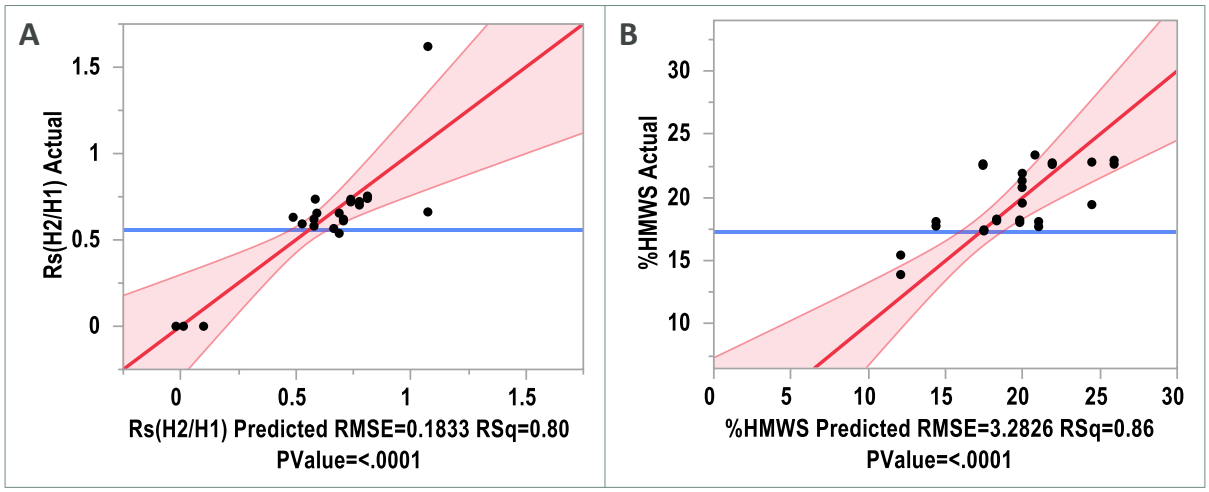

Figure 9.5 HT SEC 2x2x3 FFD DoE actual-by-predicted plot.
HT SEC 2x2x3 full factorial DoE actual-by-predicted plot for A) BsAb-1 shoulder H1/H2 resolution Rs(H2/H1), and B) %HMWS. The model p-value < 0.0001, RMSE = 0.1833, R^2 = 0.80 (A) and p-value < 0.0001, RMSE = 3.2826, R^2 = 0.86 (B) are evidence of the model significancy and goodness-of-fit.

$$\mathrm{Exp}\left(0.5 \bullet \mathrm{Log}\left(\mathrm{Desirability}\left(\begin{bmatrix}-0.1\\0.3\\0.7\end{bmatrix},\begin{bmatrix}0.066\\0.5\\0.982\end{bmatrix},\mathrm{Rs(H2/H1)}\right)^{\wedge}\right) + 0.5 \bullet \mathrm{Log}\left(\mathrm{Desirability}\left(\begin{bmatrix}25\\30\\35\end{bmatrix},\begin{bmatrix}0.018\\1\\0.018\end{bmatrix},\mathrm{\%HMWS}\right)^{\wedge}\right)\right) \quad (6.4)$$

Equation 9.4 HT SEC 2x2x3 DoE desirability formula for BsAb-1.

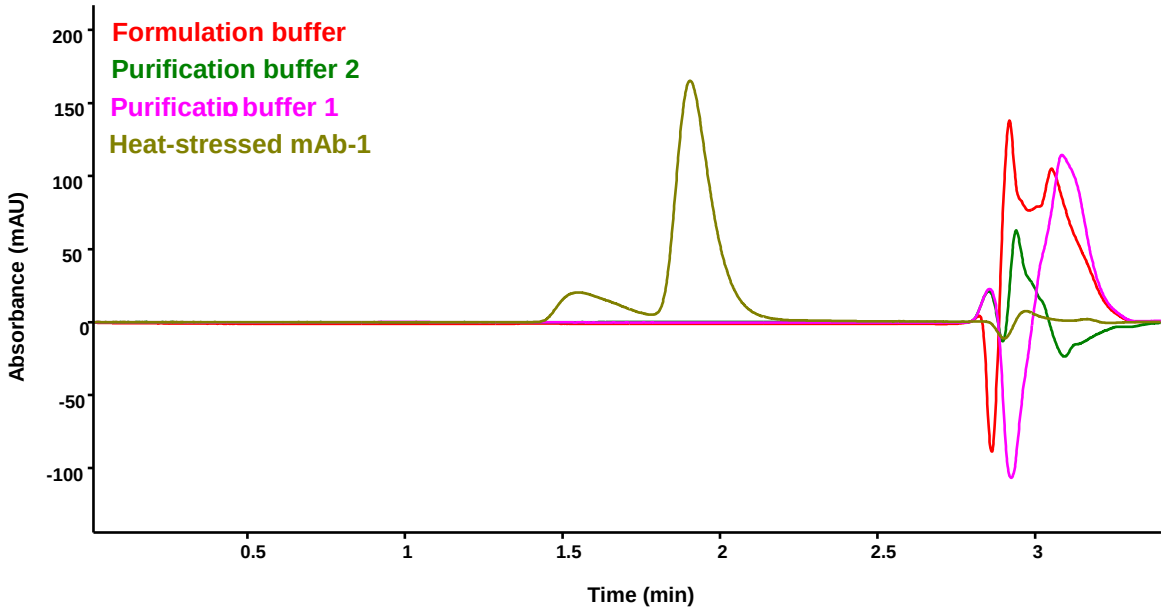

Figure 9.6 HT SEC specificity assessment.

HT SEC chromatogram overlay of a sample of heat-stressed mAb-1 (gold) against the mAb formulation buffer (red), PhyTip purification wash buffer (pink) and GlyHCl-2.6 elution buffer (green). The mAb-1 sample was diluted to 1 mg/mL before analysis and the injection volume was 5 µL, whereas the buffers injection volume was 20 µL.

Table 9.8 HT SEC throughput gain by injection overlapping.

Run time		
µ (n = 12)	**Single injection**	**Overlapped injections**
	4.2 min	3.5 min
Time gained = 0.7 min		

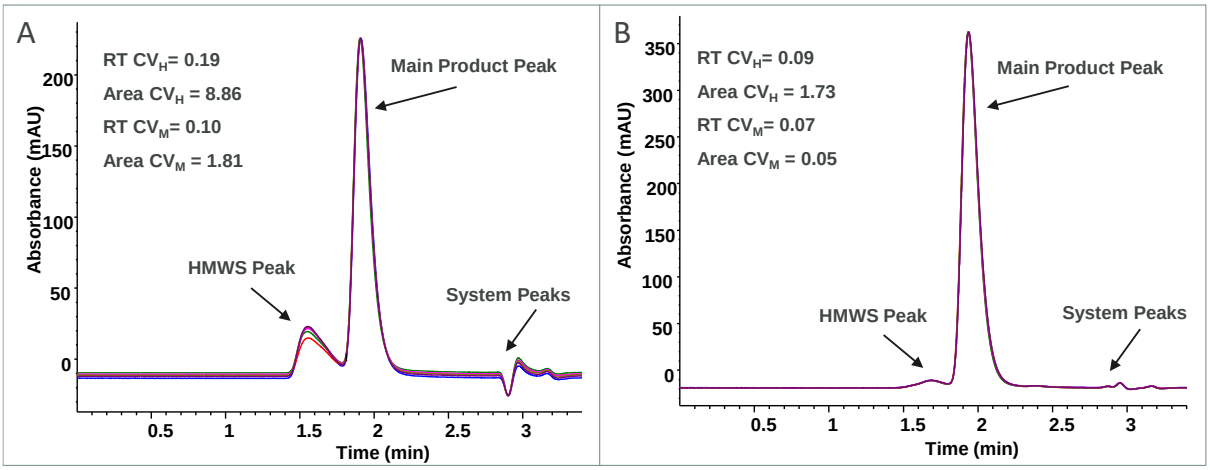

Figure 9.7 HT SEC repeatability study.

Chromatogram overlay of six replicate injections of a sample of A) mAb-1 and B) mAb-2 showing the separation of HMWS peak, main product peak, and system peaks. The reporting the CV of the retention time and area of the HMWS (RT CV_H, Area CV_H) and main product peak (RT CV_M, Area CV_M) were reported for each molecule. The CV of mAb-1 HMWS and main product peak retention time were 0.19 and 0.1 and peak area 8.86 and 1.81, respectively (A). B) The CV of mAb-2 HMWS and main product peak retention time were 0.09 and 0.07 and area 1.73 and .0.05, respectively (B). The samples were diluted to 1 mg/mL before the analysis and the injection volume was kept constant at 5 mL.

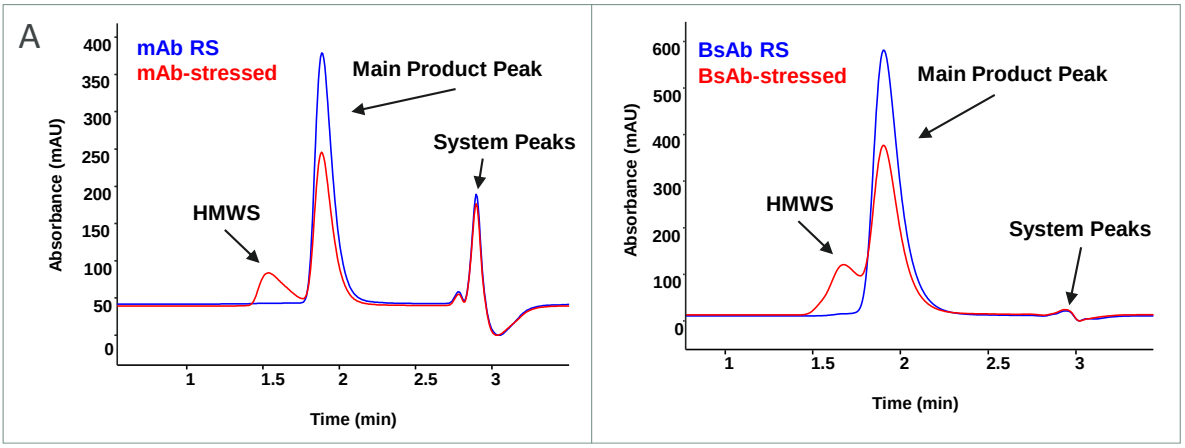

Figure 9.8 HT SEC stability-indicating capability.

Chromatogram overlay of the stressed sample (red) against its RS (blue) for both mAb-1 (A) and BsAb-1 (B) analysed by HT SEC. The UV trace shows the separation of HMWS, main product peak and system peaks in both molecules. The %HMWS of the stressed samples (A/B, red) is increased when compared to the mAb-1 RS (A, blue) and BsAb-1 RM (B, blue). The samples were diluted to 1 mg/mL before analysis.

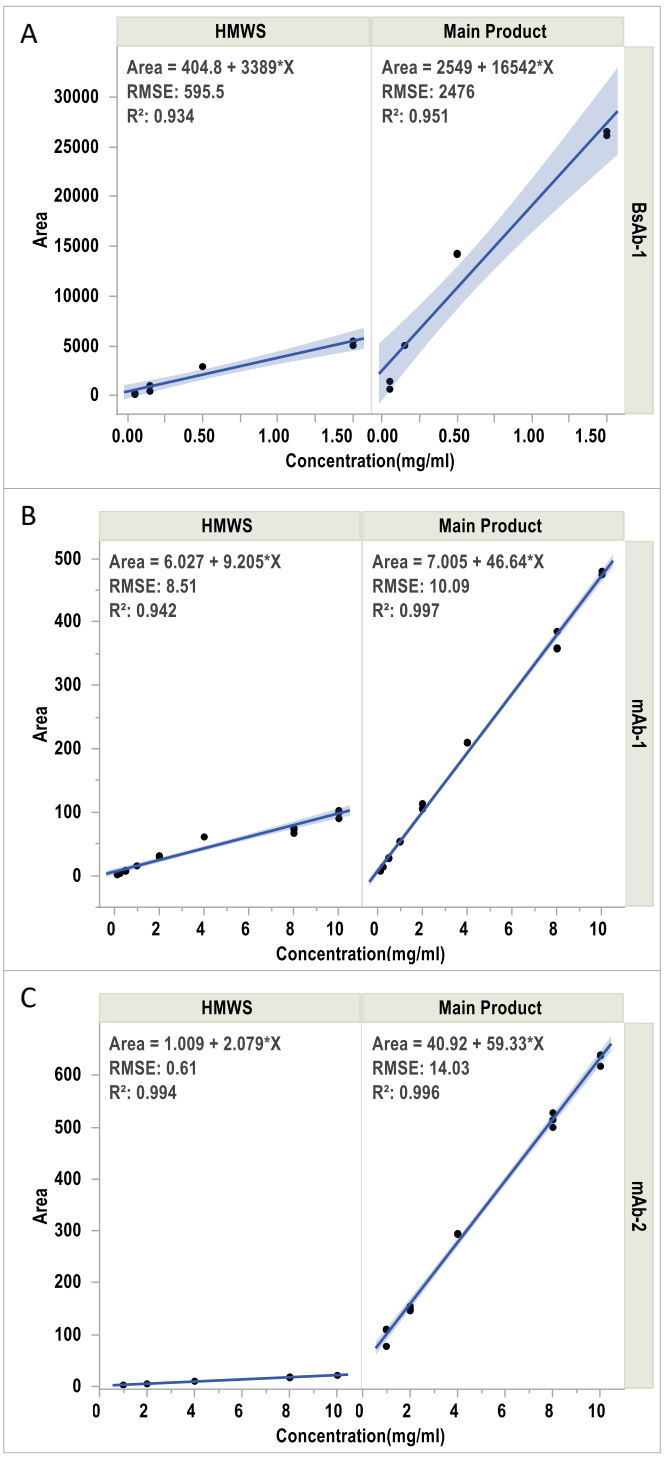

Figure 9.9 Linearity test of the UV absorbance response *vs.* %HMWS.
HT SEC method linearity study comprising of 5 concentration levels each analysed in triplicate and performed for the three molecules used for method development: BsAb-1, mAb-1 and mAb-2. Linear regression analysis of the peak area *vs.* the sample concentration was plotted for A) BsAb-1 samples displaying 0.2, 0.4, 0.8, 1.7, and 2.5 mg/mL concentration range and 10 µL injection volume; B) mAb-1 and C) mAb-2 samples with concentrations 10, 8, 4, 2, and 1 mg/mL and 0.1 µL injection volume.

Table 9.9 HT SEC accuracy study.

Molecule	N	Inj. V	C mg/ml	Load ug	Peak Name	Area	% Area	Mean %Area	CV %Area	Grand Mean %Area	CV Accuracy
BsAb-1	1	10	0.05	0.50	HMWS	108.58	14.59	15.04	4.23	16.26	4.92
BsAb-1	2	10	0.05	0.50	HMWS	260.62	15.49	15.04	4.23	16.26	4.92
BsAb-1	2	10	0.15	1.50	HMWS	438.57	16.07	16.36	2.46	16.26	4.92
BsAb-1	1	10	0.15	1.50	HMWS	1004.54	16.64	16.36	2.46	16.26	4.92
BsAb-1	2	10	0.50	5.00	HMWS	2903.92	17.01	17.05	0.29	16.26	4.92
BsAb-1	1	10	0.50	5.00	HMWS	2941.61	17.08	17.05	0.29	16.26	4.92
BsAb-1	1	10	1.50	15.00	HMWS	5017.63	16.12	16.62	4.21	16.26	4.92
BsAb-1	2	10	1.50	15.00	HMWS	5473.11	17.11	16.62	4.21	16.26	4.92
mAb-1	1	0.1	0.13	0.01	HMWS	1.10	14.32	18.53	20.13	20.03	11.84
mAb-1	2	0.1	0.13	0.01	HMWS	1.70	19.83	18.53	20.13	20.03	11.84
mAb-1	3	0.1	0.13	0.01	HMWS	2.00	21.43	18.53	20.13	20.03	11.84
mAb-1	3	0.1	0.25	0.03	HMWS	3.20	19.48	20.49	6.64	20.03	11.84
mAb-1	1	0.1	0.25	0.03	HMWS	3.50	19.95	20.49	6.64	20.03	11.84
mAb-1	2	0.1	0.25	0.03	HMWS	4.00	22.04	20.49	6.64	20.03	11.84
mAb-1	2	0.1	0.50	0.05	HMWS	6.70	20.75	21.73	3.99	20.03	11.84
mAb-1	1	0.1	0.50	0.05	HMWS	7.50	22.03	21.73	3.99	20.03	11.84
mAb-1	3	0.1	0.50	0.05	HMWS	8.00	22.40	21.73	3.99	20.03	11.84
mAb-1	1	0.1	1.00	0.10	HMWS	15.10	21.62	22.32	3.10	20.03	11.84
mAb-1	3	0.1	1.00	0.10	HMWS	15.10	23.00	22.32	3.10	20.03	11.84
mAb-1	2	0.1	1.00	0.10	HMWS	15.20	22.34	22.32	3.10	20.03	11.84
mAb-1	2	0.1	2.00	0.20	HMWS	28.50	21.39	21.57	0.85	20.03	11.84
mAb-1	3	0.1	2.00	0.20	HMWS	29.40	21.75	21.57	0.85	20.03	11.84
mAb-1	1	0.1	2.00	0.20	HMWS	31.10	21.56	21.57	0.85	20.03	11.84
mAb-1	2	0.1	4.00	0.40	HMWS	60.80	22.45	22.49	0.26	20.03	11.84
mAb-1	1	0.1	4.00	0.40	HMWS	60.90	22.56	22.49	0.26	20.03	11.84
mAb-1	3	0.1	4.00	0.40	HMWS	60.90	22.47	22.49	0.26	20.03	11.84
mAb-1	1	0.1	8.00	0.80	HMWS	66.50	15.70	16.25	3.32	20.03	11.84
mAb-1	3	0.1	8.00	0.80	HMWS	72.40	16.78	16.25	3.32	20.03	11.84
mAb-1	2	0.1	8.00	0.80	HMWS	74.80	16.28	16.25	3.32	20.03	11.84
mAb-1	1	0.1	10.00	1.00	HMWS	89.70	15.90	16.90	5.24	20.03	11.84
mAb-1	2	0.1	10.00	1.00	HMWS	98.70	17.21	16.90	5.24	20.03	11.84
mAb-1	3	0.1	10.00	1.00	HMWS	102.40	17.59	16.90	5.24	20.03	11.84
mAb-2	1	0.1	1.00	0.10	HMWS	2.60	3.21	2.67	18.25	3.21	9.09
mAb-2	2	0.1	1.00	0.10	HMWS	2.60	2.27	2.67	18.25	3.21	9.09
mAb-2	3	0.1	1.00	0.10	HMWS	2.80	2.54	2.67	18.25	3.21	9.09
mAb-2	2	0.1	2.00	0.20	HMWS	4.90	3.24	3.25	2.33	3.21	9.09
mAb-2	3	0.1	2.00	0.20	HMWS	4.90	3.18	3.25	2.33	3.21	9.09
mAb-2	1	0.1	2.00	0.20	HMWS	5.30	3.33	3.25	2.33	3.21	9.09
mAb-2	2	0.1	4.00	0.40	HMWS	9.90	3.26	3.33	2.12	3.21	9.09
mAb-2	3	0.1	4.00	0.40	HMWS	10.20	3.33	3.33	2.12	3.21	9.09
mAb-2	1	0.1	4.00	0.40	HMWS	10.40	3.40	3.33	2.12	3.21	9.09
mAb-2	2	0.1	8.00	0.80	HMWS	16.60	3.54	3.49	1.75	3.21	9.09

mAb-2	3	0.1	8.00	0.80	HMWS	17.90	3.42	3.49	1.75	3.21	9.09
mAb-2	1	0.1	8.00	0.80	HMWS	18.20	3.52	3.49	1.75	3.21	9.09
mAb-2	3	0.1	10.00	1.00	HMWS	21.20	3.32	3.32	0.08	3.21	9.09
mAb-2	1	0.1	10.00	1.00	HMWS	21.70	3.32	3.32	0.08	3.21	9.09
mAb-2	2	0.1	10.00	1.00	HMWS	21.90	3.33	3.32	0.08	3.21	9.09
BsAb-1	1	10	0.05	0.50	MP	635.72	85.41	84.96	0.75	83.74	0.96
BsAb-1	2	10	0.05	0.50	MP	1421.57	84.51	84.96	0.75	83.74	0.96
BsAb-1	1	10	0.15	1.50	MP	5031.07	83.36	83.65	0.48	83.74	0.96
BsAb-1	2	10	0.15	1.50	MP	5031.07	83.93	83.65	0.48	83.74	0.96
BsAb-1	2	10	0.50	5.00	MP	14163.78	82.99	82.96	0.06	83.74	0.96
BsAb-1	1	10	0.50	5.00	MP	14279.62	82.92	82.96	0.06	83.74	0.96
BsAb-1	1	10	1.50	15.00	MP	26100.95	83.88	83.39	0.84	83.74	0.96
BsAb-1	2	10	1.50	15.00	MP	26511.38	82.89	83.39	0.84	83.74	0.96
mAb-1	3	0.1	0.03	0.00	MP	1.10	100.00	100.00	0.00	83.97	10.03
mAb-1	2	0.1	0.03	0.00	MP	1.20	100.00	100.00	0.00	83.97	10.03
mAb-1	1	0.1	0.03	0.00	MP	1.30	100.00	100.00	0.00	83.97	10.03
mAb-1	3	0.1	0.06	0.01	MP	2.70	100.00	100.00	0.00	83.97	10.03
mAb-1	2	0.1	0.06	0.01	MP	2.80	100.00	100.00	0.00	83.97	10.03
mAb-1	1	0.1	0.06	0.01	MP	3.30	100.00	100.00	0.00	83.97	10.03
mAb-1	2	0.1	0.13	0.01	MP	6.80	80.17	81.47	4.58	83.97	10.03
mAb-1	1	0.1	0.13	0.01	MP	6.90	85.68	81.47	4.58	83.97	10.03
mAb-1	3	0.1	0.13	0.01	MP	7.30	78.57	81.47	4.58	83.97	10.03
mAb-1	3	0.1	0.25	0.03	MP	13.40	80.52	79.51	1.71	83.97	10.03
mAb-1	1	0.1	0.25	0.03	MP	14.00	80.05	79.51	1.71	83.97	10.03
mAb-1	2	0.1	0.25	0.03	MP	14.00	77.97	79.51	1.71	83.97	10.03
mAb-1	2	0.1	0.50	0.05	MP	26.60	79.25	78.27	1.11	83.97	10.03
mAb-1	3	0.1	0.50	0.05	MP	27.50	77.60	78.27	1.11	83.97	10.03
mAb-1	1	0.1	0.50	0.05	MP	28.00	77.97	78.27	1.11	83.97	10.03
mAb-1	2	0.1	1.00	0.10	MP	52.70	77.66	77.68	0.89	83.97	10.03
mAb-1	3	0.1	1.00	0.10	MP	53.90	77.00	77.68	0.89	83.97	10.03
mAb-1	1	0.1	1.00	0.10	MP	54.70	78.39	77.68	0.89	83.97	10.03
mAb-1	2	0.1	2.00	0.20	MP	104.70	78.61	78.43	0.23	83.97	10.03
mAb-1	3	0.1	2.00	0.20	MP	105.80	78.25	78.43	0.23	83.97	10.03
mAb-1	1	0.1	2.00	0.20	MP	113.30	78.44	78.43	0.23	83.97	10.03
mAb-1	1	0.1	4.00	0.40	MP	208.90	77.44	77.51	0.08	83.97	10.03
mAb-1	2	0.1	4.00	0.40	MP	210.10	77.55	77.51	0.08	83.97	10.03
mAb-1	3	0.1	4.00	0.40	MP	210.10	77.54	77.51	0.08	83.97	10.03
mAb-1	1	0.1	8.00	0.80	MP	357.20	84.30	83.75	0.64	83.97	10.03
mAb-1	3	0.1	8.00	0.80	MP	359.00	83.22	83.75	0.64	83.97	10.03
mAb-1	2	0.1	8.00	0.80	MP	384.80	83.72	83.75	0.64	83.97	10.03
mAb-1	1	0.1	10.00	1.00	MP	474.30	84.10	83.10	1.06	83.97	10.03
mAb-1	2	0.1	10.00	1.00	MP	474.50	82.79	83.10	1.06	83.97	10.03
mAb-1	3	0.1	10.00	1.00	MP	479.70	82.42	83.10	1.06	83.97	10.03
mAb-2	2	0.1	0.03	0.00	MP	1.00	100.00	100.00	0.00	98.34	1.68
mAb-2	3	0.1	0.03	0.00	MP	1.00	100.00	100.00	0.00	98.34	1.68
mAb-2	1	0.1	0.03	0.00	MP	1.10	100.00	100.00	0.00	98.34	1.68

mAb-2	1	0.1	0.06	0.01	MP	2.30	100.00	100.00	0.00	98.34	1.68
mAb-2	2	0.1	0.06	0.01	MP	2.50	100.00	100.00	0.00	98.34	1.68
mAb-2	3	0.1	0.06	0.01	MP	2.60	100.00	100.00	0.00	98.34	1.68
mAb-2	2	0.1	0.13	0.01	MP	4.50	100.00	100.00	0.00	98.34	1.68
mAb-2	1	0.1	0.13	0.01	MP	4.80	100.00	100.00	0.00	98.34	1.68
mAb-2	3	0.1	0.13	0.01	MP	4.80	100.00	100.00	0.00	98.34	1.68
mAb-2	1	0.1	0.25	0.03	MP	7.80	100.00	100.00	0.00	98.34	1.68
mAb-2	2	0.1	0.25	0.03	MP	10.10	100.00	100.00	0.00	98.34	1.68
mAb-2	1	0.1	0.50	0.05	MP	23.10	100.00	100.00	0.00	98.34	1.68
mAb-2	2	0.1	0.50	0.05	MP	23.20	100.00	100.00	0.00	98.34	1.68
mAb-2	3	0.1	0.50	0.05	MP	23.30	100.00	100.00	0.00	98.34	1.68
mAb-2	1	0.1	1.00	0.10	MP	77.20	96.79	97.33	0.50	98.34	1.68
mAb-2	3	0.1	1.00	0.10	MP	108.80	97.46	97.33	0.50	98.34	1.68
mAb-2	2	0.1	1.00	0.10	MP	110.30	97.74	97.33	0.50	98.34	1.68
mAb-2	2	0.1	2.00	0.20	MP	145.80	96.76	96.75	0.08	98.34	1.68
mAb-2	3	0.1	2.00	0.20	MP	148.70	96.82	96.75	0.08	98.34	1.68
mAb-2	1	0.1	2.00	0.20	MP	154.30	96.67	96.75	0.08	98.34	1.68
mAb-2	1	0.1	4.00	0.40	MP	293.00	96.60	96.67	0.07	98.34	1.68
mAb-2	2	0.1	4.00	0.40	MP	294.80	96.74	96.67	0.07	98.34	1.68
mAb-2	3	0.1	4.00	0.40	MP	295.40	96.67	96.67	0.07	98.34	1.68
mAb-2	1	0.1	8.00	0.80	MP	499.40	96.48	96.51	0.06	98.34	1.68
mAb-2	3	0.1	8.00	0.80	MP	513.90	96.58	96.51	0.06	98.34	1.68
mAb-2	2	0.1	8.00	0.80	MP	527.60	96.46	96.51	0.06	98.34	1.68
mAb-2	3	0.1	10.00	1.00	MP	617.30	96.68	96.68	0.00	98.34	1.68
mAb-2	2	0.1	10.00	1.00	MP	637.60	96.67	96.68	0.00	98.34	1.68
mAb-2	1	0.1	10.00	1.00	MP	639.30	96.68	96.68	0.00	98.34	1.68

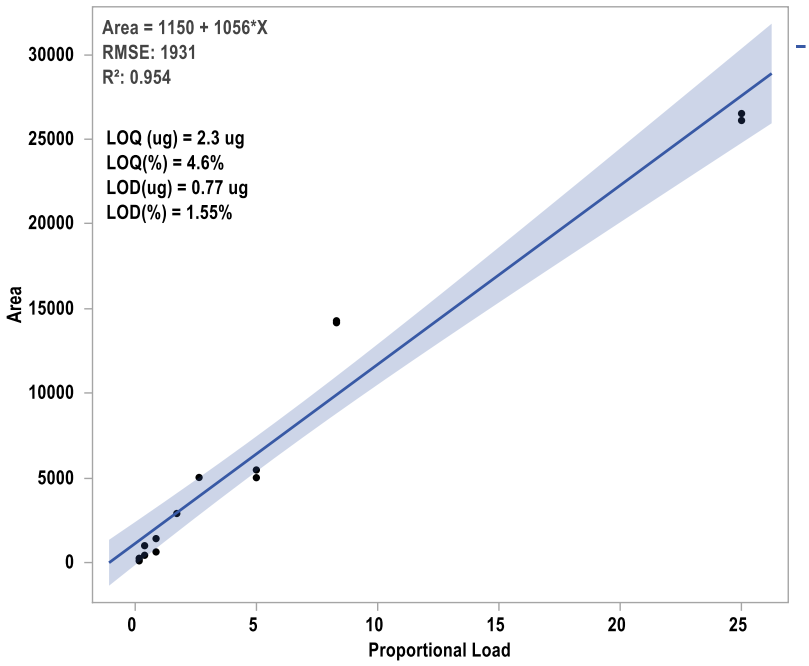

Figure 9.10 Determination of the HT SEC method LOQ and LOD from a calibration curve.

Linear regression analysis of the average peak area *vs.* the proportional protein load (µg) calculated for 10 µL injection of BsAb-1 samples displaying a concentration of 0.2, 0.4, 0.8, 1.7, and 2.5 mg/mL, each analysed in triplicate.

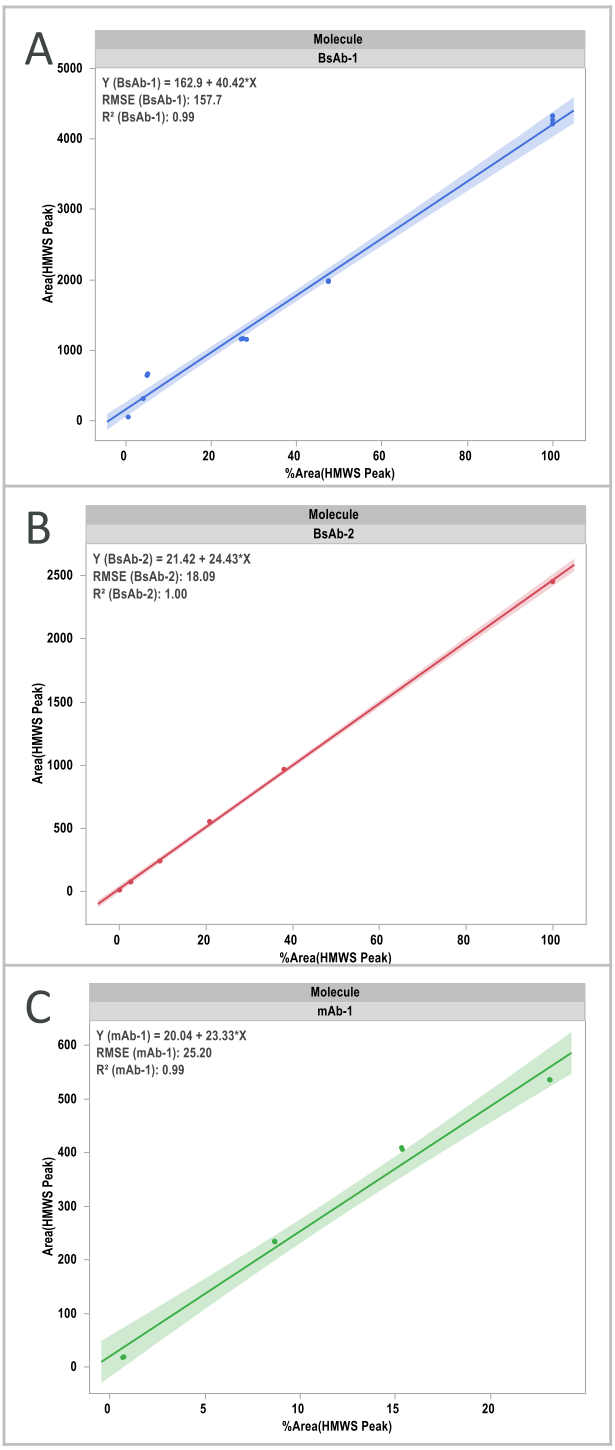

Figure 9.11 Proof-of-concept application of the HT SEC method.

Linear regression analysis displaying the area *vs.* the %area of the HMWS peak of A) BsAb-1, B) BsAb-2, and C) mAb-1 blends analysed by HT SEC. The samples were analysed in triplicate with a concentration of 1 mg/mL and an injection volume of 5 µL. The mAb-1 RS sample was stressed at 70 °C for 1 hour to induce the formation of HMWS. The %HMWS of BsAb-1, BsAb-1 and mAb-1 by the AZ SEC SOP 35%, 22% and 17%, respectively. The HMWS peak was separated from the main product peak by AZ SEC SOP, the peaks fractions were collected and enriched to 1 mg/mL. The sample blends were obtained by spiking the HMWS fraction into the main product peak fraction at different ratios, namely 0, 10, 20, 40, and 60% for BsAb-1 and BsAb-2, and 0, 35, and 65% for mAb-1.

Table 9.10 Analysis conditions of HT CEX method development DoE1.

Factors
Columns: Agilent, Sepax, Phenomenex, Waters
pH (5.5, 6.0, 6.5)
Response
Experimental Peak Capacity (ePC)
Constant
Cbuffer: 20 mM Na3PO4 buffer
Csalt(t0): 40 mM NaCl
F: 0.17 mL/min
gt: 15 min
gshape: linear, 40-500mM NaCl
Temperature: 25 °C
Injection Volume: 5 µL
Sample concentration: 1 mg/mL
UV: 210 nm, 280 nm

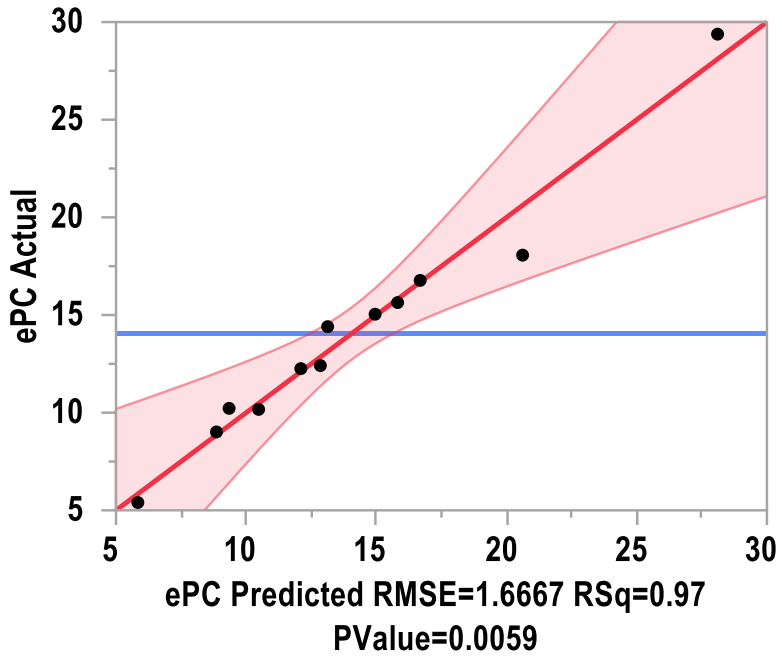

Figure 9.12 HT CEX Method development DoE1 actual-by-predicted plot.
HT CEX 2x4 factorial DoE1 actual-by-predicted plot displaying the ePC experimental values *vs.* the model estimates. The model p-value = 0.0059, RMSE = 1.6667, R^2 = 0.97 are evidence of the model significancy and goodness-of-fit.

Table 9.11 Analysis conditions of the HT CEX DoE2.

Factors
C_{buffer} (mM): 10, 20, 40
$C_{salt(t_0)}$ (mM): 10 40, 80
F (mL/min): 0.13, 0.17, 0.21
Response
Experimental Peak Capacity (ePC)
Constant
Column: Phenomenex
Buffer pH: 6.5
g_t: 15 min
g_{shape}: linear, $C_{salt(t_0)}$ up to 500mM NaCl
Temperature: 25 °C
Injection Volume: 5 µL
Sample concentration: 1 mg/mL
UV: 210 nm, 280 nm

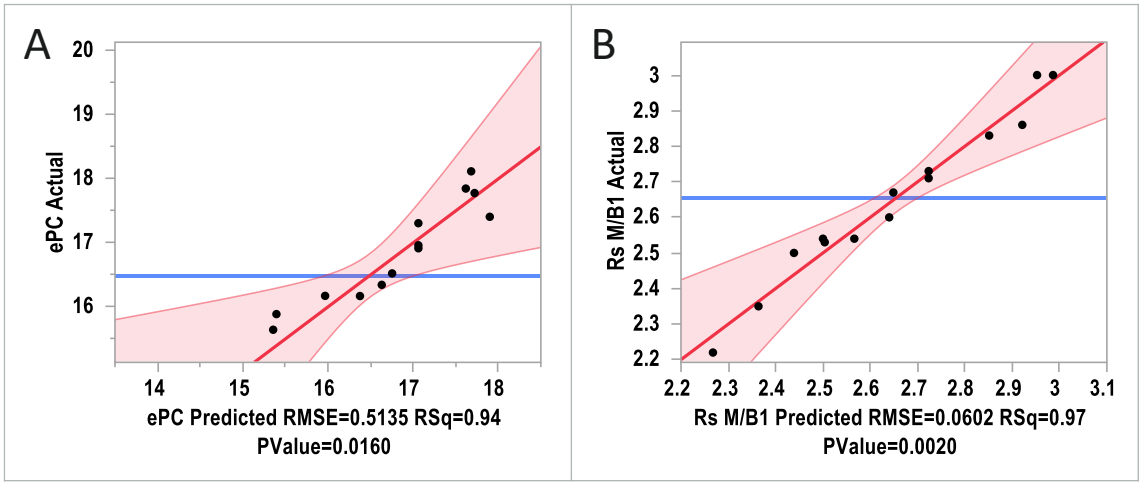

Figure 9.13 HT CEX method development DoE2 actual-by-predicted plot.

HT CEX BBD DoE2 actual-by-predicted plot displaying the ePC experimental values *vs.* the model estimates for A) ePC and B) $Rs_{(M/B1)}$ responses. The ePC model p-value = 0.016, RMSE = 0.5135, and R^2= 0.94, and $Rs_{(M/B1)}$ model p-value = 0.002, RMSE = 0.0602, R^2 = 0.97 are evidence of the model significancy and goodness-of-fit.

$$\text{Exp}\left(\begin{array}{l} 0.3333333333 \bullet \text{Log}\left(\text{Desirability}\left(\begin{bmatrix}2.2\\2.65\\3.1\end{bmatrix}, \begin{bmatrix}0.066\\0.5\\0.982\end{bmatrix}, \text{Rs M/B1}\right)\right) \\ + 0.6666666667 \bullet \text{Log}\left(\text{Desirability}\left(\begin{bmatrix}13.5\\16\\18.5\end{bmatrix}, \begin{bmatrix}0.066\\0.5\\0.982\end{bmatrix}, \text{ePC}\right)\right) \end{array}\right) \tag{6.5}$$

Equation 9.5 HT CEX DoE2 Desirability Formula.

Table 9.12 HT CEX DoE2 parameter estimates analysed for each response.

ePC DoE2 Parameter estimates				
Term	**Estimate**	**Std Error**	**t Ratio**	**Prob>|t|**
Intercept	17.06242	0.296444	57.56	**<.0001***
C_{buffer} [mM](10,30)	-0.842521	0.181534	-4.64	**0.0056***
$C_{salt(t0)}$ [mM](0,80)	0.4099375	0.181534	2.26	**0.0735**
F (mL/min)(0.13,0.21)	1.0472912	0.181534	5.77	**0.0022***
C_{buffer} [mM]*$C_{salt(t0)}$ [mM]	0.2692	0.256728	1.05	0.3424
C_{buffer} [mM]*F (mL/min)	0.1696075	0.256728	0.66	0.5381
$C_{salt(t0)}$ [mM]*F (mL/min)	0.115075	0.256728	0.45	0.6727
C_{buffer} [mM]*C_{buffer} [mM]	-0.126319	0.267211	-0.47	0.6563
$C_{salt(t0)}$ [mM]*$C_{salt(t0)}$ [mM]	-0.018801	0.267211	-0.07	0.9466
F*F (mL/min)	-0.933844	0.267211	-3.49	**0.0174***
Rs(M/B1) DoE2 Parameter estimates				
Term	**Estimate**	**Std Error**	**t Ratio**	**Prob>|t|**
Intercept	2.7233333	0.034777	78.31	**<.0001***
C_{buffer} [mM](10,30)	-0.13625	0.021297	-6.40	**0.0014***
$C_{salt(t0)}$ [mM](0,80)	0.105	0.021297	4.93	**0.0044***
F (mL/min)(0.13,0.21)	0.20625	0.021297	9.68	**0.0002***
C_{buffer} [mM]*$C_{salt(t0)}$ [mM]	-0.0725	0.030118	-2.41	**0.0611**
C_{buffer} [mM]*F (mL/min)	-0.02	0.030118	-0.66	0.5360
$C_{salt(t0)}$ [mM]*F (mL/min)	-0.0375	0.030118	-1.25	0.2683
C_{buffer} [mM]*C_{buffer} [mM]	-0.119167	0.031348	-3.80	**0.0126***
$C_{salt(t0)}$ [mM]*$C_{salt(t0)}$ [mM]	0.0033333	0.031348	0.11	0.9195
F (mL/min)*F (mL/min)	-0.014167	0.031348	-0.45	0.6703

* = factors found to be significant with a probability of $p \leq 0.05$

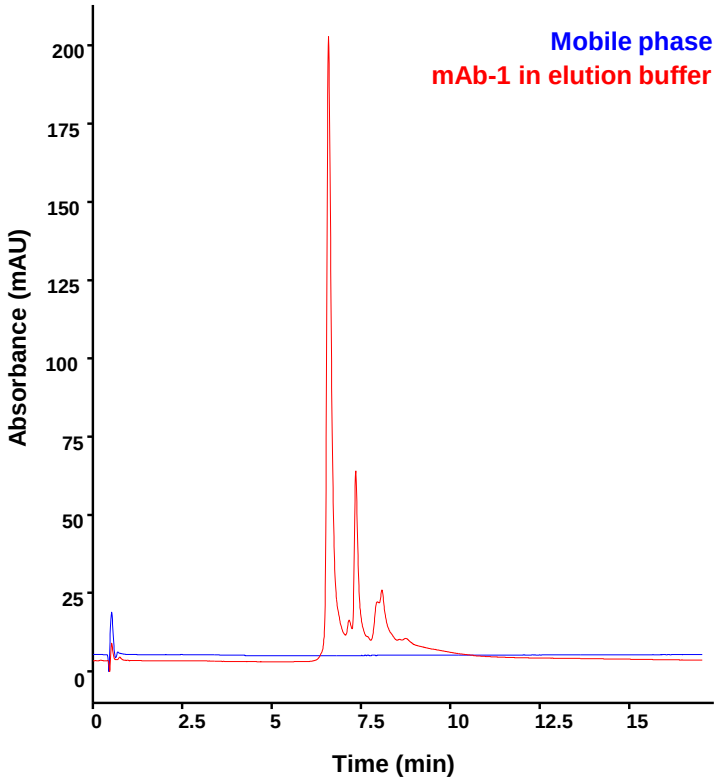

Figure 9.14 HT CEX specificity test.

HT CEX chromatogram overlay of 5 µL injection of a sample of a mAb-1 dissolved in PhyTip purification GlyHCl-2.6 buffer (red) against 20 uL injection of mobile phase (blue). The sample was diluted to 2 mg/mL before analysis.

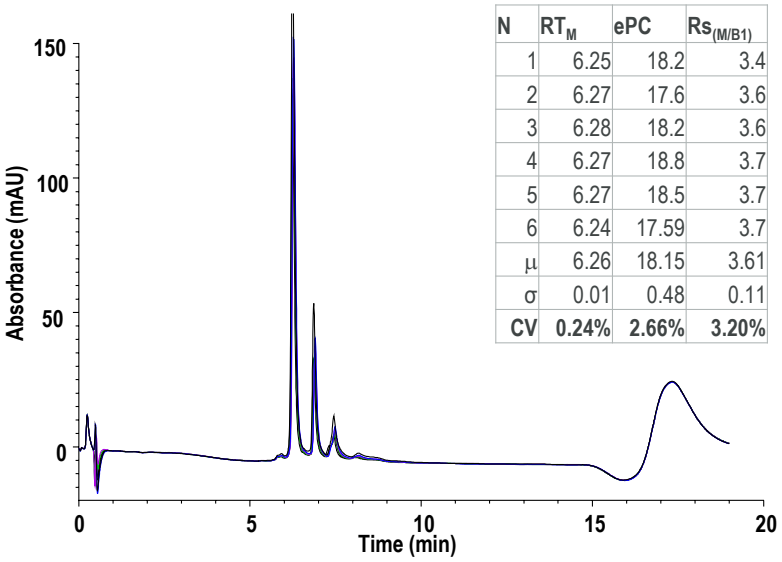

N	RT_M	ePC	$Rs_{(M/B1)}$
1	6.25	18.2	3.4
2	6.27	17.6	3.6
3	6.28	18.2	3.6
4	6.27	18.8	3.7
5	6.27	18.5	3.7
6	6.24	17.59	3.7
µ	6.26	18.15	3.61
σ	0.01	0.48	0.11
CV	**0.24%**	**2.66%**	**3.20%**

Figure 9.15 HT CEX repeatability study.

Chromatograms overlay of 6 replicate injections of a sample of mAb-1 analysed by HT CEX. The sample concentration was 1 mg/mL and the injection volume was 5 µL.

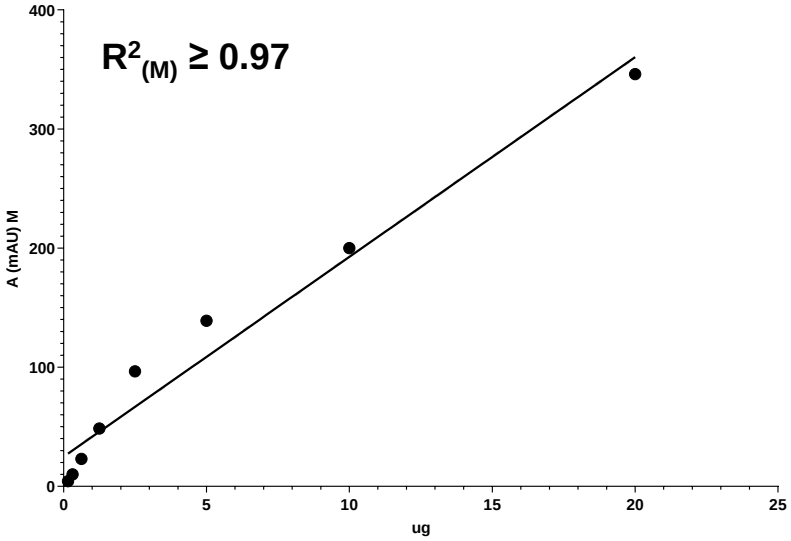

Figure 9.16 HT CEX linearity.

Linear regression analysis of the main species peak area *vs.* the column loading was performed to assess the linearity of the HT CEX method. The linearity was assessed over 8 different concentrations (4, 2, 1, 0.5, 0.25, 0.12, 0.06, 0.03, 0.01 mg/mL) of mAb-1 analysed by HT CEX. The injection volume was 5 µL, corresponding to 20, 10, 5, 2.5, 0.6 0.3 and 0.1 µg column loading.

Appendix B

Supplementary information related to Chapter 4

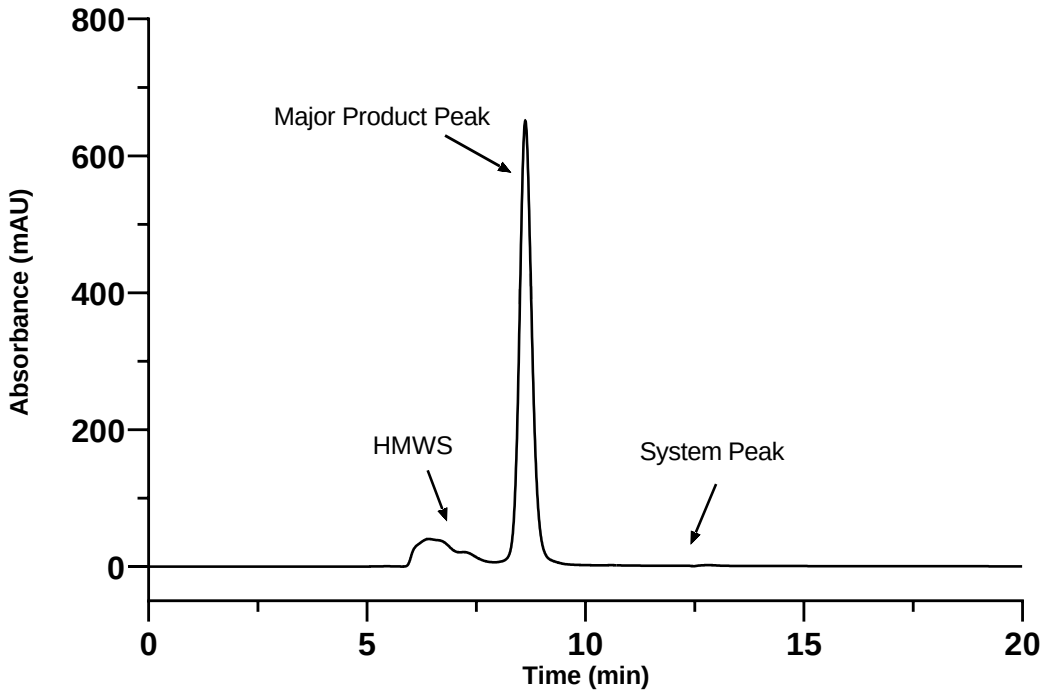

Figure 10.1 SEC profile of heat-stressed mAb-1 analysed by the AZ SOP SEC method. Chromatogram of mAb-1stressed by heat exposure analysed by the AZ SOP SEC method and reporting 17.4% HMWS impurities and 82.6% main product. The system peaks corresponding to the mobile phase salts and formulation buffer components were not integrated.

Table 10.1 2D SEC-CEX-UV column screening and mobile phase composition selection DoE table.

[Na3PO4](mM)	[NaCl] (mM)	Column	Resolution	%HMWS
50	0	Agilent	1.73	3.31
50	200	Agilent	1.82	22.23
50	0	Agilent	1.45	0.83
50	200	Agilent	1.85	21.48
125	100	Agilent	1.84	15.73
125	100	Agilent	1.91	16.13
200	200	Agilent	1.80	17.05
200	0	Agilent	1.99	15.01
200	200	Agilent	1.86	17.08
200	0	Agilent	2.03	15.52
50	0	Waters	0	0.09
50	200	Waters	1.97	17
50	0	Waters	0	0.09
50	200	Waters	1.95	17.33
125	100	Waters	1.86	15.91
125	100	Waters	1.86	16.64
200	200	Waters	1.86	16.49
200	0	Waters	1.87	14.49
200	0	Waters	1.82	14.9
200	200	Waters	1.82	16.32
50	200	Phenomenex	1.21	2.95
50	0	Phenomenex	0.89	1.72
50	0	Phenomenex	0.90	0.53
50	200	Phenomenex	0.97	2.33
125	100	Phenomenex	0.99	4.41
125	100	Phenomenex	0.91	3.93
200	200	Phenomenex	1.08	7.23
200	0	Phenomenex	1.21	5.27
200	200	Phenomenex	1.04	6.44
200	0	Phenomenex	0.92	6.26

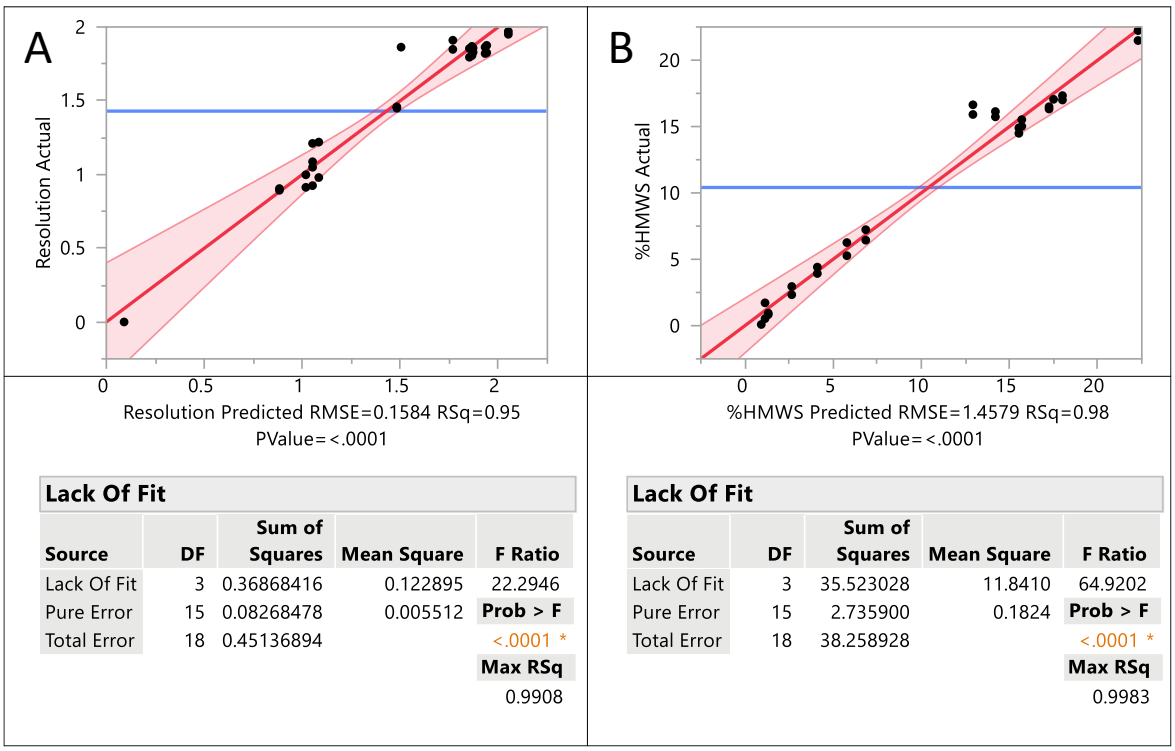

Lack Of Fit

Source	DF	Sum of Squares	Mean Square	F Ratio
Lack Of Fit	3	0.36868416	0.122895	22.2946
Pure Error	15	0.08268478	0.005512	**Prob > F**
Total Error	18	0.45136894		<.0001 *
				Max RSq
				0.9908

Lack Of Fit

Source	DF	Sum of Squares	Mean Square	F Ratio
Lack Of Fit	3	35.523028	11.8410	64.9202
Pure Error	15	2.735900	0.1824	**Prob > F**
Total Error	18	38.258928		<.0001 *
				Max RSq
				0.9983

Figure 10.2 Actual-by-predicted plot for resolution (A) and %HMWS (B) with the respective lack of fit tables reporting the DoE Model summary for each response.

The Lack of Fit report demonstrates that the model fit the data well. The sources of variation are the lack of fit, the pure error and the total error. The table reports the degree of freedom (DF) and the sum of squares of each source of error; the mean square corresponding to the sum of squares divided by the DF, the F ratio, the p-value, and the maximum R^2 (Max RSq).

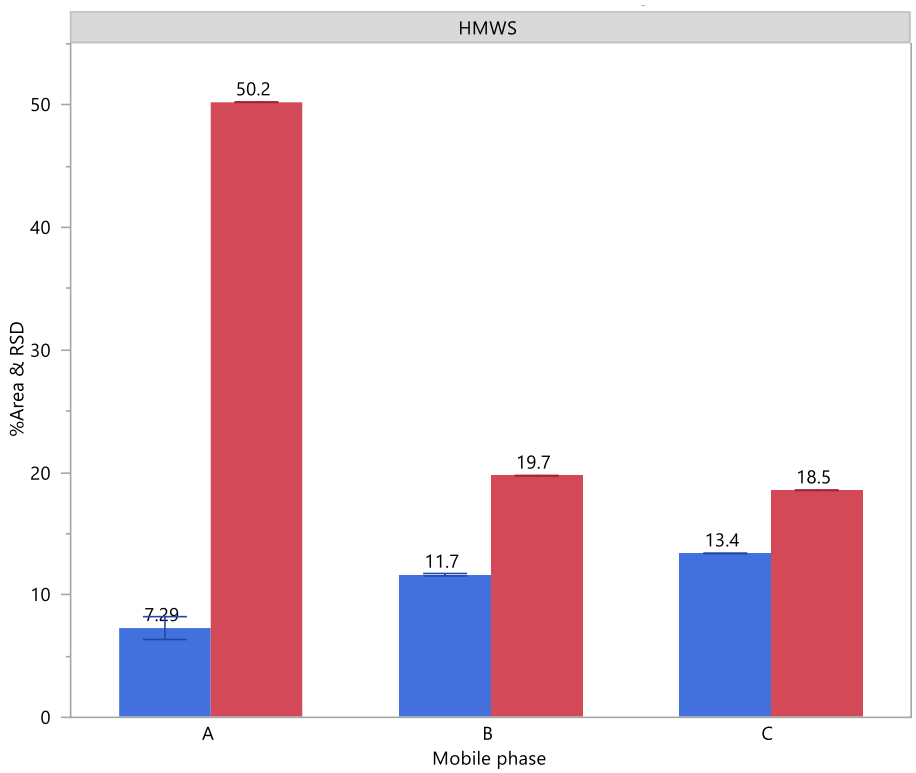

Figure 10.3 [1]D SEC DoE verification.

Bar chart reporting the mean %area (red) and RSD (equivalent of CV) and the HMWS (blue) impurities obtained for the analysis of a heat-stressed mAb-1 sample in duplicate by using mobile phases composed of 50 mM (A), 100 mM (B), and 200 mM (C) Na_3PO_4 buffer. The injection volume and the sample concentration were 5 mL and 1 mg/mL, respectively.

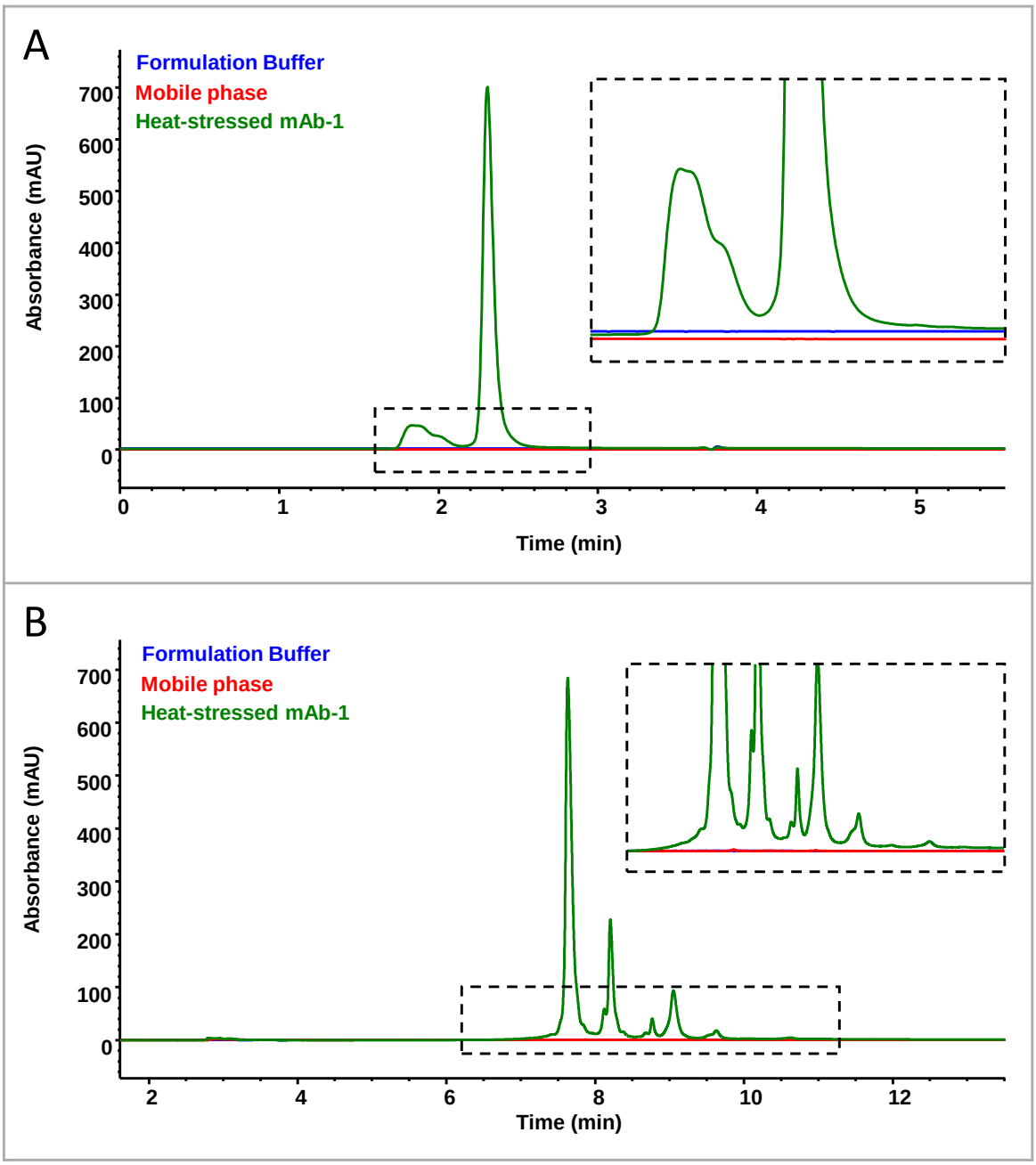

Figure 10.4 SEC-CEX-UV specificity test.

A) ^{1}D SEC UV and B) ^{2}D CEX trace overlay of 10 µL injection of formulation buffer and mobile phase against a heat-stressed mAb-1 sample. Stress conditions involved exposure of mAb-1 to 70 °C for 60 min. The sample was diluted to 1 mg/mL before injection.

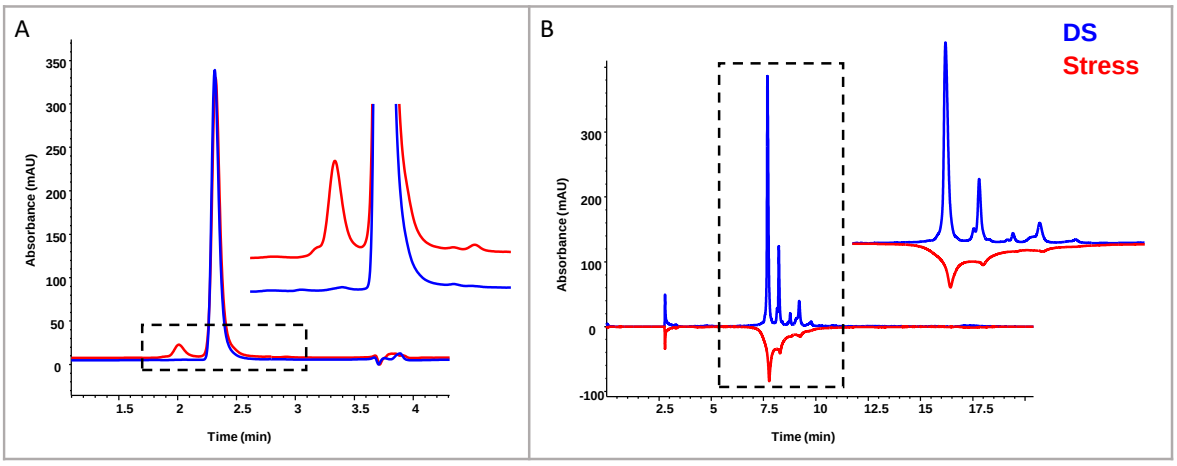

Figure 10.5 2D SEC-CEX-UV stability-indicating study.
A) [1]D SEC and B) [2]D CEX chromatograms overlay of the mAb-1 reference standard (blue) versus AAPH stress sample (red). The injection volume was 10 µL and the sample was diluted to 1 mg/mL before analysis.

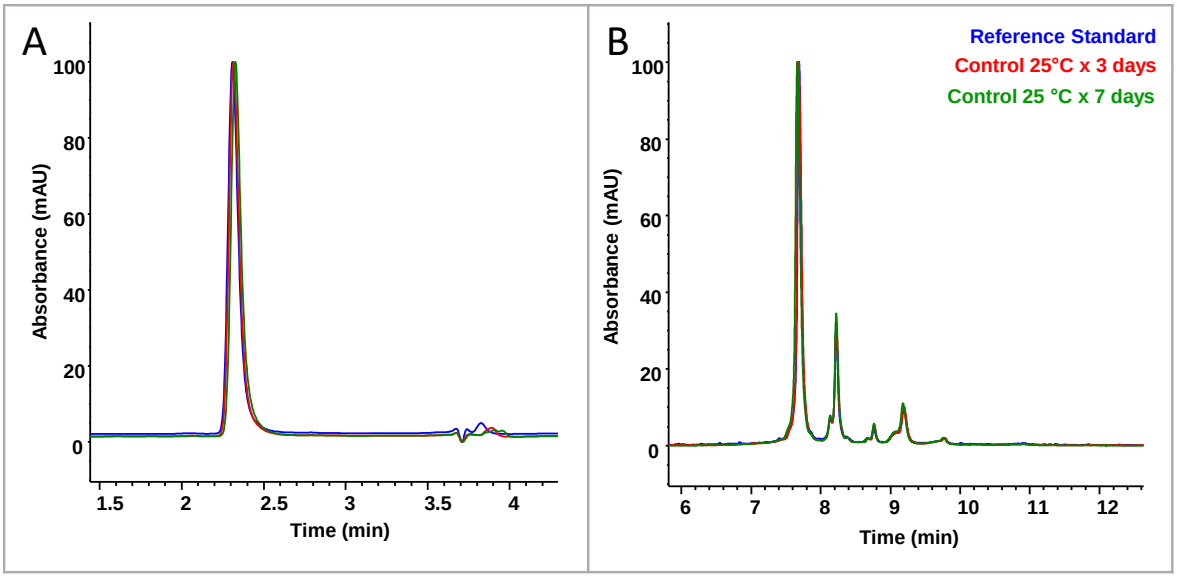

Figure 10.6 SEC-CEX-UV RS-control samples overlay over time.
A) [1]D SEC and B) [2]D CEX chromatogram overlay of mAb-1 RS (blue) against the control samples aliquoted after 3 (red) and 7 (green) days of incubation at 25 °C. The injection volume was 10 µL and the sample was diluted to 1 mg/mL before analysis.

Table 10.2 T-test evaluating the difference between the mean %peak area of mAb-1 size and charge variants for the RS and control samples.

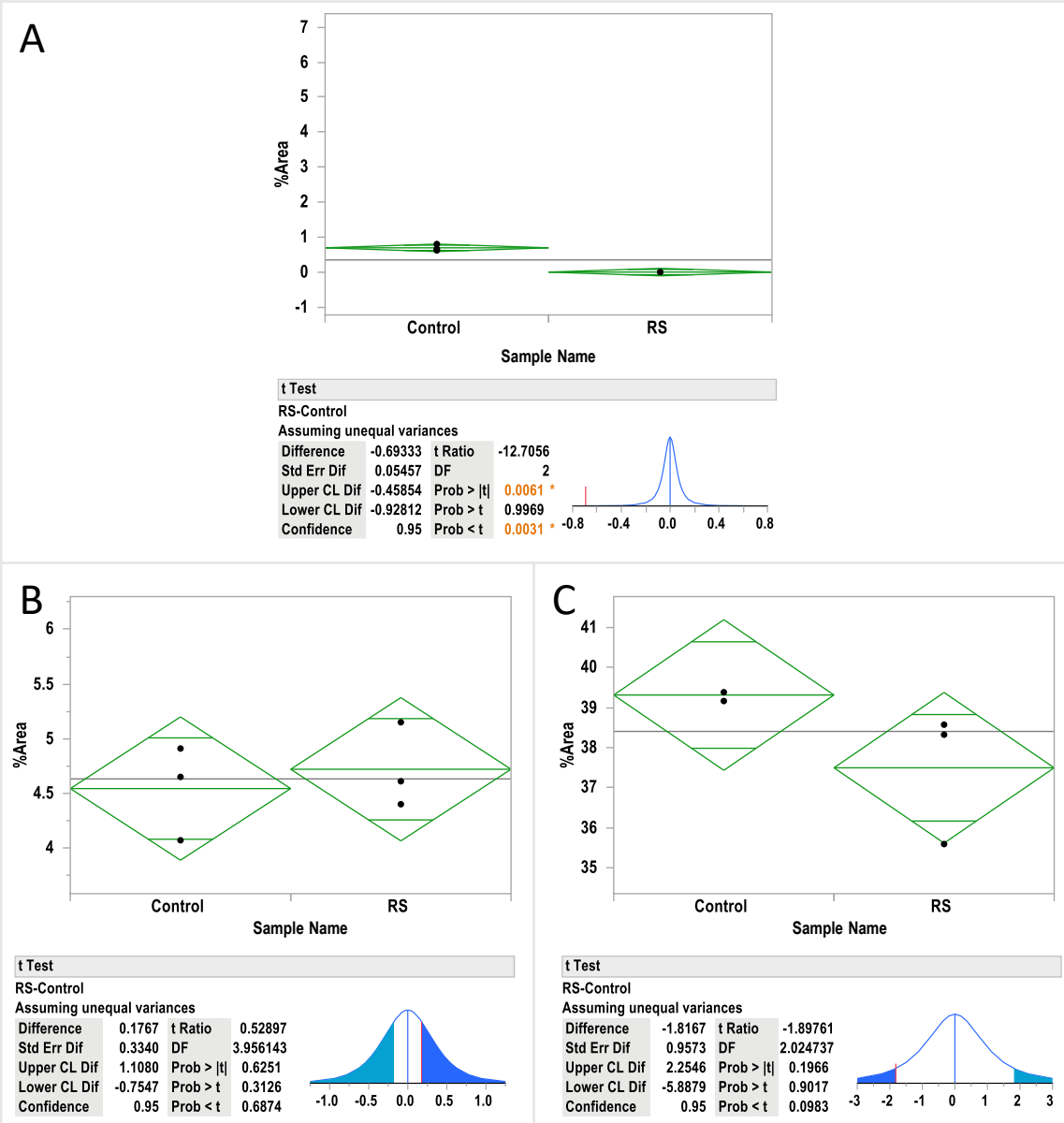

At the top, mean diamonds illustrating the group mean (middle line) and confidence intervals at 95% (top and bottom lines) of the % area of the LMWS (A), acid species (B), and basic species (C) peak analysed across the replicates (n=3) of the control, and RS samples. Assuming equal variances across the observations, the height of each diamond is proportional to the reciprocal of the square root of the number of observations in the group (n=3). At the bottom, the t-test of the %LMWS (A), %acid species (B), and %basic species (C) confirmed that no significant difference between mAb-1 RS and control samples were observed (p-value > 0.05).

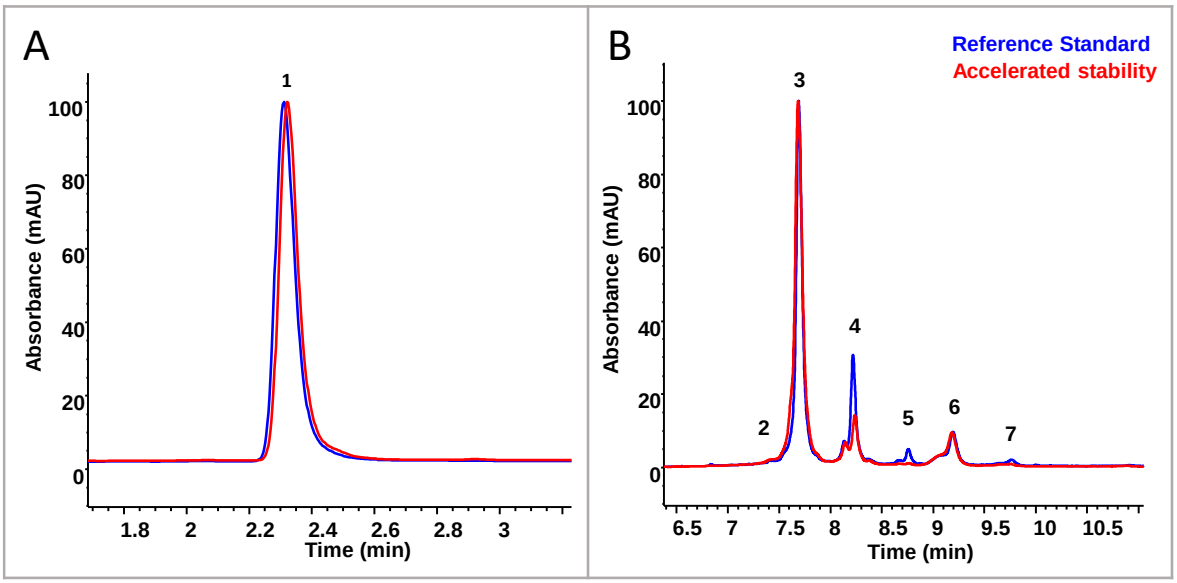

Figure 10.7 ^{2}D accelerated stability study SEC-CEX-UV chromatograms.
A) ^{1}D SEC and B) ^{2}D CEX chromatogram overlay of mAb-1 RS before (blue) and after the accelerated stability study (red) carried on by stressing the mAb at 37 °C for 30 days. The injection volume was 10 µL and the sample was diluted to 1 mg/mL before analysis.

Table 10.3 ANOVA test for the %LMWS observed during the accelerated stability study.

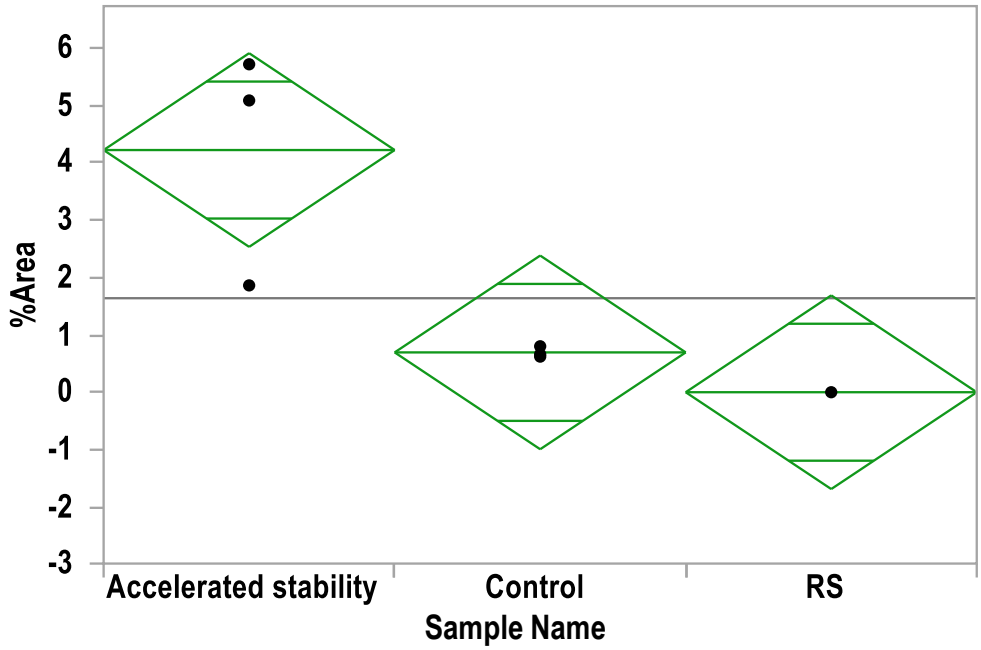

Oneway Anova

Summary of Fit

Rsquare	0.782083
Adj Rsquare	0.709444
Root Mean Square Error	1.193534
Mean of Response	1.636667
Observations (or Sum Wgts)	9

Analysis of Variance

Source	DF	Sum of Squares	Mean Square	F Ratio	Prob > F
Treatment	2	30.674867	15.3374	10.7667	0.0103 *
Error	6	8.547133	1.4245		
C. Total	8	39.222000			

Means for Oneway Anova

Level	Number	Mean	Std Error	Lower 95%	Upper 95%
Accelerated stability	3	4.21667	0.68909	2.531	5.9028
Control	3	0.69333	0.68909	-0.993	2.3795
RS	3	0.00000	0.68909	-1.686	1.6861

Std Error uses a pooled estimate of error variance

At the top, mean diamonds illustrating the group mean (middle line) and confidence intervals at 95% (top and bottom lines) of the % area of the LMWS peak analysed across the sample replicates (n=3) of accelerated stability, control, and RS samples. Assuming equal variances across the observations, the height of each diamond is proportional to the reciprocal of the square root of the number of observations in the group (n=3). At the bottom, the ANOVA test of the %LMWS confirmed that the %LMWS resulting from the accelerated stability study was significantly higher than the control and RS samples (p-value < 0.05).

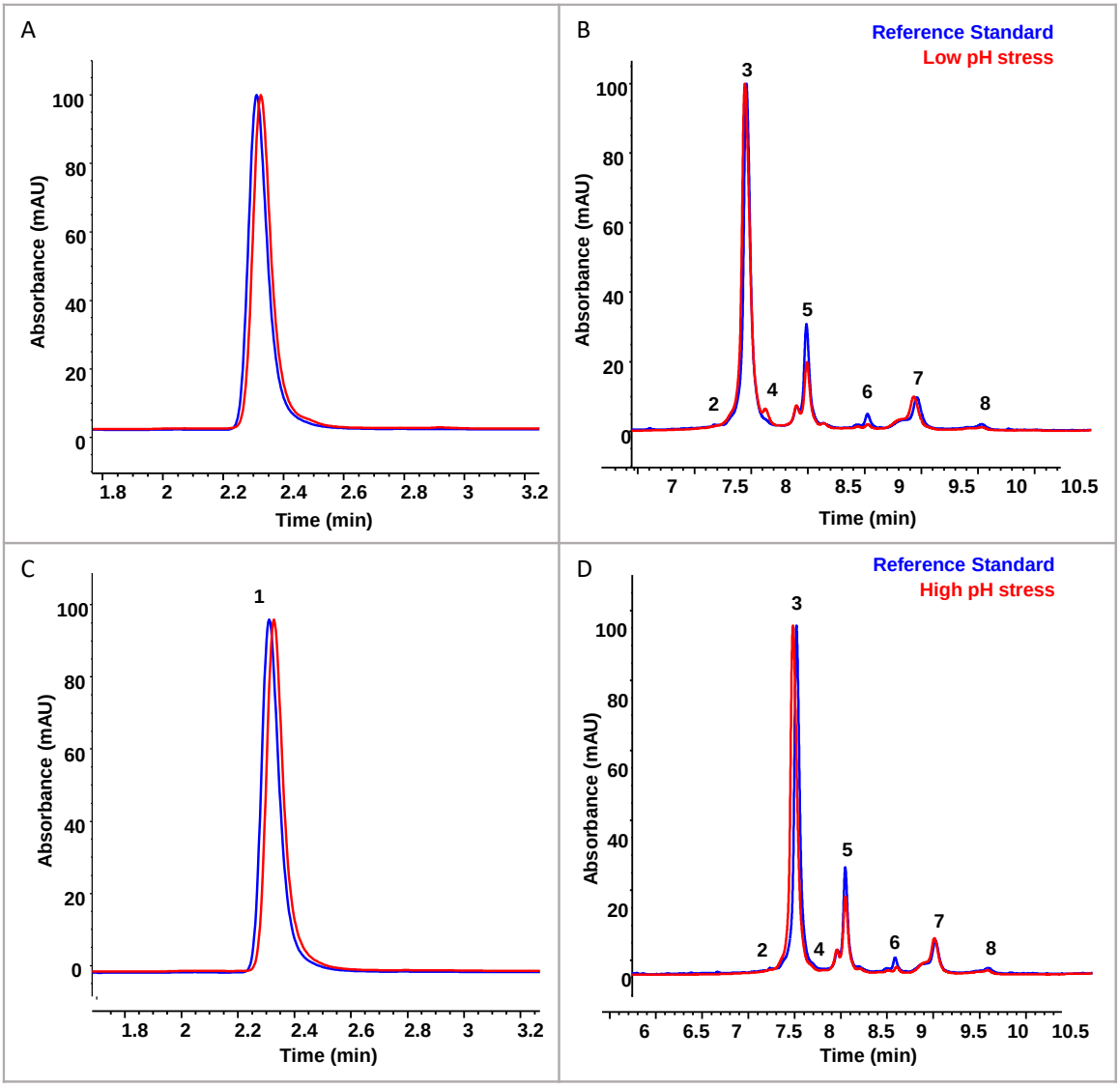

Figure 10.8 2D low and high pH treatment SEC-CEX-UV chromatograms overlays.
A, C) [1]D SEC and B, D) [2]D CEX chromatogram overlays of mAb-1 RS (blue) against the stressed material (red) at low pH (top) and high pH (bottom). The injection volume was 10 µL and the sample was diluted to 1 mg/mL before analysis.

Table 10.4 ANOVA test for the %LMWS observed during the low pH stress.

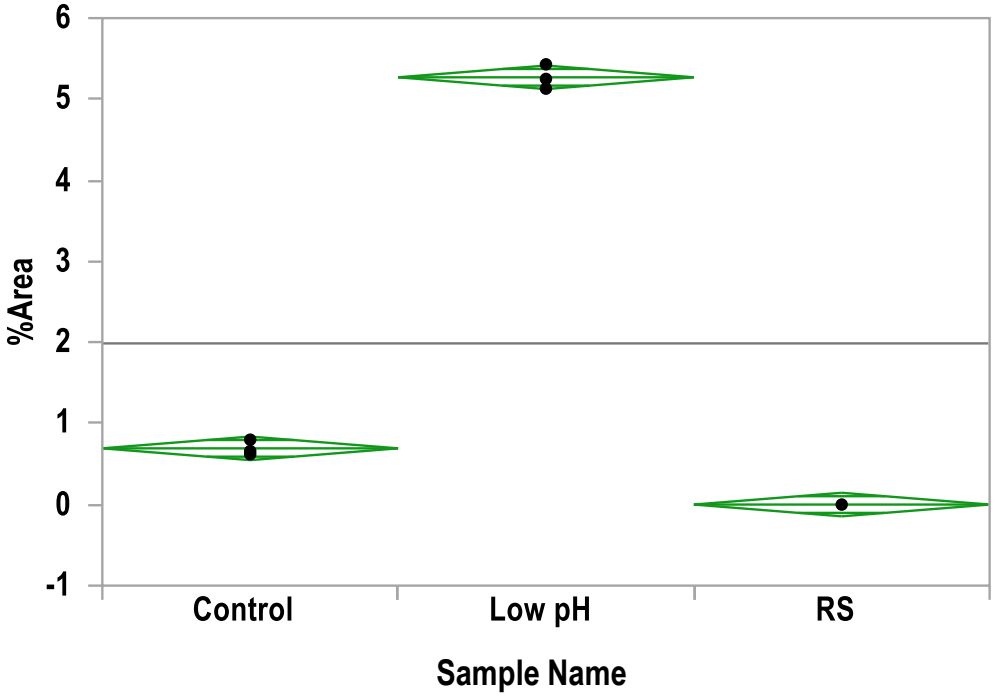

Oneway Anova

Summary of Fit

Rsquare	0.998712
Adj Rsquare	0.998282
Root Mean Square Error	0.102848
Mean of Response	1.987778
Observations (or Sum Wgts)	9

Analysis of Variance

Source	DF	Sum of Squares	Mean Square	F Ratio	Prob > F
Treatment	2	49.199489	24.5997	2325.606	<.0001 *
Error	6	0.063467	0.0106		
C. Total	8	49.262956			

Means for Oneway Anova

Level	Number	Mean	Std Error	Lower 95%	Upper 95%
Control	3	0.69333	0.05938	0.548	0.8386
Low pH	3	5.27000	0.05938	5.125	5.4153
RS	3	0.00000	0.05938	-0.145	0.1453

Std Error uses a pooled estimate of error variance

At the top, mean diamonds illustrating the group mean (middle line) and confidence intervals at 95% (top and bottom lines) of the % area of the LMWS peak analysed across the sample replicates (n=3) of control, low pH and RS samples. Assuming equal variances across the observations, the height of each diamond is proportional to the reciprocal of the square root of the number of observations in the group (n=3). At the bottom, the ANOVA test demonstrated that the %LMWS resulting from low pH stress was significantly higher (p-value < 0.05) than the control and RS sample.

Table 10.5 ANOVA test for the %LMWS observed during the high pH stress.

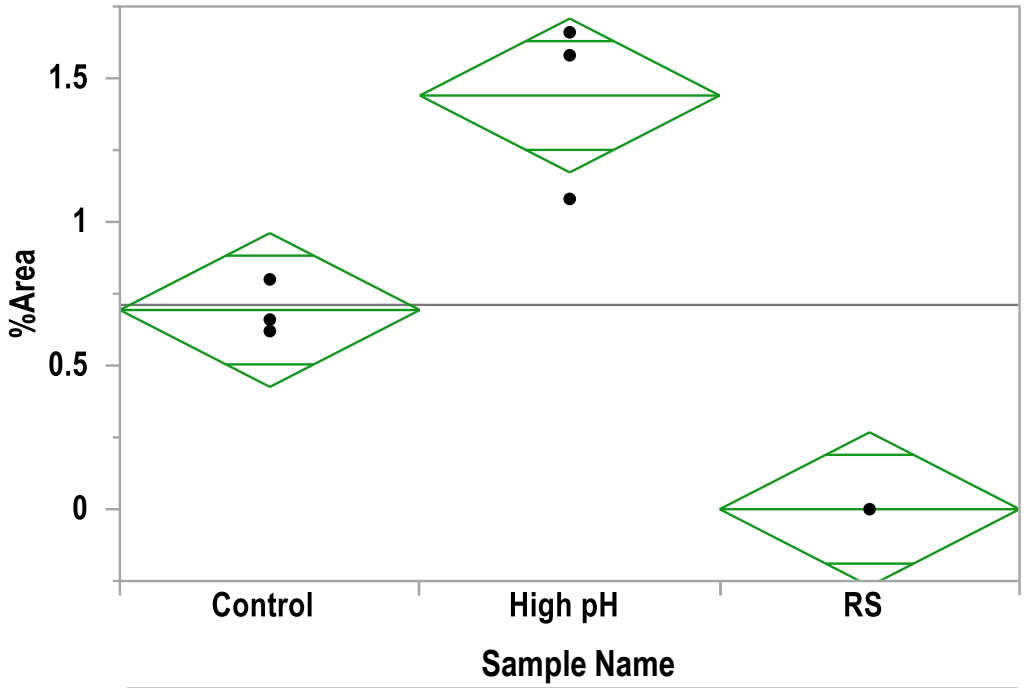

Oneway Anova

Summary of Fit

Rsquare	0.935243
Adj Rsquare	0.913657
Root Mean Square Error	0.189502
Mean of Response	0.711111
Observations (or Sum Wgts)	9

Analysis of Variance

Source	DF	Sum of Squares	Mean Square	F Ratio	Prob > F
Treatment	2	3.1118222	1.55591	43.3267	0.0003 *
Error	6	0.2154667	0.03591		
C. Total	8	3.3272889			

Means for Oneway Anova

Level	Number	Mean	Std Error	Lower 95%	Upper 95%
Control	3	0.69333	0.10941	0.426	0.9610
High pH	3	1.44000	0.10941	1.172	1.7077
RS	3	0.00000	0.10941	-0.268	0.2677

Std Error uses a pooled estimate of error variance

At the top, mean diamonds illustrating the group mean (middle line) and confidence intervals at 95% (top and bottom lines) of the % area of the LMWS peak analysed across the sample replicates (n=3) of control, high pH and RS samples. Assuming equal variances across the observations, the height of each diamond is proportional to the reciprocal of the square root of the number of observations in the group (n=3). At the bottom, the ANOVA test demonstrated that the %LMWS resulting from high pH stress was significantly higher (p-value < 0.05) than the control and RS samples.

Table 10.6 ANOVA test for the %acidic species observed during the low pH stress.

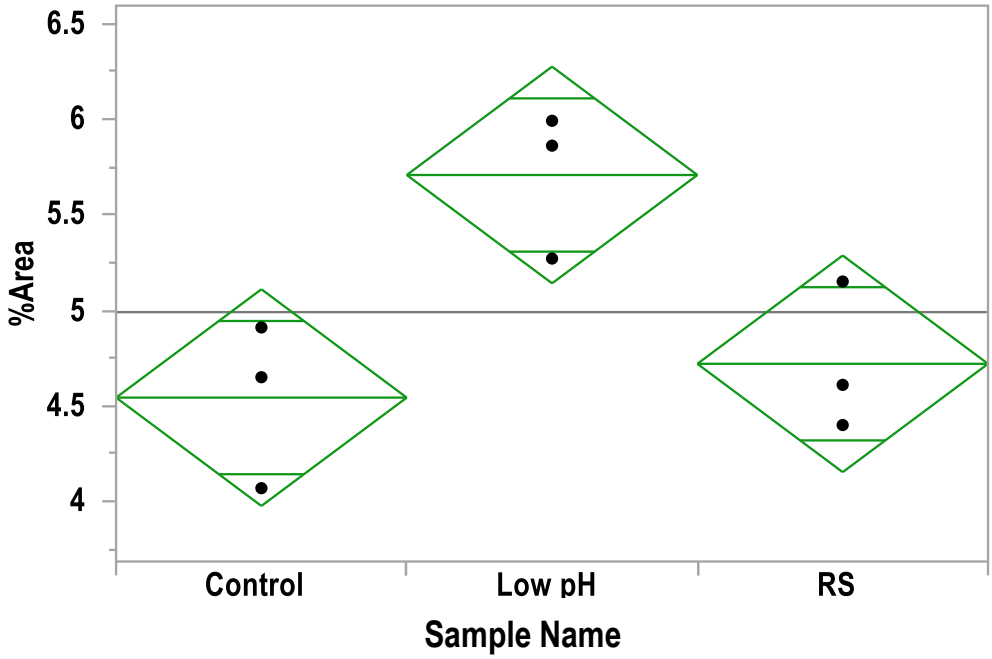

Oneway Anova

Summary of Fit

Rsquare	0.709876
Adj Rsquare	0.613168
Root Mean Square Error	0.400777
Mean of Response	4.99
Observations (or Sum Wgts)	9

Analysis of Variance

Source	DF	Sum of Squares	Mean Square	F Ratio	Prob > F
Treatment	2	2.3580667	1.17903	7.3404	0.0244 *
Error	6	0.9637333	0.16062		
C. Total	8	3.3218000			

Means for Oneway Anova

Level	Number	Mean	Std Error	Lower 95%	Upper 95%
Control	3	4.54333	0.23139	3.9771	5.1095
Low pH	3	5.70667	0.23139	5.1405	6.2729
RS	3	4.72000	0.23139	4.1538	5.2862

Std Error uses a pooled estimate of error variance

At the top, mean diamonds illustrating the group mean (middle line) and confidence intervals at 95% (top and bottom lines) of the % area of the acidic species peak analysed across the sample replicates (n=3) of control, low pH, and RS samples. Assuming equal variances across the observations, the height of each diamond is proportional to the reciprocal of the square root of the number of observations in the group (n=3). At the bottom, the ANOVA test demonstrated that the %acidic species peak resulting as a consequence of low pH stress was significantly higher than the control and RS samples (p-value < 0.05).

Table 10.7 ANOVA test for the %acidic species observed during the high pH stress.

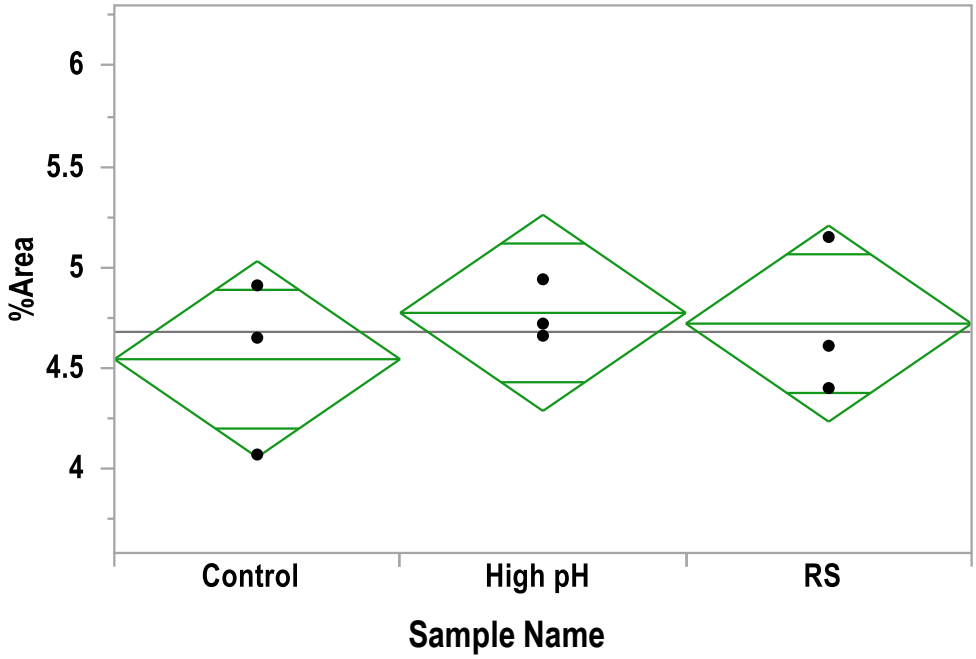

Oneway Anova

Summary of Fit

Rsquare	0.108737
Adj Rsquare	-0.18835
Root Mean Square Error	0.344658
Mean of Response	4.678889
Observations (or Sum Wgts)	9

Analysis of Variance

Source	DF	Sum of Squares	Mean Square	F Ratio	Prob > F
Treatment	2	0.08695556	0.043478	0.3660	0.7080
Error	6	0.71273333	0.118789		
C. Total	8	0.79968889			

Means for Oneway Anova

Level	Number	Mean	Std Error	Lower 95%	Upper 95%
Control	3	4.54333	0.19899	4.0564	5.0302
High pH	3	4.77333	0.19899	4.2864	5.2602
RS	3	4.72000	0.19899	4.2331	5.2069

Std Error uses a pooled estimate of error variance

At the top, mean diamonds illustrating the group mean (middle line) and confidence intervals at 95% (top and bottom lines) of the % area of the acidic species peak analysed across the sample replicates (n=3) of control, high pH, and RS samples. Assuming equal variances across the observations, the height of each diamond is proportional to the reciprocal of the square root of the number of observations in the group (n=3). At the bottom, the ANOVA test demonstrated that the variation of %acidic species peak resulting as a consequence of high pH stress was not significant (p-value > 0.05).

Table 10.8 ANOVA test for the %acidic species observed during the stress conditions applied during the accelerated stability study.

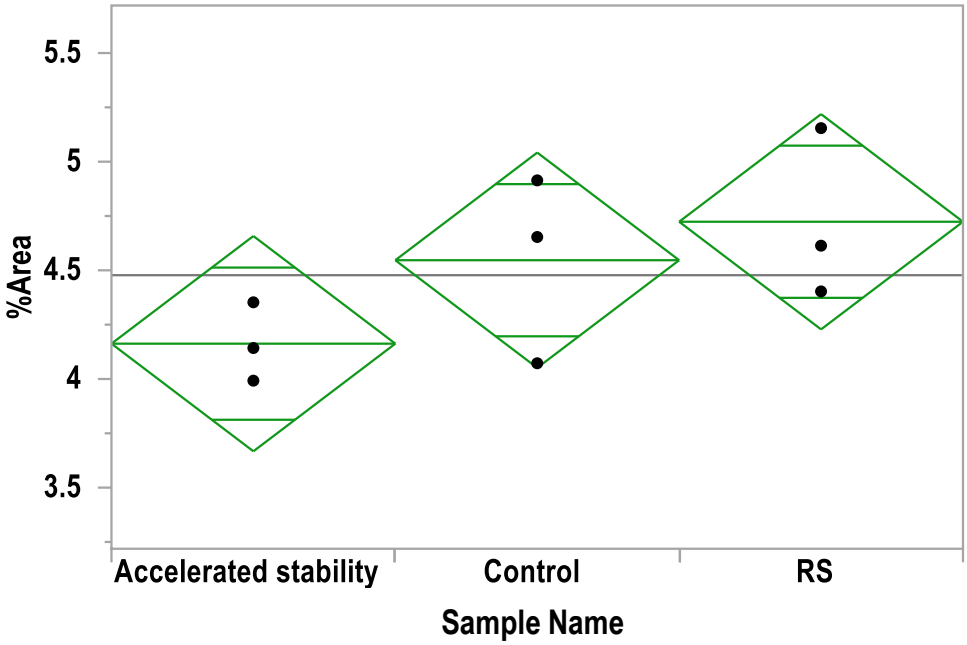

Oneway Anova

Summary of Fit

Rsquare	0.400968
Adj Rsquare	0.20129
Root Mean Square Error	0.349921
Mean of Response	4.474444
Observations (or Sum Wgts)	9

Analysis of Variance

Source	DF	Sum of Squares	Mean Square	F Ratio	Prob > F
Treatment	2	0.4917556	0.245878	2.0081	0.2150
Error	6	0.7346667	0.122444		
C. Total	8	1.2264222			

Means for Oneway Anova

Level	Number	Mean	Std Error	Lower 95%	Upper 95%
Accelerated stability	3	4.16000	0.20203	3.6657	4.6543
Control	3	4.54333	0.20203	4.0490	5.0377
RS	3	4.72000	0.20203	4.2257	5.2143

Std Error uses a pooled estimate of error variance

At the top, mean diamonds illustrating the group mean (middle line) and confidence intervals at 95% (top and bottom lines) of the % area of the acidic species peak analysed across the sample replicates (n=3) of accelerated stability, control, and RS samples. Assuming equal variances across the observations, the height of each diamond is proportional to the reciprocal of the square root of the number of observations in the group (n=3). At the bottom, the ANOVA test demonstrated that the variation of %acidic species peak resulting from stress the stress conditions applied during the accelerated stability study was not significant (p-value > 0.05).

Table 10.9 ANOVA test for the %basic species observed during low pH stress.

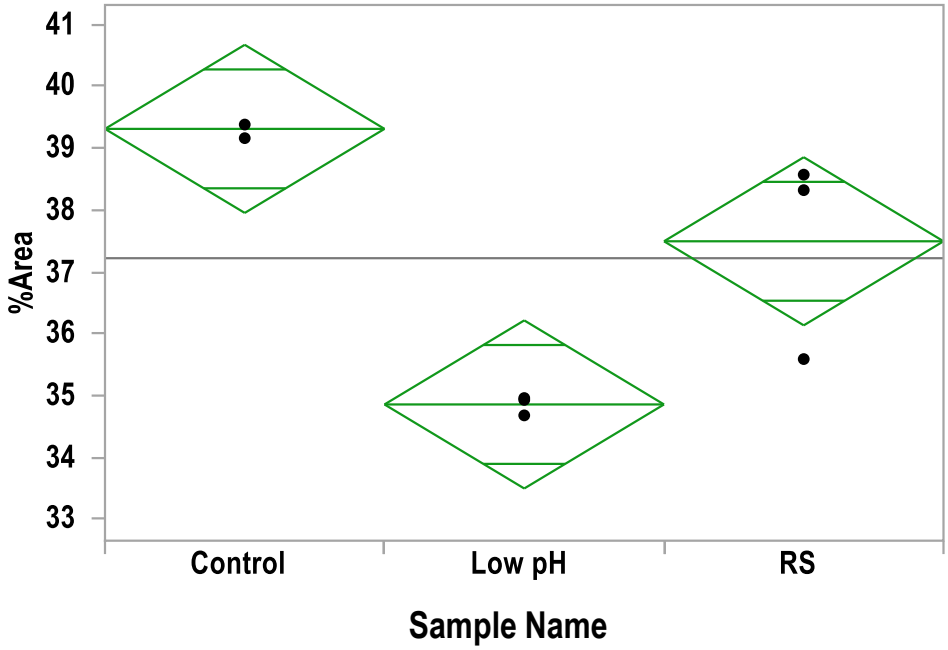

Oneway Anova

Summary of Fit

Rsquare	0.844339
Adj Rsquare	0.792452
Root Mean Square Error	0.961451
Mean of Response	37.22
Observations (or Sum Wgts)	9

Analysis of Variance

Source	DF	Sum of Squares	Mean Square	F Ratio	Prob > F
Treatment	2	30.084467	15.0422	16.2726	0.0038 *
Error	6	5.546333	0.9244		
C. Total	8	35.630800			

Means for Oneway Anova

Level	Number	Mean	Std Error	Lower 95%	Upper 95%
Control	3	39.3100	0.55509	37.952	40.668
Low pH	3	34.8567	0.55509	33.498	36.215
RS	3	37.4933	0.55509	36.135	38.852

Std Error uses a pooled estimate of error variance

At the top, mean diamonds illustrating the group mean (middle line) and confidence intervals at 95% (top and bottom lines) of the % area of the basic species peak analysed across the sample replicates (n=3) of accelerated stability, control, low pH, and RS samples. Assuming equal variances across the observations, the height of each diamond is proportional to the reciprocal of the square root of the number of observations in the group (n=3). At the bottom, the ANOVA test demonstrated that the %basic species peak resulting as a consequence of low pH stress was significantly lower than the control and RS samples (p-value < 0.05).

Table 10.10 ANOVA test for the %basic species observed during high pH stress.

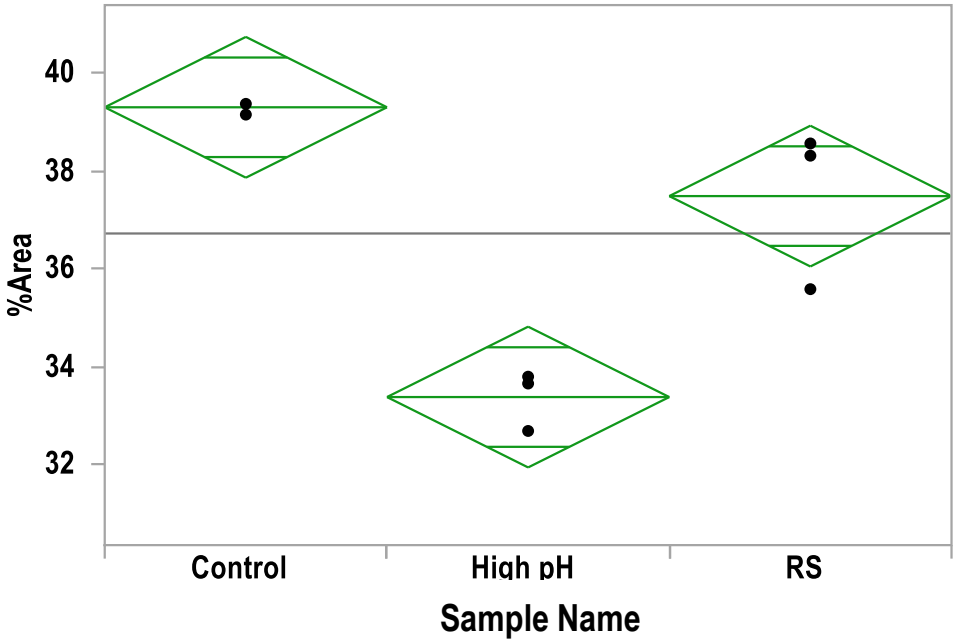

Oneway Anova

Summary of Fit

Rsquare	0.898779
Adj Rsquare	0.865038
Root Mean Square Error	1.018981
Mean of Response	36.72889
Observations (or Sum Wgts)	9

Analysis of Variance

Source	DF	Sum of Squares	Mean Square	F Ratio	Prob > F
Treatment	2	55.317756	27.6589	26.6380	0.0010 *
Error	6	6.229933	1.0383		
C. Total	8	61.547689			

Means for Oneway Anova

Level	Number	Mean	Std Error	Lower 95%	Upper 95%
Control	3	39.3100	0.58831	37.870	40.750
High pH	3	33.3833	0.58831	31.944	34.823
RS	3	37.4933	0.58831	36.054	38.933

Std Error uses a pooled estimate of error variance

At the top, mean diamonds illustrating the group mean (middle line) and confidence intervals at 95% (top and bottom lines) of the % area of the basic species peak analysed across the sample replicates (n=3) of accelerated stability, control, high pH, and RS samples. Assuming equal variances across the observations, the height of each diamond is proportional to the reciprocal of the square root of the number of observations in the group (n=3). At the bottom, the ANOVA test demonstrated that the %basic species peak resulting as a consequence of high pH stress was significantly lower than the control and RS samples (p-value < 0.05).

Table 10.11 ANOVA test for the %basic species observed under the accelerated stability study stress conditions.

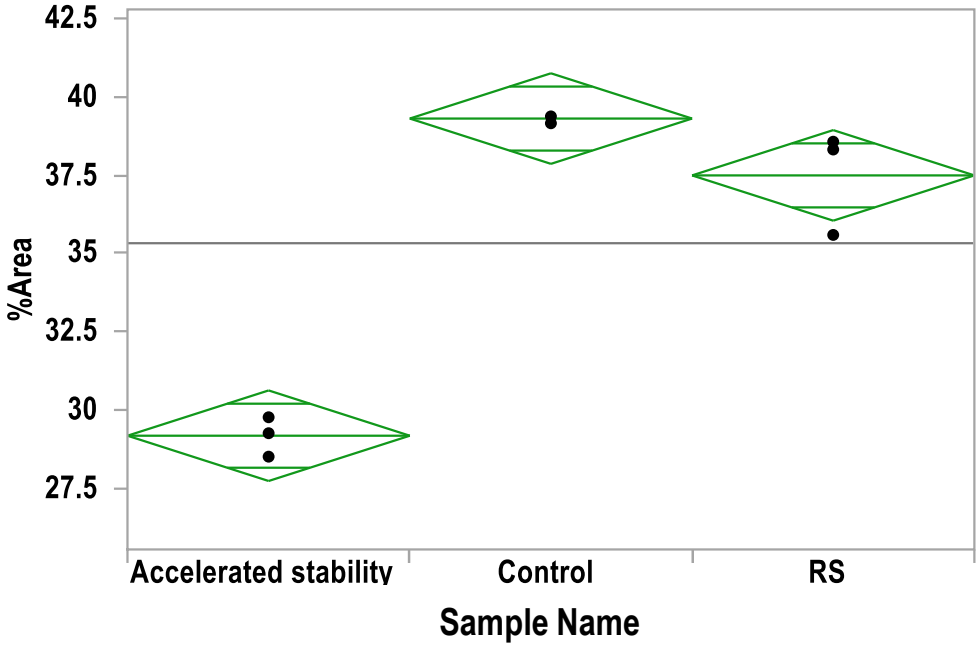

Oneway Anova

Summary of Fit

Rsquare	0.965314
Adj Rsquare	0.953752
Root Mean Square Error	1.024896
Mean of Response	35.32444
Observations (or Sum Wgts)	9

Analysis of Variance

Source	DF	Sum of Squares	Mean Square	F Ratio	Prob > F
Treatment	2	175.39776	87.6989	83.4901	<.0001 *
Error	6	6.30247	1.0504		
C. Total	8	181.70022			

Means for Oneway Anova

Level	Number	Mean	Std Error	Lower 95%	Upper 95%
Accelerated stability	3	29.1700	0.59172	27.722	30.618
Control	3	39.3100	0.59172	37.862	40.758
RS	3	37.4933	0.59172	36.045	38.941

Std Error uses a pooled estimate of error variance

At the top, mean diamonds illustrating the group mean (middle line) and confidence intervals at 95% (top and bottom lines) of the % area of the basic species peak analysed across the sample replicates (n=3) of accelerated stability, control, and RS samples. Assuming equal variances across the observations, the height of each diamond is proportional to the reciprocal of the square root of the number of observations in the group (n=3). At the bottom, the ANOVA test demonstrated that the %basic species peak resulting as a consequence of the stress conditions applied in the accelerated stability study was significantly lower than the control and RS samples (p-value < 0.05).

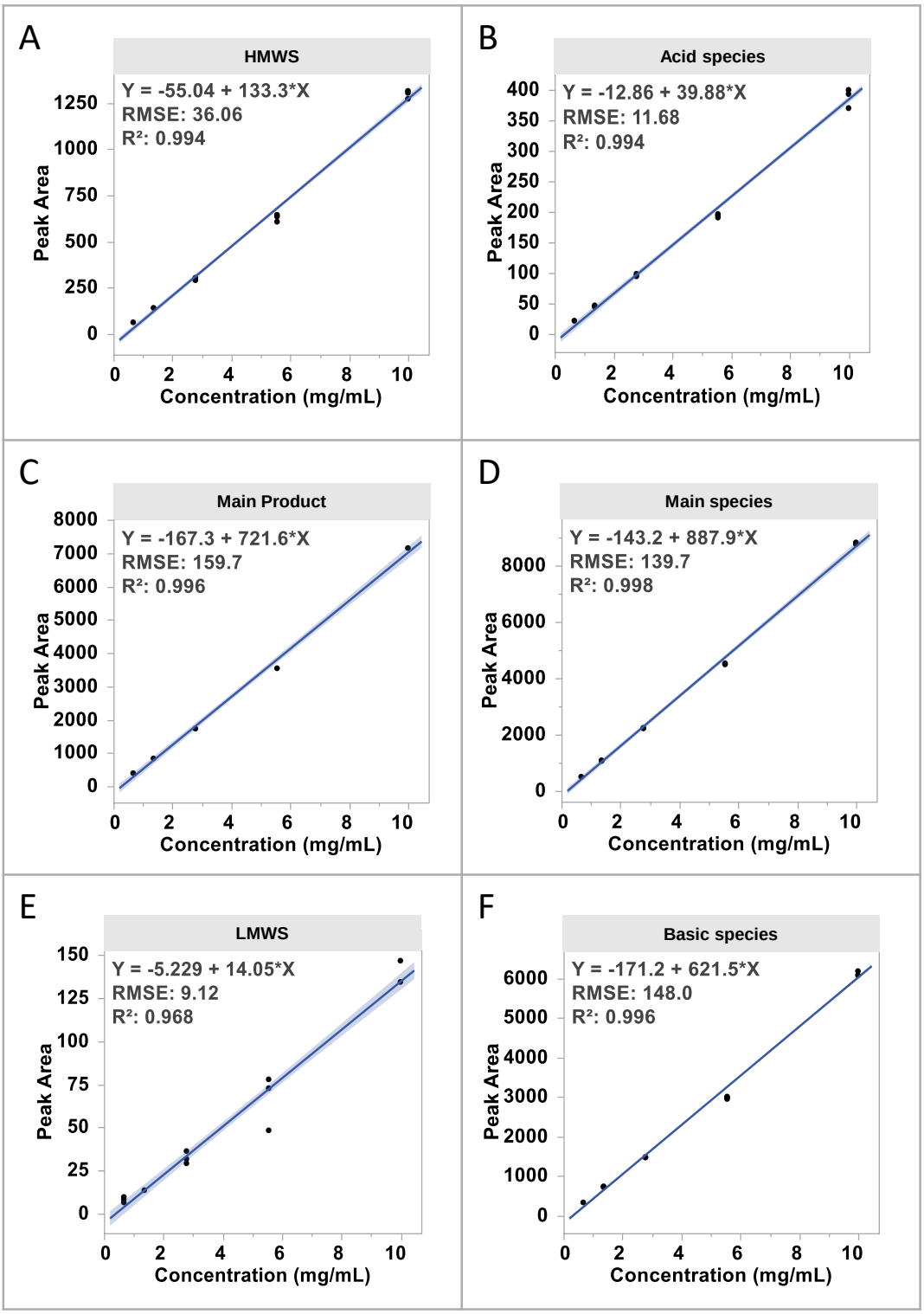

Figure 10.9 Linearity study.

Linear regression analysis was performed to evaluate whether the area of the size and charge variants peaks is proportional to the sample concentration (0.66, 1.34, 2.76, 5.53, 9.97 mg/mL). The injection volume was kept constant at 4 µL throughout the study. Linear regression data including equation, RMSE, and R^2 were plotted for the A) HMWS, C) main product, E) LMWS peaks of size variants analysed in the ^{1}D by SEC and for the B) acidic species, D) main species, F) basic species peaks analysed in the ^{2}D by CEX.

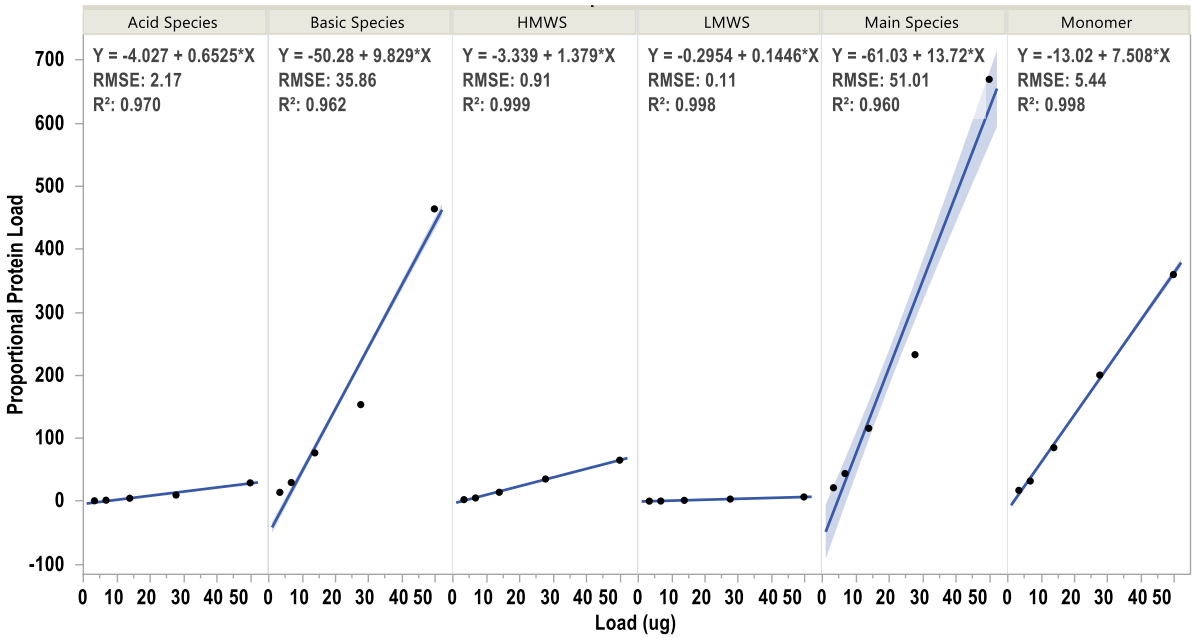

Figure 10.10 Peak area *vs.* proportional protein load for LOQ determination.

Table 10.12 Method assessment accuracy data for the analysis of heat-stressed mAb-1.

The peak names are reported for the main product (MP), high molecular weight peaks (HMWS) acquired in the [1]D and acidic species (AS), basic species (BS) and main species (MS) peaks acquired in the [2]D.

N°	C (mg/ml)	Peak Name	% Area	Mean (%Area)	Std Dev (%Area)	CV (%Area)	Grand Mean (%Area)	Grand Std Dev (%Area)	CV Accuracy
1	0.66	AS	2.50	2.48	0.03	1.16	2.23	0.56	1.30
1	0.66	HMWS	13.34	13.33	0.07	0.53	13.65	1.33	0.52
1	0.66	MP	84.67	84.99	0.29	0.35	85.22	1.31	0.35
1	0.66	MS	58.69	58.70	0.08	0.14	59.07	1.31	0.14
2	0.66	AS	2.45	2.48	0.03	1.16	2.23	0.56	1.30
2	0.66	BS	38.75	38.70	0.12	0.31	38.68	0.91	0.31
2	0.66	HMWS	13.39	13.33	0.07	0.53	13.65	1.33	0.52
2	0.66	MP	85.25	84.99	0.29	0.35	85.22	1.31	0.35
2	0.66	MS	58.78	58.70	0.08	0.14	59.07	1.31	0.14
3	0.66	AS	2.50	2.48	0.03	1.16	2.23	0.56	1.30
3	0.66	BS	38.54	38.70	0.12	0.31	38.68	0.91	0.31
3	0.66	HMWS	13.25	13.33	0.07	0.53	13.65	1.33	0.52
3	0.66	MP	85.05	84.99	0.29	0.35	85.22	1.31	0.35
3	0.66	MS	58.62	58.70	0.08	0.14	59.07	1.31	0.14
1	1.34	AS	2.37	2.46	0.08	3.23	2.23	0.56	3.56
1	1.34	BS	39.73	39.35	0.33	0.85	38.68	0.91	0.86
1	1.34	HMWS	14.09	14.10	0.03	0.23	13.65	1.33	0.24
1	1.34	MP	85.32	85.24	0.72	0.84	85.22	1.31	0.84
1	1.34	MS	57.90	58.19	0.34	0.58	59.07	1.31	0.57
2	1.34	AS	2.49	2.46	0.08	3.23	2.23	0.56	3.56
2	1.34	BS	38.94	39.35	0.33	0.85	38.68	0.91	0.86
2	1.34	HMWS	14.08	14.10	0.03	0.23	13.65	1.33	0.24
2	1.34	MP	85.92	85.24	0.72	0.84	85.22	1.31	0.84
2	1.34	MS	58.56	58.19	0.34	0.58	59.07	1.31	0.57
3	1.34	AS	2.52	2.46	0.08	3.23	2.23	0.56	3.56
3	1.34	BS	39.37	39.35	0.33	0.85	38.68	0.91	0.86
3	1.34	HMWS	14.14	14.10	0.03	0.23	13.65	1.33	0.24
3	1.34	MP	84.49	85.24	0.72	0.84	85.22	1.31	0.84
3	1.34	MS	58.11	58.19	0.34	0.58	59.07	1.31	0.57
1	2.78	AS	2.56	2.51	0.05	1.84	2.23	0.56	2.07
1	2.78	BS	38.64	38.89	0.18	0.47	38.68	0.91	0.47
1	2.78	HMWS	14.13	14.32	0.28	1.93	13.65	1.33	2.03
1	2.78	MP	85.26	85.03	0.30	0.36	85.22	1.31	0.35
1	2.78	MS	58.80	58.61	0.17	0.29	59.07	1.31	0.29
2	2.78	AS	2.48	2.51	0.05	1.84	2.23	0.56	2.07
2	2.78	BS	38.97	38.89	0.18	0.47	38.68	0.91	0.47
2	2.78	HMWS	14.20	14.32	0.28	1.93	13.65	1.33	2.03
2	2.78	MP	85.15	85.03	0.30	0.36	85.22	1.31	0.35
2	2.78	MS	58.56	58.61	0.17	0.29	59.07	1.31	0.29
3	2.78	AS	2.48	2.51	0.05	1.84	2.23	0.56	2.07
3	2.78	BS	39.05	38.89	0.18	0.47	38.68	0.91	0.47
3	2.78	HMWS	14.64	14.32	0.28	1.93	13.65	1.33	2.03
3	2.78	MP	84.69	85.03	0.30	0.36	85.22	1.31	0.35
3	2.78	MS	58.47	58.61	0.17	0.29	59.07	1.31	0.29
1	5.5	AS	2.60	2.54	0.05	2.05	2.23	0.56	2.33
1	5.5	BS	38.61	38.78	0.13	0.33	38.68	0.91	0.33
1	5.5	HMWS	14.45	14.87	0.38	2.55	13.65	1.33	2.77
1	5.5	MP	84.91	84.50	0.36	0.43	85.22	1.31	0.43

1	5.5	MS	58.78	58.68	0.09	0.16	59.07	1.31	0.16
2	5.5	AS	2.51	2.54	0.05	2.05	2.23	0.56	2.33
2	5.5	BS	38.85	38.78	0.13	0.33	38.68	0.91	0.33
2	5.5	HMWS	14.99	14.87	0.38	2.55	13.65	1.33	2.77
2	5.5	MP	84.35	84.50	0.36	0.43	85.22	1.31	0.43
2	5.5	MS	58.65	58.68	0.09	0.16	59.07	1.31	0.16
3	5.5	AS	2.51	2.54	0.05	2.05	2.23	0.56	2.33
3	5.5	BS	38.89	38.78	0.13	0.33	38.68	0.91	0.33
3	5.5	HMWS	15.18	14.87	0.38	2.55	13.65	1.33	2.77
3	5.5	MP	84.23	84.50	0.36	0.43	85.22	1.31	0.43
3	5.5	MS	58.60	58.68	0.09	0.16	59.07	1.31	0.16
1	10.76	AS	2.44	2.53	0.08	3.21	2.23	0.56	3.66
1	10.76	BS	39.90	39.90	0.13	0.33	38.68	0.91	0.34
1	10.76	HMWS	14.84	15.10	0.23	1.52	13.65	1.33	1.68
1	10.76	MP	83.45	83.29	0.15	0.18	85.22	1.31	0.18
1	10.76	MS	57.65	57.57	0.19	0.33	59.07	1.31	0.32
2	10.76	AS	2.57	2.53	0.08	3.21	2.23	0.56	3.66
2	10.76	BS	39.74	39.90	0.13	0.33	38.68	0.91	0.34
2	10.76	HMWS	15.17	15.10	0.23	1.52	13.65	1.33	1.68
2	10.76	MP	83.27	83.29	0.15	0.18	85.22	1.31	0.18
2	10.76	MS	57.70	57.57	0.19	0.33	59.07	1.31	0.32
3	10.76	AS	2.59	2.53	0.08	3.21	2.23	0.56	3.66
3	10.76	BS	40.05	39.90	0.13	0.33	38.68	0.91	0.34
3	10.76	HMWS	15.28	15.10	0.23	1.52	13.65	1.33	1.68
3	10.76	MP	83.15	83.29	0.15	0.18	85.22	1.31	0.18
3	10.76	MS	57.35	57.57	0.19	0.33	59.07	1.31	0.32

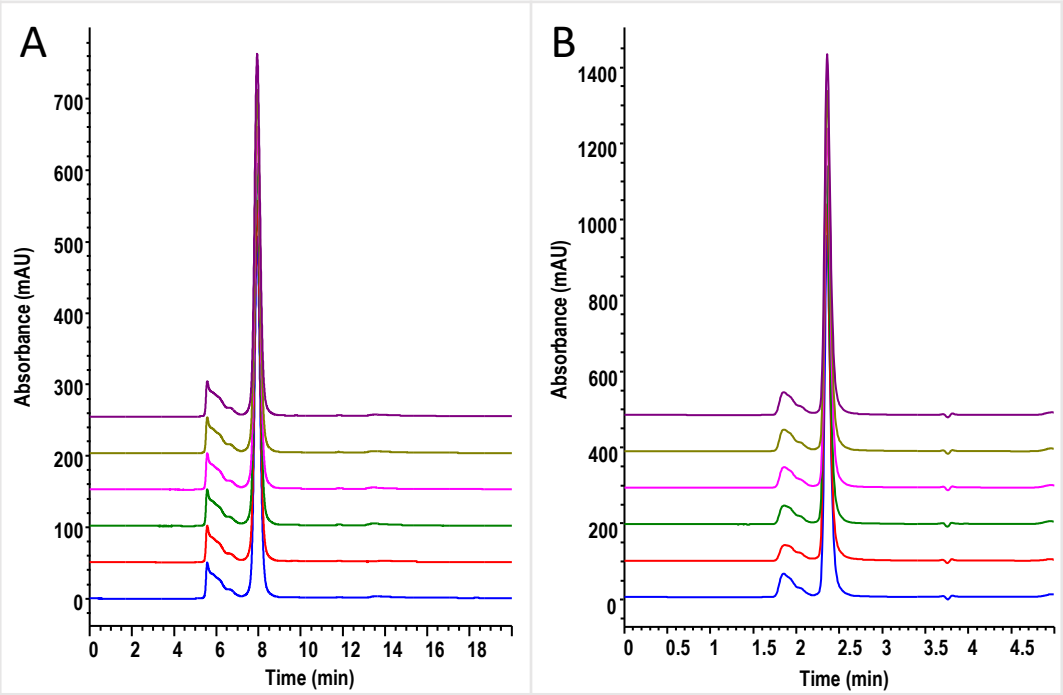

Figure 10.11 Comparison of %HMWS quantitation obtained by SEC-CEX-UV method *vs.* the AZ SOP SEC.

Chromatogram overlay of 6 technical replicate injections of a heat-stressed mAb-1 sample obtained by A) SEC-CEX-UV and B) AZ SOP SEC analysis. The samples were stressed by exposure at 70 °C for 60 min, divided into two aliquots and analysed by the two methods. The mean %HMWS and CVs were reported for each method.

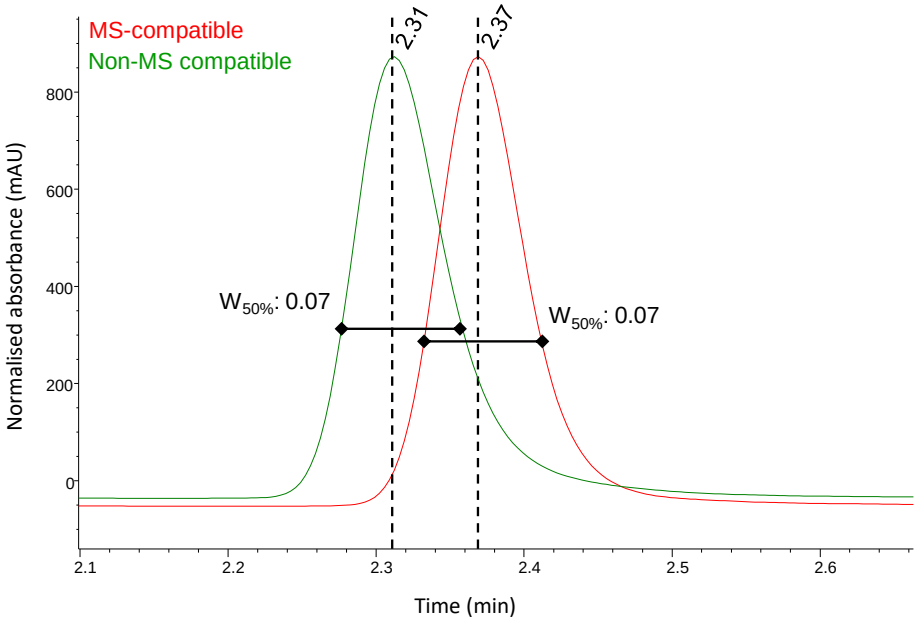

Figure 10.12 Overlay of the mAb-1 RS ^{1}D SEC profiles obtained by using volatile and non-volatile buffers.

Comparison of mAb-1 RS SEC UV trace obtained by using MS-compatible (red) and non-volatile (green) mobile phases. The injection volume was 10 µL and the sample was diluted to 1 mg/mL before analysis.

Table 10.13 MS peak assignment.

Sample Name	RT	Modification	Accuracy (ppm)
RS	9.8	2PyroQ+G0F+G1FS1	20.01
RS	11.2	2PyroQ+G0F+G0F	5.76
RS	11.2	2PyroQ+G0F+G1F	5.89
RS	11.2	2PyroQ+G0F+G0	3.87
RS	11.2	2PyroQ+G1F+G1F	23.88
RS	11.2	2PyroQ+G0F+G1F-GN	-16.36
RS	11.8	2PyroQ+Man6+G1FS1	5.00
RS	11.8	2PyroQ+G2+G1F-GN	-29.81
RS	11.8	G2FS2+Man4	18.31
RS	11.8	G2F+G0F-GN	27.50
RS	12.9	2PyroQ+G0F+G0F+1Ox	9.76
RS	12.9	2PyroQ+G0F+G1F+1Ox	14.36
RS	12.9	2PyroQ+G0+G0F+1Ox	15.41
RS	13.5	2PyroQ+Man6+G1F+Nac+Ox	5.41
RS	13.5	2PyroQ+G2+G1F-GN+Ox	-1.22
RS	14.3	2PyroQ+G0F+G0F+2Ox	24.61
RS	15.7	2PyroQ+Man5+G2S1	3.86
RS	15.7	2PyroQ+Man6+G1FS1	-17.92
Control	9.8	2PyroQ+G0F+G1FS1	31.97
Control	11.2	2PyroQ+G0F+G0F	8.00
Control	11.2	2PyroQ+G0F+G1F	8.53
Control	11.2	2PyroQ+G0+G0F	1.70
Control	11.2	2PyroQ+G1F+G1F	15.29
Control	11.2	2PyroQ+G0F+G-GN	-14.46
Control	11.7	2PyroQ+G0F+G0F	16.41
Control	11.7	2PyroQ+Man6+G1FS1	5.07
Control	11.7	2PyroQ+G2+G1F-GN	29.06
Control	13.0	2PyroQ+G0F+G0F+Ox	20.81
Control	13.0	2PyroQ+G0F+G1F+Ox	6.98
Control	13.0	2PyroQ+G0+G0F+1Ox	14.52
Control	13.4	1PyroQ+G0+G0F	3.39
Control	13.4	2PyroQ+Man6+G1F+Nac+Ox	14.27
Control	13.4	2PyroQ+G2+G1F-GN+Ox	0.41
Control	15.5	2PyroQ+G0F+G0F+2Ox	20.47
Control	15.7	2PyroQ+Man5+G2S1	1.02
Control	15.7	2PyroQ+Man6+G1FS1	-25.02
Low pH	9.9	2PyroQ+G0F+G1FS1	44.00
Low pH	11.2	2PyroQ+G0F+G0F	7.93
Low pH	11.2	2PyroQ+G0F+G1F	7.79
Low pH	11.2	2PyroQ+G0+G0F	-6.24
Low pH	11.2	2PyroQ+G1F+G1F	16.24
Low pH	11.2	2PyroQ+G0F+G-GN	-32.66
Low pH	11.7	2PyroQ+G0F+G0F	-9.70
Low pH	11.7	2PyroQ+Man6+G1FS1	5.48
Low pH	11.7	2PyroQ+G2+G1F-GN	-3.52
Low pH	12.9	2PyroQ+G0F+G0F+Ox	14.10

Low pH	12.9	2PyroQ+G0F+G1F+Ox	-7.11
Low pH	12.9	2PyroQ+G0+G0F+1Ox	8.28
Low pH	13.4	1PyroQ+G0+G0F	-2.44
Low pH	13.4	2PyroQ+G2+G1F-GN+Ox	16.80
Low pH	14.3	2PyroQ+G0F+G0F+2Ox	5.01
Low pH	15.7	2PyroQ+Man5+G2S1	10.15
Low pH	15.7	2PyroQ+Man6+G1F1	0.20
High pH	9.9	2PyroQ+G0F+G1FS1	28.93
High pH	11.3	2PyroQ+G0F+G0F	7.93
High pH	11.3	2PyroQ+G0F+G1F	-2.37
High pH	11.3	2PyroQ+G0+G0F	-3.05
High pH	11.3	2PyroQ+G1F+G1F	15.97
High pH	11.3	2PyroQ+G0F+G-GN	-24.17
High pH	11.7	2PyroQ+G0F+G0F	8.14
High pH	11.7	2PyroQ+G0F+G1F	-8.81
High pH	11.7	2PyroQ+Man6+G1FS1	5.00
High pH	11.7	2PyroQ+G0+G0F	2.44
High pH	11.7	2PyroQ+G2+G1F-GN+Ox	-2.78
High pH	11.7	G2FS2+Man4	8.98
High pH	13.7	2PyroQ+G0F+G0F+Ox	12.14
High pH	13.7	2PyroQ+G0F+G1F+Ox	23.43
High pH	13.7	2PyroQ+G0+G0F+1Ox	20.09
High pH	14.5	2PyroQ+G0F+G0F+2Ox	-15.12
High pH	15.8	2PyroQ+Man5+G2S1	8.33
High pH	15.8	2PyroQ+Man6+G1FS1	-18.60
AAPH stress	11.5	2PyroQ+G0F+G0F+5Ox	10.64
AAPH stress	11.5	2PyroQ+G0F+G1F+6Ox	8.80
AAPH stress	13.2	1PyroQ+G0F+G0F+6Ox	5.22
AAPH stress	11.5	2PyroQ+G0F+G0F+6Ox	-12.87
AAPH stress	11.5	2PyroQ+G0F+G0F+5Ox	15.38
AAPH stress	13.0	2PyroQ+G0F+G0F+7Ox	20.46
H_2O_2 stress	10.3	Fab[Q^{13}-C^{230}-SOH+H_2O]+2Ox	16.35
H_2O_2 stress	10.8	2PyroQ+G0F+G0F-Fab-5Ox	-0.96
H_2O_2 stress	11.5	2PyroQ+G0F+G0F+6Ox	41.74
H_2O_2 stress	11.5	2PyroQ+G1F-G1F+7Ox	-39.73
H_2O_2 stress	11.5	2PyroQ+G0F+G0F+7Ox	-0.27
H_2O_2 stress	13.5	2PyroQ+G0F+G0F+7Ox	37.81
Accelerated stability	9.90	2PyroQ+G0F+G1FS1	27.10
Accelerated stability	10.8	2PyroQ+G0F+G0F	9.63
Accelerated stability	10.8	2PyroQ+G0F+G1F	9.82
Accelerated stability	10.8	2PyroQ+G0F+G-GN	-23.15
Accelerated stability	10.8	2PyroQ+G0+G0F	-4.75
Accelerated stability	10.8	2PyroQ+G1F+G1F	24.09
Accelerated stability	11.2	2PyroQ+G0F+G0F	7.70
Accelerated stability	11.2	2PyroQ+G0F+G1F	6.00
Accelerated stability	11.2	2PyroQ+G0+G0F	-4.64
Accelerated stability	11.2	2PyroQ+G1F+G1F	18.68
Accelerated stability	11.2	2PyroQ+G0F+G-GN	-27.77
Accelerated stability	11.7	2PyroQ+G0F+G0F	14.24

Accelerated stability	11.7	2PyroQ+Man6+G1FS1	4.46
Accelerated stability	11.7	2PyroQ+G2+G1F-GN	-19.44
Accelerated stability	11.7	2PyroQ+G2+G1F-GN+Ox	0.14
Accelerated stability	13.1	1PyroQ+G0+G0F	8.34
Accelerated stability	13.1	2PyroQ+G0F+G1F+Ox	-4.88
Accelerated stability	13.1	2PyroQ+G0+G0F+1Ox	23.14
Accelerated stability	15.8	2PyroQ+Man5+G2S1	12.52
Accelerated stability	15.8	2PyroQ+Man6+G1FS1	-1.28

Appendix C

Supplementary information related to Chapter 5

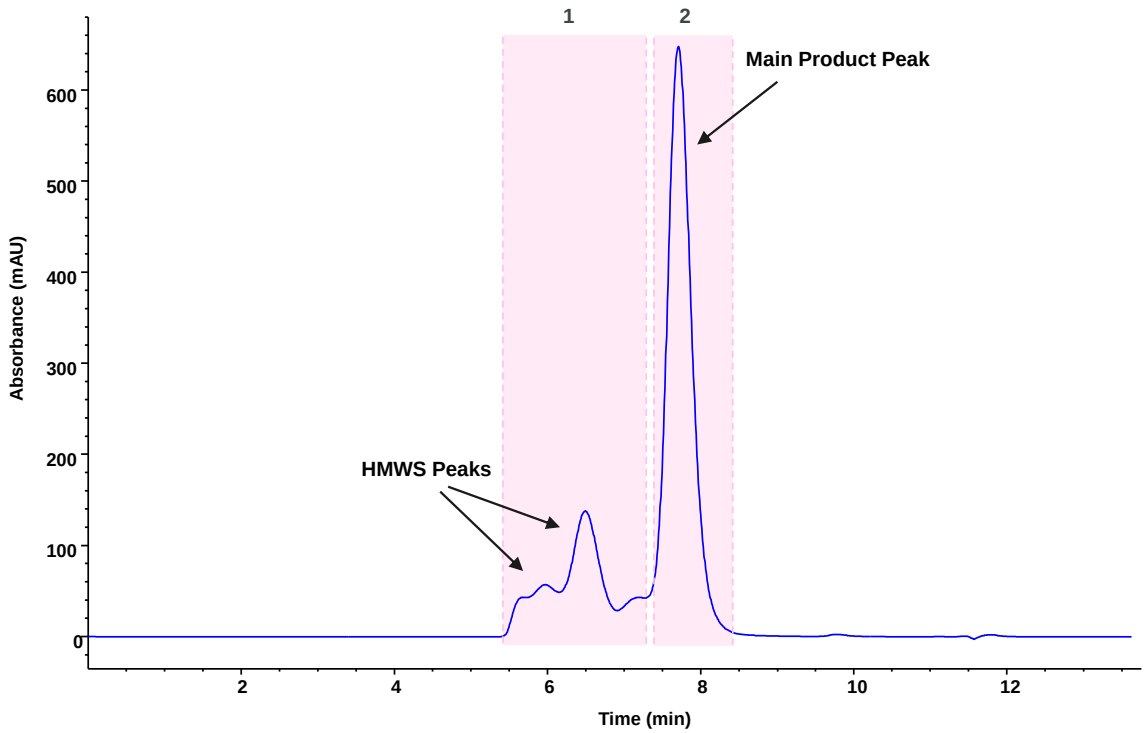

Figure 11.1 BsAb-1 SEC profile displaying the time window of the HMWS impurities and main product peak fractions.

Separation of BsAb-1 HMWS impurities from the main product peak by AZ SEC SOP. The pink shaded areas correspond to the time window used to fractionate the HMWS (1) and the main product peak (2) separately. The SEC method was run as per AZ SOP.

Peptide: XXXXC23X-XXXXXXXXXXXXXXXXXXXXXXXXXXXXC88XXXXXXXXXXXXXXX

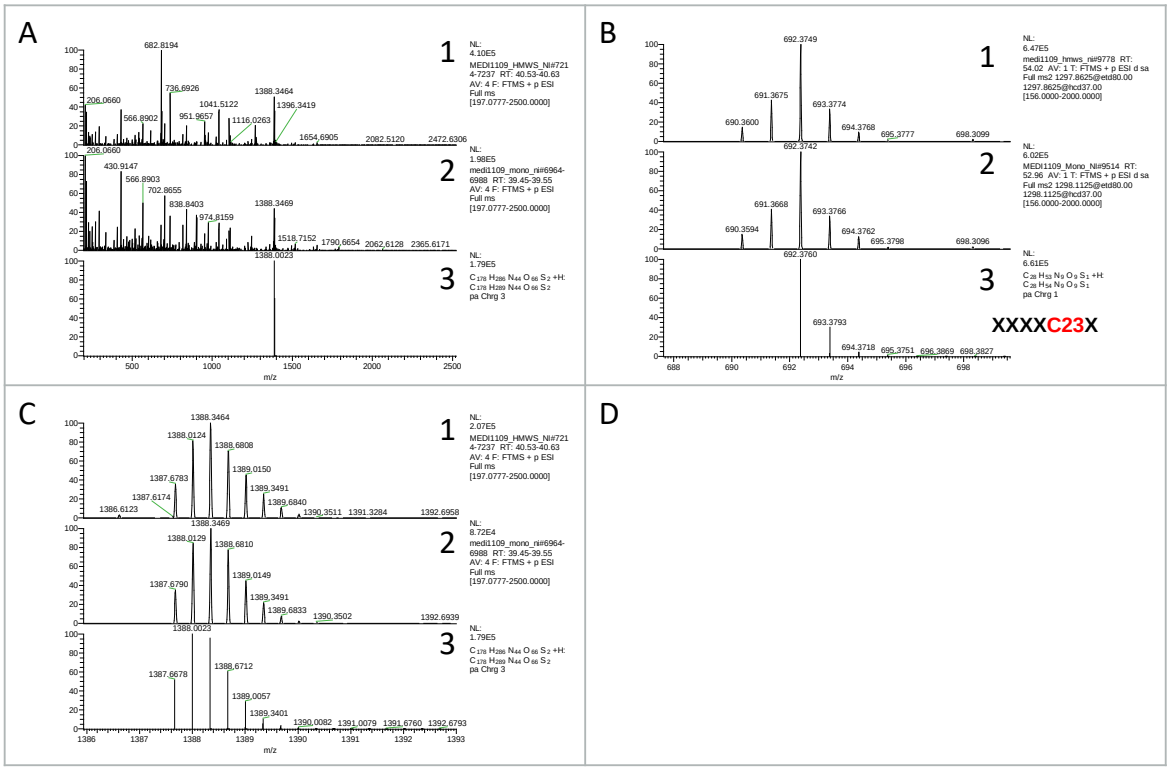

Figure 11.2 EThcD-assisted MS/MS spectra of the Cys23-Cys88 disulphide bond linked peptide.

A) Full MS spectra of the Cys23-Cys88 disulphide bond linked peptide observed in the SEC fraction 1 (A1) and fraction 2 (A2) with $[M+3H]^{3+}$ (1388 m/z) species detected in both fractions and $[M+3H]^{3+}$ matching the theoretical charge state distribution for $[M+3H]^{3+}$ (A3); B) Zoom of the isotopic charge distribution of $[M+3H]^{3+}$ observed in fraction 1 (B1) and 2 (B2) matching the theoretical charge state distribution for $[M+3H]^{3+}$; C) EThcD MS/MS spectra showing the fragment of the peptide containing Cys23 observed in fraction 1 (C1) and 2 (C2) and matching the theoretical charge state distribution for $[M+1H]^{1+}$ (C3).

Peptide: XXXXXXXC134XXXXXXXX-XXXC194XXXXXXXXXXXXX

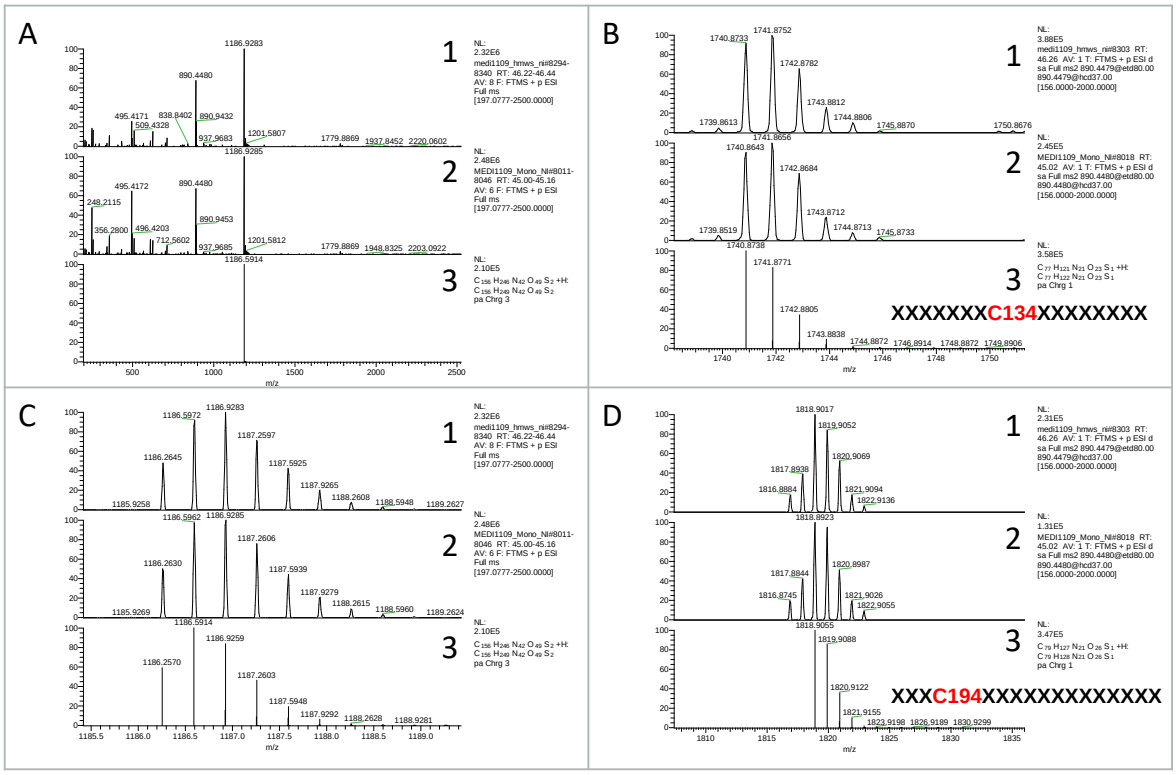

Figure 11.3 EThcD-assisted MS/MS spectra of the Cys134-Cys194 disulphide bond linked peptide.

A) Full MS spectra of the Cys134-Cys194 disulphide bond linked observed in the SEC fraction 1 (A1) and fraction 2 (A2) with $[M+2H]^{2+}$ (1186 m/z) species detected in both fractions matching the theoretical charge state distribution for $[M+2H]^{2+}$ (A3); B) Zoom of the isotopic charge distribution of $[M+2H]^{2+}$in fraction 1 (B1) and 2 (B2) matching the theoretical charge state distribution for $[M+2H]^{2+}$ (B3); C) EThcD MS/MS spectra showing the fragments of Cys134 observed in both fractions fraction 1 (C1) and 2 (C2) and matching the theoretical charge state distribution for $[M+1H]^{1+}$ (C3); D) EThcD MS/MS spectra showing the fragments of Cys194 observed in both fractions fraction 1 (D1) and 2 (D2) and matching the theoretical charge state distribution for $[M+1H]^{1+}$ (D3).

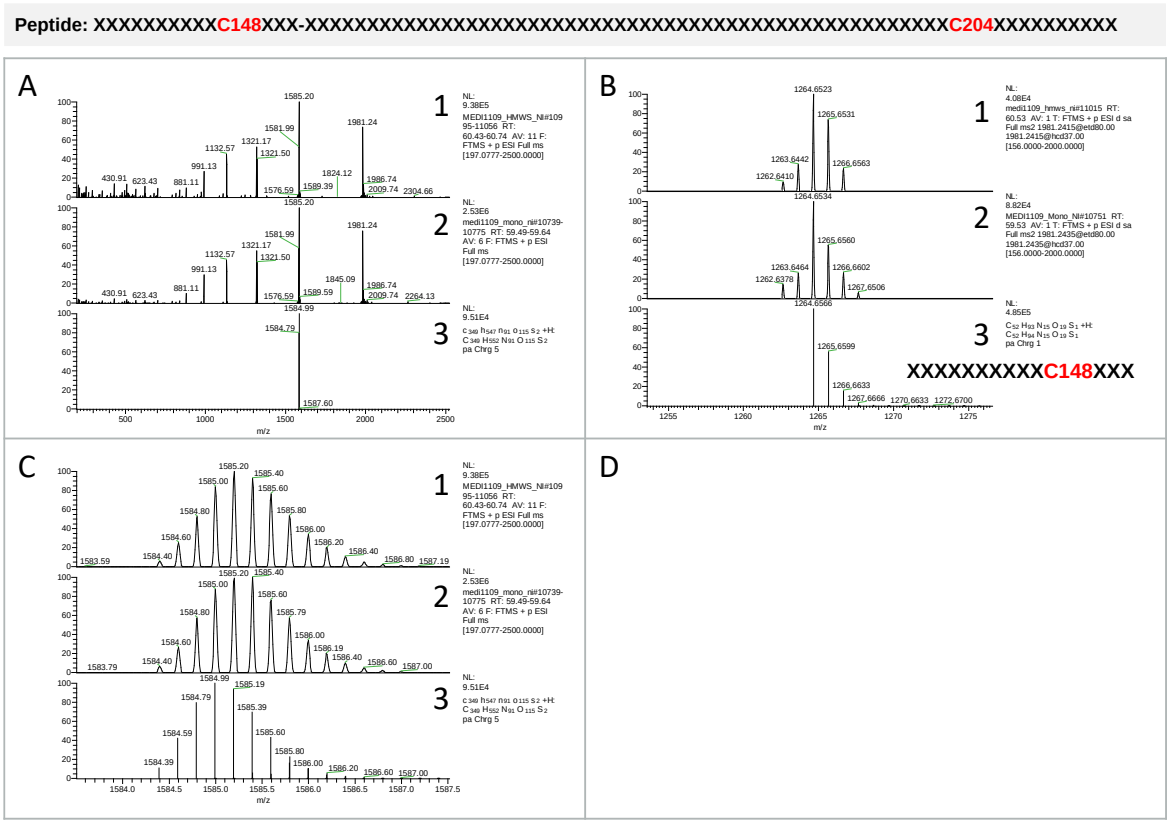
Peptide: XXXXXXXXXXC148XXX-XXXXXXXXXX

Peptide: XXXXXC265XXXXXXXXXXXXXC325X

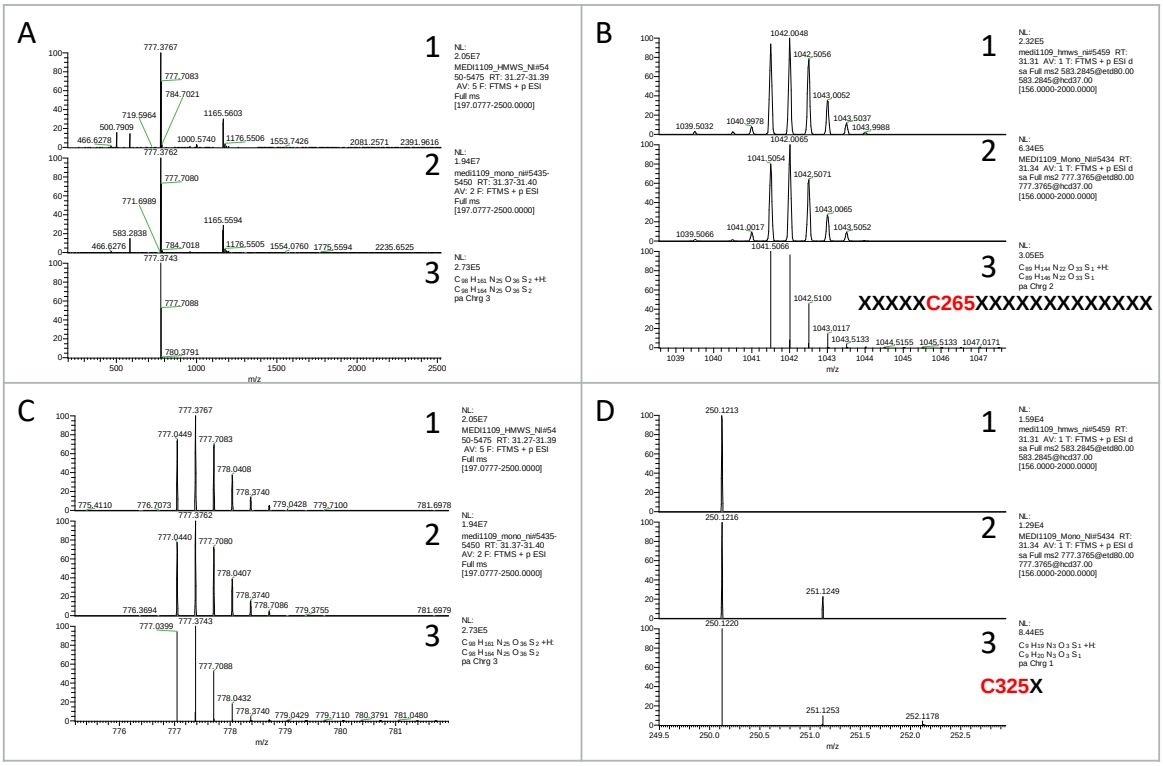

Figure 11.5 EThcD-assisted MS/MS spectra of the Cys265-Cys325 disulphide bond linked peptide.

A) Full MS spectra of the Cys265-Cys325 disulphide bond linked peptide observed in the SEC fraction 1 (A1) and fraction 2 (A2) with $[M+3H]^{3+}$ (777 m/z) species detected in both fractions matching the theoretical charge state distribution for $[M+3H]^{3+}$ (A3); B) Zoom of the isotopic charge distribution of $[M+3H]^{3+}$in fraction 1 (B1) and 2 (B2) matching the theoretical charge state distribution for $[M+3H]^{3+}$ (B3); C) EThcD MS/MS spectra showing the fragments of Cys265 observed in both fractions fraction 1 (C1) and 2 (C2) and matching the theoretical charge state distribution for $[M+2H]^{2+}$ (C3); D) EThcD MS/MS spectra showing the fragments of Cys325 observed in both fractions fraction 1 (D1) and 2 (D2) and matching the theoretical charge state distribution for $[M+1H]^{1+}$ (D3).

Peptide: XXXXXXC371XXX-XXXXXXXXC698XXXXXXXXXXXXXX

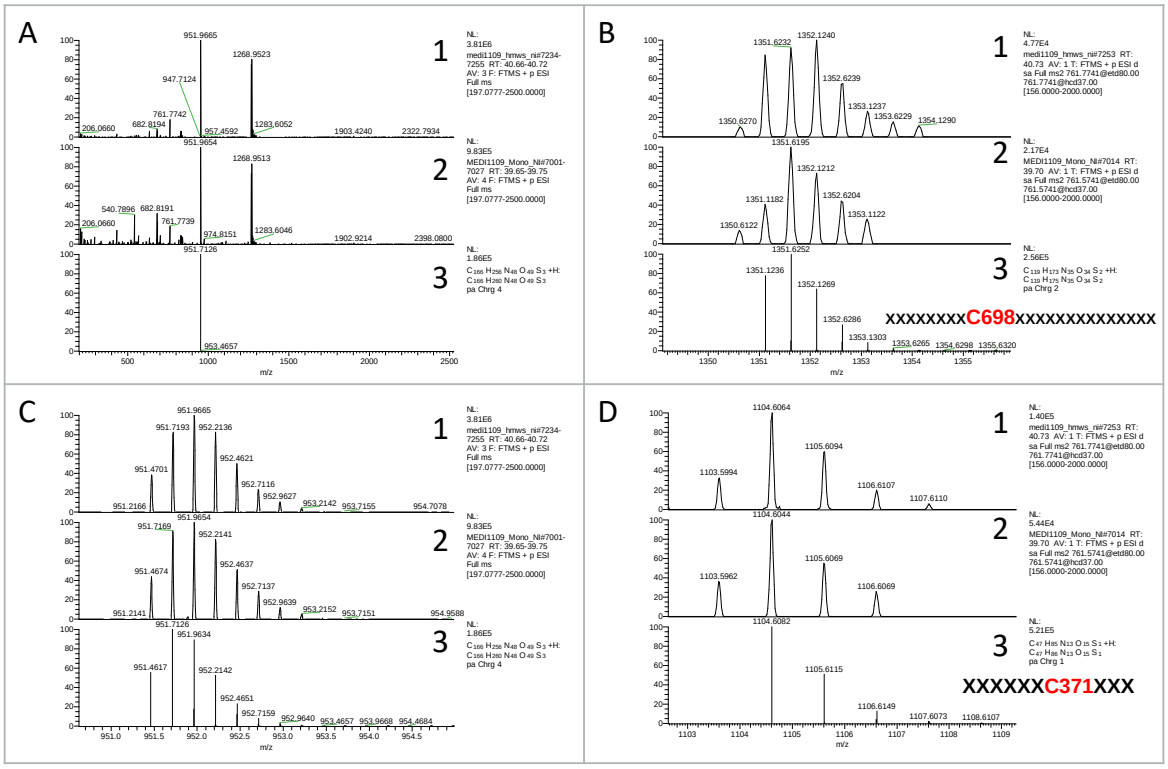

Figure 11.6 EThcD-assisted MS/MS spectra of the Cys371-Cys698 disulphide bond linked peptide.

A) Full MS spectra of the Cys371-Cys698 disulphide bond linked peptide observed in the SEC fraction 1 (A1) and fraction 2 (A2) with $[M+4H]^{4+}$ (951 m/z) species detected in both fractions matching the theoretical charge state distribution for $[M+4H]^{4+}$ (A3); B) Zoom of the isotopic charge distribution of $[M+4H]^{4+}$in fraction 1 (B1) and 2 (B2) matching the theoretical charge state distribution for $[M+4H]^{4+}$ (B3); C) EThcD MS/MS spectra showing the fragments of Cys698 observed in both fractions fraction 1 (C1) and 2 (C2) and matching the theoretical charge state distribution for $[M+2H]^{2+}$ (C3); D) EThcD MS/MS spectra showing the fragments of Cys371 observed in both fractions fraction 1 (D1) and 2 (D2) and matching the theoretical charge state distribution for $[M+1H]^{1+}$ (D3).

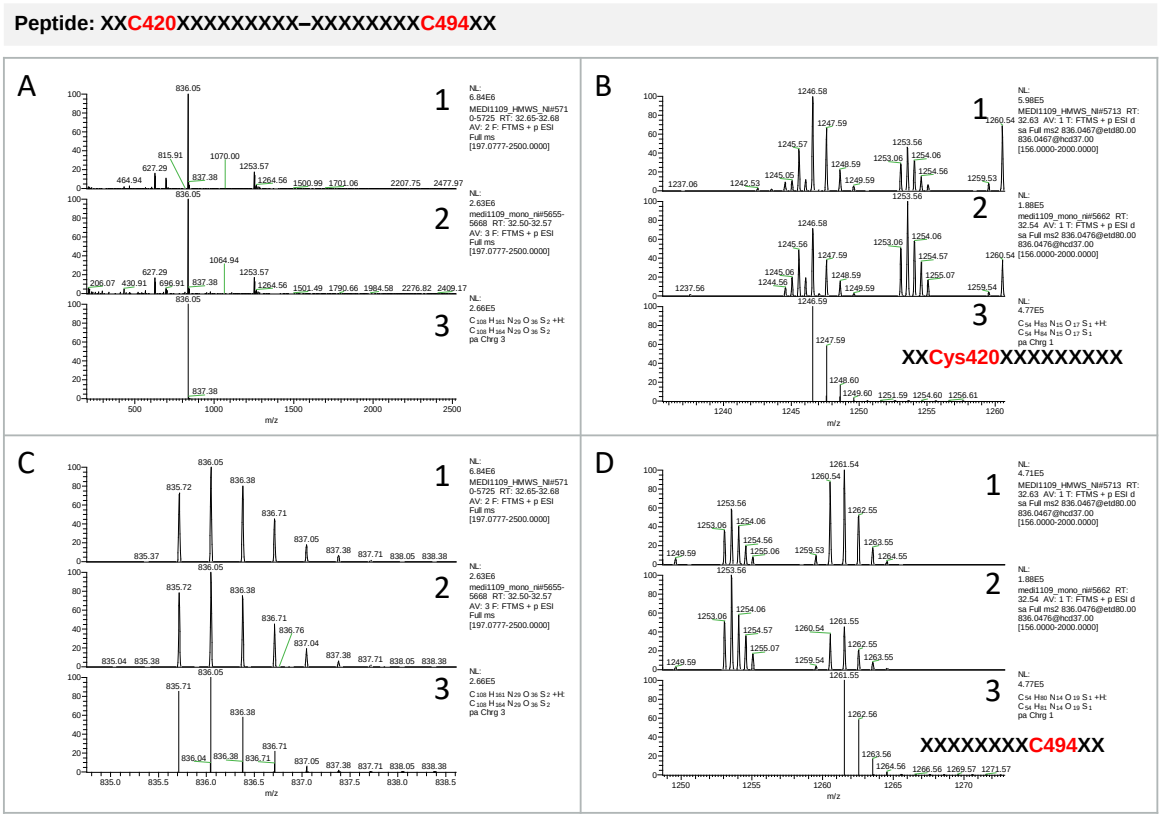

Figure 11.7 EThcD-assisted MS/MS spectra of the Cys420-Cys494 disulphide bond linked peptide.

A) Full MS spectra of the Cys420-Cys494 disulphide bond linked peptide observed in the SEC fraction 1 (A1) and fraction 2 (A2) with $[M+3H]^{3+}$ (836 m/z) species detected in both fractions matching the theoretical charge state distribution for $[M+3H]^{3+}$ (A3); B) Zoom of the isotopic charge distribution of $[M+3H]^{3+}$ in fraction 1 (B1) and 2 (B2) matching the theoretical charge state distribution for $[M+3H]^{3+}$ (B3); C) EThcD MS/MS spectra showing the fragments of Cys420 observed in both fractions fraction 1 (C1) and 2 (C2) and matching the theoretical charge state distribution for $[M+1H]^{1+}$ (C3); D) EThcD MS/MS spectra showing the fragments of Cys494 observed in both fractions fraction 1 (D1) and 2 (D2) and matching the theoretical charge state distribution for $[M+1H]^{1+}$ (D3).

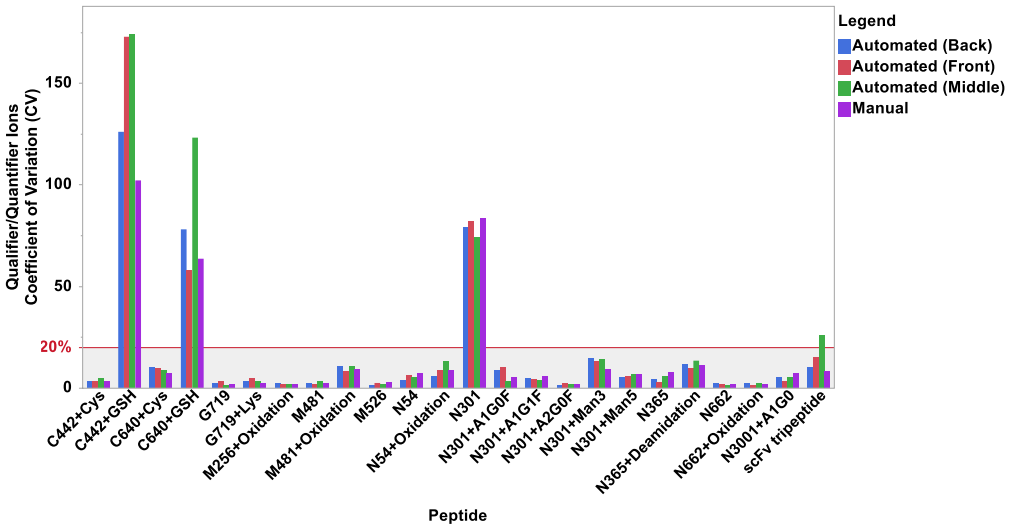

Figure 11.8 Comparison of the qualifier/quantifier ion ratio CVs obtained when using the manual and automated sample preparation procedures.

Bar chart comparing the qualifier/quantifier ion ratio CVs obtained across the 6 sample replicates analysed when using the manual and automated sample preparation procedures. The sample groups were colour-coded to facilitate the visualisation of the sample groups under investigation. Namely, the data obtained by using manual sample preparation (purple) was compared to the automated procedure. The latter comprised of 3 groups corresponding to 6 replicate samples analysed at the front (red), middle (green), and back (blue) of the plate. This was done to evaluate the variability of the automated procedure across a 96-DWP.

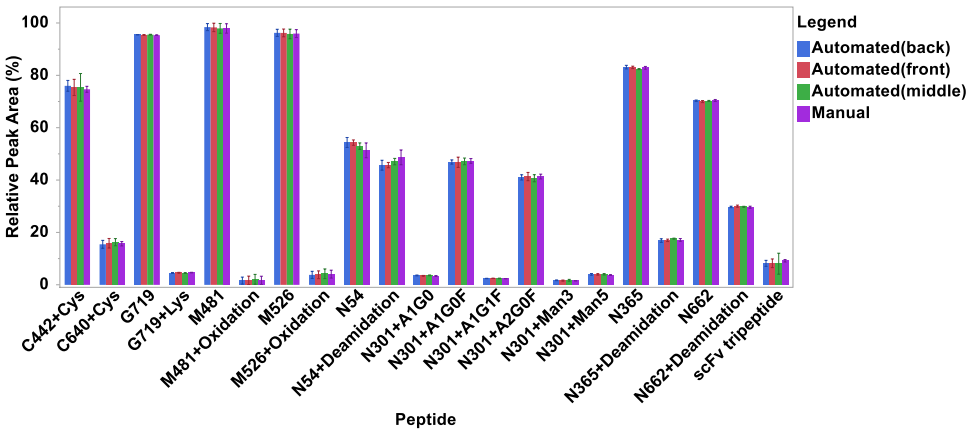

Figure 11.9 Comparison of the MAM relative quantitation data of BsAb-1 PTMs obtained when using the manual *vs.* the automated sample preparation procedures.

Bar chart comparing the relative quantitation of BsAb-1 PTMs obtained across the 6 sample replicates analysed when using the manual and automated sample preparation procedures. The sample groups were colour-coded to facilitate the visualisation of the sample groups under investigation. Namely, the data obtained by using manual sample preparation (purple) was compared to the automated procedure. The latter comprised of 3 groups corresponding to 6 replicate samples analysed at the front (red), middle (green), and back (blue) of the plate. This was done to evaluate the variability of the automated procedure across a 96-DWP.

Table 11.1 ANOVA test for the sample plate position.

Site-specific Modification	Source.	DF	Sum of Squares	Mean Square	F Ratio	Prob > F
C442+Cys	Sample Group	2	1.19624	0.5981	0.0441	0.9570
	Error	13	176.37093	13.5670		
	C. Total	15	177.56718			
C640+Cys	Sample Group	2	1.643740	0.82187	0.3192	0.7323
	Error	13	33.469937	2.57461		
	C. Total	15	35.113677			
G719	Sample Group	2	0.03960629	0.019803	0.9853	0.3996
	Error	13	0.26127917	0.020098		
	C. Total	15	0.30088546			
G719+Lys	Sample Group	2	0.03960629	0.019803	0.9853	0.3996
	Error	13	0.26127917	0.020098		
	C. Total	15	0.30088546			
M481	Sample Group	2	0.665228	0.33261	0.1260	0.8827
	Error	13	34.320294	2.64002		
	C. Total	15	34.985522			
M481+Oxidation	Sample Group	2	0.665228	0.33261	0.1260	0.8827
	Error	13	34.320294	2.64002		
	C. Total	15	34.985522			
M526	Sample Group	2	0.576985	0.28849	0.1168	0.8907
	Error	13	32.117206	2.47055		
	C. Total	15	32.694191			
M526+Oxidation	Sample Group	2	0.576985	0.28849	0.1168	0.8907
	Error	13	32.117206	2.47055		
	C. Total	15	32.694191			
N54	Sample Group	2	6.332828	3.16641	1.6003	0.2392
	Error	13	25.722231	1.97863		
	C. Total	15	32.055059			
N54+Deamidation	Sample Group	2	6.332828	3.16641	1.6003	0.2392
	Error	13	25.722231	1.97863		
	C. Total	15	32.055059			
N301+A1G0	Sample Group	2	0.10539276	0.052696	2.1021	0.1618
	Error	13	0.32588436	0.025068		
	C. Total	15	0.43127713			
N301+A1G0F	Sample Group	2	0.309870	0.15494	0.0711	0.9317
	Error	13	28.331982	2.17938		
	C. Total	15	28.641852			
N301+A1G1F	Sample Group	2	0.01013787	0.005069	0.5404	0.5951
	Error	13	0.12194124	0.009380		
	C. Total	15	0.13207911			
N301+A2G0F	Sample Group	2	1.136096	0.56805	0.3082	0.7400

	Error	13	23.961192	1.84317		
	C. Total	15	25.097288			
N301+Man3	Sample Group	2	0.05025678	0.025128	0.4092	0.6724
	Error	13	0.79823692	0.061403		
	C. Total	15	0.84849370			
N301+Man5	Sample Group	2	0.0044441	0.002222	0.0261	0.9743
	Error	13	1.1072128	0.085170		
	C. Total	15	1.1116569			
N365	Sample Group	2	1.6407700	0.820385	3.3723	0.0661
	Error	13	3.1625363	0.243272		
	C. Total	15	4.8033064			
N365+Deamidation	Sample Group	2	1.6407700	0.820385	3.3723	0.0661
	Error	13	3.1625363	0.243272		
	C. Total	15	4.8033064			
N662	Sample Group	2	0.2957513	0.147876	1.5237	0.2544
	Error	13	1.2616500	0.097050		
	C. Total	15	1.5574014			
N662+Deamidation	Sample Group	2	0.2957513	0.147876	1.5237	0.2544
	Error	13	1.2616500	0.097050		
	C. Total	15	1.5574014			
scFv tripeptide	Sample Group	2	0.073150	0.03658	0.0057	0.9943
	Error	13	83.453104	6.41947		
	C. Total	15	83.526254			

Table 11.2 T-test of the manual *vs.* the automated sample preparation procedures.

C442+Cys	**t Test** Manual-Automated Assuming unequal variances Difference -0.6665 t Ratio -0.5059 Std Err Dif 1.3175 DF 6.407666 Upper CL Dif 2.5082 Prob > |t| 0.6299 Lower CL Dif -3.8413 Prob > t 0.6851 Confidence 0.95 Prob < t 0.3149 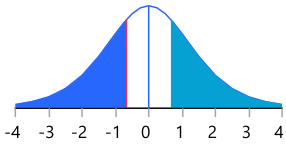
C640+Cys	**t Test** Manual-Automated Assuming unequal variances Difference -0.2239 t Ratio -0.2782 Std Err Dif 0.8047 DF 7.100803 Upper CL Dif 1.6735 Prob > |t| 0.7888 Lower CL Dif -2.1213 Prob > t 0.6056 Confidence 0.95 Prob < t 0.3944 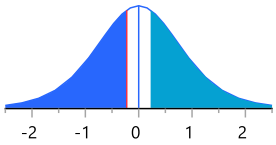
G719	**t Test** Manual-Automated Assuming unequal variances Difference -0.09273 t Ratio -1.16575 Std Err Dif 0.07955 DF 9.802127 Upper CL Dif 0.08499 Prob > |t| 0.2713 Lower CL Dif -0.27045 Prob > t 0.8644 Confidence 0.95 Prob < t 0.1356 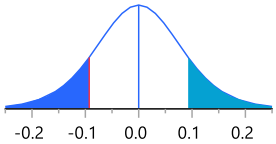
G719+Lys	**t Test** Manual-Automated Assuming unequal variances Difference 0.09273 t Ratio 1.165755 Std Err Dif 0.07955 DF 9.802127 Upper CL Dif 0.27045 Prob > |t| 0.2713 Lower CL Dif -0.08499 Prob > t 0.1356 Confidence 0.95 Prob < t 0.8644 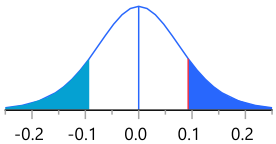
M481	**t Test** Manual-Automated Assuming unequal variances Difference 0.5821 t Ratio 0.625839 Std Err Dif 0.9300 DF 9.968325 Upper CL Dif 2.6552 Prob > |t| 0.5455 Lower CL Dif -1.4911 Prob > t 0.2727 Confidence 0.95 Prob < t 0.7273 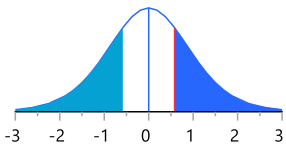
M481+Oxidation	**t Test** Manual-Automated Assuming unequal variances Difference -0.5821 t Ratio -0.62584 Std Err Dif 0.9300 DF 9.968325 Upper CL Dif 1.4911 Prob > |t| 0.5455 Lower CL Dif -2.6552 Prob > t 0.7273 Confidence 0.95 Prob < t 0.2727 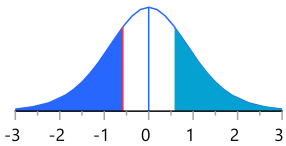
M526	**t Test** Manual-Automated Assuming unequal variances Difference 0.3400 t Ratio 0.382237 Std Err Dif 0.8894 DF 9.988648 Upper CL Dif 2.3220 Prob > |t| 0.7103 Lower CL Dif -1.6420 Prob > t 0.3551 Confidence 0.95 Prob < t 0.6449 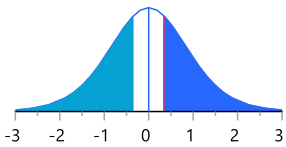

M526+Oxidation

t Test

Manual-Automated

Assuming unequal variances

Difference	-0.3400	t Ratio	-0.38224
Std Err Dif	0.8894	DF	9.988648
Upper CL Dif	1.6420	Prob > |t|	0.7103
Lower CL Dif	-2.3220	Prob > t	0.6449
Confidence	0.95	Prob < t	0.3551

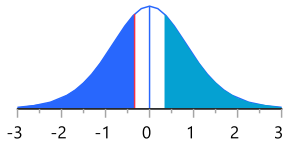

N54

t Test

Manual-Automated

Assuming unequal variances

Difference	-3.4652	t Ratio	-2.7818
Std Err Dif	1.2457	DF	6.530095
Upper CL Dif	-0.4762	Prob > |t|	0.0292 *
Lower CL Dif	-6.4543	Prob > t	0.9854
Confidence	0.95	Prob < t	0.0146 *

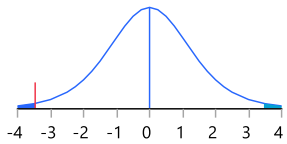

N54+Deamidation

t Test

Manual-Automated

Assuming unequal variances

Difference	3.46523	t Ratio	2.781803
Std Err Dif	1.24568	DF	6.530095
Upper CL Dif	6.45431	Prob > |t|	0.0292 *
Lower CL Dif	0.47615	Prob > t	0.0146 *
Confidence	0.95	Prob < t	0.9854

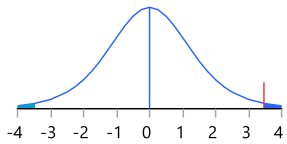

N301+A1G0

t Test

Manual-Automated

Assuming unequal variances

Difference	-0.06762	t Ratio	-0.73434
Std Err Dif	0.09209	DF	9.442163
Upper CL Dif	0.13921	Prob > |t|	0.4806
Lower CL Dif	-0.27446	Prob > t	0.7597
Confidence	0.95	Prob < t	0.2403

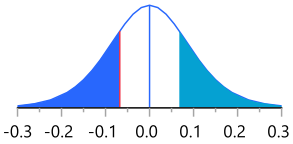

N301+A1G0F

t Test

Manual-Automated

Assuming unequal variances

Difference	0.4546	t Ratio	0.508224
Std Err Dif	0.8944	DF	7.021388
Upper CL Dif	2.5682	Prob > |t|	0.6269
Lower CL Dif	-1.6591	Prob > t	0.3134
Confidence	0.95	Prob < t	0.6866

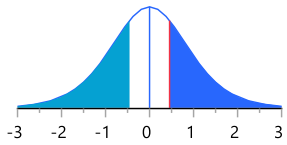

N301+A1G1F

t Test

Manual-Automated

Assuming unequal variances

Difference	-0.11047	t Ratio	-2.02127
Std Err Dif	0.05466	DF	9.485797
Upper CL Dif	0.01221	Prob > |t|	0.0724
Lower CL Dif	-0.23316	Prob > t	0.9638
Confidence	0.95	Prob < t	0.0362 *

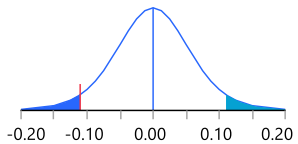

N301+A2G0F

t Test

Manual-Automated

Assuming unequal variances

Difference	0.0412	t Ratio	0.053863
Std Err Dif	0.7651	DF	7.937459
Upper CL Dif	1.8079	Prob > |t|	0.9584
Lower CL Dif	-1.7255	Prob > t	0.4792
Confidence	0.95	Prob < t	0.5208

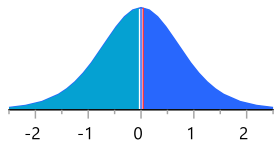

N301+Man3

t Test

Manual-Automated

Assuming unequal variances

Difference	-0.08162	t Ratio	-0.90898
Std Err Dif	0.08980	DF	5.619233
Upper CL Dif	0.14176	Prob > |t|	0.4007
Lower CL Dif	-0.30500	Prob > t	0.7997
Confidence	0.95	Prob < t	0.2003

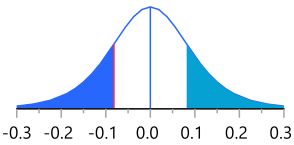

N301+Man5

t Test

Manual-Automated

Assuming unequal variances

Difference	-0.22999	t Ratio	-2.00418
Std Err Dif	0.11476	DF	6.632099
Upper CL Dif	0.04444	Prob > |t|	0.0874
Lower CL Dif	-0.50443	Prob > t	0.9563
Confidence	0.95	Prob < t	0.0437 *

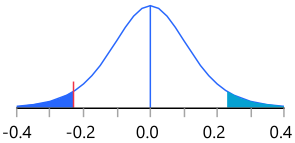

N365

t Test

Manual-Automated

Assuming unequal variances

Difference	-0.18365	t Ratio	-0.63752
Std Err Dif	0.28806	DF	9.895889
Upper CL Dif	0.45911	Prob > |t|	0.5383
Lower CL Dif	-0.82641	Prob > t	0.7309
Confidence	0.95	Prob < t	0.2691

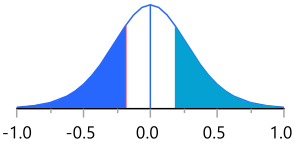

N365+Deamidation

t Test

Manual-Automated

Assuming unequal variances

Difference	0.18365	t Ratio	0.637519
Std Err Dif	0.28806	DF	9.895889
Upper CL Dif	0.82641	Prob > |t|	0.5383
Lower CL Dif	-0.45911	Prob > t	0.2691
Confidence	0.95	Prob < t	0.7309

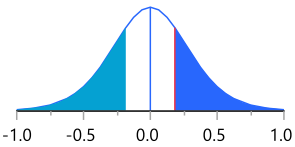

N662

t Test

Manual-Automated

Assuming unequal variances

Difference	0.33817	t Ratio	1.635497
Std Err Dif	0.20677	DF	9.592956
Upper CL Dif	0.80155	Prob > |t|	0.1343
Lower CL Dif	-0.12520	Prob > t	0.0671
Confidence	0.95	Prob < t	0.9329

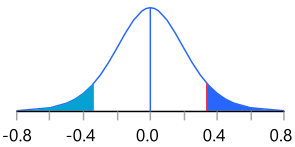

N662+Deamidation

t Test

Manual-Automated

Assuming unequal variances

Difference	-0.33817	t Ratio	-1.6355
Std Err Dif	0.20677	DF	9.592956
Upper CL Dif	0.12520	Prob > |t|	0.1343
Lower CL Dif	-0.80155	Prob > t	0.9329
Confidence	0.95	Prob < t	0.0671

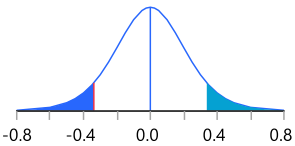

scFv tripeptide

t Test

Manual-Automated

Assuming unequal variances

Difference	0.9532	t Ratio	1.344962
Std Err Dif	0.7088	DF	5.816823
Upper CL Dif	2.7008	Prob > |t|	0.2287
Lower CL Dif	-0.7943	Prob > t	0.1144
Confidence	0.95	Prob < t	0.8856

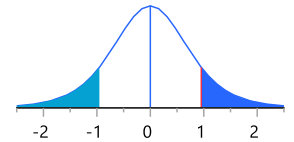

Table 11.3 Summary of the variability gauge analysis for BsAb-1 PTMs quantitation by manual and automated sample preparation.

	μ	σ	CV	Median	N
Relative Peak Area	38.05	34.8	91.6	29.70	252
Site-specific PTM[C442+Cys]	74.98	2.20	2.94	74.85	12
Site-specific PTM[C640+Cys]	15.79	1.33	8.45	15.61	12
Site-specific PTM[G719]	95.38	0.14	0.15	95.39	12
Site-specific PTM[G719+Lys]	4.62	0.14	3.03	4.61	12
Site-specific PTM[M481]	97.98	1.57	1.60	98.61	12
Site-specific PTM[M481+Oxidation]	2.02	1.57	7.46	1.39	12
Site-specific PTM[M526]	95.74	1.48	1.55	96.24	12
Site-specific PTM[M526+Oxidation]	4.26	1.48	34.72	3.76	12
Site-specific PTM[N54]	53.07	2.74	5.16	53.43	12
Site-specific PTM[N54+Deamidation]	46.93	2.74	5.84	46.57	12
Site-specific PTM[N301+A1G0]	3.43	0.16	4.55	3.43	12
Site-specific PTM[N301+A1G0F]	47.08	1.50	3.18	47.29	12
Site-specific PTM[N301+A1G1F]	2.40	0.11	4.47	2.37	12
Site-specific PTM[N301+A2G0F]	41.31	1.26	3.06	41.26	12
Site-specific PTM[N301+Man3]	1.60	0.15	9.65	1.58	12
Site-specific PTM[N301+Man5]	3.86	0.22	5.81	3.83	12
Site-specific PTM[N365]	82.94	0.49	0.59	82.90	12
Site-specific PTM[N365+Deamidation]	17.06	0.49	2.84	17.10	12
Site-specific PTM[N662]	70.20	0.38	0.55	70.30	12
Site-specific PTM[N662+Deamidation]	29.80	0.38	1.29	29.70	12
Site-specific PTM[scFv tripeptide]	8.70	1.27	14.62	8.84	12
Site-specific PTM[C442+Cys] Group[Automated]	75.31	3.02	4.01	75.26	6
Site-specific PTM[C442+Cys] Group[Manual]	74.64	1.14	1.53	74.71	6
Site-specific PTM[C640+Cys] Group[Automated]	15.90	1.78	11.22	15.83	6
Site-specific PTM[C640+Cys] Group[Manual]	15.68	0.84	5.34	15.61	6
Site-specific PTM[G719] Group[Automated]	95.42	0.15	0.15	95.40	6
Site-specific PTM[G719] Group[Manual]	95.33	0.13	0.13	95.35	6
Site-specific PTM[G719+Lys] Group[Automated]	4.58	0.15	3.22	4.60	6
Site-specific PTM[G719+Lys] Group[Manual]	4.67	0.13	2.73	4.65	6
Site-specific PTM[M481] Group[Automated]	97.69	1.66	1.69	97.99	6
Site-specific PTM[M481] Group[Manual]	98.27	1.56	1.59	98.73	6
Site-specific PTM[M481+Oxidation] Group[Automated]	2.31	1.66	71.60	2.01	6
Site-specific PTM[M481+Oxidation] Group[Manual]	1.73	1.56	90.43	1.27	6
Site-specific PTM[M526] Group[Automated]	95.57	1.57	1.64	95.74	6
Site-specific PTM[M526] Group[Manual]	95.91	1.51	1.58	96.42	6
Site-specific PTM[M526+Oxidation] Group[Automated]	4.43	1.57	35.34	4.26	6
Site-specific PTM[M526+Oxidation] Group[Manual]	4.09	1.51	37.01	3.58	6
Site-specific PTM[N54] Group[Automated]	54.80	1.12	2.05	54.48	6
Site-specific PTM[N54] Group[Manual]	51.34	2.84	5.53	52.29	6
Site-specific PTM[N54+Deamidation] Group[Automated]	45.20	1.12	2.49	45.52	6
Site-specific PTM[N54+Deamidation] Group[Manual]	48.66	2.84	5.83	47.71	6
Site-specific PTM[N301+A1G0] Group[Automated]	3.47	0.18	5.13	3.47	6
Site-specific PTM[N301+A1G0] Group[Manual]	3.40	0.14	4.08	3.40	6
Site-specific PTM[N301+A1G0F] Group[Automated]	46.85	1.99	4.25	47.33	6

Site-specific PTM[N301+A1G0F] Group[Manual]	47.30	0.91	1.93	47.29	6
Site-specific PTM[N301+A1G1F] Group[Automated]	2.45	0.11	4.28	2.48	6
Site-specific PTM[N301+A1G1F] Group[Manual]	2.34	0.08	3.54	2.34	6
Site-specific PTM[N301+A2G0F] Group[Automated]	41.29	1.63	3.94	40.90	6
Site-specific PTM[N301+A2G0F] Group[Manual]	41.33	0.93	2.24	41.42	6
Site-specific PTM[N301+Man3] Group[Automated]	1.64	0.21	13.02	1.63	6
Site-specific PTM[N301+Man3] Group[Manual]	1.56	0.05	3.42	1.54	6
Site-specific PTM[N301+Man5] Group[Automated]	3.97	0.26	6.55	4.06	6
Site-specific PTM[N301+Man5] Group[Manual]	3.74	0.11	2.85	3.75	6
Site-specific PTM[N365] Group[Automated]	83.03	0.47	0.57	82.96	6
Site-specific PTM[N365] Group[Manual]	82.85	0.52	0.63	82.90	6
Site-specific PTM[N365+Deamidation] Group[Automated]	16.97	0.47	2.79	17.04	6
Site-specific PTM[N365+Deamidation] Group[Manual]	17.15	0.52	3.05	17.10	6
Site-specific PTM[N662] Group[Automated]	70.03	0.32	0.46	69.99	6
Site-specific PTM[N662] Group[Manual]	70.37	0.39	0.56	70.43	6
Site-specific PTM[N662+Deamidation] Group[Automated]	29.97	0.32	1.06	30.01	6
Site-specific PTM[N662+Deamidation] Group[Manual]	29.63	0.39	1.33	29.57	6
Site-specific PTM[scFv tripeptide] Group[Automated]	8.22	1.67	20.30	7.53	6
Site-specific PTM[scFv tripeptide] Group[Manual]	9.18	0.48	5.22	8.98	6

Table 11.4 Summary HMWS quantitation regression model.

Measure	Training	Validation
Number of rows	39	18
Sum of Frequencies	39	18
-LogLikelihood	126.65742	66.745611
Number of Parameters	9	9
BIC	286.28689	159.50457
AICc	277.52173	173.99122
RSquare	0.8068489	0.6811203
RASE	6.2257104	8.6286793
Lambda Penalty	0.0805884	.

Table 11.5 Summary of the factors effects in the HMWS quantitation model.

Source	Prob > ChiSquare
C442-Cys	<.0001*
C442-Cys*scFv tripeptide	0.0001*
C442-Cys*C640-Cys*scFv tripeptide	0.7849
C640-Cys*scFv tripeptide	0.8219
C640-Cys	0.8770
C442-Cys*C640-Cys	0.9115
scFv tripeptide	1.0000

Table 11.6 Summary of the Variability gauge analysis to assess the overtime stability of the tryptic digested peptides under process conditions before LC-MS injection within 48 samples.

	Mean	Std Dev	CV	Median	N°
Relative Peak Area	50	31.2611	62.5223	50	96
Site[M526]	78.1402	13.3766	17.1187	79.6713	48
Site[M526+Oxidation]	21.8597	13.3766	61.1928	20.3286	48
Site[N365]	83.0099	0.67899	0.81797	83.0241	48
Site[N365+Deamidation]	16.9900	0.67899	3.99643	16.9758	48
Site[M481]	79.52585	14.09912	17.72898	81.38873	48
Site[M481+Oxidation]	20.47415	14.09912	68.86305	18.61127	48
Site[N54]	53.10061	2.355995	4.436851	53.18983	48
Site[N54+Deamidation]	46.89939	2.355995	5.023509	46.81017	48
Site[N662]	69.75681	0.26712	0.38293	69.78085	48
Site[N662+Deamidation]	30.24319	0.26712	0.88324	30.21915	48
Site[G719]	94.48128	0.265323	0.28082	94.50076	28
Site[G719 + Lys]	5.427482	0.257038	4.735855	5.377381	48
Glycoform[A1G0]	3.608128	0.145397	4.029713	3.614516	48
Glycoform[A1G0F]	46.22296	1.330799	2.879086	46.13294	48
Glycoform[A1G1F]	2.621408	0.112037	4.273912	2.630407	48
Glycoform[A2G0]	41.49464	1.2324	2.970023	41.26873	48
Glycoform[Man3]	1.529036	0.106508	6.965689	1.543195	48
Glycoform[Man5]	4.214023	0.286245	6.792667	4.218994	48
Cys[442+Cys]	69.94729	2.840407	4.060782	70.55865	48
Cys[640+Cys]	19.78338	2.815304	14.23065	19.03611	48
Cys[scFv tripeptide]	9.732902	1.654862	17.00276	9.500876	48

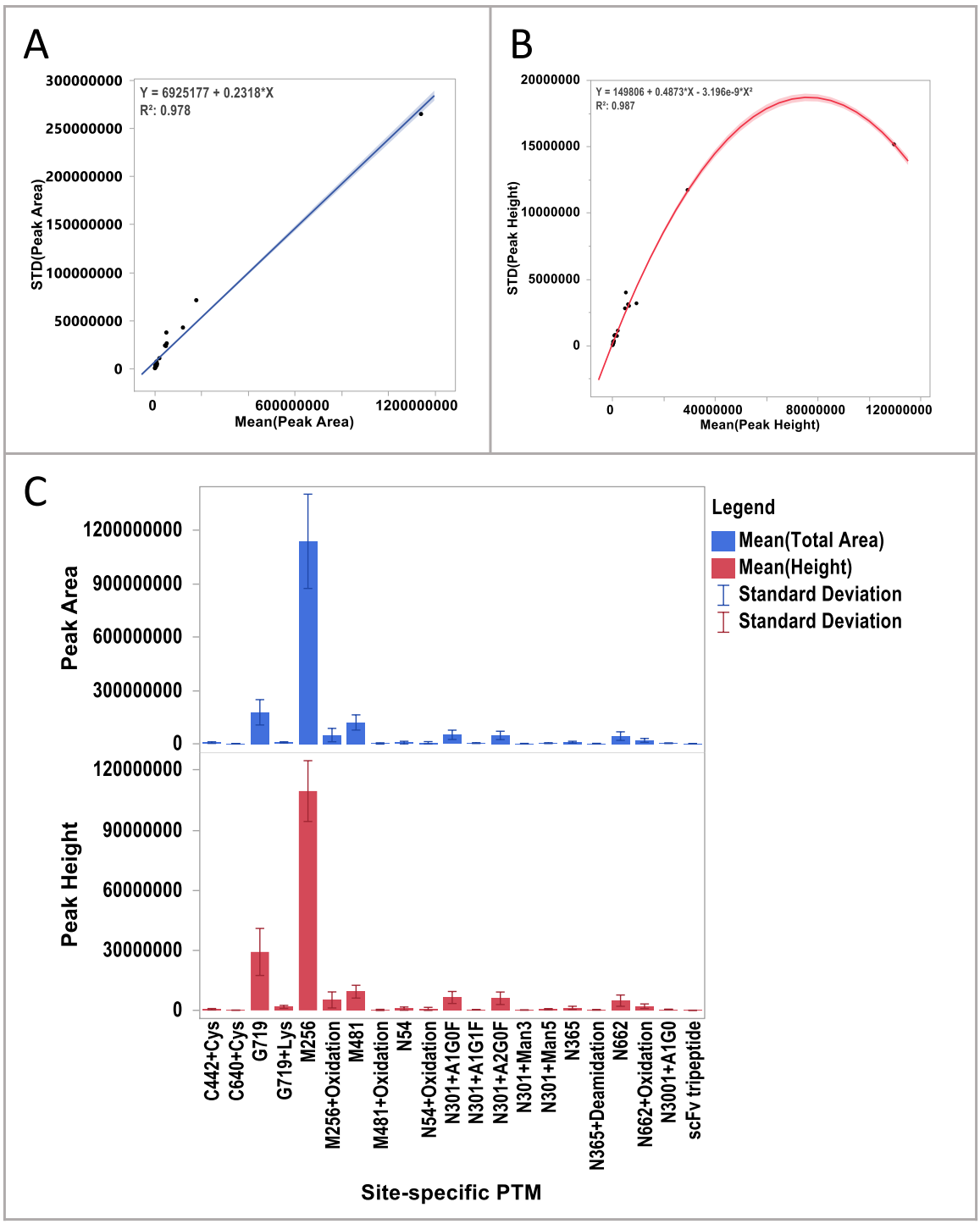

Figure 11.10 Comparison of the standard deviation observed in relation to the ms signal intensity.

A and B) Regression analysis demonstrating the relationship between the PTMs peak areas and peak height with their respective standard deviations amongst the replicate measurements, respectively; C) bar chart visualising the PTMs mean peak area (blue), the mean peak height (red) and their standard deviations amongst the measurement replicates.

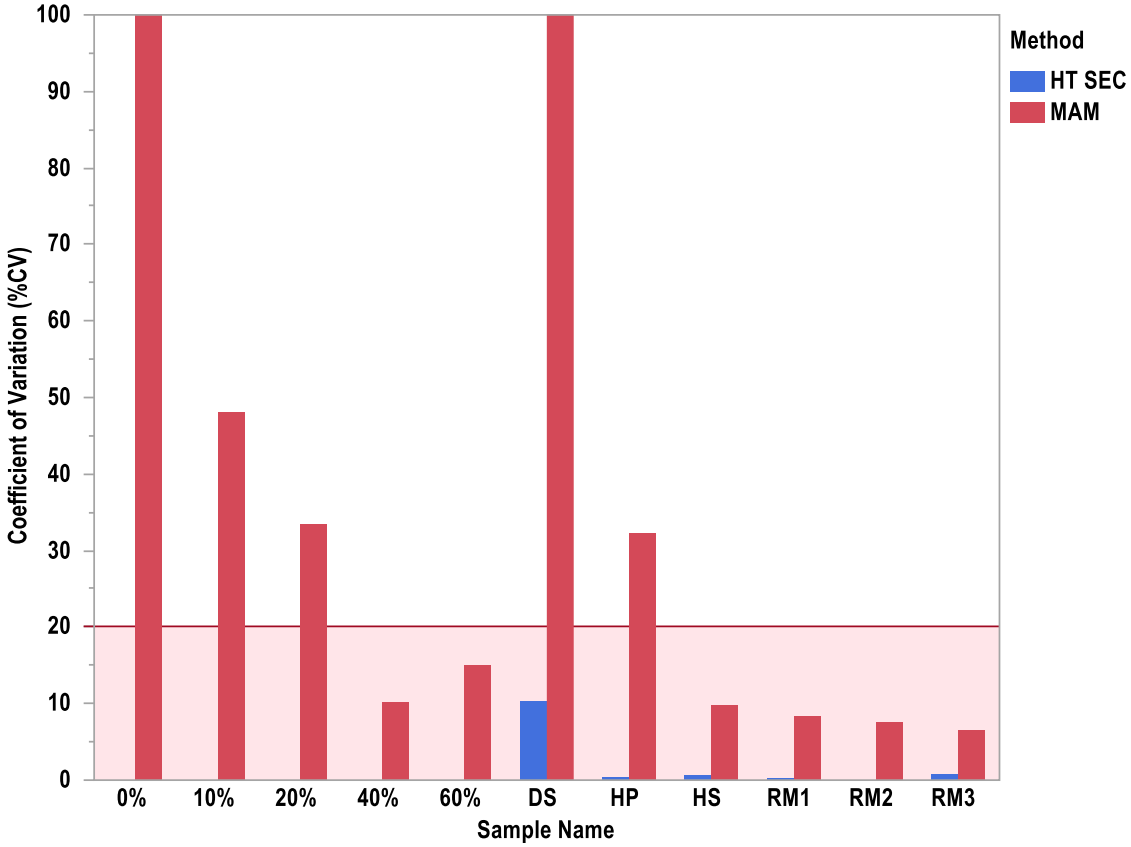

Figure 11.11 Comparison between the HT SEC and MAM method precision in quantifying BsAb-1 HMWS impurities.

Bar chart depicting the CVs of the %HMWS measured by HT SEC (blue) and MAM (red) across BsAb-1 sample replicates. The samples used for the assessment were the same as the ones described for training and testing the model (see Section 5.3.2.1).

Appendix D

Supplementary information related to Chapter 6

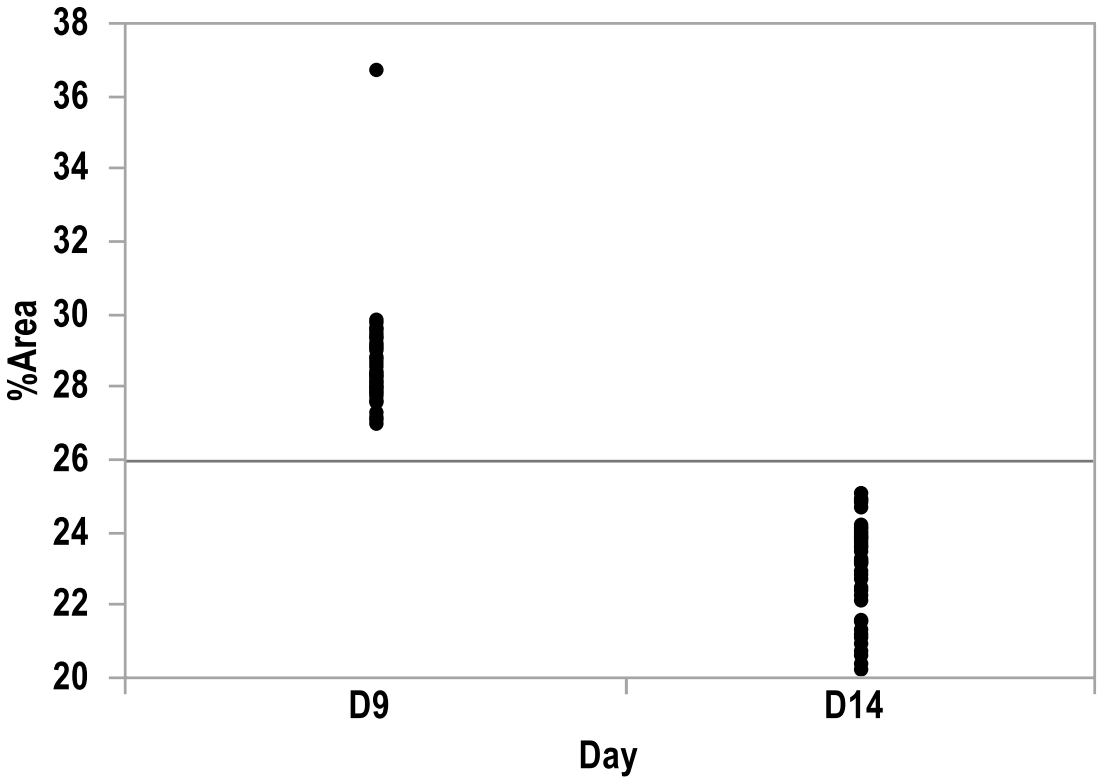

Assuming unequal variances

Difference	-5.5651	t Ratio	-22.4603
Std Err Dif	0.2478	DF	107.2211
Upper CL Dif	-5.0739	Prob > |t|	<.0001 *
Lower CL Dif	-6.0562	Prob > t	1.0000
Confidence	0.95	Prob < t	<.0001 *

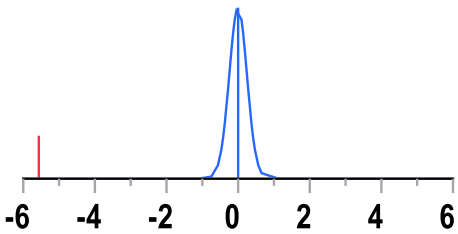

Figure 12.1 T-test of the variation in HMWS levels analysed by HT SEC on day 9 and day 14.

Representation of the % area of the HMWS peak analysed by HT SEC on day 9 and day 14 across all the samples of the second case study (top). T-test summary table (bottom) confirming that the changes in HMWS levels between the two days were significant (p-value <0.05).

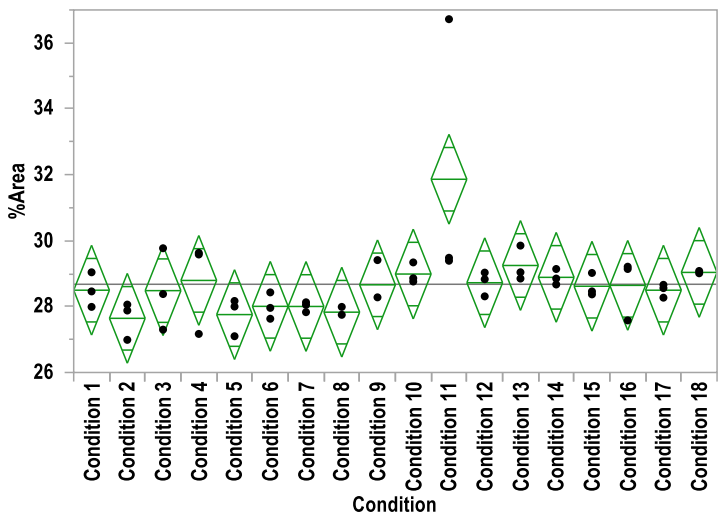

Oneway Anova

Summary of Fit

Rsquare	0.470142
Adj Rsquare	0.219932
Root Mean Square Error	1.163169
Mean of Response	28.6763
Observations (or Sum Wgts)	54

Analysis of Variance

Source	DF	Sum of Squares	Mean Square	F Ratio	Prob > F
Condition	17	43.217393	2.54220	1.8790	0.0552
Error	36	48.706667	1.35296		
C. Total	53	91.924059			

Means for Oneway Anova

Level	Number	Mean	Std Error	Lower 95%	Upper 95%
Condition 1	3	28.4967	0.67156	27.135	29.859
Condition 2	3	27.6433	0.67156	26.281	29.005
Condition 3	3	28.4833	0.67156	27.121	29.845
Condition 4	3	28.7933	0.67156	27.431	30.155
Condition 5	3	27.7567	0.67156	26.395	29.119
Condition 6	3	28.0067	0.67156	26.645	29.369
Condition 7	3	28.0033	0.67156	26.641	29.365
Condition 8	3	27.8300	0.67156	26.468	29.192
Condition 9	3	28.6600	0.67156	27.298	30.022
Condition 10	3	28.9867	0.67156	27.625	30.349
Condition 11	3	31.8633	0.67156	30.501	33.225
Condition 12	3	28.7233	0.67156	27.361	30.085
Condition 13	3	29.2467	0.67156	27.885	30.609
Condition 14	3	28.8867	0.67156	27.525	30.249
Condition 15	3	28.6167	0.67156	27.255	29.979
Condition 16	3	28.6433	0.67156	27.281	30.005
Condition 17	3	28.4967	0.67156	27.135	29.859
Condition 18	3	29.0367	0.67156	27.675	30.399

Std Error uses a pooled estimate of error variance

Figure 12.2 ANOVA of the %HMWS analysed on day 9 across the experimental conditions.

At the top, mean diamonds illustrating the group mean (middle line) and confidence intervals at 95% (top and bottom lines) of the % area of the HMWS peak analysed across the sample replicates (n=3) of each experimental condition. Assuming equal variances across the observations, the height of each diamond is proportional to the reciprocal of the square root of the number of observations in the group (n=3). At the bottom, the ANOVA test of the %HMWS calculated amongst the experimental conditions showing a lack of significance (p-value > 0.05).

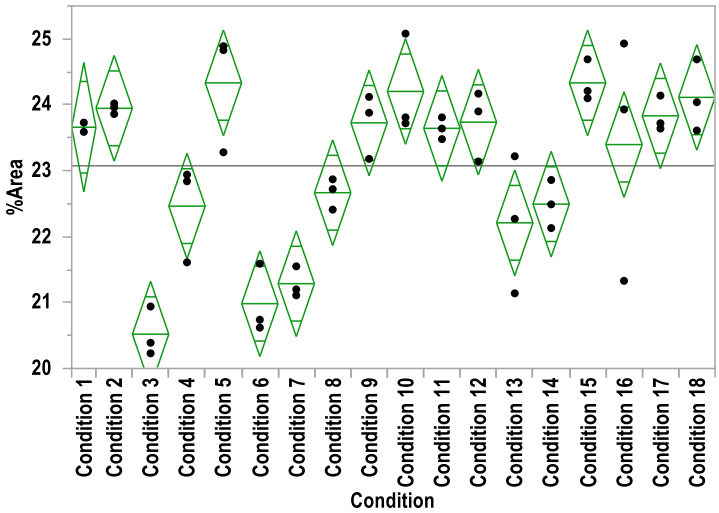

Oneway Anova

Summary of Fit

Rsquare	0.815338
Adj Rsquare	0.725645
Root Mean Square Error	0.68398
Mean of Response	23.07528
Observations (or Sum Wgts)	53

Analysis of Variance

Source	DF	Sum of Squares	Mean Square	F Ratio	Prob > F
Condition	17	72.296121	4.25271	9.0903	<.0001 *
Error	35	16.374000	0.46783		
C. Total	52	88.670121			

Means for Oneway Anova

Level	Number	Mean	Std Error	Lower 95%	Upper 95%
Condition 1	2	23.6600	0.48365	22.678	24.642
Condition 2	3	23.9467	0.39490	23.145	24.748
Condition 3	3	20.5200	0.39490	19.718	21.322
Condition 4	3	22.4633	0.39490	21.662	23.265
Condition 5	3	24.3333	0.39490	23.532	25.135
Condition 6	3	20.9833	0.39490	20.182	21.785
Condition 7	3	21.2867	0.39490	20.485	22.088
Condition 8	3	22.6667	0.39490	21.865	23.468
Condition 9	3	23.7267	0.39490	22.925	24.528
Condition 10	3	24.2033	0.39490	23.402	25.005
Condition 11	3	23.6433	0.39490	22.842	24.445
Condition 12	3	23.7367	0.39490	22.935	24.538
Condition 13	3	22.2100	0.39490	21.408	23.012
Condition 14	3	22.4933	0.39490	21.692	23.295
Condition 15	3	24.3333	0.39490	23.532	25.135
Condition 16	3	23.3967	0.39490	22.595	24.198
Condition 17	3	23.8333	0.39490	23.032	24.635
Condition 18	3	24.1133	0.39490	23.312	24.915

Std Error uses a pooled estimate of error variance

Figure 12.3 ANOVA of the %HMWS analysed on day 14 across the experimental conditions.

At the top, mean diamonds illustrating the group mean (middle line) and confidence intervals at 95% (top and bottom lines) of the % area of the HMWS peak analysed across the sample replicates (n=3) of each experimental condition. Assuming equal variances across the observations, the height of each diamond is proportional to the reciprocal of the square root of the number of observations in the group (n=3). At the bottom, the ANOVA test of the %HMWS calculated amongst the experimental conditions confirming that the %HMWS varied significantly amongst the experimental conditions (p-value < 0.05).

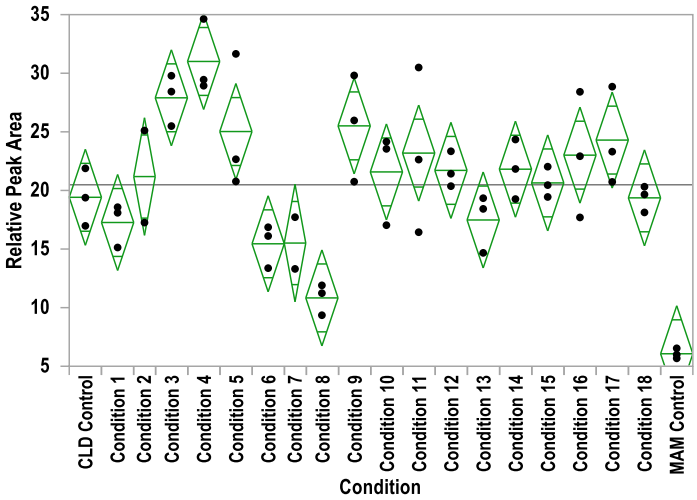

Oneway Anova

Summary of Fit

Rsquare	0.796659
Adj Rsquare	0.694989
Root Mean Square Error	3.504057
Mean of Response	20.48294
Observations (or Sum Wgts)	58

Analysis of Variance

Source	DF	Sum of Squares	Mean Square	F Ratio	Prob > F
Condition	19	1827.9926	96.2101	7.8357	<.0001 *
Error	38	466.5799	12.2784		
C. Total	57	2294.5724			

Means for Oneway Anova

Level	Number	Mean	Std Error	Lower 95%	Upper 95%
CLD Control	3	19.4146	2.0231	15.319	23.510
Condition 1	3	17.2642	2.0231	13.169	21.360
Condition 2	2	21.1838	2.4777	16.168	26.200
Condition 3	3	27.9020	2.0231	23.807	31.998
Condition 4	3	31.0038	2.0231	26.908	35.099
Condition 5	3	25.0251	2.0231	20.930	29.121
Condition 6	3	15.4475	2.0231	11.352	19.543
Condition 7	2	15.5108	2.4777	10.495	20.527
Condition 8	3	10.8302	2.0231	6.735	14.926
Condition 9	3	25.5087	2.0231	21.413	29.604
Condition 10	3	21.5796	2.0231	17.484	25.675
Condition 11	3	23.1852	2.0231	19.090	27.281
Condition 12	3	21.7099	2.0231	17.614	25.805
Condition 13	3	17.4796	2.0231	13.384	21.575
Condition 14	3	21.8128	2.0231	17.717	25.908
Condition 15	3	20.6409	2.0231	16.545	24.736
Condition 16	3	23.0098	2.0231	18.914	27.105
Condition 17	3	24.2957	2.0231	20.200	28.391
Condition 18	3	19.3656	2.0231	15.270	23.461
MAM Control	3	6.0651	2.0231	1.970	10.161

Std Error uses a pooled estimate of error variance

Figure 12.4 ANOVA of C-terminal Lys retention across the experimental conditions on day 9.

At the top, mean diamonds illustrating the group mean (middle line) and confidence intervals at 95% (top and bottom lines) of the % area of the HMWS peak analysed across the sample replicates (n=3) of each experimental condition. Assuming equal variances across the observations, the height of each diamond is proportional to the reciprocal of the square root of the number of observations in the group (n=3). At the bottom, the ANOVA test of the %HMWS calculated amongst the experimental conditions showing significance (p-value < 0.05).

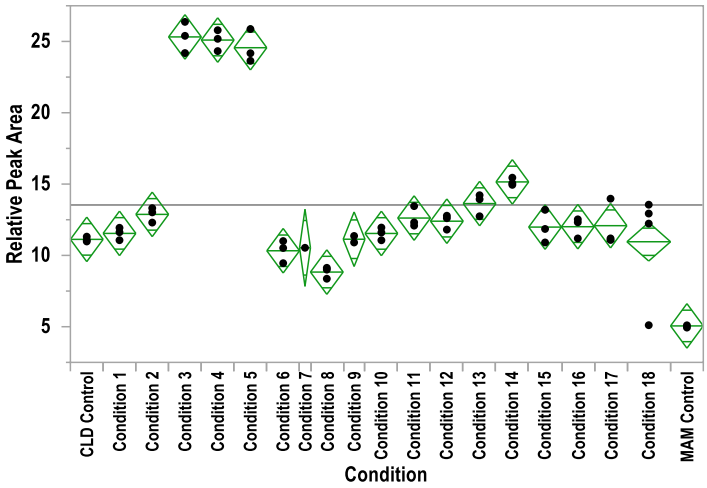

Oneway Anova

Summary of Fit

Rsquare	0.959806
Adj Rsquare	0.939709
Root Mean Square Error	1.335947
Mean of Response	13.53528
Observations (or Sum Wgts)	58

Analysis of Variance

Source	DF	Sum of Squares	Mean Square	F Ratio	Prob > F
Condition	19	1619.5019	85.2369	47.7584	<.0001 *
Error	38	67.8207	1.7848		
C. Total	57	1687.3226			

Means for Oneway Anova

Level	Number	Mean	Std Error	Lower 95%	Upper 95%
CLD Control	3	11.1231	0.7713	9.562	12.685
Condition 1	3	11.5425	0.7713	9.981	13.104
Condition 2	3	12.8757	0.7713	11.314	14.437
Condition 3	3	25.3156	0.7713	23.754	26.877
Condition 4	3	25.0963	0.7713	23.535	26.658
Condition 5	3	24.5599	0.7713	22.998	26.121
Condition 6	3	10.3253	0.7713	8.764	11.887
Condition 7	1	10.5332	1.3359	7.829	13.238
Condition 8	3	8.8313	0.7713	7.270	10.393
Condition 9	2	11.1338	0.9447	9.221	13.046
Condition 10	3	11.5383	0.7713	9.977	13.100
Condition 11	3	12.6175	0.7713	11.056	14.179
Condition 12	3	12.3976	0.7713	10.836	13.959
Condition 13	3	13.6318	0.7713	12.070	15.193
Condition 14	3	15.1513	0.7713	13.590	16.713
Condition 15	3	11.9848	0.7713	10.423	13.546
Condition 16	3	12.0113	0.7713	10.450	13.573
Condition 17	3	12.0826	0.7713	10.521	13.644
Condition 18	4	10.9558	0.6680	9.604	12.308
MAM Control	3	5.0559	0.7713	3.494	6.617

Std Error uses a pooled estimate of error variance

Figure 12.5 ANOVA of C-terminal Lys retention across the experimental conditions on day 14.

At the top, mean diamonds illustrating the group mean (middle line) and confidence intervals at 95% (top and bottom lines) of the % area of the HMWS peak analysed across the sample replicates (n=3) of each experimental condition. Assuming equal variances across the observations, the height of each diamond is proportional to the reciprocal of the square root of the number of observations in the group (n=3). At the bottom, the ANOVA test of the %HMWS calculated amongst the experimental conditions showing significance (p-value < 0.05).

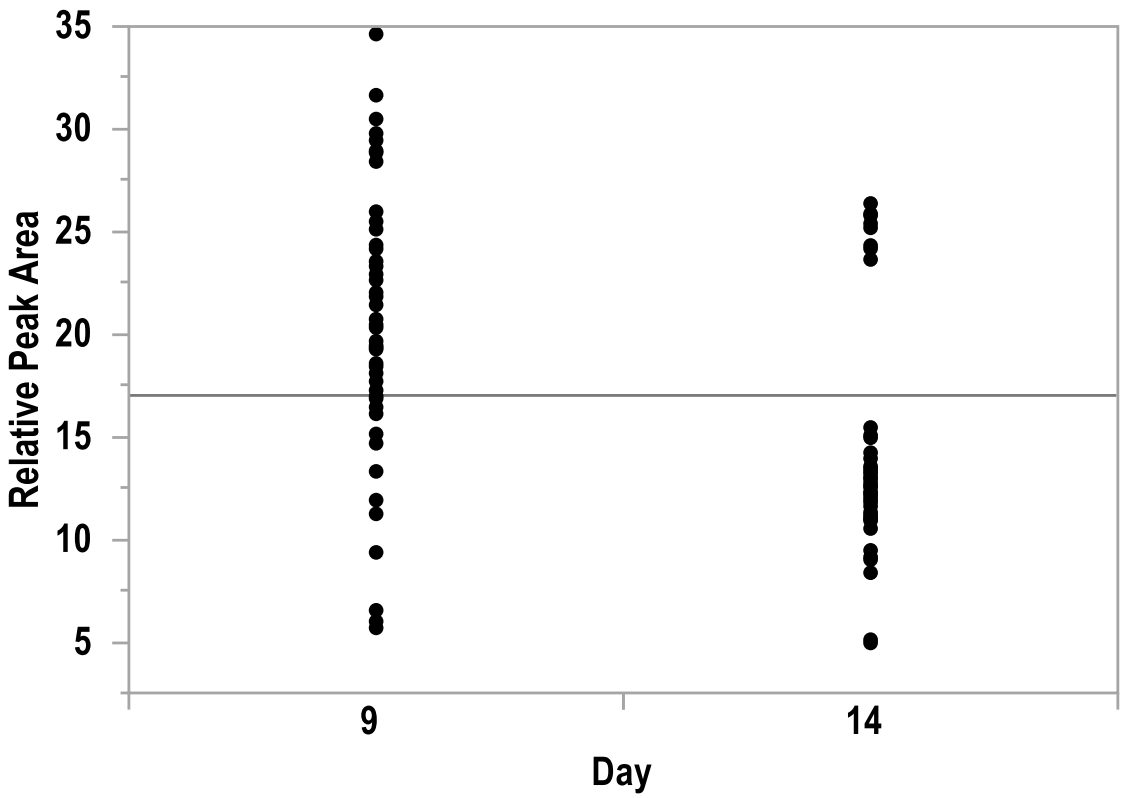

Assuming unequal variances

Difference	-6.9477	t Ratio	-6.3306
Std Err Dif	1.0975	DF	111.409
Upper CL Dif	-4.7730	Prob > |t|	<.0001 *
Lower CL Dif	-9.1223	Prob > t	1.0000
Confidence	0.95	Prob < t	<.0001 *

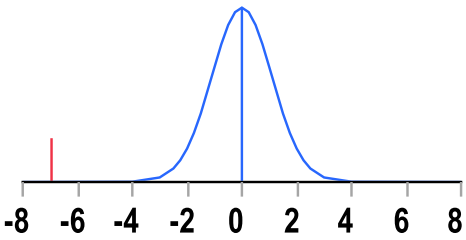

Figure 12.6 T-test of C-terminal Lys retention between day 9 and day 14.

Representation of the % area of the HMWS peak analysed on day 9 and day 14 across all the samples conditions (top). T-test summary table (bottom) confirming that the changes in HMWS levels between the two days were significant (upper confidence limit difference p-value <0.05).

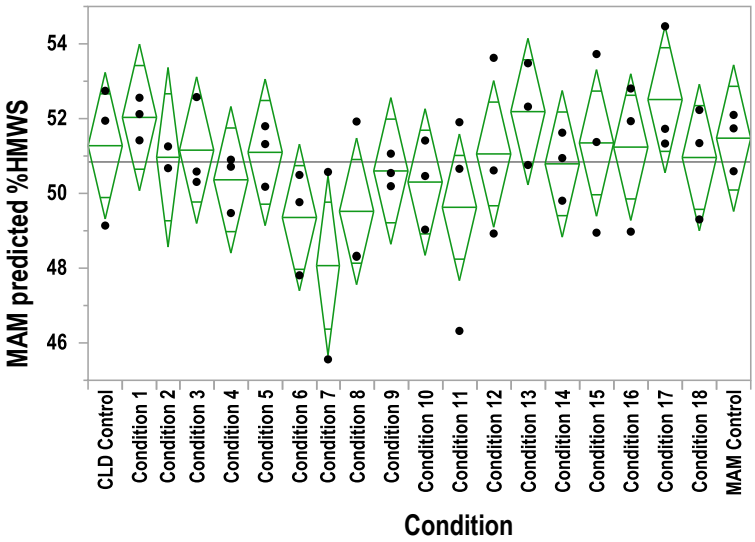

Oneway Anova

Summary of Fit

Rsquare	0.34031
Adj Rsquare	0.010465
Root Mean Square Error	1.677917
Mean of Response	50.84064
Observations (or Sum Wgts)	58

Analysis of Variance

Source	DF	Sum of Squares	Mean Square	F Ratio	Prob > F
Sample Name (%fraction2 blended)	19	55.18983	2.90473	1.0317	0.4513
Error	38	106.98537	2.81540		
C. Total	57	162.17521			

Means for Oneway Anova

Level	Number	Mean	Std Error	Lower 95%	Upper 95%
CLD Control	3	51.2757	0.9687	49.315	53.237
Condition 1	3	52.0329	0.9687	50.072	53.994
Condition 2	2	50.9654	1.1865	48.564	53.367
Condition 3	3	51.1559	0.9687	49.195	53.117
Condition 4	3	50.3628	0.9687	48.402	52.324
Condition 5	3	51.0978	0.9687	49.137	53.059
Condition 6	3	49.3556	0.9687	47.395	51.317
Condition 7	2	48.0670	1.1865	45.665	50.469
Condition 8	3	49.5194	0.9687	47.558	51.481
Condition 9	3	50.6000	0.9687	48.639	52.561
Condition 10	3	50.3030	0.9687	48.342	52.264
Condition 11	3	49.6275	0.9687	47.666	51.589
Condition 12	3	51.0554	0.9687	49.094	53.017
Condition 13	3	52.1867	0.9687	50.226	54.148
Condition 14	3	50.7906	0.9687	48.829	52.752
Condition 15	3	51.3497	0.9687	49.389	53.311
Condition 16	3	51.2378	0.9687	49.277	53.199
Condition 17	3	52.5100	0.9687	50.549	54.471
Condition 18	3	50.9595	0.9687	48.998	52.921
MAM Control	3	51.4770	0.9687	49.516	53.438

Std Error uses a pooled estimate of error variance

Figure 12.7 ANOVA of MAM predicted HMWS across the experimental conditions on day 9.

At the top, mean diamonds illustrating the group mean (middle line) and confidence intervals at 95% (top and bottom lines) of the % area of the HMWS peak analysed across the sample replicates (n=3) of each experimental condition. Assuming equal variances across the observations, the height of each diamond is proportional to the reciprocal of the square root of the number of observations in the group (n=3). At the bottom, the ANOVA test of the %HMWS calculated amongst the experimental conditions showing a lack of significance (p-value > 0.05).

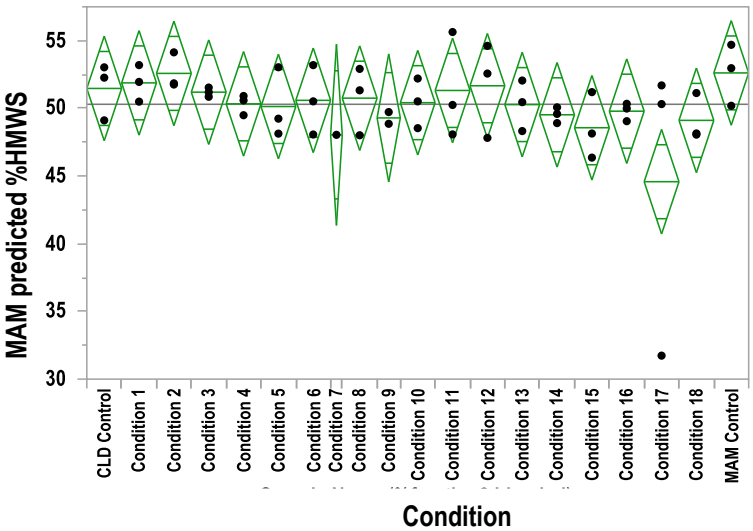

Oneway Anova

Summary of Fit

Rsquare	0.304371
Adj Rsquare	-0.05284
Root Mean Square Error	3.30198
Mean of Response	50.30011
Observations (or Sum Wgts)	57

Analysis of Variance

Source	DF	Sum of Squares	Mean Square	F Ratio	Prob > F
Sample Name (%fraction2 blended)	19	176.51236	9.2901	0.8521	0.6371
Error	37	403.41355	10.9031		
C. Total	56	579.92591			

Means for Oneway Anova

Level	Number	Mean	Std Error	Lower 95%	Upper 95%
CLD Control	3	51.4701	1.9064	47.607	55.333
Condition 1	3	51.8813	1.9064	48.019	55.744
Condition 2	3	52.5820	1.9064	48.719	56.445
Condition 3	3	51.1953	1.9064	47.333	55.058
Condition 4	3	50.3324	1.9064	46.470	54.195
Condition 5	3	50.1358	1.9064	46.273	53.999
Condition 6	3	50.5931	1.9064	46.730	54.456
Condition 7	1	48.0436	3.3020	41.353	54.734
Condition 8	3	50.7530	1.9064	46.890	54.616
Condition 9	2	49.2931	2.3349	44.562	54.024
Condition 10	3	50.4193	1.9064	46.557	54.282
Condition 11	3	51.3217	1.9064	47.459	55.184
Condition 12	3	51.6681	1.9064	47.805	55.531
Condition 13	3	50.2785	1.9064	46.416	54.141
Condition 14	3	49.5246	1.9064	45.662	53.387
Condition 15	3	48.5675	1.9064	44.705	52.430
Condition 16	3	49.7910	1.9064	45.928	53.654
Condition 17	3	44.5820	1.9064	40.719	48.445
Condition 18	3	49.1127	1.9064	45.250	52.975
MAM Control	3	52.6170	1.9064	48.754	56.480

Std Error uses a pooled estimate of error variance

Figure 12.812.9 ANOVA of MAM predicted HMWS across the experimental conditions on day 14.

At the top, mean diamonds illustrating the group mean (middle line) and confidence intervals at 95% (top and bottom lines) of the % area of the HMWS peak analysed across the sample replicates (n=3) of each experimental condition. Assuming equal variances across the observations, the height of each diamond is proportional to the reciprocal of the square root of the number of observations in the group (n=3). At the bottom, the ANOVA test of the %HMWS calculated amongst the experimental conditions showing a lack of significance (p-value > 0.05).

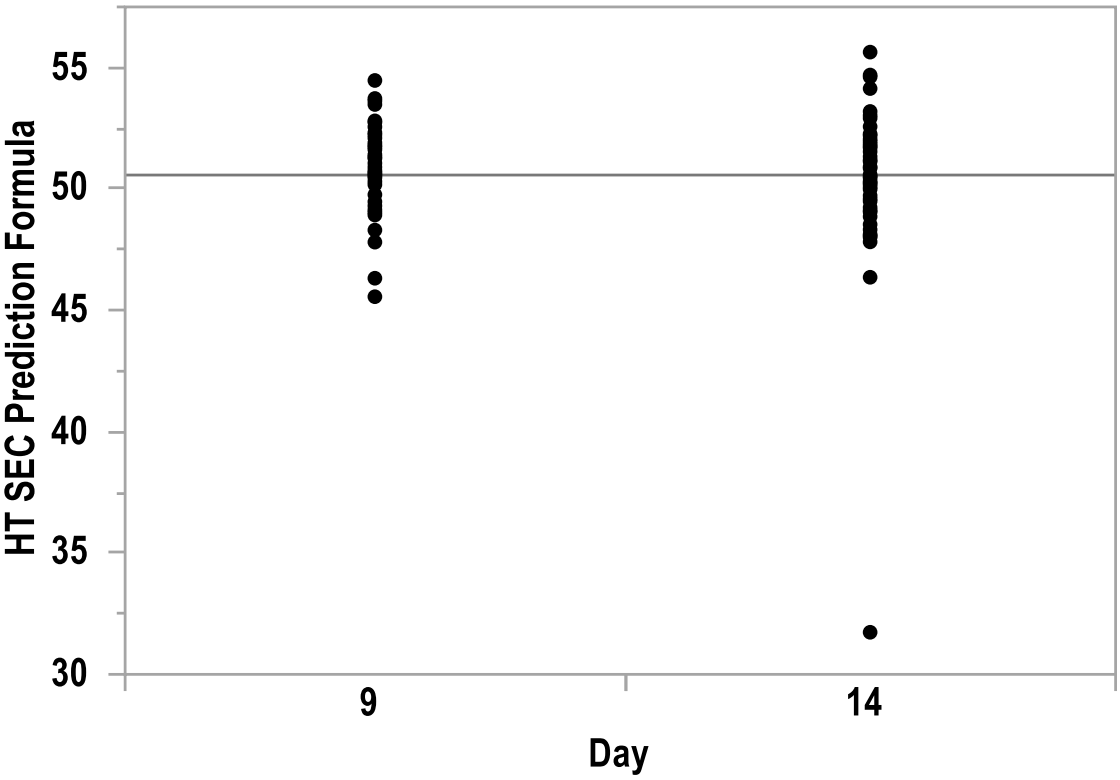

Assuming unequal variances

Difference	-0.5405	t Ratio	-1.12528
Std Err Dif	0.4803	DF	84.28623
Upper CL Dif	0.4147	Prob > |t|	0.2637
Lower CL Dif	-1.4957	Prob > t	0.8682
Confidence	0.95	Prob < t	0.1318

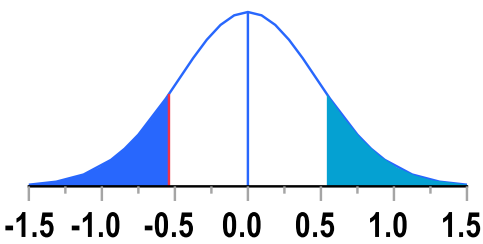

Figure 12.10 T-test of MAM predicted %HMWS between day 9 and day 14.
Representation of the % area of the MAM predicted %HMWS between day 9 and day 14 across all the samples conditions (top). T-test summary table (bottom) confirming that the changes in the MAM predicted HMWS levels between the two days were not significant (p-value >0.05).

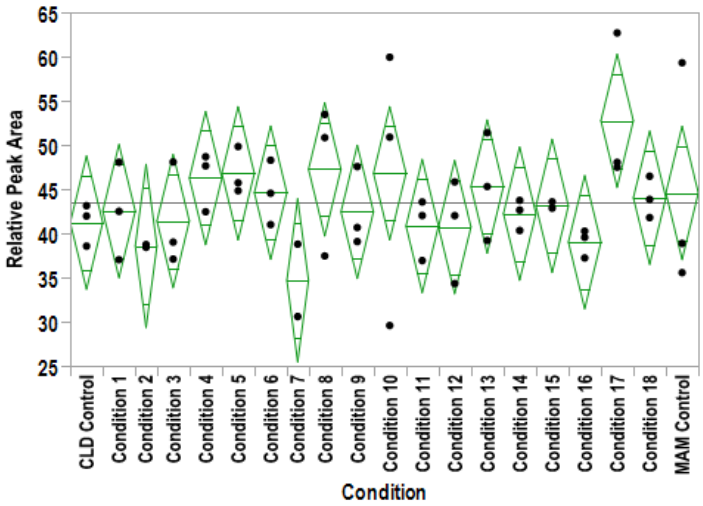

Oneway Anova

Summary of Fit

Rsquare	0.322712
Adj Rsquare	-0.01593
Root Mean Square Error	6.449464
Mean of Response	43.48542
Observations (or Sum Wgts)	58

Analysis of Variance

Source	DF	Sum of Squares	Mean Square	F Ratio	Prob > F
Condition	19	753.1334	39.6386	0.9530	0.5301
Error	38	1580.6321	41.5956		
C. Total	57	2333.7655			

Means for Oneway Anova

Level	Number	Mean	Std Error	Lower 95%	Upper 95%
CLD Control	3	41.2232	3.7236	33.685	48.761
Condition 1	3	42.5252	3.7236	34.987	50.063
Condition 2	2	38.5828	4.5605	29.351	47.815
Condition 3	3	41.3966	3.7236	33.859	48.935
Condition 4	3	46.2576	3.7236	38.720	53.796
Condition 5	3	46.7968	3.7236	39.259	54.335
Condition 6	3	44.6086	3.7236	37.071	52.147
Condition 7	2	34.6897	4.5605	25.458	43.922
Condition 8	3	47.2517	3.7236	39.714	54.790
Condition 9	3	42.4372	3.7236	34.899	49.975
Condition 10	3	46.8047	3.7236	39.267	54.343
Condition 11	3	40.8354	3.7236	33.297	48.373
Condition 12	3	40.7203	3.7236	33.182	48.258
Condition 13	3	45.2973	3.7236	37.759	52.835
Condition 14	3	42.2389	3.7236	34.701	49.777
Condition 15	3	43.1108	3.7236	35.573	50.649
Condition 16	3	39.0107	3.7236	31.473	46.549
Condition 17	3	52.7408	3.7236	45.203	60.279
Condition 18	3	44.0350	3.7236	36.497	51.573
MAM Control	3	44.5789	3.7236	37.041	52.117

Std Error uses a pooled estimate of error variance

Figure 12.11 ANOVA of deamidation of Asn54 across the experimental conditions on day 9.

At the top, mean diamonds illustrating the group mean (middle line) and confidence intervals at 95% (top and bottom lines) of the % area of the HMWS peak analysed across the sample replicates (n=3) of each experimental condition. Assuming equal variances across the observations, the height of each diamond is proportional to the reciprocal of the square root of the number of observations in the group (n=3). At the bottom, the ANOVA test of the %HMWS calculated amongst the experimental conditions showing a lack of significance (p-value > 0.05).

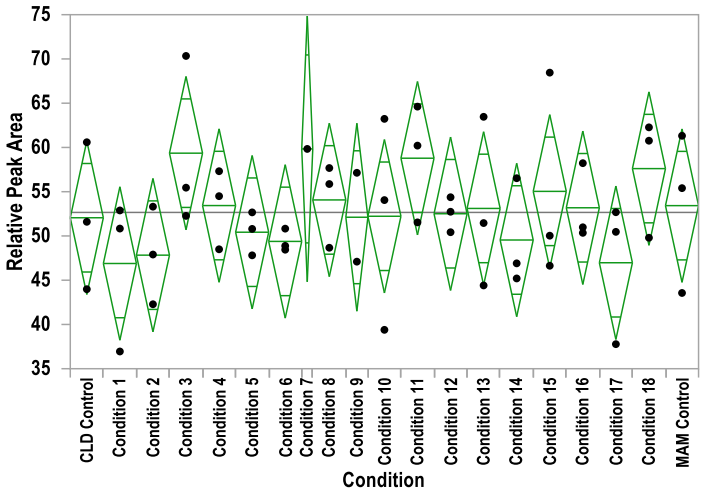

Oneway Anova

Summary of Fit

Rsquare	0.268369
Adj Rsquare	-0.10733
Root Mean Square Error	7.411037
Mean of Response	52.65896
Observations (or Sum Wgts)	57

Analysis of Variance

Source	DF	Sum of Squares	Mean Square	F Ratio	Prob > F
Condition	19	745.4194	39.2326	0.7143	0.7810
Error	37	2032.1682	54.9235		
C. Total	56	2777.5876			

Means for Oneway Anova

Level	Number	Mean	Std Error	Lower 95%	Upper 95%
CLD Control	3	52.0563	4.2788	43.387	60.726
Condition 1	3	46.8877	4.2788	38.218	55.557
Condition 2	3	47.8302	4.2788	39.161	56.500
Condition 3	3	59.3531	4.2788	50.683	68.023
Condition 4	3	53.4342	4.2788	44.765	62.104
Condition 5	3	50.4234	4.2788	41.754	59.093
Condition 6	3	49.3837	4.2788	40.714	58.053
Condition 7	1	59.8325	7.4110	44.816	74.849
Condition 8	3	54.0688	4.2788	45.399	62.738
Condition 9	2	52.1147	5.2404	41.497	62.733
Condition 10	3	52.2237	4.2788	43.554	60.893
Condition 11	3	58.7838	4.2788	50.114	67.453
Condition 12	3	52.5093	4.2788	43.840	61.179
Condition 13	3	53.1089	4.2788	44.439	61.778
Condition 14	3	49.5415	4.2788	40.872	58.211
Condition 15	3	55.0374	4.2788	46.368	63.707
Condition 16	3	53.1840	4.2788	44.514	61.854
Condition 17	3	46.9725	4.2788	38.303	55.642
Condition 18	3	57.6096	4.2788	48.940	66.279
MAM Control	3	53.4248	4.2788	44.755	62.094

Std Error uses a pooled estimate of error variance

Figure 12.12 ANOVA of deamidation of Asn54 across the experimental conditions on day 14.

At the top, mean diamonds illustrating the group mean (middle line) and confidence intervals at 95% (top and bottom lines) of the % area of the HMWS peak analysed across the sample replicates (n=3) of each experimental condition. Assuming equal variances across the observations, the height of each diamond is proportional to the reciprocal of the square root of the number of observations in the group (n=3). At the bottom, the ANOVA test of the %HMWS calculated amongst the experimental conditions showing a lack of significance (p-value > 0.05).

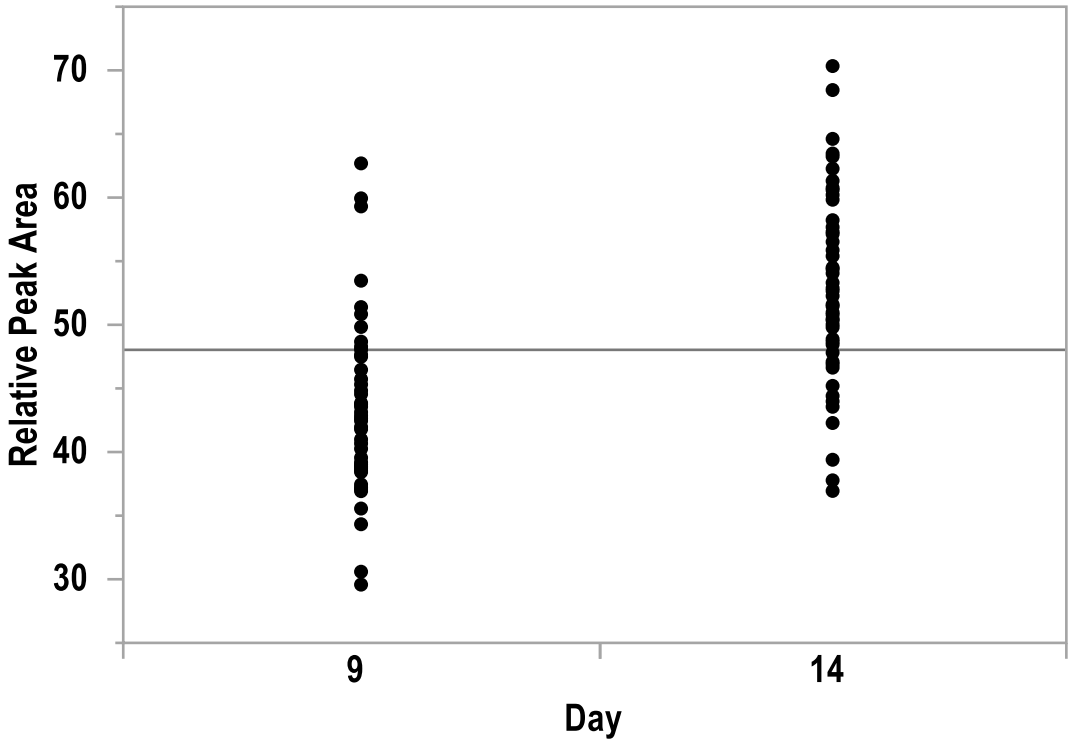

Assuming unequal variances

Difference	9.1735	t Ratio	7.307123
Std Err Dif	1.2554	DF	111.5736
Upper CL Dif	11.6611	Prob > |t|	<.0001 *
Lower CL Dif	6.6860	Prob > t	<.0001 *
Confidence	0.95	Prob < t	1.0000

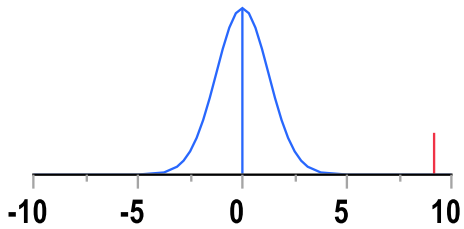

Figure 12.13 T-test of deamidation of Asn54 between day 9 and day 14.

Representation of the % area of the HMWS peak analysed on day 9 and day 14 across all the samples of the second case study (top). T-test summary table (bottom) confirming that the changes in HMWS levels between the two days were significant (upper and lower confidence limit difference p-value <0.05).

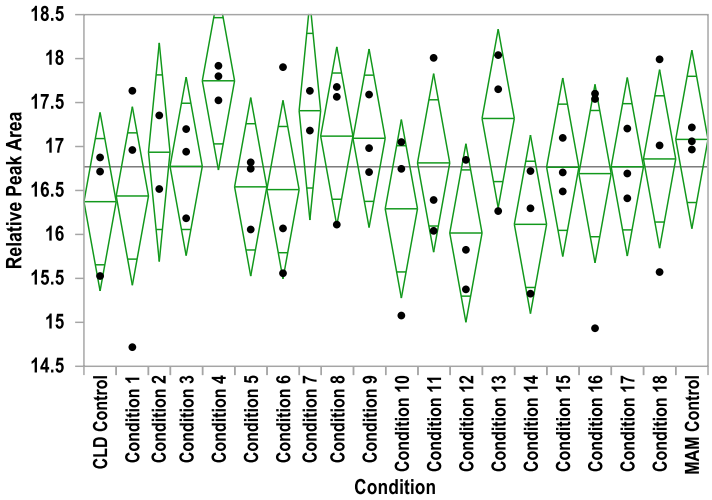

Oneway Anova

Summary of Fit

Rsquare	0.268026
Adj Rsquare	-0.09796
Root Mean Square Error	0.868741
Mean of Response	16.76933
Observations (or Sum Wgts)	58

Analysis of Variance

Source	DF	Sum of Squares	Mean Square	F Ratio	Prob > F
Condition	19	10.501330	0.552702	0.7323	0.7636
Error	38	28.679005	0.754711		
C. Total	57	39.180336			

Means for Oneway Anova

Level	Number	Mean	Std Error	Lower 95%	Upper 95%
CLD Control	3	16.3724	0.50157	15.357	17.388
Condition 1	3	16.4372	0.50157	15.422	17.453
Condition 2	2	16.9350	0.61429	15.691	18.179
Condition 3	3	16.7742	0.50157	15.759	17.790
Condition 4	3	17.7476	0.50157	16.732	18.763
Condition 5	3	16.5411	0.50157	15.526	17.556
Condition 6	3	16.5098	0.50157	15.494	17.525
Condition 7	2	17.4072	0.61429	16.164	18.651
Condition 8	3	17.1179	0.50157	16.103	18.133
Condition 9	3	17.0937	0.50157	16.078	18.109
Condition 10	3	16.2913	0.50157	15.276	17.307
Condition 11	3	16.8135	0.50157	15.798	17.829
Condition 12	3	16.0160	0.50157	15.001	17.031
Condition 13	3	17.3189	0.50157	16.304	18.334
Condition 14	3	16.1146	0.50157	15.099	17.130
Condition 15	3	16.7640	0.50157	15.749	17.779
Condition 16	3	16.6916	0.50157	15.676	17.707
Condition 17	3	16.7692	0.50157	15.754	17.785
Condition 18	3	16.8587	0.50157	15.843	17.874
MAM Control	3	17.0807	0.50157	16.065	18.096

Std Error uses a pooled estimate of error variance

Figure 12.14 ANOVA of deamidation of Asn365 across the experimental conditions on day 9.

At the top, mean diamonds illustrating the group mean (middle line) and confidence intervals at 95% (top and bottom lines) of the % area of the HMWS peak analysed across the sample replicates (n=3) of each experimental condition. Assuming equal variances across the observations, the height of each diamond is proportional to the reciprocal of the square root of the number of observations in the group (n=3). At the bottom, the ANOVA test of the %HMWS calculated amongst the experimental conditions showing a lack of significance (p-value > 0.05).

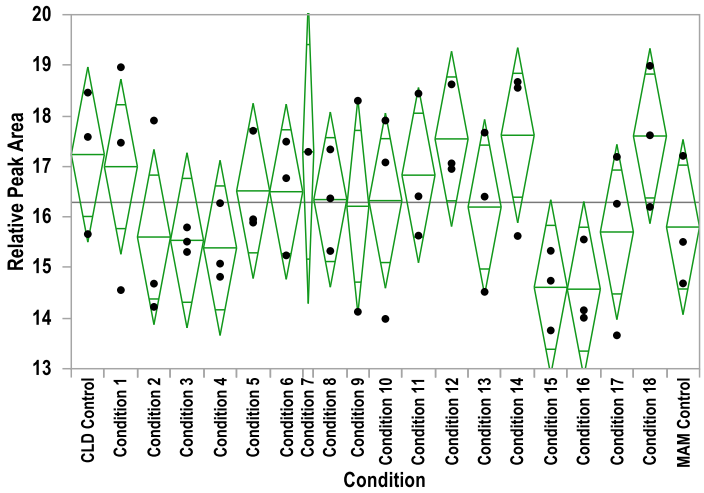

Oneway Anova

Summary of Fit

Rsquare	0.362538
Adj Rsquare	0.035192
Root Mean Square Error	1.480568
Mean of Response	16.28861
Observations (or Sum Wgts)	57

Analysis of Variance

Source	DF	Sum of Squares	Mean Square	F Ratio	Prob > F
Condition	19	46.12722	2.42775	1.1075	0.3829
Error	37	81.10701	2.19208		
C. Total	56	127.23423			

Means for Oneway Anova

Level	Number	Mean	Std Error	Lower 95%	Upper 95%
CLD Control	3	17.2345	0.8548	15.503	18.967
Condition 1	3	16.9947	0.8548	15.263	18.727
Condition 2	3	15.6036	0.8548	13.872	17.336
Condition 3	3	15.5381	0.8548	13.806	17.270
Condition 4	3	15.3892	0.8548	13.657	17.121
Condition 5	3	16.5159	0.8548	14.784	18.248
Condition 6	3	16.4993	0.8548	14.767	18.231
Condition 7	1	17.2880	1.4806	14.288	20.288
Condition 8	3	16.3438	0.8548	14.612	18.076
Condition 9	2	16.2118	1.0469	14.091	18.333
Condition 10	3	16.3237	0.8548	14.592	18.056
Condition 11	3	16.8271	0.8548	15.095	18.559
Condition 12	3	17.5439	0.8548	15.812	19.276
Condition 13	3	16.1964	0.8548	14.464	17.928
Condition 14	3	17.6160	0.8548	15.884	19.348
Condition 15	3	14.6092	0.8548	12.877	16.341
Condition 16	3	14.5727	0.8548	12.841	16.305
Condition 17	3	15.7031	0.8548	13.971	17.435
Condition 18	3	17.6009	0.8548	15.869	19.333
MAM Control	3	15.8009	0.8548	14.069	17.533

Std Error uses a pooled estimate of error variance

Figure 12.15 ANOVA of deamidation of Asn365 across the experimental conditions on day 14.

At the top, mean diamonds illustrating the group mean (middle line) and confidence intervals at 95% (top and bottom lines) of the % area of the HMWS peak analysed across the sample replicates (n=3) of each experimental condition. Assuming equal variances across the observations, the height of each diamond is proportional to the reciprocal of the square root of the number of observations in the group (n=3). At the bottom, the ANOVA test of the %HMWS calculated amongst the experimental conditions showing a lack of significance (p-value > 0.05).

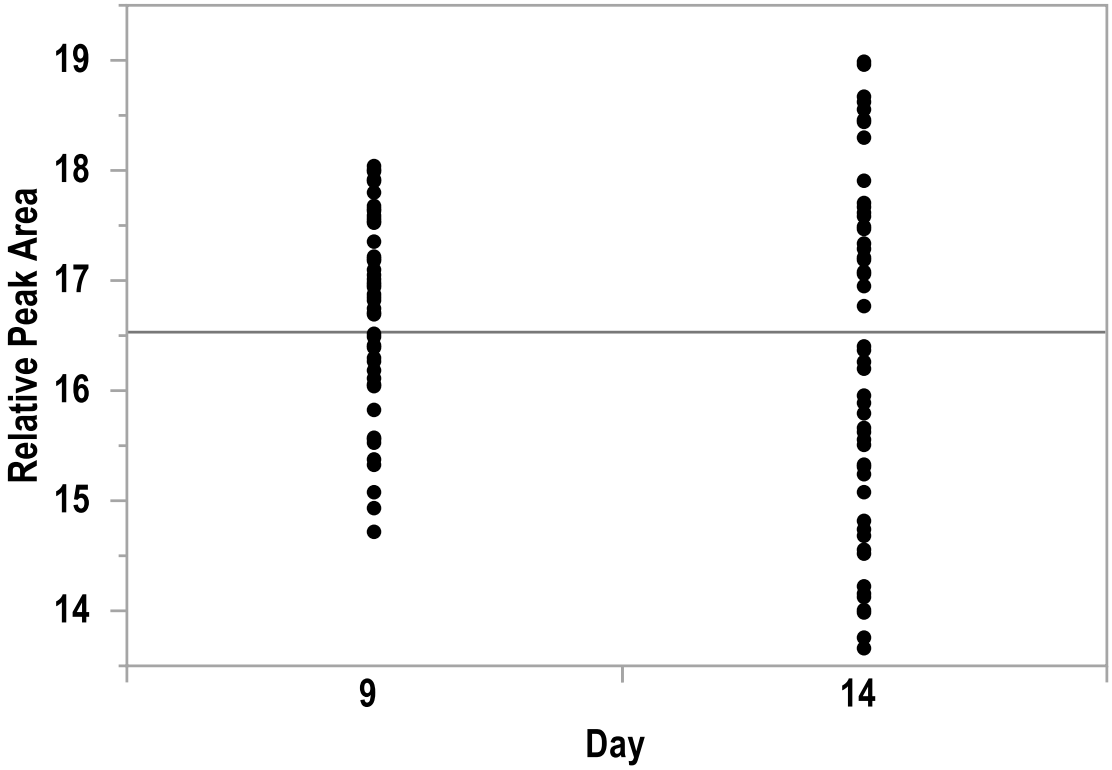

Assuming unequal variances

Difference	-0.48073	t Ratio	-2.114
Std Err Dif	0.22740	DF	86.71882
Upper CL Dif	-0.02872	Prob > |t|	0.0374 *
Lower CL Dif	-0.93273	Prob > t	0.9813
Confidence	0.95	Prob < t	0.0187 *

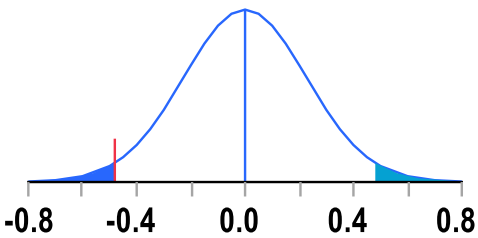

Figure 12.16 T-test of deamidation of Asn365 between day 9 and day 14.

Representation of the % area of the HMWS peak analysed on day 9 and day 14 across all the samples of the second case study (top). T-test summary table (bottom) confirming that the changes in HMWS levels between the two days were significant (upper confidence limit difference p-value <0.05).

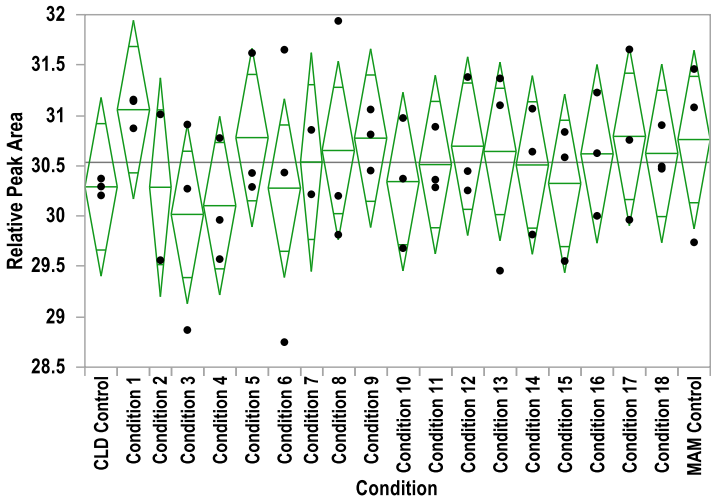

Oneway Anova

Summary of Fit

Rsquare	0.148703
Adj Rsquare	-0.27695
Root Mean Square Error	0.759103
Mean of Response	30.53348
Observations (or Sum Wgts)	58

Analysis of Variance

Source	DF	Sum of Squares	Mean Square	F Ratio	Prob > F
Condition	19	3.824922	0.201312	0.3494	0.9916
Error	38	21.896999	0.576237		
C. Total	57	25.721921			

Means for Oneway Anova

Level	Number	Mean	Std Error	Lower 95%	Upper 95%
CLD Control	3	30.2907	0.43827	29.403	31.178
Condition 1	3	31.0567	0.43827	30.170	31.944
Condition 2	2	30.2863	0.53677	29.200	31.373
Condition 3	3	30.0168	0.43827	29.130	30.904
Condition 4	3	30.1035	0.43827	29.216	30.991
Condition 5	3	30.7793	0.43827	29.892	31.666
Condition 6	3	30.2777	0.43827	29.390	31.165
Condition 7	2	30.5365	0.53677	29.450	31.623
Condition 8	3	30.6515	0.43827	29.764	31.539
Condition 9	3	30.7740	0.43827	29.887	31.661
Condition 10	3	30.3426	0.43827	29.455	31.230
Condition 11	3	30.5115	0.43827	29.624	31.399
Condition 12	3	30.6943	0.43827	29.807	31.582
Condition 13	3	30.6421	0.43827	29.755	31.529
Condition 14	3	30.5078	0.43827	29.621	31.395
Condition 15	3	30.3245	0.43827	29.437	31.212
Condition 16	3	30.6182	0.43827	29.731	31.505
Condition 17	3	30.7917	0.43827	29.904	31.679
Condition 18	3	30.6224	0.43827	29.735	31.510
MAM Control	3	30.7600	0.43827	29.873	31.647

Std Error uses a pooled estimate of error variance

Figure 12.17 ANOVA of deamidation of Asn662 across the experimental conditions on day 9.

At the top, mean diamonds illustrating the group mean (middle line) and confidence intervals at 95% (top and bottom lines) of the % area of the HMWS peak analysed across the sample replicates (n=3) of each experimental condition. Assuming equal variances across the observations, the height of each diamond is proportional to the reciprocal of the square root of the number of observations in the group (n=3). At the bottom, the ANOVA test of the %HMWS calculated amongst the experimental conditions showing a lack of significance (p-value > 0.05).

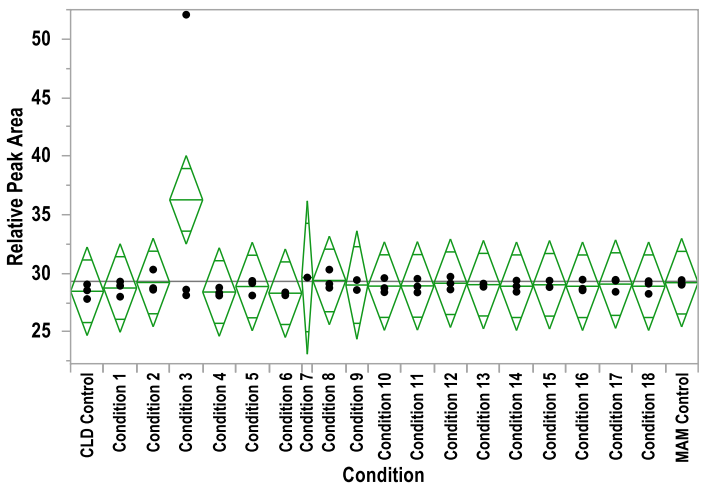

Oneway Anova

Summary of Fit

Rsquare	0.290574
Adj Rsquare	-0.07373
Root Mean Square Error	3.228381
Mean of Response	29.31518
Observations (or Sum Wgts)	57

Analysis of Variance

Source	DF	Sum of Squares	Mean Square	F Ratio	Prob > F
Condition	19	157.95046	8.3132	0.7976	0.6953
Error	37	385.63053	10.4224		
C. Total	56	543.58099			

Means for Oneway Anova

Level	Number	Mean	Std Error	Lower 95%	Upper 95%
CLD Control	3	28.4729	1.8639	24.696	32.250
Condition 1	3	28.7500	1.8639	24.973	32.527
Condition 2	3	29.2228	1.8639	25.446	32.999
Condition 3	3	36.2726	1.8639	32.496	40.049
Condition 4	3	28.4079	1.8639	24.631	32.185
Condition 5	3	28.8784	1.8639	25.102	32.655
Condition 6	3	28.3079	1.8639	24.531	32.085
Condition 7	1	29.6453	3.2284	23.104	36.187
Condition 8	3	29.3951	1.8639	25.618	33.172
Condition 9	2	29.0053	2.2828	24.380	33.631
Condition 10	3	28.9132	1.8639	25.137	32.690
Condition 11	3	28.9307	1.8639	25.154	32.707
Condition 12	3	29.1600	1.8639	25.383	32.937
Condition 13	3	29.0365	1.8639	25.260	32.813
Condition 14	3	28.9039	1.8639	25.127	32.680
Condition 15	3	29.0241	1.8639	25.247	32.801
Condition 16	3	28.9003	1.8639	25.124	32.677
Condition 17	3	29.0846	1.8639	25.308	32.861
Condition 18	3	28.9036	1.8639	25.127	32.680
MAM Control	3	29.2055	1.8639	25.429	32.982

Std Error uses a pooled estimate of error variance

Figure 12.18 ANOVA of deamidation of Asn662 across the experimental conditions on day 14.

At the top, mean diamonds illustrating the group mean (middle line) and confidence intervals at 95% (top and bottom lines) of the % area of the HMWS peak analysed across the sample replicates (n=3) of each experimental condition. Assuming equal variances across the observations, the height of each diamond is proportional to the reciprocal of the square root of the number of observations in the group (n=3). At the bottom, the ANOVA test of the %HMWS calculated amongst the experimental conditions showing a lack of significance (p-value > 0.05).

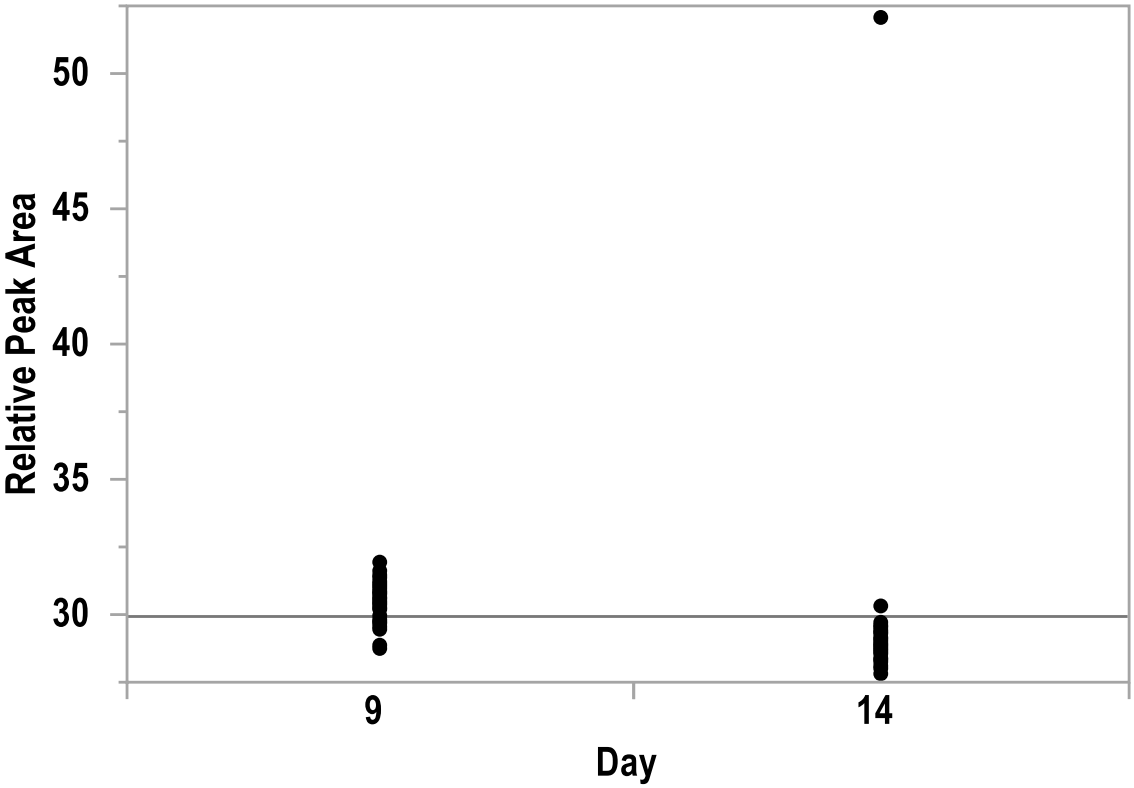

Assuming unequal variances

Difference	-1.2183	t Ratio	-2.88703
Std Err Dif	0.4220	DF	61.1086
Upper CL Dif	-0.3745	Prob > |t|	0.0054 *
Lower CL Dif	-2.0621	Prob > t	0.9973
Confidence	0.95	Prob < t	0.0027 *

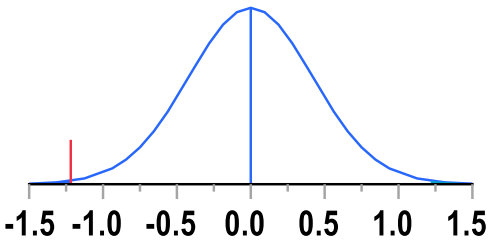

Figure 12.19 T-test of deamidation of Asn662 between day 9 and day 14.

Representation of the % area of the HMWS peak analysed on day 9 and day 14 across all the samples of the second case study (top). T-test summary table (bottom) confirming that the changes in HMWS levels between the two days were significant (upper confidence limit difference p-value <0.05).

Table 12.1 Example of PhyTip purification/HTSEC Python script 1.

Cell Line	Molecule	CLD Sample Name	Titre (mg/L)	CM Volume (mL)	Purification Plate Position	Concentration (mg/ml)	Elution Volume (uL)	e-corrected Concentration (mg/ml)	Min Load (ug)	Volume to inject (ul)	Injection Volume (ul)	Injected mass	Column loading	LOD	LOQ	%R
CAT-S	BsAb-1	A1	208.7	200	A1	0.37	160	0.4	5	13.5	10	3.7	below min mass			141.8
CAT-S	BsAb-1	A2	181.8	200	A2	0.35	160	0.4	5	14.3	10	3.5	below min mass			154
CAT-S	BsAb-1	A3	244.5	200	A3	0.46	160	0.5	5	10.9	10	4.6	below min mass			150.5
CAT-S	BsAb-1	A4	250.9	200	A4	0.41	160	0.4	5	12.2	10	4.1	below min mass			130.7
CAT-S	BsAb-1	A5	432.9	200	A5	0.69	160	0.7	5	7.2	10	6.9	within range			127.5
CAT-S	BsAb-1	A6	974.4	200	A6	1.2	160	1.2	5	4.2	10	12	within range			98.5
CAT-S	BsAb-1	A7	345.1	200	A7	1.12	160	1.1	5	4.5	10	11.2	within range			259.6
CAT-S	BsAb-1	A8	394.6	200	A8	0.61	160	0.6	5	8.2	10	6.1	within range			123.7
CAT-S	BsAb-1	A9	483.8	200	A9	0.57	160	0.6	5	8.8	10	5.7	within range			94.3
CAT-S	BsAb-1	A10	532.9	200	A10	0.73	160	0.7	5	6.8	10	7.3	within range			109.6
CAT-S	BsAb-1	A11	875.3	200	A11	1.03	160	1	5	4.9	10	10.3	within range			94.1
CAT-S	BsAb-1	A12	578.7	200	A12	0.92	160	0.9	5	5.4	10	9.2	within range			127.2
CAT-S	BsAb-1	B1	260.3	200	B1	0.45	160	0.4	5	11.1	10	4.5	below min mass			138.3
CAT-S	BsAb-1	B2	1033.4	200	B2	1.32	160	1.3	5	3.8	10	13.2	within range			102.2
CAT-S	BsAb-1	B3	471.7	200	B3	0.88	160	0.9	5	5.7	10	8.8	within range			149.2
CAT-S	BsAb-1	B4	462.8	200	B4	0.83	160	0.8	5	6	10	8.3	within range			143.5
CAT-S	BsAb-1	B5	967.7	200	B5	1.45	160	1.4	5	3.4	10	14.5	within range			119.9
CAT-S	BsAb-1	B6	134	200	B6	0.38	160	0.4	5	13.2	10	3.8	below min mass			226.9
CAT-S	BsAb-1	B7	921.3	200	B7	0.36	160	0.4	5	13.9	10	3.6	below min mass			31.3
CAT-S	BsAb-1	B8	189.4	200	B8	0.52	160	0.5	5	9.6	10	5.2	within range			219.6
CAT-S	BsAb-1	B9	963.8	200	B9	1.42	160	1.4	5	3.5	10	14.2	within range			117.9
CAT-S	BsAb-1	B10	1327.1	200	B10	1.79	160	1.8	5	2.8	10	17.9	within range			107.9
CAT-S	BsAb-1	B11	341	200	B11	0.56	160	0.6	5	8.9	10	5.6	within range			131.4

CAT-S	BsAb-1	B12	834.4	200	B12	0.88	160	0.9	5	5.7	10	8.8	within range		84.4
CAT-S	BsAb-1	C1	841.8	200	C1	0.85	160	0.8	5	5.9	10	8.5	within range		80.8
CAT-S	BsAb-1	C2	174.9	200	C2	0.36	160	0.4	5	13.9	10	3.6	below min mass		164.7
CAT-S	BsAb-1	C3	127	200	C3	0.24	160	0.2	5	20.8	10	2.4	below min mass		151.2
CAT-S	BsAb-1	C4	342.6	200	C4	0.6	160	0.6	5	8.3	10	6	within range		140.1
CAT-S	BsAb-1	C5	1266	200	C5	1.44	160	1.4	5	3.5	10	14.4	within range		91
CAT-S	BsAb-1	C6	645.6	200	C6	1.12	160	1.1	5	4.5	10	11.2	within range		138.8
CAT-S	BsAb-1	C7	774.4	200	C7	1.04	160	1	5	4.8	10	10.4	within range		107.4
CAT-S	BsAb-1	C8	833.2	200	C8	1.03	160	1	5	4.9	10	10.3	within range		98.9
CAT-S	BsAb-1	C9	209.9	200	C9	0.38	160	0.4	5	13.2	10	3.8	below min mass		144.8
CAT-S	BsAb-1	C10	424.6	200	C10	0.72	160	0.7	5	6.9	10	7.2	within range		135.7
CAT-S	BsAb-1	C11	1174.5	200	C11	1.27	160	1.3	5	3.9	10	12.7	within range		86.5
CAT-S	BsAb-1	C12	808.7	200	C12	1.35	160	1.4	5	3.7	10	13.5	within range		133.5
CAT-S	BsAb-1	D1	388.8	200	D1	0.69	160	0.7	5	7.2	10	6.9	within range		142
CAT-S	BsAb-1	D2	666.2	200	D2	1.31	160	1.3	5	3.8	10	13.1	within range		157.3
CAT-S	BsAb-1	D3	413.7	200	D3	0.72	160	0.7	5	6.9	10	7.2	within range		139.2
CAT-S	BsAb-1	D4	288.3	200	D4	0.52	160	0.5	5	9.6	10	5.2	within range		144.3
CAT-S	BsAb-1	D5	353.9	200	D5	0.59	160	0.6	5	8.5	10	5.9	within range		133.4
CAT-S	BsAb-1	D6	525.9	200	D6	0.9	160	0.9	5	5.6	10	9	within range		136.9
CAT-S	BsAb-1	D7	767	200	D7	0.9	160	0.9	5	5.6	10	9	within range		93.9
CAT-S	BsAb-1	D8	510.4	200	D8	0.82	160	0.8	5	6.1	10	8.2	within range		128.5
CAT-S	BsAb-1	D9	1081	200	D9	1.45	160	1.4	5	3.4	10	14.5	within range		107.3
CAT-S	BsAb-1	D10	1238	200	D10	1.89	160	1.9	5	2.6	10	18.9	within range		122.1
CAT-S	BsAb-1	D11	856	200	D11	1.31	160	1.3	5	3.8	10	13.1	within range		122.4
CAT-S	BsAb-1	D12	72.6	200	D12	0.13	160	0.1	5	38.5	10	1.3	below min mass	below LOQ	143.3
CAT-S	BsAb-1	E1	263.6	200	E1	0.46	160	0.5	5	10.9	10	4.6	below min mass		139.6

CAT-S	BsAb-1	E2	275.7	200	E2	0.51	160	0.5	5	9.8	10	5.1	within range		148
CAT-S	BsAb-1	E3	966.7	200	E3	1.22	160	1.2	5	4.1	10	12.2	within range		101
CAT-S	BsAb-1	E4	796.7	200	E4	0.95	160	1	5	5.3	10	9.5	within range		95.4
CAT-S	BsAb-1	E5	117.1	200	E5	0.24	160	0.2	5	20.8	10	2.4	below min mass		164
CAT-S	BsAb-1	E6	821.5	200	E6	0.88	160	0.9	5	5.7	10	8.8	within range		85.7
CAT-S	BsAb-1	E7	506.9	200	E7	0.89	160	0.9	5	5.6	10	8.9	within range		140.5
CAT-S	BsAb-1	E8	827.1	200	E8	1	160	1	5	5	10	10	within range		96.7
CAT-S	BsAb-1	E9	428.7	200	E9	0.72	160	0.7	5	6.9	10	7.2	within range		134.4
CAT-S	BsAb-1	E10	178.1	200	E10	0.36	160	0.4	5	13.9	10	3.6	below min mass		161.7
CAT-S	BsAb-1	E11	392.1	200	E11	0.66	160	0.7	5	7.6	10	6.6	within range		134.7
CAT-S	BsAb-1	E12	386.4	200	E12	0.68	160	0.7	5	7.4	10	6.8	within range		140.8
CAT-S	BsAb-1	F1	851.9	200	F1	1.15	160	1.2	5	4.3	10	11.5	within range		108
CAT-S	BsAb-1	F2	801.2	200	F2	0.95	160	1	5	5.3	10	9.5	within range		94.9
CAT-S	BsAb-1	F3	488.5	200	F3	0.92	160	0.9	5	5.4	10	9.2	within range		150.7
CAT-S	BsAb-1	F4	203.8	200	F4	0.36	160	0.4	5	13.9	10	3.6	below min mass		141.3
CAT-S	BsAb-1	F5	348.3	200	F5	0.63	160	0.6	5	7.9	10	6.3	within range		144.7
CAT-S	BsAb-1	F6	274.1	200	F6	0.5	160	0.5	5	10	10	5	within range		145.9
CAT-S	BsAb-1	F7	1372.3	200	F7	0.54	160	0.5	5	9.3	10	5.4	within range		31.5
CAT-S	BsAb-1	F8	385.7	200	F8	0.59	160	0.6	5	8.5	10	5.9	within range		122.4
CAT-S	BsAb-1	F9	215.8	200	F9	0.42	160	0.4	5	11.9	10	4.2	below min mass		155.7
CAT-S	BsAb-1	F10	983.3	200	F10	1.41	160	1.4	5	3.5	10	14.1	within range		114.7
CAT-S	BsAb-1	F11	412.1	200	F11	0.74	160	0.7	5	6.8	10	7.4	within range		143.7
CAT-S	BsAb-1	F12	131.6	200	F12	0.27	160	0.3	5	18.5	10	2.7	below min mass		164.1
CAT-S	BsAb-1	G1	196	200	G1	0.43	160	0.4	5	11.6	10	4.3	below min mass		175.5
CAT-S	BsAb-1	G2	225.5	200	G2	0.41	160	0.4	5	12.2	10	4.1	below min mass		145.5
CAT-S	BsAb-1	G3	391.5	200	G3	0.57	160	0.6	5	8.8	10	5.7	within range		116.5
CAT-S	BsAb-1	G4	300.8	200	G4	0.53	160	0.5	5	9.4	10	5.3	within range		141

CAT-S	BsAb-1	G5	291.3	200	G5	0.55	160	0.6	5	9.1	10	5.5	within range		151
CAT-S	BsAb-1	G6	395.2	200	G6	0.73	160	0.7	5	6.8	10	7.3	within range		147.8
CAT-S	BsAb-1	G7	346.8	200	G7	0.74	160	0.7	5	6.8	10	7.4	within range		170.7
CAT-S	BsAb-1	G8	62.4	200	G8	0.22	160	0.2	5	22.7	10	2.2	below min mass		282.1
CAT-S	BsAb-1	G9	618.4	200	G9	0.82	160	0.8	5	6.1	10	8.2	within range		106.1
CAT-S	BsAb-1	G10	633.5	200	G10	1.09	160	1.1	5	4.6	10	10.9	within range		137.6
CAT-S	BsAb-1	G11	320.9	200	G11	0.56	160	0.6	5	8.9	10	5.6	within range		139.6
CAT-S	BsAb-1	G12	464.4	200	G12	0.86	160	0.9	5	5.8	10	8.6	within range		148.1
CAT-S	BsAb-1	H1	468.8	200	H1	1.08	160	1.1	5	4.6	10	10.8	within range		184.3
CAT-S	BsAb-1	H2	316.3	200	H2	0.66	160	0.7	5	7.6	10	6.6	within range		166.9
CAT-S	BsAb-1	H3	753.6	200	H3	1.11	160	1.1	5	4.5	10	11.1	within range		117.8
CAT-S	BsAb-1	H4	845.6	200	H4	0.98	160	1	5	5.1	10	9.8	within range		92.7
CAT-S	BsAb-1	H5	151.4	200	H5	0.41	160	0.4	5	12.2	10	4.1	below min mass		216.6
CAT-S	BsAb-1	H6	348	200	H6	0.65	160	0.6	5	7.7	10	6.5	within range		149.4
CAT-S	BsAb-1	H7	110.3	200	H7	0.67	160	0.7	5	7.5	10	6.7	within range		485.9
CAT-S	BsAb-1	H8	136	200	H8	0.24	160	0.2	5	20.8	10	2.4	below min mass		141.2
CAT-S	BsAb-1	H9	1027.8	200	H9	1.41	160	1.4	5	3.5	10	14.1	within range		109.7
CAT-S	BsAb-1	H10	454.6	200	H10	0.91	160	0.9	5	5.5	10	9.1	within range		160.1
CAT-S	BsAb-1	H11	69.9	200	H11	0.14	160	0.1	5	35.7	10	1.4	below min mass	below LOQ	160.2
CAT-S	BsAb-1	H12	1073.5	200	H12	1.35	160	1.4	5	3.7	10	13.5	within range		100.6

This page was intentionally left blank